

Copyright
By
Jacob Dale Blair
2014

The Thesis committee for Jacob Dale Blair
Certifies that this is the approved version of the following thesis:

**Development of an Integrated Building Load and Ground Source
Heat Pump Model to Assess Heat Pump and Ground Loop
Design and Performance in a Commercial Office Building**

APPROVED BY
SUPERVISING COMMITTEE:

Glenn Y. Masada, Supervisor

Tess J. Moon, Co-Supervisor

**Development of an Integrated Building Load and Ground Source
Heat Pump Model to Assess Heat Pump and Ground Loop
Design and Performance in a Commercial Office Building**

by

Jacob Dale Blair, B.S.M.E

THESIS

Presented to the Faculty of the Graduate School
of the University of Texas at Austin
in Partial Fulfillment
of the Requirements
for the Degree of

MASTER OF SCIENCE IN ENGINEERING

THE UNIVERSITY OF TEXAS AT AUSTIN

May 2014

Dedicated to my friends and family;
you have cultivated my curiosity, making me who I am today.

Acknowledgments

The writing of this thesis would not be possible without the continuous support, feedback and encouragement of my advisor, Dr. Glenn Y. Masada. Through myriad conversations, he helped me to focus on the areas of my research that needed further exploration and let go of the areas I was making needlessly complicated.

Further support has come from my co-advisor, Dr. Tess J. Moon. Her input and recommendations have also been instrumental in moving my project to completion.

Much of the background knowledge used in the execution of this thesis has come thanks to Dr. Atila Novoselac. His courses, Energy Simulation in Building Design and HVAC Design, were indispensable.

Special thanks are due to my wife, Kelly Blair. She has patiently supported me through late nights and early mornings, and she was always ready with an encouraging word when I needed it.

Thanks are also due to father, Thomas Blair, whose conversation at Rudy's Texas Bar-B-Q® helped tip my research from the explore stage to the execution stage.

Thank you to my mother, Anne Dale Blair and my brothers, Devon Blair and Taylor Blair, for their support throughout this project.

My research lab coworkers, Jonathan Gaspredes, Sid Bala, and Sid Shah also contributed extensively through their support and conversations during the project.

The financial support from the U.S. Department of Energy Office of Energy Efficiency and Renewable Energy, Recovery Act-Geothermal Technologies Program: Ground Source Heat Pump Award No. DE-EE0002803 helped make this research possible.

The technical support provided by ClimateMaster, Inc. throughout this project was a significant boon that helped bridge the gap between theory and practice. Special thanks are owed to Mike Hammond for his extensive and frequent contributions. Thanks also to Paul Bony and Dee Brower for their input.

**Development of an Integrated Building Load and Ground Source
Heat Pump Model to Assess Heat Pump and Ground Loop
Design and Performance in a Commercial Office Building**

by

Jacob Dale Blair, MSE

The University of Texas at Austin, 2014

Supervisors: Glenn Y. Masada
Tess J. Moon

Ground source heat pumps (GSHPs) offer an efficient method for cooling and heating buildings, reducing energy usage and operating cost. In hot, arid regions such as Texas and the southwest United States, building load imbalance towards cooling causes design and performance challenges to GSHP systems in residential and commercial building applications.

An integrated building load and GSHP model is developed in this thesis to test approaches to reduce GSHP cost, to properly size ground heat exchanger (GHEX) installations and to offer methods to improve GSHP performance in commercial buildings. The integrated model is comprised of a three-story office building, heat pumps, air handling system and a GHEX. These component models were integrated in the Matlab® Simulink® modeling environment, which allows for easy model modification and expansion.

The building-load model was developed in HAMBASE, which simulates the thermal and hygric response of each zone in the building to external weather and internal loads. The building-load model was validated using the ASHRAE 140-2007 Standard

Method of Test and with results from EnergyPlus. The heat pump model was developed as a performance map, based on data commonly provided by heat pump manufacturers. This approach allows for easy expansion of the number and type of heat pump models supported. The GHEX model was developed at Oklahoma State University and is based on Eskilson's g-function model of vertical borehole operation. The GHEX model accurately represents the interaction between boreholes and the ground temperature response over short and long time-intervals. The GHEX model uses GLHEPRO files for parameter inputs.

Long time-interval simulations of the integrated model are provided to assess the sensitivity of the GSHP system to various model parameters. These studies show that: small changes in the total GHEX length reduce system cost with minimal impact on performance; increased borehole spacing improves system performance with no additional cost; supplemental heat rejection reduces installation costs and improves system performance; industry-recommended design cutoff temperatures properly size the GHEX system; and, while cooling is the greatest contributor to operating cost in the southwest and southcentral United States, heating is the limiting design case for GHEX sizing.

Table of Contents

Acknowledgments	v
Abstract	vi
Table of Contents	viii
List of Tables	xiii
List of Figures	xviii
Chapter 1 Introduction	1
1.1. GSHP Defined.....	2
1.2. Barriers to GSHP adoption.....	7
1.3. Research Objectives	9
Chapter 2 Literature Review	10
2.1. Modeling of Building Physics.....	10
2.2. Modeling a Water-Source Heat Pump	11
2.3. Modeling of Ground Heat Exchanger	13
Chapter 3 Office Building Model	17
3.1. Physical Layout	17
3.2. Building Construction	20
3.3. Fenestration	22
3.4. Load Scheduling.....	22
3.5. Internal Loads.....	23
3.5.1. People	23
3.5.2. Lighting	25
3.5.3. Equipment.....	27
3.5.4. Elevators	29
3.5.5. Modeling of Sensible Loads	30

3.5.6. Summary of Sensible and Latent Loads	31
3.6. External Loads.....	34
3.6.1. Ventilation	34
3.6.2. Infiltration.....	36
3.6.3. Weather.....	39
3.7. Temperature Control	39
Chapter 4 Integrated Building-Load + GSHP Model	42
4.1. Simulation Order	43
4.2. Building Subsystem Model	45
4.3. Thermostat and Timing Subsystem.....	48
4.4. HVAC Subsystem Model.....	49
4.4.1. Plenum Subsystem Model	52
4.4.2. Heat Pump Subsystem Model.....	55
4.4.3. Heat Pump Sizing	68
4.4.4. Heat Pump Header Subsystem Model	71
4.5. Ground Loop Subsystem Model	72
4.5.1. Ground Loop Sizing	75
4.6. Ground Loop Water Pump Subsystem Model	78
4.7. Data Storage and Processing	79
4.8. Model Simulation.....	81
Chapter 5 Validation of the Integrated Model and Subsystems.....	85
5.1. Test Overview	86
5.2. Testing Standard.....	86
5.2.1. Standards for Open-Loop Temperature Tests	87
5.2.2. Standards for Closed-Loop Temperature Tests	88
5.2.3. Summary of Testing Standards.....	90
5.3. Open-Loop Tests of HAMBASE Building Load Model	91

5.3.1. Test Set 1: Open-Loop, Constant Weather, No Internal Loads.....	92
5.3.2. Test Set 2: Open-Loop, Ambient Temperature-Step, No Internal Loads.....	97
5.3.3. Test Set 3: Open-Loop, Ambient Relative Humidity-Step, No Internal Loads	104
5.3.4. Test Set 4: Open-Loop, Weather-Sine, No Internal Loads.....	107
5.3.5. Test Set 5: Open-Loop, Actual Weather, No Internal Loads	114
5.3.6. Test Set 6: Open-Loop, Constant Weather, Actual Internal Loads	119
5.3.7. Test Set 7: Open-Loop, Actual Weather, Actual Internal Loads.....	125
5.4. Closed-Loop Comparison of Integrated Model	131
5.5. Summary of Validation Results	134
Chapter 6 Base Model Results	136
6.1. Time-Step Results	137
6.1.1. Time-Step Zone Data.....	137
6.1.2. Time-Step Ground Loop Data	141
6.2. Hourly Results.....	142
6.2.1. Hourly Temperature Data	142
6.2.2. Hourly Heating and Cooling Data	144
6.2.3. Hourly Heat Pump Efficiency Data.....	146
6.2.4. Hourly Heat Rejection Data	149
6.2.5. Hourly Heat Pump Water Temperature Data	151
6.2.6. Hourly Ground Loop Water Temperature Data	153
6.3. Monthly Results	154
6.3.1. Monthly Heating and Cooling Data.....	154
6.3.2. Monthly Ground Loop Data	156
6.3.3. Monthly Power Usage Data.....	157
6.3.4. Monthly Out-of-Setpoint Data.....	159
6.3.5. Monthly Heat Pump Efficiency Data	161
6.4. Annual Results	163

6.4.1. Annual Heating and Cooling Data.....	163
6.4.2. Annual Ground Loop Data	168
6.4.3. Annual Power Usage Data.....	171
6.4.4. Annual Out-of-Setpoint Data.....	173
6.4.5. Annual Heat Pump Efficiency Data	175
6.5. Summary of Base Model Results	179
Chapter 7 Sensitivity Studies	180
7.1. Heat Pump EWT Design Cutoff Temperature	181
7.2. Borehole Spacing	192
7.3. Borehole Depth	204
7.4. Supplemental Heat Rejection.....	214
Chapter 8 Conclusions.....	229
8.1. Recommendations for Future Work.....	231
Appendix.....	232
A.1. Additional Load Profiles	232
A.2. Additional Performance Map Data.....	236
A.3. Inlet Air Correction Factors	237
A.4. Additional GLHEPRO Data.....	239
A.4.1. Peak Load Analysis Tool.....	239
A.4.2. Use of GLHEPRO	242
A.5. Additional Validation Tests.....	245
A.5.1. Test Set 8: Open-Loop, Ambient Temperature and Relative Humidity -Sine, No Internal Loads.....	245
A.5.2. Test Set 9: Open-Loop Direct Normal Irradiance-Sine, No Internal Loads	248
A.5.3. Test Set 10: Open-Loop, Diffuse Horizontal Irradiance-Sine, No Internal Loads	252

A.5.4. Test Set 11: Open-Loop, Constant Weather, People Loads	256
A.5.5. Test Set 13: Open-Loop, Constant Weather, Equipment Loads.....	260
A.5.6. Closed-Loop Heating and Cooling Data.....	265
A.6. Additional Hourly Data for the Base Model	271
A.7. Additional Monthly Data for the Base Model.....	273
A.8. Additional Annual Data for the Base Model.....	274
A.9. Additional Data for the EWT Cutoff Sensitivity Study	276
A.10. Additional Data for the Borehole Spacing Study.....	283
A.11. Additional Data for the Borehole Depth Study.....	292
A.12. Additional Data for the SHR Study.....	301
Bibliography	319

List of Tables

Table 1: Zone dimensions, SI units (U.S. Department of Energy, 2010).....	19
Table 2: Zone dimensions, BI units (U.S. Department of Energy, 2010).....	20
Table 3: Properties of construction materials	21
Table 4: Peak heat rates resulting from people by zone	24
Table 5: Peak heat rates resulting from lighting by zone.....	26
Table 6: Peak heat rates resulting from equipment by zone	28
Table 7: Example calculation of convective fraction for Core2 zone	31
Table 8: Convective factors by zone.....	31
Table 9: Total latent and sensible heat rates by zone.....	33
Table 10: Ventilation values by zone.....	35
Table 11: Infiltration values by zone	37
Table 12: Weather inputs to HAMBASE	39
Table 13: Performance map linear interpolation, step1	61
Table 14: Performance map linear interpolation, step2	61
Table 15: Heat pump operating limits	61
Table 16: Inlet air limits for correction factor calculation.....	66
Table 17: Heat pump sizing based on EnergyPlus design days.....	68
Table 18: HVAC capacity for EnergyPlus variable air volume system	69
Table 19: Heat pump sizing based on EnergyPlus HVAC capacity.....	69
Table 20: Heat pump sizes used in the HAMBASE model	70
Table 21: HAMBASE building loads (SI units) used as GLHEPRO inputs	75
Table 22: HAMBASE building loads (BI units) used as GLHEPRO inputs.....	76
Table 23: Ground loop properties used for the base model in GLHEPRO	77
Table 24: Hourly averaging of cooling and heating values for West1	84
Table 25: Free-floating temperature results from ASHRAE 140-2007.....	87
Table 26: Benchmarks for open-loop temperature tests	88
Table 27: Closed-loop annual heating & cooling results from ASHRAE 140-2007.....	89

Table 28: Closed-loop peak heating & cooling results from ASHRAE 140-2007.....	90
Table 29: List of testing benchmarks.....	91
Table 30: Summary of open-loop validation tests.....	91
Table 31: Summary of supplementary open-loop validation tests.....	92
Table 32: Open-loop constant weather inputs.....	93
Table 33: Steady-state temperature after constant weather input.....	96
Table 34: Steady-state relative humidity after constant weather input.....	97
Table 35: Temperature results for open-loop temperature-step input.....	102
Table 36: EnergyPlus and HAMBASE time constant for ambient temperature -step input.....	103
Table 37: Relative humidity results for open-loop RH-step input.....	106
Table 38: EnergyPlus and HAMBASE time constant for ambient RH-step input.....	107
Table 39: Temperature results for open-loop weather-sine input.....	112
Table 40: Relative humidity results for open-loop weather-sine input.....	113
Table 41: Temperature results for open-loop actual weather input.....	118
Table 42: Relative humidity results for open-loop actual weather input.....	119
Table 43: Temperature results for open-loop, actual internal load input.....	123
Table 44: Relative humidity results for open-loop, actual internal load input.....	124
Table 45: Temperature results for open-loop, actual internal load and weather input.....	129
Table 46: Relative humidity results for open-loop, actual internal load and weather input.....	130
Table 47: Data for the annual total cooling energy provided in the base model.....	164
Table 48: Data for the annual total hours of cooling operation in the base model.....	165
Table 49: Data for the annual total heating energy provided in the base model.....	167
Table 50: Data for the annual total hours of heating operation in the base model.....	168
Table 51: Data for the annual total heat rejected to the ground loop in the base model.....	169
Table 52: Data for the annual extremes for heat pump EWT in the base model.....	171

Table 53: Data for the annual total power usage during cooling in the base model.....	172
Table 54: Data for the annual total power usage during heating in the base model.....	173
Table 55: Data for the annual total time out-of-setpoint in the base model	175
Table 56: Data for the annual average cooling EER in the base model	176
Table 57: Data for the annual average heating COP in the base model	178
Table 58: Ground loop specifications for heat pump EWT design cutoff temperature test.....	181
Table 59: Data for the maximum annual EWT in the EWT cutoff test.....	183
Table 60: Data for the annual average EER in the EWT cutoff test.....	190
Table 61: Summary of results for EWT cutoff test.....	192
Table 62: Ground loop specifications for the borehole spacing tests	193
Table 63: Data for the maximum annual EWT for the borehole spacing test	194
Table 64: Data for the annual average EER in the borehole spacing test.....	201
Table 65: Summary of results for borehole spacing test.....	203
Table 66: Lot size required for the borehole spacing tests	203
Table 67: Ground loop specifications for the borehole depth tests	204
Table 68: Data for the maximum annual EWT for the borehole depth test.....	205
Table 69: Data for the annual average EER in the borehole depth test	212
Table 70: Summary of results for borehole depth test.....	214
Table 71: Ground loop specifications for the SHR tests.....	215
Table 72: Data for the maximum annual EWT for the SHR test.....	217
Table 73: Data for the annual average EER in the SHR test	226
Table 74: Summary of results for SHR test.....	228
Table 75: Temperature results for open-loop temperature and RH-sine input	247
Table 76: Relative humidity results for open-loop temperature and RH-sine input.....	248
Table 77: Temperature results for open-loop DNI-sine input	251
Table 78: Relative humidity results for open-loop DNI-sine input	252
Table 79: Temperature results for open-loop DHI-sine input	255
Table 80: Relative humidity results for open-loop DHI-sine input	256

Table 81: Temperature results for open-loop constant people input	259
Table 82: Relative humidity results for open-loop constant people input	260
Table 83: Temperature results for open-loop constant people input	263
Table 84: Relative humidity results for open-loop constant people input	264
Table 85: HAMBASE and EnergyPlus annual heating and cooling data.....	265
Table 86: HAMBASE and EnergyPlus annual sensible and latent cooling data.....	266
Table 87: HAMBASE and EnergyPlus peak heating and cooling data.....	268
Table 88: HAMBASE and EnergyPlus peak sensible and latent data.....	270
Table 89: Data for the minimum annual EWT for the EWT cutoff test	276
Table 90: Data for the total annual cooling in the EWT cutoff test.....	277
Table 91: Data for the total annual heating in the EWT cutoff test.....	278
Table 92: Data for the total annual time out-of-setpoint in the EWT cutoff test.....	279
Table 93: Data for the total annual cooling power usage in the EWT cutoff test.....	280
Table 94: Data for the total annual heating power usage in the EWT cutoff test.....	281
Table 95: Data for the annual average COP in the EWT cutoff test.....	282
Table 96: Data for the average annual EWT for the borehole spacing test	284
Table 97: Data for the minimum annual EWT for the borehole spacing test	285
Table 98: Data for the total annual cooling for the borehole spacing test	286
Table 99: Data for the total annual heating for the borehole spacing test	287
Table 100: Data for the annual time out-of-setpoint for the borehole spacing test	288
Table 101: Data for the total annual cooling power usage for the borehole spacing test	289
Table 102: Data for the total annual heating power usage for the borehole spacing test	290
Table 103: Data for the annual average COP for the borehole spacing test	291
Table 104: Data for the average annual EWT for the borehole depth test	293
Table 105: Data for the minimum annual EWT for the borehole depth test	294
Table 106: Data for the total annual cooling for the borehole depth test	295
Table 107: Data for the total annual heating for the borehole depth test.....	296

Table 108: Data for the total annual time out-of-setpoint for the borehole depth test	297
Table 109: Data for the total annual cooling power usage for the borehole depth test	298
Table 110: Data for the total annual heating power usage for the borehole depth test	299
Table 111: Data for the annual average COP for the borehole depth test	300
Table 112: GLHEPRO total monthly cooling design loads for the SHR test.....	302
Table 113: GLHEPRO total monthly heating design loads for the SHR test.....	302
Table 114: GLHEPRO peak monthly cooling design loads for the SHR test	303
Table 115: GLHEPRO peak monthly heating design loads for the SHR test	303
Table 116: Data for the average annual EWT for the SHR test.....	305
Table 117: Data for the minimum annual EWT for the SHR test	306
Table 118: Data for the total annual cooling for the SHR test.....	307
Table 119: Data for the total annual time in cooling operation for the SHR test	308
Table 120: Data for the ratio of net annual heat rejected per unit GHEX length for the SHR test.....	309
Table 121: Data for the ratio of net annual cooling provided per hour of cooling operation for the SHR test.....	311
Table 122: Data for the total annual heating for the SHR test.....	312
Table 123: Data for the total annual time out-of-setpoint for the SHR test.....	313
Table 124: Data for the annual net heat rejected to the ground loop for the SHR test	315
Table 125: Data for the total annual cooling power usage for the SHR test	316
Table 126: Data for the total annual heating power usage for the SHR test.....	317
Table 127: Data for the annual average COP for the SHR test	318

List of Figures

Figure 1: Ground-source heat pump schematic for summer operation (cooling mode).....	2
Figure 2: Ground-source heat pump schematic for winter operation (heating mode).....	3
Figure 3: Air-source heat pump schematic for summer operation (cooling mode).....	4
Figure 4: Annual air and soil temperature variation for San Antonio, TX (International Ground Source Heat Pump Association, 2009, pp. 1-27)	5
Figure 5: Commercial GHEX configurations (CANMET Energy Technology Centre, 2002).....	6
Figure 6: Residential GHEX configurations (U.S. Department of Energy, 2012)	7
Figure 7: Worldwide use of ground-source heat pumps (Lund, Freeston, & Boyd, 2011)	8
Figure 8: Inputs and outputs to the heat pump performance map.....	12
Figure 9: Vertical ground heat exchanger (CANMET Energy Technology Centre, 2002, p. 14)	13
Figure 10: Cross-sectional view of u-tube	14
Figure 11: Medium office building (U.S. Department of Energy, 2010)	17
Figure 12: Aerial view of the first floor zones.....	18
Figure 13: Horizontal view of the first floor zones.....	18
Figure 14: Hourly load multiplier schedule for people.....	24
Figure 15: Hourly load multiplier schedule for lighting.....	26
Figure 16: Hourly schedule for loads resulting from equipment.....	28
Figure 17: Hourly load multiplier schedule for elevators.....	30
Figure 18: Sensible load profiles for the Core1 zone	32
Figure 19: Latent load profiles for the Core1 zone.....	32
Figure 20: Hourly on/off schedule for outdoor air ventilation	35
Figure 21: Hourly on/off schedule for HVAC system operation.....	38
Figure 22: Hourly load multiplier schedule for infiltration	38
Figure 23: Hourly temperature control setpoint schedule for heating and cooling	40

Figure 24: Example deadband operation during summer (cooling mode)	41
Figure 25: Example deadband operation during winter (heating mode)	41
Figure 26: Top-level view of integrated Simulink® model.....	42
Figure 27: Block diagram of integrated model	43
Figure 28: Setting subsystem priority in Simulink®	44
Figure 29: Testing simulation order using Simulink® Debugger.....	45
Figure 30: View of the building subsystem Simulink® model	46
Figure 31: Inputs and outputs for the building subsystem.....	47
Figure 32: View of the thermostat and timing subsystem Simulink® model.....	49
Figure 33: View of the HVAC subsystem Simulink® model (part 1)	50
Figure 34: View of the HVAC subsystem Simulink® model (part 2)	51
Figure 35: View of the plenum subsystem Simulink® model.....	52
Figure 36: Control volume for a single conditioned zone using (A) the HVAC flow path for an actual heat pump and (B) the flow path for the HAMBASE simplification	53
Figure 37: Control volume for three conditioned zones using a plenum.....	54
Figure 38: Inputs and outputs for the heat pump subsystem	56
Figure 39: View of the heat pump subsystem Simulink® model.....	57
Figure 40: Heat pump performance map data (ClimateMaster, 2010, p. 113).....	59
Figure 41: Heat pump performance data for cooling when EWT = 90°F, GPM = 15 and Airflow = 1950CFM	60
Figure 42: Antifreeze correction data (ClimateMaster, 2010, p. 100).....	62
Figure 43: Airflow rate correction factors (ClimateMaster, 2010, p. 98).....	62
Figure 44: Entering air correction data for cooling mode (ClimateMaster, 2010, p. 99)	63
Figure 45: Core1 heat pump inlet air conditions during HVAC ON for 1 year	64
Figure 46: Core1 heat pump inlet air conditions during HVAC ON for 1 year	65
Figure 47: Psychrometric chart representation of entering air correction data for cooling (ASHRAE 2009 Fundamentals HandBook, 2009, p. 1.11)	66

Figure 48: Entering air correction factors for heating (ClimateMaster, 2010, p. 99)	67
Figure 49: Entering air correction polynomials for heating.....	67
Figure 50: Results of heat pump sizing study (hourly average time out-of-setpoint)	70
Figure 51: View of the heat pump header subsystem Simulink® model	71
Figure 52: View of the GHEX subsystem Simulink® model.....	73
Figure 53: Block diagram of water-side flow path	74
Figure 54: Masked view of GHEX water pump subsystem Simulink® model.....	78
Figure 55: Unmasked view of GHEX water pump subsystem Simulink® model	79
Figure 56: Visualization of heat pump cooling/heating lag in Core1	81
Figure 57: Visualization of heat pump cooling/heating lag in West1	83
Figure 58: Open-loop responses of Core1 to constant weather inputs	93
Figure 59: Open-loop responses of East2 to constant weather inputs	94
Figure 60: Open-loop responses of South3 to constant weather inputs.....	95
Figure 61: Open-loop response of Core1 to ambient temperature-step input.....	98
Figure 62: ASHRAE psychometric chart showing perimeter zones in blue-solid and core zones in orange-dash for Test Set 2 (ASHRAE 2009 Fundamentals HandBook, p. 1.11).....	99
Figure 63: Open-loop response of East2 to ambient temperature-step input.....	100
Figure 64: Open-loop response of South3 to ambient temperature-step input	101
Figure 65: Open-loop response of Core1 to ambient relative humidity-step input	104
Figure 66: Open-loop response of East2 to ambient relative humidity-step input	105
Figure 67: Open-loop response of South3 to ambient relative humidity-step input.....	105
Figure 68: Temperature and relative humidity curves for 8/16/2004 used in Test Set 4.....	108
Figure 69: Direct and diffuse irradiance curves for 8/16/2004 used in Test Set 4	108
Figure 70: Open-loop response of Core1 to weather-sine input	109
Figure 71: Open-loop steady-state response of Core1 to weather-sine input	109
Figure 72: Open-loop steady-state response of East2 to weather-sine input	110
Figure 73: Open-loop steady-state response of South3 to weather-sine input.....	111

Figure 74: Open-loop response of Core1 to actual weather input for one year	114
Figure 75: Open-loop response of Core1 to actual weather input for Aug 15–19.....	115
Figure 76: Open-loop response of East2 to actual weather input for one year.....	115
Figure 77: Open-loop response of East2 to actual weather input for Aug 15–19.....	116
Figure 78: Open-loop response of South3 to actual weather input for one year	116
Figure 79: Open-loop response of South3 to actual weather input for Aug 15–19	117
Figure 80: Open-loop response of Core1 to actual internal loads	120
Figure 81: Open-loop steady-state response of Core1 to actual internal loads.....	121
Figure 82: Open-loop steady-state response of East2 to actual internal loads	122
Figure 83: Open-loop steady-state response of South3 to actual internal loads.....	122
Figure 84: Open-loop response of Core1 to actual internal loads and weather for one year	125
Figure 85: Open-loop winter response of Core1 to actual internal loads and weather	126
Figure 86: Open-loop summer response of Core1 to actual internal loads and weather	126
Figure 87: Open-loop winter response of East2 to actual internal loads and weather	127
Figure 88: Open-loop summer response of East2 to actual internal loads and weather	127
Figure 89: Open-loop winter response of South3 to actual internal loads and weather	128
Figure 90: Open-loop summer response of South3 to actual internal loads and weather	128
Figure 91: Comparison of HAMBASE and EnergyPlus annual heating	132
Figure 92: Comparison of HAMBASE and EnergyPlus annual total cooling.....	132
Figure 93: Comparison of HAMBASE and EnergyPlus annual sensible cooling.....	133
Figure 94: Comparison of HAMBASE and EnergyPlus annual latent cooling.....	134

Figure 95: Time-step temperature and relative humidity for Core1 for June 30, 12-3pm	137
Figure 96: Time-step cooling provided and water temperature for Core1 heat pump for June 30, 12-3pm	138
Figure 97: Time-step temperature and relative humidity for East2 for June 30, 12-3pm	139
Figure 98: Time-step cooling provided and water temperature for East2 heat pump for June 30, 12-3pm	139
Figure 99: Time-step temperature and relative humidity for South3 for June 30, 12-3pm	140
Figure 100: Time-step cooling provided and water temperature for South3 heat pump for June 30, 12-3pm	140
Figure 101: Time-step water temperature for the ground loop and heat pump return header for June 30, 5am -12am	141
Figure 102: Hourly average temperature of Core1 for first 12 months of simulation.....	143
Figure 103: Hourly average temperature of East2 for first 12 months of simulation.....	143
Figure 104: Hourly average temperature of South3 for first 12 months of simulation.....	144
Figure 105: Hourly average cooling (negative) and heating (positive) provided by the Core1 heat pump for the first 12 months of simulation	145
Figure 106: Hourly average cooling (negative) and heating (positive) provided by the East2 heat pump for the first 12 months of simulation	145
Figure 107: Hourly average cooling (negative) and heating (positive) provided by the South3 heat pump for the first 12 months of simulation.....	146
Figure 108: Hourly average efficiency ratings for the Core1 heat pump for the first 12 months of simulation (EER is associated with cooling, COP with heating)	147
Figure 109: Hourly average efficiency ratings for the East2 heat pump for the first 12 months of simulation (EER is associated with cooling, COP with heating)	148

Figure 110: Hourly average efficiency ratings for the South3 heat pump for the first 12 months of simulation (EER is associated with cooling, COP with heating)	148
Figure 111: Hourly average heat rejected to ground loop water by the Core1 heat pump (positive heat rejection is associated with cooling) for the first 12 months of simulation	149
Figure 112: Hourly average heat rejected to ground loop water by the East2 heat pump (positive heat rejection is associated with cooling) for the first 12 months of simulation	150
Figure 113: Hourly average heat rejected to ground loop water by the South3 heat pump (positive heat rejection is associated with cooling) for the first 12 months of simulation	150
Figure 114: Hourly average Core1 heat pump entrance water temperature and temperature change for the first 12 months of simulation	151
Figure 115: Hourly average East2 heat pump entrance water temperature and temperature change for the first 12 months of simulation	152
Figure 116: Hourly average South3 heat pump entrance water temperature and temperature change for the first 12 months of simulation	153
Figure 117: Hourly average ground loop entrance water temperature and temperature change for the first 12 months of simulation	154
Figure 118: Monthly totals for cooling and heating provided in Core1, East2 and South3	155
Figure 119: Monthly operating times for cooling and heating in Core1, East2 and South3	155
Figure 120: Monthly totals for heat rejected and absorbed from Core1, East2 and South3	156
Figure 121: Monthly maximum, minimum and mean heat pump entering water temperature	157
Figure 122: Monthly power usage totals in Core1, East2 and South3 for cooling and heating	158

Figure 123: Monthly power usage totals for cooling, heating and water pump operation	158
Figure 124: Heat pump cooling capacity versus entering water temperature (ClimateMaster, 2010)	159
Figure 125: Monthly total time out-of-setpoint in the base model	160
Figure 126: Monthly average cooling and heating efficiency for Core1	161
Figure 127: Monthly average cooling and heating efficiency for East2.....	162
Figure 128: Monthly average cooling and heating efficiency for South3	162
Figure 129: Annual total cooling energy provided in the base model over 15 years	164
Figure 130: Annual total hours of cooling operation in the base model over 15 years	165
Figure 131: Annual total heating energy provided in the base model over 15 years.....	166
Figure 132: Annual total hours of heating operation in the base model over 15 years	167
Figure 133: Annual total heat rejected to the ground loop in the base model over 15 years	169
Figure 134: Annual extremes for heat pump EWT in the base model over 15 years	170
Figure 135: Annual total power usage in the base model over 15 years	172
Figure 136: Annual total time out-of-setpoint in the base model over 15 years.....	174
Figure 137: Annual average cooling EER in the base model over 15 years.....	176
Figure 138: Annual average heating COP in the base model for 15 years	177
Figure 139: Annual average heating COP of all zones in the base model for 15 years	177
Figure 140: Comparison of maximum annual EWT for the EWT cutoff test	182
Figure 141: Comparison of total annual cooling for the EWT cutoff test	184
Figure 142: Comparison of total annual heating for the EWT cutoff test	185
Figure 143: Comparison of annual time out-of-setpoint for the EWT cutoff test	186
Figure 144: Comparison of total annual cooling power usage for the EWT cutoff test	187

Figure 145: Comparison of total annual heating power usage for the EWT cutoff test	188
Figure 146: Comparison of average annual EER for the EWT cutoff test	189
Figure 147: Comparison of average annual COP for the EWT cutoff test	191
Figure 148: Borefield arrangement and dimensions for borehole spacing study	193
Figure 149: Comparison of maximum annual EWT for the borehole spacing test	194
Figure 150: Comparison of total annual cooling for the borehole spacing test	195
Figure 151: Comparison of total annual heating for the borehole spacing test	196
Figure 152: Comparison of annual time out-of-setpoint for the borehole spacing test	197
Figure 153: Comparison of total annual cooling power usage for the borehole spacing test	198
Figure 154: Comparison of total annual heating power usage for the borehole spacing test	199
Figure 155: Comparison of average annual EER for the borehole spacing test	200
Figure 156: Comparison of annual average COP for the borehole spacing test	202
Figure 157: Comparison of maximum annual EWT for the borehole depth test	205
Figure 158: Comparison of total annual cooling for the borehole depth test	206
Figure 159: Comparison of total annual heating for the borehole depth test	207
Figure 160: Comparison of annual time out-of-setpoint for the borehole depth test	208
Figure 161: Comparison of total annual cooling power usage for the borehole depth test	209
Figure 162: Comparison of total annual heating power usage for the borehole depth test	210
Figure 163: Comparison of average annual EER for the borehole depth test	211
Figure 164: Comparison of annual average COP for the borehole depth test	213
Figure 165: Comparison of maximum annual EWT for the SHR test	216
Figure 166: Comparison of total annual cooling for the SHR test	218
Figure 167: Comparison of total annual time of cooling operation for the SHR test	219

Figure 168: Comparison of the ratio of net annual heat rejected per unit GHEX length for the SHR test.....	220
Figure 169: Comparison of total annual heating for the SHR test.....	221
Figure 170: Comparison of annual time out-of-setpoint for the SHR test.....	222
Figure 171: Comparison of annual net heat rejected to the ground loop for the SHR test	223
Figure 172: Comparison of total annual cooling power usage for the SHR test	224
Figure 173: Comparison of total annual heating power usage for the SHR test.....	225
Figure 174: Comparison of average annual EER for the SHR test.....	225
Figure 175: Comparison of annual average COP for the SHR test	227
Figure 176: Sensible internal load profiles for Core2 and Core3	232
Figure 177: Latent internal load profiles for Core2 and Core3	232
Figure 178: Sensible internal load profiles for North and South zones	233
Figure 179: Latent internal load profiles for North and South zones	233
Figure 180: Sensible internal load profiles for East and West zones	234
Figure 181: Latent internal load profiles for East and West zones.....	234
Figure 182: Sensible internal load profiles for Plenum zones	235
Figure 183: Performance map data fitting process	236
Figure 184: Inlet air correction factors provided by ClimateMaster	237
Figure 185: Inlet air correction factors for heat pump performance map.....	238
Figure 186: Secondary parameters used in the GLHEPRO peak load analysis tool	239
Figure 187: GLHEPRO normalized temperature response for peak cooling load	240
Figure 188: GLHEPRO normalized temperature response for peak heating load.....	240
Figure 189: Monthly total loads and peak loads generated by the peak load analysis tool	241
Figure 190: Main screen of GLHEPRO for the base model simulation.....	242
Figure 191: G-function and borehole resistance screen for the base model simulation.....	243
Figure 192: Heat pump load screen for the base model simulation.....	244

Figure 193: Temperature and relative humidity curves for 8/16/2004	245
Figure 194: Open-loop response of Core1 to temperature and RH-sine input	246
Figure 195: Open-loop response of East2 to temperature and RH-sine input	246
Figure 196: Open-loop response of South3 to temperature and RH-sine input.....	247
Figure 197: Direct normal irradiance curves for 8/16/2004	249
Figure 198: Open-loop response of Core1 to DNI-sine input.....	249
Figure 199: Open-loop steady-state response of Core1 to DNI-sine input.....	250
Figure 200: Open-loop steady-state response of East2 to DNI-sine input.....	250
Figure 201: Open-loop steady-state response of South3 to DNI-sine input	251
Figure 202: Diffuse horizontal irradiance curves for 8/16/2004	253
Figure 203: Open-loop response of Core1 to DHI-sine input.....	253
Figure 204: Open-loop steady-state response of Core1 to DHI-sine input.....	254
Figure 205: Open-loop steady-state response of East2 to DHI-sine input.....	254
Figure 206: Open-loop steady-state response of South3 to DHI-sine input	255
Figure 207: Open-loop response of Core1 to constant people input	257
Figure 208: Open-loop steady-state response of Core1 to constant people input.....	257
Figure 209: Open-loop steady-state response of East2 to constant people input	258
Figure 210: Open-loop steady-state response of South3 to constant people input	258
Figure 211: Open-loop response of Core1 to constant equipment input	261
Figure 212: Open-loop steady-state response of Core1 to constant equipment input	261
Figure 213: Open-loop steady-state response of East2 to constant equipment input	262
Figure 214: Open-loop steady-state response of South3 to constant equipment input	262
Figure 215: Comparison of HAMBASE and EnergyPlus peak heating	267
Figure 216: Comparison of HAMBASE and EnergyPlus peak total cooling.....	267
Figure 217: Comparison of HAMBASE and EnergyPlus peak sensible cooling.....	269
Figure 218: Comparison of HAMBASE and EnergyPlus peak latent cooling.....	269
Figure 219: Hourly average power usage by the Core1 heat pump for the first 12 months of simulation.....	271

Figure 220: Hourly average power usage by the East2 heat pump for the first 12 months of simulation.....	271
Figure 221: Hourly average power usage by the South3 heat pump for the first 12 months of simulation.....	272
Figure 222: Monthly average power usage by the water pumps during 15 years of simulation.....	273
Figure 223: Monthly average power usage by the building during 15 years of simulation.....	273
Figure 224: Annual average cooling EER of all zones in the base model for 15 years	274
Figure 225: Annual average Core1 heat pump efficiency in the base model for 15 years	274
Figure 226: Annual average East2 heat pump efficiency in the base model for 15 years	275
Figure 227: Annual average South3 heat pump efficiency in the base model for 15 years	275
Figure 228: Comparison of average annual EWT for the borehole spacing test	283
Figure 229: Comparison of minimum annual EWT for the borehole spacing test	283
Figure 230: Comparison of average annual EWT for the borehole depth test	292
Figure 231: Comparison of minimum annual EWT for the borehole depth test	292
Figure 232: GLHEPRO sizing loads for the SHR test.....	301
Figure 233: Comparison of average annual EWT for the SHR test	304
Figure 234: Comparison of minimum annual EWT for the SHR test	304
Figure 235: Comparison of the ratio of net annual cooling provided per hour of cooling operation for the SHR test.....	310
Figure 236: Comparison of heat rejected to the ground loop during cooling for the SHR test	314
Figure 237: Comparison of heat absorbed from the ground loop during heating for the SHR test.....	314

Chapter 1 Introduction

Worldwide electricity generation was 21,449 terawatt hours (TWh) in 2010, an increase of 39% since 2000 (The World Bank, 2013). The largest electricity generating country during this period was the United States, which generated 4,354TWh in 2010 (The World Bank, 2013). Of the electricity consumed in the United States in 2010, 14% was used for space heating and cooling in residential and commercial buildings (U.S. Energy Information Administration, 2012).

Electricity used for heating and cooling has a direct cost, paid by the end user, and an indirect cost resulting from air pollution and the negative externalities air pollution causes, paid by everyone. The direct cost of electricity used for heating and cooling for residential and commercial users in the United States was \$68.4 billion in 2010 (U.S. Energy Information Administration, 2012). Pollution in the United States resulting from electricity used in this manner totaled 3.429×10^8 tons of carbon dioxide (CO₂), 2.948×10^5 tons of nitrogen oxide (NO), and 7.220×10^5 tons of sulfur dioxide (SO₂) in 2010 (United States Government Accountability Office, Apr 2012, p. 21). This air pollution caused “Gross external damages”, the total cost to the public health and the environment, with an estimated total cost of \$8.3 billion (in year 2000 dollars, \$10.5 billion in 2010 dollars) (Muller, Mendelsohn, & Nordhaus, 2011).

As worldwide demand for electricity increases due to the industrialization of Africa and Asia, the total worldwide direct cost of electricity and indirect cost related to air pollution will similarly increase, which in turn will drive the demand for technology that is more energy efficient. Ground-source heat pumps are one such technology.

According to Fisher and Rees, utilization of ground-source heat pumps in residential applications can reduce total residential electricity consumption by up to 40% (2005). Including both residential and commercial applications, Hughes estimated that utilization of ground-source heat pumps will reduce total residential and commercial electricity usage by 30-40% (2008). These estimates correspond to a reduction in the total

electricity consumption in the United States of 4-6%, an annual savings of \$2.737 billion in direct costs, an air pollution reduction of 1.37×10^7 tons of CO_2 , 1.18×10^4 tons of NO and 2.89×10^4 tons of SO_2 , with a corresponding reduction in gross external damages totaling of \$332.1 million. Thus, the United States and the world stand to realize significant fiscal, environmental and health savings through the widespread adoption of ground-source heat pump technology.

1.1. GSHP Defined

A ground-source heat pump (GSHP) is similar to a traditional air-source heat pump in that they both use a refrigeration cycle to provide heating and cooling. A GSHP uses the ground as its external heat exchanger, where an air-source heat pump uses the external air. Figure 1 and Figure 2 show schematics for the GSHP system during summer and winter operation respectively.

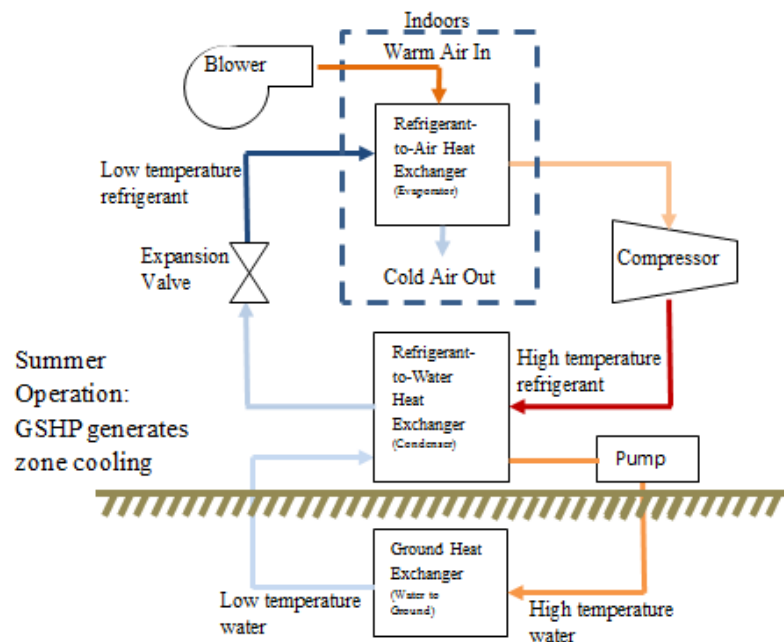


Figure 1: Ground-source heat pump schematic for summer operation (cooling mode)

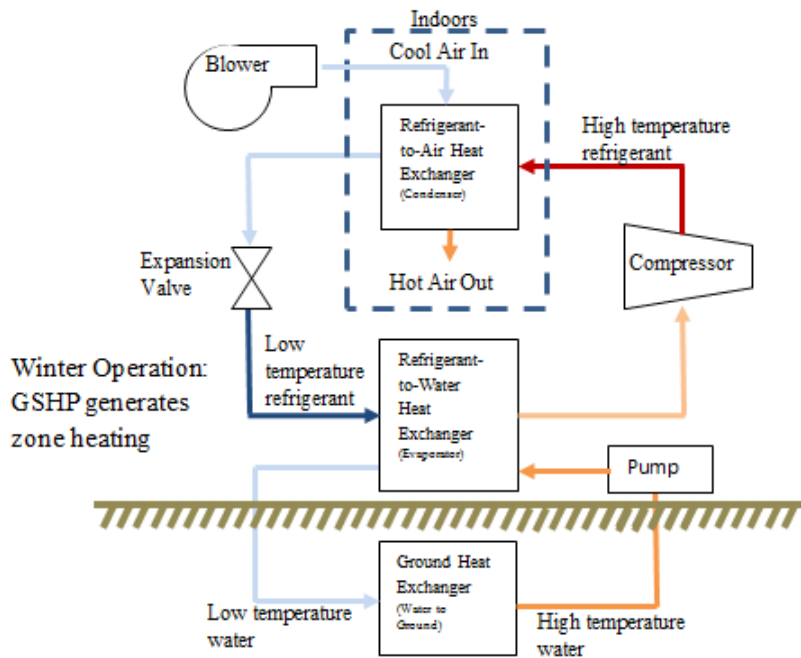


Figure 2: Ground-source heat pump schematic for winter operation (heating mode)

GSHP systems offer energy savings compared to other methods of space heating and cooling due to the larger temperature difference experienced by the external heat exchanger. During summer months, the refrigerant-to-air condenser in a traditional air-source heat pump (as shown in Figure 3) experiences a temperature difference of approximately 19.8°C (35°F), in Austin, TX, as it rejects heat to outside air temperatures that regularly exceed 37.8°C (100°F). A GSHP refrigerant-to-water condenser however, experiences a temperature difference of approximately 35.0°C (63°F), in Austin, TX, as it rejects heat to the ground temperatures that are approximately 22.2°C (72°F) year round. The greater temperature difference found in the GSHP condenser yields increased condenser efficiency and decreased compressor power used. This efficiency improvement is also found during winter months.

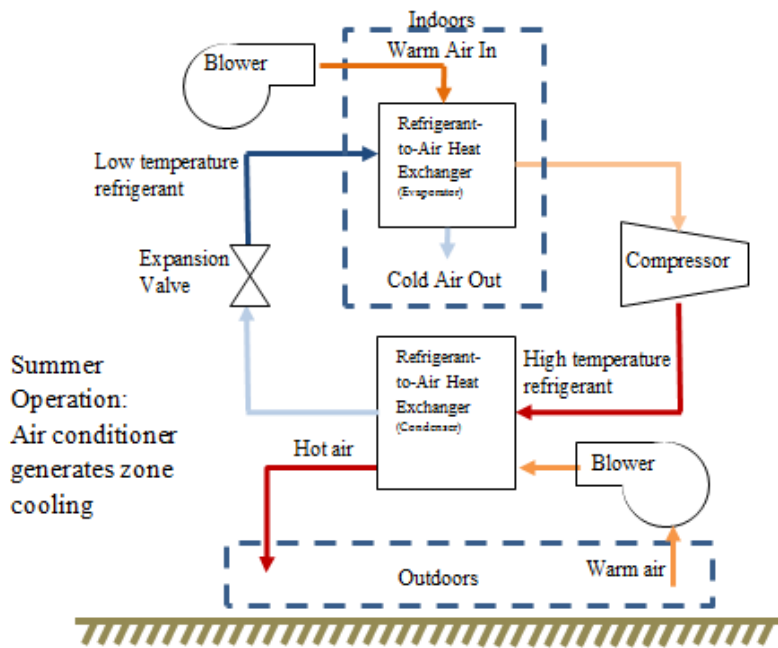


Figure 3: Air-source heat pump schematic for summer operation (cooling mode)

Figure 4 shows the difference between air and ground temperatures for San Antonio, TX, which is similar to Austin, TX in climate. The average earth temperature (black rectangles) is a constant 22.2°C (72°F). The average monthly air temperature and the monthly temperature range (vertical lines) extend from a low of -9.4°C (15°F) to a high of 38.9°C (102°F).

San Antonio, TX Silty-Clay Soil

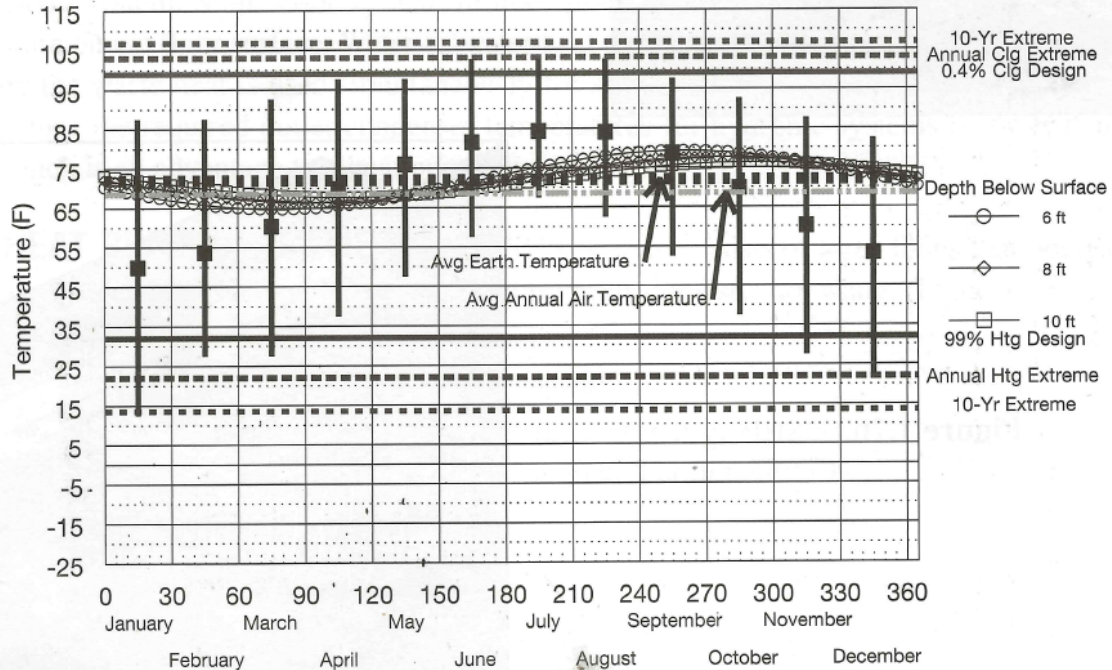


Figure 4: Annual air and soil temperature variation for San Antonio, TX (International Ground Source Heat Pump Association, 2009, pp. 1-27)

There are many types of ground heat exchangers (GHEX), classified based on the circulating fluid and physical orientation in the ground. A closed-loop system reuses the same circulating fluid in a continuous loop, typically using water or a water/antifreeze mixture as the working fluid. An open-loop system continuously intakes new fluid into the heat pump before discharging it to a separate location, using ground-water as the working fluid. While open-loop systems have been in use since the 1970's and currently represent 10-20% of U.S. GSHP systems, open-loop systems are rarely used due to the potential for environmental contamination and fouling of the water pipes by minerals (Navigant Consulting, Inc., 2009). Within the closed-loop system, there are three methods of installation, based on the location of the piping. Vertical loops place piping in vertically drilled boreholes, typically spaced 4.6 to 7.6m (15 to 25ft) apart, drilled to depths of 30.5 to 182.9m (100 to 600ft) (International Ground Source Heat Pump

Association, 2009). Horizontal loops use piping in 1.2 to 2.4m (4 to 8ft) deep horizontal trenches, dug 3.0m (10ft) apart, and “up to [45.7m] 150 feet in length per nominal ton of heat pump capacity” (International Ground Source Heat Pump Association, 2009, p. 5.1.2.2). Pond or lake loops are similar to horizontal loops, but piping is laid in a lake instead of a horizontal trench. The best GHEX layout for a particular project will depend on “Climate, soil conditions, available land, and local installation costs” (U.S. Department of Energy, 2012).

Horizontal loop installations are typically less expensive than vertically bored installations, however horizontal loops require a larger ground surface area footprint for a given amount of cooling/heating and they potentially have a lower efficiency due to ground temperature fluctuations at shallow depths (Navigant Consulting, Inc., 2009). As a result, ground surface area constraints often dictate the use of vertically bored GHEX installations. Examples of commercial installations are shown in Figure 5. Examples of residential installations are shown in Figure 6.

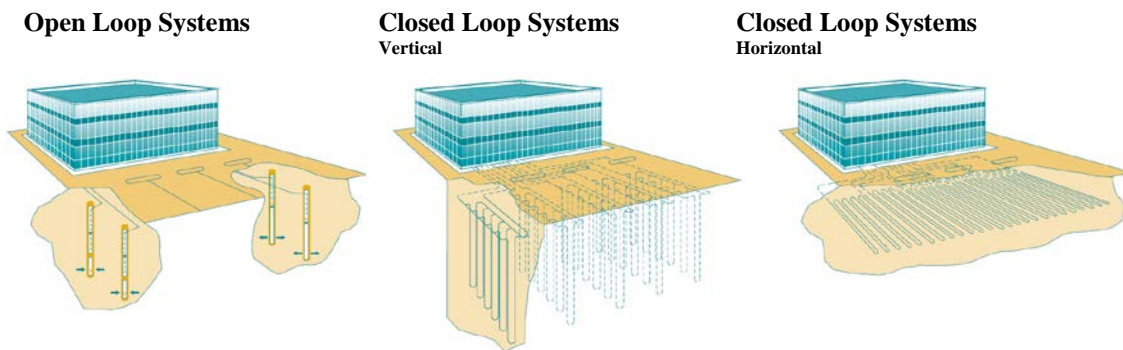


Figure 5: Commercial GHEX configurations (CANMET Energy Technology Centre, 2002)

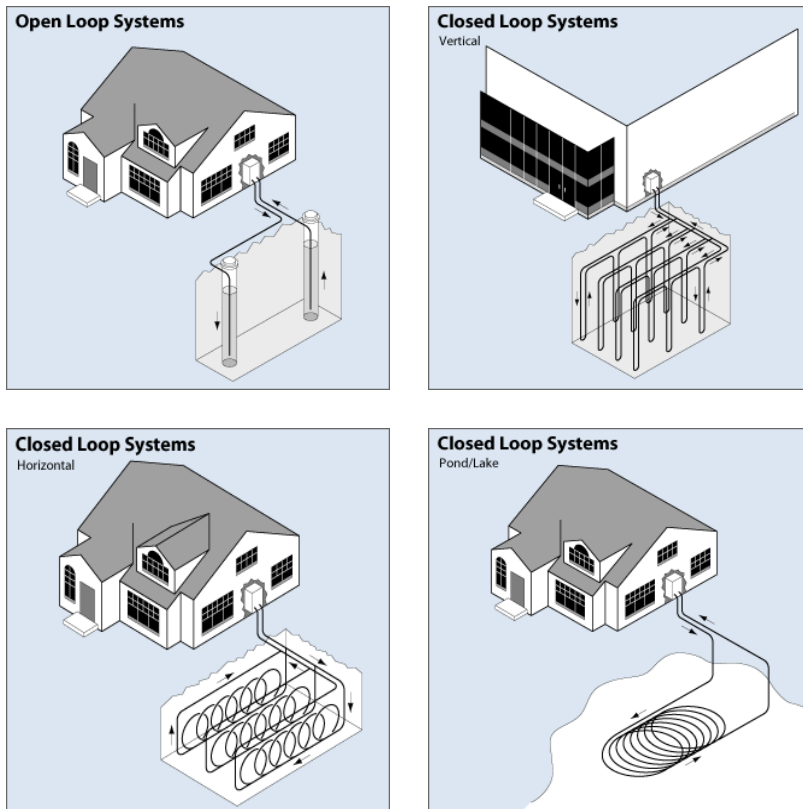


Figure 6: Residential GHEX configurations (U.S. Department of Energy, 2012)

1.2. Barriers to GSHP adoption

In their 2009 report to the U.S. Department of Energy, Navigant Consulting described the opportunity represented by GSHPs, saying “GSHPs can provide significant primary unit energy savings...often in the range of 30 to 60 percent of space-conditioning energy consumption” (2009, p. viii). The energy savings offered by GSHPs combined with various governmental tax benefits have helped increase the adoption of GSHPs worldwide as shown in Figure 7.

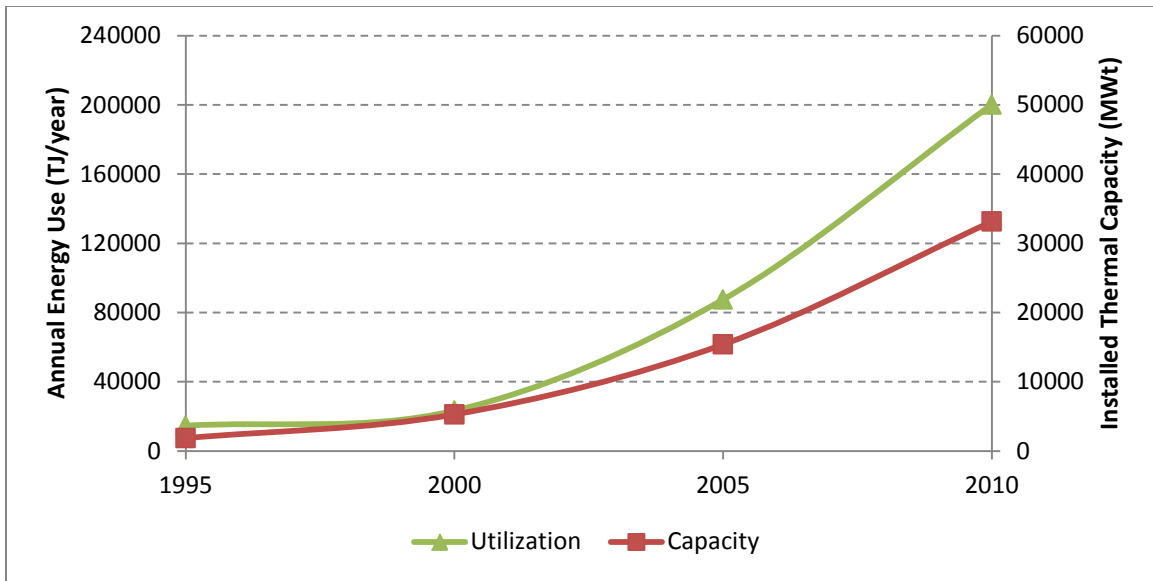


Figure 7: Worldwide use of ground-source heat pumps (Lund, Freeston, & Boyd, 2011)

While adoption of GSHPs continues to grow, the improvements in operating costs and environmental impact suggest greater usage should be observed. Many individuals have investigated the barriers limiting adoption of GSHPs, with installation cost being the most significant and prevalent barrier. In 1994, the National Earth Comfort Program (NECP) viewed GSHP cost, public awareness and infrastructure as the three primary barriers to market adoption (Hughes & Pratsch, 2001). In 1998, the Federal Energy Management Program (FEMP) identified a lack of confidence in GSHP technology, missing technical infrastructure for life-cycle analysis and installation design, and inability to predict installation costs as the main barriers for governmental adoption of GSHP technology (Hughes P. J., 2008). In 2003, a National Ground Water Association (NGWA) survey of ground water industry professionals found that end-user awareness, and cost were the most significant barriers to GSHP adoption (Hughes P. J., 2008). In 2008, NGWA informally surveyed industry experts who stated that “High first-cost” of GSHP installations was the most important barrier to consumer adoption (Hughes P. J., 2008). In 2009, Navigant Consulting identified high equipment costs, difficulty evaluating GSHP suitability and the need for installation-specific design as the three most prominent barriers to adoption (2009, p. viii).

1.3. Research Objectives

The objective of this research is to provide a GSHP model that can evaluate the efficacy of new technologies and control approaches as well as predict the life-cycle performance of planned installations. Specifically, this research will focus on commercial GSHP installations in the southwest and southcentral United States.

The model must include the following:

- Building heat and moisture physics
- Control and response of commercially available heating, ventilation and air-conditioning (HVAC) systems, specifically including heat pumps
- A ground heat exchanger model that responds to thermal input
- Integration of the building, HVAC and GHEX models
- Multi-year simulations with reasonable simulation times
- User customizability
- Easy coupling between subsystems models

The following sections describe the previous research that contributed to the development of this model in Chapter 2, the specific parameters of the commercial office building used in this work in Chapter 3, description of the component models in Chapter 4, validation of the model in Chapter 5, and model results in Chapter 6 and Chapter 7.

Chapter 2

Literature Review

Modern GSHP research began in the late 1970s with an emphasis on experimental testing, and has expanded since 1990 with increased computer simulation abilities (Spitler J. , 2005). Since 1990, many modeling environments developed to simulate building physics were modified to include GSHP technologies. The integrated model developed in this research consists of three major sections: the building and its thermal and hygric states, the heat pump that provides heating/cooling to the building, and the ground-loop acting as the heat source/sink for the system.

2.1. Modeling of Building Physics

This research forgoes the use of common modeling environments of building physics such as EQuest, EnergyPlus and TRNSYS (TRaNsient System Simulation). Evaluation of these modeling environments for the aims of this research has previously been covered (Schijndel, 2007; Gaspredes, 2011). Instead, the Matlab® and Simulink® based environment of HAMBASE (Heat Air and Moisture model for Building and Systems Evaluation) developed by de Wit (2006) is used. The HAMBASE modeling environment builds on ELAN, a heating/cooling model developed by de Wit and Driessen (1988). Verification and validation of the HAMBASE model and numerous add-on component models was undertaken by van Schijndel and others (2007). Further explanation of the development history of HAMBASE and physics assumptions in the HAMBASE model was covered by de Wit (2009).

HAMBASE simulates both heat and moisture flows in a building, providing thermal indoor climate, hygric indoor climate, and the heating/cooling energy used to maintain this climate (Wit, 2009). HAMBASE is an open and transparent modeling environment, meaning that the governing equations are accessible within the modeling files, and adding component models is straightforward. The user creates a building model

by defining zones consisting of materials, constructions, orientations, fenestration (windows), shading and internal loads. Simulation time-steps can be chosen, custom weather files can be made and control can be easily added. HAMBASE can be simulated as either a Matlab® executable or as a subroutine within a larger Simulink® model.

2.2. Modeling a Water-Source Heat Pump

A heat pump uses a refrigeration vapor compression cycle to move heat from one source to another. A water-source heat pump consists of a compressor, a refrigerant-to-air heat exchanger, an expansion valve and a refrigerant-to-water heat exchanger. An overview of the function of the heat pump and its components in both heating and cooling modes was covered in Chapter 1. Three potential modeling approaches for the heat pump were covered in detail by Gasprede: component models based on first-principals, component models based on empirical models and system-level empirical models (2011).

Component models using first-principals have been developed for compressors (Chen, Halm, Groll, & Braun, 2002; Chen, Halm, Braun, & Groll, 2002; Wang, Li, & Shi, 2005), and heat exchangers (Judge & Radermacher, 1997; Garca-Valladaresa, Perez-Segarrab, & Rigola, 2004). This approach requires performance characteristics and geometric details that are difficult to acquire, while also being computationally demanding. Semi-empirical component models improve upon the computational efficiency of first-principals models and have been developed using simplified physical representations of compressors (Winandy & Claudio Saavedra O, 2002), heat exchangers (Lee & Jones, 1997), and for an entire air-source heat pump (Fischer & Rice, 1983). While offering much faster computation times, the semi-empirical models require similar performance and geometry data as the first-principals models. Fully-empirical component models that map component inputs to outputs using curve fits have been developed for compressors (Fischer & Rice, 1983) and for heat exchangers (Pacheco-Vega, Sen, Yang, & McClain, 2001). These empirical component models offer the best combination of

computational efficiency, number of inputs and level of detail, however even these models require component geometries that are not readily available for commercial units.

To eliminate the need for component geometries, empirical models have been developed for the entire heat pump system (Spitler & Cullin, 2008). While this approach does not offer detailed tracking of internal refrigerant states, all of the inputs to this type of model are published in heat pump manufacturers' catalogues.

A similar approach to the empirical model is a performance map model (Gaspredes, 2011). This approach, utilizes the heat pump performance data published by manufacturers to relate input and output conditions. The schematic in Figure 8 shows the inputs and outputs for the performance map model.

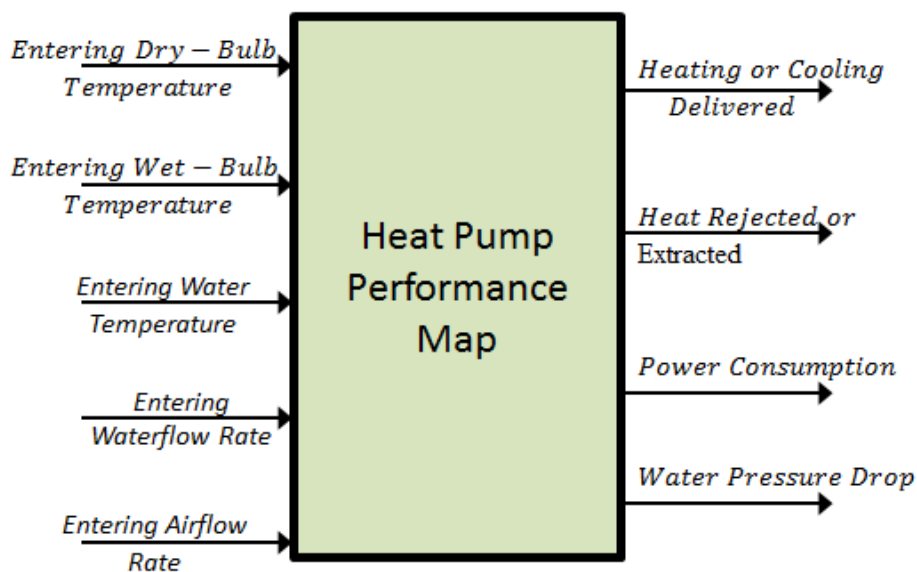


Figure 8: Inputs and outputs to the heat pump performance map

The performance map approach is computationally efficient and allows for easy inclusion of a variety of heat pumps. The only drawback to this approach is the lack of detail within the refrigeration cycle itself. For example, it is not possible to experiment with the quantity of hot water generation associated with different desuperheaters. Further discussion of correction factors (inlet air flow rate, inlet air dry bulb temperature,

inlet air wet bulb temperature, ground loop working fluid) and validation for the performance map model has been detailed by Gasprede (2011).

2.3. Modeling of Ground Heat Exchanger

Chapter 1 described the three main approaches to commercial GHEX installations as open-loop, closed-loop horizontal and closed-loop vertical. Closed-loop horizontal and closed-loop vertical installations are both widely used. The suitability of either approach depends on the ground surface area availability, ground conductivity, and financing available for a particular installation. For this research, a vertical installation was chosen. A schematic of a vertical bore GHEX is shown in Figure 9.

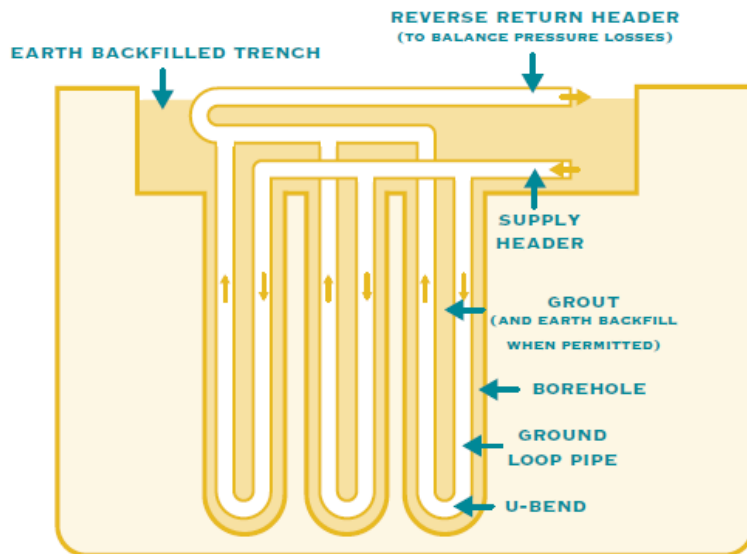


Figure 9: Vertical ground heat exchanger (CANMET Energy Technology Centre, 2002, p. 14)

Various models for a vertical GHEX were examined by Gasprede (2011). A complete model of the system typically consists of two subcomponents: one region representing the heat transfer within the borehole, including the circulating fluid, the u-

tube wall, and the grout, and a second region representing the ground surrounding the borehole. Figure 10 shows a schematic of these components.

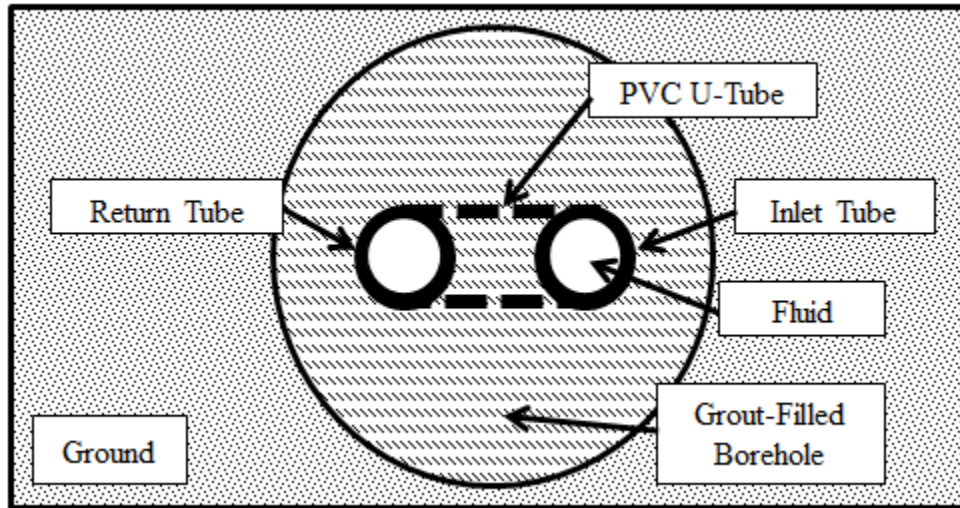


Figure 10: Cross-sectional view of u-tube

Models of the borehole fit into two groups based on the simplifying assumptions: steady-state heat transfer or installation geometry that aligns with grids created by a finite-difference model. Hellström developed an analytical solution for heat transfer between a u-tube and the ground based on a two-dimensional, steady-state model (1991). This model was later expanded to include fluid temperature distribution along the borehole, resulting in a quasi-three-dimensional heat transfer (Zeng, Diao, & Fang, 2003). Bennet et al. developed a multipole model that can calculate conductive heat flow between borehole pipes and does not require pipe or borehole symmetry (1987). This model was subsequently updated to use mean temperatures around the wall of the borehole, simplifying the application of the model (Claesson & Hellström, 2011).

Models of the ground surrounding the borehole either assume a uniform heat source and ignore the effects of the borehole or include one of the borehole modeling approaches previously described. An infinite line source model was developed by Ingersoll and Plass that treats the ground as a uniform, infinite medium (1948). A

cylindrical source model was developed based on either a constant temperature or constant heat flux assumption (Carslaw & Jaeger, 1946), which was later improved (Ingersoll & Plass, 1948), and eventually applied to vertical GHEXs (Kavanaugh S. P., 1985). A second solution to the cylindrical source model was developed based on a finite capacitance and perfect conductor assumption (Carslaw & Jaeger, 1946), which was subsequently extended to include a lumped parameter model of the borehole (Young, 2004). A finite line source model for a GHEX was developed using an analytical solution based on a semi-infinite medium, uniform initial temperature, constant heat flux and constant surface temperature assumptions (Eskilson, 1987). Various finite difference models (Rottmayer, Beckman, & Mitchell, 1997; Yavuzturk, 1999), finite element models (Muraya, O'Neal, & Heffington, 1996; Kohl & Hopkirk, 1995), and finite volume models (Young, 2004; Xu, 2007) have been developed.

Of all the ground models, only Yavuzturk (1999) and Xu (2007) are accurate for hourly or sub-hourly time-steps, and both are computationally efficient due to their use of Eskilson's G-function model of the ground's temperature response (1987). The G-function approach is a combination analytical-numerical method that finds the thermal response of ground around a single borehole to a pulse heat input, spatially superimposes the thermal response of multiple boreholes to determine a borefield's response, converts the response to a non-dimensional factor or g-function, and finally temporally superimposes g-functions to time varying heat inputs (Eskilson, 1987).

Xu's model uses a numerical one-dimensional, finite volume model during simulation to handle short time-step responses (2007). Short time-step responses are then aggregated to form long term responses. The inputs to the model are inlet water temperature and the inlet water flow rate. The parameters of the GHEX are defined using parameter files generated by GLHEPRO (Ground Loop Heat Exchanger Program–GHEX design software developed at Oklahoma State University). The model calculates heat transfer from the GHEX using the borehole temperature, and subsequently calculates the GHEX outlet water temperature by assuming that the average fluid temperature is equal to the borehole temperature, as shown in Equation (1).

$$T_{out} = 2 \cdot T_{borehole} \cdot T_{in} \quad (1)$$

where

T_{out} = ground loop outlet water temperature

$T_{borehole}$ = borehole temperature

T_{in} = ground loop inlet water temperature

While this approach is accurate when the system reaches steady-state operating conditions, during transient periods such as start-up, input fluid temperature changes rapidly, while borehole temperature changes slowly. This causes oscillations in the outlet temperature. Increasing the simulation time-step for the ground loop model minimizes this issue (Gasprede, 2011).

Chapter 3 Office Building Model

The commercial building chosen for this work is the Medium Office from the Department of Energy's (DoE) Commercial Reference Building Models (U.S. Department of Energy, 2010). It is a $4,982\text{m}^2$ ($53,628\text{ft}^2$) three-story office building, that is newly built using a steel framed-wall construction approach. The envelope of the rectangular building measures $49.9\text{m} \times 33.3\text{m} \times 11.9\text{m}$ ($163.8\text{ft} \times 109.2\text{ft} \times 39\text{ft}$). An image of the building is shown in Figure 11. The following sections discuss the dimensions, material properties, internal loads and HVAC systems for the building.

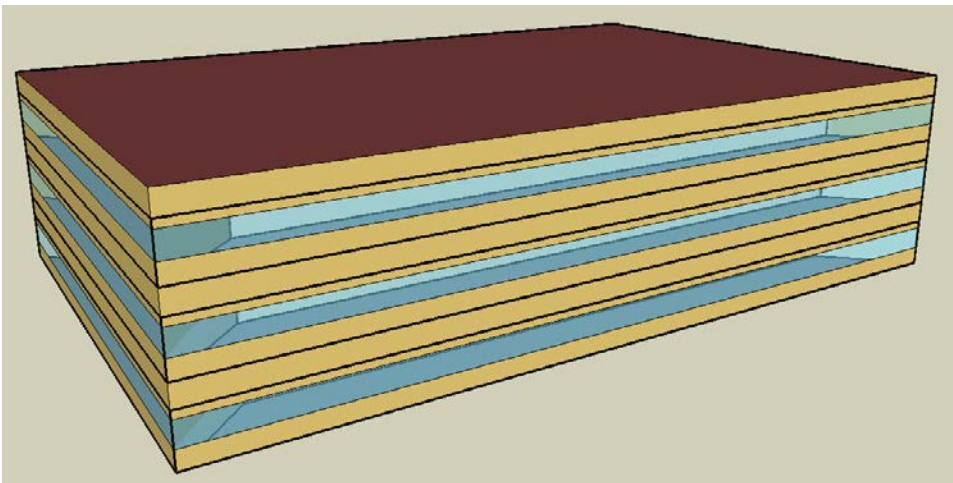


Figure 11: Medium office building (U.S. Department of Energy, 2010)

3.1. Physical Layout

The building is oriented perpendicular to the cardinal-direction compass, with sides of the building directly facing north, east, south and west. Each floor of the building model consists of six zones: a core zone, four perimeter zones (north, south, east, and west) and an unconditioned plenum zone. Zones are labeled as North1, Core2, Plenum3, etc. for the first-floor north zone, the second-floor core zone and the third-floor plenum

zone, respectively. Cross-sectional views of the building are shown in Figure 12 and Figure 13.

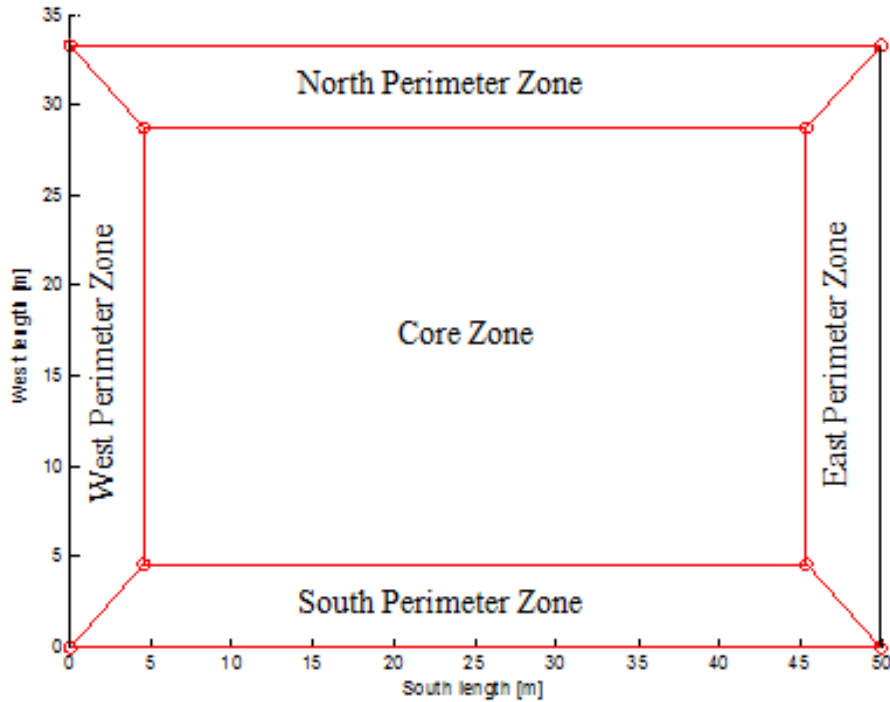


Figure 12: Aerial view of the first floor zones

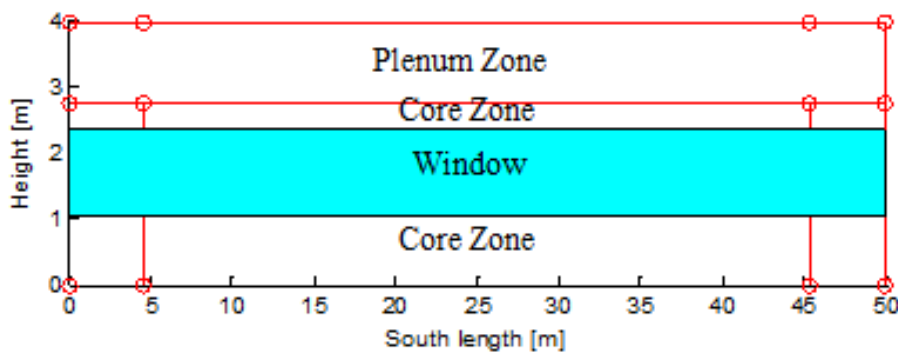


Figure 13: Horizontal view of the first floor zones

All perimeter zones have a single external wall that contains 1.3m (4.3ft) tall windows spanning their entire width, shown in blue. The core zones have no external

walls, nor windows. The plenum zones have four external walls that extend the entire width and length of the building, but have no windows.

The core zones are the largest zones in the building, with a floor area of 984m² (10,587ft²) and a total volume of 2,698m³ (95,279ft³). The east and west zones are the smallest in the building, with a floor area of 131m² (1,413ft²) and a total volume of 360m³ (12,713ft³). The north and south zones have a floor area of 207m² (2,232ft²) and a total volume of 569m³ (20,086ft³). Exact dimensions for each zone in the building are shown with SI units in Table 1 and British Imperial (BI) units in Table 2.

Table 1: Zone dimensions, SI units (U.S. Department of Energy, 2010)

Zone	Floor Area [m ²]	Volume [m ³]	Exterior Area [m ²]	Window Area [m ²]
Core1	984	2,698	-	-
South1	207	569	137	65
East1	131	360	91	44
North1	207	569	137	65
West1	131	360	91	44
Plenum1	1,661	2,025	203	-
Core2	984	2,698	-	-
South2	207	569	137	65
East2	131	360	91	44
North2	207	569	137	65
West2	131	360	91	44
Plenum2	1,661	2,025	203	-
Core3	984	2,698	-	-
South3	207	569	137	65
East3	131	360	91	44
North3	207	569	137	65
West3	131	360	91	44
Plenum3	1,661	2,025	203	-
Total	9,963	19,743	3,638	653

Table 2: Zone dimensions, BI units (U.S. Department of Energy, 2010)

Zone	Floor Area [ft ²]	Volume [ft ³]	Exterior Area [ft ²]	Window Area [ft ²]
Core1	10,587	95,280	-	-
South1	2,232	20,086	1,474	703
East1	1,413	12,716	982	468
North1	2,232	20,086	1,474	703
West1	1,413	12,716	982	468
Plenum1	17,876	71,504	2,183	-
Core2	10,587	95,280	-	-
South2	2,232	20,086	1,474	703
East2	1,413	12,716	982	468
North2	2,232	20,086	1,474	703
West2	1,413	12,716	982	468
Plenum2	17,876	71,504	2,183	-
Core3	10,587	95,280	-	-
South3	2,232	20,086	1,474	703
East3	1,413	12,716	982	468
North3	2,232	20,086	1,474	703
West3	1,413	12,716	982	468
Plenum3	17,876	71,504	2,183	-
Total	107,259	697,161	39,163	7,027

3.2. Building Construction

The building is comprised of five separate wall constructions: exterior vertical walls, a roof, floors, interior vertical walls, and plenum drop ceilings. The exterior vertical walls use a “Steel frame wall” construction, which consists of wood siding as the outer-most layer, insulation and gypsum board as the inner-most layer for a total U-value of $0.704\text{W}/\text{m}^2\cdot\text{K}$ ($0.124\text{btu}/\text{h}\cdot\text{ft}^2\cdot^\circ\text{F}$) (U.S. Department of Energy, 2010, p. 25). The roof uses an “Insulation entirely above deck” construction, which consists of a water-proof membrane as the outer-most layer, insulation, and metal decking as the inner-most layer for a total U-value of $0.358\text{W}/\text{m}^2\cdot\text{K}$ ($0.063\text{btu}/\text{h}\cdot\text{ft}^2\cdot^\circ\text{F}$) (U.S. Department of Energy, 2010, p. 23). The floors consist of 4-inch concrete and a layer of carpet. Interior vertical walls consist of two layers of gypsum board. Plenum drop ceilings consist of standard drop-in ceiling tiles. Table 3 lists the properties of the construction materials.

Table 3: Properties of construction materials

Material	Thickness [m]	Conductivity [W/m·K]	Density [kg/m ³]	Heat capacity [J/kg·K]	Emissivity	Moisture resistance [ng/(Pa·s·m)]	Moisture capacity [kg/m ³ ·Pa]	Vapor capacity x10 ⁷ [g/kg]
Wall Insulation	0.0539	0.049	265	836.8	0.7	1	5	6.6
Roof Insulation	0.0125	0.049	265	836.8	0.7	1	5	6.6
Wood Siding	0.01	0.11	544.6	1210	0.78	16	80	6.6
Gypsum Board	0.0127	0.16	784.9	830	0.92	9	6	3.5
Concrete Floor	0.102	1.311	2240	836.8	0.7	25	40	3.7
Metal Decking	0.0015	45	7680	418.4	0.7	9000000	0	0
Roof	0.0095	0.16	1121	1460	0.3	5000	0	0
Carpet	0.00635	0.03	112	1379	0.7	10000	0	0
Ceiling Tiles	0.0127	0.057	288	1339	0.7	10	20	4.2

3.3. Fenestration

Windows comprise 33% of the vertical exterior surface area, or 18% of the total exterior envelope (roof included). The exact area of windows in each zone is shown in Table 1. The window U-values of $6.927\text{W}/\text{m}^2\cdot\text{K}$ ($1.22\text{btu}/\text{h}\cdot\text{ft}^2\cdot^\circ\text{F}$) are based on “The highest U-values from [Standard] 90.1-1989” (U.S. Department of Energy, 2010, p. 28). The solar heat gain coefficient (SHGC) value of 0.25 is based on Standard 90.1-1999 (U.S. Department of Energy, 2010, p. 28). An additional window parameter called a “convection factor with/without sunblinds” is also required by HAMBASE, and a value of 0.04 is used based on “double glazing” (Wit, HAMBASE: Part II Input and Output, 2009). There are no shading devices incorporated in the building, nor does shading occur from external sources (trees, buildings, etc.).

3.4. Load Scheduling

The internal and external loads used in this model are all subject to hourly scheduling that varies by day of the week. At different times of day, each load will operate at some percentage of its peak value. On a weekday for example, a typical office building will experience approximately 0% people load at 6am, 10% at 7am, and 20% at 8am, and finally reaching 95% at 9am, as shown in Figure 14. Thus, the load generated by a particular source at a particular time is simply the product of the peak load and scheduling load multiplier factor. For example, the peak heat rate for Core1 is shown to be $6,355.2\text{W}$ ($21,684.8\text{btu}/\text{hr}$) in Table 4, so the heat rate generated by people at 8am on a weekday in Core1 is 20% (load multiplier from Figure 14) of the peak value, or $1,271.4\text{W}$ ($4,338.2\text{btu}/\text{hr}$).

Schedules in this model were taken from the DoE’s Commercial Reference Office building, which in turn was based on, “Standard 90.1-1989 Section 13, which includes schedules for use with the Energy Cost budget Method (ASHRAE 1989)” (U.S. Department of Energy, 2010). The following sections list scheduling profiles and tables of peak loads for each heat source.

3.5. Internal Loads

The building model includes four categories of heat loads found internally within zones: people, lighting, electrical equipment and elevators. Peak heating rates and calculation methods of heat transfer are explained in detail for each category in the following sections.

3.5.1. People

Zone loads resulting from people are based upon occupancy of 18.58m²/person as recommended by ASHRAE Standard 62.1-2004 (U.S. Department of Energy, 2010, p. 9). The DoE implementation uses a total heat rate of 120W/person (409.5btu/hr), which is close to the representative total heat rate of 115W (392.4btu/hr) from ASHRAE for “Seated, very light work” in an office (ASHRAE 2009 Fundamentals HandBook, 2009, p. 18.4). ASHRAE divides the total heat rate of 115W into 61% (70W, 238.8btu/hr) sensible heat and 39% latent heat (45W, 153.5btu/hr) (ASHRAE 2009 Fundamentals HandBook, 2009, p. 18.4). This model uses 120W/person to better match results with the DoE implementation.

Table 4 shows the number of people in each zone, the peak heat rate they generate, and the sensible and latent portions of the load. Figure 14 shows the hourly load multiplier schedule for people.

Table 4: Peak heat rates resulting from people by zone

Zone	Number of People	Peak Total Heat Rate [W]	Peak Sensible Heat Rate [W]	Peak Latent Heat Rate [W]
Core1	53.0	6355.2	3876.7	2478.5
South1	11.1	1336.9	815.5	521.4
East1	7.1	846.1	330.0	516.1
North1	11.1	1336.9	815.5	521.4
West1	7.1	846.1	330.0	516.1
Plenum1	0	0	0	0
Core2	53.0	6355.2	3876.7	2478.5
South2	11.1	1336.9	815.5	521.4
East2	7.1	846.1	330.0	516.1
North 2	11.1	1336.9	815.5	521.4
West2	7.1	846.1	330.0	516.1
Plenum2	0	0	0	0
Core3	53.0	6355.2	3876.7	2478.5
South3	11.1	1336.9	815.5	521.4
East3	7.1	846.1	330.0	516.1
North3	11.1	1336.9	815.5	521.4
West3	7.1	846.1	330.0	516.1
Plenum3	0	0	0	0

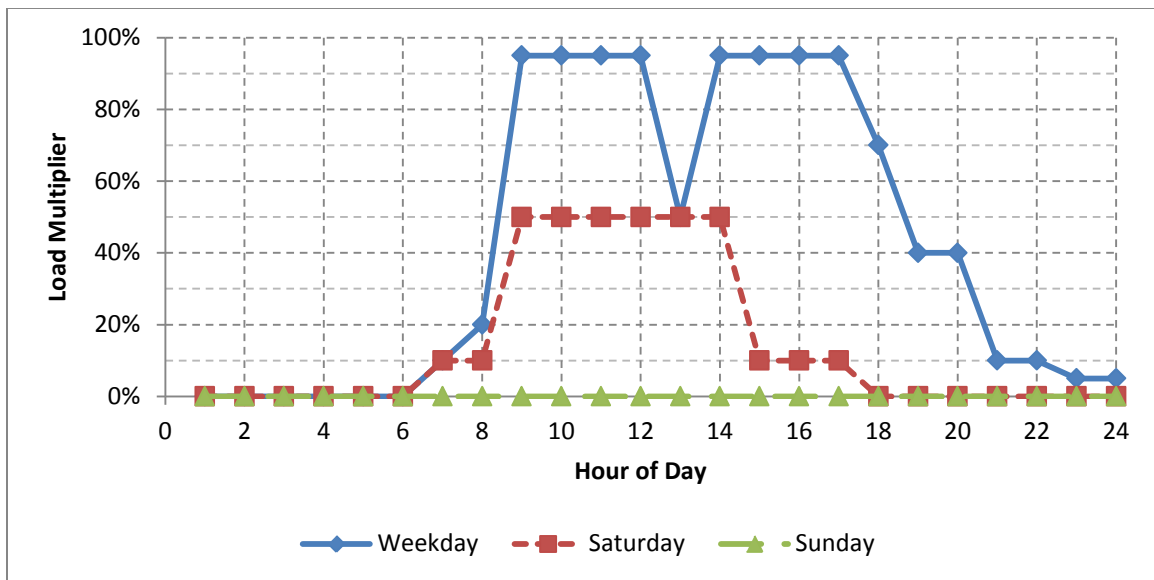


Figure 14: Hourly load multiplier schedule for people

3.5.2. Lighting

The DoE implementation uses “The building area method or the space-by-space method from [ASHRAE] Standard 90.1-2004” to estimate the heat rate resulting from lighting. This method estimates the lighting heat rate on a per unit area basis (U.S. Department of Energy, 2010, p. 30). The maximum lighting power density for offices listed by ASHRAE is 12W/m^2 (ASHRAE 2009 Fundamentals HandBook, 2009, p. 18.5). The value used in the DoE implementation is 10.76W/m^2 ($3.41\text{btu/hr}\cdot\text{ft}^2$). This model uses 10.76W/m^2 to better match results with the DoE implementation.

Lighting fixtures are typically located in the ceiling, which results in a load distribution between the unconditioned plenum space above the fixtures and the lighted space below the fixtures. This division results in the conditioned space receiving 60% of the load, while the plenum receives 40%. Lights do not produce latent heat, meaning that the entire load generated from lights is sensible. Table 5 shows the zone areas and subsequent peak heat rates due to lighting for each zone. Figure 15 shows the hourly load multiplier schedule for lighting.

Table 5: Peak heat rates resulting from lighting by zone

Zone	Area [m ²]	Peak Total Heat Rate [W]	Peak Sensible Heat Rate [W]	Peak Latent Heat Rate [W]
Core1	984	6352.7	6352.7	0
South1	207	1336.4	1336.4	0
East1	131	845.7	845.7	0
North1	207	1336.4	1336.4	0
West1	131	845.7	845.7	0
Plenum1	1,661	7148.9	7148.9	0
Core2	984	6352.7	6352.7	0
South2	207	1336.4	1336.4	0
East2	131	845.7	845.7	0
North 2	207	1336.4	1336.4	0
West2	131	845.7	845.7	0
Plenum2	1,661	7148.9	7148.9	0
Core3	984	6352.7	6352.7	0
South3	207	1336.4	1336.4	0
East3	131	845.7	845.7	0
North3	207	1336.4	1336.4	0
West3	131	845.7	845.7	0
Plenum3	1,661	7148.9	7148.9	0

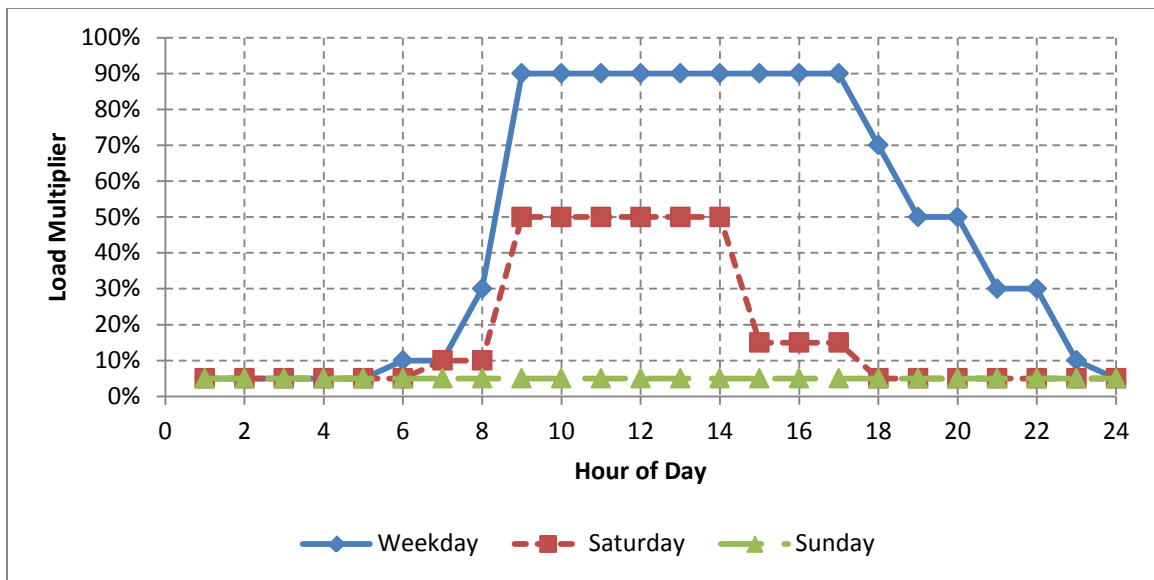


Figure 15: Hourly load multiplier schedule for lighting

3.5.3. Equipment

Heat gains resulting from equipment (computers, printers, etc.) are based on a heat gain per unit floor area method. Acceptable heat gain values range from 4.7 to 11.6W/m² (1.49 to 3.68btu/hr·ft²) with a normalized average of 8.7W/m² (2.76btu/hr·ft²) (ASHRAE 2009 Fundamentals HandBook, 2009, p. 18.10). According to Wilkins and Hosni, an office with medium load density has a heat gain of 10.8W/m² (3.42btu/hr·ft²) (ASHRAE 2009 Fundamentals HandBook, 2009, p. 18.13). The DoE implementation uses a load density of 10.76W/m² (3.41btu/hr·ft²). This model uses 10.76W/m² to better match results with the DoE implementation.

Typical equipment found in offices is assumed to not produce latent heat, meaning that the entire load generated from equipment is sensible. All equipment heat loads are assumed to be generated in the conditioned spaces, and not in the plenums. Table 6 shows the zone areas and peak heat rates from equipment for each zone. Figure 16 shows the hourly load multiplier schedule for equipment.

Table 6: Peak heat rates resulting from equipment by zone

Zone	Area [m ²]	Peak Total Heat Rate [W]	Peak Sensible Heat Rate [W]	Peak Latent Heat Rate [W]
Core1	984	10587.8	10587.8	0
South1	207	2227.3	2227.3	0
East1	131	1409.6	1409.6	0
North1	207	2227.3	2227.3	0
West1	131	1409.6	1409.6	0
Plenum1	1,661	0.0	0.0	0
Core2	984	10587.8	10587.8	0
South2	207	2227.3	2227.3	0
East2	131	1409.6	1409.6	0
North 2	207	2227.3	2227.3	0
West2	131	1409.6	1409.6	0
Plenum2	1,661	0.0	0.0	0
Core3	984	10587.8	10587.8	0
South3	207	2227.3	2227.3	0
East3	131	1409.6	1409.6	0
North3	207	2227.3	2227.3	0
West3	131	1409.6	1409.6	0
Plenum3	1,661	0.0	0.0	0

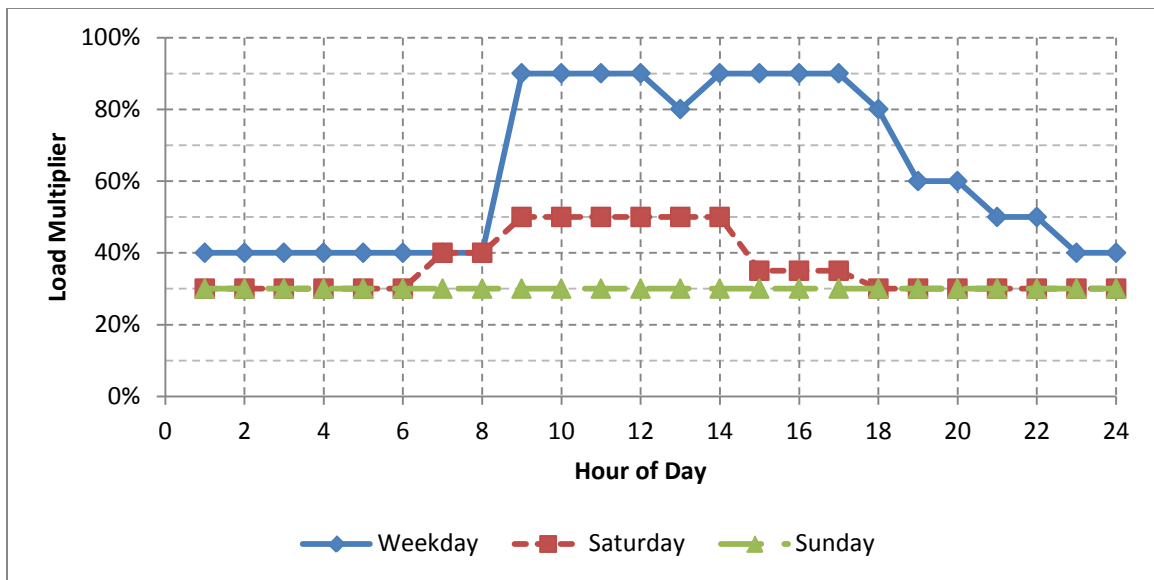


Figure 16: Hourly schedule for loads resulting from equipment

3.5.4. Elevators

The office building contains two elevators, each of which is assumed to “Use hydraulic motors with no counter weighting, weigh 2,500lb (1,134kg), travel 150fpm (46mpm), and have a mechanical efficiency of 58%” (U.S. Department of Energy, 2010, p. 15). Based on the motor power calculation from Baldor Electric Company, each motor has a power rating of 14.61kW (19.6HP), resulting in a combined power rating of 29.22kW (39.2HP) for the two elevator motors (U.S. Department of Energy, 2010, p. 15). The peak heat rate resulting from elevator operation used by the DoE implementation is 32.11kW (43.1HP).

Even though the elevator motors are not located in a particular zone, the heat generated by their operation will conduct through walls and eventually be handled by the building’s HVAC system. As a result, this model assumes that the motors are outside of the conditioned zone, but the heat generated by their operation is entirely assigned to the first-floor core zone. In such a case, the heat equivalent generated of elevator operation is given by Equation (2) (ASHRAE 2009 Fundamentals Handbook, 2009, p. 18.6).

$$q_{em} = PF_{UM}F_{LM} \quad (2)$$

where

q_{em} = heat equivalent of equipment operation [W]

P = motor power rating [W]

F_{UM} = motor use factor

F_{LM} = motor load factor

While it is unclear what motor use and load factors were used in conjunction with the 29.22kW (39.2HP) total motor power rating to yield a 32.11kW internal heat gain, 32.11kW is used in this model in order to better match the DoE results. Figure 17 shows the hourly load multiplier schedule for elevators.

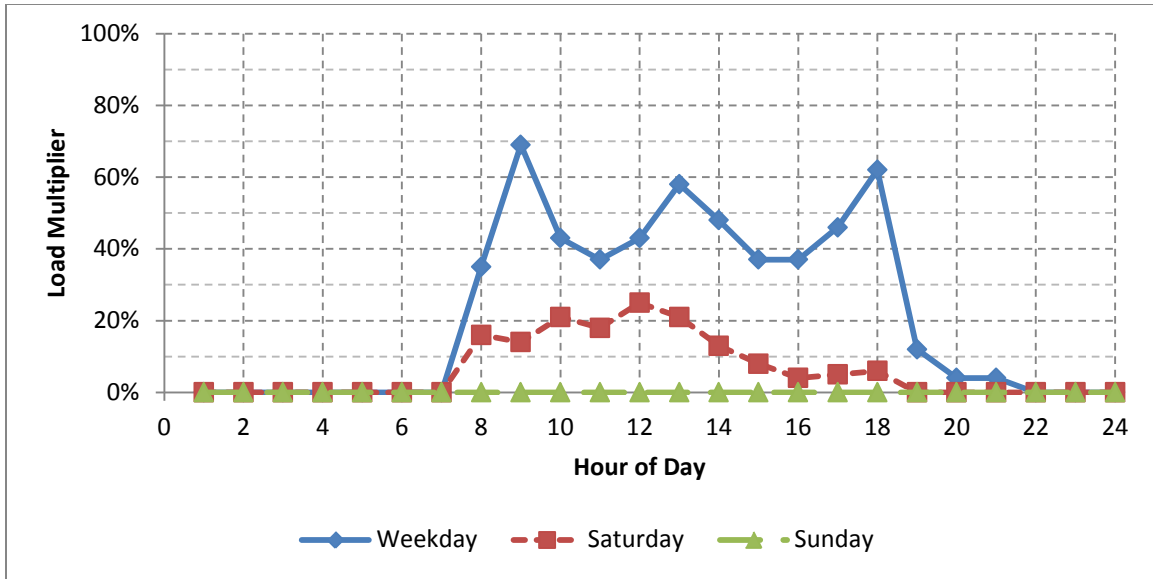


Figure 17: Hourly load multiplier schedule for elevators

3.5.5. Modeling of Sensible Loads

EnergyPlus allows sensible loads to be divided into convective and radiant components on a load-by-load basis. For example, EnergyPlus defines the sensible load resulting from electrical equipment as 50% convective and 50% radiant. This breakdown is then used by the EnergyPlus solver in the energy balance equations. HAMBASE does not have the ability to construct multiple separate internal loads in a particular zone, making it impossible to divide a particular load into convective and radiant components. Instead, HAMBASE includes a convection factor that divides the total sensible load into convective and radiant components. Example calculations for the convection factor are shown in Table 7 based on the loads in Core2. Values for the convection factor used for each zone are shown in Table 8.

Table 7: Example calculation of convective fraction for Core2 zone

Heat Source	People	Lighting	Elec.		Total	Fraction
			Equip.	Elevator		
Sensible Heat Rate [W]	3877	6353	10588	0	20818	100%
Convective Heat Rate [W]	2714	0	5294	0	8008	38%
Radiant Heat Rate [W]	1163	6353	5294	0	12810	62%

Table 8: Convective factors by zone

Zone	Peak Sensible Heat Rate [W]	Peak Radiant Heat Rate [W]	Peak Convective Heat Rate [W]	Convection Factor [%]
Core1	52927	28865	24063	45%
South1	4379	2695	1685	38%
East1	2771	1705	1066	38%
North1	4379	2695	1685	38%
West1	2771	1705	1066	38%
Plenum1	7149	0	7149	100%
Core2	20817	12810	8008	38%
South2	4379	2695	1685	38%
East2	2771	1705	1066	38%
North 2	4379	2695	1685	38%
West2	2771	1705	1066	38%
Plenum2	7149	0	7149	100%
Core3	20817	12810	8008	38%
South3	4379	2695	1685	38%
East3	2771	1705	1066	38%
North3	4379	2695	1685	38%
West3	2771	1705	1066	38%
Plenum3	7149	0	7149	100%

3.5.6. Summary of Sensible and Latent Loads

EnergyPlus gives the user the option to itemize separate heat sources and automatically include each individual heat source in simulations. HAMBASE does not have this functionality. Internal loads for HAMBASE must be in the form of total sensible heat rate and total latent heat rate (in $\text{kg}_{\text{water}}/\text{s}$) for a given zone. As a result, all individual heat sources in each zone must be summed on an hourly basis to create the

load profile for a zone that incorporates the load multiplier schedule. Examples of these load profiles are shown in Figure 18 for the sensible loads and Figure 19 for the latent loads of the Core1 zone. Additional profiles for the remaining zones can be found in Appendix A.1.

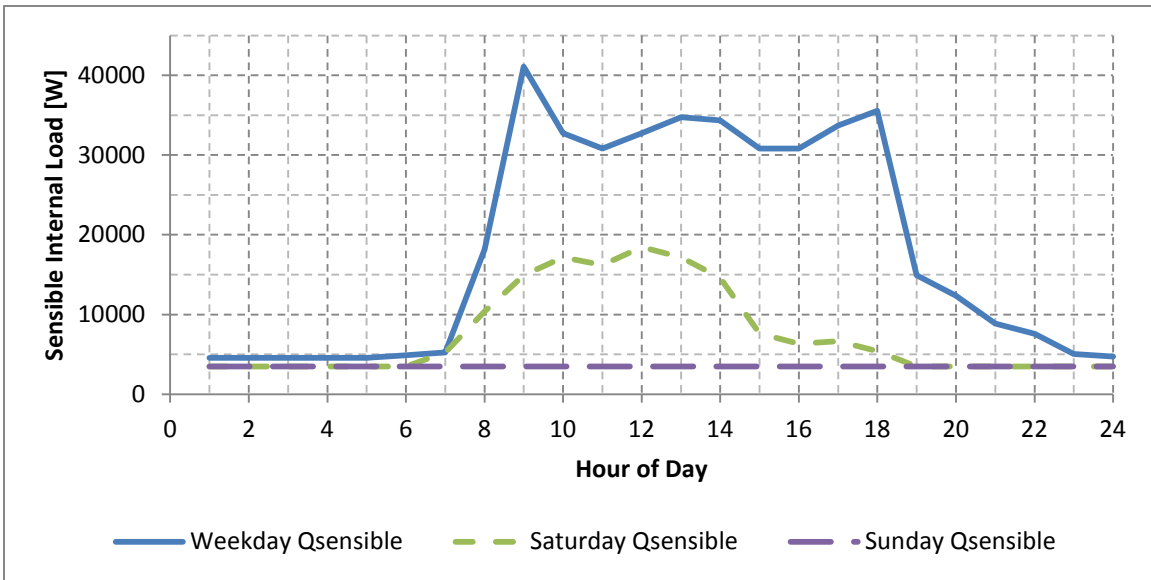


Figure 18: Sensible load profiles for the Core1 zone

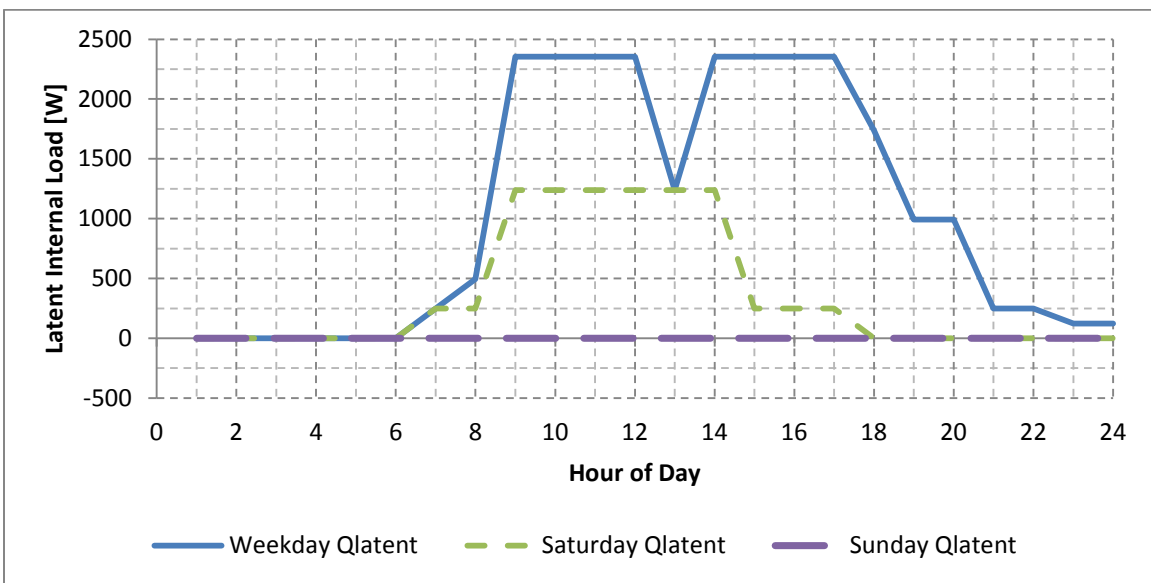


Figure 19: Latent load profiles for the Core1 zone

A summary of the total peak loads each zone is shown in Table 9. Note that the peak load values do not include scheduling, so they represent the greatest heat rate the zones could experience if all internal loads were on simultaneously.

The latent load, originally in watts, was converted to $\text{g}_{\text{water}}/\text{s}$ using Equation (3).

$$Q_{\text{latent}} = h_{fg} \cdot \dot{m}_{\text{water}} \quad (3)$$

where

$$h_{fg} = 2440.08 \cdot \frac{J}{\text{g}_w}, \text{ heat of vaporization at } 24^\circ \text{ C.}$$

Table 9: Total latent and sensible heat rates by zone

Zone	Peak Total Heat Rate [W]	Peak Sensible Heat Rate [W]	Peak Latent Heat Rate [W]	Peak Latent Heat Rate [g_w/s]
Core1	55406	52927	2479	1.014
South1	4901	4379	521	0.213
East1	3101	2771	330	0.135
North1	4901	4379	521	0.213
West1	3101	2771	330	0.135
Plenum1	7149	7149	0	0
Core2	23296	20817	2479	1.014
South2	4901	4379	521	0.213
East2	3101	2771	330	0.135
North 2	4901	4379	521	0.213
West2	3101	2771	330	0.135
Plenum2	7149	7149	0	0
Core3	23296	20817	2479	1.014
South3	4901	4379	521	0.213
East3	3101	2771	330	0.135
North3	4901	4379	521	0.213
West3	3101	2771	330	0.135
Plenum3	7149	7149	0	0

3.6. External Loads

This model includes three heat flows from sources outside of the building: infiltration, “The flow of outdoor air into a building through cracks and other unintentional openings and through the normal use of exterior doors,” ventilation, “intentional introduction of air from the outside into a building” and external weather (ASHRAE 2009 Fundamentals HandBook, 2009, p. 16.1). These three inputs are described in detail in the following sections.

3.6.1. Ventilation

Ventilation is the “Intentional introduction of air from the outside into a building” (ASHRAE 2009 Fundamentals HandBook, 2009, p. 16.1). Ventilation air is used to “Provide indoor air quality (IAQ)” (ASHRAE 2009 Fundamentals HandBook, 2009, p. 16.2). Outdoor air is required to maintain appropriate elimination of odors, concentration of carbon dioxide and concentration of other pollutants. Apte et al., Mendell and Seppanen et al. have shown that an “Outdoor air supply of about 10L/s per person is very likely to provide acceptable perceived indoor air quality in office spaces” (ASHRAE 2009 Fundamentals HandBook, 2009, p. 16:10). The ANSI/ASHRAE Standard 62.1-2013 lists 8.5L/s per person as the minimum outdoor air rate for office space in an office building (ASHRAE, 2013, p. 13). The DoE documentation uses 9.44L/s per person based on ANSI/ASHRAE Standard 62.1-1999 (U.S. Department of Energy, 2010, p. 13).

This model uses the 10L/s per person ventilation rate combined with the 18.58m²/person occupancy rate to arrive at a ventilation value of 0.538L/s per square meter for occupied, conditioned zones. Dividing the ventilation rate by a zone’s volume yields the air exchange rate, which has units of 1/time. Usually the time is in hours, so the air exchange rate is called air changes per hour (ACH). The ventilation rate for each zone in the model is shown in Table 10. Ventilation only occurs when the building is occupied, and the corresponding ventilation schedule is shown in Figure 20.

Table 10: Ventilation values by zone

Zone	Area [m ²]	Ventilation [L/s]	Ventilation [ACH]
Core1	984	529.6	0.707
South1	207	111.4	0.705
East1	131	70.5	0.705
North1	207	111.4	0.705
West1	131	70.5	0.705
Plenum1	1,661	0.0	0.000
Core2	984	529.6	0.707
South2	207	111.4	0.705
East2	131	70.5	0.705
North 2	207	111.4	0.705
West2	131	70.5	0.705
Plenum2	1,661	0.0	0.000
Core3	984	529.6	0.707
South3	207	111.4	0.705
East3	131	70.5	0.705
North3	207	111.4	0.705
West3	131	70.5	0.705
Plenum3	1,661	0.0	0.000

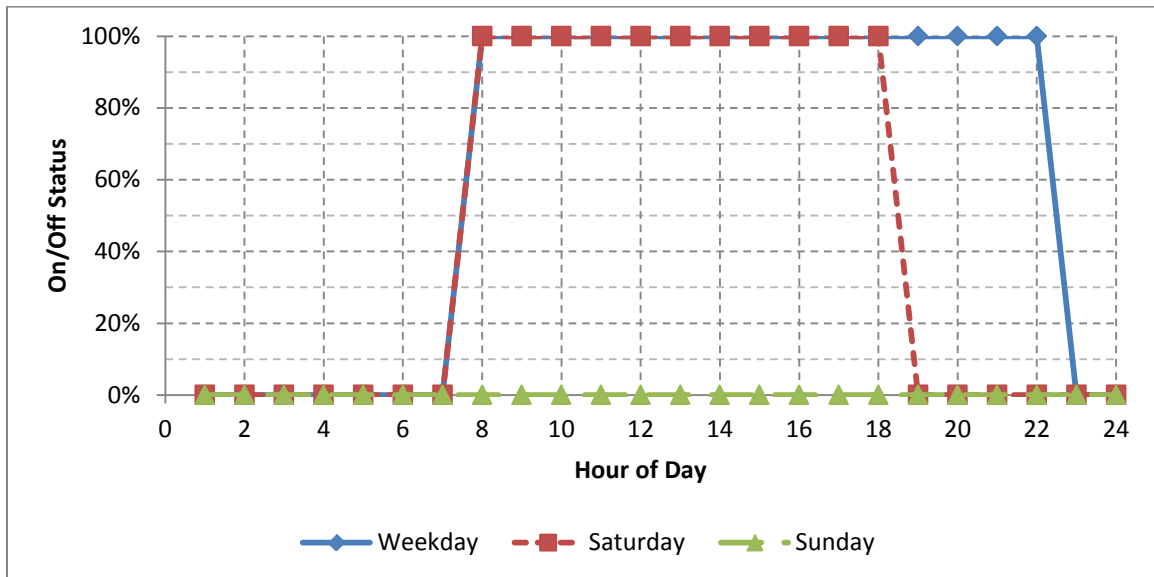


Figure 20: Hourly on/off schedule for outdoor air ventilation

3.6.2. Infiltration

Where ventilation was purposeful flow of outdoor air into a building, infiltration is the “Flow of outdoor air into a building through cracks and other unintentional openings and through the normal use of exterior doors” (ASHRAE 2009 Fundamentals HandBook, 2009, p. 16.1). Infiltration rates depend on building construction, weather conditions and HVAC operation pressures. Relationships exist relating air leakage rates to pressure difference across the exterior envelope of a building, and to average envelope crack size. The pressure difference across the building envelope varies continuously with wind speed, barometric pressure and HVAC pressurization, while envelope crack size and distribution are typically unknown.

As a result of these challenges, “Modeling approaches to infiltration are typically very simple” (U.S. Department of Energy, 2010, p. 29). In many commercial applications, it is assumed that building envelopes are airtight, but Persily and Grot found that when results are normalized by envelope area, envelope airtightness for American commercial buildings display similar levels of airflow as American houses (ASHRAE 2009 Fundamentals HandBook, 2009, p. 16.25). Another approach applies a fan pressurization test to measure flow rate through a building’s envelope at a certain supply pressure, and subsequently normalizes the flow rate by the building’s surface area. Using this method, Persily and Grot found air leakage rates, “Ranging from 1080 to 5220cm³/(s·m²) at 75Pa” (ASHRAE 2009 Fundamentals HandBook, 2009, p. 16.25). Tamura and Shaw found that air leakage values at 75Pa for tight, average and leaky walls were “500, 1500, and 3000cm³/(s·m²)” respectively (ASHRAE 2009 Fundamentals HandBook, 2009, p. 16.25). ASHRAE Standard 90.1-2004 proposed an ideal maximum building leakage of 2000cm³/(s·m²) for above-grade envelope area (exterior walls and roof) (U.S. Department of Energy, 2010, p. 29).

The actual DoE implementation used a constant flow per exterior surface area value of 0.000302m³/(s·m²) (302cm³/(s·m²)). This value applies only applies during times when the HVAC system is not in operation. When the HVAC system is on, the pressure exerted by the system serves to reduce infiltration into the building. As a result,

it was “Assumed that the uncontrolled infiltration is reduced to 25% of the [maximum] value” (U.S. Department of Energy, 2010, p. 29). Infiltration flow rates for each zone in the model are shown in Table 11. The HVAC operation schedule is shown in Figure 21, while the resulting infiltration load multiplier schedule is shown in Figure 22.

Table 11: Infiltration values by zone

Zone	Exterior Surface Area [m ²]	Infiltration, HVAC off [m ³ /s]	Infiltration, HVAC off [ACH]	Infiltration, HVAC on [ACH]
Core1	0	0.0000	0.000	0.000
South1	137	0.0413	0.262	0.065
East1	91	0.0276	0.276	0.069
North1	137	0.0413	0.262	0.065
West1	91	0.0276	0.276	0.069
Plenum1	203	0.0613	0.109	0.027
Core2	0	0.0000	0.000	0.000
South2	137	0.0413	0.262	0.065
East2	91	0.0276	0.276	0.069
North 2	137	0.0413	0.262	0.065
West2	91	0.0276	0.276	0.069
Plenum2	203	0.0613	0.109	0.027
Core3	0	0.0000	0.000	0.000
South3	137	0.0413	0.262	0.065
East3	91	0.0276	0.276	0.069
North3	137	0.0413	0.262	0.065
West3	91	0.0276	0.276	0.069
Plenum3	1864	0.5628	1.001	0.250

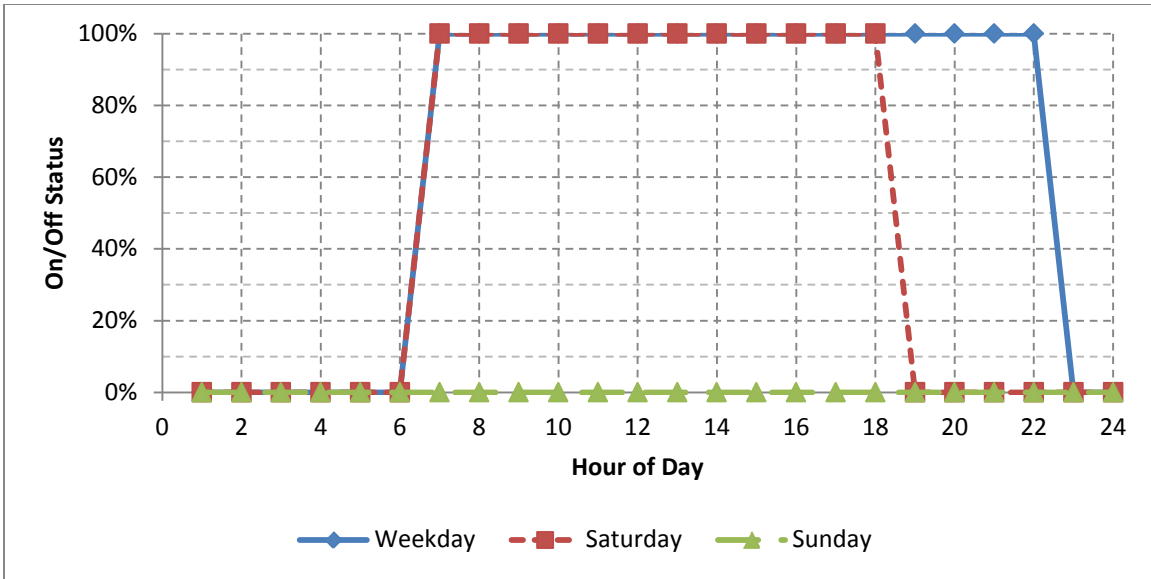


Figure 21: Hourly on/off schedule for HVAC system operation

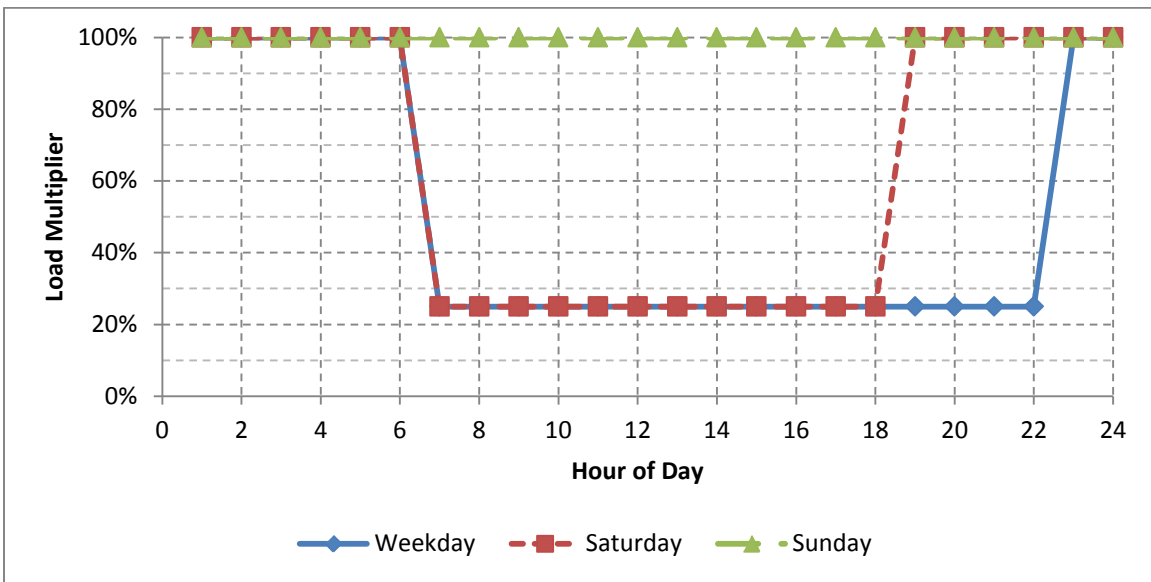


Figure 22: Hourly load multiplier schedule for infiltration

3.6.3. Weather

The weather input used in this model and in the DoE implementation is the typical meteorological year (TMY) dataset produced by the National Renewable Energy Laboratory's (NREL) Electric Systems Center under the Solar Resource Characterization Project (NREL, 2009). This dataset contains "Hourly values of solar radiation and meteorological elements for a 1-year period" (NREL, 2009). The TMY data is in its third iteration (TMY3). It is generated by looking across years of meteorological data for a given location and choosing the best representation of typical weather for a given month. TMY3 draws from the 1961-1990 and 1991-2005 National Solar Radiation Data Base archives (NREL, 2009). TMY3 offers data for 1020 locations in the United States and represents "Typical rather than extreme conditions," making it perfectly suited for an extended time simulation (NREL, 2009). HAMBASE uses seven categories of weather input from the TMY3 data, which are shown in Table 12.

Table 12: Weather inputs to HAMBASE

Weather Input	Units
Direct normal irradiance (DNI)	W/m ²
Diffuse horizontal irradiance (DHI)	W/m ²
Cloud cover	0-8
Dry bulb air temperature	°C
Relative humidity	%
Wind direction	Degrees from North
Wind velocity	m/s

3.7. Temperature Control

The temperatures in the 15 conditioned zones of the building are controlled using a dual-setpoint thermostat model. An hourly temperature control setpoint schedule for heating and cooling operation is shown in Figure 23. The heating setpoint represents the temperature below which a heat pump provides heating to a zone. The cooling setpoint represents the temperature above which a heat pump provides cooling to a zone. Both the

heating and cooling schedules show a typical night and weekend “temperature setback” energy-saving control approach. When the building is occupied, the cooling setpoint is 24°C (75.2°F) and the heating setpoint is 21°C (69.8°F). When the building is not occupied, the thermostat setpoints are relaxed to 26.7°C (80.1°F) for cooling and 15.6°C (60.1°F) for heating to minimize the amount energy used for heating and cooling.

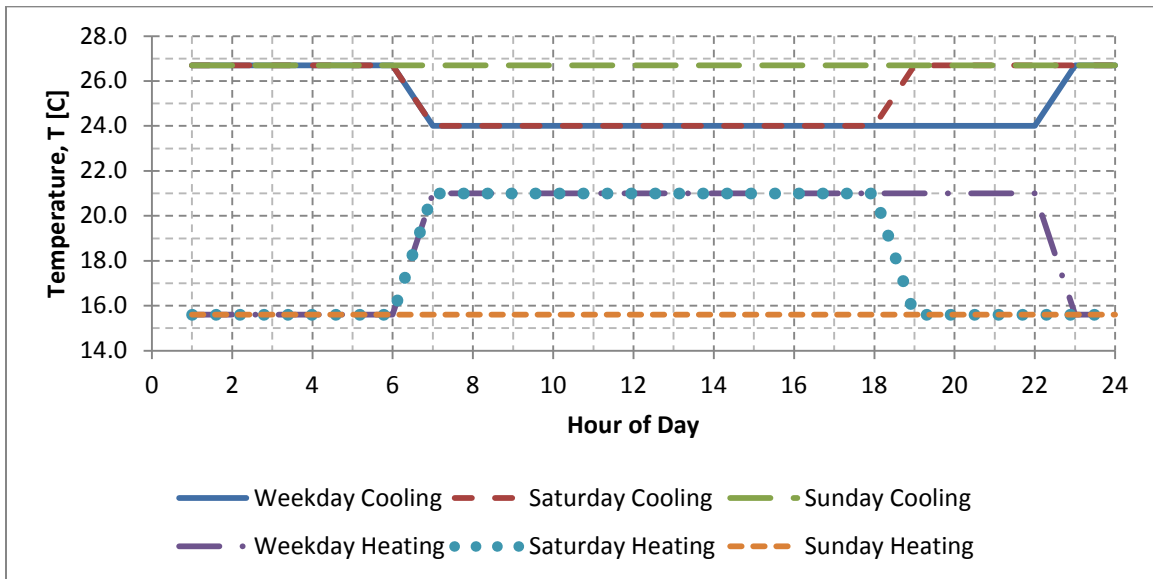


Figure 23: Hourly temperature control setpoint schedule for heating and cooling

The thermostat model includes a deadband of $\pm 1^\circ\text{C}$ (1.8°F) to eliminate the efficiency and control problems resulting from a bang-bang control. Example data showing the deadband’s operation in summer and winter are shown in Figure 24 and Figure 25 respectively. Figure 24 shows the zone temperature increasing gradually under summer loads until the upper deadband limit is reached (cooling setpoint + deadband), at which point the thermostat turns on the heat pump, cooling the zone. The heat pump provides cooling until the lower deadband limit is reached (cooling setpoint – deadband), at which point the thermostat turns off the heat pump.

Figure 25 shows the same process in reverse for heating mode in the winter. The zone temperature decreases gradually under winter conditions until the lower deadband

limit is reached (heating setpoint - deadband), at which point the thermostat turns on the heat pump, heating the zone. The heat pump provides heating until the upper deadband limit is reached (heating setpoint + deadband), at which point the thermostat turns off the heat pump.

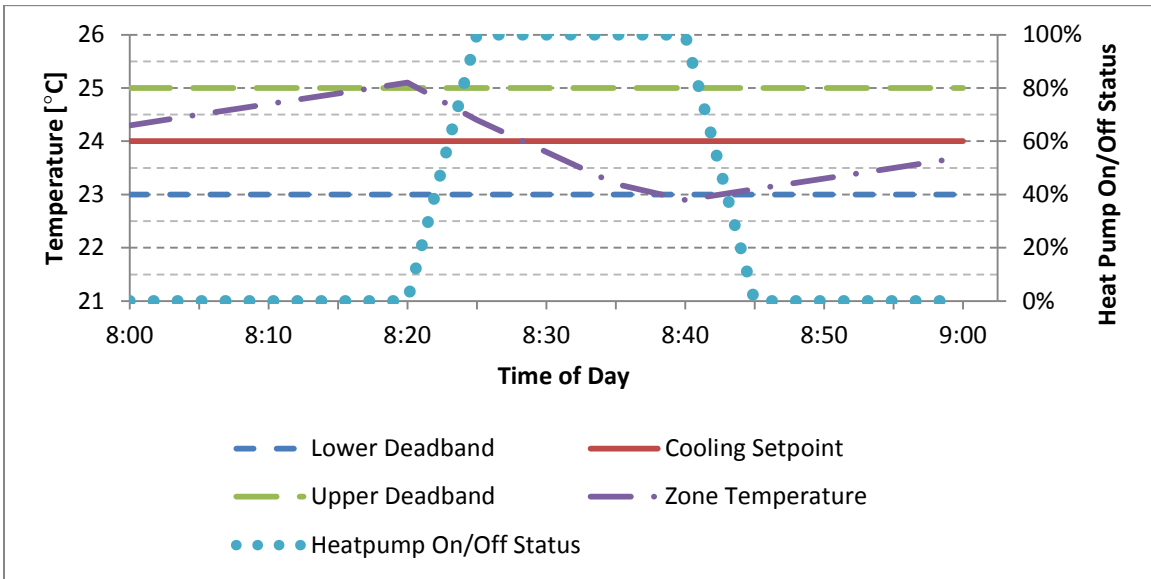


Figure 24: Example deadband operation during summer (cooling mode)

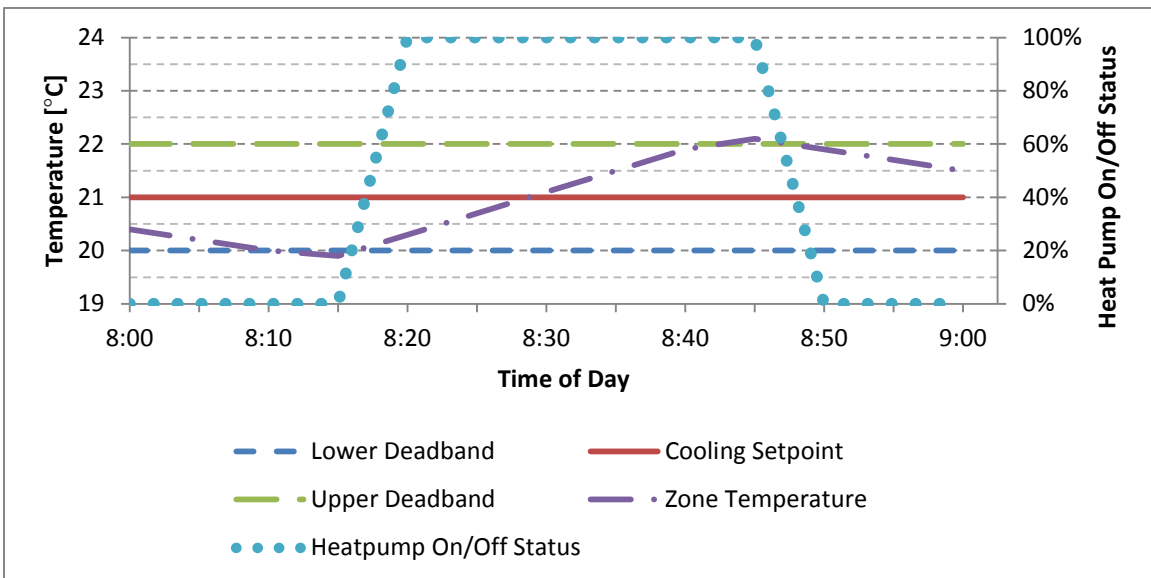


Figure 25: Example deadband operation during winter (heating mode)

Chapter 4 Integrated Building-Load + GSHP Model

The building model described in Chapter 3 was combined with an HVAC model, a GHEX model and a thermostat model to create the integrated building-load + GSHP model shown in Figure 26. The model offers easy modification to include hybrid sizing, such as a cooling tower, making the model one of the first Matlab® Simulink® based hybrid GSHP simulation tools.

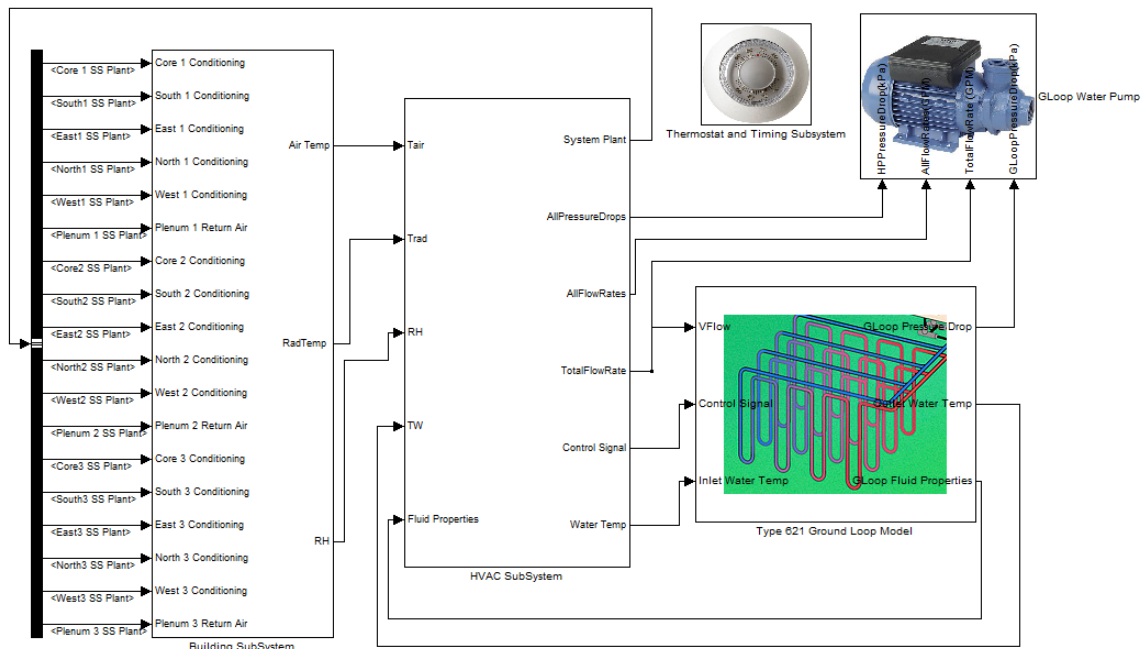


Figure 26: Top-level view of integrated Simulink® model

The following sections describe the simulation order (Section 4.1), the subsystems that comprise the integrated model, simulation data storage (Section 4.7) and model simulation details (Section 4.8). The five model subsystems include: the building subsystem in Section 4.2, the thermostat and timing subsystem in Section 4.3, the HVAC subsystem in Section 4.4, the ground loop subsystem in Section 4.5 and the water pump subsystem in Section 4.6.

4.1. Simulation Order

A block-diagram of the subsystems and signals is shown in Figure 27. The inputs to the integrated model are weather and supplemental heat rejection. Internal loads are defined within the building model.

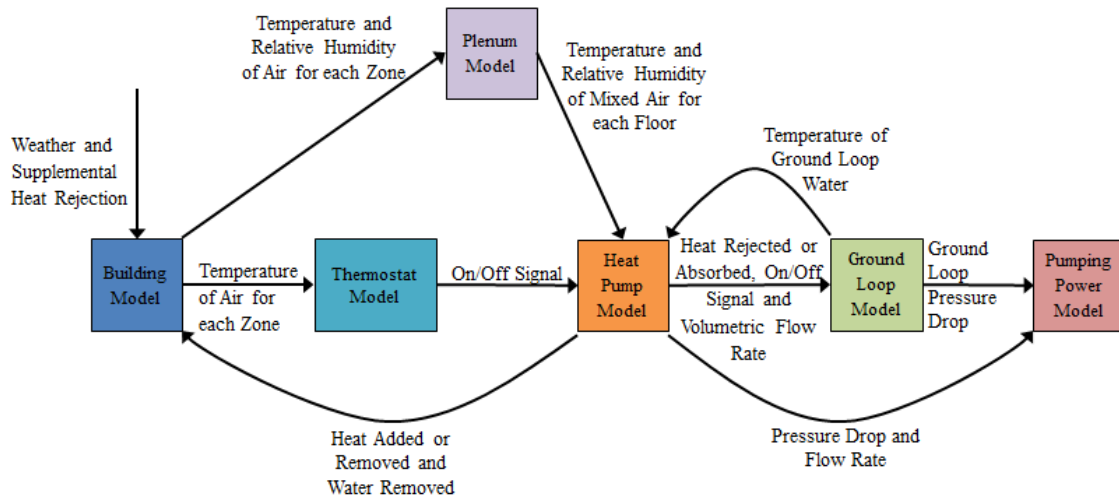


Figure 27: Block diagram of integrated model

For a given time-step, the simulation order starts with the building model and continues to the right: thermostat model, plenum model, heat pump model, ground loop model and pumping power model. Thus, the air temperature and relative humidity in each zone of the building are calculated using the current time-step's weather and internal loads, and the previous time-step's heat pump conditioning.

Model simulation order is controlled via the “Priority” setting of each Simulink® block. Right-clicking on a model block opens a block modification menu that includes “Block Properties”. The “Block Properties” menu allows the user to set simulation priority for that particular block, as shown in Figure 28. Blocks with a priority setting of one are the first to simulate, followed by blocks with priority setting of two, etc. For blocks that are not explicitly assigned a priority setting, Simulink® sets their simulation order based on the flow of data through the whole model.

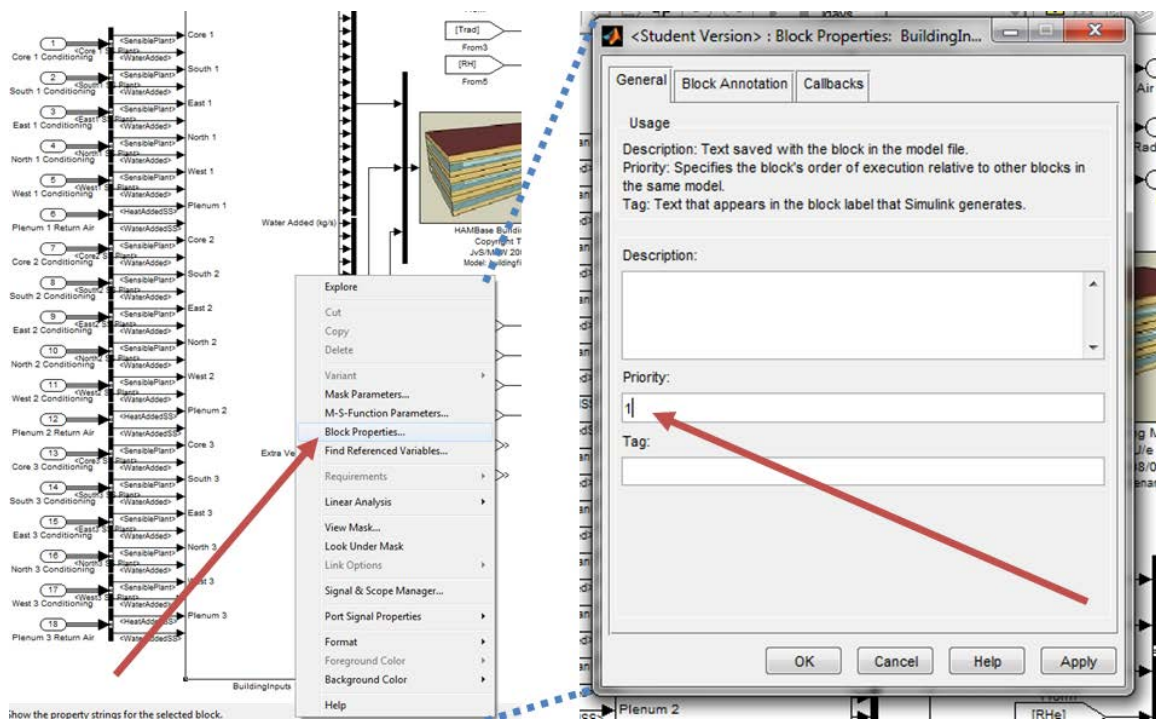


Figure 28: Setting subsystem priority in Simulink®

With priority settings chosen for particular blocks, testing the simulation order is easily completed using the Simulink® Debugger. The Debugger view shows every block in the model, sorted by simulation order. Figure 29 shows an image of this process. Using the block priority settings and the Debugger, the simulation order of the integrated model can be quickly changed.

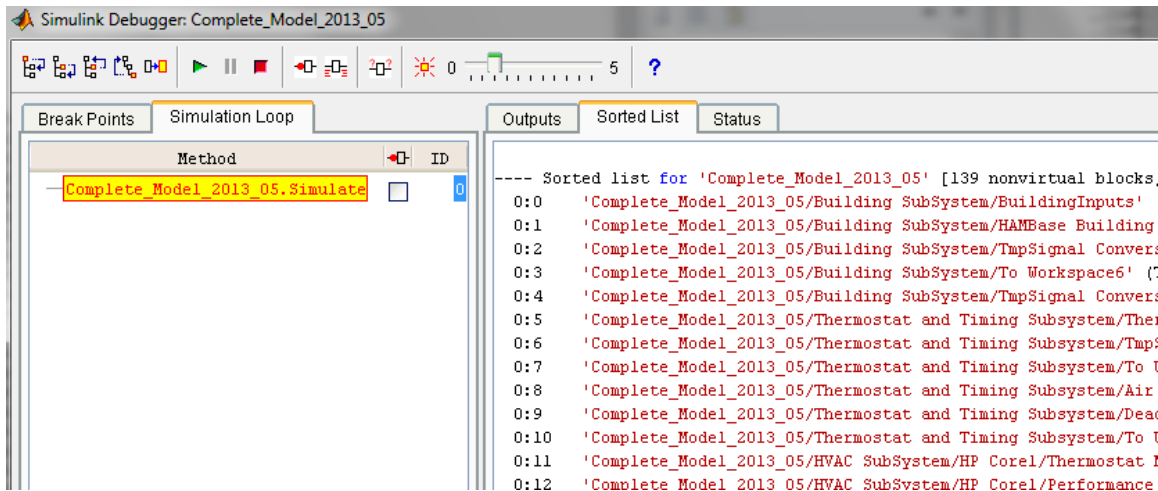


Figure 29: Testing simulation order using Simulink® Debugger

4.2. Building Subsystem Model

The building subsystem represents the physics of the building envelope and zones. Shown in Figure 30, it is comprised of three components: the HAMBASE model block, a building inputs block, and a data recording “To Workspace” block. An overview of the subsystem inputs and outputs is shown in Figure 31. An overview of the data processing used in this model can be found in Section 4.7.

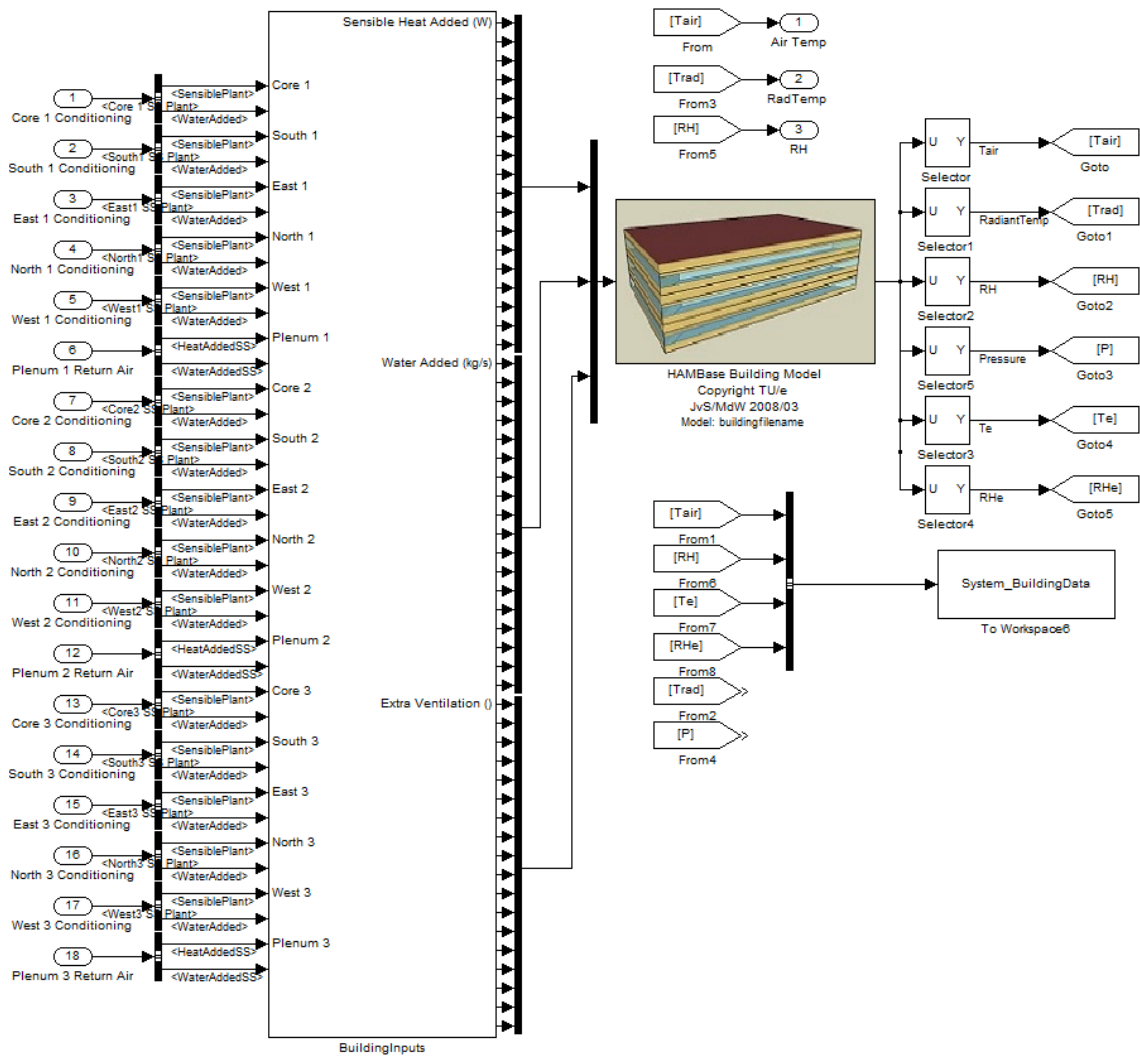


Figure 30: View of the building subsystem Simulink® model

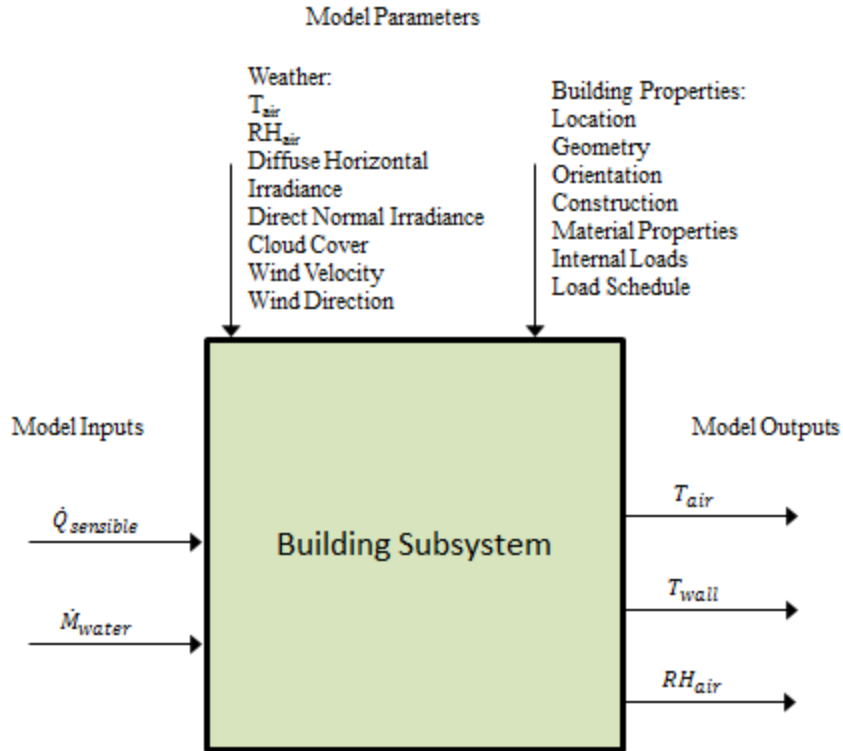


Figure 31: Inputs and outputs for the building subsystem

The HAMBASE model block uses as inputs: the sensible heat added or removed to each zone (in watts), the latent heat added or removed to each zone (in kilograms of water per second) and the extra ventilation added to each zone (in air changes per hour). The HAMBASE model block calls the HAMBASE m-file, which is a text-based representation of the building parameters that were discussed in Chapter 3. Values for the building location, geometry, orientation, envelope construction, material properties, internal loads and schedule are all stored in arrays within the HAMBASE m-file. With these parameters, the HAMBASE model block updates the air temperature, wall temperature and air relative humidity for every zone, and returns these values as block outputs.

The building input block is a pass-through structure that routes signals for the HAMBASE model block, and allows for proper simulation sequencing. The building

input block routes the conditioning provided by heat pumps to the appropriate zone input. The block also defines the initial conditions for heat pump cooling or heating. These initial conditions allow the HAMBASE model block to be the first block simulated in the model, ensuring appropriate simulation sequencing.

The data recording block stores block outputs for every simulation time-step. During one-year simulations, air temperature, humidity, wall temperature and pressure are recorded for every zone. During 15-year simulations, the only variables stored are air temperature and humidity. Reducing the number of variables is required to not overload system resources and to increase simulation speed.

4.3. Thermostat and Timing Subsystem

The thermostat and timing subsystem determines the temperature setpoints for the HVAC system based on the time of day and day of the week. The method of temperature control used in this model (a dual-setpoint, on/off control with deadband) was previously described in Section 3.7. During typical building hours the cooling setpoint is 24°C (75.2°F) and the heating setpoint is 21°C (69.8°F). When the building is not occupied, the thermostat setpoints are relaxed to 26.7°C (80.1°F) for cooling and 15.6°C (60.1°F) for heating to minimize the amount energy used for heating and cooling. The hourly setpoint schedule was previously shown in Figure 23.

The setpoint schedule is stored in an array and read by the thermostat setpoint block, shown in Figure 32. The thermostat setpoint block compares the day of week and time of day of every time-step to the thermostat schedule, and outputs the appropriate cooling and heating setpoint for each zone. The cooling and heating setpoint for a particular zone is then used as an input to the thermostat model in each zone, which is further described in Section 4.4.2.

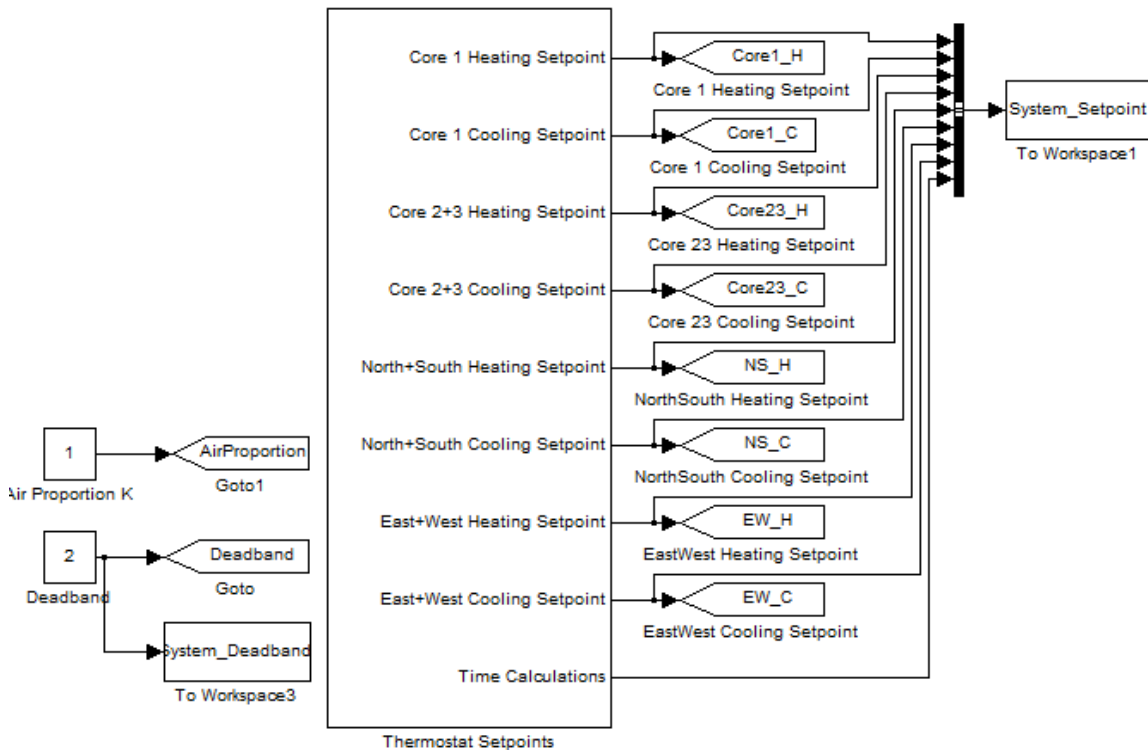


Figure 32: View of the thermostat and timing subsystem Simulink® model

4.4. HVAC Subsystem Model

The HVAC subsystem controls the sensible heating, sensible cooling and latent cooling provided to each zone in the building and the thermal energy rejected or absorbed to the ground loop. The subsystem is comprised of four components: the plenum subsystem, heat pump subsystems, a ground-loop header, signal routing and data recording blocks. A view of the entire HVAC subsystem is shown in Figure 33 and Figure 34. The inputs to the HVAC subsystem are air temperature, wall temperature and relative humidity for each zone, the total airflow rate of the HVAC system (previous time-step), and temperature of ground-loop water entering the heat pump (entering water temperature, EWT).

The component models of the HVAC subsystem are described individually in the following sections.

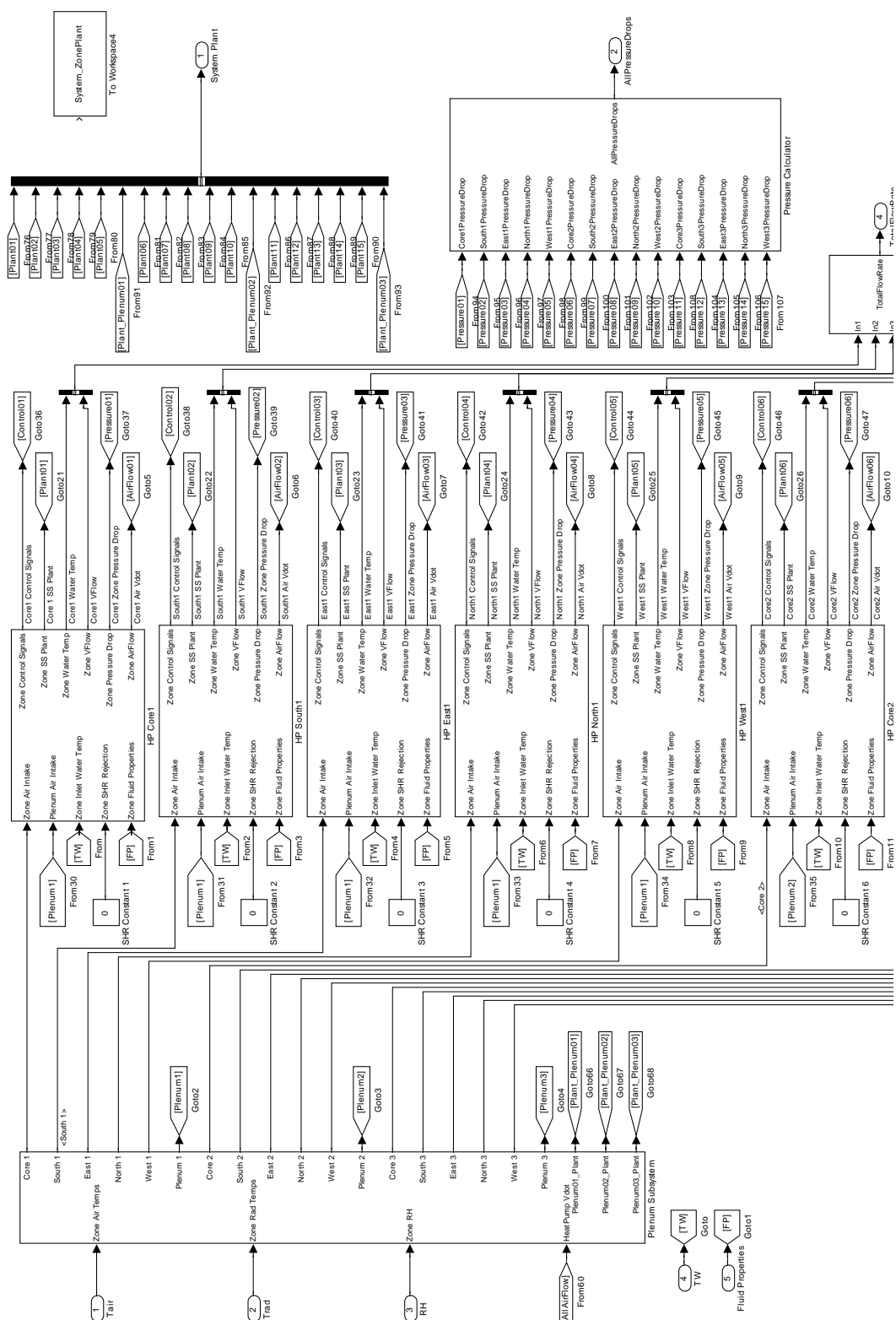


Figure 33: View of the HVAC subsystem Simulink® model (part 1)

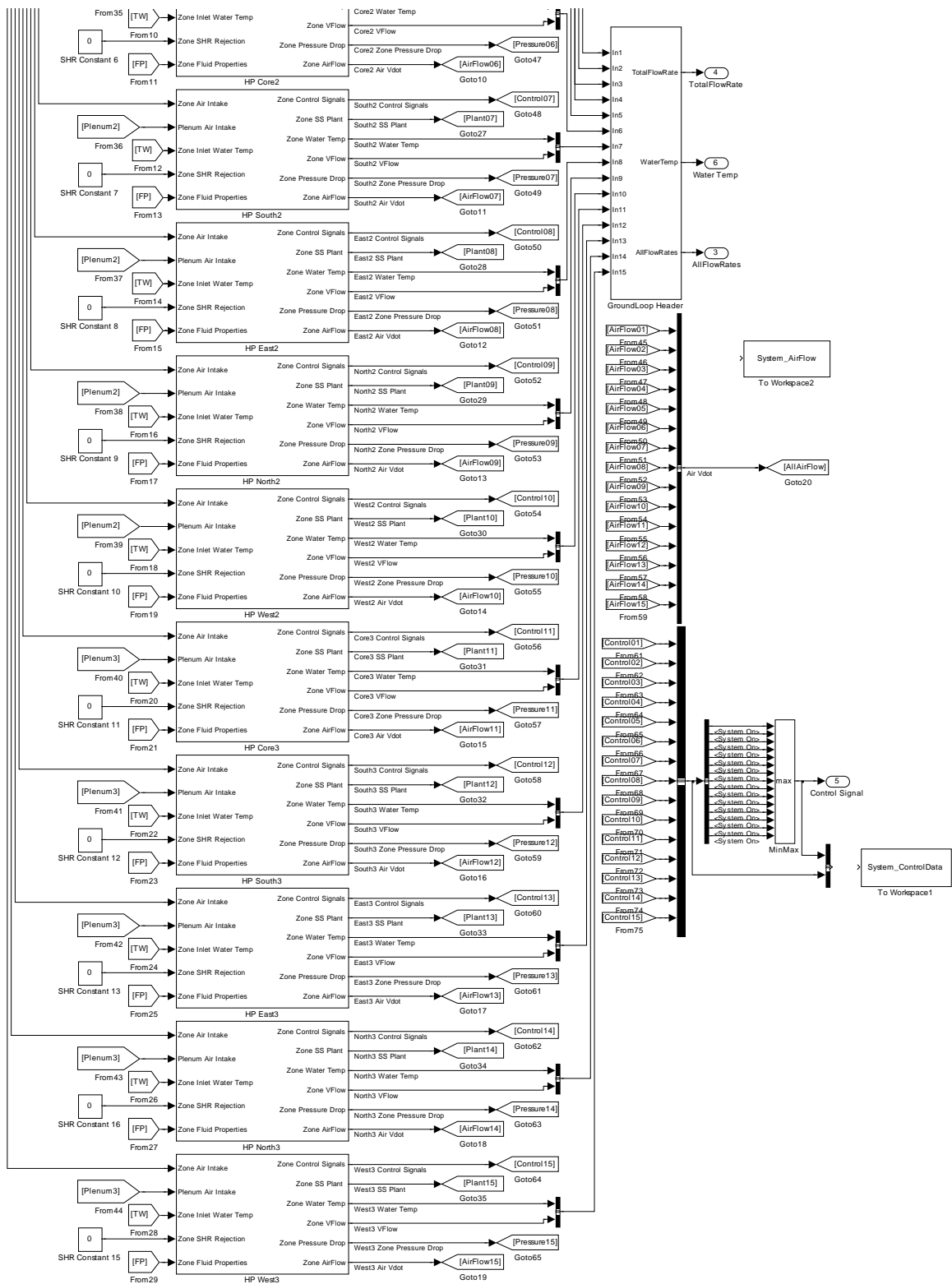


Figure 34: View of the HVAC subsystem Simulink® model (part 2)

4.4.1. Plenum Subsystem Model

The plenum subsystem functions as the return air path for the HVAC system. It is shown in Figure 35, and consists of a plenum block for each floor (for a total of three plenum blocks) and signal routing and data recording. The plenum block calculates the amount of sensible and latent heat added to the plenum as a result of return air from each zone. An explanation of the plenum block model is shown below.

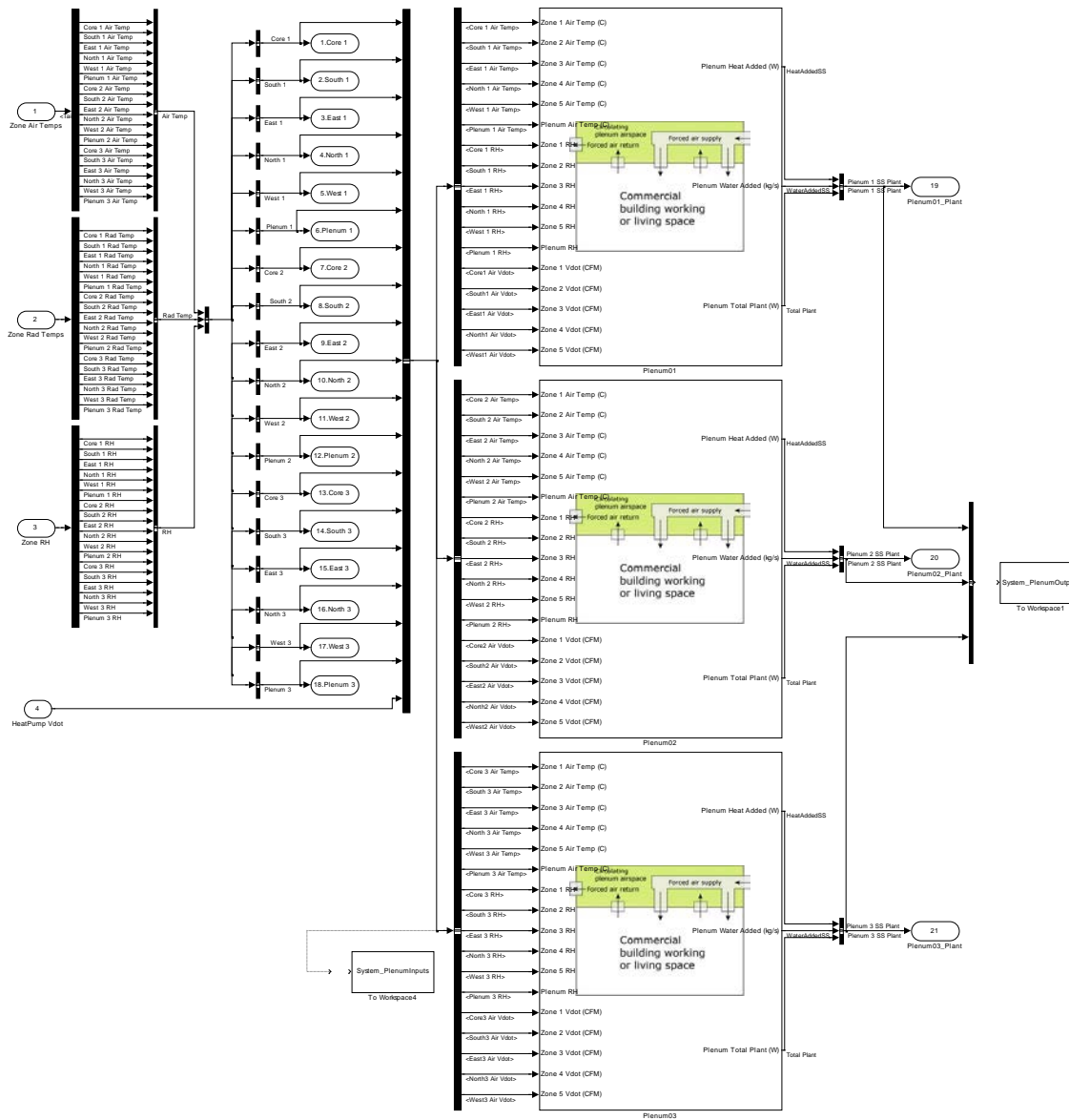


Figure 35: View of the plenum subsystem Simulink® model

For a single conditioned zone, the control volume and idealized airflow rates of the HVAC system are shown in Figure 36. Control Volume A represents the flow path of an actual heat pump implementation: infiltration from the outdoor environment exchanges directly with the zone, supply air is provided by the heat pump, zone air is returned to the heat pump and the heat pump handles the intake of ventilation air and the exhaust of some portion of the return air. Control Volume B shows the modified flow path used in HAMBASE: since ventilation air and infiltration both represent volumetric flow between the conditioned zone and the outdoor environment they are combined.

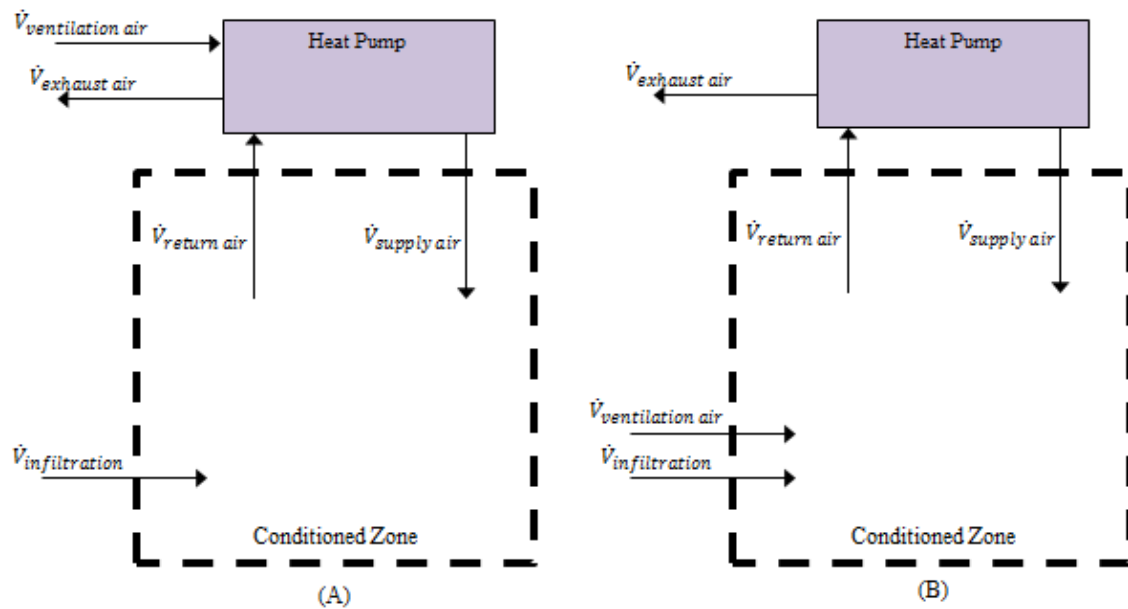


Figure 36: Control volume for a single conditioned zone using (A) the HVAC flow path for an actual heat pump and (B) the flow path for the HAMBASE simplification

When multiple conditioned zones are modelled with dedicated heat pumps, the plenum acts as a common return air path for all zones. This arrangement reduces ducting requirements and corresponding losses in efficiency. As shown in Figure 37, each of the three conditioned zones in the figure return air to the plenum, and the plenum air acts as a common air intake for all heat pumps. The plenum experiences infiltration because it has

external walls that are subject to leakage, but it does not experience ventilation because it is not a conditioned space.

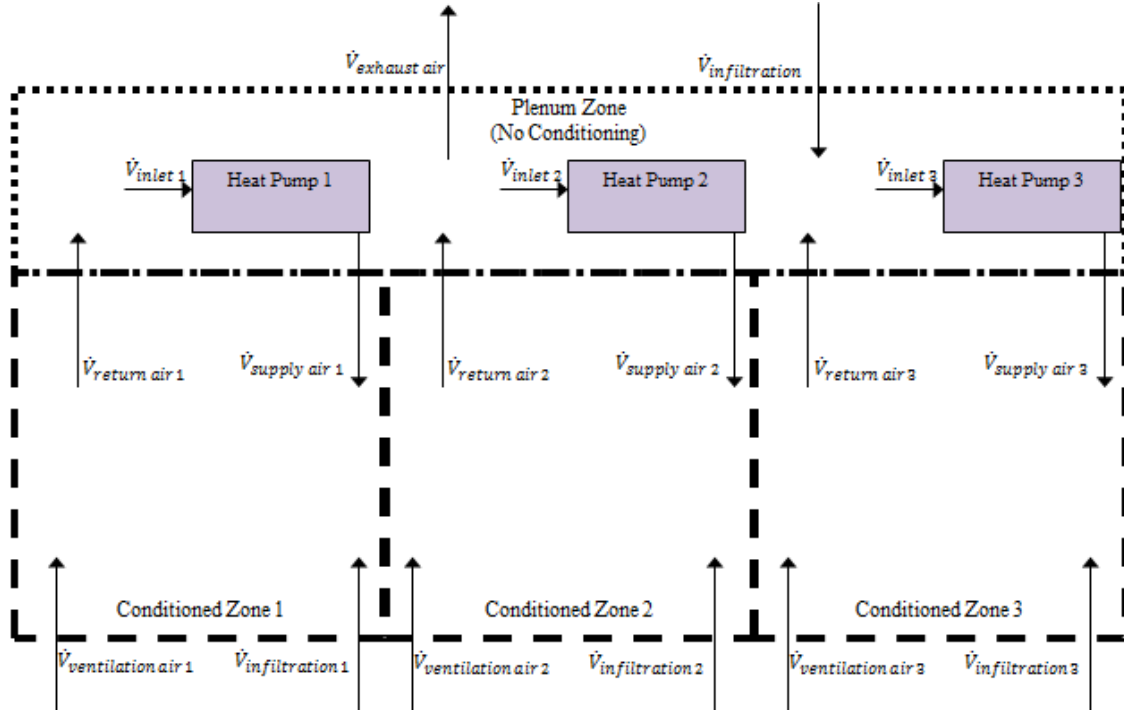


Figure 37: Control volume for three conditioned zones using a plenum

The inputs to the plenum block are the air temperature, air relative humidity and airflow rate returning from each zone. After converting relative humidity to humidity ratio (W), the mass conservation equations for the plenum can then be written as:

$$\dot{Q}_{plenum,sensible} = \sum_{i=1}^n \dot{V}_{iRA} \rho C_p \Delta T_i \text{ for } n \text{ zones} \quad (4)$$

$$\dot{Q}_{plenum,latent} = \sum_{i=1}^n h_{fg} \dot{V}_{iRA} \rho \Delta W_i \text{ for } n \text{ zones} \quad (5)$$

where the volumetric flow rate of the return air is given by:

$$\dot{V}_{iRA} = \dot{V}_{i inf} + \dot{V}_{i vent} + \dot{V}_{i supply} \text{ for zone } i. \quad (6)$$

While the volumetric flow rate shown in Equation (6) includes infiltration, the implementation in the plenum block does not include infiltration because the effects of

infiltration heat transfer are already included in the HAMBASE zone calculations. Thus, Equation (7) represents the volumetric flow rate equation used in the plenum model.

$$\dot{V}_{iRA} = \dot{V}_{i\text{vent}} + \dot{V}_{i\text{supply}} \text{ for zone } i. \quad (7)$$

The resulting sensible and latent heat rates calculated by the plenum block are then used as input conditioning for the plenum zones on the next simulation time-step.

4.4.2. Heat Pump Subsystem Model

The heat pump subsystem calculates the exact amount of heating or cooling delivered to a zone, the resulting heat rejected to the ground loop and the heat pump's power usage. Each conditioned zone in the model has a dedicated heat pump subsystem, for a total of 15 heat pump subsystems. The heat pump subsystem uses the state of the zone air, the state of the plenum air and the state of the ground loop water as inputs, and returns sensible cooling/heating, latent cooling, ground loop water temperature and power usage as outputs. A block diagram showing all of the inputs, outputs and parameters for the subsystem is shown in Figure 38.

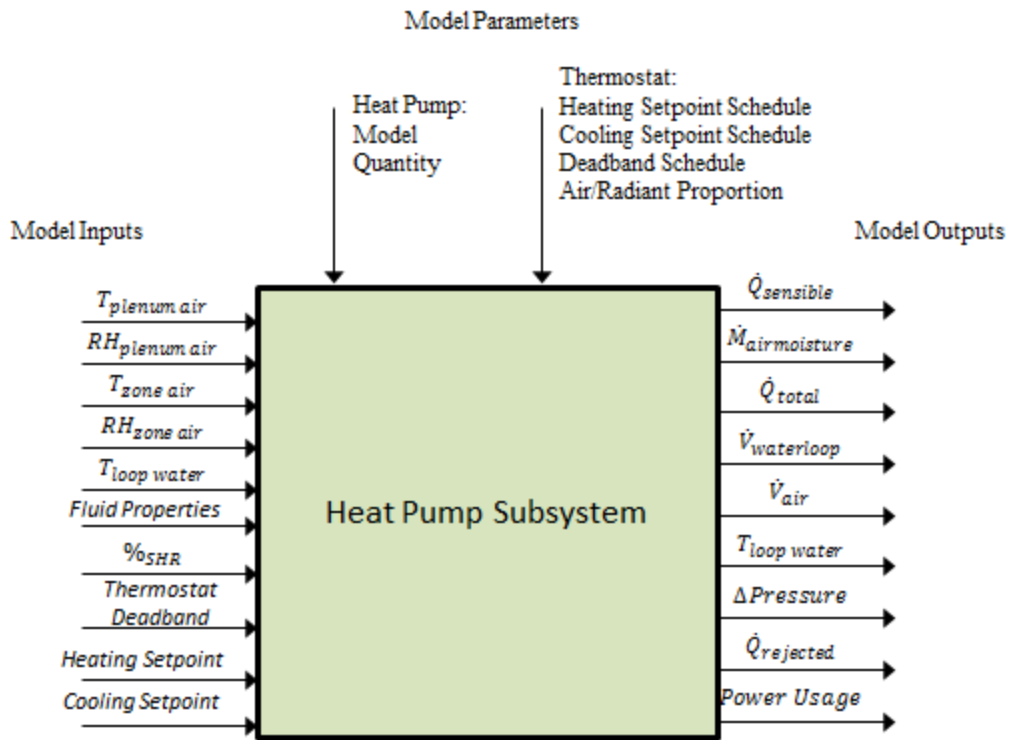


Figure 38: Inputs and outputs for the heat pump subsystem

The heat pump subsystem contains a thermostat block, a heat pump block, signal routing and data storage, as shown in Figure 39. Discussion of each of these subsystems follows Figure 39.

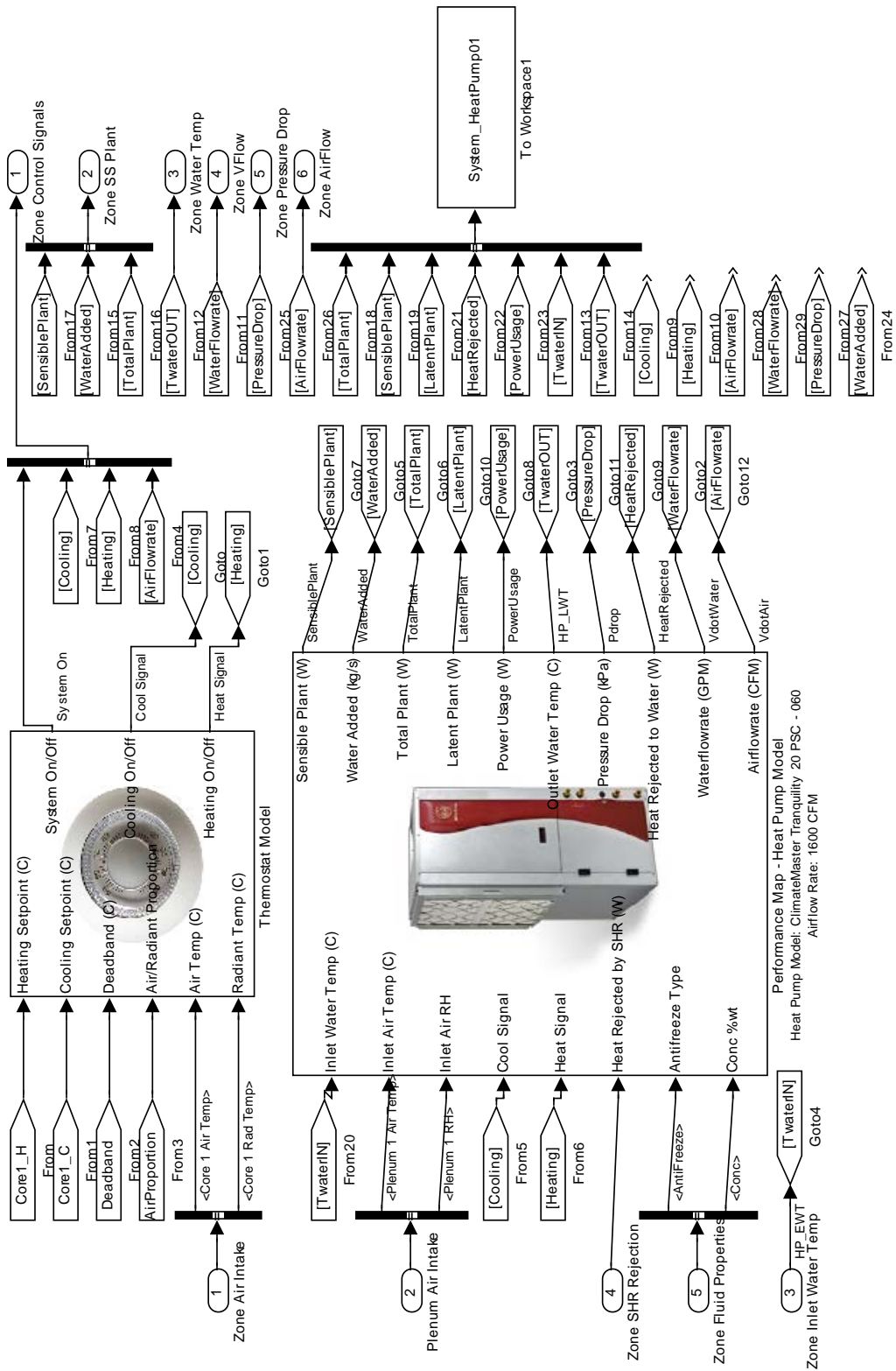


Figure 39: View of the heat pump subsystem Simulink® model

The thermostat block compares the zone temperature to the heating and cooling temperature setpoints generated by the thermostat and timing subsystem (described in Section 4.3). The block generates a binary control signal for system on/off status, cooling on/off status and heating on/off status. The thermostat includes a weighting factor, called the air proportion, α , that allows the user to define the reference zone temperature as a combination of the zone air temperature and/or the zone wall temperature. The control temperature, T_c , is given by Equation (8).

$$T_c = \alpha T_{air} + (1 - \alpha) T_{wall} \text{ where } 0 \leq \alpha \leq 1 \quad (8)$$

Thus, an air proportion value of one results in a control temperature based solely on the zone air temperature, and an air proportion value of zero results in a control temperature based solely on the zone wall temperature. In this simulation, an air proportion value of one is used.

The heat pump block contains the performance-map based calculations for heat pump operation. An example of the data used in the performance map is shown in Figure 40. The performance map uses the temperature of the ground loop water as it enters the heat pump (EWT), the volumetric flow rate of the ground loop water as it enters the heat pump and the volumetric flow rate of air through the heat pump as the operating conditions that determine block outputs. The data are specified for nominal inlet water properties (100% water in the ground loop) and nominal inlet air conditions (19.4°C T_{wb} (67°F), 26.7°C T_{db} (80°F) for cooling and 21.1°C T_{db} (70°F) for heating).

Performance Data — Tranquility® 20 Model 060 - PSC Blower

1,950 CFM Nominal (Rated) Airflow Cooling, 1,950 CFM Nominal (Rated) Airflow Heating Performance capacities shown in thousands of Btu/h

EWT °F	GPM	WPD		Cooling - EAT 80/67°F							Heating - EAT 70°F						
		PSI	FT	Airflow CFM	TC	SC	kW	HR	EER	HW	Airflow CFM	HC	kW	HE	LAT	COP	HW
20	15.0	5.0	11.6	Operation not recommended							1465	40.8	4.43	26.6	96	2.70	2.8
	15.0	5.0	11.6								1950	41.9	4.05	28.2	90	3.03	2.9
30	7.5	0.6	1.4	1465	61.8	36.2	2.64	70.8	23.4	0.8	1465	44.1	4.50	29.6	98	2.88	3.4
	7.5	0.6	1.4	1950	64.3	43.4	2.73	73.6	23.6	0.8	1950	45.3	4.11	31.4	92	3.23	3.5
	11.3	2.3	5.3	1465	63.0	36.5	2.63	72.0	23.9	0.7	1465	45.8	4.53	31.1	99	2.96	3.5
	11.3	2.3	5.3	1950	65.6	43.7	2.72	74.9	24.1	0.8	1950	47.0	4.14	33.0	92	3.33	3.6
	15.0	4.8	11.1	1465	64.9	37.4	2.60	73.8	24.9	0.7	1465	46.7	4.55	32.0	100	3.01	3.7
	15.0	4.8	11.1	1950	67.6	44.8	2.69	76.7	25.1	0.7	1950	48.0	4.16	33.9	93	3.38	3.8
40	7.5	0.5	1.2	1465	64.9	38.6	2.86	74.8	22.7	1.5	1465	50.0	4.61	34.9	102	3.18	4.0
	7.5	0.5	1.2	1950	67.5	46.2	2.96	77.6	22.9	1.6	1950	51.3	4.22	37.0	94	3.57	4.1
	11.3	2.2	5.1	1465	65.4	38.7	2.76	74.9	23.7	1.4	1465	52.1	4.65	36.8	103	3.28	4.1
	11.3	2.2	5.1	1950	68.2	46.3	2.85	77.8	23.9	1.5	1950	53.5	4.25	39.1	95	3.69	4.2
	15.0	4.5	10.4	1465	66.0	38.8	2.72	75.3	24.3	1.3	1465	53.3	4.67	37.9	104	3.34	4.3
	15.0	4.5	10.4	1950	68.8	46.4	2.81	78.3	24.5	1.3	1950	54.7	4.27	40.2	96	3.75	4.4
50	7.5	0.4	0.9	1465	65.4	39.8	3.15	76.2	20.8	2.6	1465	56.1	4.73	40.5	105	3.48	4.5
	7.5	0.4	0.9	1950	68.1	47.6	3.26	79.2	20.9	2.7	1950	57.6	4.32	43.0	97	3.91	4.7
	11.3	2.1	4.9	1465	66.1	39.8	2.97	76.2	22.2	2.3	1465	58.7	4.77	42.9	107	3.60	4.7
	11.3	2.1	4.9	1950	68.8	47.6	3.07	79.2	22.4	2.4	1950	60.3	4.37	45.5	99	4.05	4.8
	15.0	4.3	9.9	1465	66.4	39.8	2.91	76.3	22.9	2.1	1465	60.1	4.80	44.1	108	3.67	4.9
	15.0	4.3	9.9	1950	69.2	47.6	3.00	79.4	23.0	2.1	1950	61.7	4.39	46.8	99	4.12	5.0
60	7.5	0.3	0.7	1465	64.0	39.9	3.50	76.0	18.3	3.6	1465	62.5	4.84	46.3	109	3.78	5.1
	7.5	0.3	0.7	1950	66.7	47.8	3.62	79.0	18.4	3.8	1950	64.2	4.43	49.1	100	4.24	5.3
	11.3	2.1	4.9	1465	65.3	40.1	3.26	76.4	20.0	3.3	1465	65.5	4.90	49.0	111	3.82	5.4
	11.3	2.1	4.9	1950	68.3	48.1	3.36	79.4	20.0	3.4	1950	66.8	4.50	51.9	101	4.30	5.5
	15.0	4.1	9.5	1465	65.7	40.1	3.17	76.5	20.7	2.9	1465	67.1	4.93	50.5	112	3.99	5.6
	15.0	4.1	9.5	1950	68.4	48.0	3.27	79.5	20.9	3.0	1950	68.9	4.51	53.5	103	4.48	5.7
70	7.5	0.3	0.7	1465	61.6	39.2	3.84	74.7	16.0	5.0	1465	68.9	4.97	52.0	114	4.06	5.8
	7.5	0.3	0.7	1950	64.2	46.9	3.97	77.7	16.2	5.2	1950	70.7	4.54	55.2	104	4.56	5.9
	11.3	2.0	4.6	1465	63.4	39.7	3.61	75.7	17.6	4.4	1465	72.2	5.03	55.0	116	4.20	6.0
	11.3	2.0	4.6	1950	66.0	47.6	3.73	78.7	17.7	4.6	1950	74.1	4.60	58.4	105	4.72	6.2
	15.0	3.9	9.0	1465	64.1	39.9	3.49	76.1	18.4	3.9	1465	73.9	5.07	56.6	117	4.28	6.2
	15.0	3.9	9.0	1950	66.9	47.8	3.61	79.1	18.5	4.1	1950	75.9	4.63	60.1	106	4.80	6.4
80	7.5	0.2	0.5	1465	58.6	38.1	4.23	73.1	13.9	6.0	1465	75.1	5.09	57.7	117	4.32	6.3
	7.5	0.2	0.5	1950	61.1	45.6	4.37	76.0	14.0	6.2	1950	77.1	4.65	61.2	107	4.85	6.5
	11.3	1.9	4.4	1465	60.7	38.9	3.96	74.2	15.3	5.5	1465	78.6	5.16	60.8	120	4.48	6.6
	11.3	1.9	4.4	1950	63.2	46.6	4.09	77.2	15.4	5.8	1950	80.7	4.72	64.5	108	5.01	6.8
	15.0	3.6	8.3	1465	61.7	39.2	3.83	74.8	16.1	5.1	1465	80.4	5.21	62.5	121	4.53	6.8
	15.0	3.6	8.3	1950	64.3	47.0	3.96	77.8	16.2	5.3	1950	82.6	4.76	66.3	109	5.08	7.0
85	7.5	0.2	0.5	1465	56.9	37.4	4.44	72.1	12.8	6.8	1465	78.1	5.15	60.4	119	4.44	6.6
	7.5	0.2	0.5	1950	59.3	44.8	4.59	75.0	12.9	7.0	1950	80.1	4.71	64.0	108	4.98	6.8
	11.3	1.9	4.3	1465	59.1	38.3	4.16	73.3	14.2	6.2	1465	81.6	5.23	63.5	122	4.57	6.9
	11.3	1.9	4.3	1950	61.6	45.8	4.30	76.3	14.3	6.5	1950	83.7	4.79	67.4	110	5.13	7.1
	15.0	3.6	8.2	1465	60.2	38.7	4.03	73.9	14.9	5.7	1465	83.4	5.28	65.1	123	4.63	7.1
	15.0	3.6	8.2	1950	62.7	46.3	4.17	76.9	15.0	6.0	1950	85.6	4.83	69.1	111	5.20	7.3
90	7.5	0.2	0.5	1465	55.2	36.8	4.66	71.2	11.9	7.7	1465	81.0	5.22	63.0	121	4.55	6.9
	7.5	0.2	0.5	1950	57.5	44.0	4.82	74.0	11.9	8.0	1950	83.2	4.77	66.9	109	5.11	7.1
	11.3	1.8	4.2	1465	57.5	37.7	4.37	72.4	13.2	7.1	1465	84.5	5.30	66.2	123	4.67	7.2
	11.3	1.8	4.2	1950	59.9	45.1	4.51	75.3	13.3	7.4	1950	86.8	4.85	70.2	111	5.25	7.4
	15.0	3.5	8.1	1465	58.6	38.1	4.23	73.1	13.9	6.6	1465	86.3	5.35	67.7	125	4.73	7.5
	15.0	3.5	8.1	1950	61.1	45.6	4.37	76.0	14.0	6.8	1950	88.6	4.89	71.9	112	5.31	7.6
100	7.5	0.1	0.2	1465	51.7	35.3	5.15	69.3	10.0	8.5	Operation not recommended						
	7.5	0.1	0.2	1950	53.9	42.3	5.32	72.1	10.1	8.8							
	11.3	1.8	4.2	1465	54.0	36.3	4.83	70.5	11.2	8.2							
	11.3	1.8	4.2	1950	56.2	43.4	4.99	73.3	11.3	8.5							
	15.0	3.3	7.6	1465	55.2	36.7	4.67	71.1	11.8	7.9							
	15.0	3.3	7.6	1950	57.5	44.0	4.83	74.0	11.9	8.2							
110	7.5	0.1	0.2	1465	48.2	33.8	5.70	67.7	8.5	10.2	Operation not recommended						
	7.5	0.1	0.2	1950	50.2	40.5	5.89	70.4	8.5	10.6							
	11.3	1.7	3.9	1465	50.4	34.8	5.35	68.7	9.4	9.9							
	11.3	1.7	3.9	1950	52.5	41.6	5.53	71.4	9.5	10.3							
	15.0	3.1	7.2	1465	51.5	35.2	5.18	69.2	10.0	9.5							
	15.0	3.1	7.2	1950	53.7	42.2	5.35	72.0	10.0	9.9							
120	7.5	0.0	0.0	1465	45.0	32.5	6.32	66.6	7.1	12.1	Operation not recommended						
	7.5	0.0	0.0	1950	46.9	39.0	6.53	69.2	7.2	12.6							
	11.3	1.7	3.9	1465	46.9	33.3	5.93	67.2	7.9	11.7							
	11.3	1.7	3.9	1950	48.9	39.9	6.13	69.9	8.0	12.2							
	15.0	2.9	6.7	1465	48.0	33.7	5.74	67.6	8.4	11.3							
	15.0	2.9	6.7	1950	50.0	40.4	5.94	70.3	8.4	11.7							

Interpolation is permissible; extrapolation is not.
 All entering air conditions are 80°F DB and 67°F WB in cooling, and 70°F DB in heating.
 AHRI/ISO certified conditions are 80.6°F DB and 66.2°F WB in cooling and 68°F DB in heating.
 Table does not reflect fan or pump power corrections for AHRI/ISO conditions.
 All performance is based upon the lower voltage of dual voltage rated units.
 Operation below 40°F EWT is based upon a 15% methanol antifreeze solution.
 Operation below 50°F EWT requires optional insulated water/refrigerant circuit.
 See performance correction tables for operating conditions other than those listed above.
 For operation in the shaded areas, please see the Performance Data Selection Notes.

Figure 40: Heat pump performance map data (ClimateMaster, 2010, p. 113)

For inlet conditions that perfectly match with the performance data, the table can be directly read to determine outputs. An example of this process is shown in Figure 41. Given EWT of 32.2°C (90°F), water flow rate of 0.946L/s (15GPM) and airflow of 920.3L/s (1950CFM), the heat pump delivers total cooling of 17.91kW_t (61.1kBtu/hr), of which 13.4kW_t (45.6kBtu/hr) is sensible cooling, the heat pump requires 4.37kW_e (14.9kBtu/hr) of power, and the heat pump rejects 22.3kW_t (76kBtu/h) to the ground loop water, all with an EER efficiency of 14.

Performance Data — Tranquility® 20 Model 060 - PSC Blower

1,950 CFM Nominal (Rated) Airflow Cooling, 1,950 CFM Nominal (Rated) Airflow Heating

Performance capacities shown in thousands of Btu/h

EWT °F	GPM	WPD		Cooling - EAT 80/67°F							Heating - EAT 70°F						
		PSI	FT	Airflow CFM	TC	SC	KW	HR	EER	HW	Airflow CFM	HC	KW	HE	LAT	COP	HW
85	7.5	0.2	0.5	1465	56.9	37.4	4.44	72.1	12.8	6.8	1465	78.1	5.15	60.4	119	4.44	6.8
	7.5	0.2	0.5	1950	59.3	44.8	4.59	75.0	12.9	7.0	1950	80.1	4.71	64.0	108	4.98	6.8
	11.3	1.9	4.3	1465	59.1	38.3	4.16	73.3	14.2	6.2	1465	81.6	5.23	63.5	122	4.57	6.9
	11.3	1.9	4.3	1950	61.6	45.8	4.30	76.3	14.3	6.5	1950	83.7	4.79	67.4	110	5.13	7.1
	15.0	3.6	8.2	1465	60.2	38.7	4.03	73.9	14.9	5.7	1465	83.4	5.28	65.1	123	4.83	7.1
	15.0	3.6	8.2	1950	62.7	46.3	4.17	76.9	15.0	6.0	1950	85.6	4.83	69.1	111	5.20	7.3
90	7.5	0.2	0.5	1465	55.2	36.8	4.08	71.2	11.9	7.7	1465	81.0	5.22	63.0	121	4.55	6.9
	7.5	0.2	0.5	1950	57.5	44.0	4.82	74.0	11.9	8.0	1950	83.2	4.77	66.9	109	5.11	7.1
	11.3	1.8	4.2	1465	57.5	37.7	4.37	72.4	13.2	7.1	1465	84.5	5.30	66.2	123	4.67	7.2
	11.3	1.8	4.2	1950	59.9	45.1	4.51	75.3	13.3	7.4	1950	86.8	4.85	70.2	111	5.25	7.4
	15.0	3.5	8.1	1465	58.6	38.1	4.23	73.1	13.9	6.6	1465	86.3	5.35	67.7	125	4.73	7.5
	15.0	3.5	8.1	1950	61.1	45.6	4.37	76.0	14.0	6.8	1950	88.6	4.89	71.9	112	5.31	7.6
100	7.5	0.1	0.2	1465	51.7	33.3	3.13	69.3	10.0	8.3							
	7.5	0.1	0.2	1950	53.9	42.3	5.32	72.1	10.1	8.8							
	11.3	1.8	4.2	1465	54.0	36.3	4.83	70.5	11.2	8.2							
	11.3	1.8	4.2	1950	56.2	43.4	4.99	73.3	11.3	8.5							
	15.0	3.3	7.6	1465	55.2	36.7	4.67	71.1	11.8	7.9							
	15.0	3.3	7.6	1950	57.5	44.0	4.83	74.0	11.9	8.2							

Figure 41: Heat pump performance data for cooling when EWT = 90°F, GPM = 15 and Airflow = 1950CFM

Most inlet conditions will not perfectly match the performance data. Linear interpolation is used to create data for operating conditions that fall between provided data points. Two iterations of linear interpolation are required, first to match EWT and second to match water flow rate. For example, if the inlet conditions for the heat pump in Figure 41 are 86°F and 13GPM, the performance map will first interpolate using the two closest EWT values (85°F and 90°F) to generate a data set for 86°F, as shown in Table 13. The performance map then uses this EWT data to interpolate for water flow

rate using the closest GPM values (11.3GPM and 15GPM), resulting in Table 14. An example of interpolating the performance map values is shown in Appendix A.2.

Table 13: Performance map linear interpolation, step1

Step 1: Interpolation for $T_{\text{WATER,IN}}$			<i>Cooling</i>				<i>Heating</i>		
<i>EWT</i>	<i>Water Flow Rate</i>	<i>Air Flow Rate</i>	<i>Total Capacity</i>	<i>Sensible Capacity</i>	<i>Power</i>	<i>Heat Rejected</i>	<i>Capacity</i>	<i>Power</i>	<i>Heat Extracted</i>
86	7.5	1465	56.56	37.28	4.484	71.92	78.68	5.164	60.92
86	7.5	1950	58.94	44.64	4.636	74.8	80.72	4.722	64.58
86	11.3	1465	58.78	38.18	4.202	73.12	82.18	5.244	64.04
86	11.3	1950	61.26	45.66	4.342	76.1	84.32	4.802	67.96
86	15	1465	59.88	38.58	4.07	73.74	83.98	5.294	65.62
86	15	1950	62.38	46.16	4.21	76.72	86.2	4.842	69.66

Table 14: Performance map linear interpolation, step2

Step 2: Interpolation for V_{WATER}			<i>Cooling</i>				<i>Heating</i>		
<i>EWT</i>	<i>Water Flow Rate</i>	<i>Air Flow Rate</i>	<i>Total Capacity</i>	<i>Sensible Capacity</i>	<i>Power</i>	<i>Heat Rejected</i>	<i>Capacity</i>	<i>Power</i>	<i>Heat Extracted</i>
86	13	1465	59.2854	38.3638	4.1414	73.4049	83.0070	5.2670	64.7659
86	13	1950	61.7746	45.8897	4.2814	76.3849	85.1838	4.8204	68.7411

For inlet conditions that fall outside of the EWT range or water flow rate range, the heat pump turns off, providing no heating or cooling. The maximum and minimum operating limits for the heat pump are shown in Table 15.

Table 15: Heat pump operating limits

Inlet Condition	Minimum Operating Value	Maximum Operating Value
Entering Water Temperature (EWT) During Cooling	-1.1°C (30°F)	48.9°C (120°F)
Entering Water Temperature (EWT) During Heating	-1.1°C (30°F)	32.2°C (90°F)
Ground Loop Water Flow Rate	0.473L/s (7.5GPM)	0.946L/s (15GPM)

For ground loop water that is not 100% water, an antifreeze correction table is used, as shown in Figure 42. The correction values act as scaling multipliers, applied to the total cooling, sensible cooling and power usage values in the performance data. An example of using correction factors on the performance map values is shown in Appendix A.2.

Antifreeze Type	Antifreeze %	Cooling			Heating		WPD Corr. Fct. EWT 30°F
		EWT 90°F			EWT 30°F		
		Total Cap	Sens Cap	Power	Htg Cap	Power	
Water	0	1.000	1.000	1.000	1.000	1.000	1.000
Propylene Glycol	5	0.995	0.995	1.003	0.989	0.997	1.070
	15	0.986	0.986	1.009	0.968	0.990	1.210
	25	0.978	0.978	1.014	0.947	0.983	1.360
Methanol	5	0.997	0.997	1.002	0.989	0.997	1.070
	15	0.990	0.990	1.007	0.968	0.990	1.160
	25	0.982	0.982	1.012	0.949	0.984	1.220
Ethanol	5	0.998	0.998	1.002	0.981	0.994	1.140
	15	0.994	0.994	1.005	0.944	0.983	1.300
	25	0.986	0.986	1.009	0.917	0.974	1.360
Ethylene Glycol	5	0.998	0.998	1.002	0.993	0.998	1.040
	15	0.994	0.994	1.004	0.980	0.994	1.120
	25	0.988	0.988	1.008	0.966	0.990	1.200

Figure 42: Antifreeze correction data (ClimateMaster, 2010, p. 100)

The performance map data provide two inlet airflow rate conditions, 920.3L/s (1950CFM) and 691.4L/s (1465CFM). For other airflow rates an airflow rate correction factor is used, as shown in Figure 43. Data in the performance map is interpolated using the closest airflow rate between 1950CFM and 1465CFM, and then scaled appropriately.

PSC Fan Motor

Airflow % of Rated	Cooling					Heating		
	Total Capacity	Sensible Capacity	S/T	Power	Heat of Rejection	Heating Capacity	Power	Heat of Extraction
68.75%	0.9465	0.8019	0.8472	0.9614	0.9496			
75%	0.9602	0.8350	0.8696	0.9675	0.9617	0.9740	1.0936	0.9425
81.25%	0.9724	0.8733	0.8981	0.9744	0.9728	0.9810	1.0635	0.9592
87.50%	0.9831	0.9149	0.9306	0.9821	0.9829	0.9876	1.0379	0.9744
93.75%	0.9923	0.9578	0.9653	0.9906	0.9920	0.9940	1.0167	0.9880
100%	1.0000	1.0000	1.0000	1.0000	1.0000	1.0000	1.0000	1.0000
106.25%	1.0062	1.0392	1.0328	1.0102	1.0070	1.0057	0.9878	1.0105
112.50%	1.0109	1.0733	1.0617	1.0211	1.0130	1.0112	0.9800	1.0194
118.75%	1.0141	1.1001	1.0848	1.0329	1.0180	1.0163	0.9705	1.0284
125%	1.0159	1.1174	1.0999	1.0455	1.0220	1.0211	0.9614	1.0368
130%	1.0161	1.1229	1.1050	1.0562	1.0244	1.0247	0.9554	1.0430

Black area denotes where operation is not recommended.

Figure 43: Airflow rate correction factors (ClimateMaster, 2010, p. 98)

For inlet air that is not 19.4°C T_{wb} (67°F), 26.7°C T_{db} (80°F) during cooling mode, entering air correction factors are used, as shown in Figure 44. The total cooling capacity, power required and heat rejected to the ground loop water all scale directly with the entering air wet bulb temperature. The sensible cooling capacity scales with the entering air wet bulb temperature and entering air dry bulb temperature.

Cooling												
Entering Air WB°F	Total Capacity	Sensible Cooling Capacity Multiplier - Entering DB °F									Power	Heat of Rejection
		60	65	70	75	80	80.6	85	90	95		
50	0.7432	0.9111	*	*	*	*	*	*	*	*	0.9866	0.7901
55	0.8202	0.7709	0.8820	1.0192	*	*	*	*	*	*	0.9887	0.8527
60	0.8960		0.6702	0.8540	1.0473	*	*	*	*	*	0.9924	0.9146
65	0.9705			0.6491	0.8657	1.0809	1.1066	*	*	*	0.9975	0.9757
66.2	0.9882			0.5939	0.8152	1.0333	1.0592	1.2481	*	*	0.9990	0.9903
67	1.0000			0.5559	0.7801	1.0000	1.0261	1.2158	*	*	1.0000	1.0000
70	1.0438				0.6377	0.8645	0.8913	1.0847	1.2983	*	1.0042	1.0362
75	1.1159					0.8008	0.8289	0.8323	1.0578	1.2773	1.0123	1.0959

* = Sensible capacity equals total capacity
 AHRI/ISO/ASHRAE 13256-1 uses entering air conditions of Cooling - 80.6°F DB/66.2°F WB, 1 and Heating - 68°F DB/59°F WB entering air temperature

Figure 44: Entering air correction data for cooling mode (ClimateMaster, 2010, p. 99)

The entering air correction table is limited by the range of values provided. During one year of simulation, input conditions fall outside of the 10-23.9°C T_{wb} (50-75°F T_{wb}) and 15.6-35°C T_{db} (60-95°F T_{db}) range provided by the table on 0.1% of time-steps during HVAC ON status. All out-of-range conditions result from excessively low wet bulb temperature. The model handles these out-of-bounds conditions by calculating sensible cooling using the actual dry bulb temperature and 10°C T_{wb} (50°F T_{wb}), and setting latent cooling to zero.

Another 23.4% of HVAC ON time-steps have an inlet condition in the “Sensible capacity equals total capacity” region (shown with a * in Figure 44, and by data above the purple line in Figure 45). Many of these data fall just outside of the limit represented by the purple line in Figure 45 (for example, 15°C T_{wb} (59°F) with 23.9°C T_{db} (75°F)), in

which case assuming that sensible capacity equals total capacity, i.e. that there is no latent cooling, over-represents the sensible cooling and under-represents latent cooling.

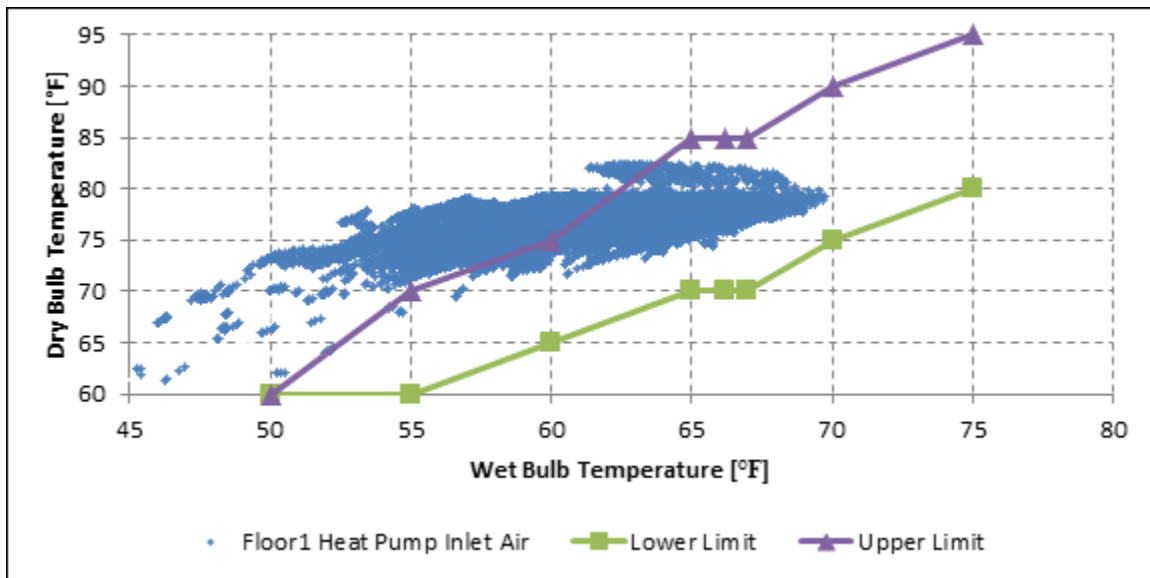


Figure 45: Core1 heat pump inlet air conditions during HVAC ON for 1 year

To allow interpolation for inlet conditions that are on or near the data boundary, additional data must be provided. The existing data points were used to extrapolate a new upper limit, shown in red in Figure 46 for HVAC ON data points (more information about the extrapolated values can be found in Appendix A.3).

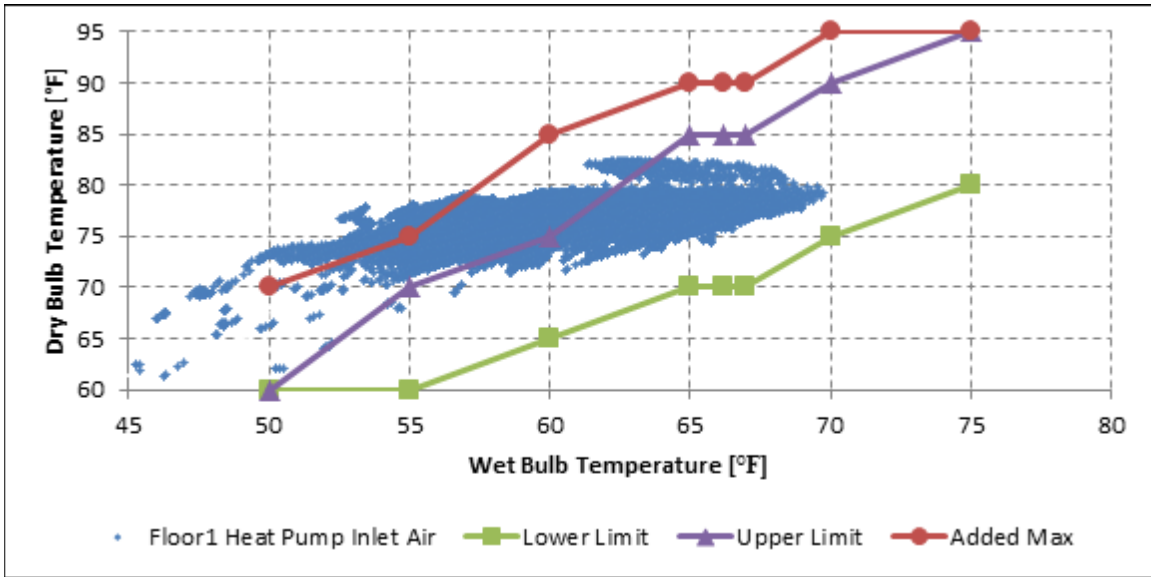


Figure 46: Core1 heat pump inlet air conditions during HVAC ON for 1 year

All of the data points from the ClimateMaster inlet air correction table were plotted in light-blue on a psychrometric chart, with the extrapolated data points plotted in purple (Figure 47). The ClimateMaster data points created natural input limits, represented by red and orange curves. These input limits (shown in Table 16) were used as a secondary “Sensible capacity equals total capacity” test for the inlet air. Conditions inside these limits resulted in the calculation of a correction factor using linear interpolation.

Using the extrapolated correction factor data in conjunction with the input condition performance limits reduced the number of “Out of interpolation range” data points from 23.4% of HVAC ON time-steps per simulation year to 1.3% (26,719 time-steps reduced to 1,537 time-steps).

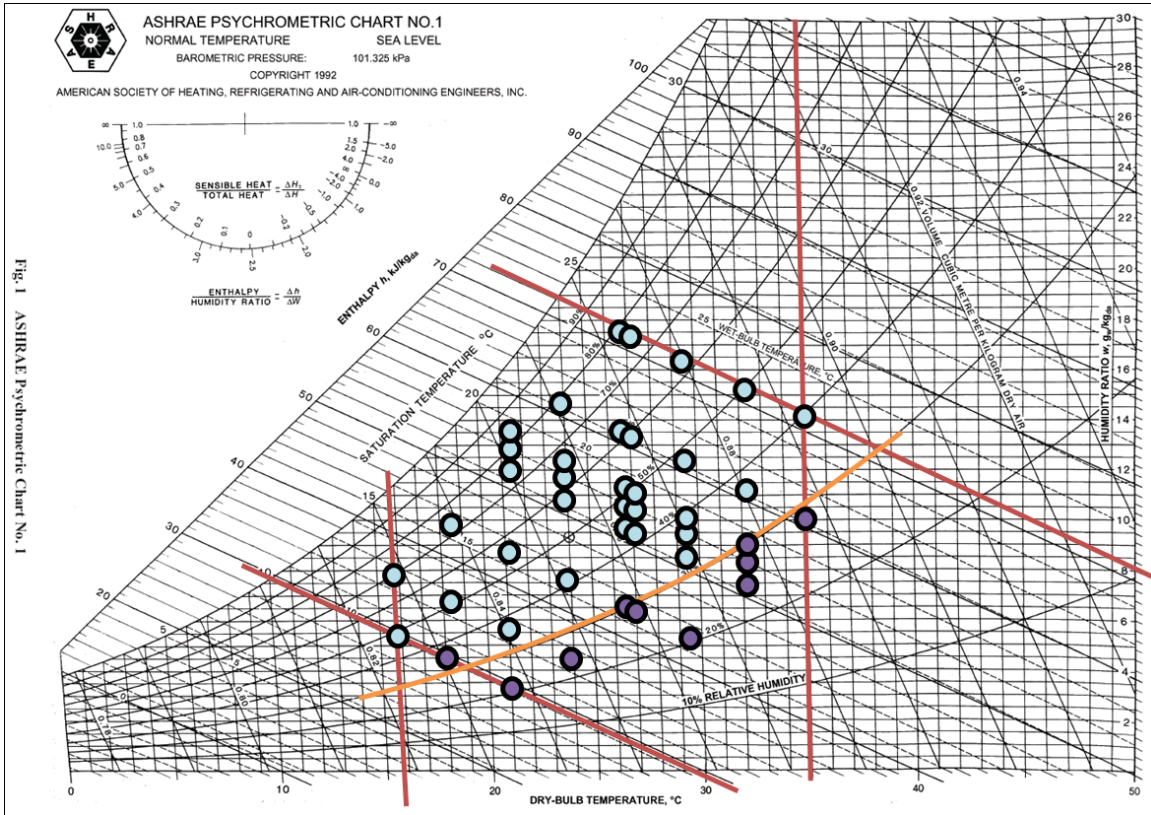


Figure 47: Psychrometric chart representation of entering air correction data for cooling (ASHRAE 2009 Fundamentals HandBook, 2009, p. 1.11)

Table 16: Inlet air limits for correction factor calculation

Inlet Condition	Test	Result	HVAC On Time-steps Affected
Dry-Bulb Temp.	$T_{db} < 15.6^{\circ}\text{C}$ (60°F)	Adjust to 15.6°C, No latent cooling	0 (0%)
Dry-Bulb Temp.	$T_{db} > 35^{\circ}\text{C}$ (95°F)	Adjust to 35°C	0 (0%)
Wet-Bulb Temp.	$T_{wb} < 10^{\circ}\text{C}$ (50°F)	Adjust to 10°C, No latent cooling	104 (0.09%)
Wet-Bulb Temp.	$T_{wb} > 24^{\circ}\text{C}$ (75°F)	Adjust to 24°C	0 (0%)
Relative Humidity	$\text{RH} < 30\%$	No latent cooling	6931 (6.06%)

Inlet air correction values for heating do not depend on wet-bulb temperature, and as a result are modelled by polynomial curve fits. The ClimateMaster correction factor data are shown in Figure 48, and the polynomial curve fits are shown in Figure 49.

Heating			
Entering Air DB°F	Heating Capacity	Power	Heat of Extraction
45	1.0514	0.7749	1.1240
50	1.0426	0.8113	1.1032
55	1.0329	0.8525	1.0802
60	1.0224	0.8980	1.0551
65	1.0114	0.9473	1.0282
68	1.0046	0.9786	1.0115
70	1.0000	1.0000	1.0000
75	0.9883	1.0556	0.9706
80	0.9764	1.1135	0.9404

Figure 48: Entering air correction factors for heating (ClimateMaster, 2010, p. 99)

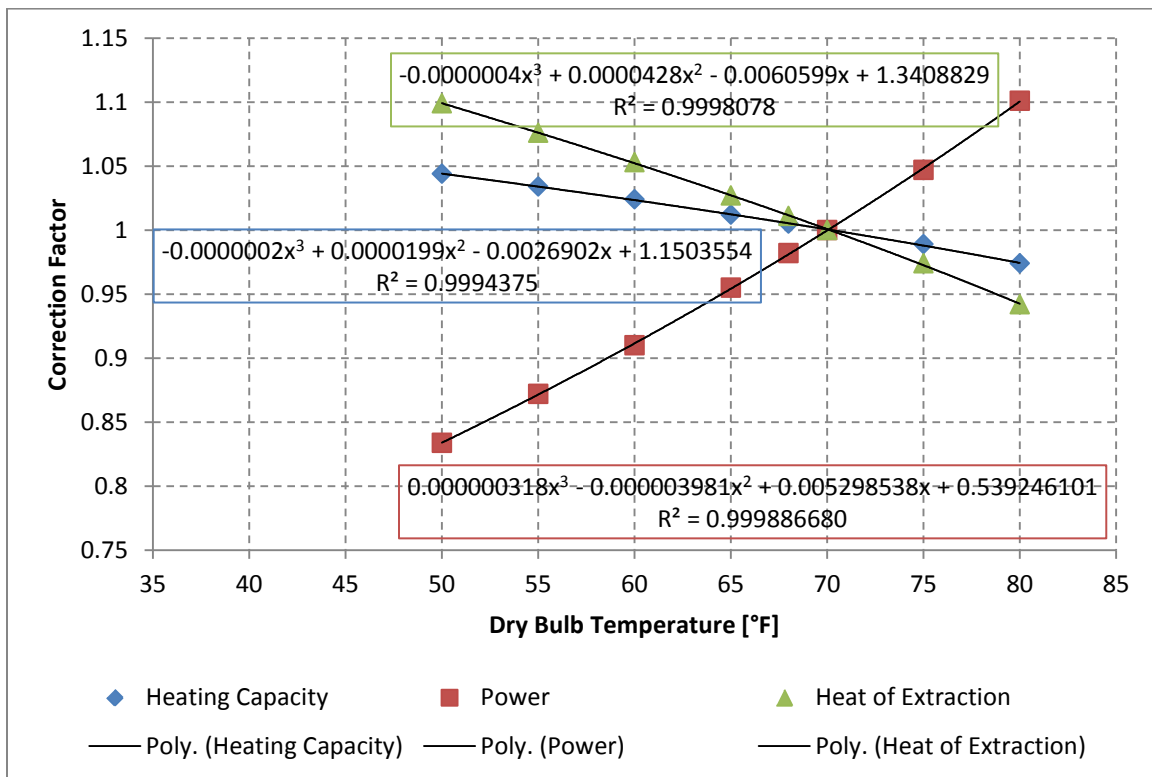


Figure 49: Entering air correction polynomials for heating

4.4.3. Heat Pump Sizing

Sizing of the heat pumps was initially based on data from the EnergyPlus simulation. EnergyPlus uses design days, a worst case for cooling and a worst case for heating, to size equipment. The heat pump sizes based on EnergyPlus design days are shown in Table 17.

Table 17: Heat pump sizing based on EnergyPlus design days

Zone	Peak Cooling Needed		Peak Heating Needed		HP Size Needed [tons]
	[kW]	[tons]	[kW]	[tons]	
Core1	44.8	12.7	4.9	1.4	13.0
South1	10.0	2.9	9.5	2.7	3.0
East1	11.8	3.4	6.2	1.8	3.5
North1	9.4	2.7	9.2	2.6	3.0
West1	14.8	4.2	6.2	1.8	4.0
Core2	41.7	11.9	8.3	2.4	12.0
South2	12.0	3.4	10.5	3.0	3.5
East2	13.1	3.7	6.9	2.0	4.0
North2	11.3	3.2	10.3	2.9	3.5
West2	16.0	4.6	6.9	2.0	5.0
Core3	43.3	12.3	23.0	6.5	13.0
South3	13.0	3.7	13.8	3.9	4.0
East3	12.8	3.6	9.0	2.6	4.0
North3	13.4	3.8	13.6	3.9	4.0
West3	17.2	4.9	9.0	2.6	5.0

The EnergyPlus design day calculation estimated peak heating and cooling loads for each zone independently, but the EnergyPlus simulation did not use heat pumps in each zone. Instead, it used a variable-air-volume (VAV) HVAC system consisting of three large air conditioners, three large natural gas heaters, and one electric reheat heaters for each conditioned zone, as shown in Table 18.

Table 18: HVAC capacity for EnergyPlus variable air volume system

VAV System	Total Cooling Capacity [kW]	Total Cooling Capacity [tons]	Total Heating Capacity [kW]	Total Heating Capacity [tons]
Floor 1	139.5	39.7	21.2	0.0
Floor 2	135.9	38.7	20.9	0.0
Floor 3	151.1	43.0	20.2	0.0

This system’s capacity was not a direct match to the HAMBASE simulation, so the VAV heating and cooling system capacities were apportioned to the zones based on each zone’s square footage. For example, the core zones represent 59% of the area of a given floor and therefore 59% of the total cooling and heating capacity of the floor’s VAV system. The cooling and heating capacities resulting from this calculation are shown in Table 19 along with the resulting heat pump sizes.

Table 19: Heat pump sizing based on EnergyPlus HVAC capacity

Zone	VAV Cooling Capacity [kW]	VAV Cooling Capacity [tons]	VAV Heating Capacity [kW]	Reheater Heating Capacity [kW]	Total Heating Capacity [tons]	HP Size Needed [tons]
Core1	82.7	23.5	12.6	39.9	14.9	24.0
South1	17.4	5.0	2.6	9.0	3.3	5.0
East1	11.0	3.1	1.7	10.5	3.5	3.5
North1	17.4	5.0	2.6	8.4	3.1	5.0
West1	11.0	3.1	1.7	13.2	4.2	4.5
Core2	80.5	22.9	12.4	36.4	13.9	24.0
South2	16.9	4.8	2.6	10.7	3.8	5.0
East2	10.7	3.1	1.7	11.7	3.8	4.0
North2	16.9	4.8	2.6	10.1	3.6	5.0
West2	10.7	3.1	1.7	14.3	4.5	5.0
Core3	89.5	25.4	12.0	38.6	14.4	26.0
South3	18.8	5.4	2.5	11.6	4.0	6.0
East3	11.9	3.4	1.6	11.4	3.7	4.0
North3	18.8	5.4	2.5	12.0	4.1	6.0
West3	11.9	3.4	1.6	15.3	4.8	5.0

These two methods of estimating heat pump sizes formed the starting point for a sizing study using the actual HAMBASE model. For each zone, a range of heat pump sizes were chosen and simulated for one year. The amount of time each zone was unable to meet the thermostat setpoint was then tabulated. The results for the first floor zones are shown in Figure 50. Floors two and three had results consistent with the first floor for all zones except the core (the first floor core has the elevator load). Based on the sizing study, the final heat pump sizes used in the HAMBASE simulation are shown in Table 20.

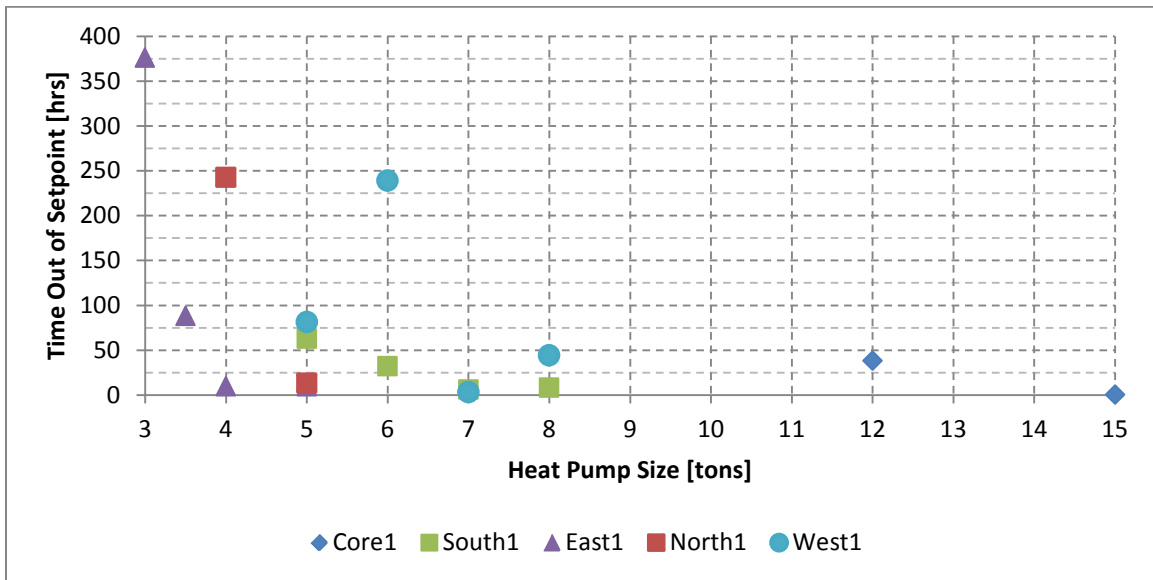


Figure 50: Results of heat pump sizing study (hourly average time out-of-setpoint)

Table 20: Heat pump sizes used in the HAMBASE model

Zone	First Floor HP Size [tons]	Second Floor HP Size [tons]	Third Floor HP Size [tons]
Core	15	10	10
South	7	7	7
East	4	4	4
North	5	5	5
West	5	5	5
Plenum	None	None	None

4.4.4. Heat Pump Header Subsystem Model

The heat pump header subsystem combines the return water from each heat pump in the system into a single flow that becomes the inlet to the ground loop. The header subsystem, shown in Figure 51, consists of a header block, signal routing and data storage. The inputs to the subsystem are the flow rate and temperature of return water from each heat pump in the building model, and the outputs of the subsystem are the flow rate and temperature of the combined return water.

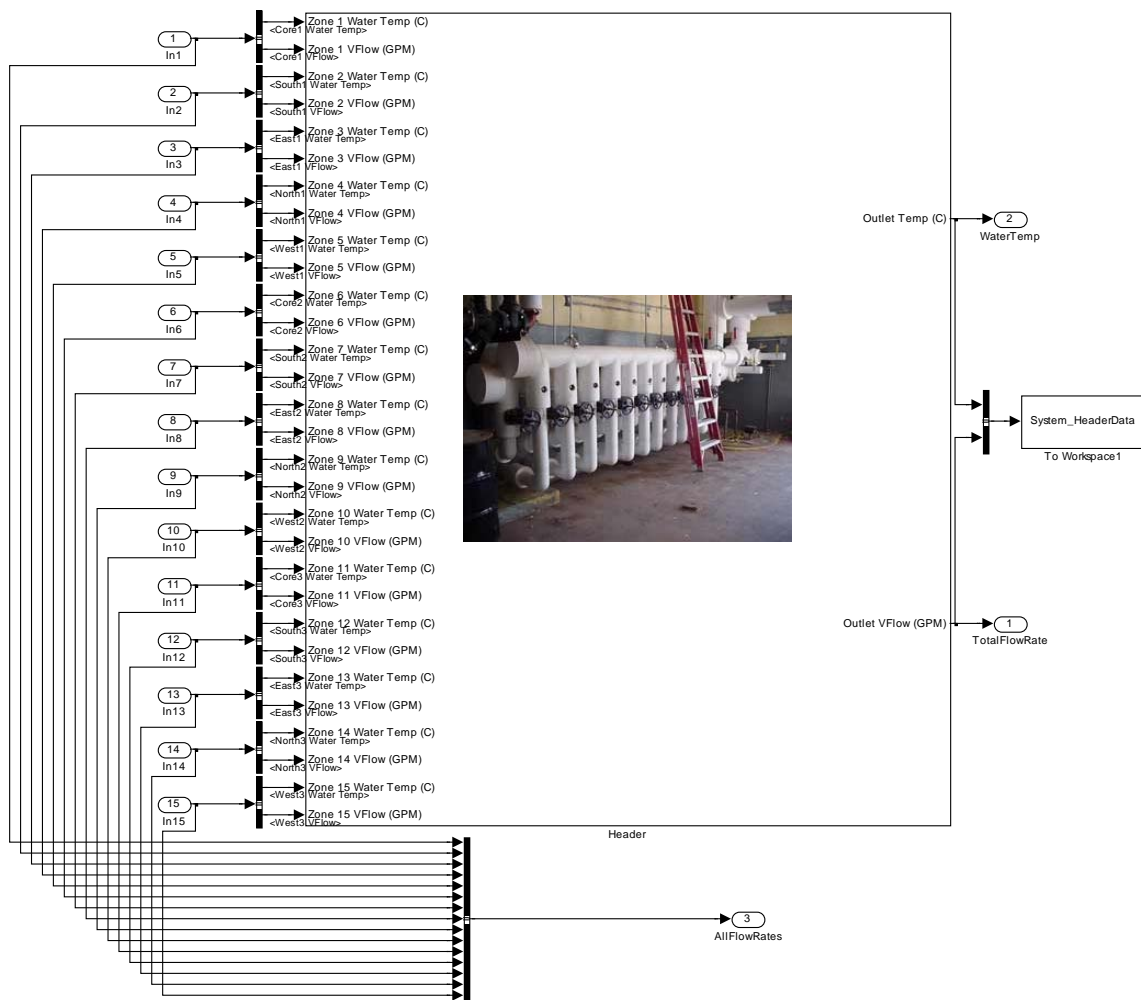


Figure 51: View of the heat pump header subsystem Simulink® model

The heat pump header block uses the temperature of the input water to interpolate a value for specific heat and density. Combining the inlet flow rate with the water density, specific heat and temperature generates a total inlet heat rate using Equation (9). The total outlet heat rate is given by Equation (10). Assuming conservation of energy in the header, the solution for the outlet temperature is given in Equation (11).

$$\sum \dot{Q}_{inlet} = \sum_{i=1}^n \dot{V}_i \rho_i C_{p_i} T_i \text{ for } n \text{ inlets} \quad (9)$$

$$\dot{Q}_{outlet} = T_{outlet} \cdot \sum_{i=1}^n \dot{V}_i \rho_i C_{p_i} \quad (10)$$

$$T_{outlet} = \frac{\sum_{i=1}^n \dot{V}_i \rho_i C_{p_i} T_i}{\sum_{i=1}^n \dot{V}_i \rho_i C_{p_i}} \text{ for } n \text{ inlets} \quad (11)$$

The outlet flow rate is generated by summing all of the inlet flow rates. The outlet temperature and outlet flow rate are then used as inputs to the ground loop subsystem covered in the next section.

4.5. Ground Loop Subsystem Model

The ground loop subsystem model calculates the temperature of the ground over time, and uses the ground temperature to calculate water temperature after it passes through the ground loop heat exchanger. The subsystem, shown in Figure 52, consists of the ground loop model, signal routing, rate-transitions and signal storage.

The inputs to the subsystem are water temperature, water flow rate and system on/off control signal. The outputs of the subsystem are water temperature, average ground temperature, total heat rejected, pressure drop across the ground loop, type of antifreeze, and antifreeze concentration. Detailed information about the ground loop model is discussed in Section 2.3.

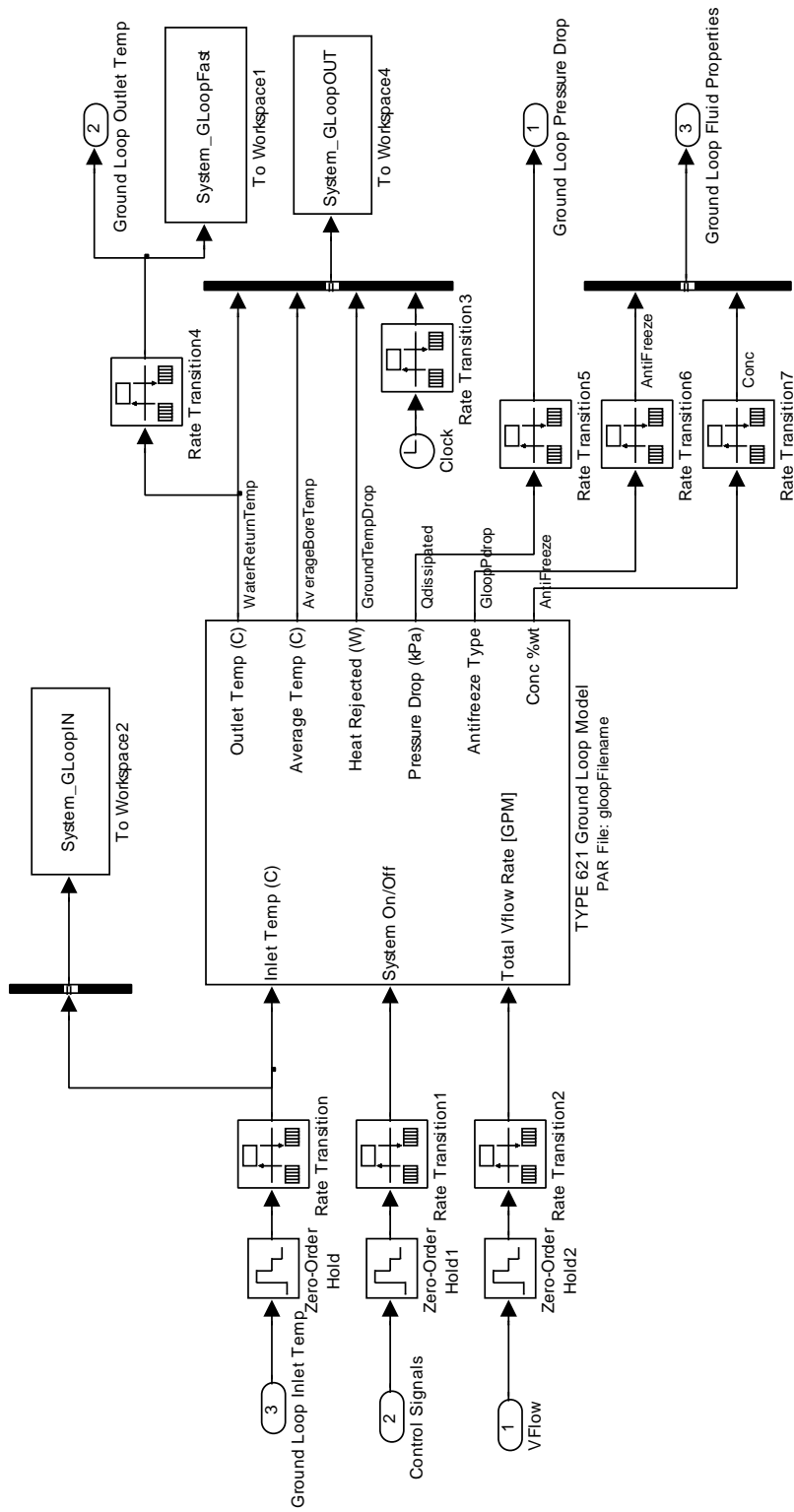


Figure 52: View of the GHEX subsystem Simulink® model

A block diagram of the water-side of the integrated model is shown in Figure 53. All heat pumps have a common entering water temperature (EWT), but unique flow rates. Each heat pump has a unique leaving water temperature (LWT). The outlet flows from all 15 heat pumps combine in the heat pump header, which generates a single outlet flow. The header outlet flows to the ground loop inlet. After passing through the GHEX, the ground loop outlet water becomes the common heat pump EWT.

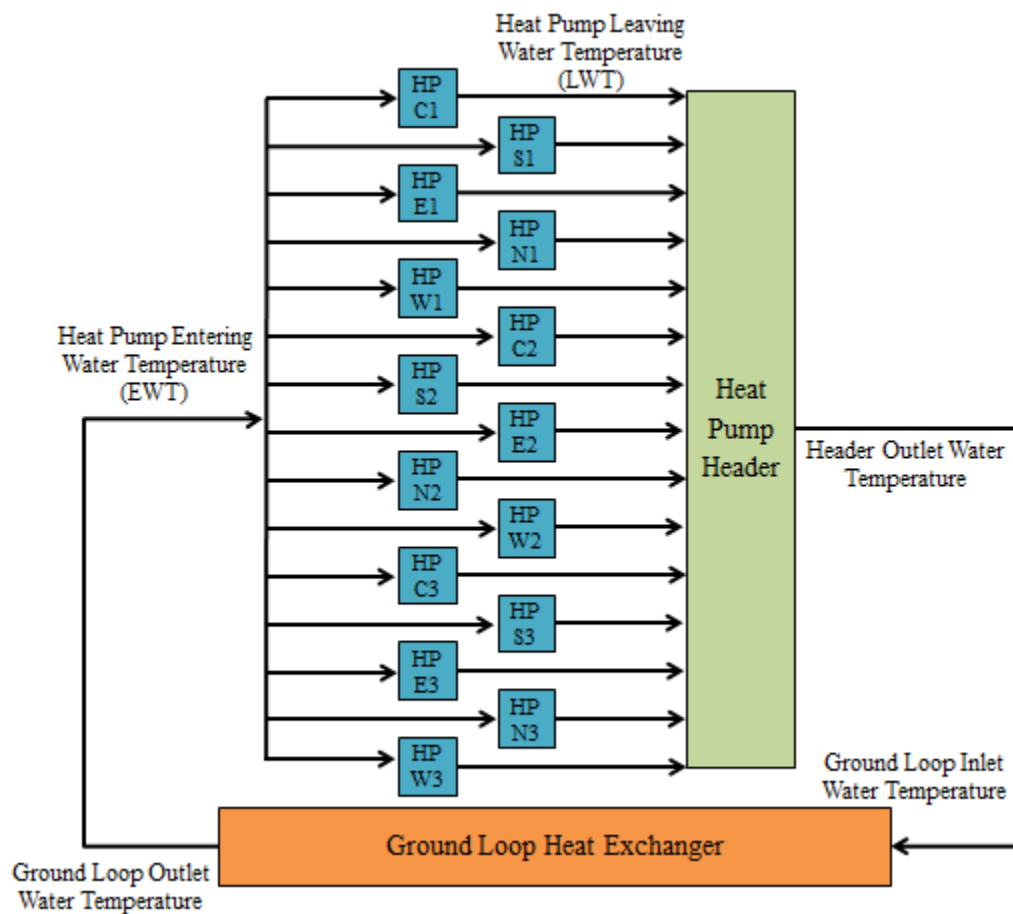


Figure 53: Block diagram of water-side flow path

4.5.1. Ground Loop Sizing

Ground loop sizing is performed using GLHEPRO. GLHEPRO calculates the required depth of the borefield by using the total thermal load on the heat pumps along with various ground soil, circulating fluid and borefield parameters. In addition to calculating the required borefield depth, GLHEPRO also simulates the operation of the borefield for a given time period and returns the maximum and minimum temperatures of the circulating fluid during that time.

To generate the first input for GLHEPRO (the total thermal load on the heat pumps), the Peak Load Analysis Tool can be used. The Peak Load Analysis Tool takes hourly cooling and heating loads for a building and converts them into a table of values that can be used as the heat pump load input to GLHEPRO. Detailed explanation of the Peak Load Analysis Tool can be found in Appendix A.4.1. .

To generate the hourly loads, the HAMBASE model was simulated without a ground loop. The hourly heating and cooling loads for all zones were combined, and the resulting hourly building totals were used in the Peak Load Analysis Tool to generate the data shown in Table 21 (SI units) and Table 22 (BI units).

Table 21: HAMBASE building loads (SI units) used as GLHEPRO inputs

Month	Total Loads [kW-h]		Peak Loads [kW]	
	Heating	Cooling	Heating	Cooling
January	15721	8606	235	164
February	6515	9275	190	184
March	3328	25620	160	246
April	239	48769	84	285
May	82	66723	27	309
June	0	87865	0	319
July	0	100035	0	326
August	0	94823	0	333
September	41	68741	19	307
October	131	53613	53	317
November	2087	25253	95	275
December	15494	11964	256	193
Duration of Peak Load [hrs]			3	9

Table 22: HAMBASE building loads (BI units) used as GLHEPRO inputs

Month	Total Loads [kBtu]		Peak Loads [kBtu/hr]	
	Heating	Cooling	Heating	Cooling
January	53639	29363	801	560
February	22230	31646	649	629
March	11356	87415	546	841
April	815	166399	287	972
May	280	227660	91	1054
June	0	299794	0	1089
July	0	341319	0	1112
August	0	323535	0	1135
September	141	234544	66	1049
October	448	182926	181	1080
November	7122	86164	323	940
December	52866	40821	874	658
Duration of Peak Load [hrs]			3	9

With the heat pump loads incorporated into GLHEPRO, the remaining inputs are material properties for the ground soil, circulating fluid and borefield geometry. A summary of all of the properties used in the GLHEPRO sizing are shown in Table 23. Images of all of the GLHEPRO inputs can be seen in Appendix A.4.2. .

Table 23: Ground loop properties used for the base model in GLHEPRO

Geometry Properties				
Dimension	SI Value	Units	BI Value	Units
Borefield Shape	Rectangle	-		
Borefield Size	10 x 16	boreholes		
Borehole Depth	171	m	561.1	ft
Total GHEX Length	27363.8	m	89776.2	ft
Borehole Spacing	6.1	m	20	ft
Borehole Diameter	127	mm	5	in
Shank Spacing	25.4	mm	1	in
U-Tube Inner Diameter	35.1	mm	1.38	in
U-Tube Outer Diameter	42.3	mm	1.666	in
Thermal Properties				
Dimension	SI Value	Units	BI Value	Units
U-Tube Conductivity	0.39	W/(m·°K)	0.225	Btu/(hr·ft ² ·°F)
U-Tube Capacitance	1542	kJ/(m ³ ·°K)	22.99	Btu/(ft ³ ·°F)
Grout Conductivity	1.7	W/(m·°K)	1	Btu/(hr·ft ² ·°F)
Grout Capacitance	3901	kJ/(m ³ ·°K)	58.17	Btu/(ft ³ ·°F)
Ground Conductivity	2.1	W/(m·°K)	1.2	Btu/(hr·ft ² ·°F)
Ground Capacitance	2343	kJ/(m ³ ·°K)	34.94	Btu/(ft ³ ·°F)
Undisturbed Ground Temp.	22	°C	72	°F
Fluid Properties				
Dimension	SI Value	Units	BI Value	Units
Antifreeze	None			
Convection Coefficient	1534	W/(m ² ·°K)	270.2	Btu/(hr·ft ² ·°F)
Fluid Factor	1	-		
Flow Rate per Borehole	0.126	L/s	2	gal/min
Total Flow Rate	20.2	L/s	320	gal/min
Simulation Properties				
Dimension	SI Value	Units	BI Value	Units
Borehole Resistance	0.103	(°K·m)/W	0.1775	(°F·hr·ft)/Btu
Max HP Entering Water Temp.	32.2	°C	90	°F
Min HP Entering Water Temp.	-6.7	°C	20	°F
Duration of Sizing	180	months		

4.6. Ground Loop Water Pump Subsystem Model

The ground loop water pump subsystem calculates the total pumping power required to move water through the heat pumps and the ground loop. The masked (icon) view of the subsystem is shown in Figure 54. The unmasked view is shown in Figure 55.

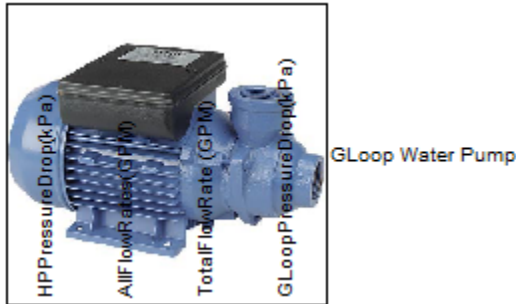


Figure 54: Masked view of GHEX water pump subsystem Simulink® model

The inputs to the subsystem are the flow rate and pressure drop across each heat pump and the flow rate and pressure drop across the ground loop. The model uses these values with Equation (12) to calculate the total pumping power. A value of 90% is used for water pump efficiency in this model.

$$P_{pump} = \sum_{i=1}^n \frac{\Delta P \cdot \dot{V}}{\eta} \text{ for } n \text{ pumps} \quad (12)$$

where

ΔP = pressure drop [Pa]

\dot{V} = volumetric flow rate [m^3/s]

η = pump efficiency

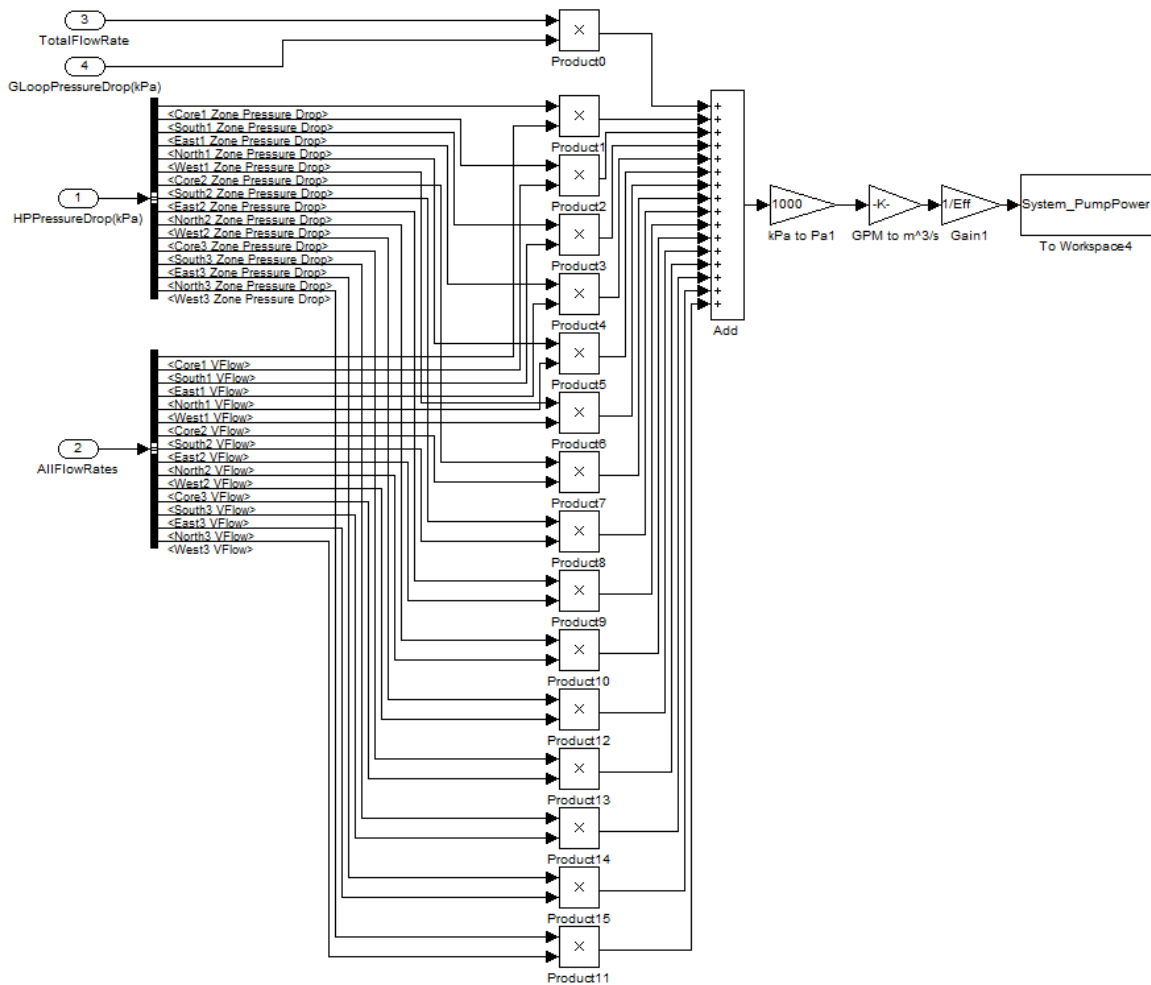


Figure 55: Unmasked view of GHEX water pump subsystem Simulink® model

4.7. Data Storage and Processing

Data storage blocks exist in every subsystem of the integrated model. The “To Workspace” block was used as the method for data storage to minimize simulation time. This block “Writes data to an internal buffer,” and upon termination of the simulation it “writes the data to the workspace” (The MathWorks, Inc., 2012, p. To Workspace). The “To File” block was considered, but this block writes to an external file on every time-step, which increases simulation time.

The integrated model includes control for the model time-step and the ground loop time-step. Both the model time-step and ground loop time-step must be a factor of 60 minutes, and the ground loop time-step must be an integer-multiple of the model time-step. For this simulation the model time-step used was 60 seconds, and the ground loop time-step was 3600 seconds (60 minutes).

The “To Workspace” blocks store initial conditions and then store data every time-step. As a result, the total number of data points generated for each variable of interest is given by Equation (13).

For a 15 years simulation, the model generates 7,884,001 data points for each variable of interest. This quantity of data requires post-simulation processing to facilitate analysis. In addition, most building-load simulation models, such as eQuest and EnergyPlus, report results using hourly averages. As a result, hourly averages are computed for all variables of interest using Equation (14). The hourly averages are then used to calculate monthly and annual totals and averages using a similar process.

$$n = 1 + \frac{y*365*24*3600}{tstep} \quad (13)$$

where

n = number of data points

y = duration of simulation, in years

$tstep$ = duration of each time-step, in seconds

$$[A] = \begin{bmatrix} A_1 \\ A_2 \\ \vdots \\ A_i \end{bmatrix} = \begin{bmatrix} \frac{1}{60} \sum_{n=1}^{60} B_n \\ \frac{1}{60} \sum_{n=61}^{120} B_n \\ \vdots \\ \frac{1}{60} \sum_{n=60i-59}^{60i} B_n \end{bmatrix} \quad (14)$$

where

[A] = array of hourly average data

[B] = array of time-step data

4.8. Model Simulation

The integrated model is solved using a 1st order, fixed time-step solver. A one-year simulation of the integrated model on the High Performance Computing cluster maintained by the Mechanical Engineering Department at the University of Texas at Austin takes approximately 7.5 hours. The machine used has two six-core, hyperthreading 3.33 GHz Xeon processors with 24 GB of shared memory (shared between 9 machines). A 15year simulation of the integrated model takes approximately 118 hours on the same computer.

The simulation for the integrated model follows the order shown in Figure 27. Within a given time-step, the subsystem dependencies all occur in series; the output of the building model is directly used as the input to the thermostat, the output of the thermostat is directly used as the input to the heat pump, and the output of the heat pump is directly used as the input to the ground loop. Between time-steps, however there is a one time-step lag (1minute), as shown for Core1 in Figure 56.

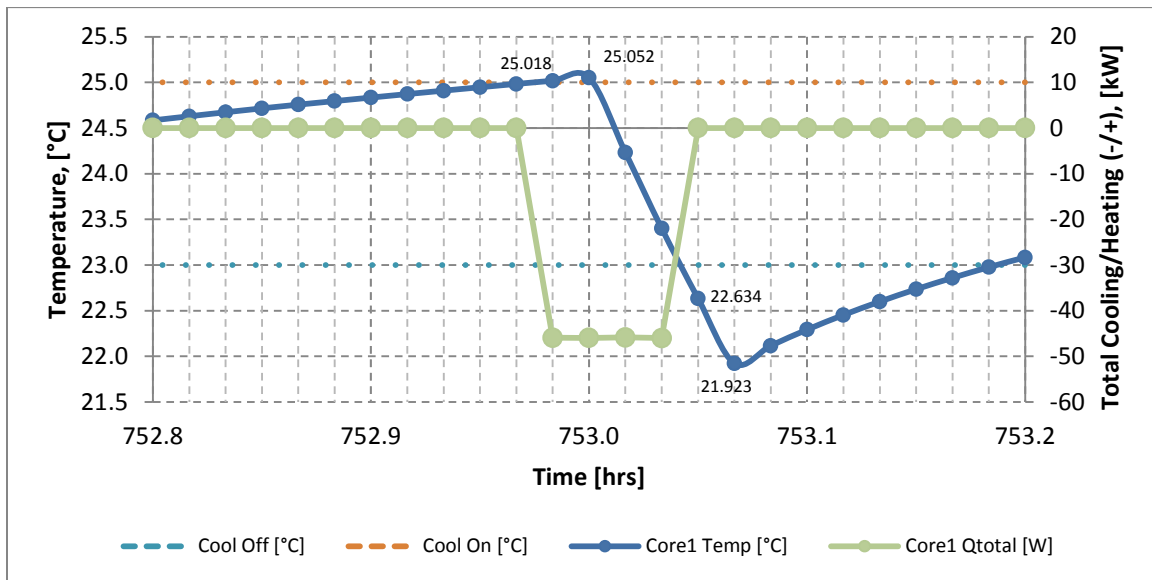


Figure 56: Visualization of heat pump cooling/heating lag in Core1

The figure shows Core1 zone temperature (shown with blue-solid) increasing gradually due to internal loads in the absence of heat pump cooling (in green-solid). The zone temperature passes above the Cooling On point (shown with orange-dash) at time 752.98hrs, and the heat pump responds during the same time-step by providing cooling. The zone temperature continues to increase during the next time-step (at time 753hrs) before the cooling takes effect in the zone at time 753.02hrs. The delay is repeated when the zone temperature falls below the Cooling Off point (shown with blue-dash) at time 753.05hrs. The heat pump responds to the Cooling Off signal in the same time-step by turning off, however the temperature in the zone continues to decline for an additional time-step (at time 753.07hrs) before the zone begins to warm due to internal loads in the absence of heat pump cooling.

The lag originates in the sampling process of HAMBASE and the Simulink® model blocks. Eliminating the lag requires altering component models, which was beyond the scope of this project (the principal files in HAMBASE are hamsimulinksfun0209.m and Wavoinit0109.m; refer to Section 4.1 for general simulation sequencing). The effect of the lag is small for appropriately sized heat pumps, and larger for oversized heat pumps. The peak cooling loads in West1 for example, require a much larger heat pump than the peak heating loads, resulting in an oversized heat pump condition during heating. Figure 57 shows the responses for West1.

When the West1 temperature falls below the Heating On setpoint (shown with black-dash), the heat pump begins providing heating. After the one time-step lag, the heating from the heat pump causes the zone temperature to increase. At 6am, this process results in overshooting the Heating Off setpoint (shown with red-dash). As the day progresses, solar irradiance and internal loads provide additional heating, amplifying the existing overshoot. By 6:30am (shown as 6.5 in the figure), the overshoot approaches the Cooling On setpoint, eventually activating cooling at approximately 6:45am (shown as 6.78 in the figure).

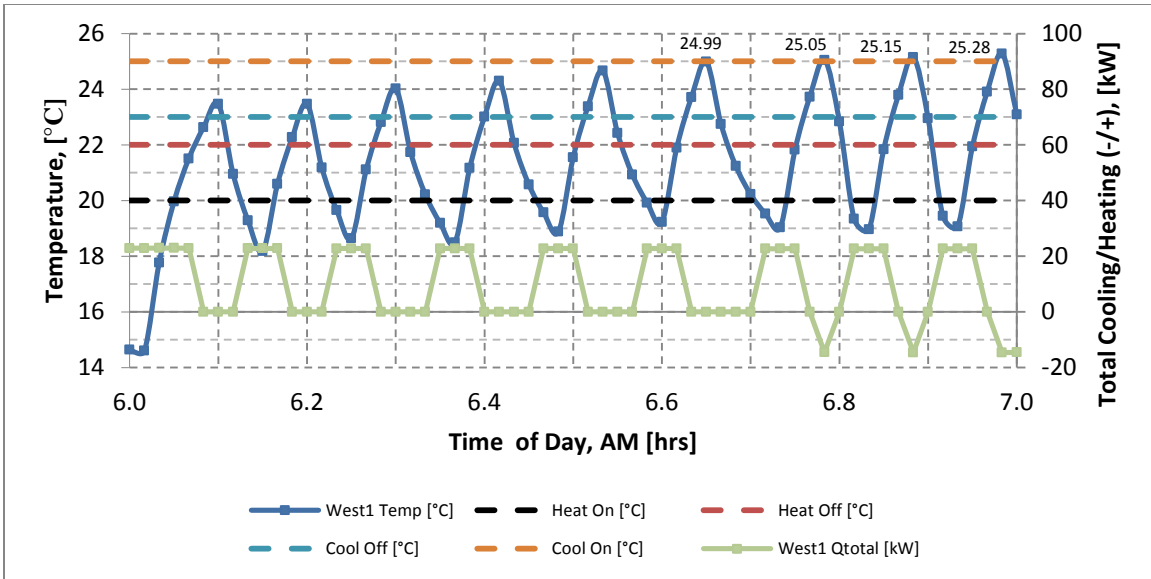


Figure 57: Visualization of heat pump cooling/heating lag in West1

The resulting system instability causes excessive heating and cooling in West1, which manifests itself in the hourly average data as a decrease in efficiency. The hourly average cooling/heating sums the time-step heating and cooling values for an hour, resulting in an hourly average heating value that is less than the total heating provided to the zone. The hourly average power usage sums an hour of time-step power usage values of both heating and cooling, resulting in an hourly average that is greater than the power usage for heating alone. Combined, the decreased value for heating provided and increased value for power usage causes a lower hourly average efficiency value than for heating alone. An example of this effect is shown below in Table 24 for West1 using the 6-7am hour of data from Figure 57. Additional information about the calculation of heat pump efficiency can be found in Section 6.2.3.

Table 24: Hourly averaging of cooling and heating values for West1

Heat Pump Value	Thermal Energy Provided [kW]	Power Usage [kW]	Efficiency [COP or EER]
Time-step Heating	660.3	130.4	5.06
Time-step Cooling	-43.8	10.9	13.74
Hourly Average	616.5	141.3	4.36

The use of variable speed cooling and heating control would minimize the system instability shown above and result in more accurate results. This type of control however, was beyond the scope of this project.

Chapter 5

Validation of the Integrated Model and Subsystems

A building load model for a residential house was developed in HAMBASE and validated by Gaspreles. This section addresses the validation of the commercial office building described in detail in Chapter 3. The viability of HAMBASE as a modeling environment was discussed in Section 2.1. Schijndel (2007), de Wit (2009) and others (Department of the Built Environment at Eindhoven University of Technology, 2012) have validated various HAMBASE models against physical data. These validation efforts included ASHRAE's "Standard Method of Test for the Evaluation of Building Energy Analysis Computer Programs" (ASHRAE, 2007). Gaspreles repeated the ASHRAE 140-2007 method of test and found that, "HAMBASE was in good agreement with the reported values for case 600," and that "HAMBASE adequately models the tested [sensitivity] cases" (2011, pp. 34, 36).

The office building discussed in this section was based on a generic medium office building created by DoE's Commercial Reference Building Models (U.S. Department of Energy, 2010). The DoE implementation exists in EnergyPlus. EnergyPlus and HAMBASE make different simplifying assumptions, necessitating a robust validation process that can isolate the effects of these differences.

In addition to the differences in the underlying physics engines, the EnergyPlus and HAMBASE models use different HVAC systems to provide cooling and heating to the zones. The EnergyPlus implementation uses three variable air volume (VAV) HVAC systems, meaning that each floor has a single direct expansion cooling coil to provide cooling and a natural gas furnace for heating. Reheat coils in each zone are then used to adjust the main supply temperature to an appropriate zone supply temperature. The HAMBASE implementation uses an individual heat pump to provide heating and cooling for each conditioned zone.

In order to validate the HAMBASE implementation, it is necessary to eliminate the effects of the HVAC system and instead to prioritize open-loop system response (e.g.

operation with no HVAC system). Closed-loop response (e.g. operation with the HVAC system operational) will only be used as a comparison of the two models.

5.1. Test Overview

The results in this section will compare EnergyPlus and HAMBASE simulation results using open-loop and closed-loop tests. The open-loop tests are designed to compare the underlying fundamental models that EnergyPlus and HAMBASE employ for heat transfer and moisture transfer by removing the HVAC system and allowing the temperature and humidity within each zone to float freely. Within these tests there are two general inputs: external weather and internal loads. The closed-loop tests are designed to give order of magnitude comparisons for heating and cooling requirements in the zones.

5.2. Testing Standard

The use of the term validation in this section does not imply that EnergyPlus results are the standard; a review of ASHRAE's 140-2007 standard shows that eight widely-used building load models result in a large range of responses to standardized building and weather inputs (2007).

Further, it is important to note that the ASHRAE 140-2007 method of test is used for "Identifying and diagnosing predictive differences from whole building energy simulation software," and that for "any given case, a tested program may fall outside [the range of values] without necessarily being incorrect" (2007, pp. 2-3).

As such, the ranges found in ASHRAE 140-2007 will be used as a reference, in which results that fall outside the range will be noted. These ranges are discussed in Section 5.2.1 and Section 5.2.2.

5.2.1. Standards for Open-Loop Temperature Tests

A summary of results from ASHRAE Standard 140-2007 for open-loop (free-floating temperature) tests is shown in Table 25. These tests turn off the HVAC system, meaning that no heating or cooling is provided to the zones. As a result, the temperatures of the zones can float to equilibrium positions. Comparing the maximum and minimum floating temperatures generated by the different energy analysis computer programs on a particular test gives a range for “acceptable” free-floating temperature deviations.

Table 25: Free-floating temperature results from ASHRAE 140-2007

Maximum Annual Hourly Zone Temperature [C°]					
Case	Min	Max	Mean	Max-Min	(Max-Min)/Min
600FF	64.9	69.5	65.2	4.6	7%
900FF	41.8	44.8	43.1	3.0	7%
650FF	63.2	68.2	64.7	5.0	8%
950FF	35.5	38.5	36.5	3.0	8%
Minimum Annual Hourly Zone Temperature [C°]					
Case	Min	Max	Mean	Max-Min	(Max-Min)/Min
600FF	-18.8	-15.6	-17.6	3.2	-17%
900FF	-6.4	-1.6	-4.2	4.8	-75%
650FF	-23	-21.6	-22.7	1.4	-6%
950FF	-20.2	-18.6	-19.6	1.6	-8%
Average Annual Hourly Zone Temperature [C°]					
Case	Min	Max	Mean	Max-Min	(Max-Min)/Min
600FF	24.2	25.9	25.1	1.7	7%
900FF	24.5	25.9	25.2	1.4	6%
650FF	18.0	19.6	18.7	1.6	9%
950FF	14.0	15.0	14.4	1.0	7%

The eight computer programs had a maximum range of 5°C (9°F) when comparing the maximum annual hourly zone temperatures, a maximum range of 4.8°C (8.6°F) when comparing minimum annual hourly zone temperatures, and a maximum range of 1.7°C (3.1°F) when comparing the average annual hourly zone temperatures. The average percentage difference for all of the maximum temperature tests was 7.5%, for the minimum temperature tests was 27%, and for the average temperature was 7%.

The open-loop tests in this section will use the ranges in the 600FF test case as the benchmark, as shown in Table 26. Any zone or test that falls outside of this range will be noted and included in the summary of differences between HAMBASE and EnergyPlus results.

Table 26: Benchmarks for open-loop temperature tests

Test Description	Test Range
Maximum Annual Hourly Zone Temperature [C°]	4.6
Minimum Annual Hourly Zone Temperature [C°]	3.2
Average Annual Hourly Zone Temperature [C°]	1.7

5.2.2. Standards for Closed-Loop Temperature Tests

A summary of heating and cooling results from ASHRAE Standard 140-2007 for closed-loop (HVAC is on) tests are shown in Table 27 and Table 28. These tests have both a heating set-point and a cooling set-point in place so that the zone temperatures are controlled to within a specified range.

The difference in annual heating energy between the computer programs with the largest and smallest annual values was 0.7MWh, and the difference in annual cooling was 0.9MWh (as shown in Table 27). From a percentage difference basis, the closed-loop tests show much greater discrepancy than the open-loop tests. The average difference in annual heating across all tests was 146%, while the average difference in annual cooling across all tests was 47%.

These values will be used as a relative point for the comparison of the EnergyPlus and HAMBASE results, but due to the different HVAC systems implemented in the EnergyPlus and HAMBASE models the values do not represent an absolute point of comparison.

Table 27: Closed-loop annual heating & cooling results from ASHRAE 140-2007

Annual Heating [MWh]					
Case	Min	Max	Mean	Max-Min	(Max-Min)/Min
610-600	0.021	0.098	0.057	0.1	367%
620-600	0.138	0.682	0.318	0.5	394%
630-620	0.267	0.551	0.421	0.3	106%
640-600	-2.166	-1.545	-1.882	0.6	-29%
900-600	-3.837	-3.126	-3.344	0.7	-19%
910-900	0.179	0.442	0.321	0.3	147%
920-900	2.07	2.505	2.227	0.4	21%
930-920	0.595	1.08	0.819	0.5	82%
Annual Sensible Cooling [MWh]					
Case	Min	Max	Mean	Max-Min	(Max-Min)/Min
610-600	-2.227	-1.272	-1.867	1.0	-43%
620-600	-2.96	-2.341	-2.614	0.6	-21%
630-620	-1.845	-0.984	-1.367	0.9	-47%
640-600	-0.32	-0.153	-0.24	0.2	-52%
900-600	-4.624	-3.833	-4.154	0.8	-17%
910-900	-1.561	-0.832	-1.231	0.7	-47%
920-900	-0.323	0.016	-0.125	0.3	-105%
930-920	-1.174	-0.682	-0.9	0.5	-42%

The difference in peak heating rate (shown in Table 28) between the computer programs with the largest and smallest peak values was 1.1kW, and the difference in peak cooling was 0.8kW. The average difference in peak heating across all tests was 521%, while the average difference in peak cooling across all tests was 60%.

These values will be used as a relative point for the comparison of the EnergyPlus and HAMBASE results, but due to the different HVAC systems implemented in the EnergyPlus and HAMBASE models the values do not represent an absolute point of comparison.

Table 28: Closed-loop peak heating & cooling results from ASHRAE 140-2007

Peak Heating [KW]					
Case	Min	Max	Mean	Max-Min	(Max-Min)/Min
610-600	-0.011	0.001	-0.003	0.0	-109%
620-600	-0.008	0.24	0.062	0.2	-3100%
630-620	-0.021	0.003	-0.003	0.0	-114%
640-600	1.546	2.6	2.03	1.1	68%
900-600	-0.587	-0.414	-0.494	0.2	-29%
910-900	0.003	0.019	0.008	0.0	533%
920-900	0.192	0.458	0.298	0.3	139%
930-920	0.027	0.047	0.034	0.0	74%
Peak Sensible Cooling [KW]					
Case	Min	Max	Mean	Max-Min	(Max-Min)/Min
610-600	-0.811	-0.116	-0.472	0.7	-86%
620-600	-2.56	-1.716	-2.118	0.8	-33%
630-620	-0.842	-0.371	-0.592	0.5	-56%
640-600	-0.08	-0.033	-0.051	0.0	-59%
900-600	-3.355	-2.81	-3.071	0.5	-16%
910-900	-1.122	-0.31	-0.714	0.8	-72%
920-900	-0.517	0.048	-0.313	0.6	-109%
930-920	-0.721	-0.387	-0.527	0.3	-46%

5.2.3. Summary of Testing Standards

A summary of the testing comparisons used in this validation are shown in Table 29. None of these values represent a PASS/FAIL testing standard, but instead are used to identify higher-discrepancy values; values which can then be incorporated in the interpretation of simulation results and recommendations based on those results.

Comparing the ASHRAE 140-2007 test results shows a general higher variance in heating calculations compared to cooling calculations. This includes the percent difference in minimum free-floating temperature versus maximum free-floating temperature, the percent difference in annual heating versus annual cooling and the percent difference in peak heating versus peak cooling.

Table 29: List of testing benchmarks

Test Description	Test Range
Maximum Annual Free-Floating Hourly Zone Temperature	4.6°C
Minimum Annual Free-Floating Hourly Zone Temperature	3.2°C
Average Annual Free-Floating Hourly Zone Temperature	1.7°C
Average Annual Heating Difference	146%
Average Annual Cooling Difference	47%
Average Peak Heating Difference	521%
Average Peak Cooling Difference	60%

5.3. Open-Loop Tests of HAMBASE Building Load Model

Various open-loop tests were used to compare the HAMBASE implementation of the building model to the EnergyPlus implementation of the building model. A summary of the tests is shown in Table 30 and Table 31. The tests in Table 30 are covered in detail in the following sections. The tests in Table 31 are referenced in the following sections, with the supporting graphs and data found in Appendix A.5.

Table 30: Summary of open-loop validation tests

Test Set	Internal Loads	Weather Input	Objective
1	None	Constant weather	Compare non-excited steady-state values
2	None	Temperature-step	Compare time constants
3	None	Relative Humidity (RH)-step	Compare time constants
4	None	Temp, RH, DNI, DHI-sine wave	Compare DC offset, phase shift and amplitude
5	None	Actual weather	Compare max and min free-floating temperatures
6	All	Constant weather	Compare max and min free-floating temperatures
7	All	Actual weather	Compare max and min free-floating temperatures

Table 31: Summary of supplementary open-loop validation tests

Test Set	Internal Loads	Weather Input	Objective
8	None	Temperature and RH-sine wave	Compare DC offset, phase shift and amplitude
9	None	DNI (Direct Normal Irradiance)-sine wave	Compare DC offset, phase shift and amplitude
10	None	DHI (Diffuse Horizontal Irradiance)-sine wave	Compare DC offset, phase shift and amplitude
11	People	Constant weather	Compare steady-state values
12	Equipment	Constant weather	Compare steady-state values

Tests 1, 2, 3, 4, 5, 8, 9 and 10 assessed the material properties of the building's construction by eliminating all internal loads and applying various external weather files. The weather file was modified to create different excitations of temperature, relative humidity and solar radiation. The input excitations used were constant, ramp, step and sinusoidal. For all of these tests the HVAC system was turned off, and ventilation was set to zero. Infiltration was kept constant throughout the tests with unique value for each zone based on the external surface area of the zone.

Tests 6, 7, 11 and 12 confirmed that the effects of sensible, latent, radiant and convective internal loads were consistent between EnergyPlus and HAMBASE.

5.3.1. Test Set 1: Open-Loop, Constant Weather, No Internal Loads

An external weather file was created with constant dry bulb temperature, humidity, wind speed and cloud cover, as listed in Table 32. Direct radiation and diffuse radiation were set to zero. Recall that the HVAC system was turned off and internal loads and ventilation were set to zero. The test was intended to measure the zonal responses of the HAMBASE and EnergyPlus building envelopes to constant external weather inputs.

Table 32: Open-loop constant weather inputs

Input Variable	Constant Value
Direct normal solar irradiance [W/m^2]	0
Diffuse horizontal solar irradiance [W/m^2]	0
Cloud cover [0 – 10]	10
Dry bulb temperature [$^{\circ}\text{C}$]	22
Relative Humidity [%]	50
Wind direction [degrees north]	0
Wind velocity [m/s]	0

The temperature and relative humidity responses for Core1 for both EnergyPlus and HAMBASE are shown in Figure 58 for a 15-day period. The data show a steady-state temperature difference of 0.70°C (1.3°F). The percent error from the expected value of 22°C (71.6°F) was $+0.5\%$ for EnergyPlus compared to -1.5% for HAMBASE. The steady-state relative humidity difference was 0.6 percentage points. The percent error from the expected value of 50% relative humidity was -0.9% for EnergyPlus and $+0.3\%$ for HAMBASE. Similar responses and % differences were found for all 18 zones in the office building.

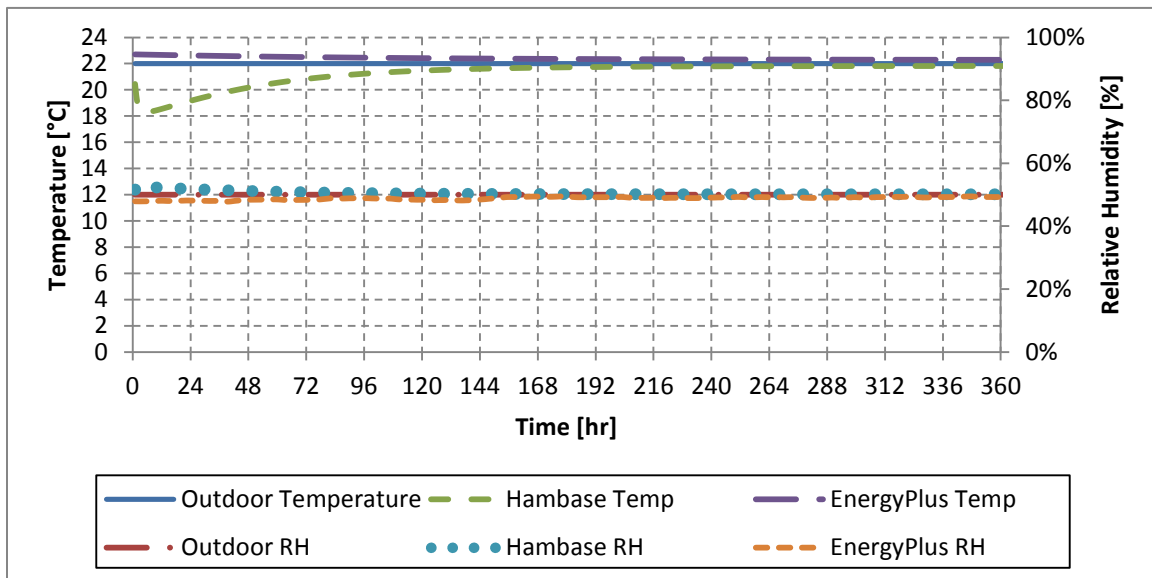


Figure 58: Open-loop responses of Core1 to constant weather inputs

While the steady-state errors of HAMBASE and EnergyPlus were of the same magnitude, HAMBASE showed a transient temperature response during the first 24 hours of simulation. HAMBASE has no built-in warm up period to eliminate start-up transience, where EnergyPlus pre-simulates 3 days of operation before beginning to collect data. Pre-simulation allows the model time to reach equilibrium, resulting in the slow monotonic response toward 22°C (71.6°F) during first 24 hours of the EnergyPlus response. HAMBASE lacks a built-in warm-up period, and as a result, it has a transient period before ultimately moving into a monotonic trend toward 22°C (71.6°F). The transient period was most pronounced in first-floor zones, as shown by the responses of East2 in Figure 59 and South3 in Figure 60.

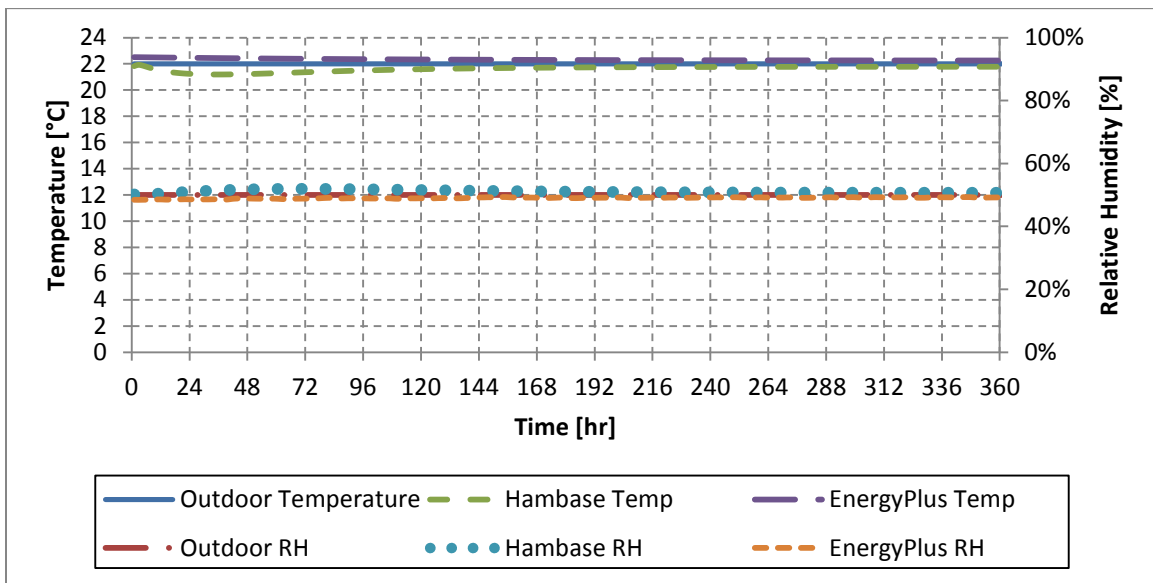


Figure 59: Open-loop responses of East2 to constant weather inputs

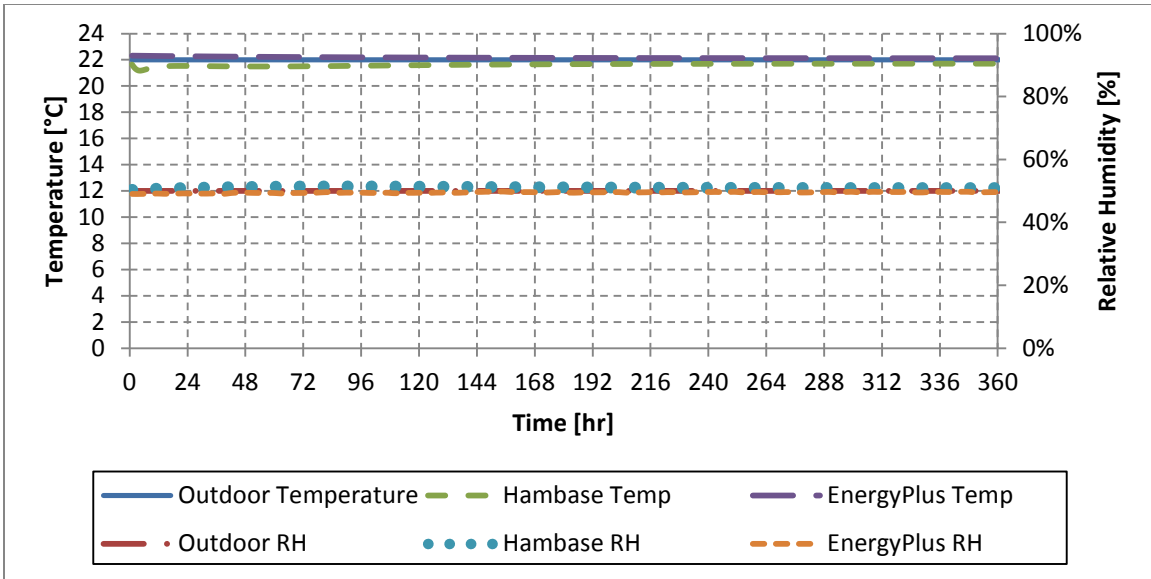


Figure 60: Open-loop responses of South3 to constant weather inputs

The steady-state temperature of all 18 zones is shown in Table 33. For all zones the HAMBASE model showed a steady-state temperature less than ambient temperature of 22°C (71.6°F), while the EnergyPlus model showed a steady-state temperature greater than ambient temperature for all zones except the four first-floor perimeter zones. On average, a zone by zone comparison shows the HAMBASE zone temperatures to be 0.44°C (0.8°F) lower than EnergyPlus temperatures.

Table 33: Steady-state temperature after constant weather input

Zone	Steady-State Temperature [°C]		Absolute Error [°C]		Percent Error	
	HB	EP	HB	EP	HB	EP
Core1	21.8	22.3	-0.2	0.3	-0.8%	1.3%
South1	21.8	22.0	-0.2	0.0	-0.8%	-0.1%
East1	21.8	22.0	-0.2	0.0	-0.8%	-0.1%
North1	21.8	22.0	-0.2	0.0	-0.8%	-0.1%
West1	21.8	22.0	-0.2	0.0	-0.8%	-0.1%
Plenum1	21.8	22.4	-0.2	0.4	-0.9%	1.9%
Core2	21.8	22.6	-0.2	0.6	-1.1%	2.6%
South2	21.8	22.3	-0.2	0.3	-1.0%	1.2%
East2	21.8	22.2	-0.2	0.2	-1.0%	1.1%
North2	21.8	22.3	-0.2	0.3	-1.0%	1.2%
West2	21.8	22.2	-0.2	0.2	-1.0%	1.1%
Plenum2	21.7	22.5	-0.3	0.5	-1.2%	2.2%
Core3	21.7	22.4	-0.3	0.4	-1.5%	1.7%
South3	21.7	22.1	-0.3	0.1	-1.3%	0.5%
East3	21.7	22.1	-0.3	0.1	-1.3%	0.5%
North3	21.7	22.1	-0.3	0.1	-1.3%	0.6%
West3	21.7	22.1	-0.3	0.1	-1.3%	0.5%
Plenum3	21.6	22.0	-0.4	0.0	-1.9%	0.1%
Average	21.8	22.2	-0.2	0.2	-1.1%	0.9%

The steady-state relative humidity of the building's 18 zones is shown in Table 34. For all zones the HAMBASE model showed a steady-state relative humidity greater than the ambient relative humidity of 50%, while the EnergyPlus model showed a steady-state relative humidity less than the ambient relative humidity except in the four first-floor perimeter zones. On average, a zone by zone comparison shows the HAMBASE relative humidity to be 1.2 percentage points lower than EnergyPlus relative humidity.

Table 34: Steady-state relative humidity after constant weather input

Zone	Steady-State RH [%]		Absolute Error [%]		Percent Error	
	HB	EP	HB	EP	HB	EP
Core1	50.1	49.8	0.1	-0.2	0.2%	-0.4%
South1	50.5	50.0	0.5	0.0	1.1%	0.0%
East1	50.5	50.1	0.5	0.1	1.1%	0.1%
North1	50.5	50.0	0.5	0.0	1.1%	0.0%
West1	50.5	50.1	0.5	0.1	1.1%	0.1%
Plenum1	50.6	48.7	0.6	-1.3	1.3%	-2.6%
Core2	50.1	48.9	0.1	-1.1	0.2%	-2.2%
South2	50.7	49.2	0.7	-0.8	1.3%	-1.6%
East2	50.7	49.2	0.7	-0.8	1.3%	-1.6%
North2	50.7	49.2	0.7	-0.8	1.3%	-1.7%
West2	50.7	49.2	0.7	-0.8	1.3%	-1.6%
Plenum2	50.8	48.5	0.8	-1.5	1.7%	-2.9%
Core3	50.1	49.5	0.1	-0.5	0.3%	-0.9%
South3	50.9	49.6	0.9	-0.4	1.8%	-0.8%
East3	50.9	49.6	0.9	-0.4	1.8%	-0.7%
North3	50.9	49.6	0.9	-0.4	1.8%	-0.8%
West3	50.9	49.6	0.9	-0.4	1.8%	-0.7%
Plenum3	51.3	49.9	1.3	-0.1	2.5%	-0.1%
Average	50.6	49.5	0.6	-0.5	0.0%	0.0%

Data from the open-loop constant weather input tests show steady-state agreement between HAMBASE and EnergyPlus for both temperature and relative humidity. HAMBASE results trended lower in temperature and higher in relative humidity than EnergyPlus.

Based on this test, steady-state conditions will not contribute significantly to different heating and cooling totals in the two models.

5.3.2. Test Set 2: Open-Loop, Ambient Temperature-Step, No Internal Loads

The constant weather file was altered to create a temperature-step input with temperature of 22°C (71.6°F) for 7 days before a step decrease to 10°C (50°F). All other weather inputs were held constant to values shown in Table 32. Recall, the HVAC system

was turned off and internal loads and ventilation were set to zero. Figure 61 shows the responses for Core1.

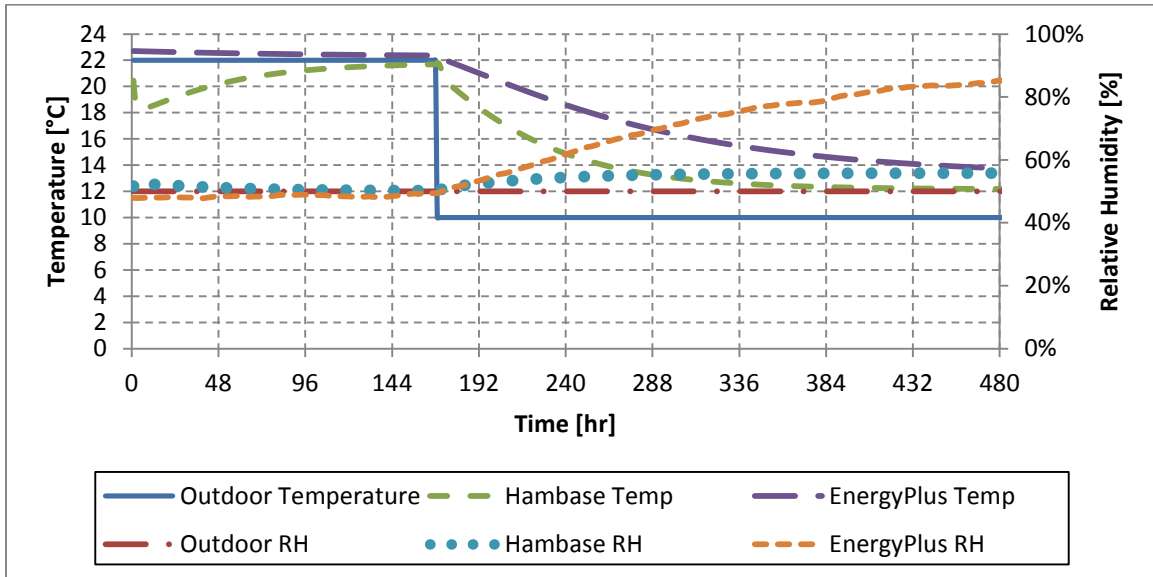


Figure 61: Open-loop response of Core1 to ambient temperature-step input

The HAMBASE Core1 temperature response is faster with a time constant of 45.33 hours compared to 88 hours for EnergyPlus. Both HAMBASE and EnergyPlus have a steady-state temperature of approximately 12°C (53.6°F) because the ground temperature remains at 22°C (71.6°F) which provides a warming effect to the zone.

The relative humidity for core zones in EnergyPlus went to 100% due to the absence of moisture transport properties in conjunction with ventilation turned off and no exterior walls to allow infiltration. The ASHRAE psychrometric chart shown in Figure 62 shows this process using an orange dashed line. The moisture content in the air stays constant while the temperature drops to 10°C (50°F), resulting in a relative humidity of approximately 100%.

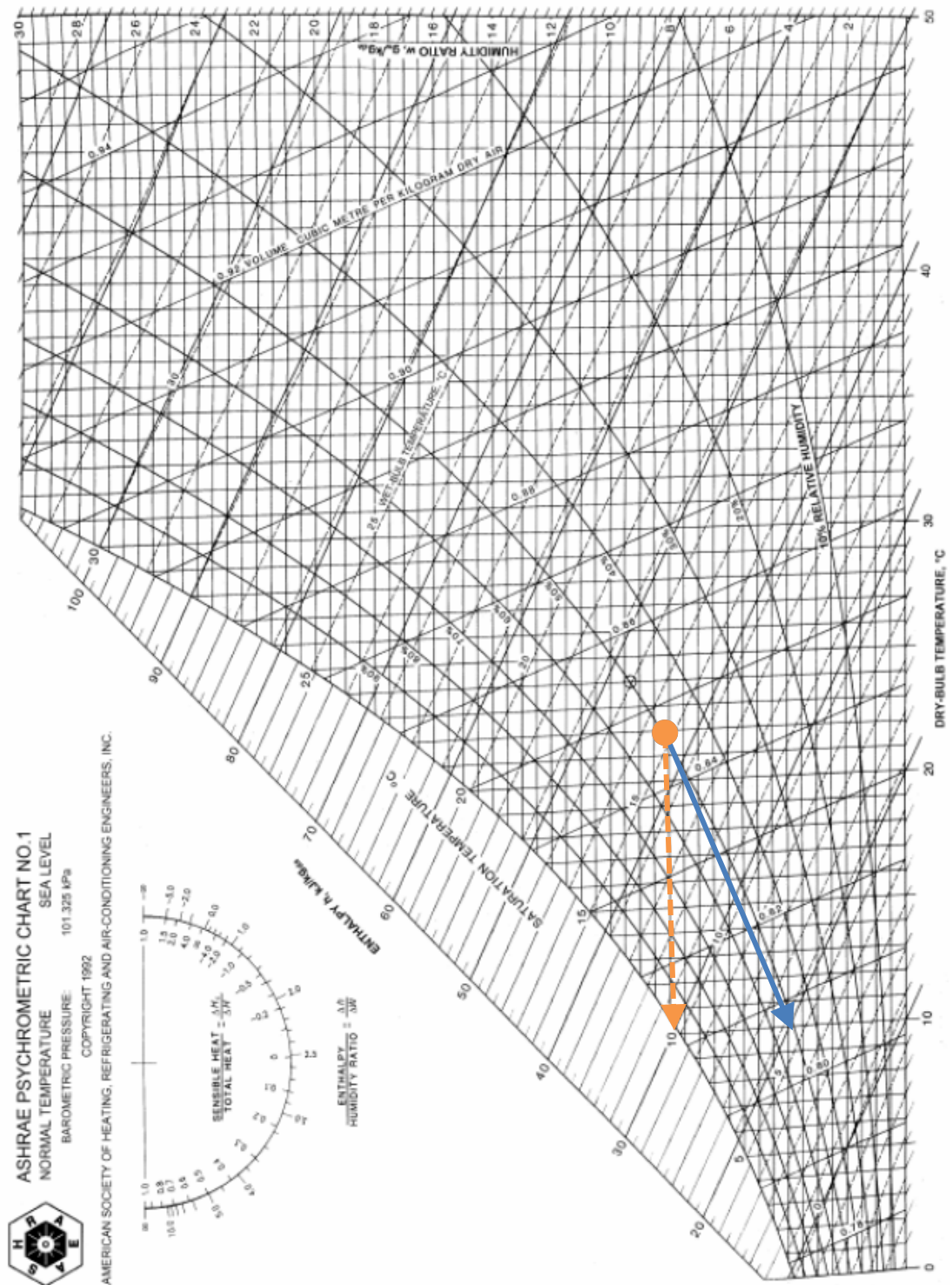


Figure 62: ASHRAE psychrometric chart showing perimeter zones in blue-solid and core zones in orange-dash for Test Set 2 (ASHRAE 2009 Fundamentals Handbook, p. 1.11)

The relative humidity response in HAMBASE also increases in the absence of ventilation and infiltration, but it only approaches 60% as opposed to the expected 100%. The results of Test Set 11 in Appendix A.5.4. show that the core zone responds with 100% relative humidity to an internal moisture source. This leads to the conclusion that the physics of the core zones in HAMBASE and EnergyPlus are similarly moisture impenetrable, but HAMBASE is less responsive to changes in relative humidity resulting from temperature change.

Looking at the response of a perimeter zone, as shown in Figure 63 and Figure 64, reveals the impact of infiltration on the relative humidity response. Where the Core1 zone lacked any external walls and as a result infiltration, the East2 and South3 zones both have one external wall, allowing infiltration to equalize relative humidity in the zone. These responses match the process shown with the blue-solid line on the psychrometric chart in Figure 62.

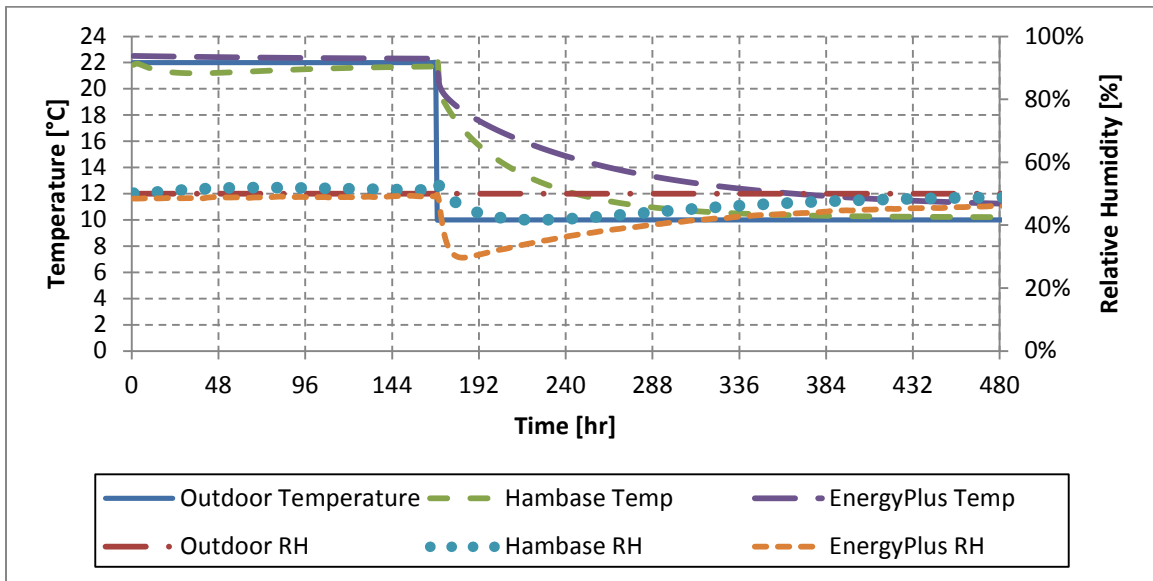


Figure 63: Open-loop response of East2 to ambient temperature-step input

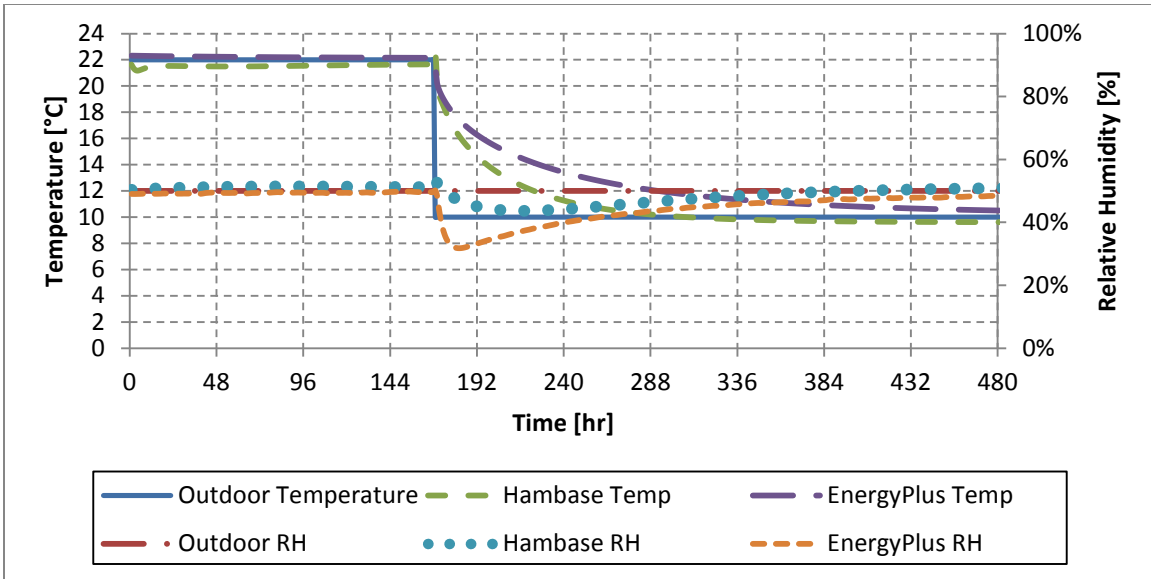


Figure 64: Open-loop response of South3 to ambient temperature-step input

The steady-state temperature values for all zones are shown in Table 35. The effect of the 22°C (71.6°F) ground temperature is seen in the higher steady-state values for the first-floor zones in both HAMBASE and EnergyPlus. The steady-state values for HAMBASE are lower than EnergyPlus in every zone, which is consistent with the results of Test Set 1. The HAMBASE values for third-floor zones are lower than the outdoor air temperature, implying that the sky temperature for HAMBASE is lower than in EnergyPlus.

Table 35: Temperature results for open-loop temperature-step input

Zone	Steady-State Temperature [°C]		Absolute Error [°C]		Percent Error	
	HB	EP	HB	EP	HB	EP
Core1	12.2	13.6	2.2	3.6	21.7%	36.3%
South1	11.3	12.3	1.3	2.3	13.4%	23.0%
East1	11.3	12.2	1.3	2.2	13.2%	22.3%
North1	11.3	12.3	1.3	2.3	13.4%	23.1%
West1	11.3	12.2	1.3	2.2	13.2%	22.3%
Plenum1	11.1	12.4	1.1	2.4	10.6%	24.2%
Core2	10.4	11.9	0.4	1.9	4.3%	18.5%
South2	10.2	11.2	0.2	1.2	2.1%	12.0%
East2	10.2	11.2	0.2	1.2	2.1%	11.7%
North2	10.2	11.2	0.2	1.2	2.1%	12.1%
West2	10.2	11.2	0.2	1.2	2.1%	11.7%
Plenum2	10.0	11.2	0.0	1.2	-0.2%	12.2%
Core3	9.6	10.8	-0.4	0.8	-3.9%	8.2%
South3	9.6	10.5	-0.4	0.5	-3.9%	4.5%
East3	9.6	10.4	-0.4	0.4	-3.9%	4.4%
North3	9.6	10.5	-0.4	0.5	-3.9%	4.6%
West3	9.6	10.4	-0.4	0.4	-3.9%	4.4%
Plenum3	9.3	10.3	-0.7	0.3	-7.0%	2.6%
Average	10.4	11.4	0.7	1.4	6.9%	14.3%

Comparing the time constants for a given model across different zones shows consistency between HAMBASE and EnergyPlus, as seen in Table 36. Both programs show the largest time constant value (slowest response) for the first-floor zones and smallest value (fastest response) for the third-floor zones, which is consistent with their distance from the ground heat-source. On a given floor, both programs show the core zones responded approximately 10% slower than the perimeter zones, which is consistent with the zones sizes.

Comparing the time constants between the programs shows HAMBASE responding approximately twice as quickly as EnergyPlus in every zone. While this difference is significant, a time constant standard does not exist. Changing material properties of the HAMBASE model to better match the EnergyPlus response is an option to improve the time constant match, but this approach was rejected in favor of using

identical material values between the programs. The faster response exhibited by HAMBASE will result in higher estimates of the annual heating and cooling values.

Table 36: EnergyPlus and HAMBASE time constant for ambient temperature-step input

Zone	Hambase Time Constant [hr]	EnergyPlus Time Constant [hr]
Core1	54.3	113.0
South1	43.7	94.3
East1	43.3	93.3
North1	43.7	94.3
West1	43.3	93.3
Plenum1	50.0	104.7
Core2	50.7	102.3
South2	44.7	90.7
East2	44.3	89.7
North2	44.7	90.7
West2	44.3	89.7
Plenum2	46.7	94.3
Core3	45.3	88.0
South3	39.7	76.7
East3	39.7	75.7
North3	39.7	76.7
West3	39.7	75.7
Plenum3	38.3	67.7
Average	44.2	89.5

Test 2 showed a difference between EnergyPlus and HAMBASE in the case of humidity response to temperature change, sky temperature and time constant. These differences will cause HAMBASE to have lower relative humidity values, more heat-loss from radiation exchange with the sky, and faster temperature effects from the outdoor air. The radiation and time constant differences will cause HAMBASE to experience greater cooling and heating loads than EnergyPlus.

Based on this test, external temperature will contribute significantly to different heating and cooling totals in the two models.

5.3.3. Test Set 3: Open-Loop, Ambient Relative Humidity-Step, No Internal Loads

The constant weather file was altered to create a relative humidity-step input with a relative humidity value of 30% for 7 days before a step decrease to 80%. All other weather inputs were held constant to values shown in Table 32. Recall, the HVAC system was turned off and internal loads and ventilation were set to zero. Figure 65 shows the response for Core1.

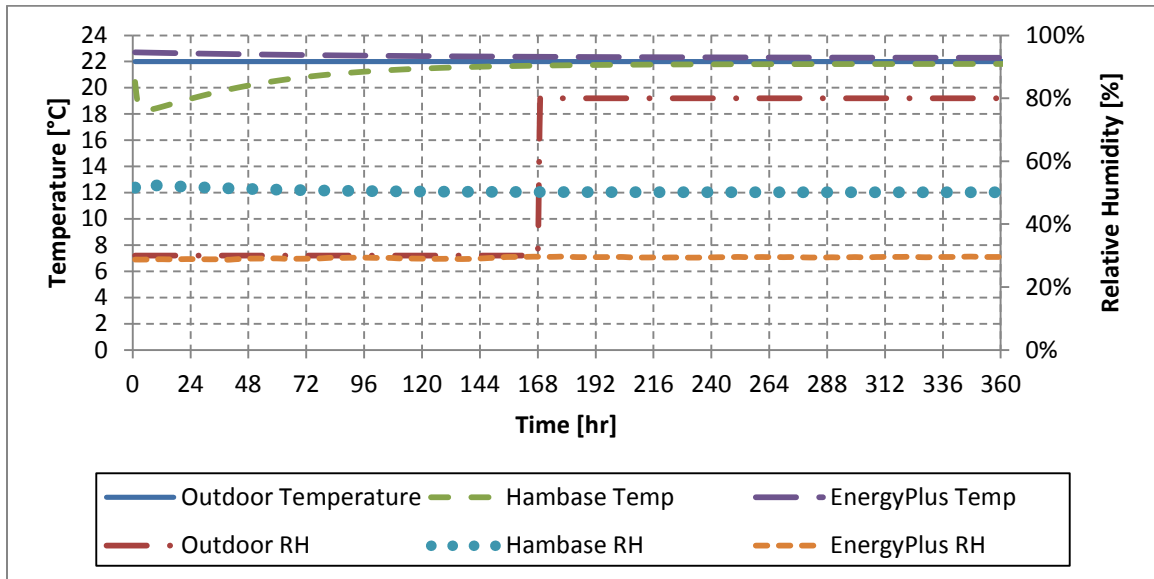


Figure 65: Open-loop response of Core1 to ambient relative humidity-step input

Consistent with the results from Test Set 2, no moisture transport occurs in the core zones, so the change in outdoor air moisture does not cause a response in Core1 for either EnergyPlus or HAMBASE. The difference in steady-state relative humidity value results from the warm-up period built into EnergyPlus. The warm-up period changes initial conditions for all the zones, while the initial conditions for HAMBASE remain at 22°C (71.6°F) and 50% relative humidity.

The response of perimeter zones, as shown in Figure 66 and Figure 67, shows EnergyPlus responding faster than HAMBASE when moisture transport occurs via infiltration. Both programs approach steady-state relative humidity of 80%, as shown in

Table 37. The HAMBASE values in all zones and the first-floor values from EnergyPlus climb above 80% due to the slightly lower air temperatures in these zones.

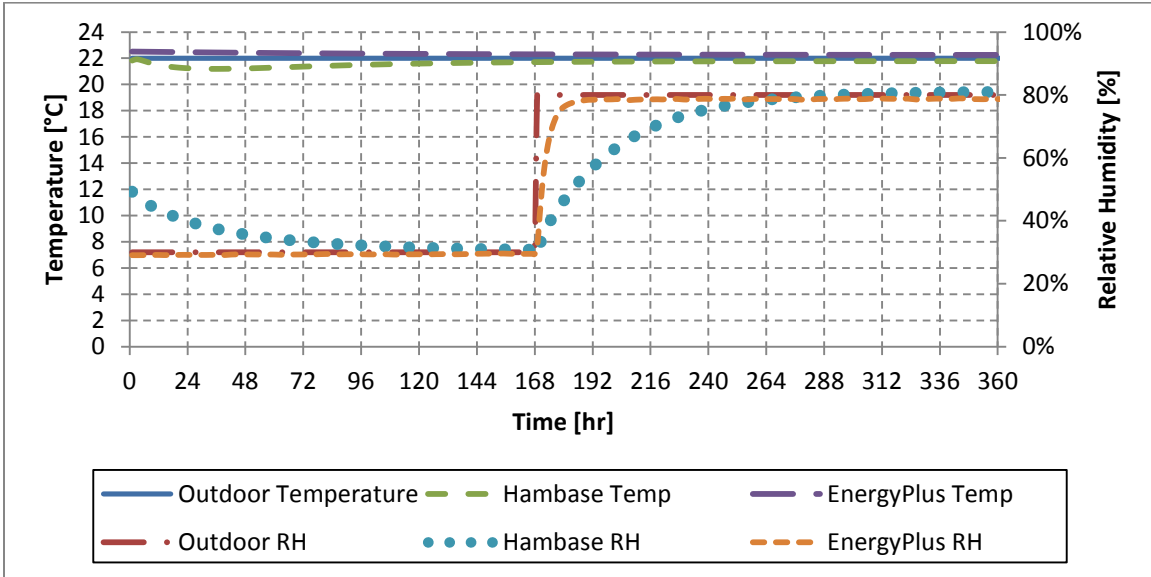


Figure 66: Open-loop response of East2 to ambient relative humidity-step input

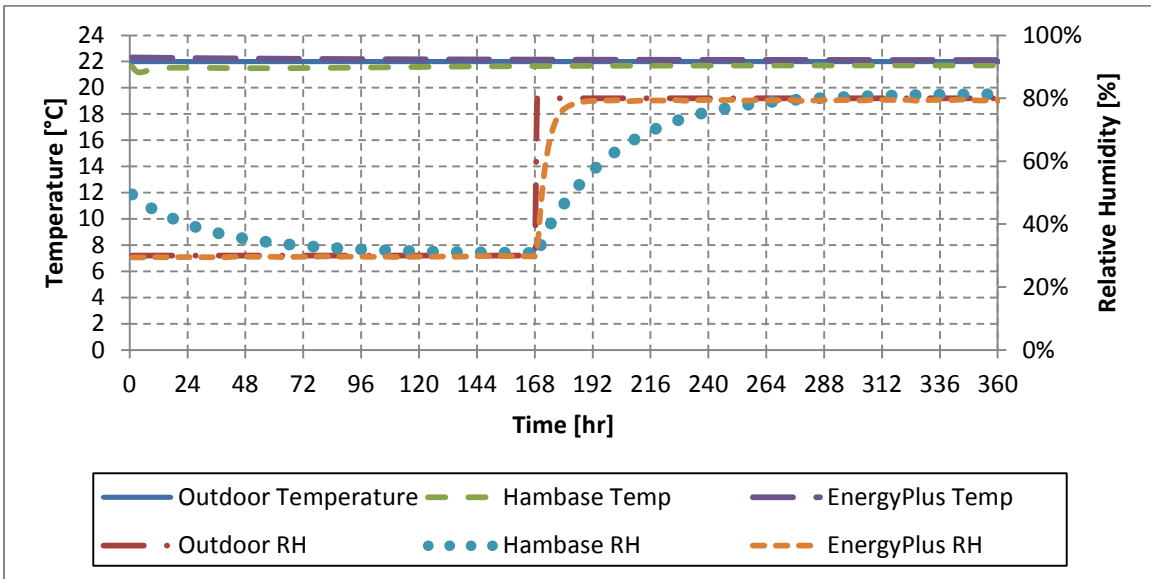


Figure 67: Open-loop response of South3 to ambient relative humidity-step input

Table 37: Relative humidity results for open-loop RH-step input

Zone	Steady-State Relative Humidity [%]		Absolute Error [%]		Percent Error	
	HB	EP	HB	EP	HB	EP
Core1	50.1	29.9	N/A	N/A	N/A	N/A
South1	80.8	80.0	0.8	0.0	1.0%	0.0%
East1	80.8	80.1	0.8	0.1	1.0%	0.1%
North1	80.8	80.0	0.8	0.0	1.0%	0.0%
West1	80.8	80.1	0.8	0.1	1.0%	0.1%
Plenum1	80.7	77.9	0.7	-2.1	0.8%	-2.6%
Core2	50.1	29.3	N/A	N/A	N/A	N/A
South2	81.0	78.7	1.0	-1.3	1.3%	-1.6%
East2	81.0	78.7	1.0	-1.3	1.3%	-1.6%
North2	81.0	78.7	1.0	-1.3	1.3%	-1.7%
West2	81.0	78.7	1.0	-1.3	1.3%	-1.6%
Plenum2	81.0	77.7	1.0	-2.3	1.2%	-2.9%
Core3	50.1	29.7	N/A	N/A	N/A	N/A
South3	81.4	79.4	1.4	-0.6	1.7%	-0.8%
East3	81.4	79.4	1.4	-0.6	1.7%	-0.7%
North3	81.4	79.3	1.4	-0.7	1.7%	-0.8%
West3	81.4	79.4	1.4	-0.6	1.7%	-0.7%
Plenum3	82.0	79.9	2.0	-0.1	2.5%	-0.1%
Average	75.9	70.9	0.9	0.7	1.2%	0.9%

Time constants for all zones except core zones are listed in Table 38. EnergyPlus consistently responds between 6 and 8 times faster than HAMBASE in all zones. Changing material properties and infiltration rates in HAMBASE could bring the response rates into better agreement, but this option was rejected in favor of using the same properties and rates in both programs.

Test 3 showed differences between EnergyPlus and HAMBASE in the case of steady-state relative humidity and time constant for relative humidity response. These differences will cause HAMBASE to remove less net moisture than EnergyPlus, all other things being equal.

Based on this test, external humidity will contribute significantly to different latent cooling totals in the two models.

Table 38: EnergyPlus and HAMBASE time constant for ambient RH-step input

Zone	Hambase Time Constant [Hr]	EnergyPlus Time Constant [Hr]
Core1	N/A	N/A
South1	22.33	4.00
East1	22.33	4.00
North1	22.33	4.00
West1	22.33	4.00
Plenum1	63.67	9.67
Core2	N/A	N/A
South2	32.67	4.00
East2	32.33	4.00
North2	32.67	4.00
West2	32.33	4.00
Plenum2	64.00	9.67
Core3	N/A	N/A
South3	33.00	4.00
East3	32.67	4.00
North3	33.00	4.00
West3	32.67	4.00
Plenum3	8.67	1.33
Average	32.47	4.58

5.3.4. Test Set 4: Open-Loop, Weather-Sine, No Internal Loads

The constant weather file was altered to create a combined temperature, relative humidity, DNI and DHI-sine input. The TMY3 weather data was reviewed to find a representative summer day. With the day of August 16 chosen, the weather data was then used for sine-wave curve-fits. The temperature and relative humidity data are shown in Figure 68, while the direct normal irradiance (DNI) and diffuse horizontal irradiance (DHI) data are shown in Figure 69. The remainder of the constant weather file from Table 32 remained unchanged. The temperature and relative humidity data were used independently in Test Set 8, shown in Appendix A.5.1. . The DNI and DHI data were used independently in Test Set 9, shown in Appendix A.5.2. , and Test Set 10, shown in Appendix A.5.3. .

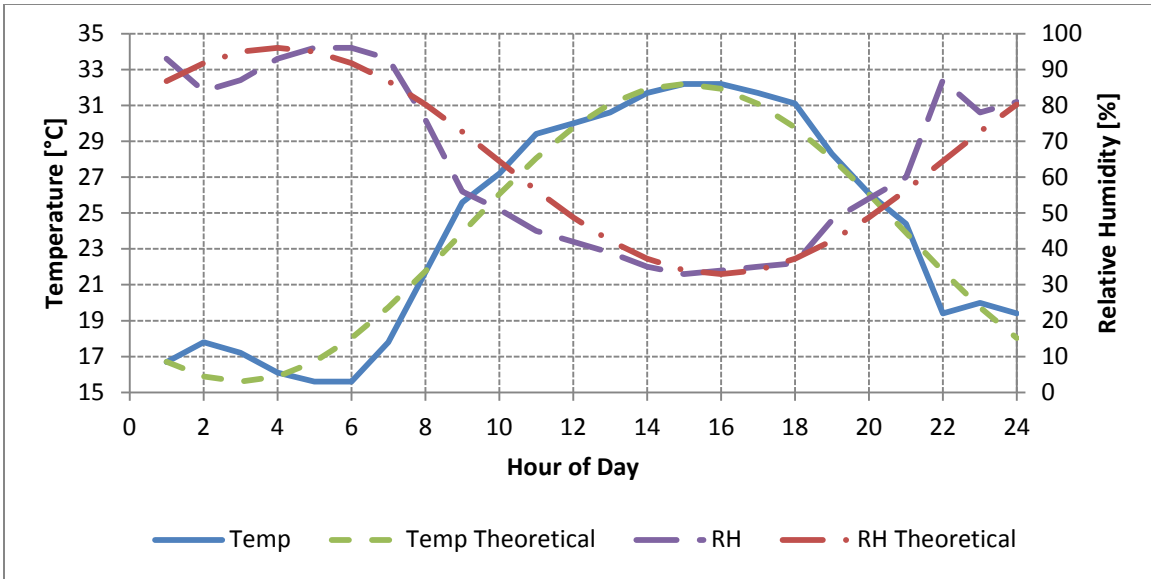


Figure 68: Temperature and relative humidity curves for 8/16/2004 used in Test Set 4

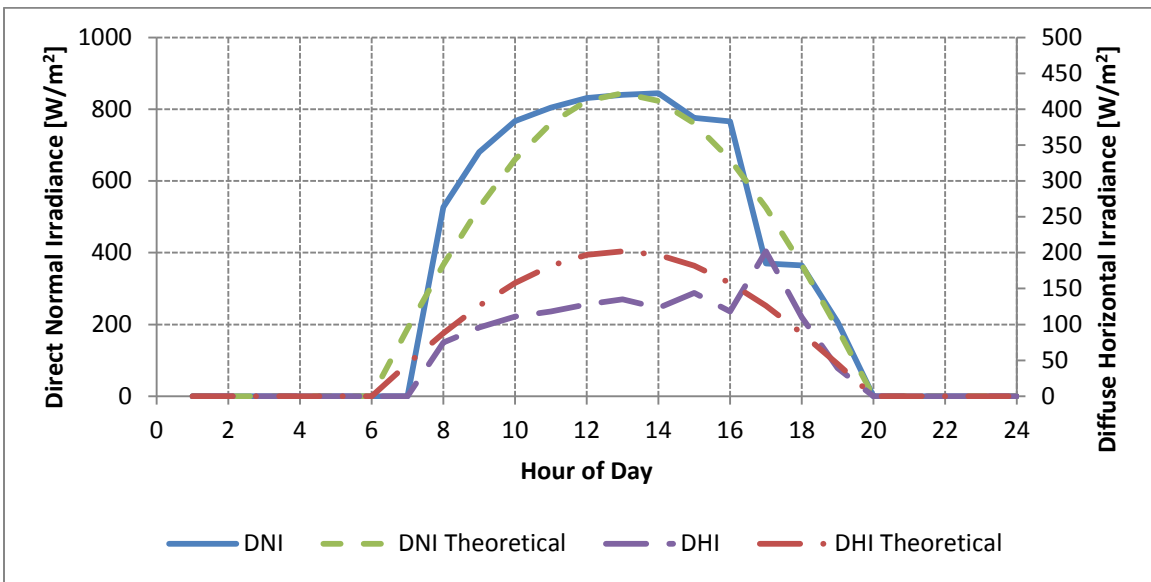


Figure 69: Direct and diffuse irradiance curves for 8/16/2004 used in Test Set 4

The complete response of Core1 is shown in Figure 70. The faster temperature response of HAMBASE can be seen in the greater amplitude of the Core1 temperature oscillations; 3.4°C (6.1°F) for HAMBASE versus 1.1°C (2.0°F) for EnergyPlus. The lower steady-state temperature value of HAMBASE can be seen in lower center

amplitude; 28°C (82.4°F) compared to 30°C (86.0°F) for EnergyPlus. The effect of EnergyPlus' warm-up period and HAMBASE's lack of warm-up period can be seen in the responses over the first six days; 22°C (71.6°F) initial temperature for HAMBASE, 29°C (84.2°F) for EnergyPlus.

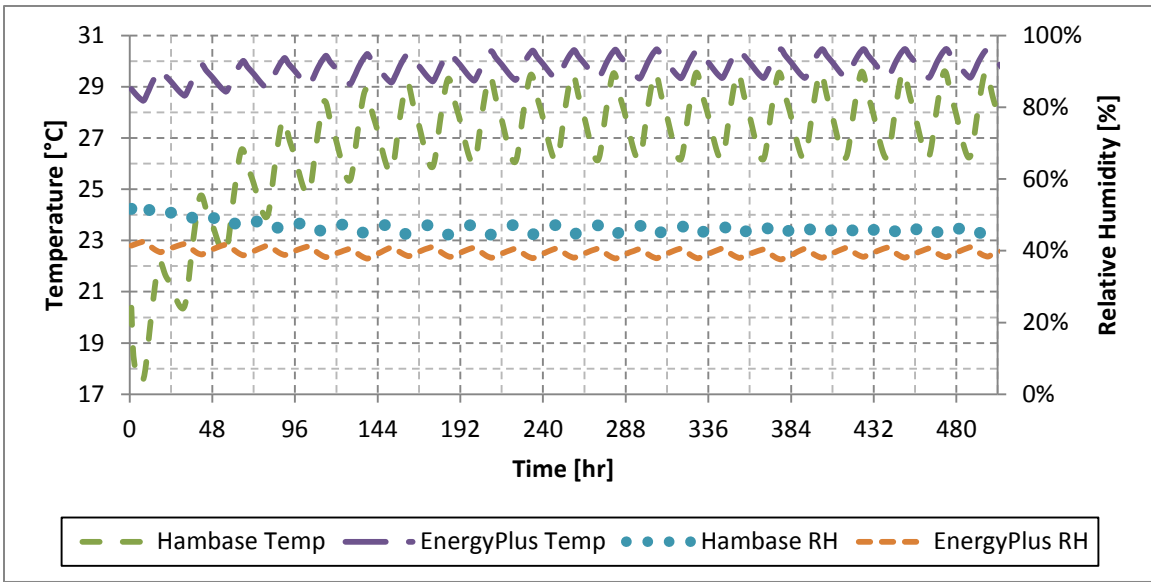


Figure 70: Open-loop response of Core1 to weather-sine input

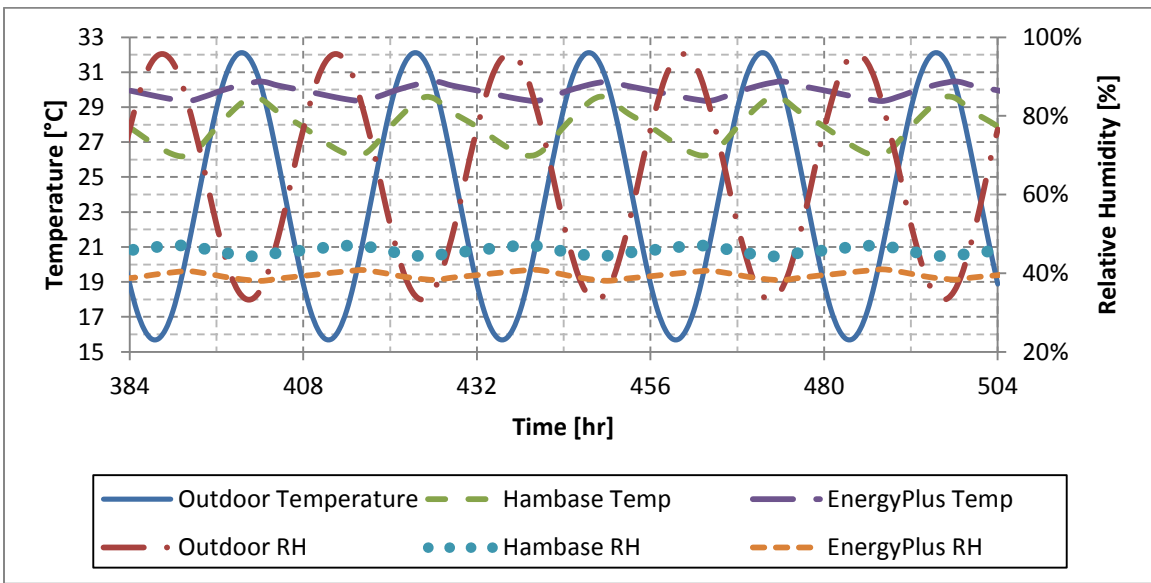


Figure 71: Open-loop steady-state response of Core1 to weather-sine input

A five-day view of steady-state response for Core1 is shown in Figure 71. The frequency of the HAMBASE and EnergyPlus responses align, as do the locations of the peaks and troughs. The locations of peaks and troughs for the Core zones correspond to a lagged peak outdoor air temperature because of the cores insulation from direct exposure to DNI, DHI and direct outdoor air.

Five-day steady-state response for East2 and South3 are shown in Figure 72 and Figure 73, respectively. For both zones, the effect of sun position on DNI can be seen in the altered temperature response. For East2, direct sunlight in the morning causes a bimodal response; one early in the morning from DNI and a second in early afternoon from high outdoor temperature and high DHI. For South3, the peak temperature response directly aligns with peak temperature, as South3 does not receive significant DNI during summer months.

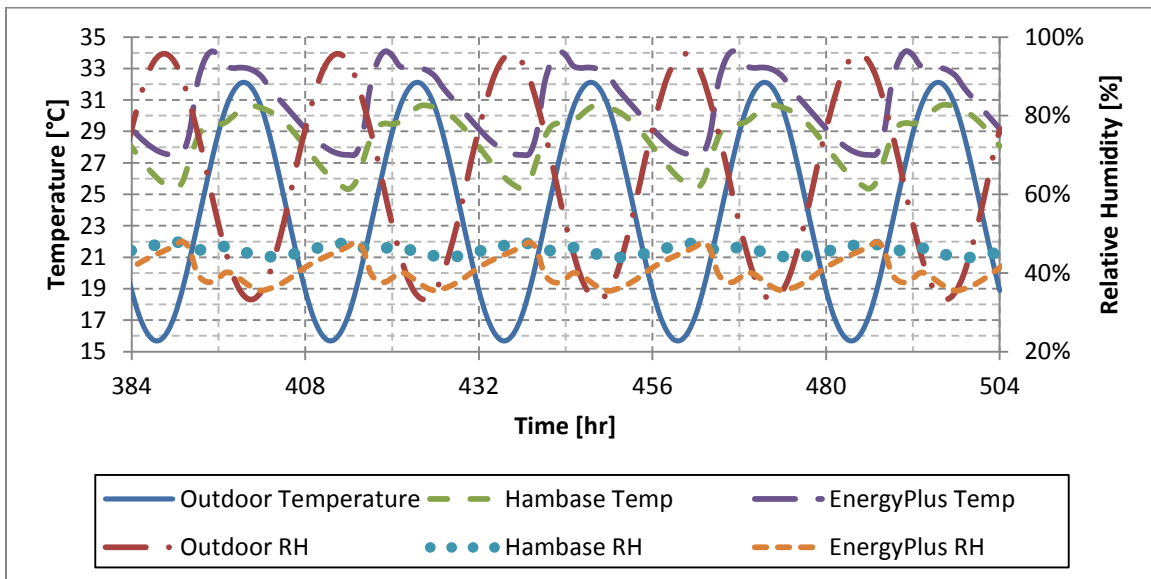


Figure 72: Open-loop steady-state response of East2 to weather-sine input

The amplitude of the temperature response for perimeter zones is almost identical between HAMBASE and EnergyPlus, resulting from a greater sensitivity to DNI and DHI by EnergyPlus (DNI and DHI are individually analyzed in Appendix A.5.2. and A.5.3.).

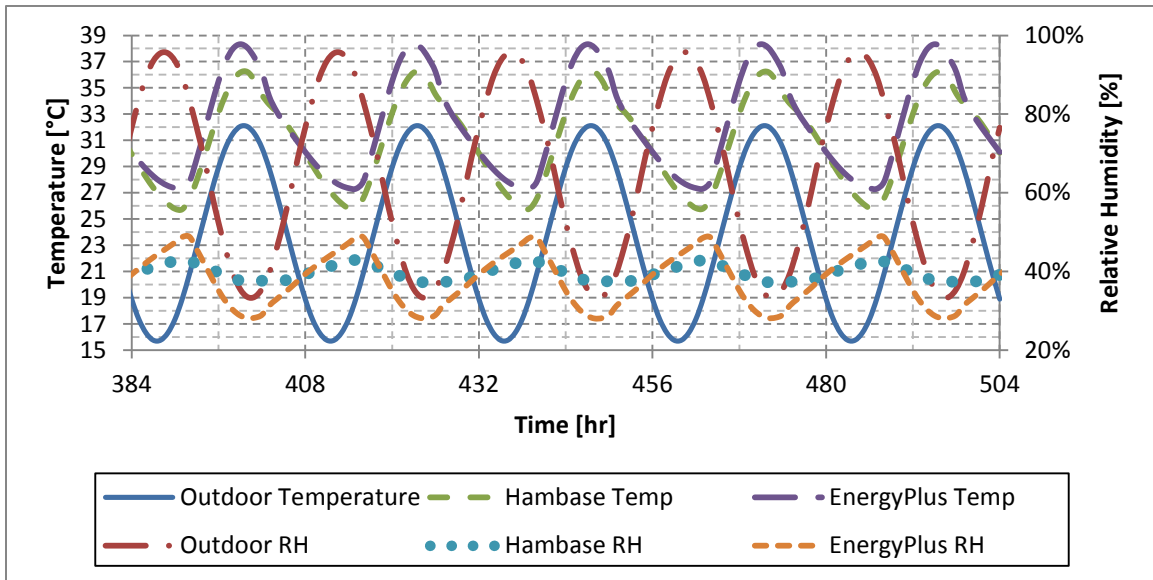


Figure 73: Open-loop steady-state response of South3 to weather-sine input

The amplitude of the temperature response for all zones, in addition to the steady-state maximum and minimum temperatures, is shown in Table 39. The steady-state temperatures for HAMBASE are again lower than EnergyPlus, but the increased temperature responsiveness of HAMBASE (seen in the core zones) was approximately balanced by EnergyPlus' sensitivity to solar irradiance (seen in the perimeter zones).

Table 39: Temperature results for open-loop weather-sine input

Zone	Steady-State Max Temperature [°C]			Steady-State Min Temperature [°C]			Steady-State Amplitude (Max-Min) [°C]		
	HB	EP	Diff.	HB	EP	Diff.	HB	EP	Diff.
Core1	29.6	30.5	-0.9	26.2	29.3	-3.1	3.4	1.1	2.3
South1	24.4	25.0	-0.6	22.6	23.5	-0.9	1.8	1.5	0.2
East1	23.7	25.4	-1.7	22.6	23.4	-0.8	1.1	1.9	-0.8
North1	23.6	24.4	-0.7	22.6	23.4	-0.8	1.1	1.0	0.1
West1	25.2	25.7	-0.4	22.6	23.4	-0.8	2.6	2.2	0.4
Plenum1	23.7	24.6	-0.9	23.0	24.3	-1.3	0.7	0.3	0.4
Core2	23.6	24.8	-1.2	23.3	24.6	-1.3	0.3	0.2	0.0
South2	24.3	25.3	-1.0	23.0	23.9	-0.9	1.3	1.4	-0.1
East2	23.7	25.6	-1.9	22.9	23.8	-0.9	0.8	1.8	-1.0
North2	23.6	24.7	-1.1	22.9	23.8	-0.9	0.7	0.9	-0.2
West2	24.8	25.8	-1.1	23.0	23.8	-0.9	1.8	2.0	-0.2
Plenum2	23.8	24.7	-0.9	23.4	24.4	-1.0	0.5	0.3	0.1
Core3	24.3	24.6	-0.3	23.4	24.2	-0.8	0.9	0.4	0.4
South3	24.7	25.1	-0.4	23.0	23.6	-0.5	1.6	1.5	0.1
East3	24.0	25.2	-1.1	23.0	23.5	-0.5	1.0	1.7	-0.6
North3	24.0	24.4	-0.4	23.0	23.5	-0.5	1.0	0.9	0.1
West3	25.2	25.6	-0.4	23.0	23.5	-0.5	2.2	2.0	0.1
Plenum3	25.8	24.1	1.7	22.8	23.1	-0.3	3.0	1.0	2.0
Average	24.6	25.3	-0.7	23.1	24.1	-0.9	1.4	1.2	0.2

Results for relative humidity are shown in Table 40. Relative humidity response corresponds with results from previous tests.

Table 40: Relative humidity results for open-loop weather-sine input

Zone	Steady-State Max. RH [%]			Steady-State Min. RH [%]			Steady-State Amplitude (Max-Min) [%]		
	HB	EP	Diff.	HB	EP	Diff.	HB	EP	Diff.
Core1	47.0	41.0	6.1	44.3	38.1	6.2	2.8	2.9	-0.2
South1	47.0	45.7	1.3	45.1	41.6	3.5	1.9	4.1	-2.2
East1	47.4	45.9	1.5	46.2	40.9	5.3	1.1	5.0	-3.9
North1	47.5	46.1	1.4	46.5	43.2	3.3	1.0	2.9	-1.9
West1	47.0	45.9	1.1	44.3	40.2	4.1	2.6	5.7	-3.0
Plenum1	46.4	43.7	2.7	46.0	42.6	3.3	0.5	1.1	-0.6
Core2	49.4	43.4	6.0	49.3	42.4	6.8	0.1	0.9	-0.8
South2	46.2	44.7	1.5	45.2	41.0	4.2	1.0	3.7	-2.7
East2	46.6	44.9	1.7	45.9	40.3	5.6	0.6	4.5	-3.9
North2	46.7	44.9	1.8	46.2	42.4	3.8	0.5	2.5	-2.0
West2	46.2	44.8	1.4	44.7	39.8	4.9	1.5	5.0	-3.5
Plenum2	45.6	43.4	2.2	45.3	42.3	3.0	0.3	1.1	-0.7
Core3	49.4	44.5	4.9	48.9	43.0	5.9	0.5	1.5	-1.0
South3	45.6	45.5	0.1	44.5	41.5	2.9	1.1	3.9	-2.8
East3	45.9	45.7	0.2	45.2	41.4	3.9	0.7	4.3	-3.6
North3	46.0	45.7	0.4	45.4	43.0	2.4	0.6	2.6	-2.0
West3	45.6	45.6	-0.1	44.0	40.4	3.6	1.6	5.2	-3.7
Plenum3	46.0	46.7	-0.8	42.0	43.9	-2.0	4.0	2.8	1.2
Average	46.7	44.9	1.9	45.5	41.6	3.9	1.2	3.3	-2.1

The results of tests 1-4 show that HAMBASE has good agreement with EnergyPlus for steady-state temperature and steady-state relative humidity. The main differences between the models show that HAMBASE has faster temperature response to changes in outdoor air temperature, slower temperature response to solar irradiance, and slower response to relative humidity.

Based on these tests, temperature, humidity and solar irradiance will contribute significantly to different heating and cooling totals in the two models.

5.3.5. Test Set 5: Open-Loop, Actual Weather, No Internal Loads

In Test Set 5, the actual TMY3 weather file was used. The HVAC system was still turned off and internal loads and ventilation were still set to zero. Figure 74 and Figure 75 show the temperature and relative humidity response of Core1 for one year and five days, respectively.

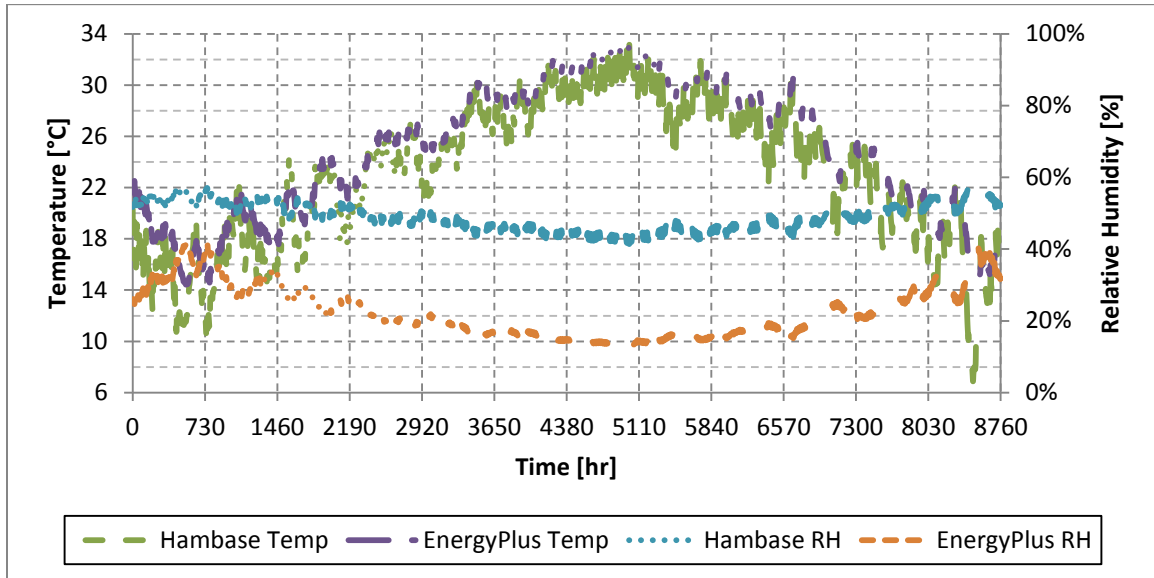


Figure 74: Open-loop response of Core1 to actual weather input for one year

The results of Test Sets 1-4 explain the results seen in the core zones. The core zones are not exposed to DNI or DHI, meaning that temperature responds faster in HAMBASE as seen by the thickness (amplitude) of the temperature plot in Figure 74. HAMBASE has lower temperatures. Relative humidity in HAMBASE is less responsive and has an initial condition of 50% with no warm-up period, meaning that it starts around 50% RH and basically remains there. The warm-up period in EnergyPlus results in lower initial relative humidity and the greater responsiveness results in a larger range of values. The humidity in core zones does not change rapidly in either program due to the absence of moisture transport.

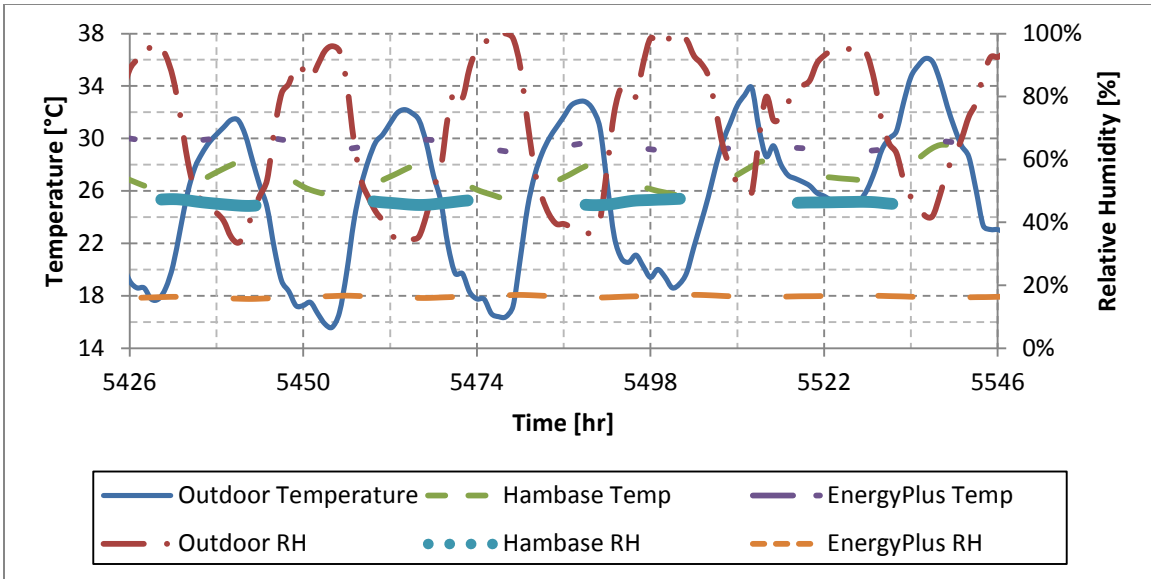


Figure 75: Open-loop response of Core1 to actual weather input for Aug 15–19

The results for the perimeter zones, shown in Figure 76 through Figure 79, again display the effect infiltration and radiation have on the zone responses. The temperature and relative humidity for East2 and South3 are much more responsive than Core1.

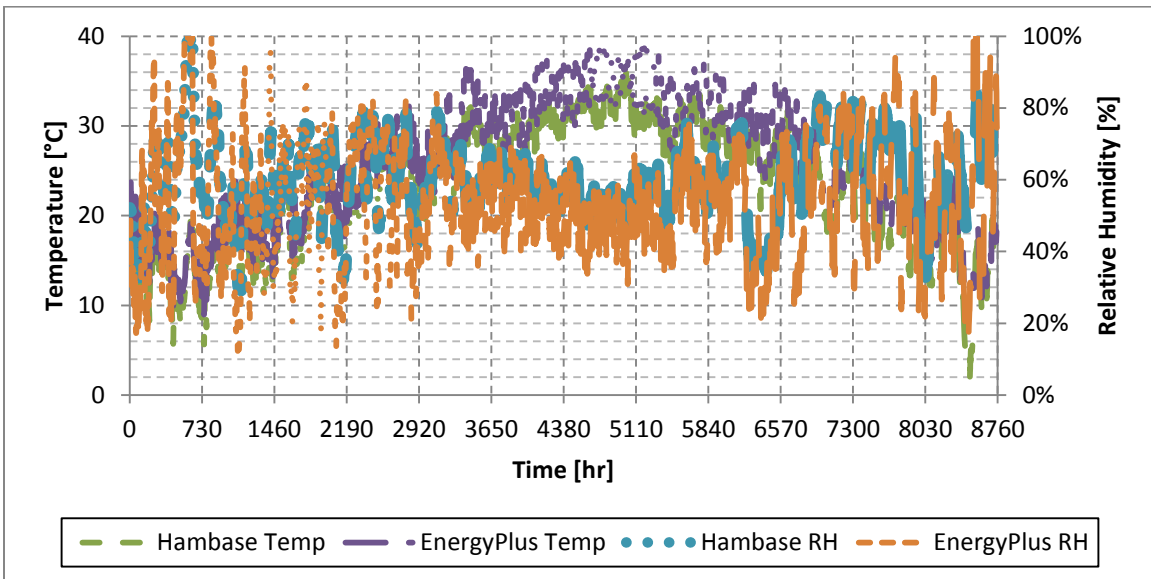


Figure 76: Open-loop response of East2 to actual weather input for one year

The temperature responses for the two programs more closely match due to EnergyPlus' sensitivity to solar radiation. East2 again shows bimodal temperature peaks due to early morning DNI and early afternoon DHI and outdoor air temperatures.

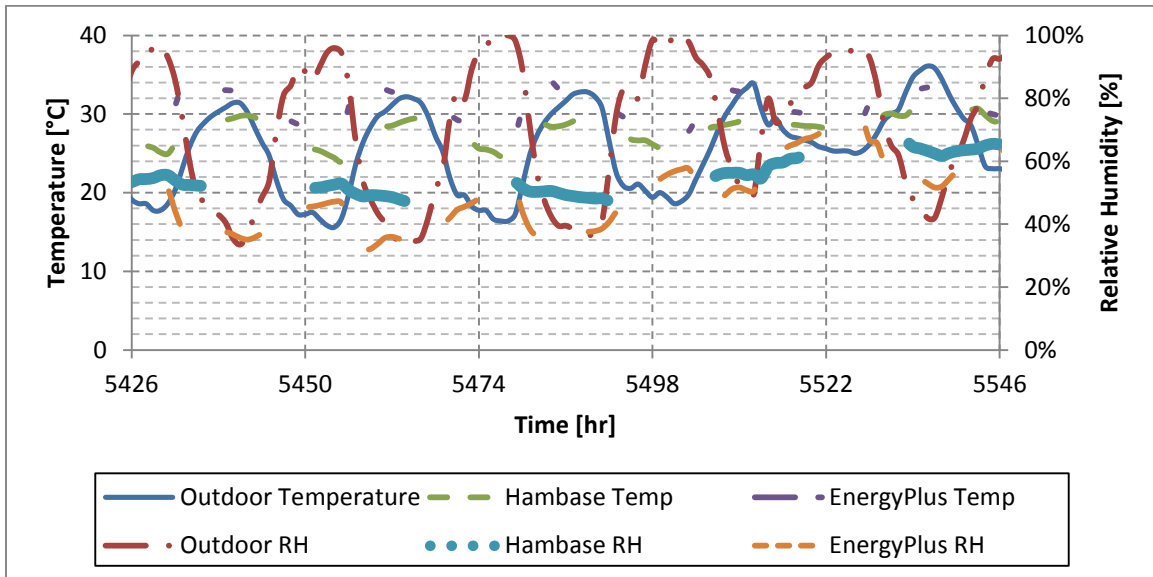


Figure 77: Open-loop response of East2 to actual weather input for Aug 15–19

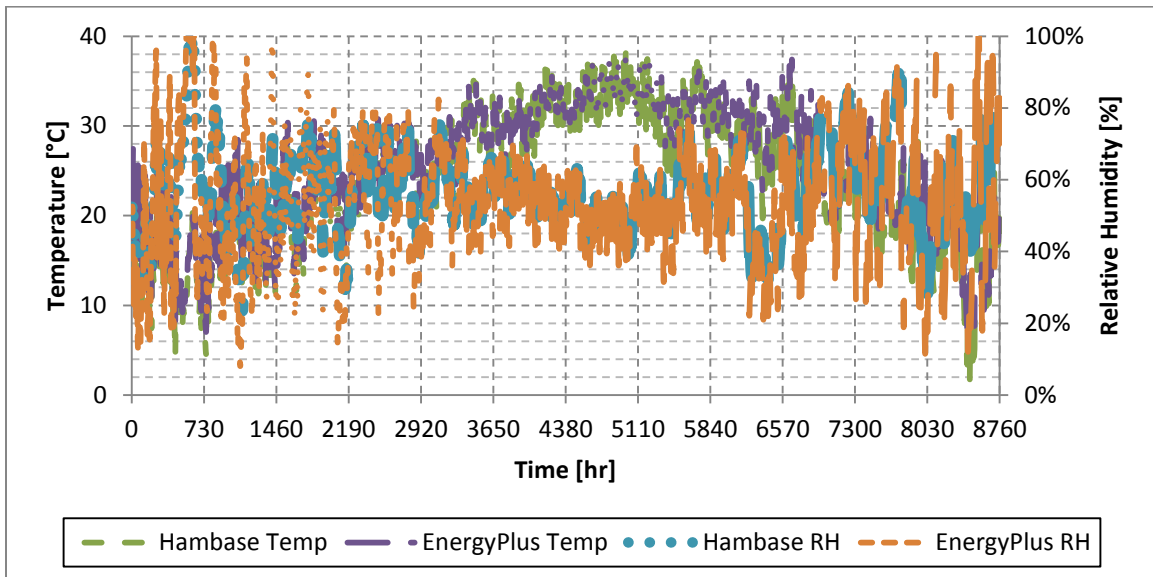


Figure 78: Open-loop response of South3 to actual weather input for one year

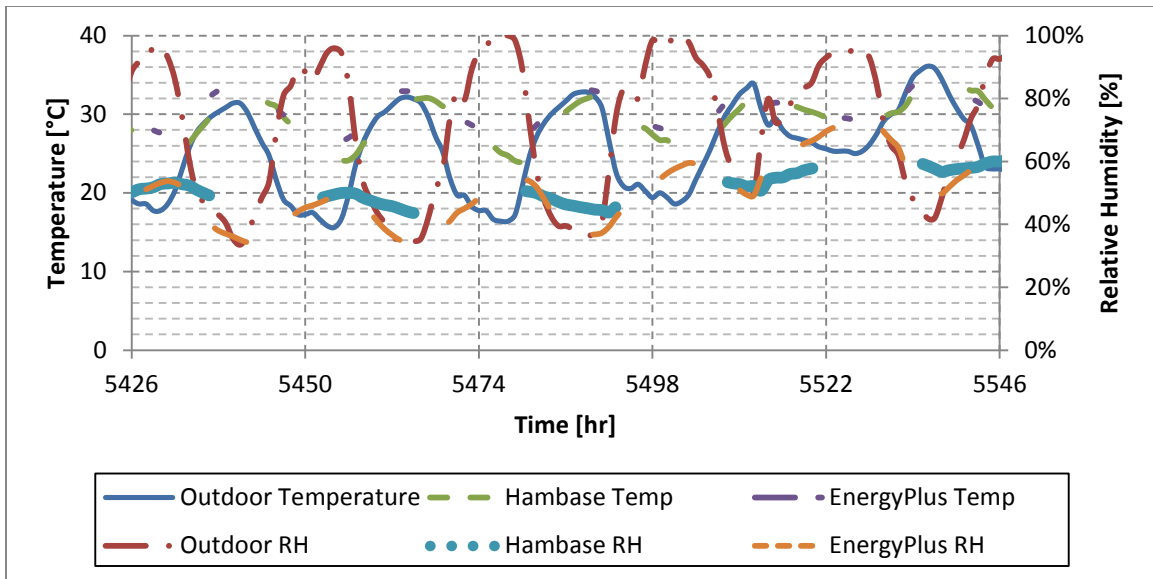


Figure 79: Open-loop response of South3 to actual weather input for Aug 15–19

Comparing the annual maximum and minimum temperatures, as seen in Table 41, brings together the testing standards and open-loop tests. Annual maximum temperatures show close alignment between HAMBASE and EnergyPlus. Every zone except for Plenum3 falls within the ASHRAE test range of 4.6°C shown in Section 5.2.3.

The annual minimum temperatures do not show a similar level of alignment. Results from the previous open-loop tests revealed HAMBASE to have a greater sensitivity to outdoor air temperature, and EnergyPlus to have a greater sensitivity to solar irradiance. During winter conditions, these respective sensitivities combine to form lower zone temperatures in HAMBASE than in EnergyPlus, which corresponds to a greater difference in annual minimum hourly temperature.

The annual average temperatures show closer alignment than the minimum temperatures. While 10 of the 18 zones fall outside of the ASHRAE test range of 1.7°C, this result is directly in line with the lower minimum temperatures found in HAMBASE.

Table 41: Temperature results for open-loop actual weather input

Zone	Annual Max. Hourly Temperature [°C]			Annual Min. Hourly Temperature [°C]			Annual Avg. Hourly Temperature [°C]		
	HB	EP	Diff.	HB	EP	Diff.	HB	EP	Diff.
Core1	33.2	33.3	-0.1	6.9	13.2	-6.3	23.0	24.9	-1.8
South1	36.0	36.5	-0.5	3.0	10.2	-7.2	23.1	25.1	-2.0
East1	35.9	39.1	-3.2	2.7	8.9	-6.2	22.7	24.8	-2.1
North1	36.1	35.3	0.8	2.7	8.9	-6.2	22.4	23.9	-1.5
West1	42.4	41.8	0.7	2.8	9.3	-6.5	23.3	25.0	-1.7
Plenum1	34.9	35.3	-0.3	4.6	11.2	-6.7	23.2	25.2	-1.9
Core2	34.7	35.9	-1.2	4.3	10.1	-5.8	23.5	25.5	-2.0
South2	35.8	37.2	-1.4	2.3	8.1	-5.9	23.4	25.4	-2.0
East2	36.1	40.5	-4.4	2.0	7.4	-5.3	23.1	25.2	-2.1
North2	36.2	37.1	-1.0	2.0	7.5	-5.4	22.8	24.5	-1.7
West2	40.9	43.1	-2.2	2.1	7.7	-5.5	23.6	25.4	-1.8
Plenum2	36.3	36.7	-0.4	3.1	8.7	-5.6	23.8	25.3	-1.5
Core3	39.2	37.9	1.3	2.2	6.9	-4.7	24.4	25.2	-0.7
South3	39.2	38.3	0.9	0.8	5.4	-4.6	24.0	25.2	-1.1
East3	39.2	40.3	-1.1	0.6	4.6	-4.1	23.7	25.0	-1.2
North3	39.5	38.6	0.9	0.6	4.7	-4.1	23.5	24.3	-0.8
West3	44.1	44.4	-0.3	0.7	4.9	-4.3	24.2	25.1	-0.9
Plenum3	47.9	41.2	6.7	-0.8	2.6	-3.4	25.1	24.2	1.0
Average	38.2	38.5	-0.3	2.4	7.8	-5.4	23.5	25.0	-1.5

Based on this test, HAMBASE is consistently displaying lower minimum temperatures and equivalent maximum temperatures. This finding aligns with the results from tests 1-4. The result of this difference will be an increased need for heating in HAMBASE than in EnergyPlus, because the temperature response of the conditioned zones is so much faster in HAMBASE.

The relative humidity data for each zone is shown in Table 42. On average there is close alignment between EnergyPlus and HAMBASE, but EnergyPlus has larger extremes. In particular, the core zones and plenum zones show the largest discrepancy between EnergyPlus and HAMBASE. These results agree with previous tests that showed EnergyPlus was much more responsive to humidity changes.

Table 42: Relative humidity results for open-loop actual weather input

Zone	Annual Max. Hourly RH [%]			Annual Min. Hourly RH [%]			Annual Avg. Hourly RH [%]		
	HB	EP	Diff.	HB	EP	Diff.	HB	EP	Diff.
Core1	58.3	44.5	13.8	41.4	13.0	28.4	49.0	22.6	26.4
South1	98.5	100.0	-1.5	20.4	7.2	13.2	59.9	54.3	5.6
East1	99.1	100.0	-0.9	22.4	10.0	12.5	61.3	54.9	6.4
North1	99.1	100.0	-0.9	23.4	11.0	12.4	62.4	57.5	4.9
West1	98.8	100.0	-1.2	21.3	7.8	13.5	59.0	54.3	4.7
Plenum1	89.9	100.0	-10.1	33.1	12.2	20.9	59.8	53.8	6.0
Core2	55.6	54.5	1.1	43.1	11.3	31.8	49.0	22.4	26.6
South2	99.9	100.0	-0.1	23.8	7.5	16.3	58.9	53.2	5.8
East2	100.0	100.0	0.0	25.8	10.1	15.7	60.1	53.7	6.4
North2	100.0	100.0	0.0	26.7	10.9	15.8	61.0	55.5	5.5
West2	100.0	100.0	0.0	24.7	8.0	16.8	58.3	53.3	5.0
Plenum2	91.3	100.0	-8.7	33.0	12.5	20.6	57.8	53.3	4.6
Core3	56.1	68.3	-12.2	40.2	10.1	30.0	48.5	23.3	25.1
South3	98.6	100.0	-1.4	23.5	8.0	15.5	56.7	53.9	2.8
East3	99.1	100.0	-0.9	25.5	10.7	14.8	57.9	54.4	3.5
North3	99.2	100.0	-0.8	26.4	11.5	14.9	58.7	56.2	2.5
West3	98.8	100.0	-1.2	24.4	8.4	16.0	56.2	54.1	2.1
Plenum3	100.0	100.0	0.0	12.2	9.6	2.6	53.9	57.1	-3.2
Average	91.2	92.6	-1.4	27.3	10.0	17.3	63.9	82.6	7.8

Based on this test, external weather will contribute significantly to different heating and cooling totals in the two models.

5.3.6. Test Set 6: Open-Loop, Constant Weather, Actual Internal Loads

Test Set 6 shifts the focus from external weather to internal loads. For this test, all of the actual loads, including both their magnitudes and schedules, were used. Detailed description of the loads and schedules can be found in Section 3.5, and a summary of the internal load profiles found in Section 3.5.6. The constant weather file described previously in Table 32 was used to eliminate weather effects.

Similar tests for internal loads were also completed and can be found in Appendix A.5.4. for people loads and Appendix A.5.5. for equipment loads.

The temperature and relative humidity response for Core1 is shown in Figure 80 with 22 days of data and in Figure 81 with six days of data. The effect of the warm-up period in EnergyPlus can be seen by the initial zone conditions; 26°C (78.8°F) for EnergyPlus and 22°C (71.6°F) for HAMBASE. Once the models reach steady-state they behave in a similar periodic manner, with both peaks and troughs matching. The amplitude of the HAMBASE response is larger than EnergyPlus again, just as was found in the weather tests. HAMBASE both gains and loses temperature faster than EnergyPlus.

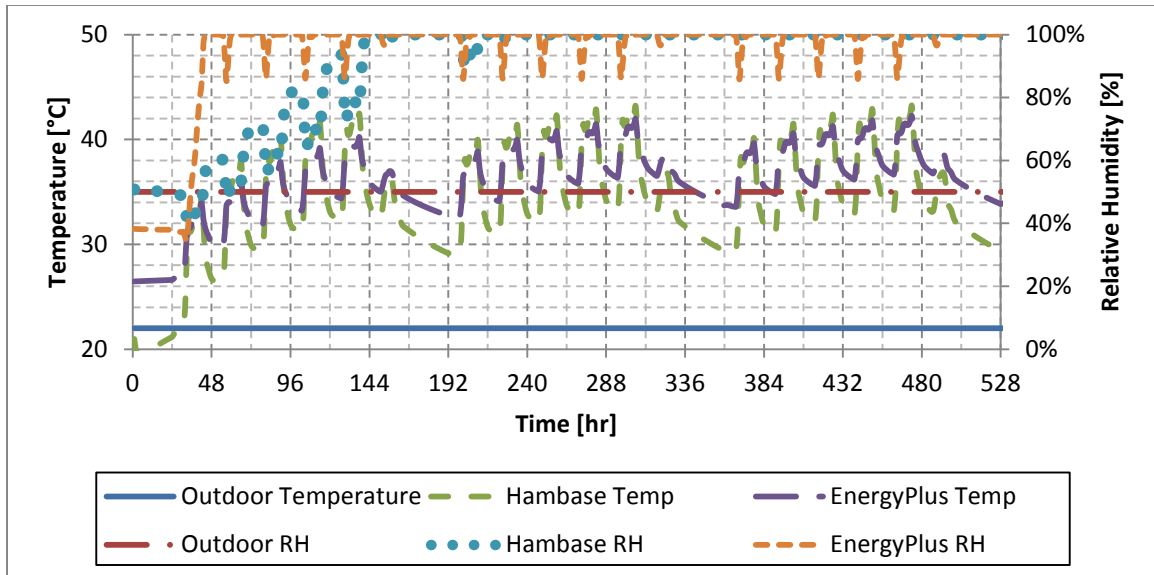


Figure 80: Open-loop response of Core1 to actual internal loads

The detailed data in Figure 81 further highlights the difference in temperature response, as the HAMBASE zone temperature closely matches the spikes in the load schedule while the EnergyPlus zone temperature is smoother.

The relative humidity response of both EnergyPlus and HAMBASE goes to 100% due to the large latent load from people and the lack of moisture transport in the core zones when ventilation is off.

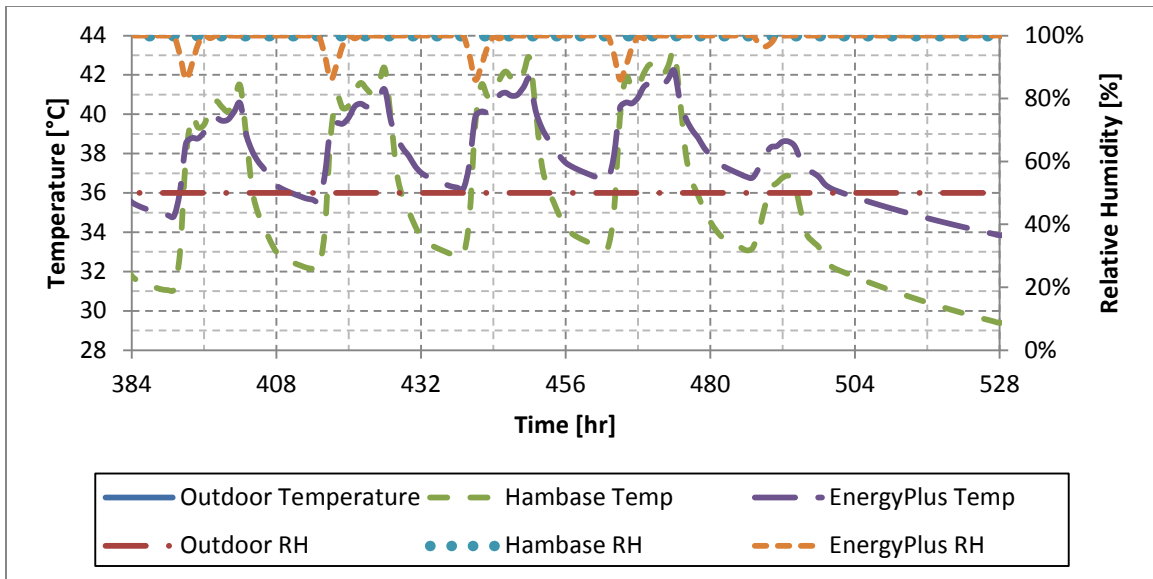


Figure 81: Open-loop steady-state response of Core1 to actual internal loads

The responses for perimeter zones East2 and South3 are shown in Figure 82 and Figure 83 respectively. In these zones, the trends of the HAMBASE temperatures match the trends of the EnergyPlus temperatures in everything but the steady-state value. They have similar periods, similar peaks and troughs and similar amplitudes. The faster temperature response of HAMBASE can still be seen during the Sunday operation in hours 504 to 528. During this period of no internal loads, the HAMBASE temperatures fall-off toward the outdoor air temperature faster than in EnergyPlus.

The relative humidity responses for HAMBASE and EnergyPlus have similar steady-state values, but where the EnergyPlus response oscillates with an amplitude of 10%, the HAMBASE response barely moves. There are three factors contributing to the value of the zone relative humidity: infiltration of outdoor air, internal latent loads and changing indoor air temperature. Based on the lack of sensitivity of HAMBASE to relative humidity in general, this response is reasonable.

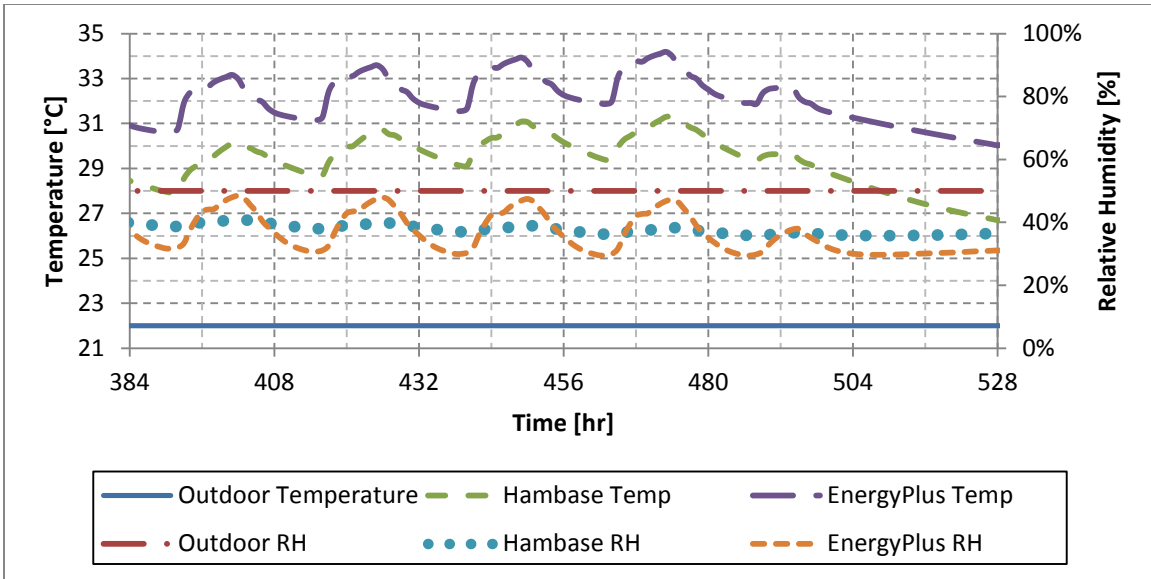


Figure 82: Open-loop steady-state response of East2 to actual internal loads

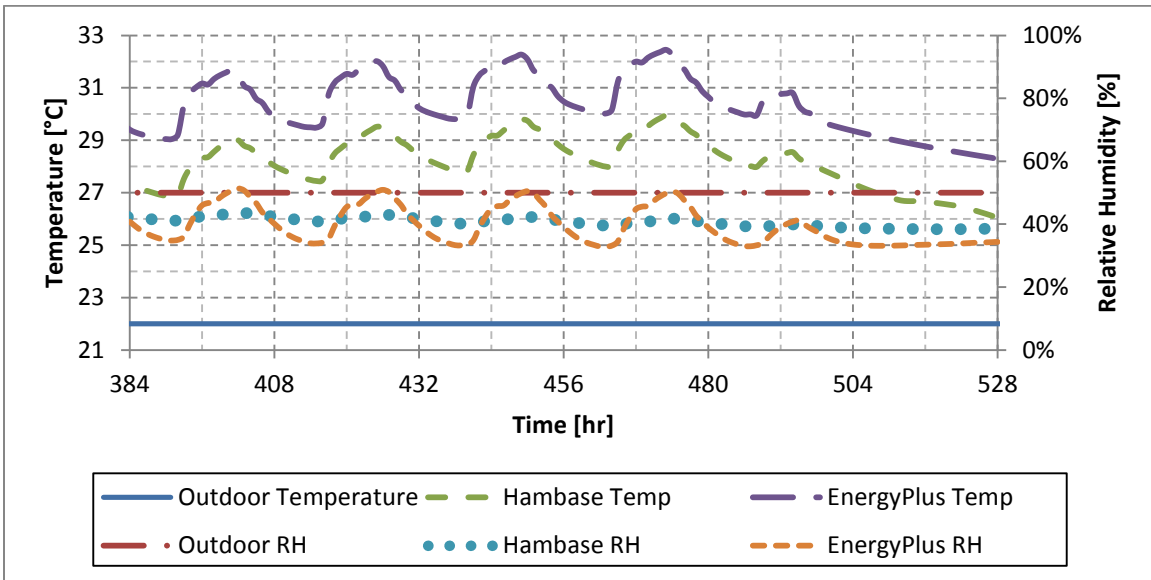


Figure 83: Open-loop steady-state response of South3 to actual internal loads

A summary of the temperature results for Test Set 6 are shown in Table 43. The maximum and minimum temperatures in EnergyPlus are consistently higher than in HAMBASE, but HAMBASE has slightly greater amplitude. This implies that the two

programs have an approximately equivalent sensitivity to internal loads, but the external temperature sensitivity of HAMBASE prevents a closer match.

Table 43: Temperature results for open-loop, actual internal load input

Zone	Steady-State Max Temperature [°C]			Steady-State Min Temperature [°C]			Steady-State Amplitude (Max-Min) [°C]		
	HB	EP	Diff.	HB	EP	Diff.	HB	EP	Diff.
Core1	43.2	42.3	0.9	29.4	33.8	-4.4	13.8	8.5	5.3
South1	32.0	34.2	-2.2	26.1	29.6	-3.5	5.9	4.6	1.3
East1	31.7	34.0	-2.2	26.0	29.4	-3.4	5.7	4.6	1.2
North1	32.0	34.2	-2.3	26.1	29.6	-3.5	5.9	4.6	1.3
West1	31.7	34.0	-2.2	26.0	29.4	-3.4	5.7	4.6	1.2
Plenum1	35.5	36.1	-0.6	27.9	32.1	-4.2	7.6	4.0	3.6
Core2	36.0	38.8	-2.8	28.9	33.5	-4.6	7.1	5.3	1.8
South2	31.4	34.5	-3.0	26.6	30.2	-3.6	4.8	4.3	0.6
East2	31.3	34.2	-2.9	26.5	30.0	-3.5	4.8	4.2	0.5
North2	31.4	34.5	-3.0	26.6	30.2	-3.6	4.8	4.3	0.5
West2	31.3	34.2	-2.9	26.5	30.0	-3.5	4.8	4.2	0.5
Plenum2	33.2	34.2	-1.0	27.5	31.0	-3.5	5.7	3.2	2.5
Core3	33.8	36.0	-2.2	27.8	30.8	-3.0	6.1	5.2	0.9
South3	30.0	32.5	-2.5	25.8	28.3	-2.5	4.1	4.2	0.0
East3	29.8	32.3	-2.5	25.8	28.2	-2.4	4.0	4.1	-0.1
North3	30.0	32.5	-2.5	25.8	28.3	-2.5	4.1	4.2	0.0
West3	29.8	32.3	-2.5	25.8	28.2	-2.4	4.0	4.1	-0.1
Plenum3	30.2	29.7	0.5	25.5	26.9	-1.3	4.7	2.9	1.8
Average	32.5	34.5	-2.0	26.7	30.0	-3.3	5.8	4.5	1.3

A summary of the relative humidity results for Test Set 6 are shown in Table 44. The maximum relative humidity values in EnergyPlus are higher, the minimum values are lower and the amplitude values are greater than in HAMBASE.

Table 44: Relative humidity results for open-loop, actual internal load input

Zone	Steady-State Max. RH [%]			Steady-State Min. RH [%]			Steady-State Amplitude (Max-Min) [%]		
	HB	EP	Diff.	HB	EP	Diff.	HB	EP	Diff.
Core1	100.0	100.0	0.0	100.0	85.9	14.1	0.0	14.1	-14.1
South1	41.6	49.7	-8.1	36.4	30.4	6.0	5.2	19.4	-14.2
East1	41.7	49.1	-7.4	36.6	30.5	6.1	5.1	18.6	-13.5
North1	41.6	49.7	-8.0	36.4	30.3	6.1	5.2	19.4	-14.2
West1	41.7	49.1	-7.4	36.6	30.5	6.1	5.1	18.6	-13.5
Plenum1	31.4	27.7	3.7	25.4	22.1	3.3	6.0	5.6	0.4
Core2	100.0	100.0	0.0	100.0	97.4	2.6	0.0	2.6	-2.6
South2	41.0	49.6	-8.7	35.8	29.2	6.5	5.2	20.4	-15.2
East2	40.8	49.0	-8.1	35.8	29.3	6.4	5.1	19.7	-14.6
North2	41.0	49.6	-8.7	35.8	29.2	6.5	5.2	20.4	-15.2
West2	40.8	49.0	-8.1	35.8	29.3	6.4	5.1	19.7	-14.6
Plenum2	32.5	29.5	3.0	27.8	24.5	3.4	4.7	5.0	-0.3
Core3	100.0	100.0	0.0	100.0	96.6	3.4	0.0	3.4	-3.4
South3	43.6	51.8	-8.2	38.4	32.8	5.6	5.2	19.0	-13.9
East3	43.4	51.2	-7.7	38.4	32.8	5.6	5.0	18.4	-13.3
North3	43.6	51.8	-8.2	38.4	32.8	5.6	5.2	19.0	-13.8
West3	43.4	51.2	-7.7	38.4	32.8	5.6	5.0	18.4	-13.3
Plenum3	39.7	37.4	2.3	31.8	31.6	0.2	7.9	5.8	2.1
Average	50.4	55.3	-4.9	46.0	40.4	5.5	4.5	14.9	-10.4

The results of the open-loop, actual internal load test show a close match between EnergyPlus and HAMBASE in terms of their responsiveness to internal loads. The differences in response are attributable to the results of previous open-loop tests, specifically the faster temperature response of HAMBASE and the faster humidity response of EnergyPlus.

Based on this test, internal loads will not contribute significantly to different heating and cooling totals in the two models.

5.3.7. Test Set 7: Open-Loop, Actual Weather, Actual Internal Loads

The final open-loop test uses the actual weather file and the actual internal loads as the inputs to the model. The response of the Core1 zone is shown in Figure 84 for a full year of data. Detailed six-day responses during winter conditions and summer conditions are shown in Figure 85 and Figure 86 respectively.

The responses to Test Set 7 are a superposition of the responses found in Test Set 5 and Test Set 6. HAMBASE and EnergyPlus still display different initial conditions resulting from the warm-up period in EnergyPlus. HAMBASE still displays greater responsiveness to outdoor temperature, as evidenced by the larger amplitude of temperature oscillations and the faster night and weekend temperature fall-off. EnergyPlus still displays greater relative humidity responsiveness, as evidenced by the nightly fluctuations in relative humidity by EnergyPlus.

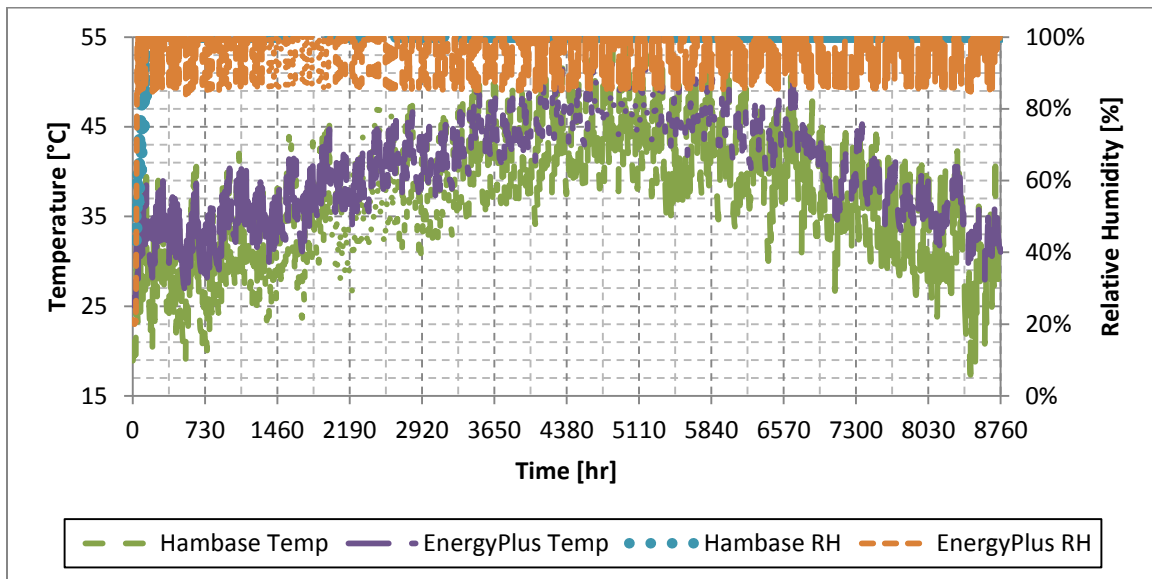


Figure 84: Open-loop response of Core1 to actual internal loads and weather for one year

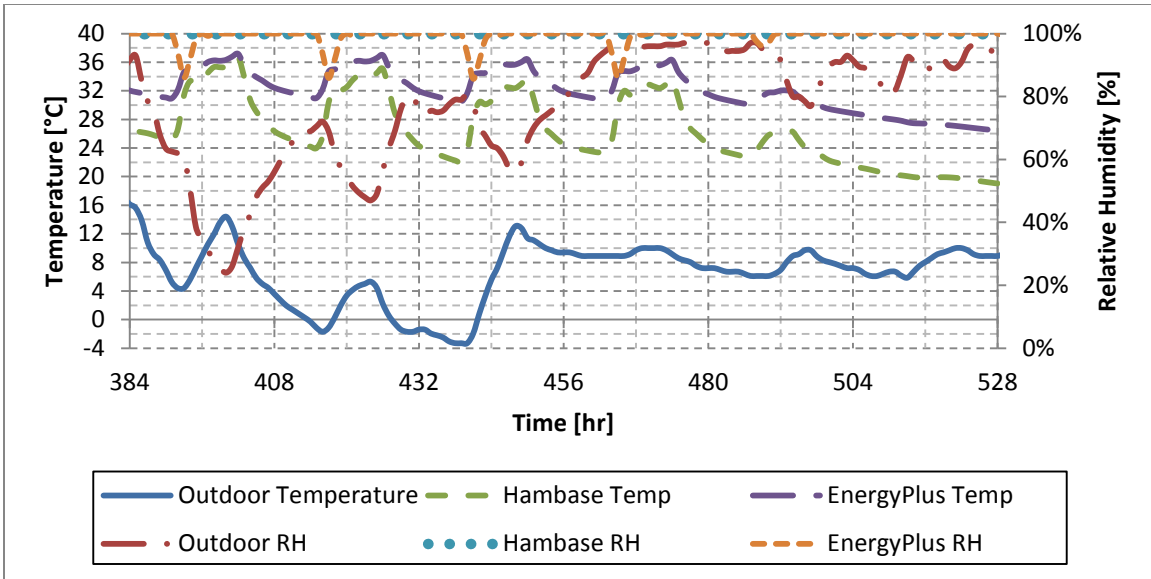


Figure 85: Open-loop winter response of Core1 to actual internal loads and weather

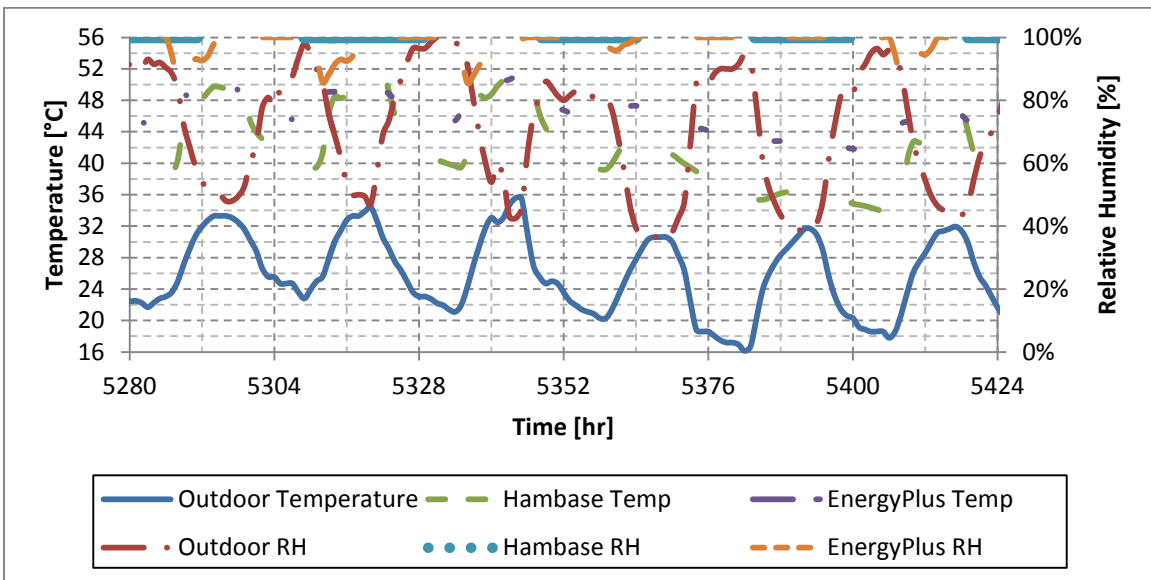


Figure 86: Open-loop summer response of Core1 to actual internal loads and weather

Looking at the perimeter zones continues the superposition trend. EnergyPlus' greater sensitivity to DNI can be seen by comparing summer and winter responses in East2 in Figure 87 and Figure 88. Winter DNI is less than summer DNI, and the EnergyPlus zone temperature amplitude is greater in summer (Figure 88) than in winter

(Figure 87) as a result. HAMBASE, with its smaller sensitivity to DNI, has a less pronounced response.

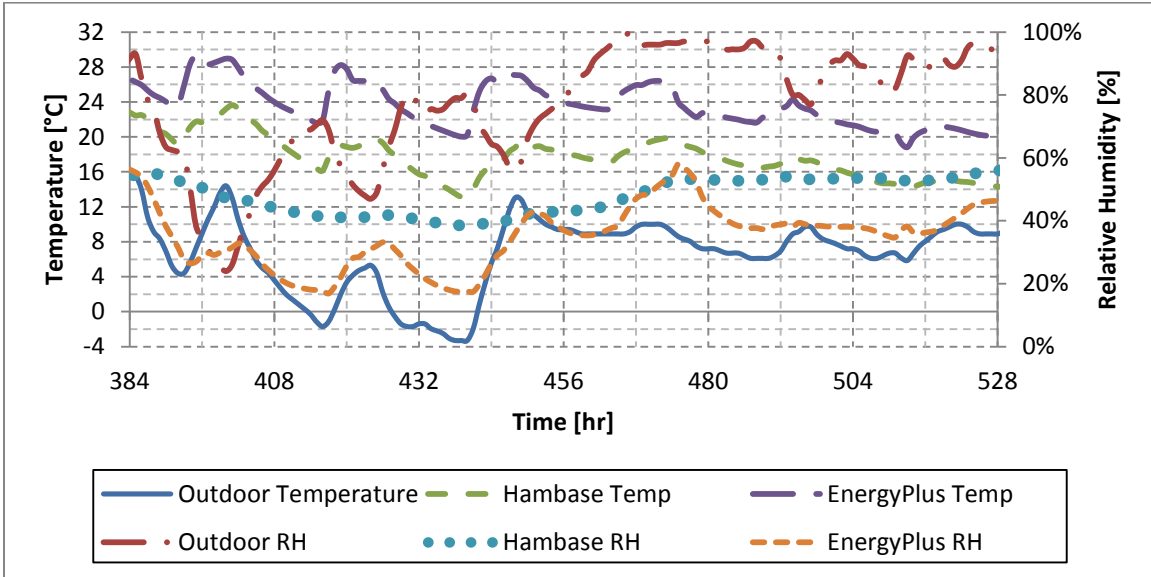


Figure 87: Open-loop winter response of East2 to actual internal loads and weather

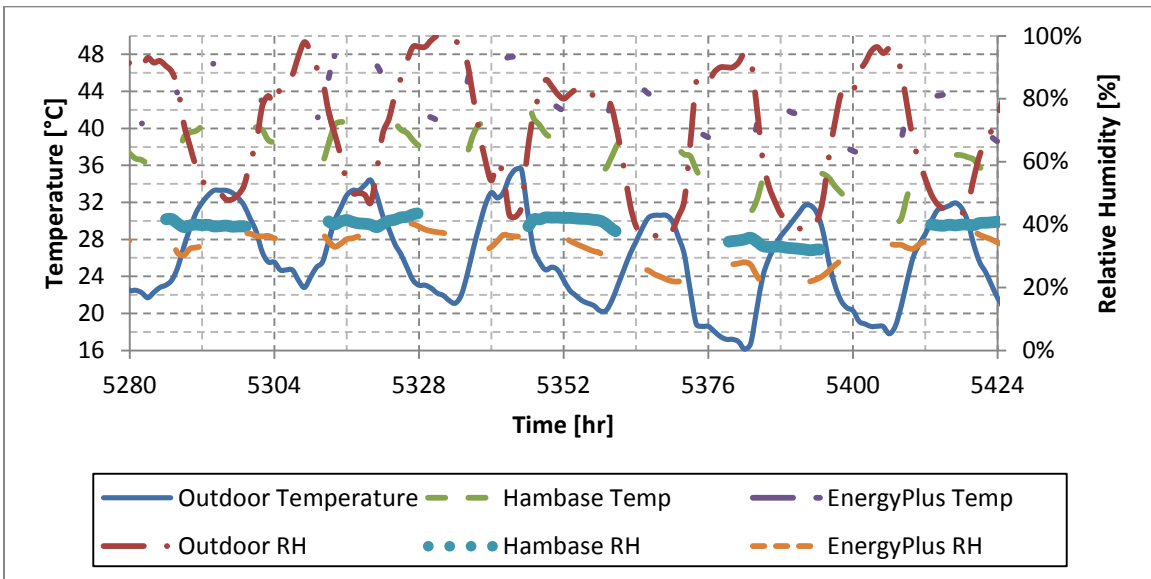


Figure 88: Open-loop summer response of East2 to actual internal loads and weather

The response of South3 also shows this effect, seen in Figure 89 and Figure 90.

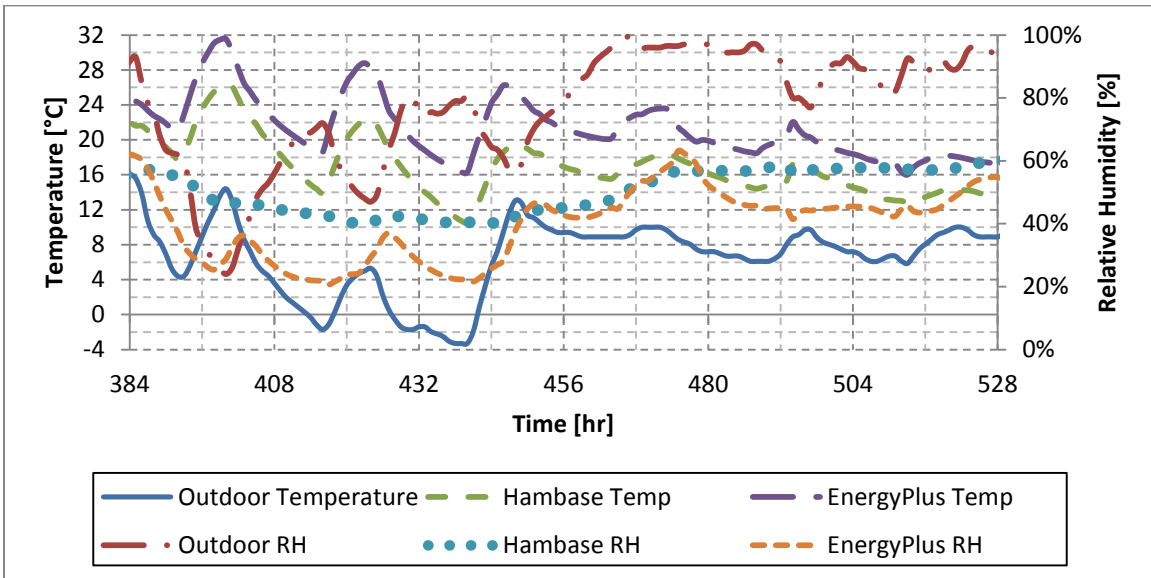


Figure 89: Open-loop winter response of South3 to actual internal loads and weather

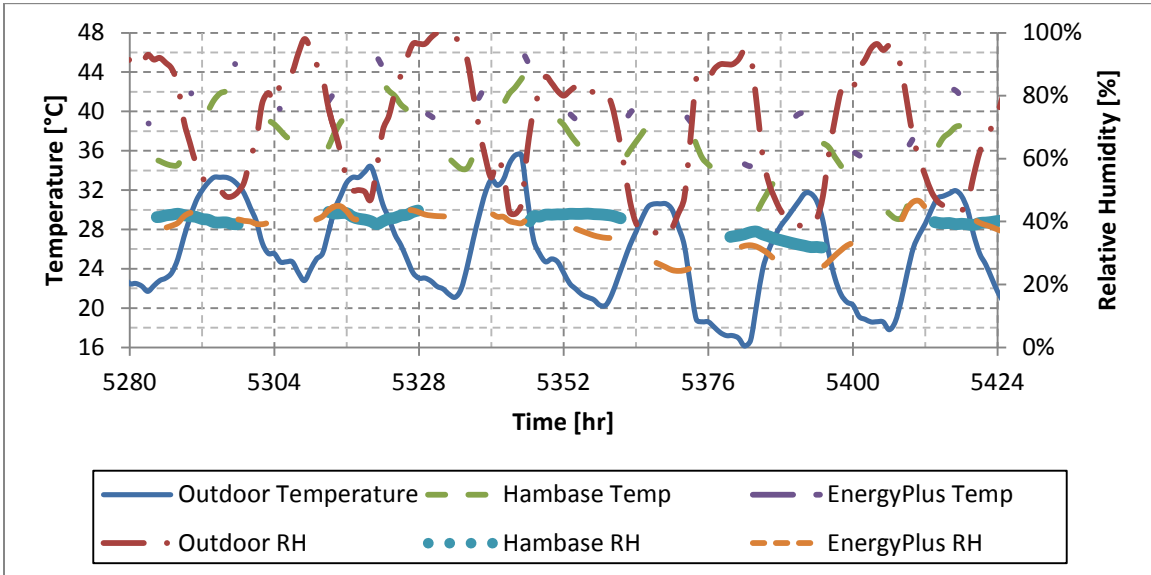


Figure 90: Open-loop summer response of South3 to actual internal loads and weather

The south zone only experiences significant DNI during winter. During summer, the sun is too high in the sky to provide significant DNI to a south zone. As a result, the

temperature response amplitude for EnergyPlus in the winter is almost identical to the amplitude in summer, even though the summer air temperature is approximately 20°C greater than the winter air temperature. HAMBASE is less responsive to DNI and more responsive to outdoor air temperature, so the summer temperature response amplitude is greater than the winter amplitude.

Temperature results for each zone are shown in Table 45.

Table 45: Temperature results for open-loop, actual internal load and weather input

Zone	Annual Max. Hourly Temperature [°C]			Annual Min. Hourly Temperature [°C]			Annual Avg. Hourly Temperature [°C]		
	HB	EP	Diff.	HB	EP	Diff.	HB	EP	Diff.
Core1	54.5	52.9	1.5	17.2	25.1	-7.8	36.4	40.1	-3.6
South1	45.6	47.7	-2.1	9.0	18.8	-9.7	30.2	34.8	-4.6
East1	45.2	49.5	-4.4	8.6	17.5	-9.0	29.6	34.4	-4.8
North1	46.1	46.9	-0.8	8.7	17.9	-9.2	29.4	33.8	-4.3
West1	52.2	52.6	-0.4	8.7	17.9	-9.2	30.2	34.5	-4.3
Plenum1	48.5	48.4	0.2	13.3	23.3	-10.1	33.1	36.9	-3.8
Core2	48.4	51.4	-3.0	14.7	23.9	-9.2	34.4	39.0	-4.6
South2	45.4	49.2	-3.8	9.1	17.5	-8.3	30.8	35.4	-4.6
East2	45.3	51.1	-5.8	8.9	16.7	-7.8	30.4	35.1	-4.7
North2	45.8	48.8	-3.0	8.8	17.1	-8.3	30.2	34.7	-4.4
West2	50.4	54.0	-3.6	8.8	16.9	-8.1	30.9	35.2	-4.3
Plenum2	47.4	48.1	-0.6	11.4	19.6	-8.2	32.6	35.7	-3.1
Core3	50.7	50.5	0.2	10.9	17.7	-6.9	33.6	36.2	-2.5
South3	47.1	48.3	-1.2	6.4	12.9	-6.5	30.3	33.4	-3.1
East3	47.1	49.0	-1.9	6.2	12.2	-6.0	29.9	33.1	-3.2
North3	47.5	48.2	-0.6	6.0	12.4	-6.4	29.7	32.6	-2.9
West3	52.1	53.5	-1.3	6.1	12.4	-6.3	30.4	33.2	-2.8
Plenum3	56.3	48.6	7.8	4.4	8.6	-4.2	31.5	30.7	0.8
Average	48.7	49.9	-1.3	9.3	17.1	-7.8	31.3	34.9	-3.6

The maximum annual temperature results show that every zone except East2 and Plenum3 falls within the ASHRAE test range of 4.6°C, as was the case in test 5. The minimum annual temperature results for HAMBASE are significantly lower than those seen in EnergyPlus. While the difference between the two programs falls outside of the

ASHRAE test range of 3.2°C, these results are in line with the results of previous tests. Just as in test 5, HAMBASE responds faster to outdoor temperature and slower to solar DNI, resulting in lower temperatures. The average annual temperature results also miss the ASHRAE test range of 1.7°C; however they are closer than the annual minimum test results, and also explained by the faster temperature response of HAMBASE.

Relative humidity results for each zone are shown in Table 46.

Table 46: Relative humidity results for open-loop, actual internal load and weather input

Zone	Annual Max. Hourly RH [%]			Annual Min. Hourly RH [%]			Annual Avg. Hourly RH [%]		
	HB	EP	Diff.	HB	EP	Diff.	HB	EP	Diff.
Core1	100.0	100.0	0.0	42.6	20.0	22.7	99.5	98.2	1.3
South1	75.7	76.3	-0.6	18.1	8.0	10.1	44.8	39.3	5.6
East1	76.2	76.1	0.0	19.5	9.7	9.9	46.0	39.4	6.6
North1	76.0	76.5	-0.4	20.4	9.9	10.5	46.6	40.7	5.9
West1	75.9	76.2	-0.3	18.6	9.7	8.9	44.4	39.0	5.4
Plenum1	54.0	56.2	-2.2	14.2	5.6	8.5	33.8	27.6	6.2
Core2	100.0	100.0	0.0	49.5	20.2	29.2	99.4	99.4	0.0
South2	75.8	78.5	-2.7	19.2	8.5	10.7	43.4	37.9	5.5
East2	76.1	78.1	-2.0	20.4	9.5	11.0	44.2	37.9	6.3
North2	76.2	78.5	-2.3	21.3	9.6	11.7	44.8	38.9	6.0
West2	76.0	78.1	-2.1	19.6	9.6	10.1	42.9	37.6	5.4
Plenum2	56.5	62.3	-5.8	15.6	6.3	9.3	34.7	29.4	5.3
Core3	100.0	100.0	0.0	48.6	21.7	26.9	99.5	98.9	0.6
South3	80.3	82.7	-2.4	20.8	10.8	10.1	44.7	41.6	3.1
East3	80.7	82.4	-1.7	22.2	11.5	10.8	45.6	41.6	4.0
North3	80.9	82.7	-1.9	23.2	11.6	11.6	46.2	42.6	3.6
West3	80.4	82.4	-2.0	21.3	11.6	9.7	44.3	41.2	3.0
Plenum3	80.9	81.9	-1.0	6.9	6.1	0.9	37.5	39.0	-1.6
Average	79.0	80.5	-1.5	23.5	11.1	12.4	55.5	69.4	4.0

The relative humidity results are the opposite of temperature. The greater responsiveness of EnergyPlus causes lower minimum relative humidity values and greater maximum relative humidity values. These results agree with the findings from earlier tests.

Based on this test, the greater responsiveness of HAMBASE to temperature will result in significantly different heating totals for the two models, while the greater responsiveness of EnergyPlus to humidity will result in significantly different latent cooling totals for the two models.

5.4. Closed-Loop Comparison of Integrated Model

Closed-loop evaluation of the integrated model compared the annual heating and annual cooling in one year of HAMBASE simulation to the same values in EnergyPlus simulation. A comparison of peak heating and peak cooling can be found in Appendix A.5.6. . For this test the HVAC system was on, all internal loads were on, and the actual weather file was used. For details on the parameters used in this test refer to Chapter 3.

There is not a pass/fail standard for this comparison. The ASHRAE 140-2007 standard method of test gives a range of cooling and heating values, but this range results from a single-zone building, with simple materials and HVAC equipment. Thus, the ranges shown previously in Table 29 merely serve to highlight differences between EnergyPlus and HAMBASE.

The annual heating for HAMBASE and EnergyPlus is shown by zone in Figure 91. As predicted by the open-loop tests, HAMBASE shows greater heating in every zone except West3. Detailed values can be found in Appendix A.5.6. . A zone by zone comparison of annual heating using the 146% range from ASHRAE 140-2007 shows that Core1, South1, North1 and Core2 have especially high differences. The remaining zones, as well as the total heating for the building (a 50% difference; 42.6MWh for HAMBASE versus 28.3MWh for EnergyPlus), fall within the 146% range.

The higher heating values shown in HAMBASE will cause slightly lower ground loop temperatures over time, all else being equal, because of the extra heat taken out of the ground compared to EnergyPlus.

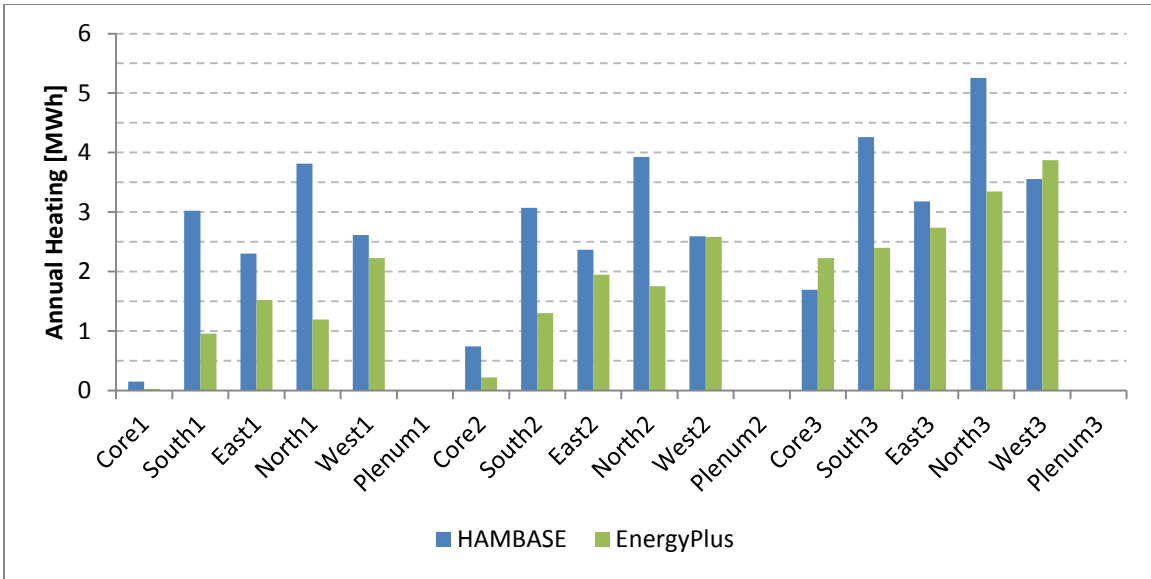


Figure 91: Comparison of HAMBASE and EnergyPlus annual heating

The annual total cooling for HAMBASE and EnergyPlus is shown by zone in Figure 92. HAMBASE shows a greater total cooling in every zone. Detailed values can be found in Appendix A.5.6. .

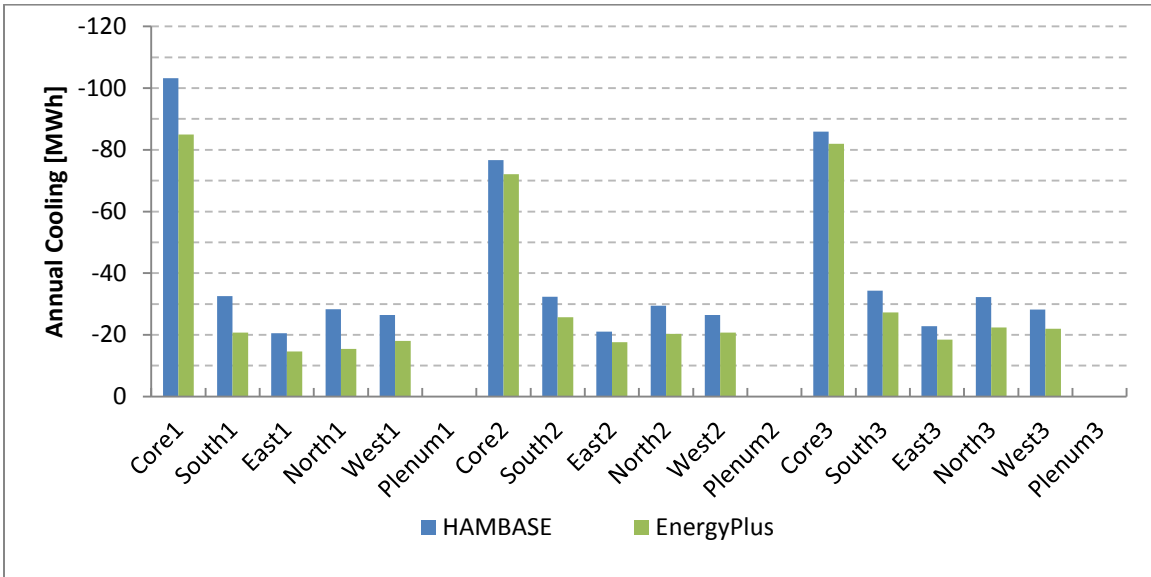


Figure 92: Comparison of HAMBASE and EnergyPlus annual total cooling

A zone by zone comparison of total cooling using the 47% range from ASHRAE 140-2007 shows that South1 and North1 have especially high differences. The remaining zones, as well as the total cooling for the building (a 24% difference; 600.4MWh for HAMBASE versus 482.4MWh for EnergyPlus), fall within the 47% range.

The higher cooling values shown in HAMBASE will cause slightly higher ground loop temperatures over time, all else being equal, because of the extra heat rejected to the ground compared to EnergyPlus.

The annual sensible cooling for HAMBASE and EnergyPlus is shown by zone in Figure 93. HAMBASE shows a closer match to EnergyPlus when looking at sensible cooling instead of total cooling. Detailed values can be found in Appendix A.5.6. .

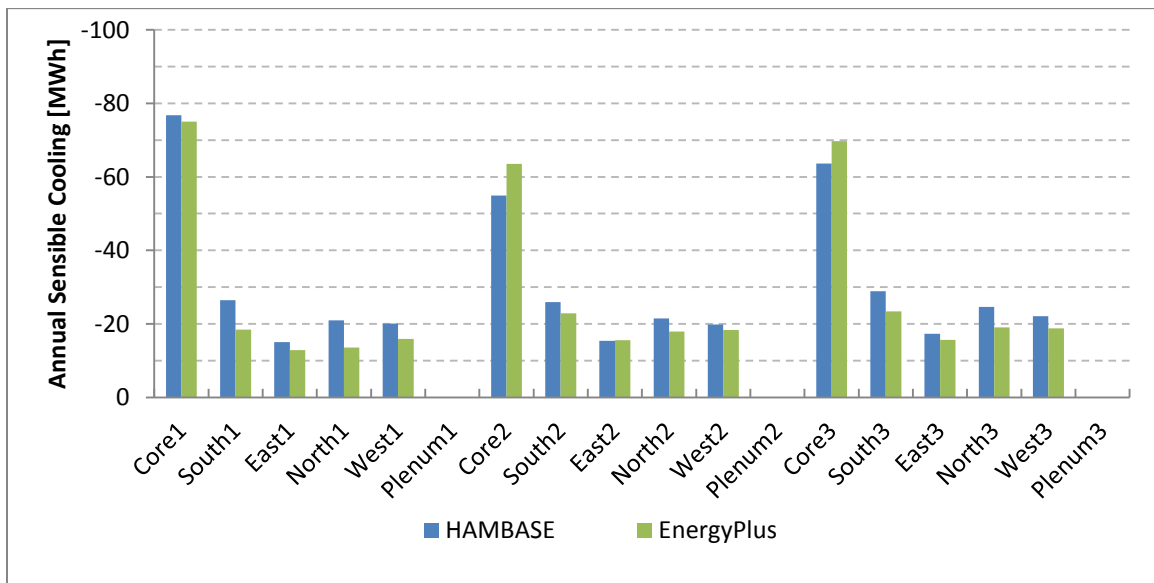


Figure 93: Comparison of HAMBASE and EnergyPlus annual sensible cooling

A zone by zone comparison of sensible cooling using the 47% range from ASHRAE 140-2007 shows that North1 has an especially high difference. The remaining zones, as well as the total sensible cooling for the building (an 8% difference; 453.3MWh for HAMBASE versus 420.4MWh for EnergyPlus), fall within the 47% range.

The annual latent cooling for HAMBASE and EnergyPlus is shown by zone in Figure 94. HAMBASE shows a greater latent cooling in every zone, as predicted by the open-loop tests. Detailed values can be found in Appendix A.5.6. .

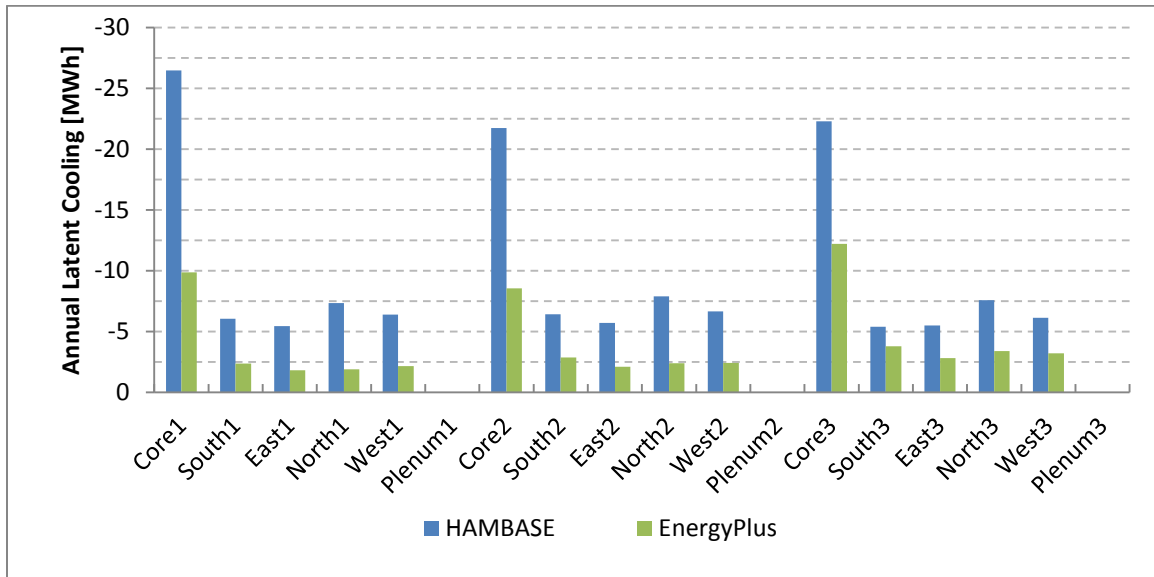


Figure 94: Comparison of HAMBASE and EnergyPlus annual latent cooling

A zone by zone comparison of latent cooling using the 47% range from ASHRAE 140-2007 shows that every zone except South3 has an especially high difference. In addition, the total latent cooling for the building (a 137% difference; 147.1MWh for HAMBASE versus 62.0MWh for EnergyPlus) falls outside the 47% range.

The differences in latent cooling values shown in HAMBASE will cause slightly higher ground loop temperatures over time, all else being equal, because of the extra heat rejected to the ground compared to EnergyPlus.

5.5. Summary of Validation Results

Open-loop (HVAC OFF) and closed-loop (HVAC ON) tests were run that compared the responses of HAMBASE and EnergyPlus to various inputs. The open-loop tests showed HAMBASE to have a greater sensitivity to outdoor air temperature, with an

overall time constant approximately double that of EnergyPlus. These tests also showed HAMBASE to have a smaller sensitivity to Direct Normal Irradiance (DNI) and outdoor air humidity than EnergyPlus.

The closed-loop tests showed HAMBASE to have greater annual heating, approximately equal sensible cooling and greater latent cooling. A comparison of the total building closed-loop test results shows that HAMBASE and EnergyPlus have a level of match labeled acceptable by the ASHRAE 140-2007 method of test for total annual heating, total annual cooling and total sensible cooling. This method of test showed the total latent cooling to be outside of the normal range.

Based on these validation tests HAMBASE has been shown to be in agreement with EnergyPlus in general; however the differences in total annual cooling and total annual heating will significantly affect the ground-loop temperature of the integrated model over time. On an annual basis, HAMBASE requires a net of 557.8MWh of cooling (-600.4MWh of total cooling combined with +42.6MWh of total heating) compared to a net of 454.1MWh of cooling in EnergyPlus (-482.4MWh of cooling combined with +28.3MWh of heating). Requiring 23% more net cooling per year will cause the ground loop in HAMBASE to be larger than it would be in EnergyPlus, resulting in higher installation costs and higher operation costs every year.

Chapter 6

Base Model Results

This section presents simulation results for the base model. The base model uses a 10x16 ground loop heat exchanger installation, with boreholes on 6.1meter (20ft) centers. The ground loop was sized using GLHEPRO using an entering water temperature cutoff of 32.2°C (90°F), resulting in borehole depth of 170.7meters (560ft) and 3.175cm (1.25in) diameter u-tubes. An overview of sizing the ground loop using GLHEPRO was provided in Section 4.4.3. A detailed list of all GLHEPRO data can be found in Appendix A.4.

The results in this chapter are divided into four sections: time-step results (Section 6.1), hourly results (Section 6.2), monthly results (Section 6.3) and annual results (Section 6.4). Analysis of time-step results is required to see the dependencies of the model, however there are too many data points in a 15year simulation for analysis of time-step data to be useful. As a result, time-step results are best viewed on a three to 24 hour interval. Analysis of hourly average data allows for comparison to other building load modeling software, and this scale allows nuanced viewing of one year of data. In order to view longer time periods of simulation, monthly averages are used. Monthly averages still reveal seasonal effects in the model, while still revealing behavior over 15years of simulation. Annual averages allow for the easiest table views, and as a result quantitative comparisons, of the model's change in performance over time.

In the following sections, qualitative comparisons will be made for all four sets of results, while quantitative comparisons will be limited to the annual results.

6.1. Time-Step Results

Time-step values are used to examine qualitative trends during one day or less of simulation. The building physics model used a time-step of 60 seconds, meaning that data was sampled every 60 seconds. Analyzing this data reveals both the integration of the subsystems and the dynamic nature of the model.

6.1.1. Time-Step Zone Data

Three hours of temperature and humidity time-step data for Core1 on June 30th of the first year of simulation are shown in Figure 95. The data show the temperature in the zone increasing until it passes the cooling-on threshold, at which point the temperature decreases due to heat pump operation shown in Figure 96.

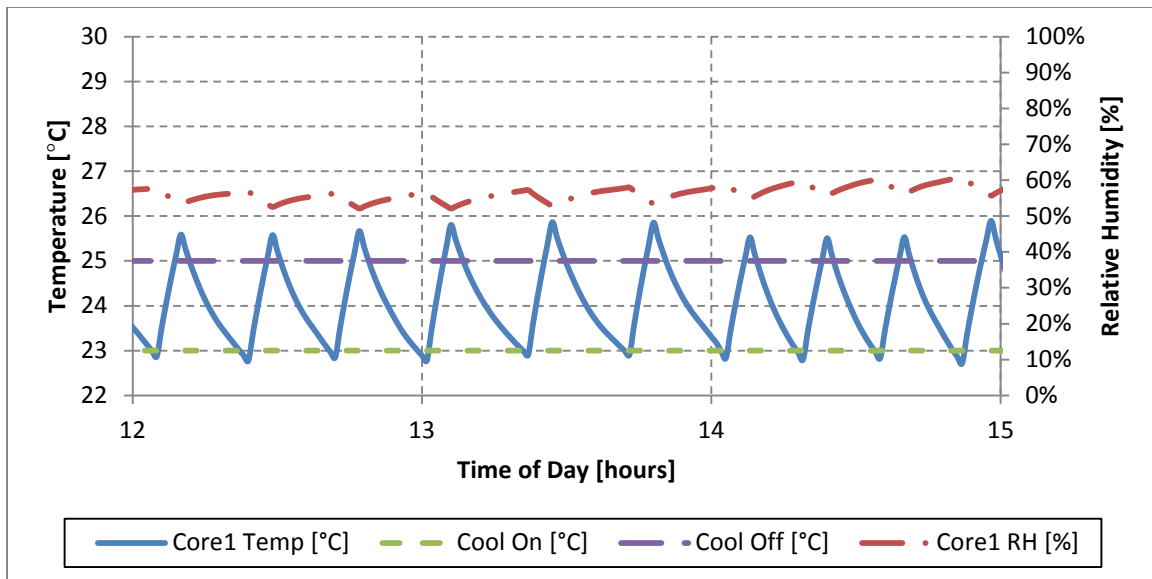


Figure 95: Time-step temperature and relative humidity for Core1 for June 30, 12-3pm

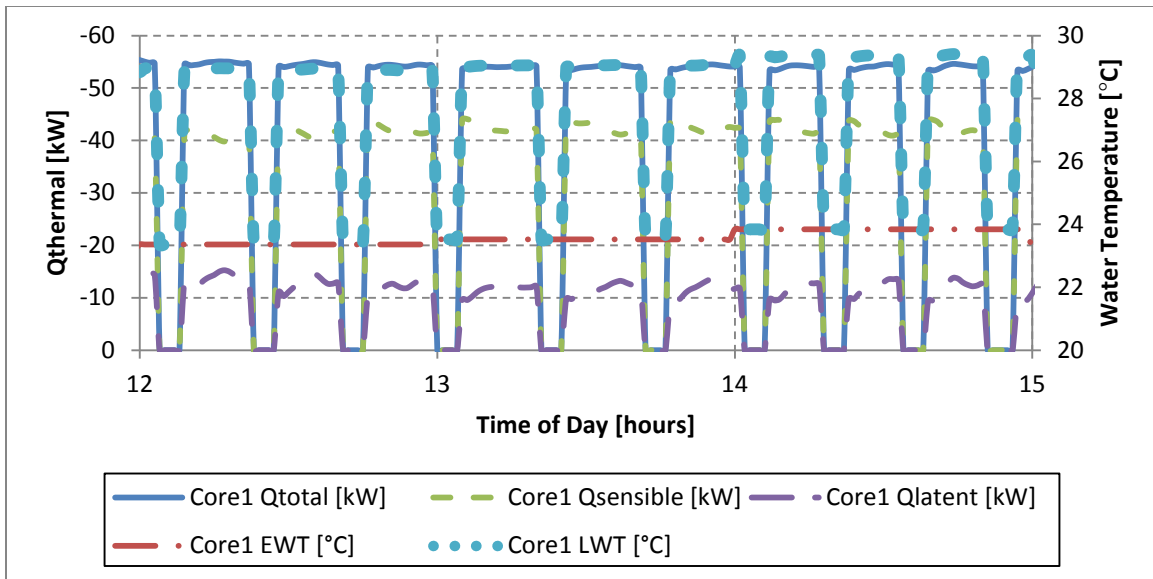


Figure 96: Time-step cooling provided and water temperature for Core1 heat pump for June 30, 12-3pm

When the heat pump turns on, 54.6 kW of cooling are provided to the zone (total cooling is shown in blue-solid, sensible cooling in green-dash and latent cooling in purple-dash in Figure 96). The cooling lowers the zone air temperature and rejects heat to the circulating water, which causes an increase in water temperature. This increase is shown by the jumps in LWT (leaving water temperature) whenever the heat pump provides cooling. The same causal relationship is shown for East2 in Figure 97 and Figure 98, and again for South3 in Figure 99 and Figure 100.

Comparing the responses for Core1 to East2 and South3 reveals the effects of heat pump sizing on overall system performance. All of the zones gain heat quickly, shown by the steep, positive slope of the zone temperature when the heat pump is off. The Core1 zone shows 3 or 4 cooling cycles during an hour, compared to 4 or 5 cooling cycles per hour for East2 and 7 or 8 cooling cycles per hour for South3. This implies that the heat pump in Core1 is better sized to its internal loads than either East2 or South3.

As a result of this finding, smaller heat pumps for East2 and South3 were considered, but smaller heat pumps were unable to meet the peak load requirements for

the zones. In actual applications, additional control would be added to these zones to better optimize their performance.

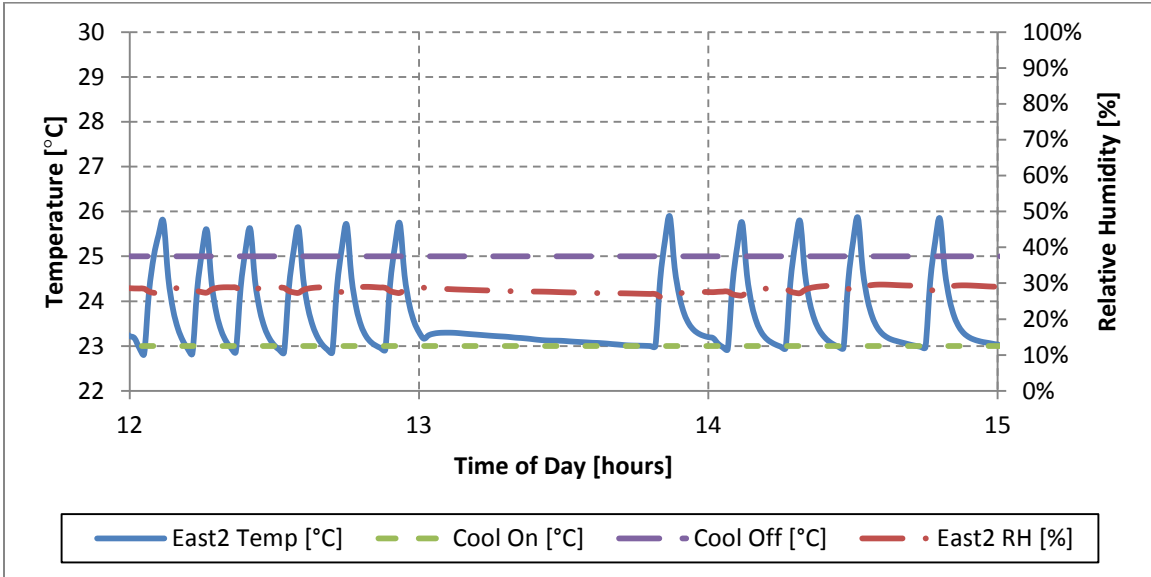


Figure 97: Time-step temperature and relative humidity for East2 for June 30, 12-3pm

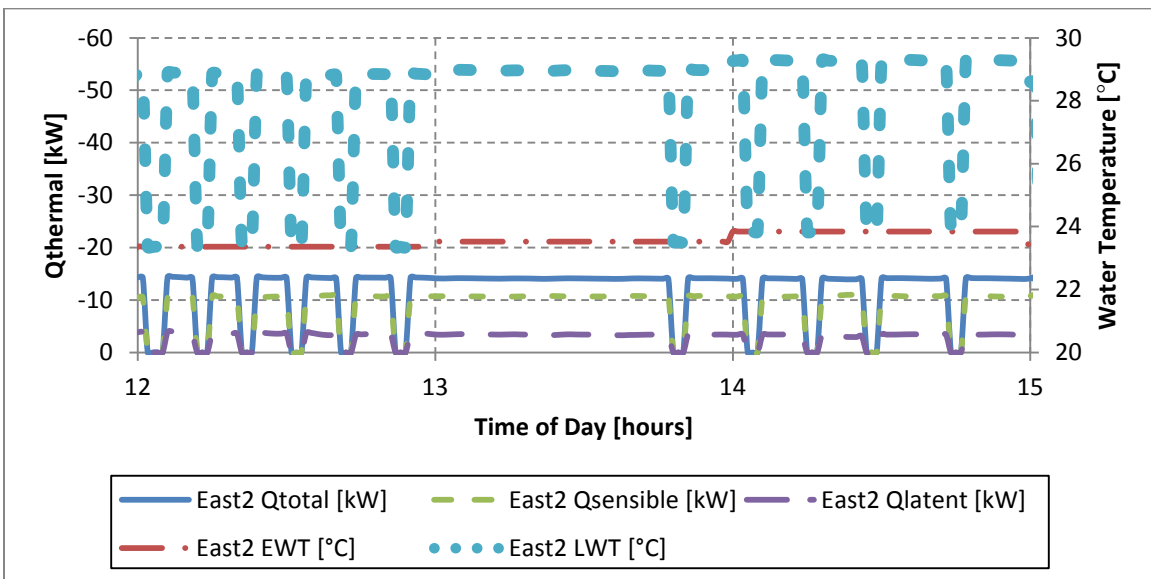


Figure 98: Time-step cooling provided and water temperature for East2 heat pump for June 30, 12-3pm

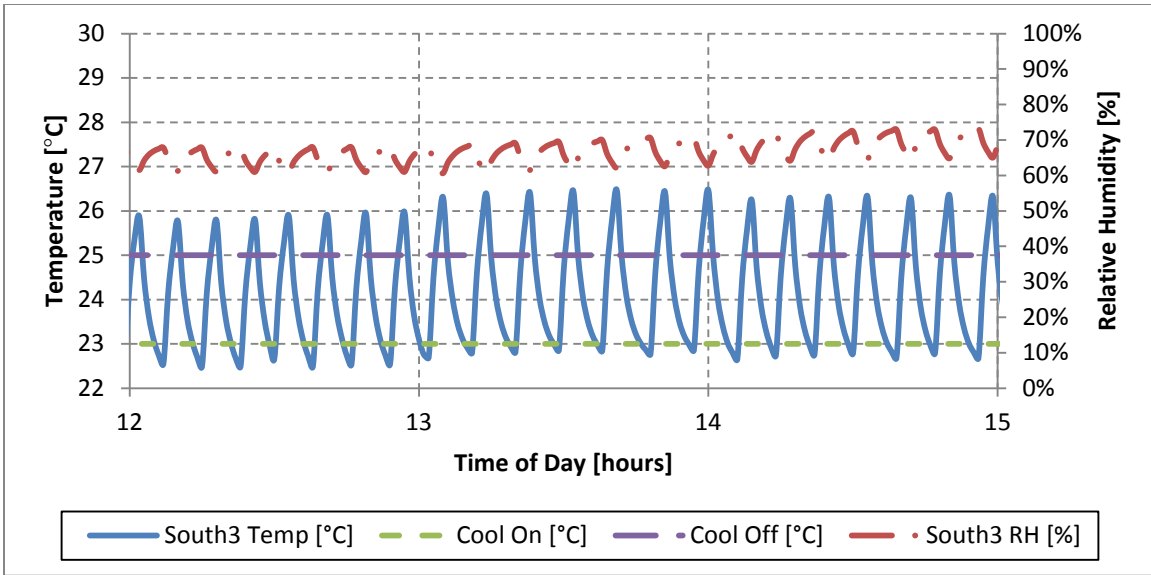


Figure 99: Time-step temperature and relative humidity for South3 for June 30, 12-3pm

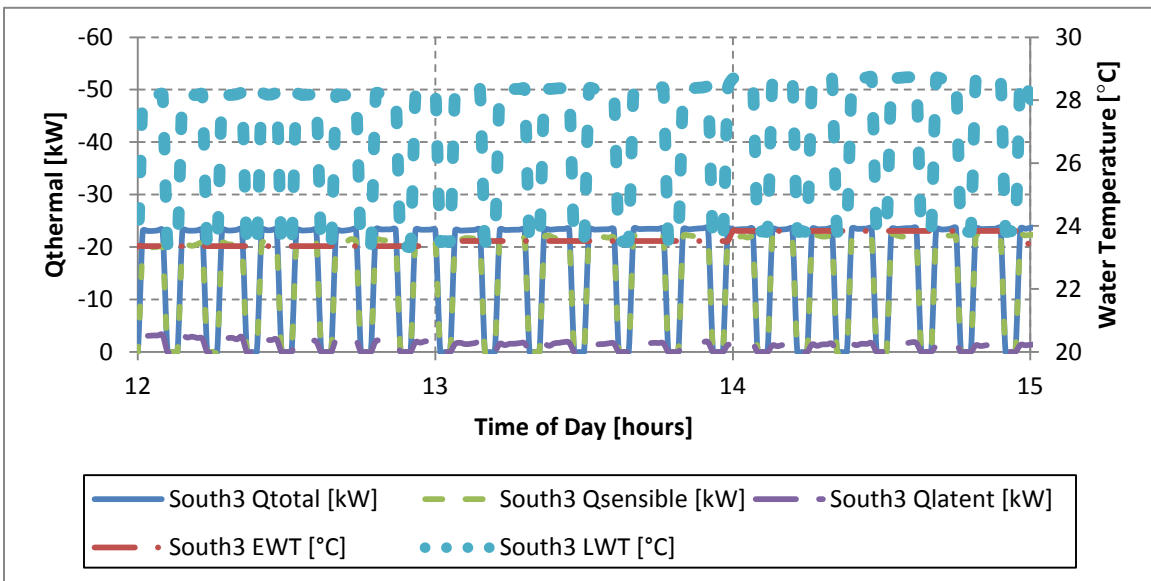


Figure 100: Time-step cooling provided and water temperature for South3 heat pump for June 30, 12-3pm

6.1.2. Time-Step Ground Loop Data

The ground loop operates on a 60-minute time-step. The time-step is large relative to the building because of the significant thermal mass of the ground and to reduce instabilities of the steady-state ground loop temperature model, as discussed in Section 2.3.

As the heat pumps begin providing cooling, the temperature of the return water increases (shown as LWT in light blue dots in Figure 96, Figure 98 and Figure 100). The return water from all 15 heat pumps combines in the heat pump header, whose temperature is shown in blue in Figure 101. The header temperature fluctuates at 60-second intervals because it is based on the heat pump time-steps. The header temperature is averaged hourly to form the inlet water temperature to the ground loop, shown in green in Figure 101. The ground loop rejects heat to the ground, and returns cooler water, shown in purple in Figure 101. The ground loop outlet then becomes the heat pump entering water, shown as EWT in red in Figure 96, Figure 98 and Figure 100.

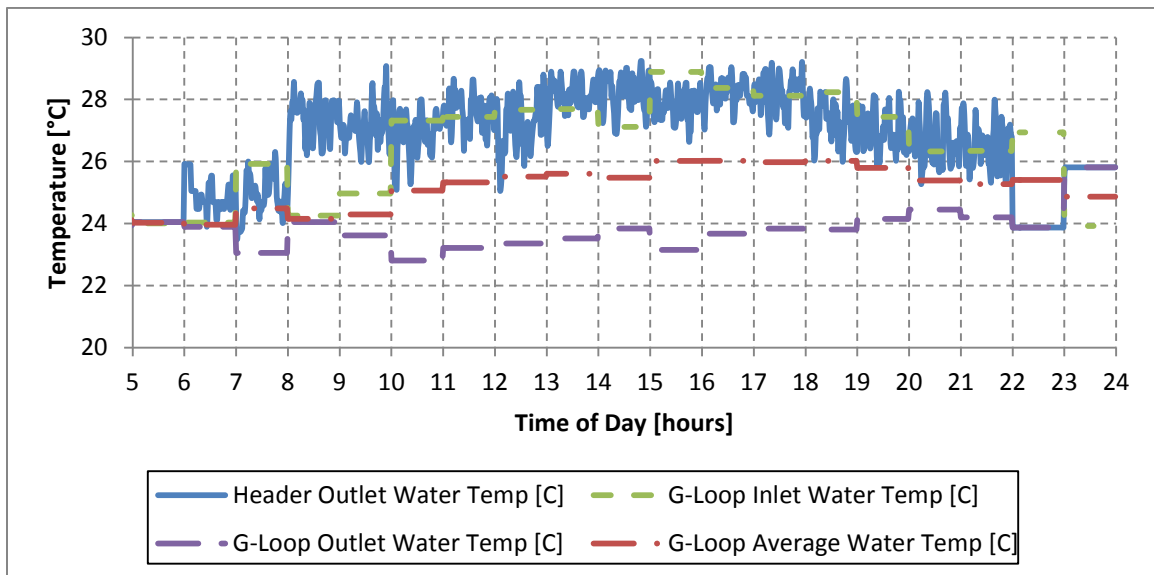


Figure 101: Time-step water temperature for the ground loop and heat pump return header for June 30, 5am -12am

6.2. Hourly Results

Hourly values are used to examine qualitative trends during one year of simulation. Hourly averages are the typical way cooling and heating loads are communicated in building load modeling software such as eQuest and EnergyPlus, so converting the time-step data to hourly averages allows easy comparison between models. Hourly averaging also reduces data storage requirements, allowing compressed transfer times and easier storage. An overview of the data processing used in this model can be found in Section 4.7. This section presents hourly averages of the time-step data for the first year of operation, January 1 through December 31.

6.2.1. Hourly Temperature Data

Hourly average temperature data for Core1, East2 and South3 are shown in Figure 102, Figure 103 and Figure 104, respectively. In all three figures, the zone air temperature is shown in blue, the heating setpoint temperature is shown in purple, the cooling setpoint temperature in red, the heating setback temperature is shown in green and the cooling setback temperature in light blue. During summer operation, Core1 temperature is generally between the cooling setpoint and cooling setback position due to the difficulty maintaining zone temperature when large internal loads are combined with high outdoor air temperatures. East2 and South3, in contrast, have smaller internal loads, resulting in lower temperatures.

The opposite effect can be seen during winter operation. East2 and South3 temperatures regularly fall below the heating setpoint due to the small internal loads combined with low outdoor temperatures. In contrast, the large internal loads of Core1 maintain temperatures above the heating setpoint except for a few extreme cases.

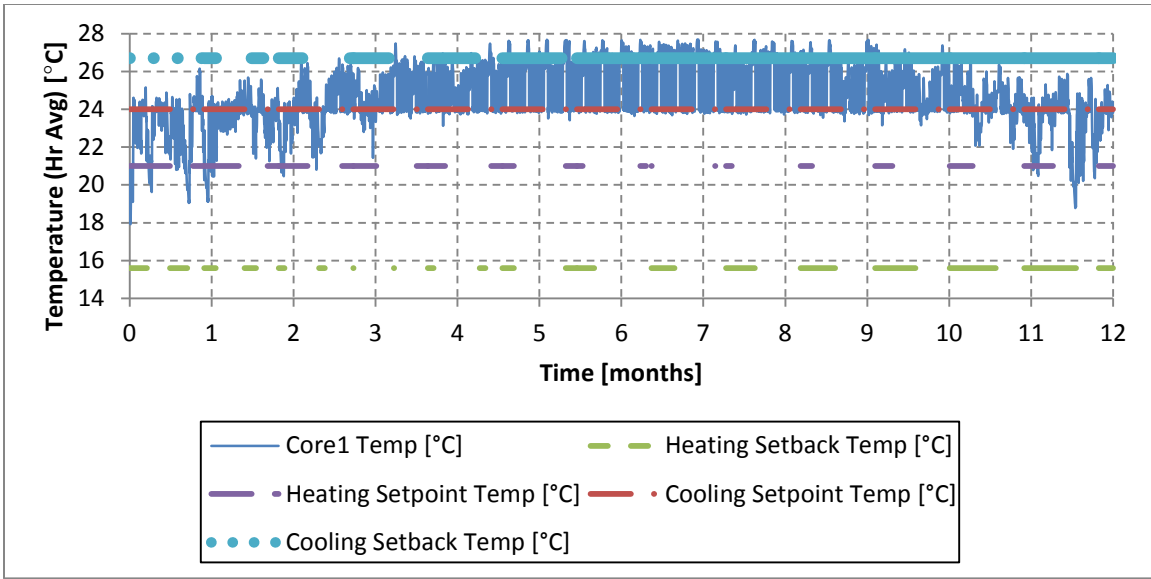


Figure 102: Hourly average temperature of Core1 for first 12 months of simulation

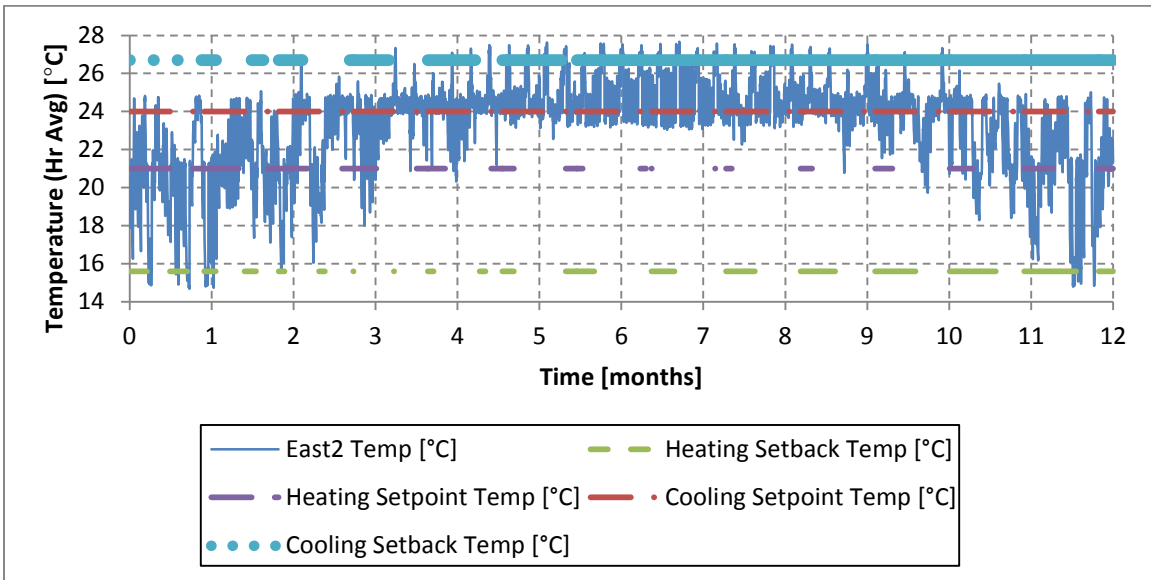


Figure 103: Hourly average temperature of East2 for first 12 months of simulation

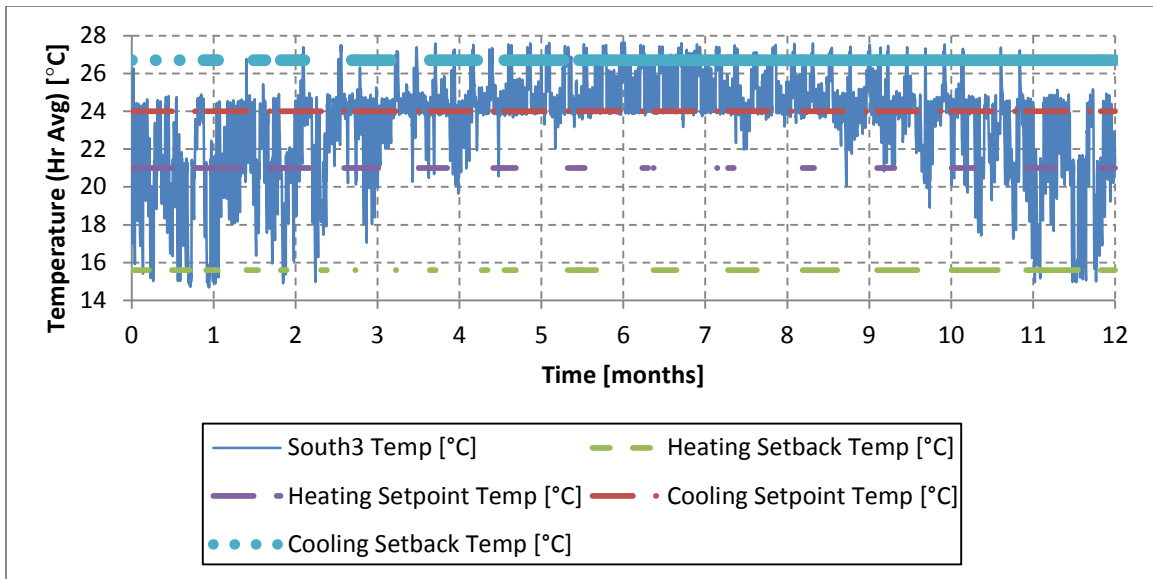


Figure 104: Hourly average temperature of South3 for first 12 months of simulation

6.2.2. Hourly Heating and Cooling Data

The air temperature in a zone is controlled by heating and cooling added to the zone by the heat pump. Hourly average data for heating and cooling provided to Core1, East2 and South3 are shown in Figure 105, Figure 106 and Figure 107, respectively. Cooling is shown as a negative value and heating is shown as a positive value. Comparing the cooling and heating loads for Core1 in Figure 105 to the temperature in Figure 102 shows the integration between the two systems: when zone temperatures are high, the heat pump provides cooling, when zone temperatures are low, the heat pump provides heating.

Comparing the cooling and heating loads between the zones reveals the effect of heat pump sizing. The 15-ton capacity heat pump in Core1 provides almost 57kW of cooling, compared to 15kW from the 4-ton unit in East2 and 23kW from the 7-ton unit in South3.

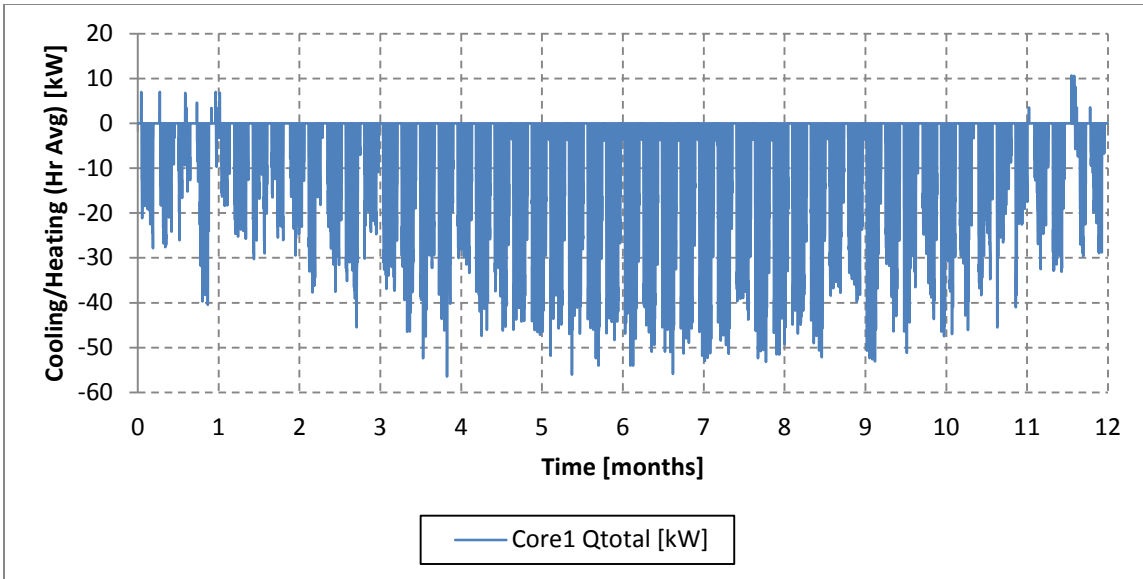


Figure 105: Hourly average cooling (negative) and heating (positive) provided by the Core1 heat pump for the first 12 months of simulation

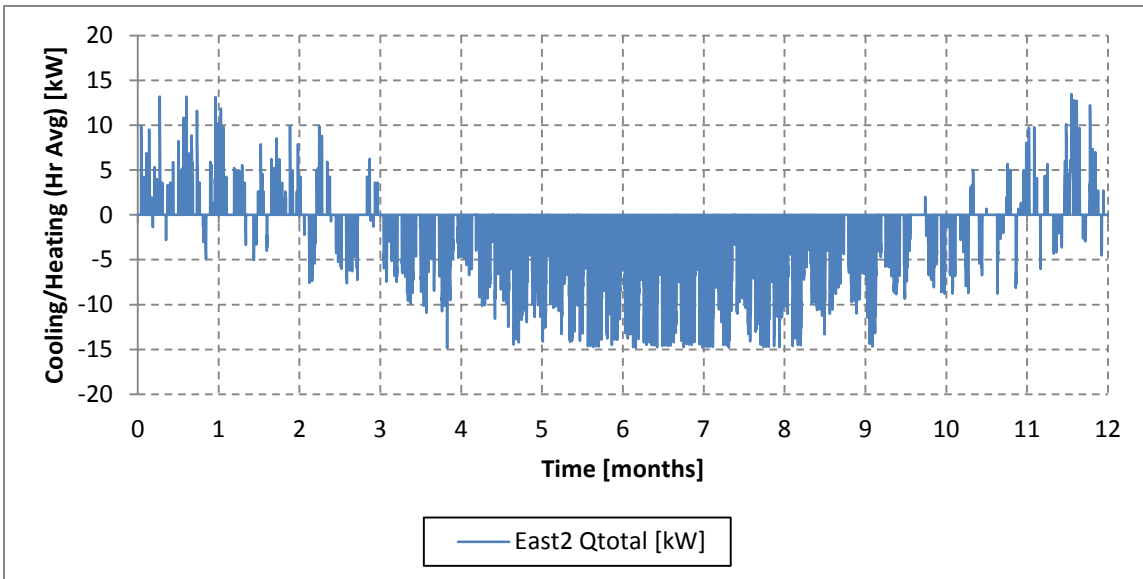


Figure 106: Hourly average cooling (negative) and heating (positive) provided by the East2 heat pump for the first 12 months of simulation

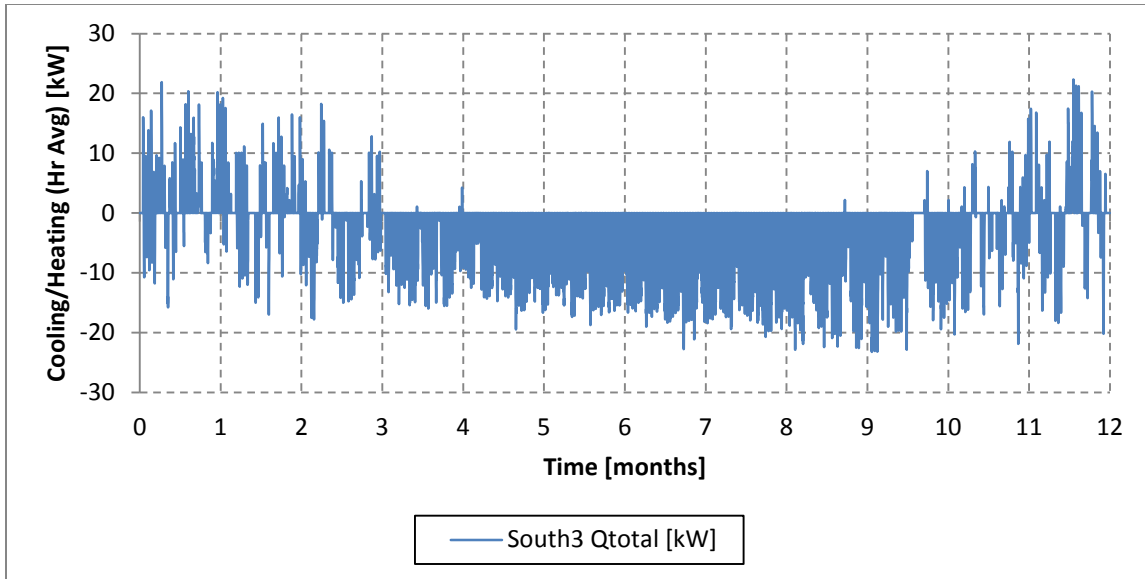


Figure 107: Hourly average cooling (negative) and heating (positive) provided by the South3 heat pump for the first 12 months of simulation

6.2.3. Hourly Heat Pump Efficiency Data

The heat rejected and absorbed by each heat pump is an important variable for comparing and evaluating between heat pumps, but it is lacking the ability for easy comparison to other HVAC equipment. The hourly average efficiency of the heat pump takes into account the amount of energy required to generate heating and cooling, and therefore gives a better tool of comparison. Efficiency during heating operation is measured using COP (Coefficient of Performance), which is calculated using Equation (15). Efficiency during cooling operation is measured using EER (Energy Efficiency Ratio), which is calculated using Equation (16).

$$COP = \eta_{heating} = \frac{\text{Heat Added } [W_t h]}{\text{Power Used } [W_e h]} \quad (15)$$

$$EER = \eta_{cooling} = \frac{\text{Heat Removed } [Btu]}{\text{Power Used } [W_e h]} \quad (16)$$

Hourly average data for COP and EER in Core1, East2 and South3 are shown in Figure 108, Figure 109 and Figure 110, respectively. Plots of the power usage for Core1, East2 and South3 are shown in Appendix A.6.

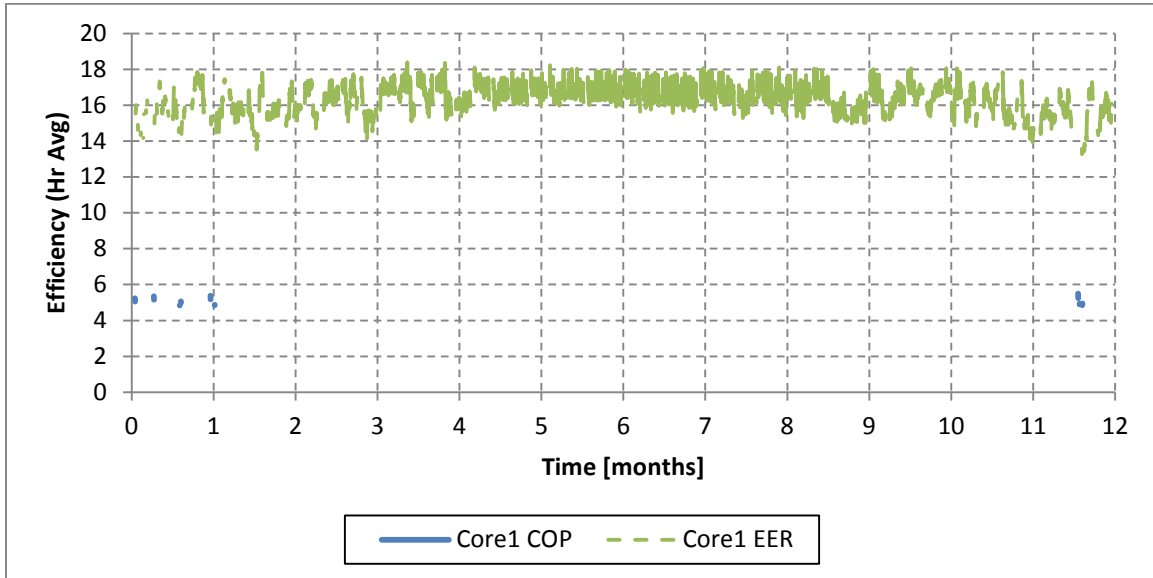


Figure 108: Hourly average efficiency ratings for the Core1 heat pump for the first 12 months of simulation (EER is associated with cooling, COP with heating)

The EER behaves in a similar manner for all three zones. During January, February and March, the low outdoor air temperature combined with high internal loads causes hourly averages that include both heating and cooling, which reduces the total cooling provided, while maintaining high total power usage. This results in high fluctuations of the EER during these months. Beginning in April, the EER becomes more consistent. Over the course of the summer, the EER gradually declines as the ground loop water temperature increases. Finally during November and December, the low outdoor air temperature brings back the high fluctuations in EER.

The COP also behaves in a similar manner for all three zones, but it is much more consistent than EER. There are few hours that consist of majority heating, resulting in very few opportunities for COP calculation, and within those hours (early mornings, late

nights), internal loads and solar irradiance are not yet high, resulting in few hours with both heating and cooling.

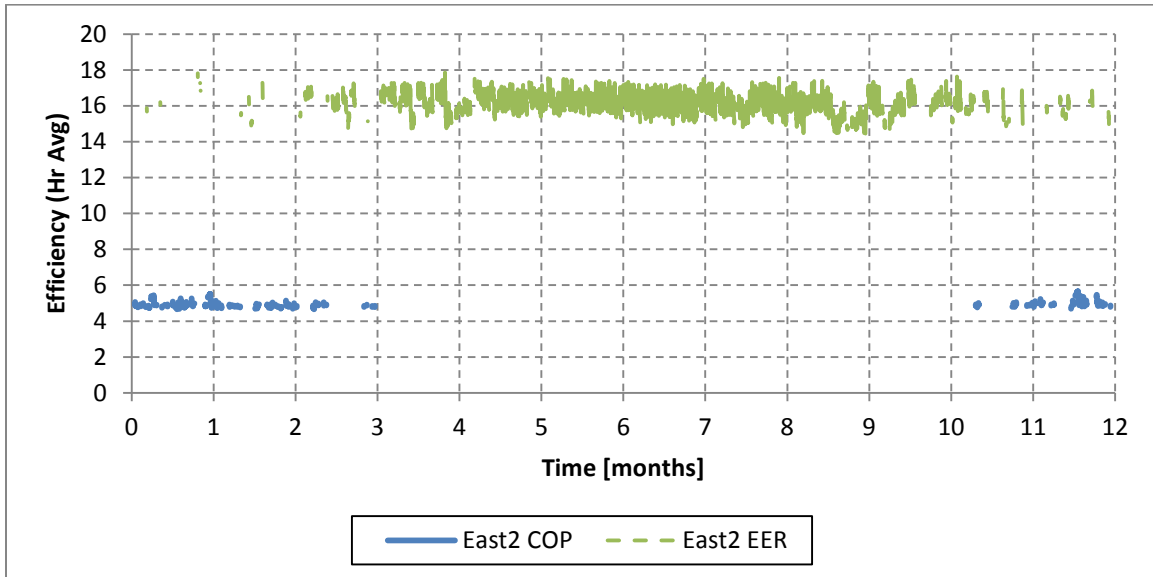


Figure 109: Hourly average efficiency ratings for the East2 heat pump for the first 12 months of simulation (EER is associated with cooling, COP with heating)

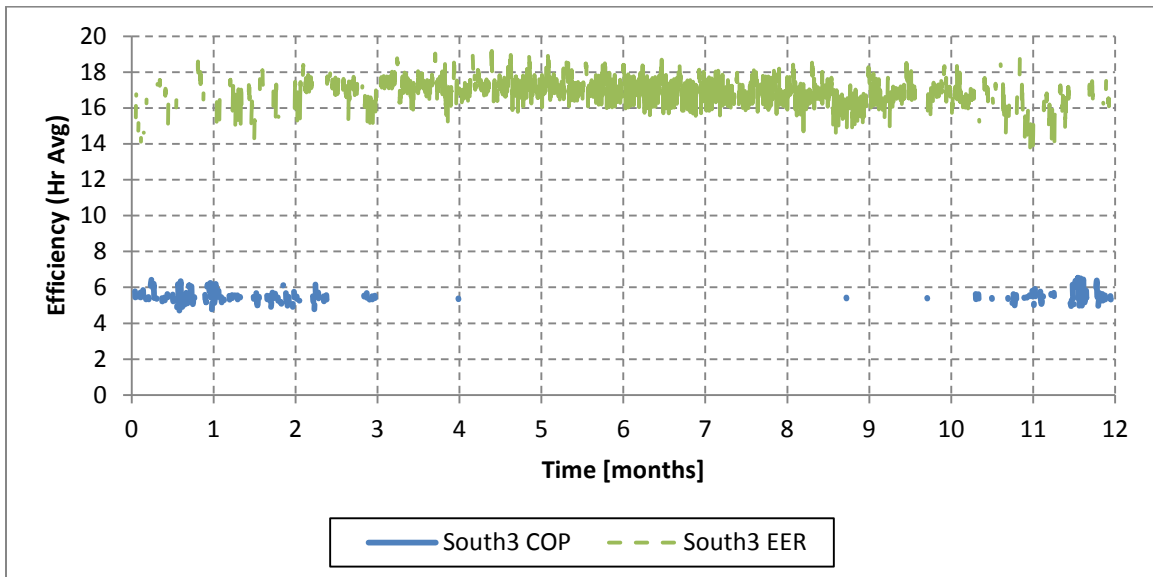


Figure 110: Hourly average efficiency ratings for the South3 heat pump for the first 12 months of simulation (EER is associated with cooling, COP with heating)

6.2.4. Hourly Heat Rejection Data

The heating and cooling provided by heat pumps in Section 6.2.2 uses a refrigeration cycle as described in Section 1.1. The refrigeration cycle absorbs heat from the ground loop water during heating and rejects heat to the ground loop water during cooling. Hourly average data for heat absorbed from and heat rejected to the ground loop water by Core1, East2 and South3 are shown in Figure 111, Figure 112 and Figure 113, respectively. Heat rejected to the ground loop during cooling operation is shown as positive, while heat absorbed from the ground loop during heating operation is shown as negative.

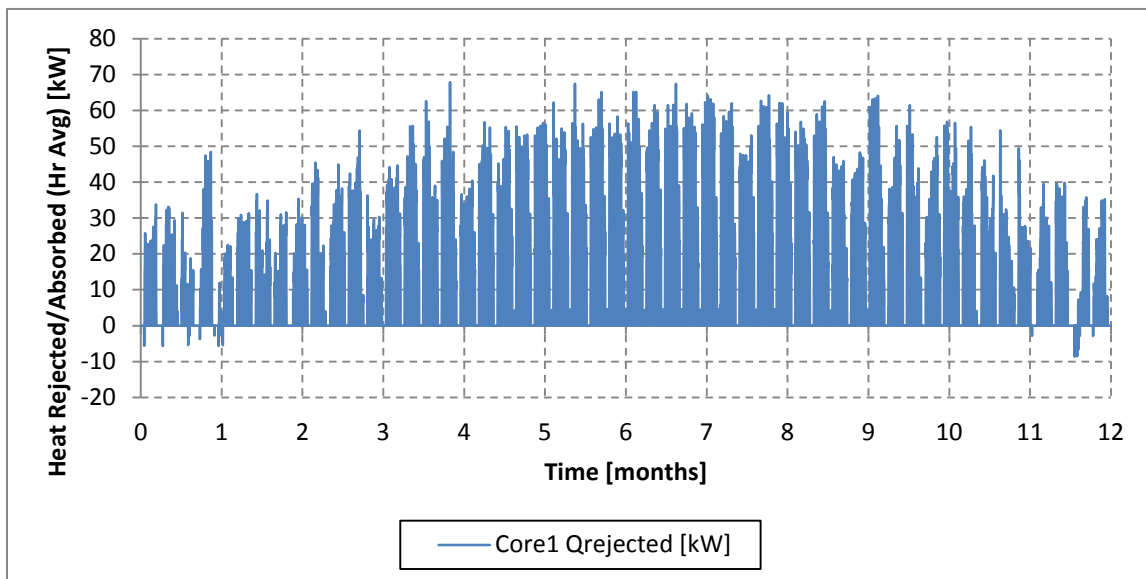


Figure 111: Hourly average heat rejected to ground loop water by the Core1 heat pump (positive heat rejection is associated with cooling) for the first 12 months of simulation

Comparing the plots of heat rejected to the plots of heating/cooling provided (for example: Figure 112 and Figure 106) reveals the effect of the refrigeration cycle. During cooling, the compressor does work on the refrigerant prior to the refrigerant's heat exchange with the ground loop (see Figure 1). As a result, the heat rejected values are slightly greater than the cooling provided values.

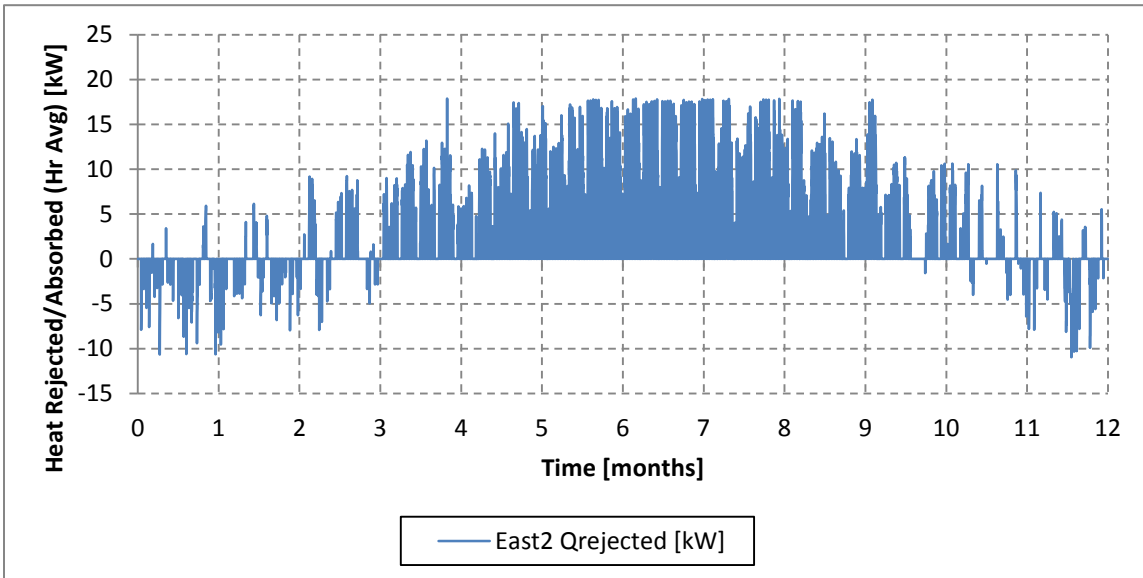


Figure 112: Hourly average heat rejected to ground loop water by the East2 heat pump (positive heat rejection is associated with cooling) for the first 12 months of simulation

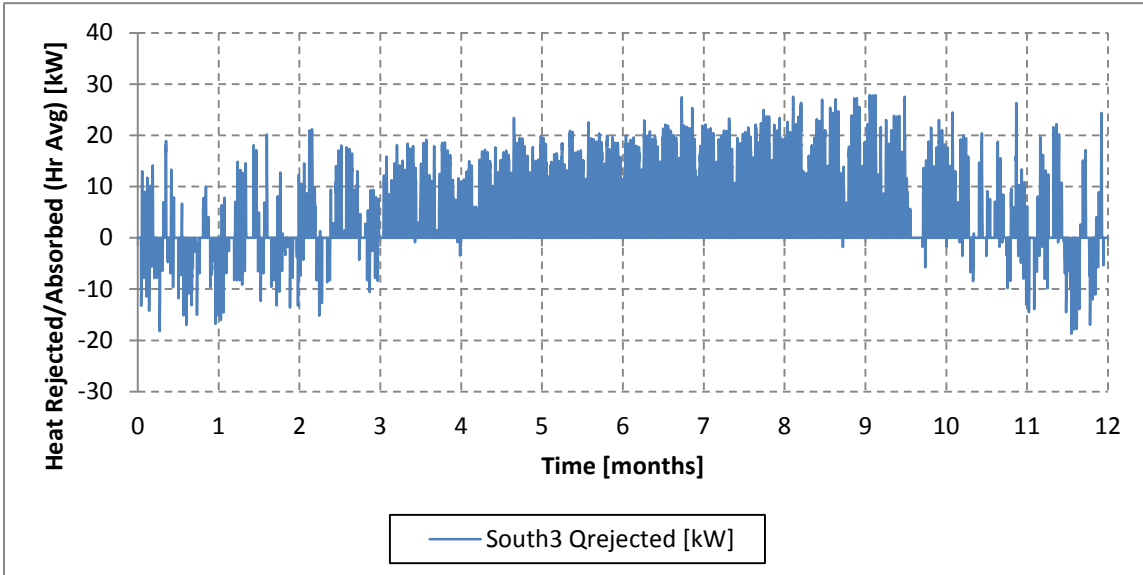


Figure 113: Hourly average heat rejected to ground loop water by the South3 heat pump (positive heat rejection is associated with cooling) for the first 12 months of simulation

During heating, the compressor does work on the refrigerant after the refrigerant's heat exchange with the ground loop (see Figure 2). Instead, refrigerant passes through the expansion valve prior to exchanging with the ground loop, resulting in heat absorbed values slightly less than the heating provided values.

6.2.5. Hourly Heat Pump Water Temperature Data

The absorbed and rejected heat shown in the previous section causes a temperature difference from the heat pump water inlet to heat pump water outlet. During heating operation, the temperature difference is negative as heat is absorbed from the water. During cooling operation, the temperature difference is positive as heat is rejected to the water. Hourly average data for heat pump temperature difference in Core1, East2 and South3 are shown in green in Figure 114, Figure 115 and Figure 116, respectively. The entering water temperature (EWT) for each head pump is included in blue as a comparison. Note that EWT is the same for all heat pumps, as discussed in Section 4.5.

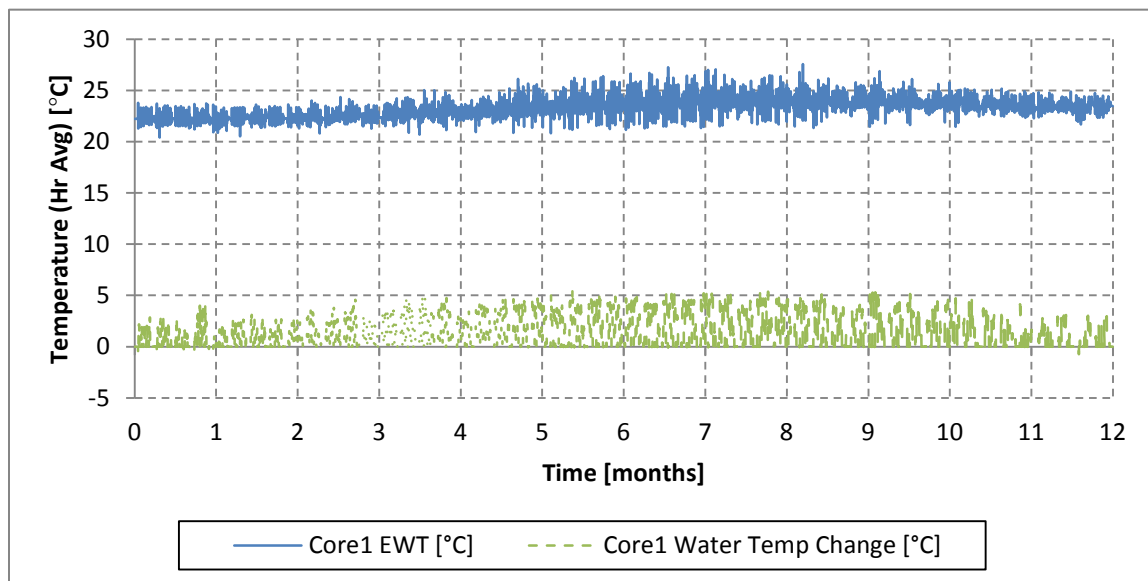


Figure 114: Hourly average Core1 heat pump entrance water temperature and temperature change for the first 12 months of simulation

Comparing Core1 to East2 and South3 shows all three zones to be cooling dominated, shown by the positive temperature difference for the majority of the year. The very few instances of negative temperature difference in Core1 show limited use of heating operation. East2 and South3, in contrast, show at least some negative temperature difference from November to March (months 10 to 12 and 0 to 3).

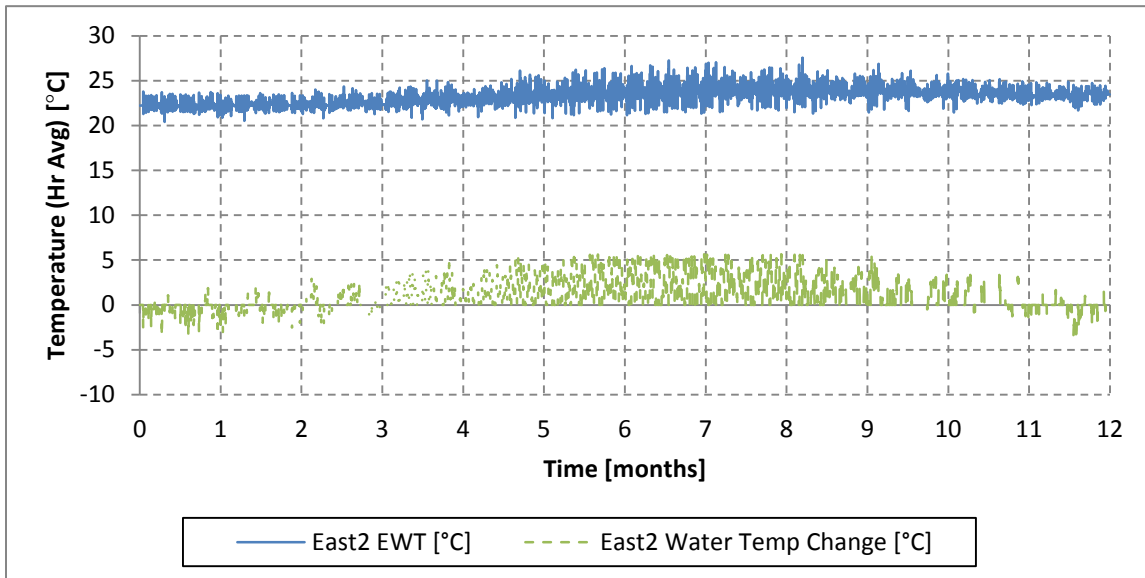


Figure 115: Hourly average East2 heat pump entrance water temperature and temperature change for the first 12 months of simulation

The magnitude of temperature difference is a result of water flow rate and magnitude of heat rejected/absorbed. Core1 and East2 both show a maximum temperature difference of approximately 5°C (9°F), compared to 4°C (7.2°F) in South3. South3 uses a 7ton heat pump compared to the 4ton heat pump used in East2, which results in a 0.63L/s (10GPM) greater flow rate through South3 than through East2 (1.39L/s (22GPM) versus 0.76L/s (12GPM)). So while South3 rejects approximately 2.5kW more heat than East2, this 2.5kW represents a 14% increase in heat compared to an 83% increase in flow rate, which causes the temperature change across the heat pump to be lower in South3 than in East2.

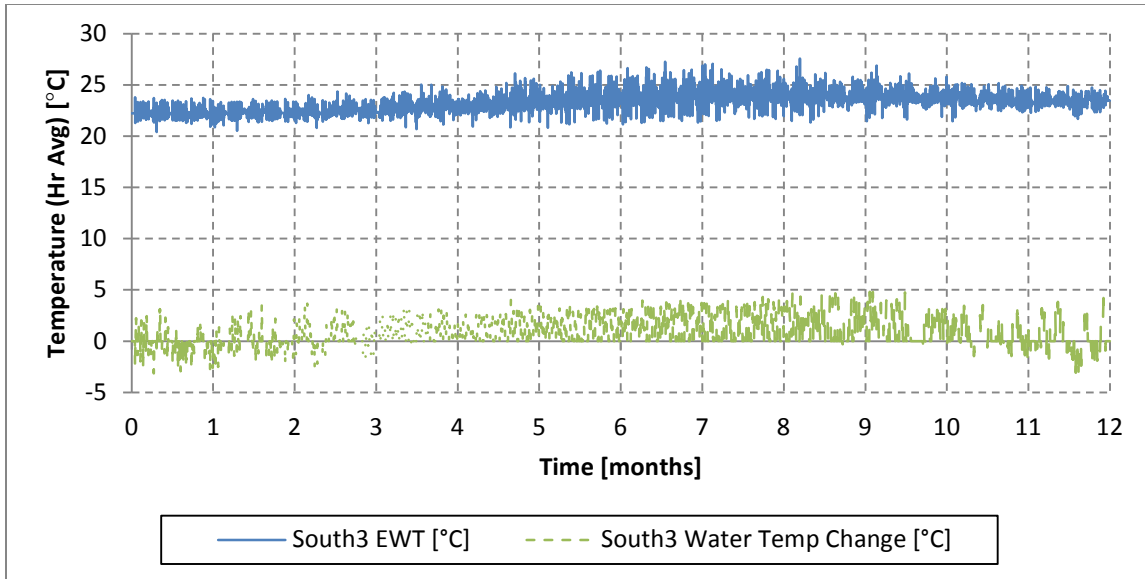


Figure 116: Hourly average South3 heat pump entrance water temperature and temperature change for the first 12 months of simulation

6.2.6. Hourly Ground Loop Water Temperature Data

The water leaving the heat pumps combines in a header before entering the ground loop heat exchanger (refer to Figure 53 for an overview of the water flow path). The undisturbed ground temperature in Austin, Texas is approximately 22°C (71.6°F), so when the water entering the ground loop is greater than 22°C, the ground loop water cools down, and when the water entering the ground loop is less than 22°C, the ground loop water heats up. Hourly average data for this relationship are shown in Figure 117.

When the water entering the ground loop (shown in blue) is below the undisturbed ground temperature (shown in purple), the ground loop temperature change (shown in green) is positive. This means that the water leaving the ground loop has a higher temperature than the water entering the ground loop. The opposite can be seen when the ground loop entering water temperature is greater than the ground temperature.

During the year of simulation shown, the entering water temperature gradually increases, resulting in the ending water temperature being slightly greater than the ground temperature.

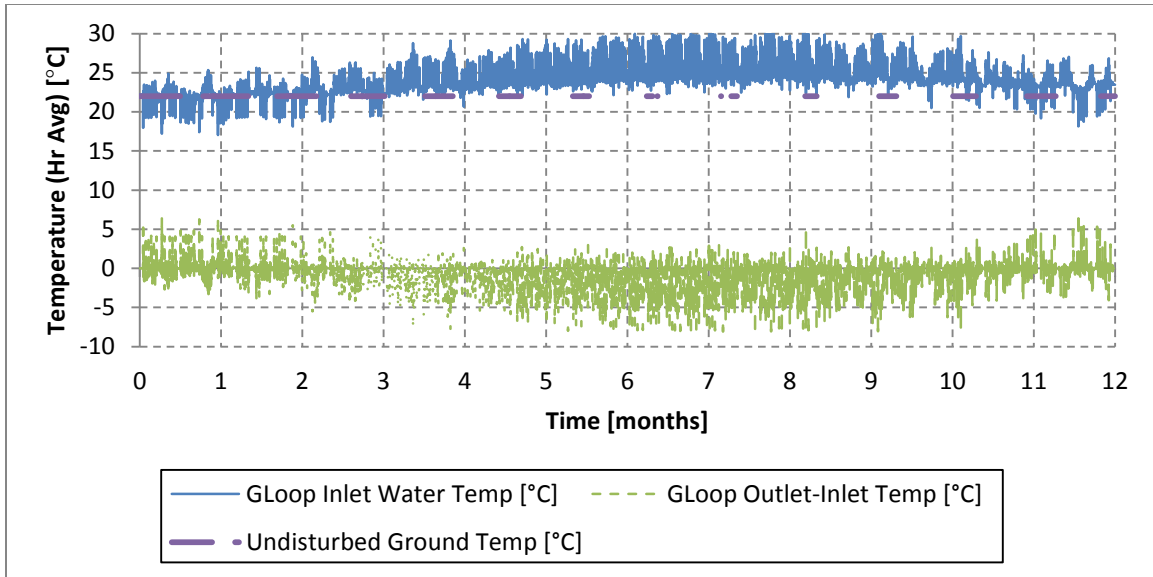


Figure 117: Hourly average ground loop entrance water temperature and temperature change for the first 12 months of simulation

6.3. Monthly Results

Monthly values are used to examine qualitative seasonal trends over the duration of the 15-year simulation. Monthly averages, monthly totals, monthly maximums and monthly minimum all serve to smooth the hourly data into a format viewable on a 15-year scale, while maintaining sensitivity to seasonal changes. The monthly values are computed by analyzing 730hrs of hourly data (8760hrs in a standard year, divided by 12months) and using the appropriate calculation (average, maximum, etc.) for each variable of interest.

6.3.1. Monthly Heating and Cooling Data

Heat pump heating and cooling values for Core1, East2 and South3 are shown in Figure 118 as total energy provided (in MWh) and in Figure 119 as total operating hours. Data in both figures show consistency from year-to-year in the amount of cooling and heating provided to the zones. These results also show the significant load imbalance in

this building. The cooling loads for every zone are significantly larger than the heating loads, as seen in the total energy provided and the total hours of operation for cooling versus heating modes.

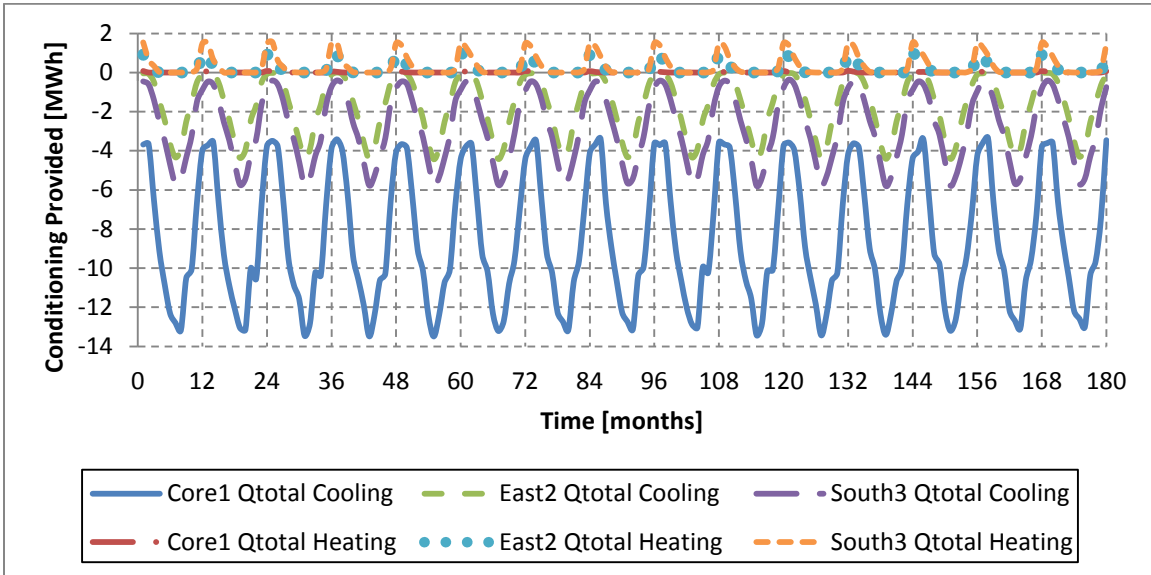


Figure 118: Monthly totals for cooling and heating provided in Core1, East2 and South3

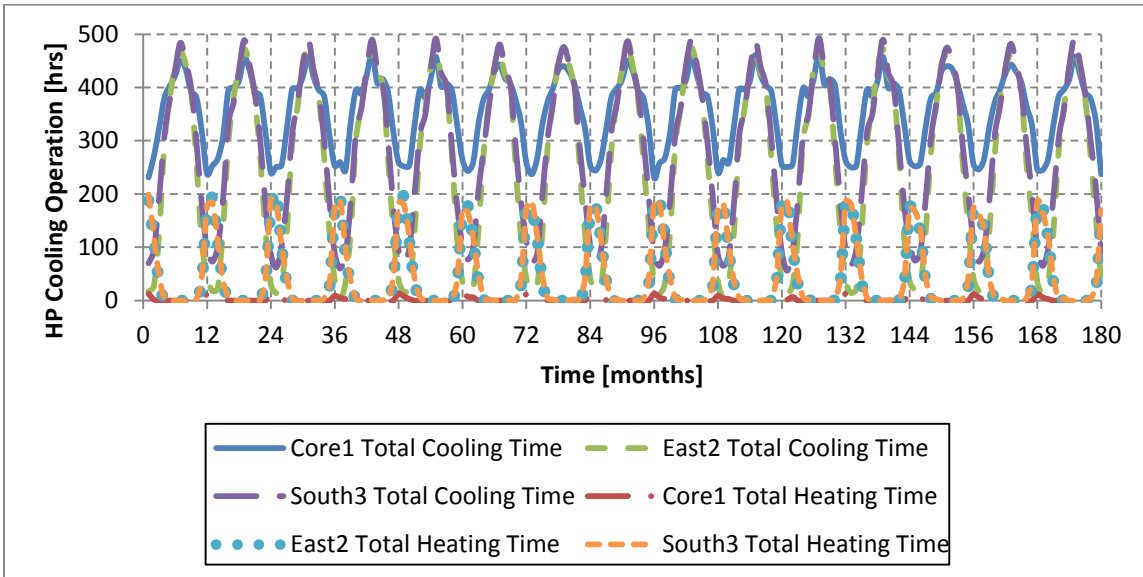


Figure 119: Monthly operating times for cooling and heating in Core1, East2 and South3

6.3.2. Monthly Ground Loop Data

The total heat rejected to the ground loop by the heat pumps during zone cooling and the total heat absorbed from the ground loop by the heat pumps during zone heating are shown in Figure 120. The difference in heat rejection and heat absorption again emphasizes the load imbalance experienced by the ground loop.

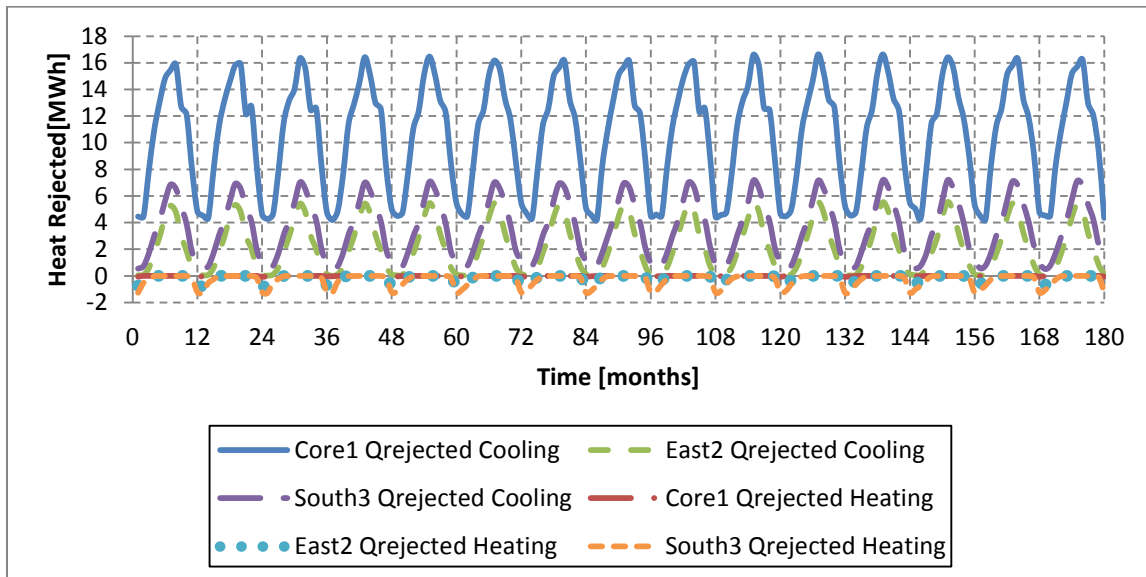


Figure 120: Monthly totals for heat rejected and absorbed from Core1, East2 and South3

The load imbalance manifests itself in changes in the ground loop water temperature. Figure 121 shows the monthly minimum, maximum and mean temperatures for the ground loop water as it enters the heat pump (heat pump entering water temperature, or HP EWT). The EWT values increase during the 15-year simulation because of the net quantity of heat rejected to the ground.

While the macro trend is increasing, the natural oscillations of the seasons can be seen on a yearly basis. This trend is most clear in the maximum EWT, shown in purple. EWT is low during January, it increases through the summer, and then it falls back down during October, November and December.

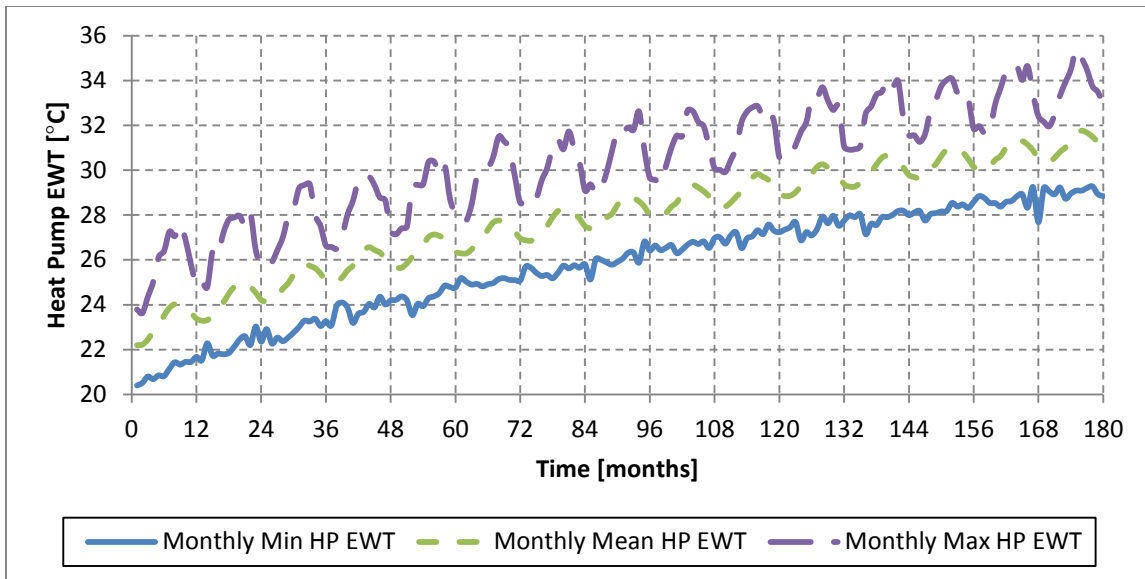


Figure 121: Monthly maximum, minimum and mean heat pump entering water temperature

6.3.3. Monthly Power Usage Data

As heat pump EWT increases, the heat pump compressor needs to work harder to generate a given amount of cooling. Figure 122 shows the monthly power usage for Core1, East2 and South3 for heating and cooling operation, and Figure 123 shows the total power usage for the building. The effect of seasonal change on cooling and heating power usage is clearly displayed. Summer months experience peak power usage for cooling in all zones, while winter months experience minimum power usage for cooling. Winter months show peak power usage for heating in all zones, while summer months show minimum power usage for heating.

The total power usage resulting from cooling operation increases every year of the 15-year simulation, which means that the cost of cooling the building increases every year.

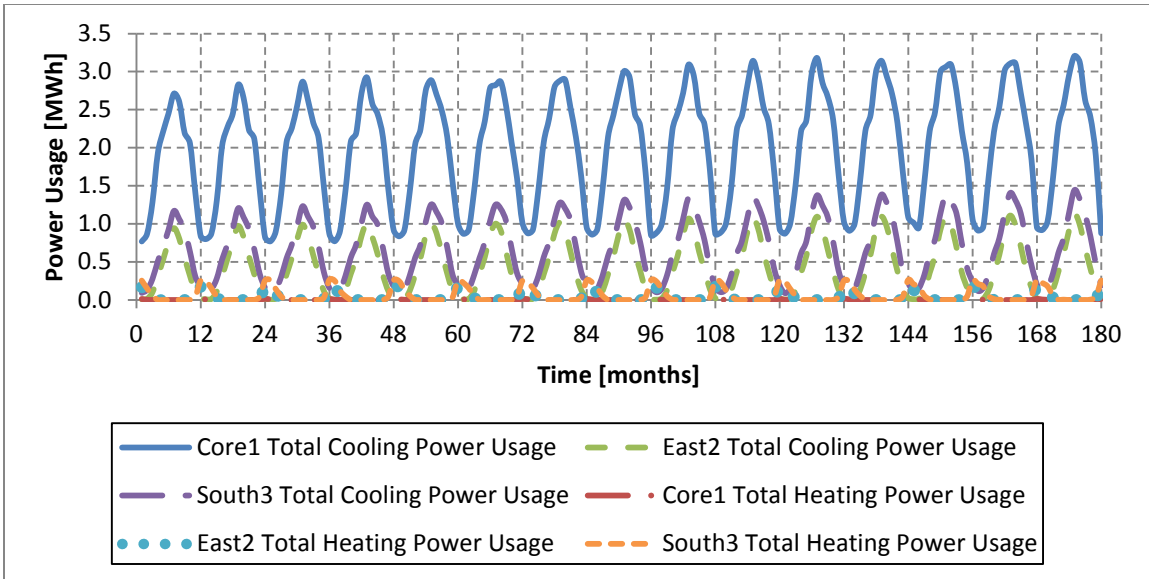


Figure 122: Monthly power usage totals in Core1, East2 and South3 for cooling and heating

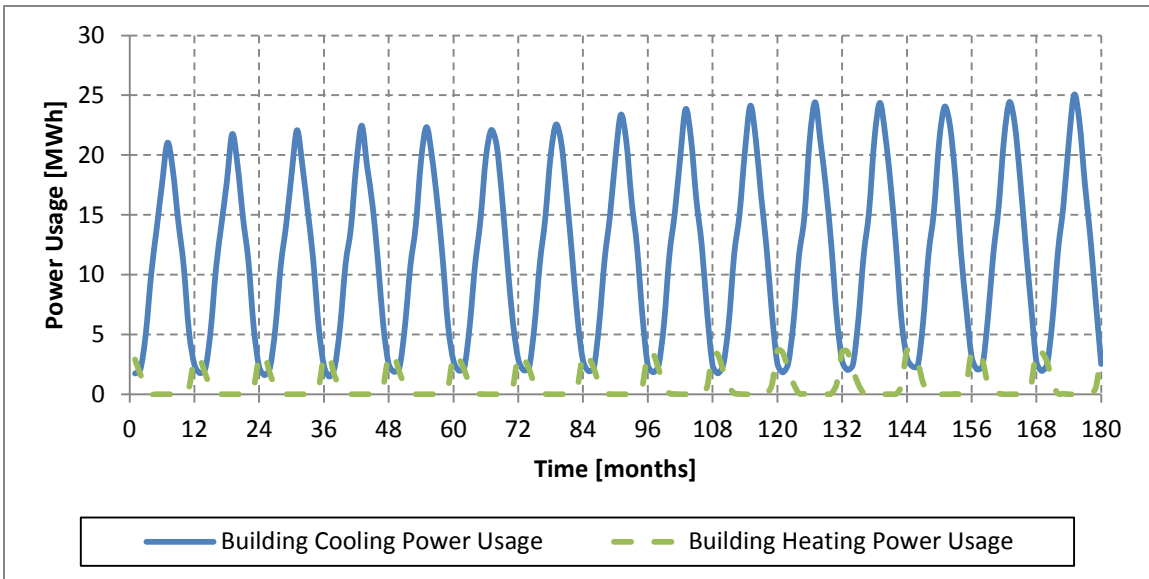


Figure 123: Monthly power usage totals for cooling, heating and water pump operation

6.3.4. Monthly Out-of-Setpoint Data

In addition to increasing the total cost of operation, increasing heat pump EWT affects the ability of the HVAC system to meet temperature setpoint. The heat pump equipment shuts down to protect itself when entering water temperatures exceed 48.9°C (120°F) during cooling mode and 32.2°C (90°F) during heating mode. During shutdown, the heat pump provides neither heating nor cooling to the zone, resulting in free-floating temperature until the EWT returns to safe conditions.

The increasing EWT still affects time out-of-setpoint if EWT values stay below the shutdown threshold. The total cooling capacity of the heat pump is inversely dependent on the entering water temperature, meaning that as the entering water temperature increases the total cooling capacity decreases. The relationship between total cooling capacity and EWT is shown Figure 124 for the ClimateMaster Tranquility TS series 5ton heat pump.

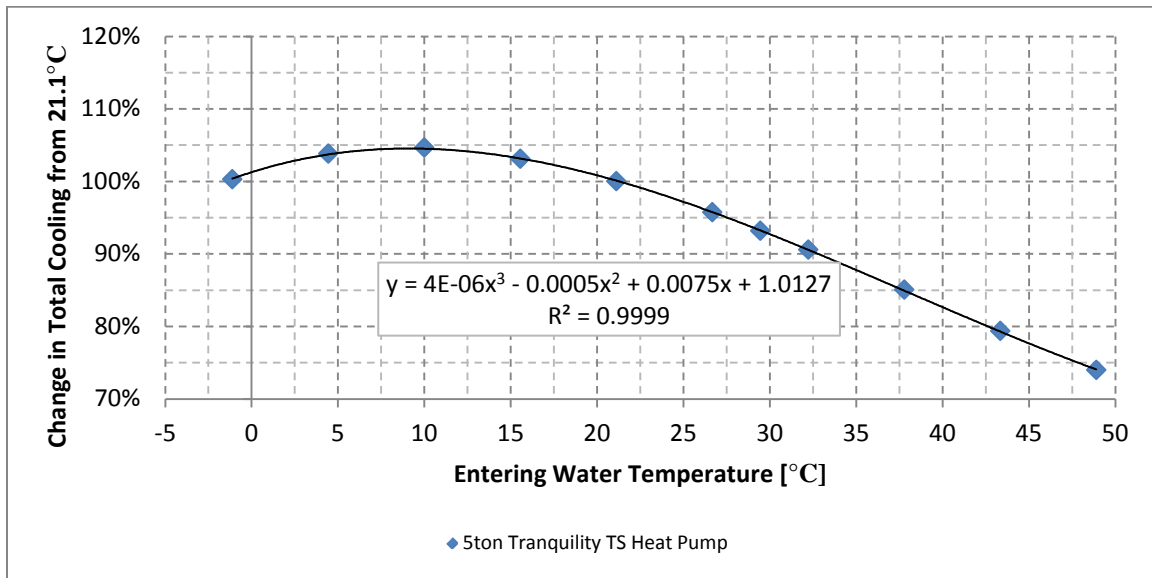


Figure 124: Heat pump cooling capacity versus entering water temperature (ClimateMaster, 2010)

The figure shows that for EWT that begins at 21.1°C (70°F), decreasing the EWT increases the total cooling available from the heat pump (seen as values greater than

100%), while increasing the EWT decreases the total cooling available from the heat pump (seen as values less than 100%). Because the integrated model uses on/off control and not variable speed control, this change in total cooling available directly results in a change in total cooling provided, even when the loads experienced by a zone remain constant. The values shown in the figure are averages of performance map data for the given EWT and only apply for the 5ton Tranquility TS heat pump, but the general trend applies to all heat pumps.

Thus, as total cooling capacity of the heat pump declines, the total cooling delivered to the zone declines, and the average zone air temperature increases. Eventually, the time-out-of setpoint for the model reflects these changes, as shown in Figure 125.

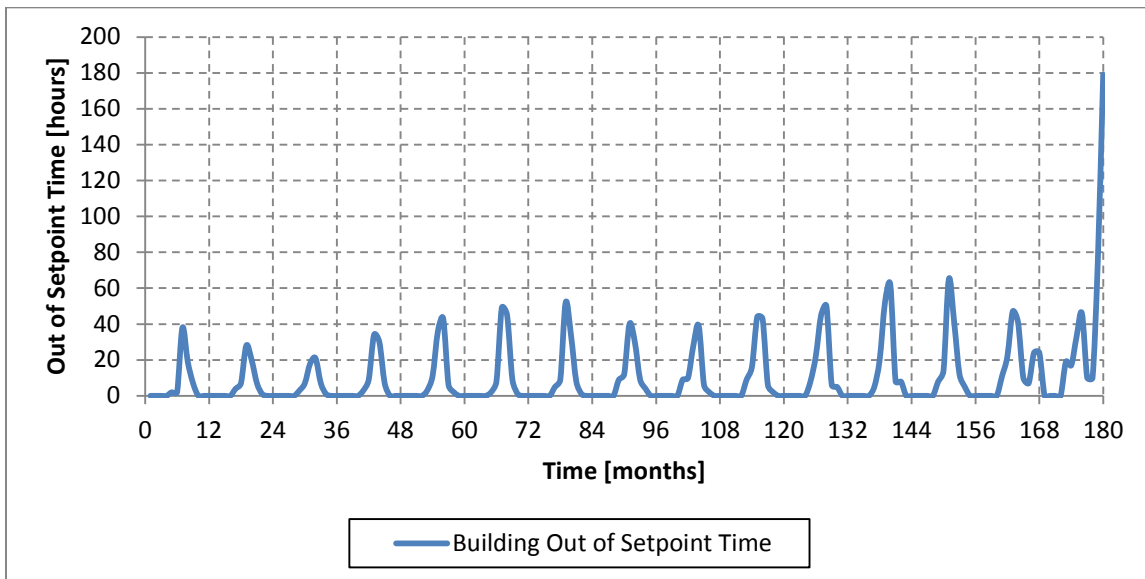


Figure 125: Monthly total time out-of-setpoint in the base model

The time-out-of-setpoint has consistent shape every year until year 14 (shown as 156 to 168 months). At the end of year 14, certain hours experience EWT greater than the 32.2°C (90°F) limit for heat pump operation in heating mode. As shown in Figure 121, beginning in month 160, the maximum EWT (shown in purple) is above 32.2°C for the remainder of the simulation. The bump in hours out-of-setpoint at month 168 in

Figure 125 represents heat pumps attempting to operate in heating mode, but being prevented due to excessively high EWT. This situation repeats in year 15 (month 168 through 180), where a spike in time out-of-setpoint indicates

6.3.5. Monthly Heat Pump Efficiency Data

Another measure of the increasing power usage of the heat pumps is heat pump efficiency. While the amount of cooling and heating provided by the heat pumps holds relatively constant from year-to-year, the increasing amount of power required to run the heat pump results in a decline in cooling efficiency. Cooling and heating efficiency values (EER and COP respectively) are shown in Figure 126 for Core1, Figure 127 for East2 and Figure 128 for South3.

All three figures show year-over-year declines in cooling efficiency and the effect of seasonal recovery. During the beginning of each year, EER increases as the ground temperature decreases. Heating the building requires the heat pumps to absorb energy from the ground loop, which lowers the ground loop water temperature. As a result, the EER improves in February, March and April (for example see months 14, 15 and 16).

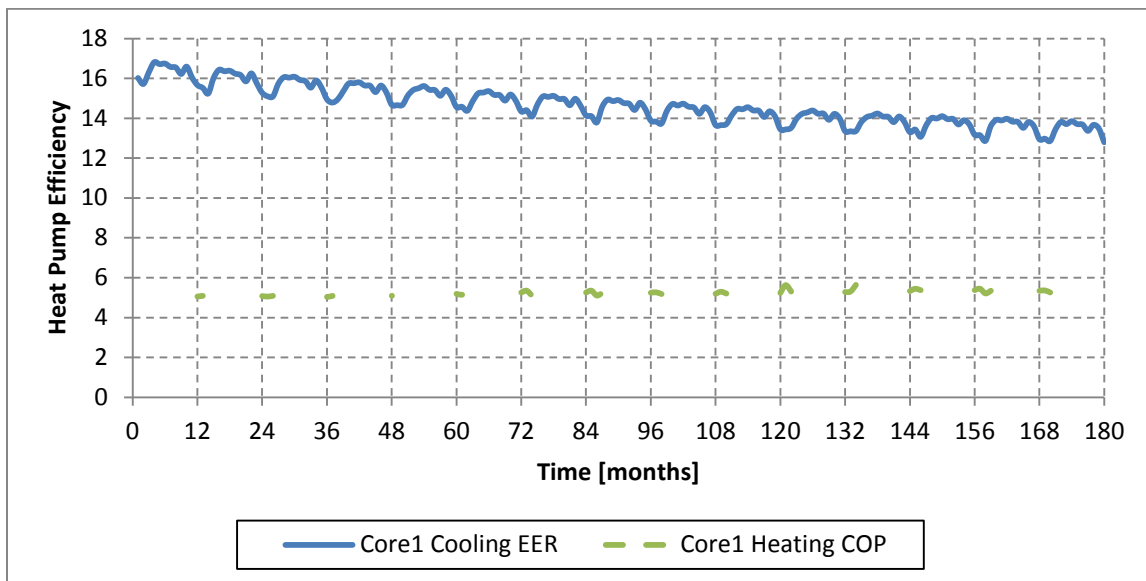


Figure 126: Monthly average cooling and heating efficiency for Core1

During summer months, EER decreases as the ground temperature increases. Cooling the building requires the heat pumps to reject energy to the ground loop, which increases the ground loop water temperature. As a result, the EER degrades during summer (for example see months 6, 7 and 8).

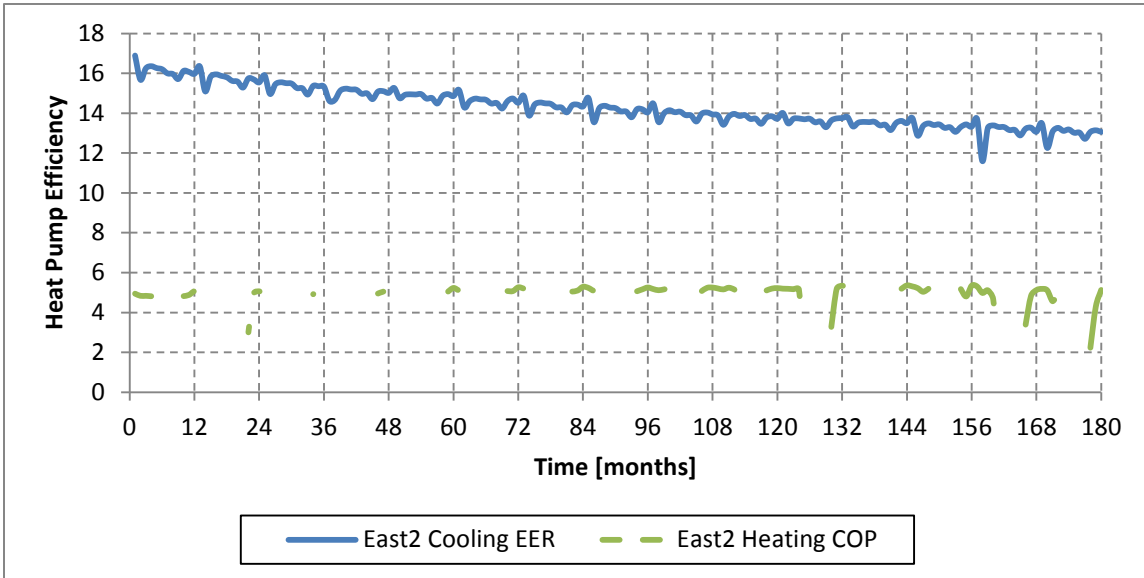


Figure 127: Monthly average cooling and heating efficiency for East2

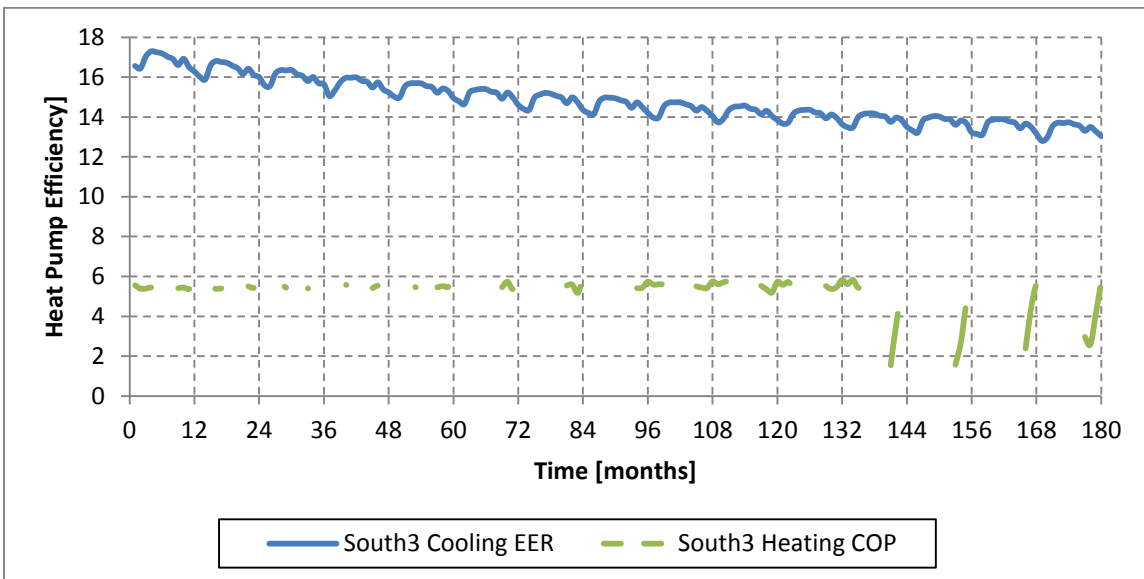


Figure 128: Monthly average cooling and heating efficiency for South3

Heating efficiency in all of the zones improved gradually during the first 10 years of the simulation. In the final years, fluctuations in heating efficiency occur. These declines are an artifact of hourly averaging. When a zone experiences both heating and cooling in a particular hour, the heating and cooling values cancel each other out in the hourly total, but the total energy usage does not cancel. This process occurs throughout the 15-year simulation, but in the final years the increasing EWT exacerbates this effect. This effect was discussed in detail in Section 4.8.

6.4. Annual Results

Annual values are used to examine trends over the duration of the 15-year simulation and to quantitatively examine changes in system performance. Annual averages, annual totals, annual maximums and annual minimums all serve to smooth the hourly data into a format easily viewed and analyzed on a 15-year scale. The annual values are computed by analyzing 8760 hours of hourly data and using the appropriate calculation (average, maximum, etc.) for each variable of interest.

6.4.1. Annual Heating and Cooling Data

The total annual cooling energy provided by the building's heat pumps is shown in Figure 129. Totals for each floor are also shown. There is a slight decrease in the annual amount of cooling provided to the building over time, from 600 MWh during the first year to 591 MWh in year 15, a 1.4% decrease over 15 years. This general decline is not continuous, with year 4 and year 10 showing the majority of the decrease, as shown in Table 47. While not continuous, the general decline is uniform across the building, with all 15 zones showing a decrease in total annual cooling over the 15-year period.

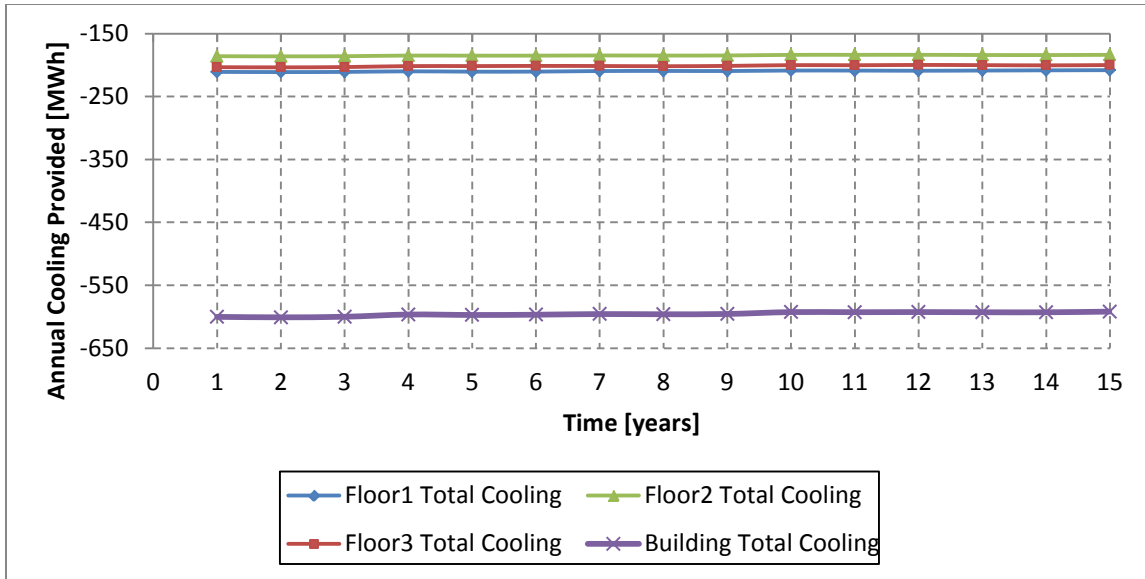


Figure 129: Annual total cooling energy provided in the base model over 15 years

Table 47: Data for the annual total cooling energy provided in the base model

Time [years]	Annual Total Cooling by Zone [MWh]																Total
	C1	S1	E1	N1	W1	C2	S2	E2	N2	W2	C3	S3	E3	N3	W3		
1	-103.3	-32.5	-20.5	-28.3	-26.3	-76.6	-32.3	-21.1	-29.4	-26.5	-85.9	-34.3	-22.8	-32.2	-28.2	-600.2	
2	-103.4	-32.5	-20.5	-28.3	-26.4	-76.7	-32.4	-21.1	-29.5	-26.5	-86.0	-34.3	-22.8	-32.3	-28.2	-600.9	
3	-103.2	-32.4	-20.6	-28.4	-26.3	-76.5	-32.4	-21.1	-29.4	-26.4	-85.7	-34.3	-22.7	-32.3	-28.1	-600.0	
4	-102.9	-32.2	-20.5	-28.2	-26.2	-75.9	-32.3	-21.1	-29.3	-26.4	-85.0	-34.0	-22.7	-32.1	-27.9	-596.5	
5	-103.3	-32.3	-20.4	-28.2	-26.2	-76.2	-32.3	-21.0	-29.2	-26.4	-85.1	-34.0	-22.5	-32.1	-27.9	-597.2	
6	-103.3	-32.5	-20.3	-28.1	-26.2	-76.2	-32.4	-20.9	-29.2	-26.3	-85.0	-34.0	-22.4	-32.0	-27.9	-596.8	
7	-102.7	-32.3	-20.3	-28.1	-26.1	-76.1	-32.2	-20.9	-29.2	-26.2	-85.2	-33.9	-22.5	-32.0	-27.9	-595.7	
8	-102.4	-32.3	-20.3	-28.2	-26.1	-76.1	-32.3	-20.9	-29.3	-26.2	-85.3	-34.0	-22.5	-32.1	-27.9	-596.1	
9	-102.5	-32.3	-20.4	-28.2	-26.1	-76.0	-32.3	-21.0	-29.3	-26.3	-84.9	-34.0	-22.5	-32.1	-27.9	-595.6	
10	-102.3	-32.1	-20.3	-28.0	-25.9	-75.5	-32.2	-20.9	-29.1	-26.2	-84.3	-33.8	-22.4	-31.8	-27.7	-592.6	
11	-102.5	-32.1	-20.3	-28.0	-25.9	-75.7	-32.1	-20.9	-29.0	-26.1	-84.5	-33.8	-22.4	-31.9	-27.7	-592.8	
12	-102.6	-32.2	-20.3	-28.0	-26.0	-75.5	-32.2	-20.9	-29.0	-26.1	-84.3	-33.8	-22.3	-31.8	-27.6	-592.5	
13	-102.4	-32.3	-20.2	-28.0	-25.9	-75.9	-32.2	-20.8	-29.0	-26.0	-84.6	-33.8	-22.2	-31.8	-27.7	-592.9	
14	-101.9	-32.2	-20.2	-28.1	-25.9	-75.8	-32.3	-20.8	-29.1	-26.1	-84.6	-33.9	-22.3	-31.9	-27.7	-592.9	
15	-101.7	-32.2	-20.3	-28.0	-25.9	-75.5	-32.2	-20.9	-29.1	-26.0	-84.2	-34.0	-22.4	-31.8	-27.6	-591.9	

The total annual hours of heat pump operation in cooling mode is relatively unchanged during the 15year simulation. The cooling hours show a slight drop from 49,671 hours in year one to 49,542 hours in year 15, a 0.3% decrease over 15years (shown in Figure 130). The total cooling time shows inconsistent fluctuations from year to year; a year of decreased total cooling hours is followed by a year of increased total cooling hours and vice versa (as shown in Table 48). The change in annual cooling hours

is also non-uniform. South1, South2, Core2 and Core3 show moderate decreases in total annual cooling hours during the 15year simulation, while East1 and North1 show slight increases in total annual cooling hours during the 15year simulation.

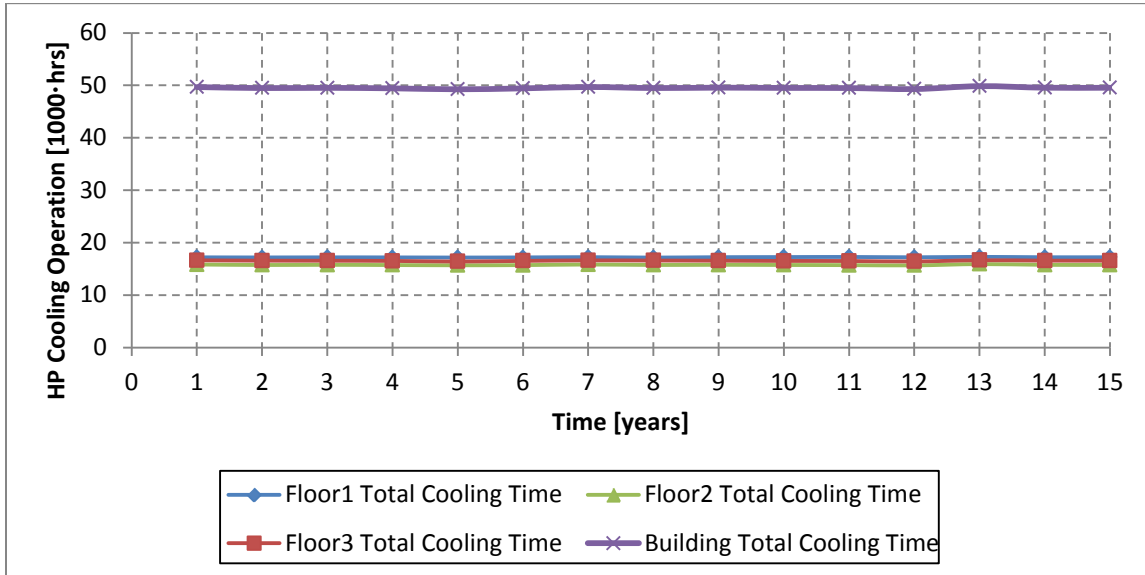


Figure 130: Annual total hours of cooling operation in the base model over 15 years

Table 48: Data for the annual total hours of cooling operation in the base model

Time [years]	Annual Total Cooling Time by Zone [hours]																Total
	C1	S1	E1	N1	W1	C2	S2	E2	N2	W2	C3	S3	E3	N3	W3		
1	4246	3464	3182	3015	3295	3588	3262	3007	2838	3139	3793	3387	3156	3017	3282	49671	
2	4251	3451	3169	3012	3296	3567	3220	3001	2823	3128	3768	3383	3149	2997	3267	49482	
3	4264	3415	3195	3038	3288	3581	3225	3004	2844	3118	3742	3368	3149	3021	3271	49523	
4	4301	3399	3182	3030	3276	3576	3209	3013	2830	3100	3757	3349	3157	3007	3245	49431	
5	4282	3429	3169	3014	3270	3587	3216	2977	2806	3099	3745	3351	3120	2963	3220	49248	
6	4274	3455	3157	3011	3288	3598	3241	2957	2794	3129	3773	3375	3133	2974	3265	49424	
7	4258	3467	3188	3023	3297	3595	3263	3006	2828	3138	3786	3386	3151	3003	3290	49679	
8	4236	3429	3172	3018	3302	3575	3227	2992	2814	3135	3773	3385	3157	3000	3271	49486	
9	4272	3423	3195	3053	3285	3583	3224	3012	2832	3124	3746	3364	3148	3022	3278	49561	
10	4315	3422	3198	3036	3280	3571	3208	3004	2838	3120	3752	3348	3153	3005	3255	49505	
11	4312	3450	3199	3034	3278	3597	3212	2989	2821	3094	3765	3346	3157	2992	3240	49486	
12	4277	3442	3190	3020	3280	3582	3218	2977	2794	3096	3754	3350	3139	2952	3220	49291	
13	4271	3489	3200	3024	3308	3618	3285	3004	2839	3165	3804	3390	3156	3005	3290	49848	
14	4255	3453	3184	3023	3299	3576	3226	2999	2817	3147	3774	3379	3152	2990	3274	49548	
15	4259	3433	3200	3031	3296	3566	3224	3004	2839	3127	3726	3383	3165	3015	3274	49542	

The total annual heating energy provided by the building's heat pumps is shown in Figure 131, along with totals for each floor. Compared to the total annual cooling energy, total annual heating energy is less consistent from year to year.

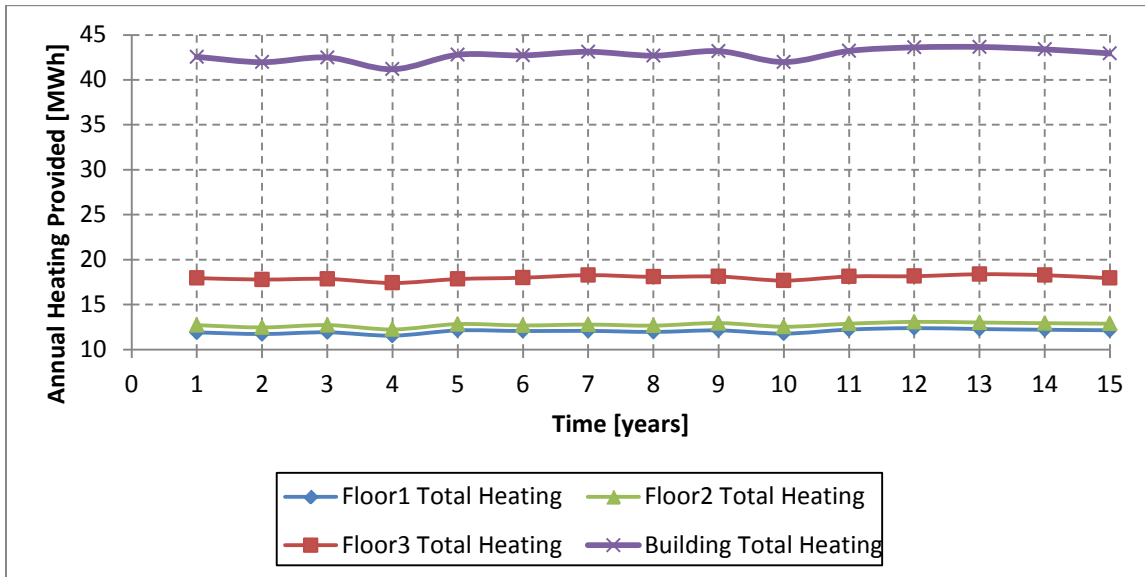


Figure 131: Annual total heating energy provided in the base model over 15 years

The total annual heating energy increases slightly over time, beginning at 42.6MWh in year one and ending at 42.9MWh in year 15, a 0.9% increase over the 15years. This change is neither continuous nor uniform. Table 49 shows that the annual heating increased year-over-year in half of the years, and it decreased year-over-year in the other half. The table also shows that Core1, North1, Core2, South2, North2, Core3, South3, East3 and North3 experience a decrease in total annual heating energy over the 15year period, while the remaining zones experience a slight increase during this time.

Table 49: Data for the annual total heating energy provided in the base model

Time [years]	Annual Total Heating by Zone [MWh]																Total
	C1	S1	E1	N1	W1	C2	S2	E2	N2	W2	C3	S3	E3	N3	W3		
1	0.2	3.0	2.3	3.8	2.6	0.7	3.1	2.4	3.9	2.6	1.7	4.3	3.2	5.3	3.6	42.6	
2	0.1	3.0	2.3	3.7	2.6	0.6	3.1	2.3	3.8	2.6	1.7	4.2	3.2	5.2	3.6	42.0	
3	0.1	3.0	2.3	3.8	2.7	0.6	3.1	2.4	3.9	2.7	1.7	4.2	3.2	5.2	3.6	42.5	
4	0.1	2.9	2.2	3.6	2.7	0.6	3.0	2.3	3.8	2.6	1.5	4.1	3.1	5.1	3.6	41.2	
5	0.2	3.0	2.3	3.8	2.8	0.7	3.1	2.4	3.9	2.7	1.6	4.2	3.2	5.2	3.7	42.8	
6	0.1	3.0	2.3	3.8	2.8	0.7	3.1	2.4	3.9	2.7	1.7	4.2	3.1	5.2	3.8	42.7	
7	0.1	3.0	2.3	3.7	2.8	0.7	3.1	2.4	3.8	2.8	1.7	4.3	3.2	5.2	3.9	43.1	
8	0.1	3.0	2.3	3.7	2.8	0.6	3.1	2.3	3.8	2.8	1.7	4.2	3.2	5.1	3.9	42.7	
9	0.1	3.0	2.4	3.7	2.9	0.6	3.1	2.4	3.9	2.9	1.7	4.2	3.2	5.1	3.9	43.2	
10	0.1	3.0	2.3	3.6	2.8	0.6	3.0	2.3	3.7	2.9	1.5	4.1	3.1	5.0	3.9	42.0	
11	0.1	3.1	2.4	3.7	2.9	0.7	3.0	2.3	3.8	3.0	1.5	4.3	3.2	5.2	4.0	43.2	
12	0.2	3.1	2.4	3.8	2.9	0.7	3.1	2.4	3.9	3.0	1.6	4.2	3.2	5.1	4.0	43.6	
13	0.1	3.2	2.4	3.7	2.9	0.7	3.1	2.4	3.8	3.0	1.7	4.3	3.2	5.1	4.0	43.7	
14	0.1	3.1	2.4	3.6	2.9	0.6	3.1	2.4	3.8	3.1	1.7	4.3	3.2	5.1	4.0	43.4	
15	0.1	3.1	2.4	3.7	2.8	0.6	3.0	2.4	3.8	3.0	1.7	4.2	3.2	5.0	3.9	42.9	

The annual time spent in heating mode is similarly inconsistent, as shown in Figure 132. The annual time spent in heating mode begins at 7771hrs in year one, decreases to 7559hrs in year three, increases to 7986hrs in year 11, and finally ends at 7460hrs in year 15 (see Table 50). The 7460hrs in year 15 represent a 4.0% decrease in total annual heating hours over the 15year interval; however the majority of this drop occurs during the final year of simulation.

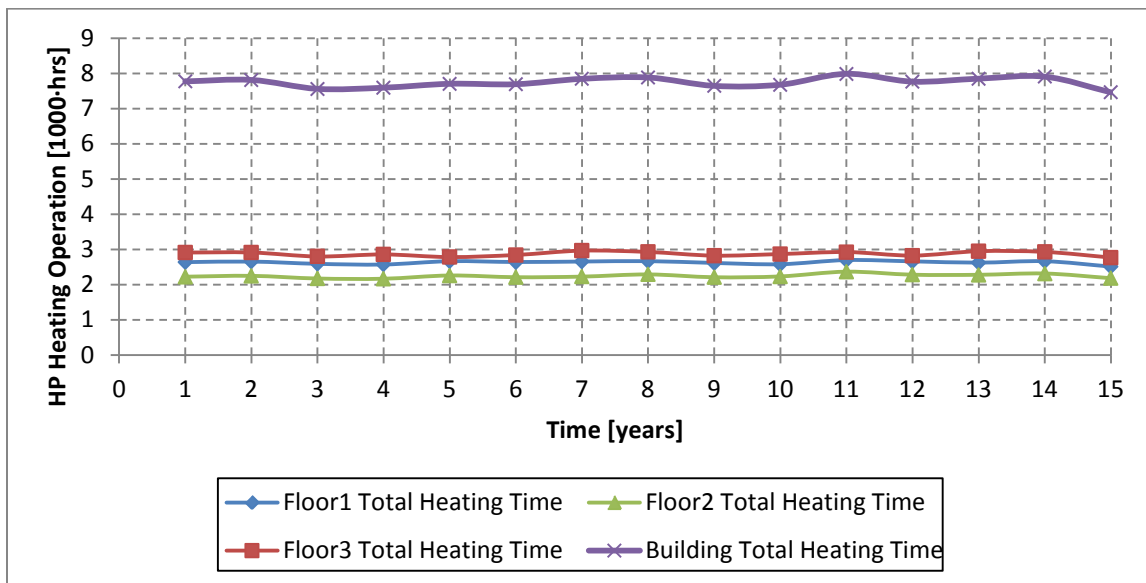


Figure 132: Annual total hours of heating operation in the base model over 15 years

Table 50: Data for the annual total hours of heating operation in the base model

Time [years]	Annual Total Heating Time by Zone [hours]															Total
	C1	S1	E1	N1	W1	C2	S2	E2	N2	W2	C3	S3	E3	N3	W3	
1	27	554	654	696	706	78	459	539	584	564	149	595	682	747	737	7771
2	23	567	638	702	723	74	468	550	588	568	163	577	691	737	743	7812
3	18	537	633	683	718	73	438	529	572	560	168	545	656	708	721	7559
4	21	533	609	677	730	75	430	528	576	557	151	563	666	729	747	7592
5	26	545	648	699	746	70	461	547	595	585	144	560	649	706	722	7703
6	25	542	633	697	744	79	439	538	579	574	155	553	649	717	767	7691
7	23	554	639	685	753	70	443	525	588	600	151	587	671	738	817	7844
8	22	555	644	688	757	71	465	540	588	624	153	573	668	729	804	7881
9	18	534	632	690	740	71	433	526	565	613	163	542	645	715	757	7644
10	20	536	618	676	728	73	434	520	567	638	151	559	650	723	784	7677
11	22	562	650	706	756	73	465	544	598	686	127	583	677	733	804	7986
12	24	552	653	702	729	69	458	540	578	635	140	562	646	699	777	7764
13	23	552	632	677	739	71	448	519	586	654	152	577	666	734	819	7849
14	21	558	654	697	733	70	457	542	578	667	157	575	674	724	798	7905
15	22	525	616	653	695	71	428	512	551	619	161	543	628	684	752	7460

The final year of simulation experiences average heat pump EWT of 31.1°C (88.0°F) (shown in Figure 134) and maximum EWT values greater than the 32.2°C (90°F) limit for heat pump operation in heating mode during every month of the year (as previously shown in Figure 121). EWT values greater than the 32.2°C cause the heat pump to shut down during heating mode, resulting in a sharp decline in total annual heating hours during year 15. For more detail on heat pump shutdown, see Section 6.4.4.

6.4.2. Annual Ground Loop Data

The annual total heat rejected to the ground loop is shown in Figure 133. The annual total heat rejected during cooling increases from 723.2MWh in year 1 to 738.9MWh in year 15, a 2.2% increase over the 15year interval, as shown in Table 51. This increase is driven by the increase in average EWT, shown in Figure 134. As EWT increases, the heat pump compressor rejects more heat to the ground loop per unit of cooling supplied to the zone. Since the amount of cooling required stays fairly constant over time (see Figure 129), the total annual heat rejected to the ground loop during cooling increases. The annual total during cooling increases every year of the simulation except for year 4 and year 10, the two years that showed large decreases in total annual cooling provided (see Figure 129).

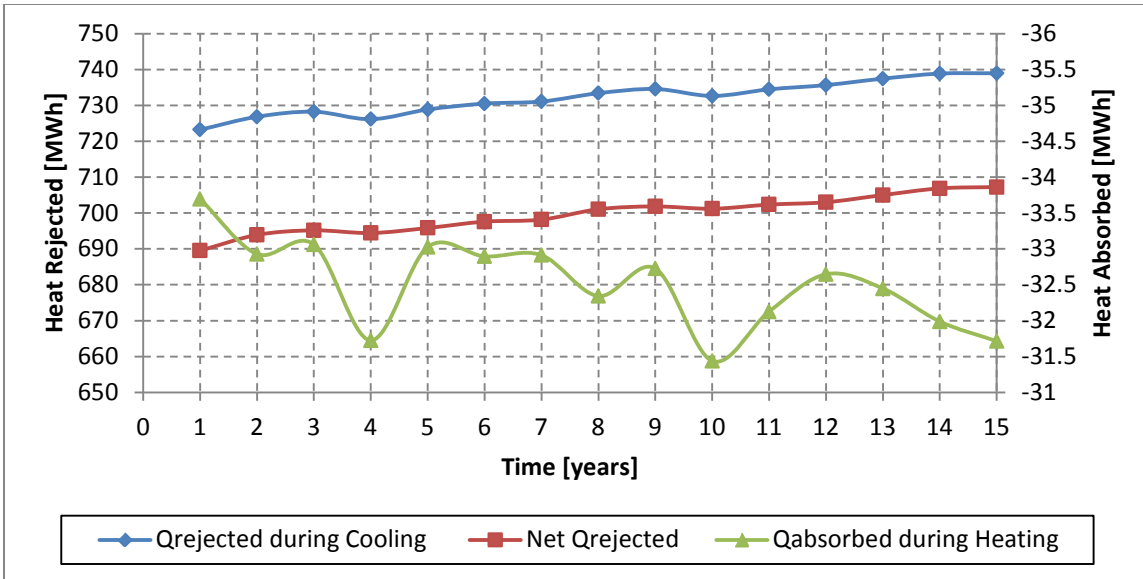


Figure 133: Annual total heat rejected to the ground loop in the base model over 15 years

Table 51: Data for the annual total heat rejected to the ground loop in the base model

Time [years]	Total Heat Rejected during Cooling [MWh]	Total Heat Absorbed during Heating [MWh]	Total Net Heat Rejected [MWh]
1	723.2	-33.7	689.5
2	726.8	-32.9	693.9
3	728.2	-33.1	695.2
4	726.1	-31.7	694.4
5	728.9	-33.0	695.8
6	730.5	-32.9	697.6
7	731.1	-32.9	698.2
8	733.4	-32.3	701.0
9	734.6	-32.7	701.8
10	732.6	-31.4	701.2
11	734.5	-32.1	702.3
12	735.7	-32.6	703.0
13	737.4	-32.4	705.0
14	738.9	-32.0	706.9
15	738.9	-31.7	707.2
Percent Change	2.2%	-5.9%	2.6%

The annual total heat absorbed from the ground loop during heating operation is volatile, as it trends with the annual total heat provided by the heat pumps (see Figure 131). While the year over year data is inconsistent, the general trend in annual total heat absorbed is decreasing. The annual total heat absorbed during the first year of simulation was 33.7MWh, which decreased to 31.7MWh during year 15, a 5.9% reduction over the 15year interval.

The annual total net heat rejected to the ground loop represents the combined effect of heat rejection during cooling operation and heat absorption during heating operation. The net heat rejected is calculated by summing the annual total heat rejected with the annual total heat absorbed. Since the annual cooling and heating loads are so imbalanced toward cooling, the net heat rejected is dominated by the annual total heat rejected, or cooling operation. The annual total net heat rejected increases every year except year 4 and year 10, starting in year 1 at 689.5MWh and ending at 707.2MWh after year 15. This represents a 2.6% increase over the 15year period.

The net heat rejected to the ground loop every year causes ground heating, which is clearly shown in Figure 134.

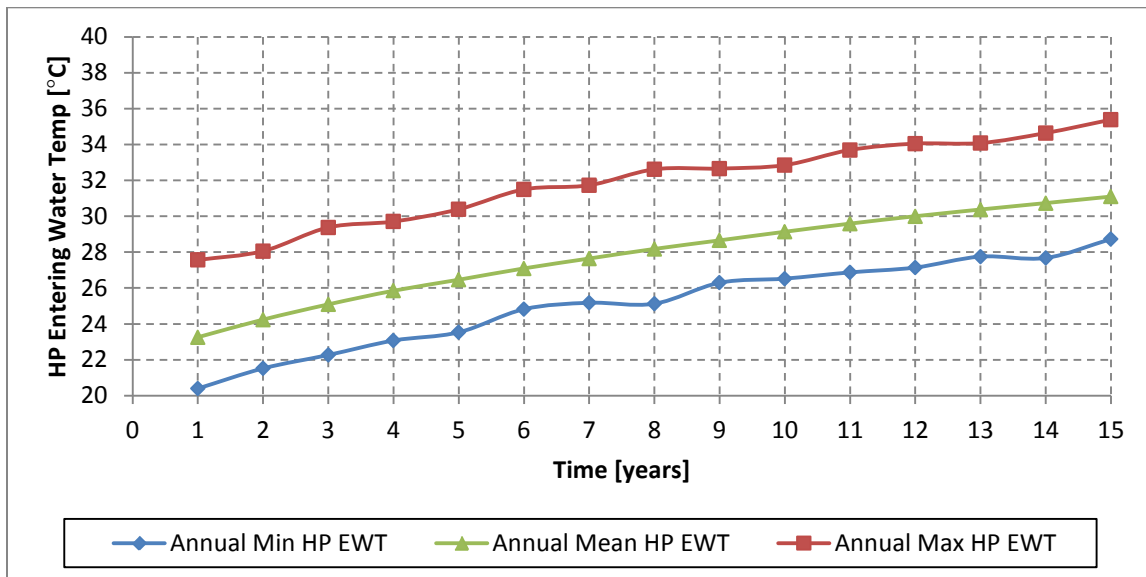


Figure 134: Annual extremes for heat pump EWT in the base model over 15 years

The annual average heat pump entering water temperature increases from 23.3°C in year 1 to 31.1°C in year 15, a 33.7% increase over the 15-year simulation. The annual minimum EWT and annual maximum EWT show similar growth. Detailed data for the entering water temperature is shown in Table 52.

Table 52: Data for the annual extremes for heat pump EWT in the base model

Time [years]	Annual Min HP EWT [°C]	Annual Mean HP EWT [°C]	Annual Max HP EWT [°C]
1	20.4	23.3	27.6
2	21.5	24.2	28.1
3	22.3	25.1	29.4
4	23.1	25.8	29.7
5	23.5	26.5	30.4
6	24.8	27.1	31.5
7	25.2	27.6	31.7
8	25.1	28.2	32.6
9	26.3	28.7	32.7
10	26.5	29.1	32.9
11	26.9	29.6	33.7
12	27.1	30.0	34.0
13	27.8	30.4	34.1
14	27.7	30.7	34.6
15	28.7	31.1	35.4
Percent Change	40.8%	33.7%	28.4%

6.4.3. Annual Power Usage Data

The increasing entering water temperature increases the amount of energy required to operate the heat pump per unit of cooling or heating provided. The increasing total power usage for heating and for cooling is shown in Figure 135.

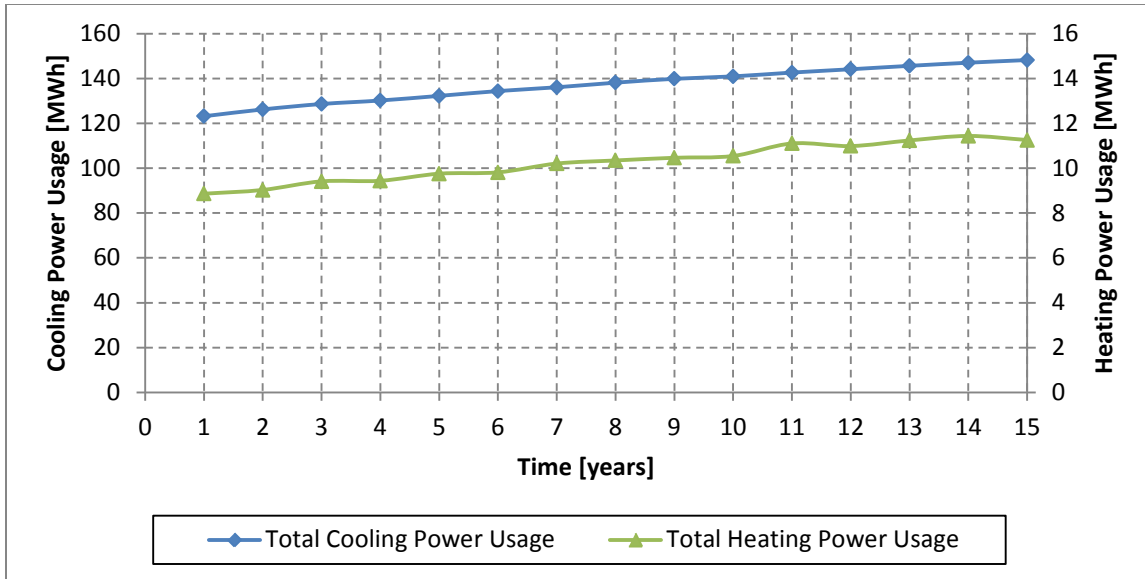


Figure 135: Annual total power usage in the base model over 15 years

The annual total cooling power usage begins at 123.1MWh during year 1 and increases steadily to 148.2MWh in year 15, a 20.4% increase over the 15year interval (see Table 53). The total heating power usage begins at 8.9MWh in year 1 and increases every year except year 12 and year 15. It eventually reaches 11.3MWh during year 15, which represents a 27.0% increase over that time (see Table 54).

Table 53: Data for the annual total power usage during cooling in the base model

Time [years]	Annual Total Power Usage during Cooling by Zone [MWh]															
	C1	S1	E1	N1	W1	C2	S2	E2	N2	W2	C3	S3	E3	N3	W3	Total
1	21.3	6.8	4.3	5.8	5.5	15.8	6.7	4.5	6.1	5.5	17.2	6.9	4.7	6.4	5.6	123.1
2	21.8	7.0	4.5	6.0	5.6	16.1	7.0	4.6	6.2	5.6	17.6	7.1	4.8	6.6	5.7	126.2
3	22.2	7.1	4.6	6.1	5.7	16.4	7.1	4.7	6.3	5.7	17.9	7.3	4.9	6.7	5.8	128.6
4	22.6	7.2	4.6	6.1	5.7	16.6	7.2	4.8	6.4	5.8	18.0	7.4	5.0	6.8	5.9	130.2
5	23.0	7.4	4.7	6.2	5.8	16.9	7.4	4.8	6.5	5.9	18.3	7.5	5.0	6.9	6.0	132.2
6	23.3	7.5	4.8	6.3	5.9	17.1	7.5	4.9	6.6	6.0	18.6	7.6	5.1	7.0	6.1	134.4
7	23.5	7.6	4.8	6.4	6.0	17.4	7.6	5.0	6.7	6.0	18.9	7.8	5.2	7.1	6.2	136.1
8	23.8	7.7	4.9	6.5	6.1	17.6	7.7	5.1	6.8	6.1	19.2	7.9	5.3	7.2	6.2	138.1
9	24.1	7.8	5.0	6.6	6.1	17.8	7.8	5.1	6.9	6.2	19.4	8.0	5.3	7.3	6.3	139.8
10	24.4	7.9	5.0	6.6	6.2	17.9	7.9	5.2	6.9	6.3	19.4	8.1	5.4	7.3	6.4	140.9
11	24.7	8.0	5.1	6.7	6.3	18.2	8.0	5.2	7.0	6.3	19.7	8.2	5.5	7.4	6.4	142.6
12	25.0	8.1	5.1	6.8	6.3	18.3	8.1	5.3	7.1	6.4	19.9	8.3	5.5	7.5	6.5	144.1
13	25.2	8.2	5.2	6.8	6.4	18.6	8.2	5.3	7.1	6.4	20.2	8.4	5.5	7.5	6.6	145.6
14	25.3	8.3	5.2	6.9	6.4	18.7	8.3	5.4	7.2	6.5	20.3	8.5	5.6	7.6	6.6	147.0
15	25.5	8.4	5.3	7.0	6.5	18.8	8.4	5.5	7.3	6.5	20.4	8.6	5.7	7.7	6.7	148.2

Table 54: Data for the annual total power usage during heating in the base model

Time [years]	Annual Total Power Usage during Heating by Zone [MWh]															Total
	C1	S1	E1	N1	W1	C2	S2	E2	N2	W2	C3	S3	E3	N3	W3	
1	0.03	0.60	0.47	0.78	0.88	0.15	0.79	0.59	0.48	0.59	0.32	0.77	0.60	1.00	0.81	8.9
2	0.02	0.60	0.46	0.76	1.02	0.12	0.77	0.58	0.47	0.65	0.31	0.75	0.59	0.98	0.93	9.0
3	0.02	0.61	0.47	0.77	1.15	0.12	0.78	0.59	0.48	0.75	0.32	0.75	0.59	0.98	1.04	9.4
4	0.02	0.59	0.45	0.73	1.28	0.11	0.74	0.57	0.45	0.83	0.28	0.73	0.57	0.95	1.14	9.4
5	0.03	0.61	0.47	0.75	1.39	0.13	0.77	0.58	0.46	0.87	0.29	0.74	0.58	0.95	1.14	9.8
6	0.03	0.62	0.47	0.74	1.38	0.13	0.75	0.57	0.45	0.85	0.31	0.74	0.57	0.95	1.26	9.8
7	0.03	0.65	0.47	0.73	1.44	0.13	0.74	0.57	0.45	1.00	0.31	0.75	0.58	0.95	1.40	10.2
8	0.02	0.67	0.49	0.72	1.46	0.12	0.73	0.57	0.45	1.10	0.30	0.75	0.58	0.94	1.45	10.3
9	0.02	0.69	0.52	0.73	1.47	0.11	0.75	0.58	0.46	1.15	0.31	0.74	0.58	0.94	1.39	10.5
10	0.02	0.73	0.55	0.70	1.50	0.11	0.72	0.57	0.44	1.25	0.27	0.73	0.56	0.92	1.49	10.5
11	0.03	0.82	0.63	0.71	1.61	0.12	0.72	0.57	0.45	1.34	0.26	0.75	0.57	0.93	1.58	11.1
12	0.03	0.82	0.67	0.72	1.54	0.12	0.74	0.58	0.46	1.23	0.28	0.75	0.58	0.92	1.54	11.0
13	0.03	0.91	0.70	0.71	1.54	0.13	0.72	0.57	0.45	1.34	0.30	0.76	0.59	0.92	1.57	11.2
14	0.02	0.92	0.77	0.70	1.53	0.11	0.71	0.59	0.47	1.41	0.29	0.79	0.60	0.91	1.59	11.4
15	0.02	0.92	0.77	0.70	1.49	0.11	0.72	0.59	0.48	1.35	0.29	0.77	0.60	0.90	1.55	11.3

6.4.4. Annual Out-of-Setpoint Data

The annual total time out-of-setpoint for each floor and for the total building is shown in Figure 135. During the first year of simulation each floor of the building shows a non-zero time out-of-setpoint, which results from the difficulty of sizing heat pumps for a limited-control application. Specifically, West1 and West2 experience internal loads that are impossible to handle with a single-sized heat pump using on-off control. These zones are small, meaning that their internal loads are not particularly substantial, but the zone orientation results in high solar irradiance values. The high solar irradiance requires a large heat pump for cooling (the West zones all use 5ton heat pumps compared to the similarly sized East zones that use 4ton heat pumps – see Section 4.4.3 for more information on heat pump sizing), but this larger heat pump is then over-sized during winter, causing excess heat to be added to the zone. As a result, even in year one of simulation, West1 and West2 experience out-of-setpoint conditions during winter due to excessively high zone temperatures.

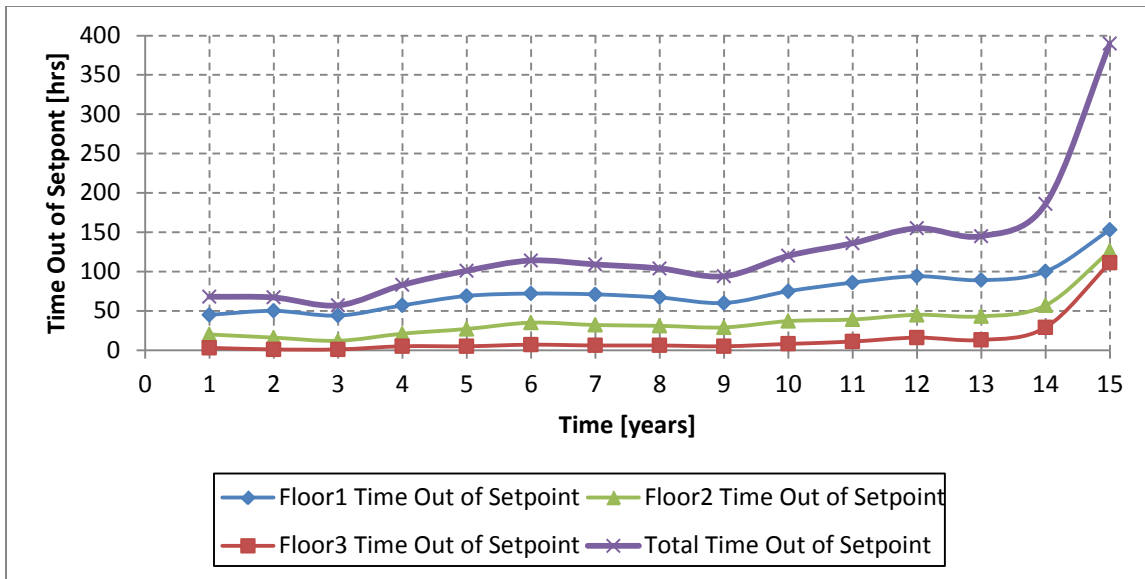


Figure 136: Annual total time out-of-setpoint in the base model over 15 years

The total time out-of-setpoint for year one of simulation was 68hrs (see Table 55). The total time out-of-setpoint increases for the first 8 years of simulation due to increasing EWT. As EWT increases, the total heating capacity of the heat pumps increase, which exacerbates the excessive heating condition in West1, West2 and West3. This can also be seen by the increasing annual total heating in the West zones shown in Table 49. In year 10, South1 and North1 begin behaving like the West zones; increased EWT increases their heat pump heating capacity sufficiently to cause an excessive heating condition.

At year 14, an additional type of out-of-setpoint condition is experienced: heat pump shutdown due to excessively high EWT. In year 14 and year 15, when EWT (previously shown in Figure 134) is above the 32.2°C (90°F) limit for heat pump operation in heating mode, the heat pump shuts down, resulting in zone temperature below setpoint. During heat pump shutdown the ground loop continues to circulate and it eventually drops below 32.2°C, at which point the heat pumps can again provide heating. The combined effects of heat pump shutdown due to excessively high EWT with high EWT increasing the heat pump heating capacity cause the total time out-of-setpoint during year 15 to be 390hours, which is a 473.5% increase over the 15year simulation.

Table 55: Data for the annual total time out-of-setpoint in the base model

Time [years]	Annual Total Out-of-Setpoint Time by Zone [hours]															Total
	C1	S1	E1	N1	W1	C2	S2	E2	N2	W2	C3	S3	E3	N3	W3	
1	0	0	0	0	45	0	0	0	0	20	0	0	0	2	1	68
2	0	0	0	0	50	0	0	0	0	16	0	0	0	0	1	67
3	0	0	0	0	44	0	0	0	0	12	0	0	0	0	1	57
4	0	0	0	1	56	0	0	0	0	21	0	0	0	0	5	83
5	0	0	0	1	68	0	0	0	0	27	0	0	0	0	5	101
6	0	0	0	1	71	0	0	0	0	35	0	0	0	0	7	114
7	0	0	0	2	69	0	0	0	0	32	0	0	0	0	6	109
8	0	0	0	1	66	0	0	0	0	31	0	0	0	0	6	104
9	0	0	0	1	59	0	0	0	0	29	0	0	0	0	5	94
10	0	0	0	3	72	0	0	0	1	36	0	0	0	0	8	120
11	0	2	0	4	80	0	0	0	0	39	0	0	0	0	11	136
12	0	2	0	5	87	0	0	0	0	45	0	0	0	0	16	155
13	0	2	0	5	82	0	0	0	0	43	0	0	0	0	13	145
14	0	5	2	10	83	1	4	3	4	45	1	5	5	5	13	186
15	1	16	17	30	89	8	15	19	24	60	11	17	22	28	33	390

6.4.5. Annual Heat Pump Efficiency Data

The annual average heat pump efficiency for the building and for each floor is shown for cooling with EER in Figure 137. Cooling efficiency decreases continuously from year to year and uniformly throughout the building during the 15year simulation because of the increasing EWT values, shown previously in Figure 134. As the EWT increases the total cooling available decreases per unit of power required, resulting in lower efficiency (previously discussed in Section 6.3.4).

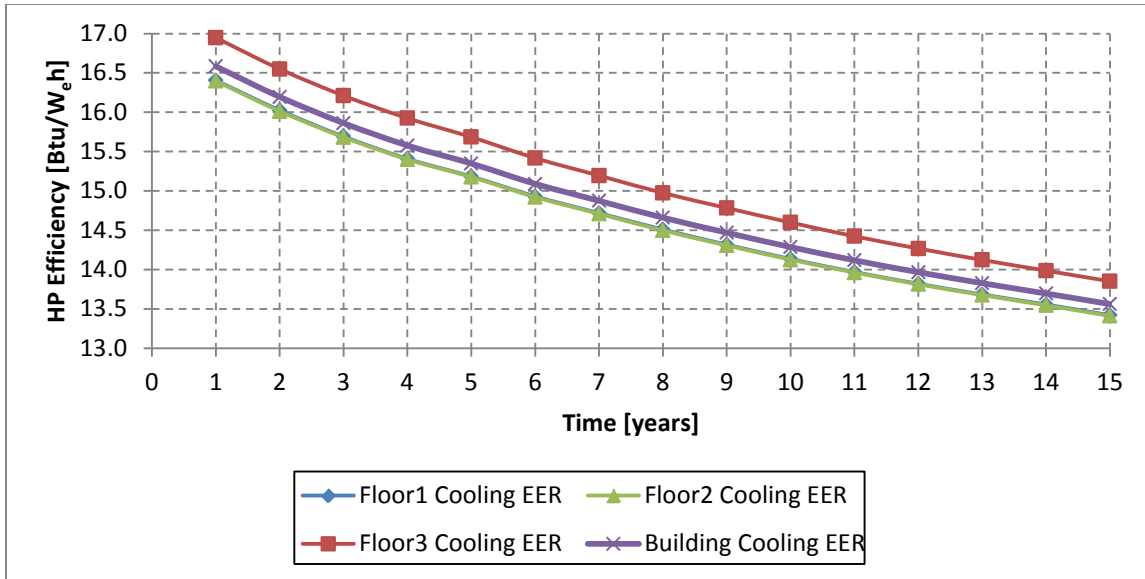


Figure 137: Annual average cooling EER in the base model over 15 years

The annual average EER in year 1 is 16.6Btu/W_eh, and it decreases to a 13.6Btu/W_eh in year 15, an 18.2% reduction across the 15years (see Table 56).

Table 56: Data for the annual average cooling EER in the base model

Time [years]	Annual Average EER by Zone [Btu/W _e h]															
	C1	S1	E1	N1	W1	C2	S2	E2	N2	W2	C3	S3	E3	N3	W3	Avg.
1	16.5	16.4	16.1	16.6	16.5	16.6	16.4	16.0	16.5	16.5	17.0	16.9	16.5	17.1	17.1	16.6
2	16.2	15.9	15.7	16.2	16.1	16.2	15.9	15.6	16.2	16.1	16.7	16.4	16.1	16.7	16.8	16.2
3	15.8	15.5	15.3	15.9	15.8	15.9	15.5	15.3	15.9	15.8	16.4	16.1	15.8	16.4	16.4	15.9
4	15.6	15.2	15.1	15.6	15.6	15.6	15.2	15.0	15.6	15.5	16.1	15.7	15.5	16.1	16.2	15.6
5	15.4	15.0	14.8	15.4	15.3	15.4	15.0	14.8	15.4	15.3	15.9	15.5	15.3	15.9	15.9	15.3
6	15.1	14.7	14.6	15.2	15.1	15.2	14.7	14.5	15.1	15.1	15.6	15.2	15.0	15.7	15.7	15.1
7	14.9	14.5	14.4	15.0	14.9	15.0	14.5	14.3	14.9	14.9	15.4	14.9	14.8	15.4	15.4	14.9
8	14.7	14.3	14.2	14.8	14.7	14.7	14.2	14.1	14.7	14.7	15.2	14.7	14.6	15.2	15.2	14.7
9	14.5	14.1	14.0	14.6	14.5	14.6	14.1	13.9	14.5	14.5	15.0	14.5	14.4	15.0	15.0	14.5
10	14.3	13.9	13.8	14.4	14.3	14.4	13.9	13.7	14.4	14.3	14.8	14.3	14.2	14.8	14.9	14.3
11	14.2	13.7	13.6	14.2	14.1	14.2	13.7	13.6	14.2	14.1	14.6	14.1	14.0	14.7	14.7	14.1
12	14.0	13.5	13.5	14.1	14.0	14.1	13.5	13.4	14.0	14.0	14.5	14.0	13.8	14.5	14.5	14.0
13	13.9	13.4	13.3	14.0	13.9	13.9	13.4	13.3	13.9	13.8	14.3	13.8	13.7	14.4	14.4	13.8
14	13.8	13.2	13.2	13.8	13.7	13.8	13.2	13.2	13.8	13.7	14.2	13.7	13.6	14.2	14.3	13.7
15	13.6	13.1	13.1	13.7	13.6	13.7	13.1	13.0	13.7	13.6	14.1	13.5	13.4	14.1	14.1	13.6

The annual average heat pump efficiency for the building and for each floor is shown for heating with COP in Figure 138. Heat pump heating efficiency increases as EWT increases, so the negative slope shown in Figure 138 requires additional

explanation. Figure 139 shows the annual average COP for each zone over the 15 year simulation.

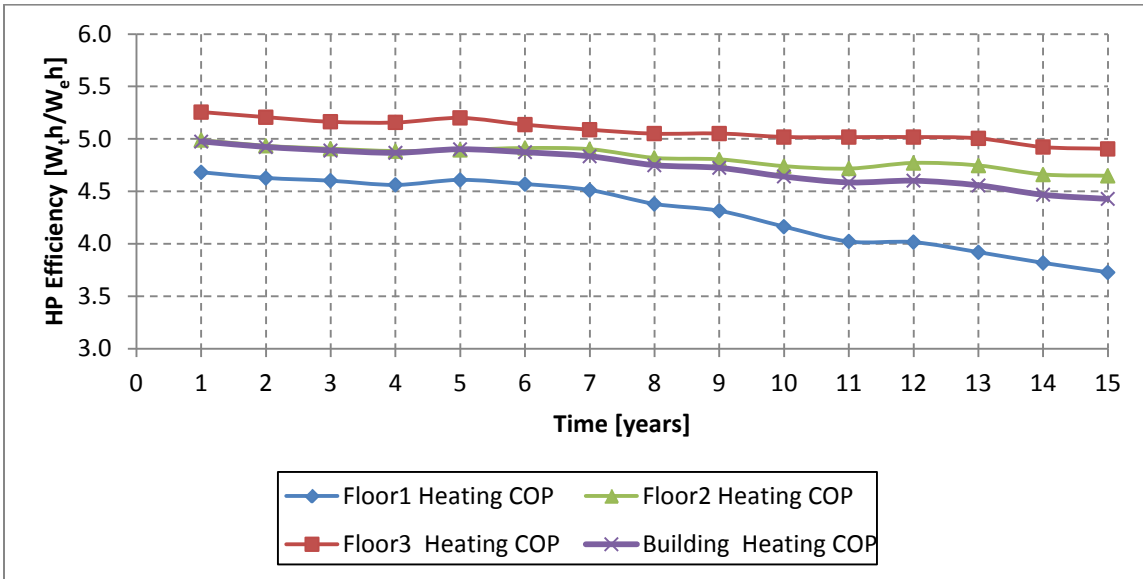


Figure 138: Annual average heating COP in the base model for 15 years

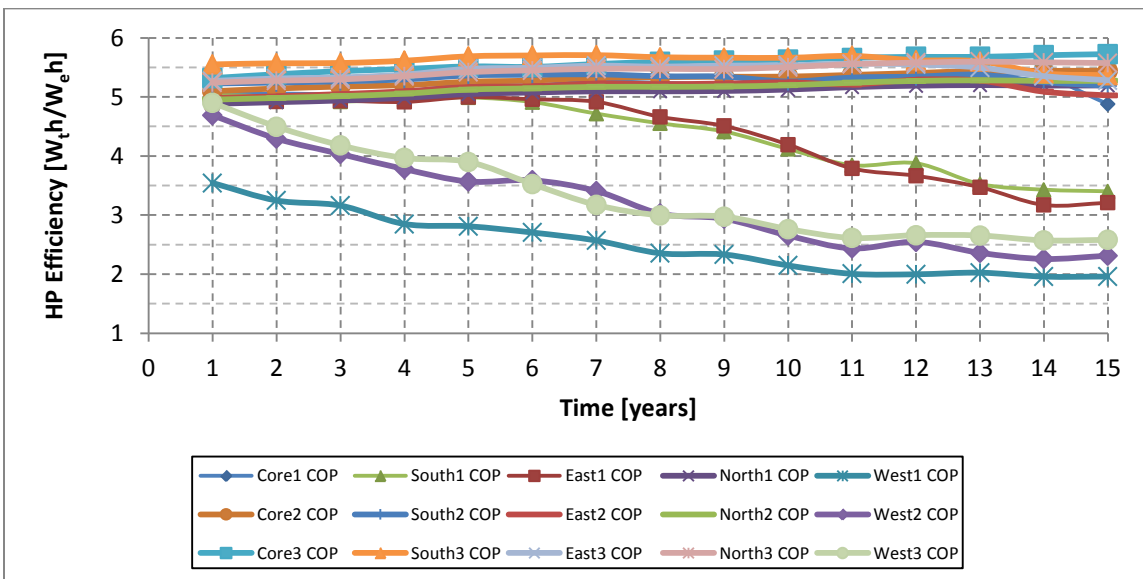


Figure 139: Annual average heating COP of all zones in the base model for 15 years

According to the figure, the majority of zones in the model do perform as expected; they increase gradually from approximately 5.0W_th/W_eh to 5.5W_th/W_eh. Five zones however, show precipitous decline in COP: West1, West2, West3, South1 and East1.

More specifically, Core and North zones collectively show a 5.0% increase in COP across the 15year interval, starting at an average COP of 5.1 during year one and ending at an average COP of 5.3 in year 15. Heat pump efficiency in East2, East3, South2 and South3 zones remains relatively constant, starting at an average COP of 5.3 during year one and ending at an average COP of 5.2 during year 15 (a 0.8% decrease over the 15year simulation). The five zones showing precipitous decline in heat pump efficiency (West1, West2, West3, South1 and East1) have an average COP of 4.6 during year one and an average COP of 2.7 during year 15 (a 41.6% decrease over that time). Detailed annual average COP data for each zone is shown in Table 57.

Table 57: Data for the annual average heating COP in the base model

Time [years]	Annual Average COP by Zone [W _{th} /W _{eh}]															
	C1	S1	E1	N1	W1	C2	S2	E2	N2	W2	C3	S3	E3	N3	W3	Avg.
1	5.0	5.0	4.9	4.9	3.5	5.1	5.2	5.0	5.0	4.7	5.3	5.6	5.3	5.2	4.9	5.0
2	5.1	5.0	4.9	4.9	3.2	5.1	5.2	5.0	5.0	4.3	5.4	5.6	5.3	5.3	4.5	4.9
3	5.0	4.9	4.9	4.9	3.2	5.2	5.3	5.0	5.0	4.0	5.4	5.6	5.3	5.3	4.2	4.9
4	5.1	5.0	4.9	5.0	2.8	5.2	5.3	5.1	5.1	3.8	5.5	5.6	5.4	5.4	4.0	4.9
5	5.2	5.0	5.0	5.0	2.8	5.3	5.4	5.2	5.1	3.6	5.5	5.7	5.5	5.4	3.9	4.9
6	5.2	4.9	5.0	5.1	2.7	5.3	5.4	5.2	5.1	3.6	5.5	5.7	5.5	5.4	3.5	4.9
7	5.3	4.7	4.9	5.1	2.6	5.3	5.4	5.2	5.2	3.4	5.6	5.7	5.5	5.5	3.2	4.8
8	5.2	4.6	4.7	5.1	2.4	5.3	5.3	5.2	5.2	3.0	5.6	5.7	5.5	5.5	3.0	4.7
9	5.2	4.4	4.5	5.1	2.3	5.3	5.3	5.2	5.2	2.9	5.6	5.7	5.5	5.5	3.0	4.7
10	5.2	4.1	4.2	5.1	2.1	5.3	5.3	5.2	5.2	2.7	5.6	5.7	5.5	5.5	2.8	4.6
11	5.3	3.8	3.8	5.2	2.0	5.4	5.3	5.2	5.2	2.4	5.7	5.7	5.6	5.6	2.6	4.6
12	5.3	3.9	3.7	5.2	2.0	5.4	5.3	5.3	5.3	2.5	5.7	5.6	5.5	5.6	2.7	4.6
13	5.4	3.5	3.5	5.2	2.0	5.4	5.4	5.3	5.3	2.4	5.7	5.6	5.5	5.6	2.7	4.6
14	5.3	3.4	3.2	5.2	2.0	5.4	5.2	5.1	5.3	2.3	5.7	5.4	5.4	5.6	2.6	4.5
15	4.9	3.4	3.2	5.2	2.0	5.4	5.2	5.0	5.3	2.3	5.7	5.4	5.3	5.6	2.6	4.4

The cause of the decreasing COP (in West1, West2, West3, South1 and East1) and the cause of the constant COP (in East2, East3, South2 and South3) is the same as the cause of the time out-of-setpoint explored in the previous section. As EWT increases, the total heating capacity of each heat pump increases. For a heat pump which was sized for

cooling loads, this additional heating capacity causes the heat pump to overshoot the heating setpoint sufficiently to activate heat pump operation in cooling mode. Adding cooling to the zone during winter months (the only time the zones will be using heating) results in overshooting the cooling setpoint sufficiently to again activate heat pump operation in heating mode. Time-step data of this effect is shown in Section 4.8.

This system instability is an artifact of the control used in this model; a heat pump that only uses on/off control will be oversized for either heating or cooling if the peak cooling and peak heating loads are not balanced. In actual HVAC installations, variable fan speed control allows the heat pump provide reduced heating, eliminating the system instability.

The zones that show the expected increase in COP, the Core and North zones, all experience sufficiently high heating loads to eliminate the problems caused by increased total heating capacity. Instead, the increased heating capacity helps these zones meet their heating needs while using less total power.

6.5. Summary of Base Model Results

Analysis of the base model simulation utilized time-step data, hourly-average data, monthly-average data and annual-average data. Taken as a whole, these different data showed the interconnectedness of the integrated model and the model's corresponding ability to incorporate the effect of changes in environmental conditions over long time-scales.

These data also showed the limitations of the base model as currently constructed: simple on/off control is insufficient for an accurate representation of HVAC performance in a commercial building. This limitation will be considered during review of the results of sensitivity studies in Chapter 7.

Chapter 7 Sensitivity Studies

This chapter investigates the base model's sensitivity to changes in various model parameters. In Section 7.1, the EWT design temperature is increased from 32.2°C (90°F) to the equipment limit of 48.9°C (120°F) in increments of 2.8°C (5°F). Section 7.2 increases the borehole spacing from 6.1m (20ft) to 10.7m (35ft) in 1.5m (5ft) increments. Section 7.3 increases and decreases borehole depth by 5% from base model value. Section 7.4 incorporates supplemental heating and cooling to reduce the installation cost of the GHEX.

Comparison of the test cases to the base model is made using installation costs and cost of operation over the 15year simulation. In actual installations, the total installation cost includes the vertical bore, the exterior header & purge equipment and the HVAC equipment. For this study, the HVAC equipment and the exterior header & purge equipment are assumed to be constant from case to case. As a result "Installation costs" in this chapter only include drilling costs. Drilling costs are based on a cost of 23\$/m (7\$/ft) that was recommended by Hammond (2011). Kavanaugh, Green and Mescher found drilling costs in Texas to range from 22.18\$/m (6.76\$/ft) to 45.93\$/m (14\$/ft), with an average cost for vertical bore installations of 38.62\$/m (11.77\$/ft), based on 16 installations in Texas, Illinois, Tennessee and Georgia (2012). Multiplying the drilling cost by the total GHEX length yields the installation cost for each test case.

The 15year cost of operation is based on the average residential price of electricity for the state of Texas, which is \$ 0.1145/kWh (\$0.3356/kBtu) (U.S. Department of Energy, 2013). Multiplying the cost of electricity by the total power usage for heating and cooling during all 15years yields the total cost of operation.

7.1. Heat Pump EWT Design Cutoff Temperature

The sizing of the GHEX used GLHEPRO, which was previously discussed in Section 4.4.3. After defining ground parameters, u-tube parameters and geometric parameters of the GHEX, the last parameter to be defined before sizing is the design cutoff temperature for the heat pump entering water. The GLHEPRO default value of 32.2°C (90°F) is typically used for small GHEX installations, but values of 35°C (95°F) are often used for commercial projects (Hammond, 2011). The maximum temperature limit for the heat pump equipment is 48.9°C (120°F), which creates a natural upper-bound for variation of the EWT design cutoff temperature.

All of the tests used the same field geometry as the base model: a 10x16 rectangular borefield, with boreholes located on 6.1m (20ft) centers. Using different maximum EWT values in a 15-year sizing resulted in the borehole depths and total GHEX length shown in Table 58.

Table 58: Ground loop specifications for heat pump EWT design cutoff temperature test

Test Case	Designed EWT Cutoff [°C]	Spacing [m]	Field Dimensions [boreholes]	Depth [m]	Total Length [m]	Installation Costs [\$]
Base Model (90°F Case)	32.2	6.1	10x16	170.7	27310	627,200
95°F Case	35.0	6.1	10x16	138.4	22141	508,480
100°F Case	37.8	6.1	10x16	117.7	18824	432,320
105°F Case	40.6	6.1	10x16	103.6	16581	380,800
110°F Case	43.3	6.1	10x16	91.4	14630	336,000
115°F Case	46.1	6.1	10x16	81.1	12972	297,920
120°F Case	48.9	6.1	10x16	74.4	11899	273,280

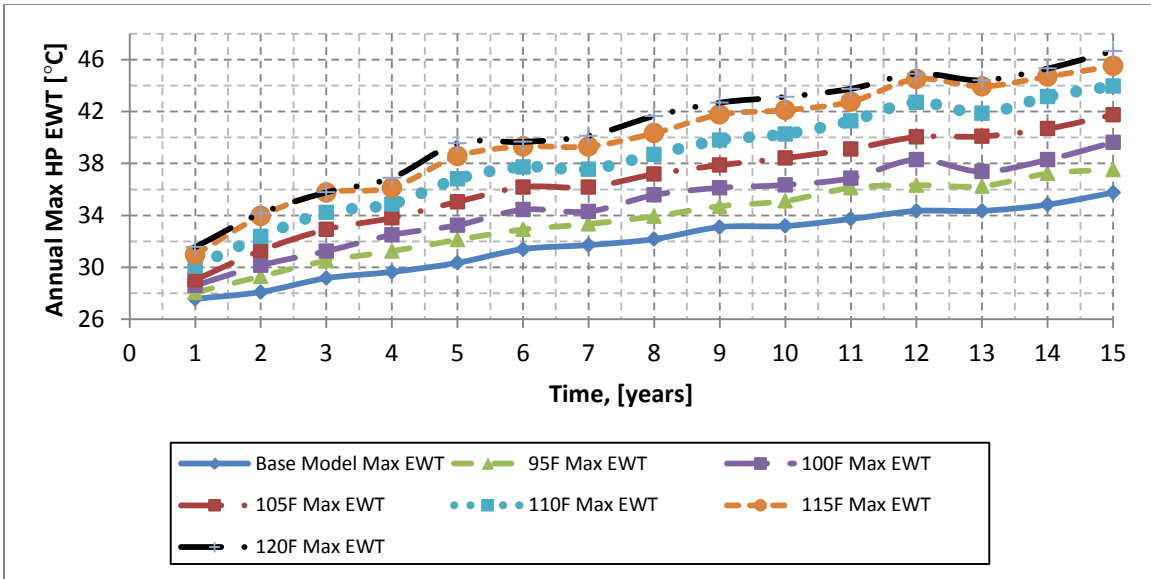


Figure 140: Comparison of maximum annual EWT for the EWT cutoff test

Figure 140 shows the response of maximum annual EWT values for each test over the duration of the 15-year simulation. The tests with higher design cutoff temperatures show higher maximum EWT values during every year of simulation. Across the 15-year interval, the base model experienced an increase in maximum annual EWT of 29.7%, compared to 33.7% for the 95°F case, 38.5% for the 100°F case, 43.8% for the 105°F case, 46.2% for the 110°F case, 46.9% for the 115°F case and 47.9% for the 120°F case. Data for the maximum annual EWT can be found in Table 59. The response of the average annual EWT and the minimum annual EWT can be found in Appendix A.9.

Table 59: Data for the maximum annual EWT in the EWT cutoff test

Time [years]	Base Model [°C]	95F Case [°C]	100F Case [°C]	105F Case [°C]	110F Case [°C]	115F Case [°C]	120F Case [°C]
1	27.6	28.1	28.6	29.0	30.1	31.0	31.6
2	28.1	29.3	30.2	31.3	32.4	33.9	34.2
3	29.2	30.5	31.2	32.9	34.2	35.8	35.8
4	29.6	31.2	32.5	33.8	34.9	36.1	36.9
5	30.3	32.1	33.2	35.0	36.8	38.6	39.5
6	31.4	32.9	34.4	36.2	37.7	39.3	39.7
7	31.7	33.3	34.3	36.2	37.5	39.3	40.1
8	32.2	33.9	35.6	37.2	38.7	40.3	41.6
9	33.1	34.7	36.1	37.9	39.8	41.8	42.7
10	33.2	35.1	36.3	38.4	40.3	42.1	43.1
11	33.7	36.1	36.9	39.1	41.3	42.7	43.7
12	34.3	36.3	38.3	40.0	42.7	44.5	44.9
13	34.3	36.3	37.4	40.1	41.9	43.9	44.4
14	34.8	37.2	38.3	40.7	43.1	44.7	45.3
15	35.8	37.5	39.6	41.7	44.0	45.5	46.7
Abs. Change %	8.2	9.5	11.0	12.7	13.9	14.5	15.1
Change % per Year	29.7%	33.7%	38.5%	43.8%	46.2%	46.9%	47.9%
	2.12%	2.41%	2.75%	3.13%	3.30%	3.35%	3.42%

Figure 141 shows the response of total annual cooling values for each test over the duration of the 15year simulation.

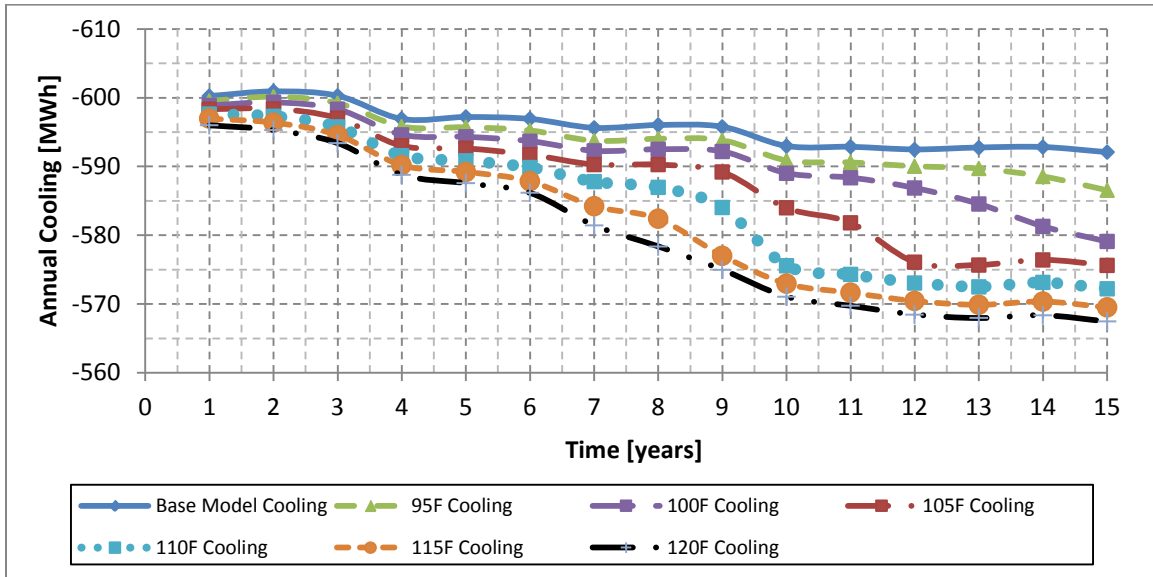


Figure 141: Comparison of total annual cooling for the EWT cutoff test

All tests show a similar initial value for total annual cooling. The tests with higher design cutoff temperature experience slightly higher EWT values during year one, resulting in slightly lower total cooling capacity (an effect previously discussed in Section 6.3.4). All of the tests show similar behavior until year 6, after which the 120°F, 115°F and 110°F cases show a substantial drop in cooling. The 105°F case makes it to year 9, the 100°F makes it to year 11 and the 95°F makes it to year 13 before showing a drop in cooling in excess of that experienced by the base model.

Over the 15year simulation, the base model experienced a decrease in total annual cooling of 1.4%, compared to 2.2% for the 95°F case, 3.3% for the 100°F case, 3.8% for the 105°F case, 4.2% for the 110°F case, 4.6% for the 115°F case and 4.8% for the 120°F case. Additional data can be found in Table 90 of Appendix A.9.

The total annual heating values for each test show a similar response to the total annual cooling values, except with more pronounced changes (shown in Figure 142).

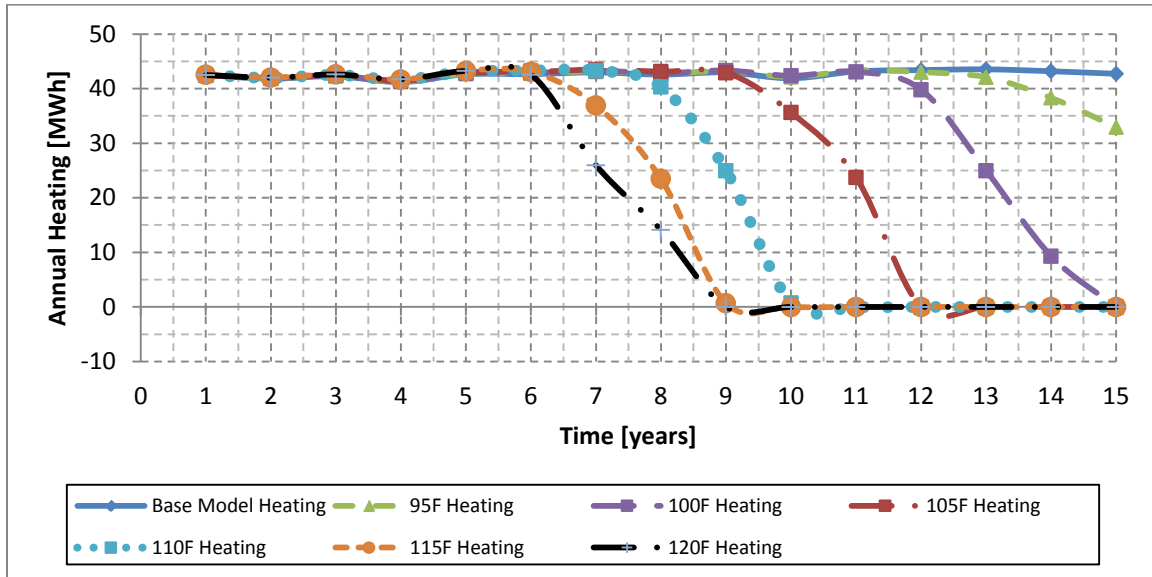


Figure 142: Comparison of total annual heating for the EWT cutoff test

Beginning in year 7, heating in the 120°F case begins to fail, evidenced by the decrease in annual heating provided to 0MWh by year 9. The 115°F case also begins to fail in year 7. The 110°F case begins to fail in year 8, the 105°F case in year 10, the 100°F case in year 12 and the 95°F case in year 14. All tests except the Base Model and the 95°F case show a complete failure of the heating system by the end of the 15year simulation

The decrease in total annual heating is a result of heat pump shutdown, which was previously described in Chapter 6. The limit on EWT for heating mode is 32.2°C (90°F). While the maximum EWT values exceed 32.2°C as soon as year 2, the reduced cooling loads and increased heating loads during winter months cause reduced ground temperatures, which partially recharge the ground loop. Over time the ground temperature continues to increase, resulting in EWT values greater than 32.2°C for the entire year, at which point the heat pump ceases all heating operation. Additional data can be found in Table 91 of Appendix A.9.

As a result of the heat pump shutdown during heating mode, the time out-of-setpoint increases, as shown in Figure 143.

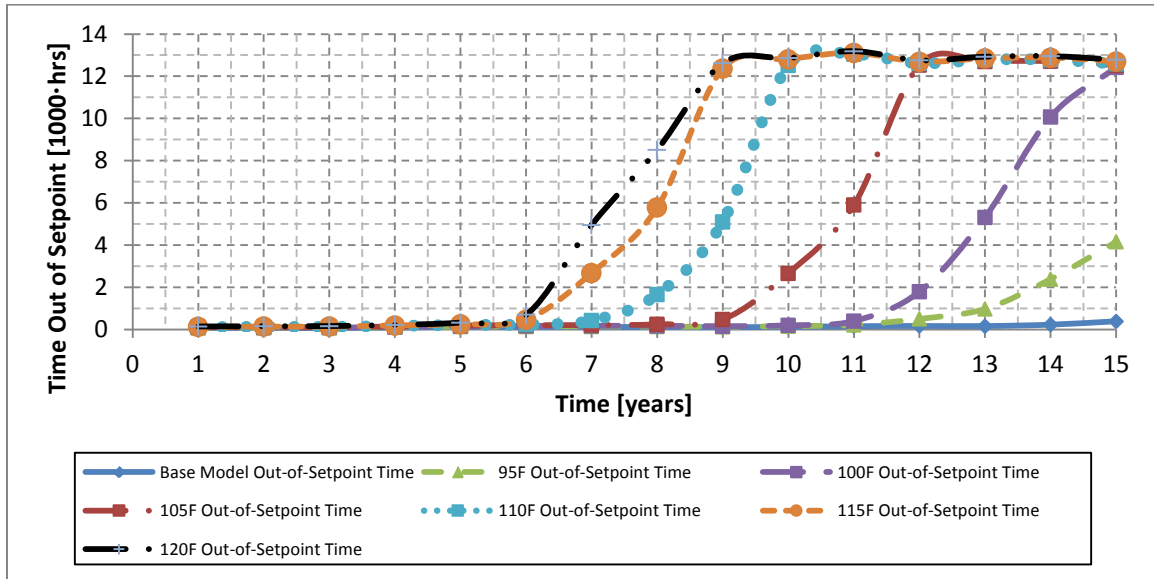


Figure 143: Comparison of annual time out-of-setpoint for the EWT cutoff test

The zones exhibit a slow increase in the time the heat pump is unable to meet the thermostat requirements during years one through 6. At year 7, the heating mode begins to fail, causing the time out-of-setpoint to increase significantly. The total number of hours out-of-setpoint for the test cases that reach this point are: 12784hours for case 120°F, 12695hours for case 115°F, 12594hours for case 110°F, 12521hours for case 105°F and 12421hours for case 100°F. Additional data can be found in Table 92 of Appendix A.9.

The total annual power usage for cooling is shown in Figure 144. The energy used for cooling increases steadily as the average EWT increases. The heat pump cooling capacity decreases as EWT increases, necessitating more hours of operation to provide the same cooling. The energy required to run the compressor also increases as EWT increases.

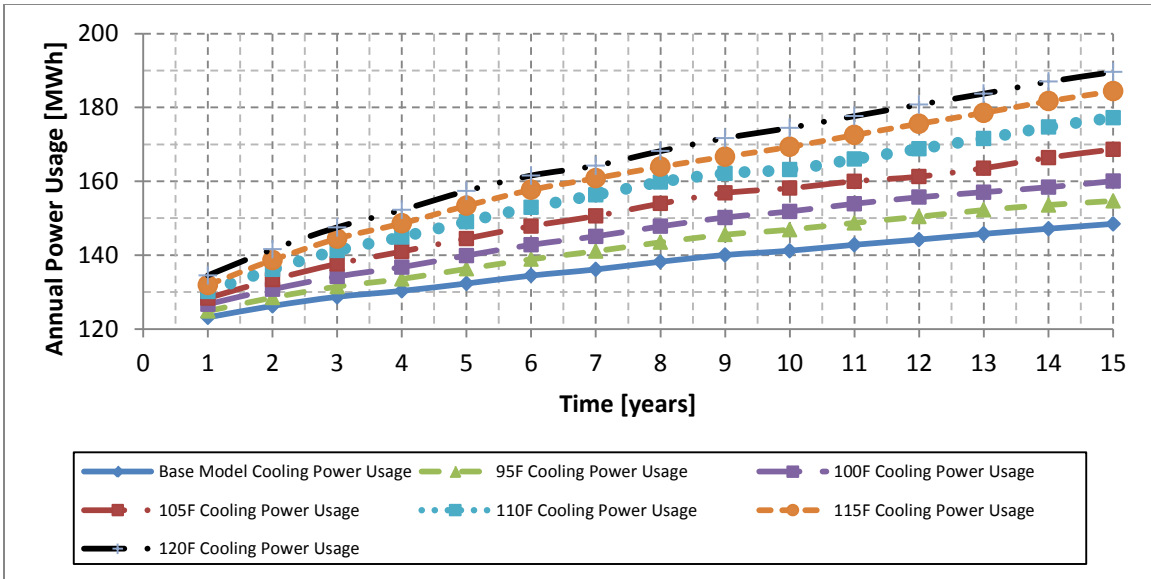


Figure 144: Comparison of total annual cooling power usage for the EWT cutoff test

Over the 15year simulation, the base model experienced an increase in total annual power usage for cooling of 20.6%, compared to 23.9% for the 95°F case, 26.3% for the 100°F case, 31.4% for the 105°F case, 36.2% for the 110°F case, 39.8% for the 115°F case and 40.9% for the 120°F case. Additional data can be found in Table 93 of Appendix A.9.

The total annual power usage for heating is shown in Figure 145. The energy used for heating increases gradually until the heat pump begins to fail due to high EWT. The increased energy usage is a result of increased EWT; as the EWT increases so does the power usage. Additional data can be found in Table 94 of Appendix A.9.

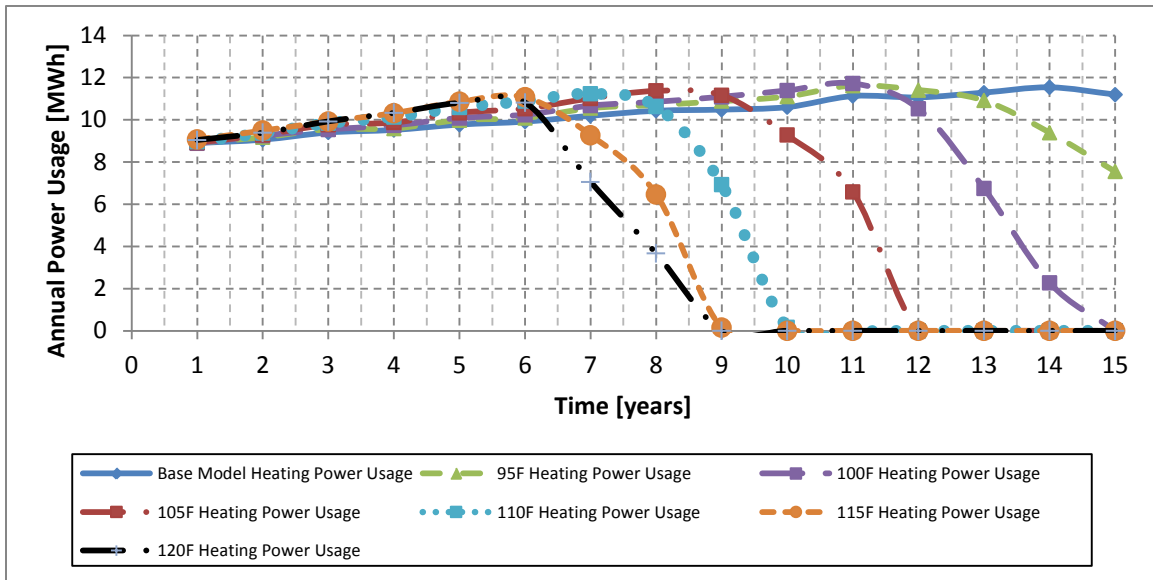


Figure 145: Comparison of total annual heating power usage for the EWT cutoff test

The increasing electricity usage values over time during cooling cause a steady decline in heat pump efficiency. Figure 146 shows this decline.

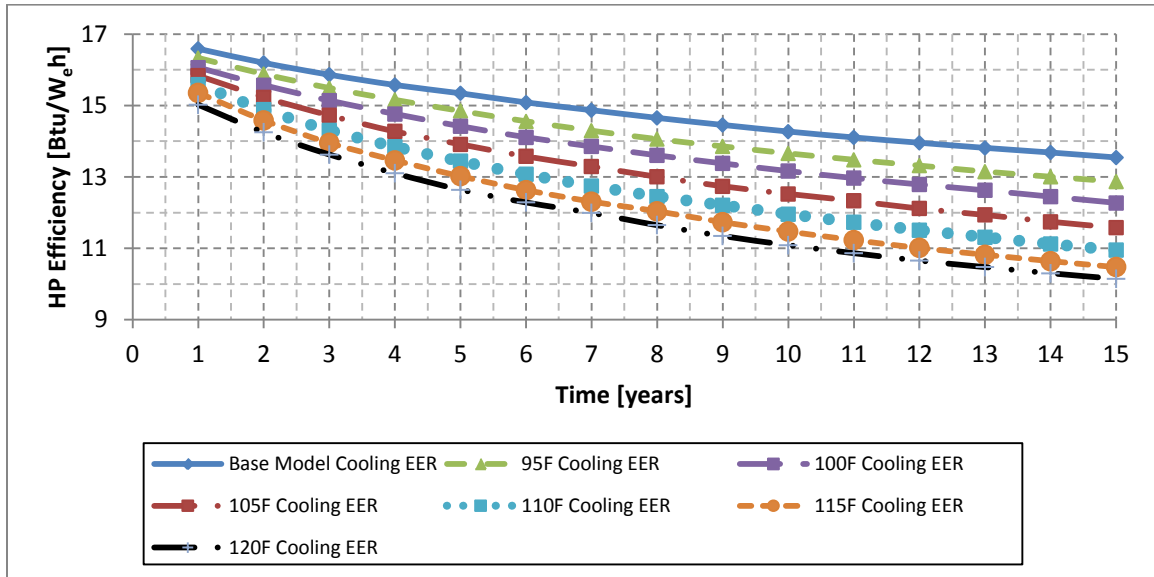


Figure 146: Comparison of average annual EER for the EWT cutoff test

The base model, with 32.2°C (90°F) EWT design cutoff temperature, has the highest heat pump efficiency throughout the simulation, and it also has the slowest rate of change in heat pump efficiency. In year one, the base model has an EER of 16.6, which decreases to an EER of 13.5 during year 15, an 18.3% reduction. The 95F case by comparison, starts year one with an EER of 16.3 and decreases to an EER of 12.9 during year 15, a 21.2% reduction. This means that the base mode will provide the best cooling with the lowest cost of operation of the different EWT cutoff cases. Data for all of the test cases are shown in Table 60.

Table 60: Data for the annual average EER in the EWT cutoff test

Time [years]	Base Model (90F) [Btu/Wh]	95F Case [Btu/Wh]	100F Case [Btu/Wh]	105F Case [Btu/Wh]	110F Case [Btu/Wh]	115F Case [Btu/Wh]	120F Case [Btu/Wh]
1	16.6	16.3	16.1	15.8	15.6	15.4	15.0
2	16.2	15.9	15.6	15.2	14.9	14.6	14.2
3	15.9	15.5	15.1	14.7	14.3	14.0	13.6
4	15.6	15.2	14.8	14.3	13.8	13.5	13.1
5	15.3	14.8	14.4	13.9	13.4	13.0	12.6
6	15.1	14.6	14.1	13.6	13.1	12.6	12.3
7	14.9	14.3	13.9	13.3	12.7	12.3	12.0
8	14.7	14.1	13.6	13.0	12.5	12.0	11.6
9	14.5	13.9	13.4	12.7	12.2	11.7	11.3
10	14.3	13.7	13.2	12.5	12.0	11.5	11.1
11	14.1	13.5	13.0	12.3	11.7	11.2	10.9
12	14.0	13.3	12.8	12.1	11.5	11.0	10.7
13	13.8	13.1	12.6	11.9	11.3	10.8	10.5
14	13.7	13.0	12.4	11.7	11.1	10.6	10.3
15	13.5	12.9	12.3	11.6	10.9	10.5	10.1
Abs. Change	-3.0	-3.5	-3.8	-4.3	-4.6	-4.9	-4.9
% Change	-18.3%	-21.2%	-23.6%	-26.9%	-29.8%	-31.8%	-32.5%
% per Year	-1.31%	-1.51%	-1.68%	-1.92%	-2.13%	-2.27%	-2.32%

The heat pump efficiency in heating mode, measured in COP, is shown in Figure 147. All of the tests show a small, gradual decline in COP over time, despite the fact that increasing EWT causes COP to increase. The reason for this discrepancy is heating overshoot, as was previously discussed in Section 6.4.5. As the heat pumps begin to fail, COP drops to zero because zero heating energy is provided to the building. Additional data can be found in Table 95 of Appendix A.9.

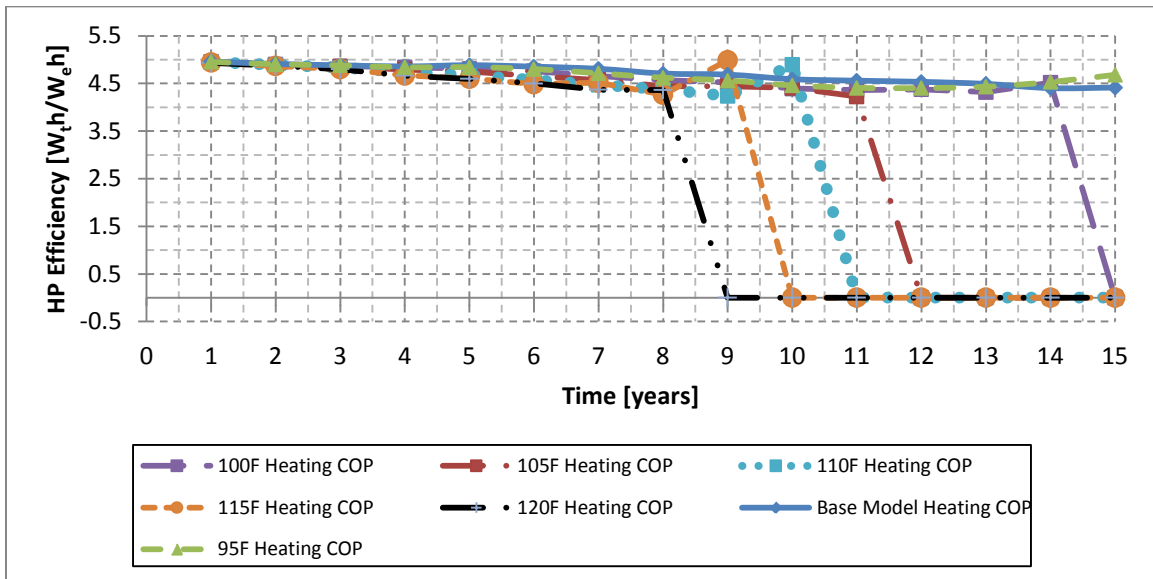


Figure 147: Comparison of average annual COP for the EWT cutoff test

A summary of the results for the EWT cutoff test is shown in Table 61. The operational costs confirm the heat pump efficiency results from Figure 146: the base model has the lowest cost of operation. While the base model has the lowest operational costs, the operational savings between the base model and the test cases does little to cover the substantial difference in installation cost. While the EWT cutoff test cases all exhibit higher average annual time out-of-setpoint, the savings in installation costs permit the investment in other methods of meeting the heating demand.

Table 61: Summary of results for EWT cutoff test

Test	Installation Costs [\$]	15-Year Operation Costs [\$]	15-Year Savings [\$]	Average Annual Time Out-of-Setpoint [hrs]
Base Model (90°F Case)	627,200	253,459	N/A	139
95°F Case	508,480	261,231	229,668	626
100°F Case	432,320	266,108	377,111	2093
105°F Case	380,800	272,524	473,735	4052
110°F Case	336,000	279,696	556,163	5630
115°F Case	297,920	286,778	625,241	6608
120°F Case	273,280	293,465	667,834	7015

The results of the EWT design cutoff temperature sensitivity test show that significant total savings can be realized through the use of higher design cutoff temperatures, however these design values will result in an under-designed system that requires supplemental HVAC equipment for heating and/or cooling. Furthermore, these results show that the use of the recommended design cutoff temperatures of 90°F and 95°F results in an appropriately designed system; one that experiences an acceptable amount of time out-of-setpoint.

7.2. Borehole Spacing

Borehole spacing represents a cost-neutral method of affecting ground loop performance. The borefield used in this paper is shown in Figure 148. The variable “a” represents the centerline distance between the boreholes, and it also can be used to find the amount of ground surface area dedicated to each borehole (represented by the yellow square in Figure 148). As “a” increases, the volume of earth interacting with one particular borehole also increases, which results in slower temperature change in the ground. A building that has a sufficiently large lot size can increase borehole spacing and thereby improve ground loop efficiency at no incremental cost.

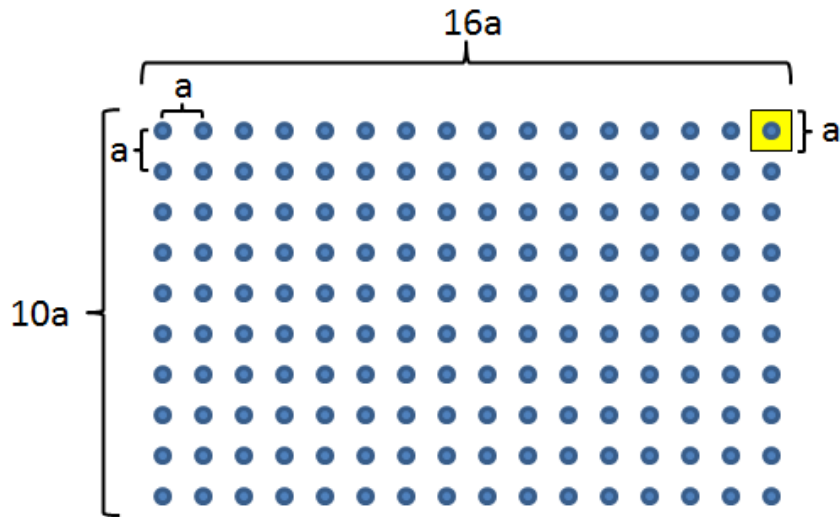


Figure 148: Borefield arrangement and dimensions for borehole spacing study

Table 62 shows the design parameters for the borehole spacing study. Every test used an identical EWT design cutoff temperature of 32.2°C (90°F), an identical field orientation of 10x16 boreholes and an identical depth of 170.7m. As a result, every test has an identical installation cost of \$627,200. The only difference between each test is the borehole spacing (variable “a” in Figure 148).

Table 62: Ground loop specifications for the borehole spacing tests

Test Case	Designed EWT Cutoff [°C]	Spacing [m]	Field Dimensions [boreholes]	Depth [m]	Total Length [m]	Installation Costs [\$]
Base Model (20ft Case)	32.2	6.1	10x16	170.7	27310	627,200
25ft Case	32.2	7.6	10x16	170.7	27310	627,200
30ft Case	32.2	9.1	10x16	170.7	27310	627,200
35ft Case	32.2	10.7	10x16	170.7	27310	627,200

Figure 149 shows the response of maximum annual EWT values for each test over the duration of the 15year simulation. Data for the maximum annual EWT is shown in Table 63.

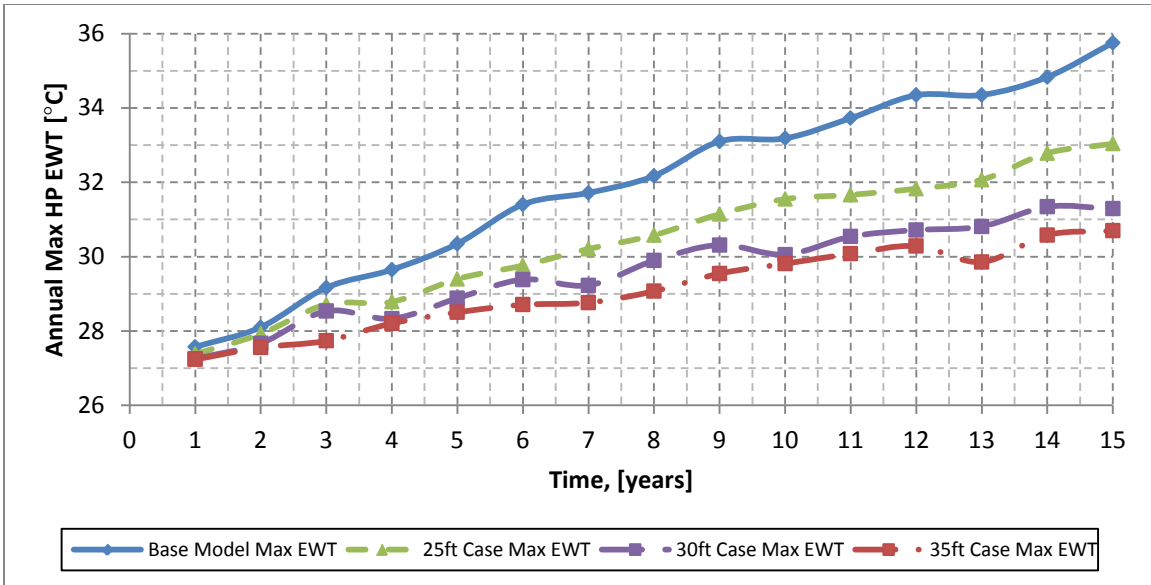


Figure 149: Comparison of maximum annual EWT for the borehole spacing test

Table 63: Data for the maximum annual EWT for the borehole spacing test

Time [years]	Base Model (20ft Case) [°C]	25ft Case [°C]	30ft Case [°C]	35ft Case [°C]
1	27.6	27.4	27.3	27.2
2	28.1	27.9	27.7	27.6
3	29.2	28.7	28.5	27.7
4	29.6	28.8	28.3	28.2
5	30.3	29.4	28.9	28.5
6	31.4	29.8	29.4	28.7
7	31.7	30.2	29.2	28.8
8	32.2	30.6	29.9	29.1
9	33.1	31.1	30.3	29.5
10	33.2	31.5	30.1	29.8
11	33.7	31.7	30.5	30.1
12	34.3	31.8	30.7	30.3
13	34.3	32.1	30.8	29.9
14	34.8	32.8	31.3	30.6
15	35.8	33.0	31.3	30.7
Abs. Change	8.2	5.7	4.0	3.5
% Change	29.7%	20.6%	14.8%	12.7%
% per Year	2.12%	1.47%	1.06%	0.91%

The tests with higher borehole spacing show lower maximum EWT values during every year of simulation. Across the 15year interval, the base model experienced an increase in maximum annual EWT of 29.7%, compared to 20.6% for the 25ft case, 14.8% for the 30ft case and 12.7% for the 35ft case. Thus, changing the borehole spacing from 6.1m (20ft) to 7.6m (25ft) reduced the 15year increase in maximum annual EWT from 8.2°C (14.8°F) to 5.7°C (10.3°F), a 30.9% reduction. Similarly, changing the borehole spacing from 6.1m (20ft) to 9.1m (30ft) resulted in a 50.7% reduction in EWT increase and changing the borehole spacing from 6.1m (20ft) to 10.7m (35ft) resulted in a 57.7% reduction in EWT increase. The response of the average annual EWT and the minimum annual EWT can be found in Appendix A.10.

Figure 150 shows the response of total annual cooling values for each test over the duration of the 15year simulation.

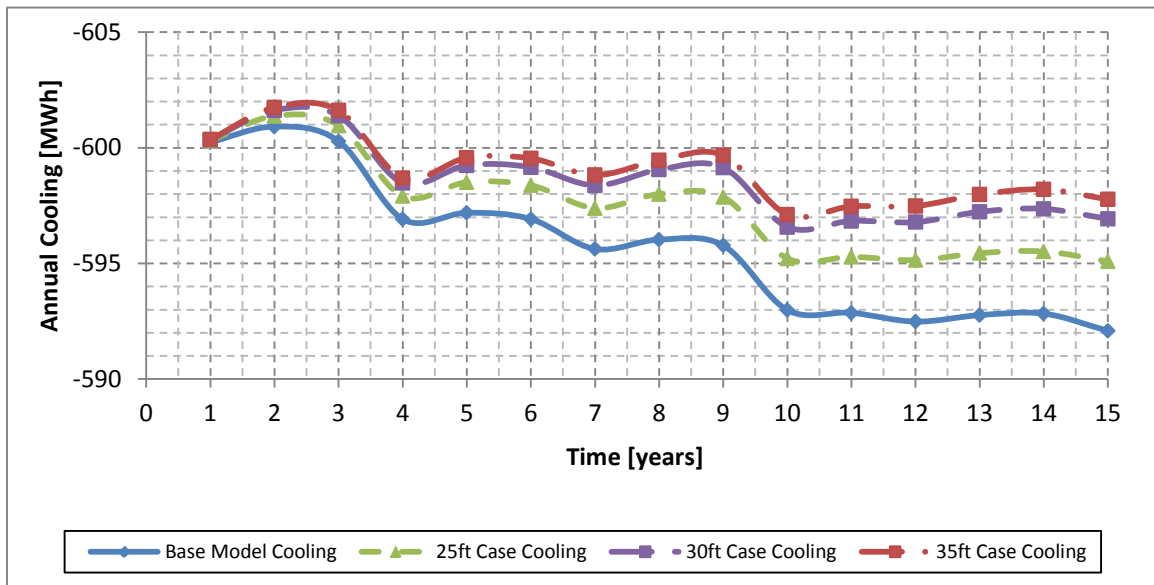


Figure 150: Comparison of total annual cooling for the borehole spacing test

All tests show a similar initial value for total annual cooling. The tests with higher borehole spacing experience slightly lower EWT values during year one, resulting in slightly higher total cooling capacity (an effect previously discussed in Section 6.3.4). All

of the tests show similar behavior until year 4, after which the base model (20ft case) shows a smaller recovery in cooling compared to the other test cases. The 25ft case follows the 30ft and 35ft cases until year 10, after which it shows a smaller recovery in cooling. The differences between the tests result from their changes in EWT; lower EWT values correspond to higher total cooling capacity and slightly higher annual cooling values.

Over the 15year simulation, the base model experienced a decrease in total annual cooling of 1.4%, compared to 0.9% for the 25ft case, 0.6% for the 30ft case and 0.4% for the 35ft case. Additional data can be found in Appendix A.10.

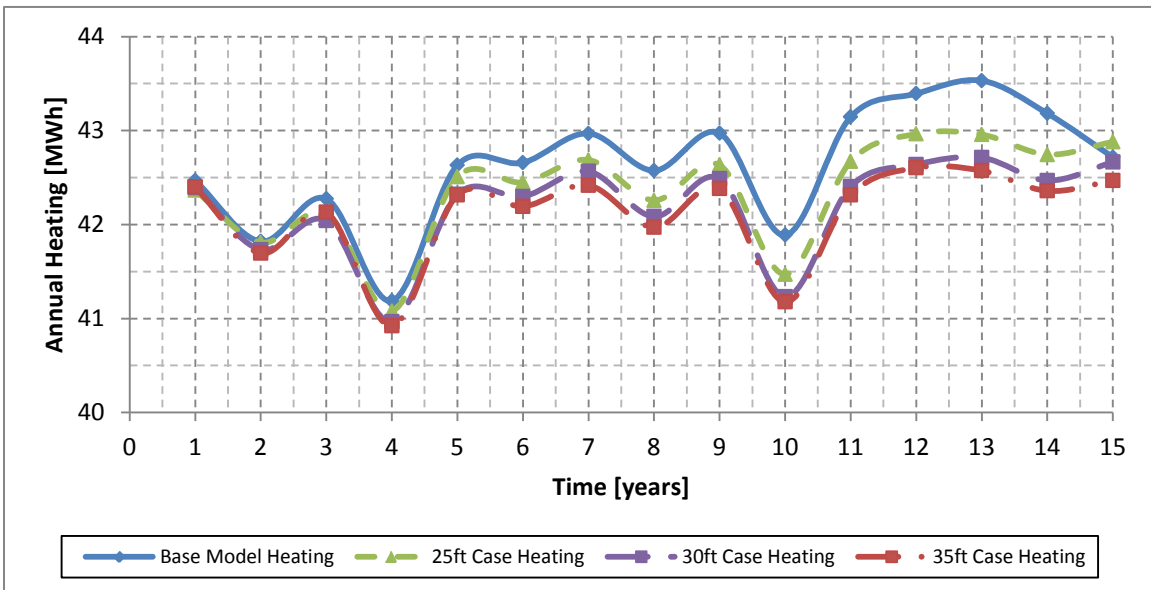


Figure 151: Comparison of total annual heating for the borehole spacing test

The total annual heating values for each test show the opposite response to the total annual cooling values, as seen in Figure 151. Through year 5, all four test cases show similar values for total annual heating. Beginning in year 6, the higher EWT values in the base model cause an increase in the total heating capacity, which results in greater total annual heating. The base model maintains greater total annual heating until year 15,

when excessively high EWT values cause heat pump shutdown during heating mode and reduced total annual heating. Data for this figure can be found in Appendix A.10.

As a result of heat pump shutdown during heating mode in the base model, the time out-of-setpoint increases for the base model but remains steady for the other test cases, as shown in Figure 152.

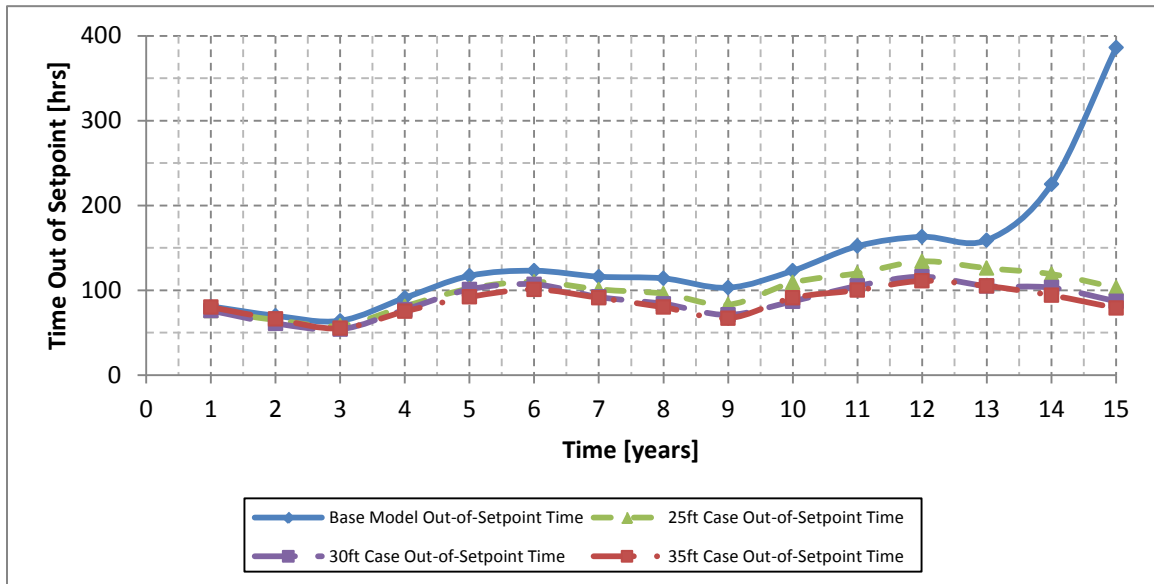


Figure 152: Comparison of annual time out-of-setpoint for the borehole spacing test

All of the test cases show gradual changes in annual time out-of-setpoint from year to year. The base model (20ft case) shows a large increase in annual time out-of-setpoint across the 15year simulation due to heat pump shutdown in years 14 and 15. The other three test cases, however, show little change across the 15year simulation. The 25ft case increases from 76hrs to 103hrs, a 35.5% increase, the 30ft case increases from 76hrs to 87hrs, a 14.5% increase, and the 35ft case actually decreases from 80hrs to 79hrs, a 1.3% decrease. Thus, the expanded borehole spacing reduces the increase in EWT over time, which significantly reduces time out-of-setpoint during year 14 and 15. Data for this figure can be found in Appendix A.10.

The total annual power usage for cooling is shown in Figure 153. The energy used for cooling increases steadily as the average EWT increases. The heat pump cooling capacity decreases as EWT increases, necessitating more hours of operation to provide the same cooling. The energy required to run the compressor also increases as EWT increases.

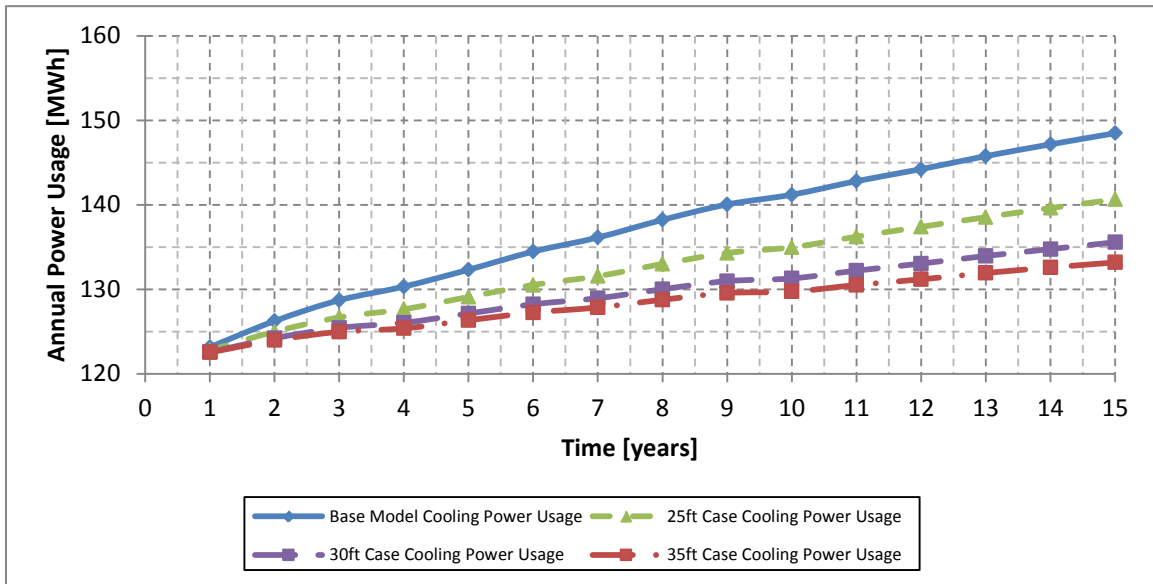


Figure 153: Comparison of total annual cooling power usage for the borehole spacing test

Over the 15year simulation, the base model experienced an increase in total annual power usage for cooling of 20.6%, compared to 14.5% for the 25ft case, 10.6% for the 30ft case and 8.7% for the 35ft case. Thus, changing the borehole spacing from 6.1m (20ft) to 7.6m (25ft) reduced the total power usage for cooling during the 15year simulation from 2.06GWh to 1.99GWh, a 3.5% reduction. Similarly, changing the borehole spacing from 6.1m (20ft) to 9.1m (30ft) reduced the total power usage from 2.06GWh to 1.94GWh, a 5.6% reduction, and changing the borehole spacing from 6.1m (20ft) to 10.7m (35ft) reduced the total power usage from 2.06GWh to 1.93GWh, a 6.5% reduction. Data for this figure can be found in Appendix A.10.

The total annual power usage for heating is shown in Figure 154. The energy used for heating increases gradually throughout the 15-year interval. The increased energy usage is a result of increased EWT; as the EWT increases so does the power usage during heating. The base model shows a sharp decline in total annual heating in year 15 because of heat pump shutdown during heating mode.

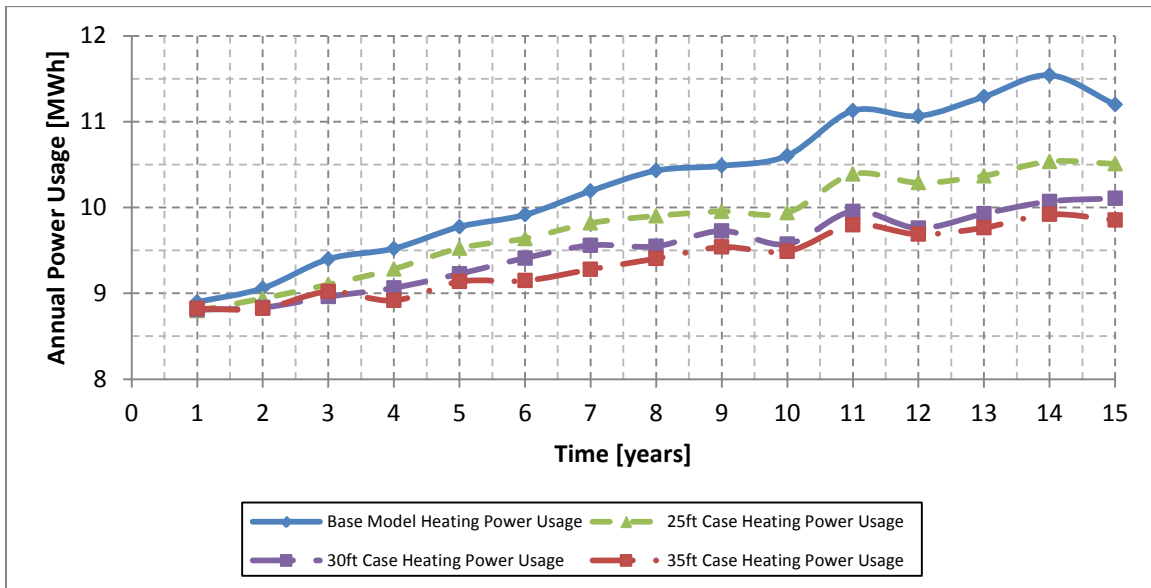


Figure 154: Comparison of total annual heating power usage for the borehole spacing test

Increasing borehole spacing results in a reduction in total power usage during the 15-year simulation. Changing the borehole spacing from 6.1m (20ft) to 7.6m (25ft) reduced the total power usage for heating during the 15-year simulation from 154.5MWh to 147.0MWh, a 4.9% reduction. Similarly, changing the borehole spacing from 6.1m (20ft) to 9.1m (30ft) reduced the total power usage from 154.5MWh to 142.5MWh, a 7.7% reduction, and changing the borehole spacing from 6.1m (20ft) to 10.7m (35ft) reduced the total power usage from 154.5MWh to 140.6MWh, a 9.0% reduction. Data for this figure can be found in Appendix A.10.

The increasing electricity usage values over time during cooling result in steady decline for heat pump efficiency, as shown in Figure 155. Cooling efficiency is directly proportional to total cooling provided and inversely proportional to power usage, so the results agree with the previous data in this section.

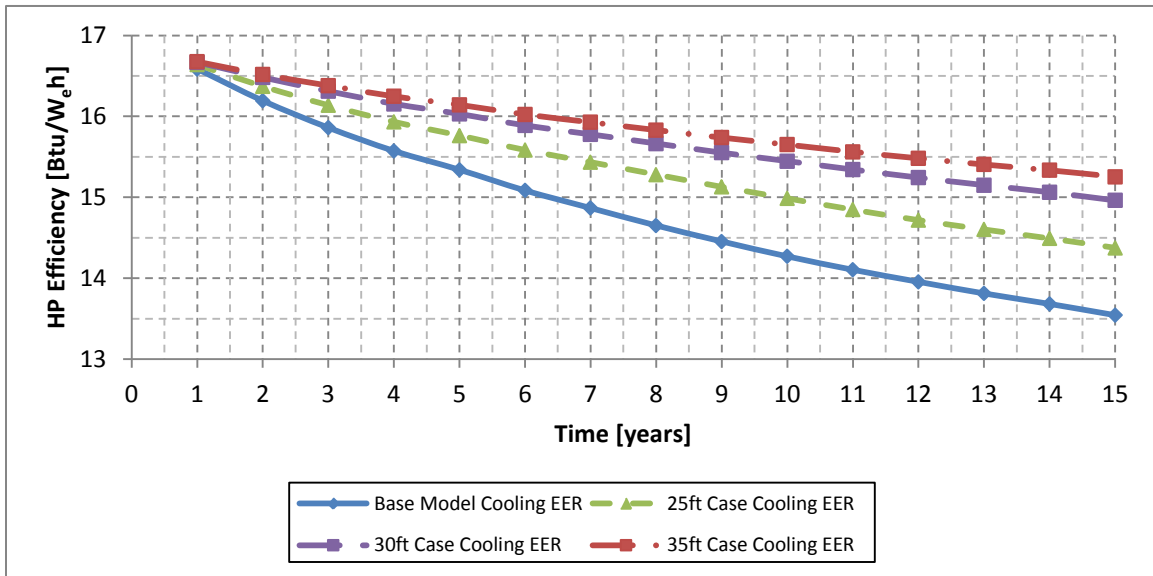


Figure 155: Comparison of average annual EER for the borehole spacing test

The base model, with 20ft borehole spacing, has the lowest heat pump efficiency throughout the simulation, and it also has the fastest rate of change in heat pump efficiency. After 15years of simulation, the 35ft case has the highest EER (15.3Btu/W_eh) followed by the 30ft case (15.0Btu/W_eh), the 25ft case (14.4Btu/W_eh) and finally the base model (13.5Btu/W_eh). This means that the base mode will provide the worst cooling with the highest cost of operation of the different borehole spacing cases. Data for all of the test cases are shown in Table 64.

Table 64: Data for the annual average EER in the borehole spacing test

Time [years]	Base Model (20ft Case) [Btu/Wh]	25ft Case [Btu/Wh]	30ft Case [Btu/Wh]	35ft Case [Btu/Wh]
1	16.6	16.6	16.7	16.7
2	16.2	16.4	16.5	16.5
3	15.9	16.1	16.3	16.4
4	15.6	15.9	16.2	16.2
5	15.3	15.8	16.0	16.1
6	15.1	15.6	15.9	16.0
7	14.9	15.4	15.8	15.9
8	14.7	15.3	15.7	15.8
9	14.5	15.1	15.6	15.7
10	14.3	15.0	15.4	15.7
11	14.1	14.8	15.3	15.6
12	14.0	14.7	15.2	15.5
13	13.8	14.6	15.2	15.4
14	13.7	14.5	15.1	15.3
15	13.5	14.4	15.0	15.3
Abs. Change	-3.0	-2.3	-1.7	-1.4
% Change	-18.3%	-13.6%	-10.2%	-8.5%
% per Year	-1.31%	-0.97%	-0.73%	-0.61%

The heat pump efficiency in heating mode, measured in COP, is shown in Figure 156. All of the tests show a small, gradual decline in COP over time, despite the fact that increasing EWT causes COP to increase. The reason for this discrepancy is heating overshoot, as was previously discussed in Section 6.4.5.

Similarly to EER, the base model shows the worst efficiency of the test cases. Over the 15year simulation, the 35ft case has the highest COP, beginning at $4.96W_t h/W_e h$ and ending at $4.85W_t h/W_e h$ (a 2.3% reduction). The 30ft case initially has a COP of $4.96W_t h/W_e h$ and ends at $4.80W_t h/W_e h$ (a 3.3% reduction). The 25ft case initially has a COP of $4.96W_t h/W_e h$ and ends at $4.66W_t h/W_e h$ (a 6.0% reduction). The base model (20ft case) initially has a COP of $4.96W_t h/W_e h$ and ends at $4.41W_t h/W_e h$ (an 11.1% reduction). Data for the COP in all test cases can be found in Appendix A.10.

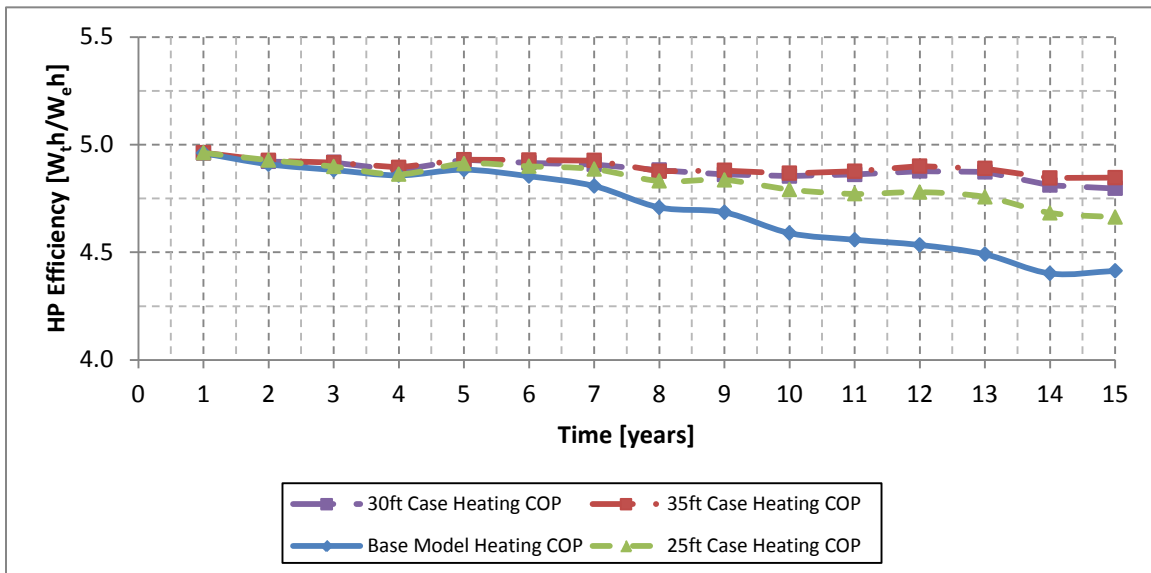


Figure 156: Comparison of annual average COP for the borehole spacing test

A summary of the results for the borehole spacing test is shown in Table 65. The operational costs confirm the heat pump efficiency results from this section: increasing the borehole spacing reduces the cost of operation.

Table 65: Summary of results for borehole spacing test

Test	Installation Costs [\$]	15-Year Operation Costs [\$]	15-Year Savings [\$]	Average Annual Time Out-of-Setpoint [hrs]
Base Model (20ft Case)	627,200	253,459	N/A	139
25ft Case	627,200	244,437	9,022	99
30ft Case	627,200	238,939	14,520	88
35ft Case	627,200	236,580	16,879	86

These results show that borehole spacing is a cost-neutral approach to improving GHEX longevity (as measured by the lower EWT values over time and lower time out-of-setpoint over time) and decreasing operational costs. The only limiting factor for implementation of increased borehole spacing is lot size. The lot size required for each test's borefield is calculated in Table 66. Changing the borehole spacing from 6.1m (20ft) to 7.6m (25ft) requires a 56% increase in borefield area, 6.1m (20ft) to 9.1m (30ft) requires a 125% increase in borefield area and changing the borehole spacing from 6.1m (20ft) to 10.7m (35ft) requires a 206% increase in borefield area.

Table 66: Lot size required for the borehole spacing tests

Test Case	Field Length [bore-holes]	Field Length [m]	Field Width [bore-holes]	Field Width [m]	Field Area [m ²]	Field Area [acres]
Base Model (20ft Case)	10	61	16	98	5,946	1.47
25ft Case	10	76	16	122	9,290	2.30
30ft Case	10	91	16	146	13,378	3.31
35ft Case	10	107	16	171	18,209	4.50

7.3. Borehole Depth

Borehole depth is the most basic measure of cost for a vertically bored GHEX system. GLHEPRO calculates a borehole depth for a GHEX system based on loads and temperatures. This study aims to measure the sensitivity of a GLHEPRO sized GHEX system to small changes in borehole depth.

Table 67 shows the design parameters for the borehole depth study. Every test used an identical EWT design cutoff temperature of 32.2°C (90°F), an identical field orientation of 10x16 boreholes and identical borehole spacing of 6.1m (20ft). The only parameter that changed from test to test was the borehole depth: the base model used a depth of 170.7m (560ft), the -5% case used a depth of 162.5m (533ft), the +5% case used a depth of 179.5m (589ft) and the +10% case used a depth of 188.1m (617ft).

Table 67: Ground loop specifications for the borehole depth tests

Test Case	Designed EWT Cutoff [°C]	Spacing [m]	Field Dimensions [boreholes]	Depth [m]	Total Length [m]	Installation Costs [\$]
Base Model	32.2	6.1	10x16	170.7	27310	627,200
-5% Case	32.2	6.1	10x16	162.5	25993	596,960
+5% Case	32.2	6.1	10x16	179.5	28724	659,680
+10% Case	32.2	6.1	10x16	188.1	30090	691,040

Figure 157 shows the response of maximum annual EWT values for each test over the duration of the 15year simulation. Data for the maximum annual EWT is shown in Table 68.

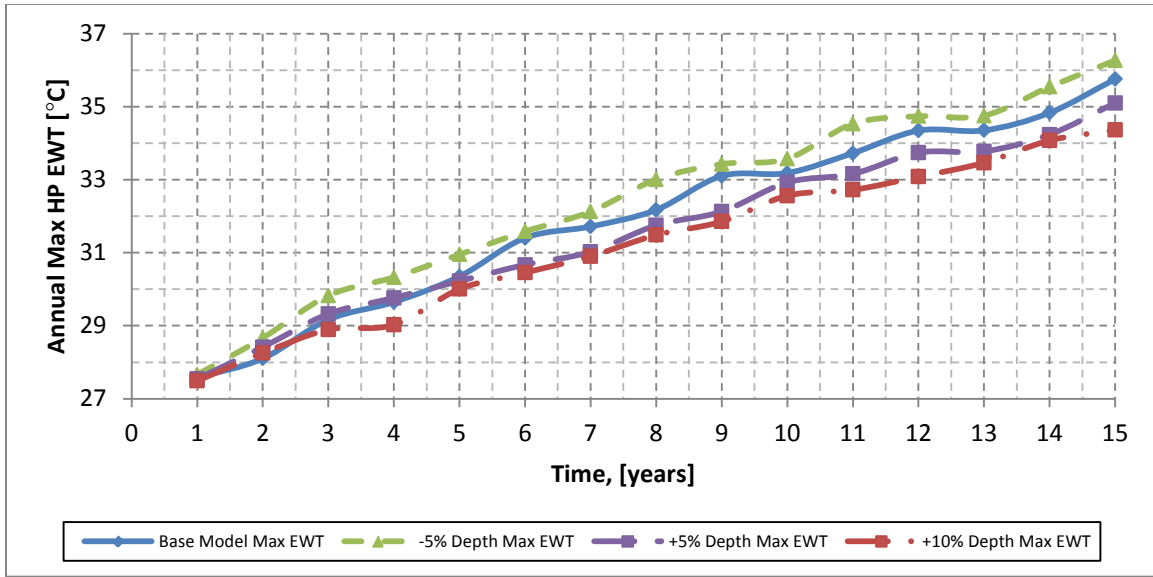


Figure 157: Comparison of maximum annual EWT for the borehole depth test

Table 68: Data for the maximum annual EWT for the borehole depth test

Time [years]	Base Model (171m Depth) [°C]	-5% Case (162m Depth) [°C]	+5% Case (180m Depth) [°C]	+10% Case (188m Depth) [°C]
1	27.6	27.7	27.5	27.5
2	28.1	28.7	28.4	28.3
3	29.2	29.8	29.3	28.9
4	29.6	30.3	29.8	29.0
5	30.3	31.0	30.2	30.0
6	31.4	31.6	30.7	30.5
7	31.7	32.1	31.0	30.9
8	32.2	33.0	31.7	31.5
9	33.1	33.4	32.1	31.9
10	33.2	33.6	32.9	32.6
11	33.7	34.5	33.2	32.7
12	34.3	34.7	33.7	33.1
13	34.3	34.8	33.8	33.5
14	34.8	35.5	34.2	34.1
15	35.8	36.3	35.1	34.4
Abs. Change	8.2	8.6	7.6	6.9
% Change	29.7%	31.1%	27.4%	25.0%
% per Year	2.12%	2.22%	1.96%	1.79%

Increasing the borehole depth resulted in lower maximum EWT values, while decreasing the borehole depth resulted in higher maximum EWT values. Across the 15year interval, the base model experienced an increase in maximum annual EWT of 29.7%, compared to 31.1% for the -5% case, 27.4% for the +5% case and 25.0% for the +10% case. Thus, decreasing the borehole depth by 5% caused an additional 5.2% increase in the maximum annual EWT across the 15year simulation (8.2°C increase in the base model compared to an 8.6°C increase in the -5% case). Increasing the borehole depth by 5% caused a 7.6% smaller increase in the maximum annual EWT across the 15year simulation (8.2°C increase in the base model compared to a 7.6°C increase in the +5% case). Increasing the borehole depth by 10% caused a 16.0% smaller increase in the maximum annual EWT across the 15year simulation (8.2°C increase in the base model compared to a 6.9°C increase in the +10% case). The response of the average annual EWT and the minimum annual EWT can be found in Appendix A.11.

Figure 158 shows the response of total annual cooling values for each test over the duration of the 15year simulation.

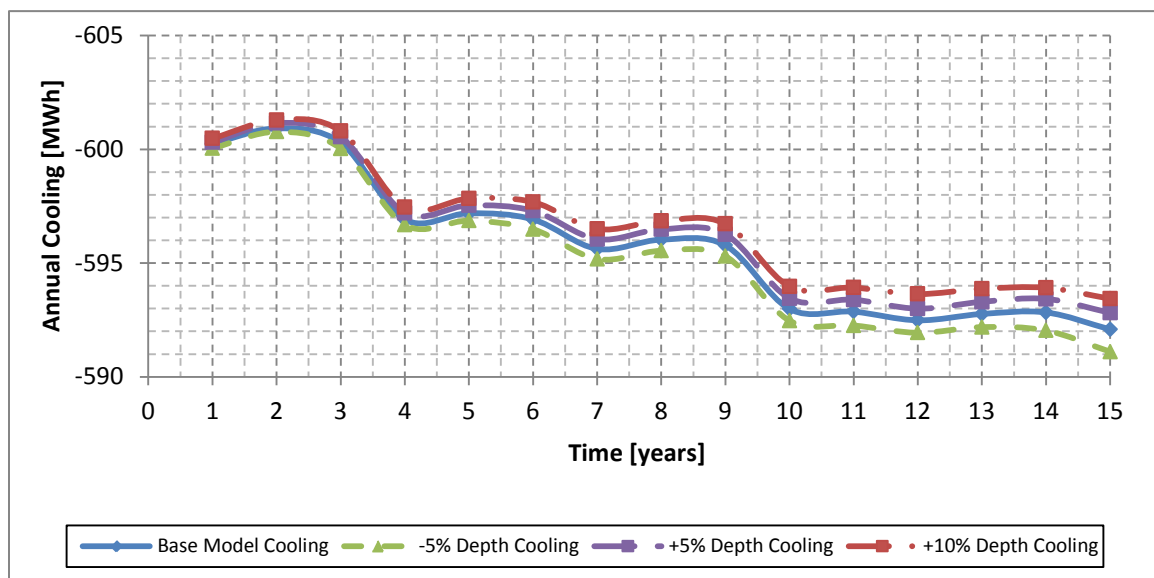


Figure 158: Comparison of total annual cooling for the borehole depth test

All tests show a similar initial value for total annual cooling. The tests with greater borehole depth experience slightly lower EWT values during year one, resulting in slightly higher total cooling capacity (an effect previously discussed in Section 6.3.4). All of the tests show similar behavior throughout the simulation, with the differences between tests slowly widening every year. The differences between the tests result from their changes in EWT; lower EWT values correspond to higher total cooling capacity and slightly higher annual cooling values.

Over the 15year simulation, the base model experienced a decrease in total annual cooling of 1.36%, compared to a decrease of 1.49% for the -5% case, a decrease of 1.25% for the +5% case and a decrease of 1.17% for the +10% case. Additional data can be found in Appendix A.11.

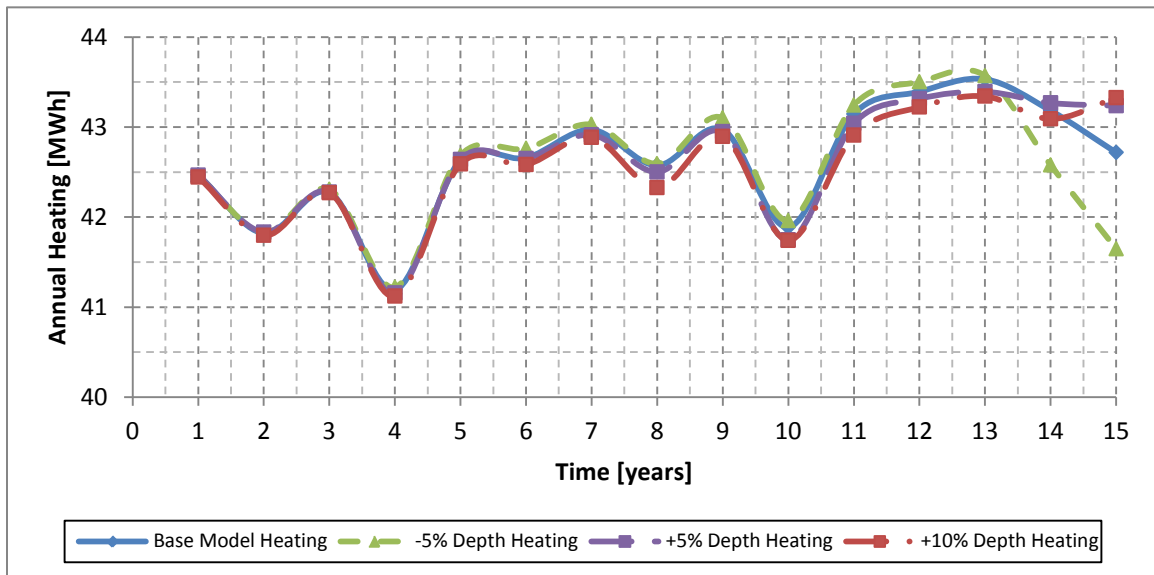


Figure 159: Comparison of total annual heating for the borehole depth test

The total annual heating values for each test are shown in Figure 159. Through year 13, all four test cases show similar values for total annual heating. In year 14, increased EWT values in the shorter depth test cases (base model and -5% case) cause heat pump shutdown, resulting in lower annual heating totals. The longer depth test cases (+5% case and +10% case) experience lower EWT values, which do not exceed the heat

pump shutdown limit. As a result their annual heating totals do not change significantly. Data for this figure can be found in Appendix A.11.

As a result of heat pump shutdown during heating mode in the base model, the time out-of-setpoint increases for the shorter depth test cases but remains steady for the longer depth test cases, as shown in Figure 160.

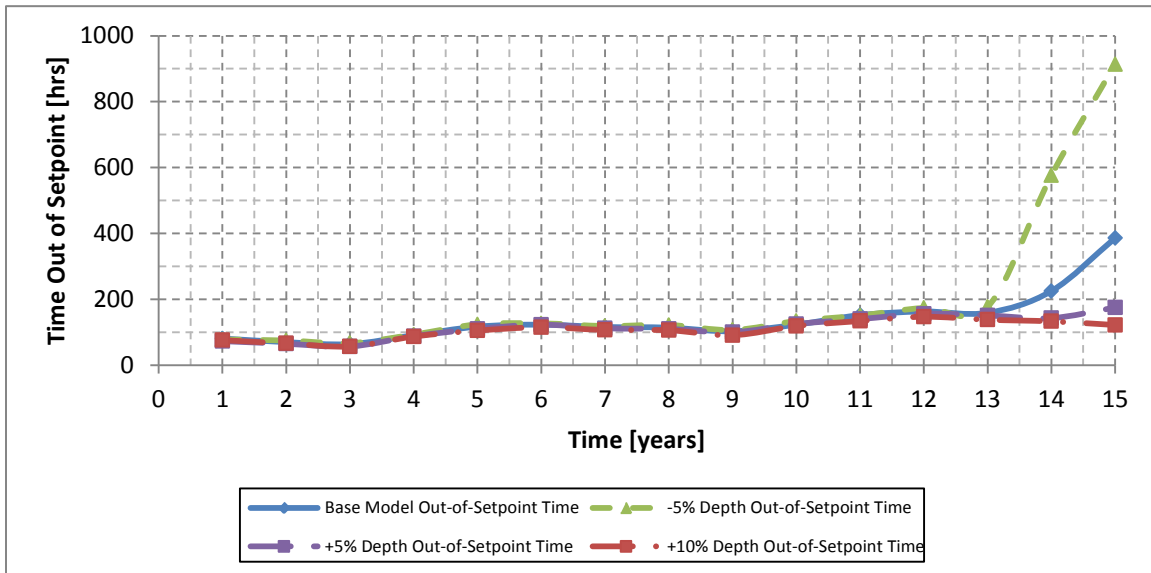


Figure 160: Comparison of annual time out-of-setpoint for the borehole depth test

All of the test cases show gradual changes in annual time out-of-setpoint from year to year. The base model (171m depth) and the -5% case (162m depth) show a large increase in annual time out-of-setpoint across the 15year simulation due to heat pump shutdown in years 14 and 15. The other two test cases show little change across the 15year simulation. The -5% case increases from 78hrs to 914hrs, a 1072% increase, the base model increases from 81hrs to 386hrs, a 377% increase, the +5% case increases from 73hrs to 175hrs, a 140% increase and the +10% case increases from 76hrs to 122hrs, a 61% decrease. Thus, small additions to the borehole depth reduce the increase in EWT over time, which significantly reduces time out-of-setpoint during year 14 and 15. Data for this figure can be found in Appendix A.11.

The total annual power usage for cooling is shown in Figure 161. The energy used for cooling increases steadily as the average EWT increases. The heat pump cooling capacity decreases as EWT increases, necessitating more hours of operation to provide the same cooling. The energy required to run the compressor also increases as EWT increases. Thus, increasing borehole depth causes a reduction in cooling power usage, and decreasing borehole depth causes an increase in cooling power usage.

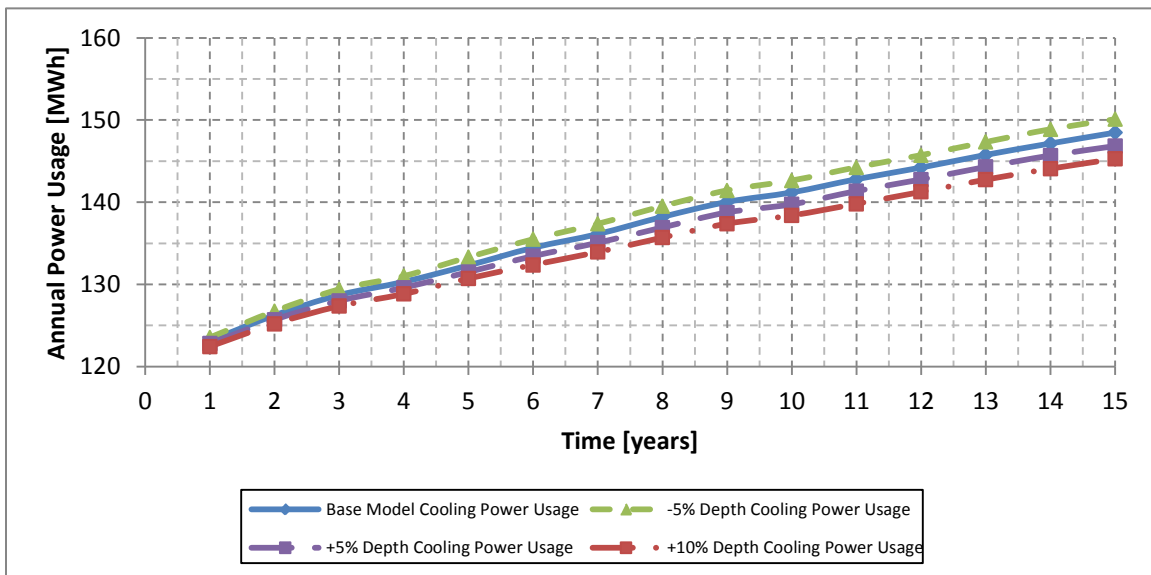


Figure 161: Comparison of total annual cooling power usage for the borehole depth test

Over the 15year simulation, the test case with the shortest depth (-5%) experienced an increase in total annual power usage for cooling of 21.5%, compared to 20.6% for the base model, 19.6% for the +5% case and 18.6% for the +10% case. Thus, decreasing the borehole depth by 5% (from 171m (560ft) to 162m (533ft)) increased the total power usage for cooling during the 15year simulation from 2.06GWh to 2.08GWh, a 0.9% increase. Increasing the borehole depth by 5% (from 171m (560ft) to 180m (589ft)) reduced the total power usage from 2.06GWh to 2.04GWh, a 0.8% reduction, increasing the borehole depth by 10% (from 171m (560ft) to 188m (617ft)) reduced the total power usage from 2.06GWh to 2.03GWh, a 1.6% reduction. Data for the cooling power usage can be found in Appendix A.11.

The total annual power usage for heating is shown in Figure 162. The energy used for heating increases gradually throughout the 15-year interval. The increased energy usage is a result of increased EWT; as the EWT increases so does the power usage during heating. The shorter test cases (-5% depth and the base model) show a sharp decline in total annual heating in year 15 because of heat pump shutdown during heating mode.

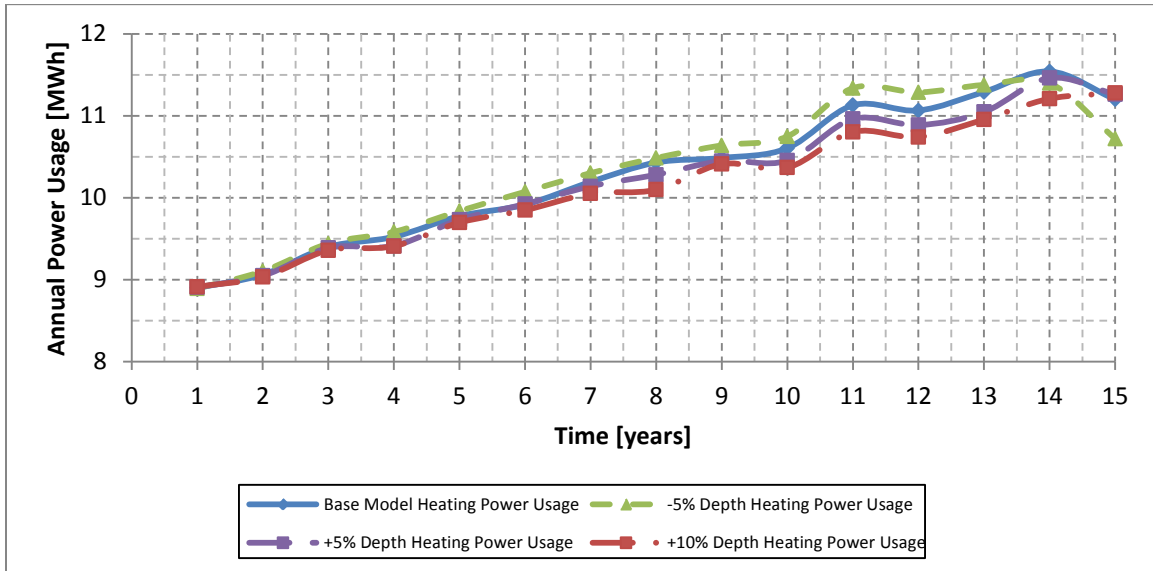


Figure 162: Comparison of total annual heating power usage for the borehole depth test

Increasing borehole depth results in a reduction in total power usage during the 15-year simulation. Increasing the borehole depth by 5% (from 171m (560ft) to 180m (589ft)) reduced the total heating power usage from 154.5MWh to 153.3MWh, a 0.8% reduction over the 15-year simulation. Increasing the borehole depth by 10% (from 171m (560ft) to 188m (617ft)) reduced the total heating power usage from 154.5MWh to 152.2MWh, a 1.5% reduction over the 15-year simulation. Decreasing the borehole depth by 5% (from 171m (560ft) to 162m (533ft)) increased the total power usage for heating during the 15-year simulation from 154.5MWh to 155.2MWh, a 0.5% increase over the 15-year simulation. Data for the heating power usage can be found in Appendix A.11.

The increasing electricity usage values over time during cooling result in steady decline for heat pump efficiency, as shown in Figure 163.

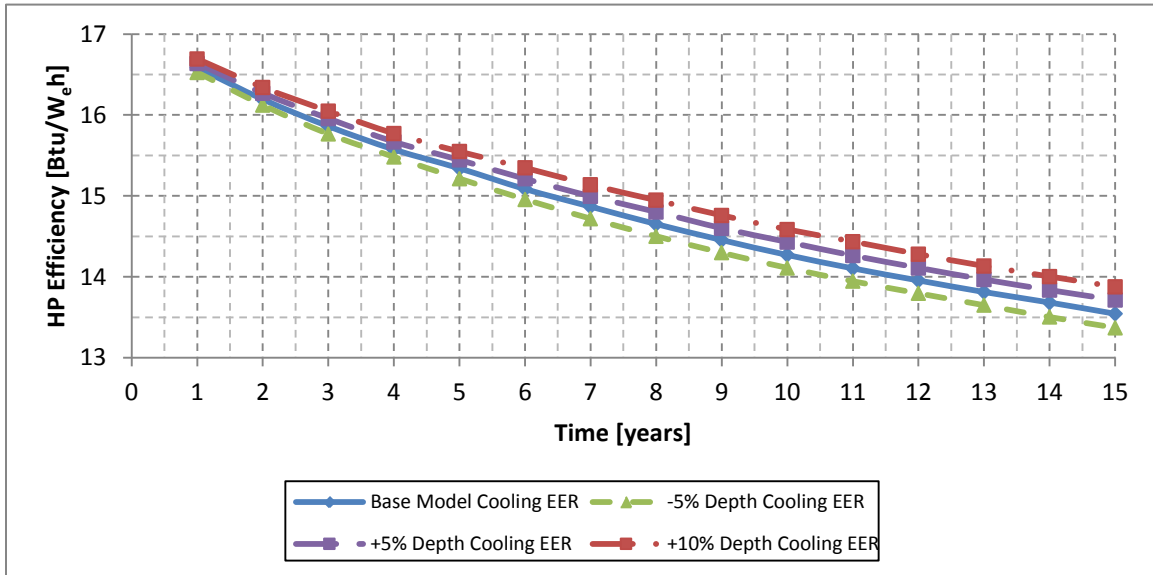


Figure 163: Comparison of average annual EER for the borehole depth test

The figure shows that as the borehole depth increases, the cooling efficiency increases, and that as borehole depth decreases, the cooling efficiency decreases. The shortest GHEX, the -5% case, has the lowest EER throughout the simulation, while the longest GHEX, the +10% case, has the highest EER throughout the simulation. After 15 years of simulation the +10% case decreased from 16.7Btu/W_eh to 13.9Btu/W_eh, a 16.9% decline. In contrast, the +5% case decreased from 16.6Btu/W_eh to 13.7Btu/W_eh (a 17.6% decline), the base model decreased from 16.6Btu/W_eh to 13.5Btu/W_eh (an 18.3% decline) and the -5% case decreased from 16.5Btu/W_eh to 13.4Btu/W_eh (a 19.1% decline). Data for all of the test cases are shown in Table 69.

Table 69: Data for the annual average EER in the borehole depth test

Time [years]	Base Model (171m Depth) [Btu/Wh]	-5% Case (162m Depth) [Btu/Wh]	+5% Case (180m Depth) [Btu/Wh]	+10% Case (188m Depth) [Btu/Wh]
1	16.6	16.5	16.6	16.7
2	16.2	16.1	16.3	16.3
3	15.9	15.8	16.0	16.0
4	15.6	15.5	15.7	15.8
5	15.3	15.2	15.4	15.5
6	15.1	15.0	15.2	15.3
7	14.9	14.7	15.0	15.1
8	14.7	14.5	14.8	14.9
9	14.5	14.3	14.6	14.8
10	14.3	14.1	14.4	14.6
11	14.1	13.9	14.3	14.4
12	14.0	13.8	14.1	14.3
13	13.8	13.6	14.0	14.1
14	13.7	13.5	13.8	14.0
15	13.5	13.4	13.7	13.9
Abs. Change	-3.0	-3.2	-2.9	-2.8
% Change	-18.3%	-19.1%	-17.6%	-16.9%
% per Year	-1.31%	-1.36%	-1.25%	-1.20%

The heat pump efficiency in heating mode, measured in COP, is shown in Figure 164. All of the tests show a general decline in COP over time, despite the fact that increasing EWT causes COP to increase. The reason for this discrepancy is heating overshoot, as was previously discussed in Section 6.4.5. Time-step data of this effect is shown in Section 4.8.

Similarly to EER, the test cases with shorter GHEX show the worse efficiency than the cases with longer GHEX. Over the 15year simulation, the +10% case has the highest COP, beginning at $4.95W_t h/W_e h$ and ending at $4.47W_t h/W_e h$ (a 9.9% reduction). The +5% case initially has a COP of $4.96W_t h/W_e h$ and ends at $4.45W_t h/W_e h$ (a 10.3% reduction). The base model initially has a COP of $4.96W_t h/W_e h$ and ends at $4.41W_t h/W_e h$ (an 11.0% reduction). Finally, the -5% case initially has a COP of $4.96W_t h/W_e h$ and ends at $4.45W_t h/W_e h$ (a 10.5% reduction). The decline in COP values for the -5% case and the base model ought to be larger, except for the increase in COP during year 15. This increase is a result of heat pump shutdown during heating mode due to excessively high EWT values. Data for the COP in all test cases can be found in Appendix A.11.

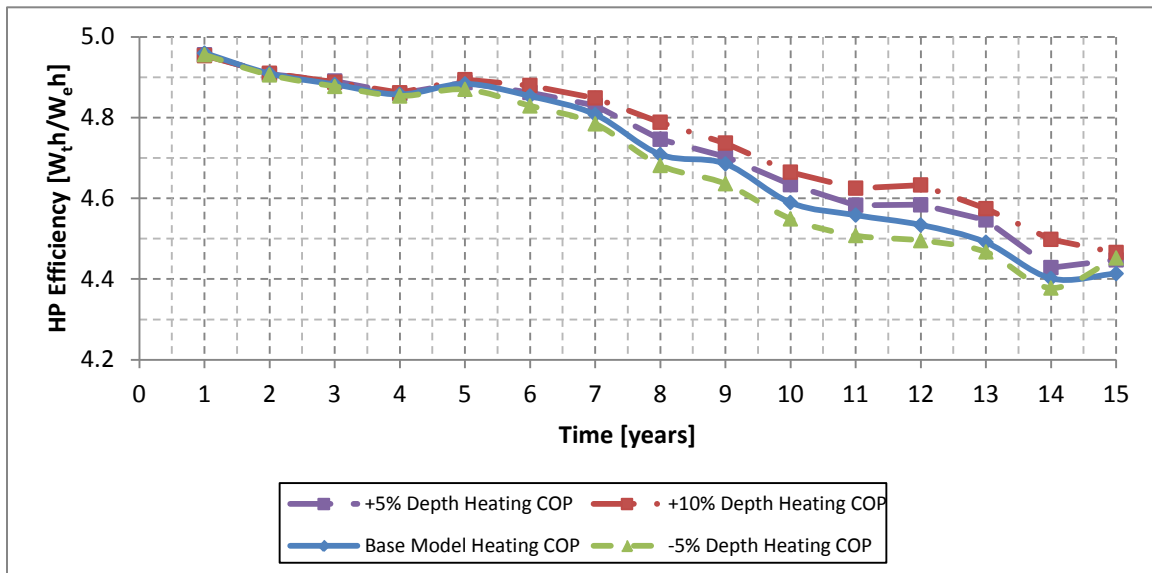


Figure 164: Comparison of annual average COP for the borehole depth test

A summary of the results for the borehole depth test is shown in Table 70. These results show that installation costs dominate the cost effectiveness calculation of borehole depth. The operational savings generated through higher efficiency from a larger GHEX system are an order of magnitude smaller than the increased costs associated with the installation of the GHEX system. The cost of an additional 5% of total GHEX length is approximately \$30,000 for the system in this model, and the extra 5% GHEX length generates approximately \$2,000 in operational savings over the 15-year time period. As a result, increasing total GHEX length in order to improve system efficiency is not a cost effective approach. In fact, the cost difference between installation and operation suggests that shortening the total GHEX length to reduce installation costs combined with the installation of a supplemental source of conditioning is a viable approach. The use of supplemental conditioning is investigated in the next section.

Table 70: Summary of results for borehole depth test

Test Case	Installation Costs [\$]	15-Year Operation Costs [\$]	15-Year Savings [\$]	Average Annual Time Out-of-Setpoint [hrs]
Base Model (171m Depth)	627,200	253,459	N/A	139
-5% Case (162m Depth)	596,960	255,559	28,140	203
+5% Case (180m Depth)	659,680	251,421	-30,442	115
+10% Case (188m Depth)	691,040	249,341	-59,722	107

7.4. Supplemental Heat Rejection

The ground loop portion of GSHP systems accounts for 26% of the total GSHP installation cost for commercial systems (Kavanaugh, Green, & Mescher, 2012). While the HVAC equipment costs account for 74% of the total GSHP installation cost, much of the HVAC equipment cost will be incurred regardless of the type of heating and cooling

system used. Thus minimizing ground loop costs helps to bring GSHP capital costs in line with costs of non-GSHP systems.

The previous section showed that small changes in ground loop length have a significant impact on the installation cost and a relatively small effect on the cost of operation for a GSHP system. The use of a supplemental heat rejection (SHR) device further extends this concept. A supplemental heat rejection device could be a cooling tower or a solar water heater that is used to supplement the heat rejection/absorption of the ground loop. This approach allows the GHEX system to be smaller, as it is designed to meet a reduced portion of the heating or cooling loads.

In this study, supplemental heat rejection is used to meet 10%, 20%, 30% and 40% of the heat pumps' heat rejection requirements for the respective test cases (note that heat absorption of the ground loop was unchanged). The cooling and heating design loads used to size the ground loop in GLHEPRO were subsequently reduced to 90%, 80%, 70% and 60% of the base model, respectively. The EWT design cutoff temperature and the borehole spacing were unchanged from the base model. The heat pump equipment sizing was also unchanged, as the heat pump must still meet 100% of the zone cooling and heating loads. Table 71 shows the design parameters used in the supplemental heat rejection study.

Table 71: Ground loop specifications for the SHR tests

Test Case	Design Cooling [MWh]	Design Heating [kWh]	Spacing [m]	Field Dimensions [boreholes]	Depth [m]	Total Length [m]	Installation Costs [\$]
Base Model	601.3	43.6	6.1	10x16	171	27310	627,200
10% SHR Case	541.2	39.3	6.1	10x16	158	25359	582,400
20% SHR Case	481.0	34.9	6.1	10x16	140	22433	515,200
30% SHR Case	420.9	30.5	6.1	10x16	124	19800	454,720
40% SHR Case	360.8	26.2	6.1	10x16	110	17556	403,200

Figure 165 shows the response of maximum annual EWT values for each test over the duration of the 15 year simulation. Each subsequent SHR test case has a reduced GHEX length combined with a lower total heat rejected to the ground loop. Thus, the base model has the longest GHEX with the highest net heat rejected, while the 40% SHR case has the shortest GHEX with the lowest net heat rejected. Even though GLHEPRO was used to size each test case, Figure 165 shows that reduced heat rejection is more influential on the annual maximum EWT over time than the shorter GHEX length.

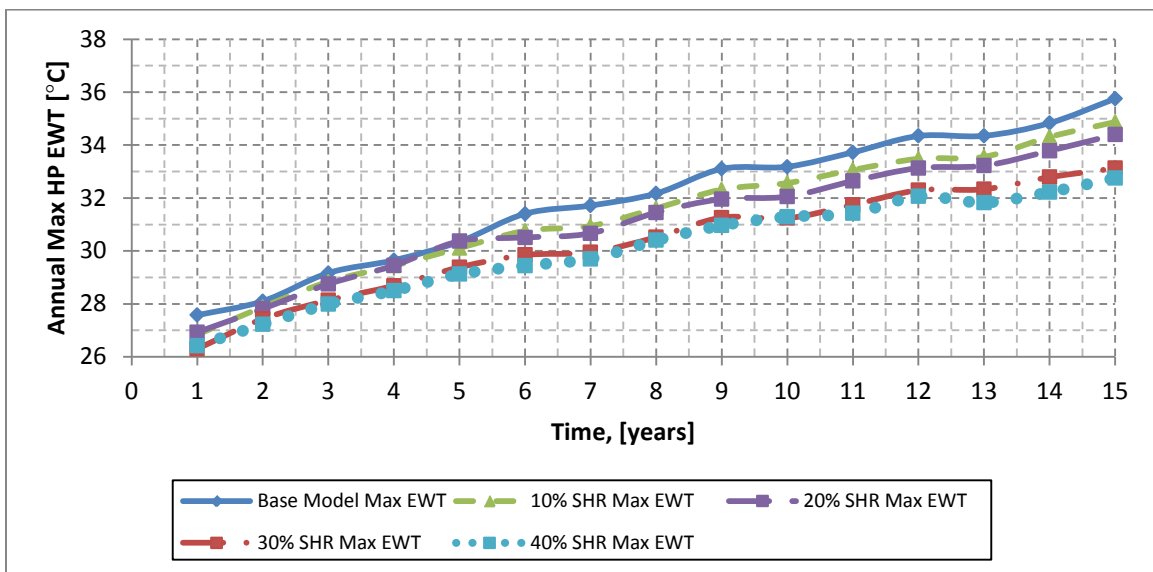


Figure 165: Comparison of maximum annual EWT for the SHR test

The base model has the highest maximum EWT for every year of simulation, while the 40% SHR case has the lowest maximum EWT. The 10% SHR and 20% SHR cases show similar EWT values over time, as do the 30% SHR and 40% SHR cases. Over the 15 year simulation, the base model increased maximum EWT values by 29.7%, compared to 29.9% for the 10% SHR case, 27.7% for the 20% SHR case, 25.9% for the 30% SHR case and 24.0% for the 40% SHR case. Data for the maximum annual EWT is shown in Table 72. The response of the average annual EWT and the minimum annual EWT can be found in Appendix A.12.

Table 72: Data for the maximum annual EWT for the SHR test

Time [years]	Base Model [°C]	10% SHR [°C]	20% SHR [°C]	30% SHR [°C]	40% SHR [°C]
1	27.6	26.8	26.9	26.3	26.4
2	28.1	27.9	27.8	27.4	27.2
3	29.2	28.8	28.8	28.1	28.0
4	29.6	29.4	29.4	28.7	28.5
5	30.3	30.1	30.4	29.4	29.1
6	31.4	30.8	30.5	29.8	29.4
7	31.7	30.9	30.7	29.9	29.7
8	32.2	31.6	31.4	30.5	30.4
9	33.1	32.3	32.0	31.3	31.0
10	33.2	32.6	32.1	31.2	31.3
11	33.7	33.1	32.6	31.7	31.4
12	34.3	33.5	33.1	32.3	32.1
13	34.3	33.6	33.2	32.3	31.8
14	34.8	34.3	33.8	32.8	32.2
15	35.8	34.9	34.4	33.1	32.8
Abs. Change	8.2	8.0	7.5	6.8	6.3
% Change	29.7%	29.9%	27.7%	25.9%	24.0%
% per Year	2.12%	2.14%	1.98%	1.85%	1.71%

Figure 166 shows the response of total annual cooling values for each test over the duration of the 15year simulation. The internal and external loads acting on the model do not change from test case to test case, so the annual cooling values should be similar from case to case. As EWT increases the total cooling capacity of a heat pump decreases, so the total annual cooling for the base model should decrease the most over the 15year simulation, while the 40% SHR case should experience the smallest decrease in total annual cooling (an effect previously discussed in Section 6.3.4).

Over the 15year simulation, the base model experienced a decrease in total annual cooling of 1.36%, compared to a decrease of 20% for the 10% SHR case, a decrease of 1.14% for the 20% SHR case, a decrease of 1.01% for the 30% SHR case and a decrease of 0.97% for the 40% SHR case. Data for total cooling can be found in Appendix A.12.

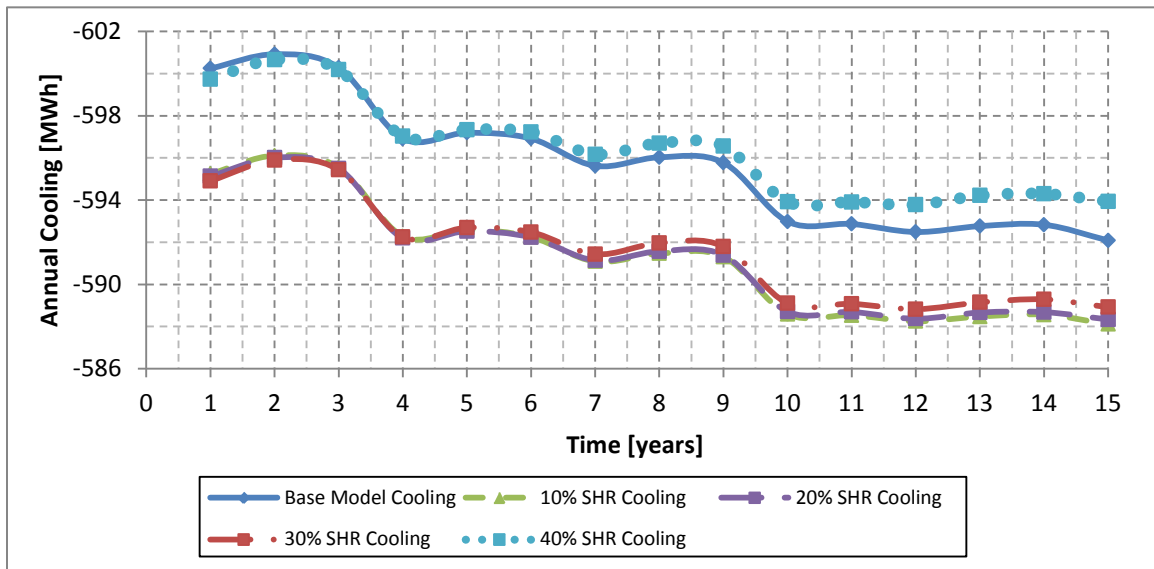


Figure 166: Comparison of total annual cooling for the SHR test

An explanation for the difference in total cooling during year one between the base model and 40% SHR case which have initial annual cooling of approximately 600MWh and the other three cases which have initial annual cooling of 595MWh is unclear. The total hours of operation in cooling, shown in Figure 167, match the total cooling results of Figure 166, but do not explain why the 10% SHR, 20% SHR and 30%

SHR require 200 fewer hours of cooling per year than the base model and the 40% SHR case. Data for the time of operation can be found in Appendix A.12.

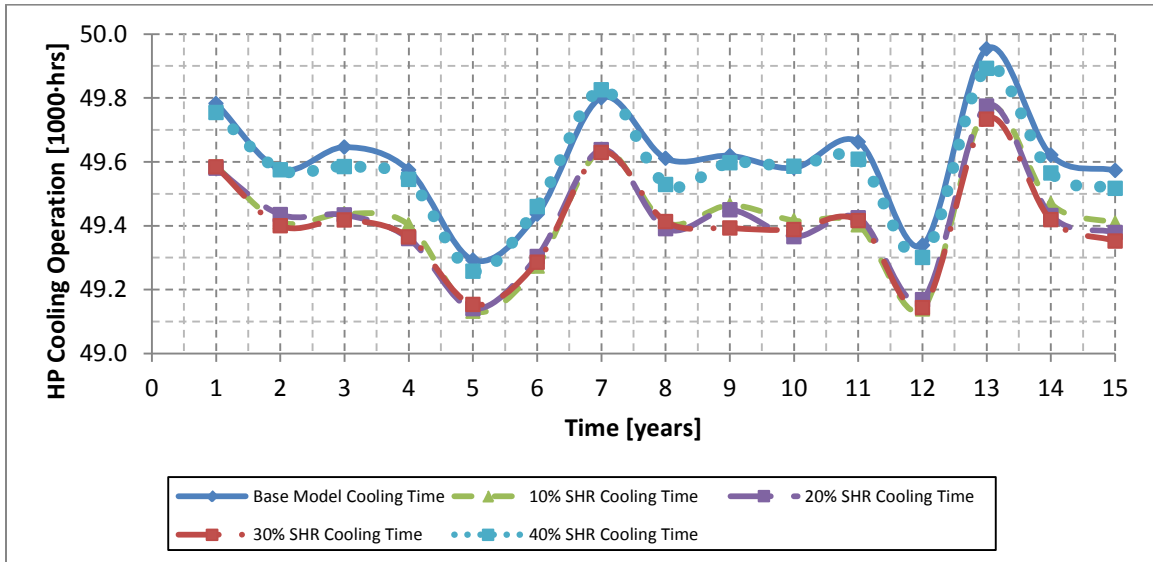


Figure 167: Comparison of total annual time of cooling operation for the SHR test

Additionally, the ratio of net heat rejected to the ground per unit GHEX length, shown in Figure 168, behaves as expected. The SHR test cases in Figure 168 reject less total heat to the ground during year one per unit length of GHEX installation, which results in less ground heating and lower EWT values. Supporting data for the net annual heat rejected per GHEX length ratio can be found in Appendix A.12.

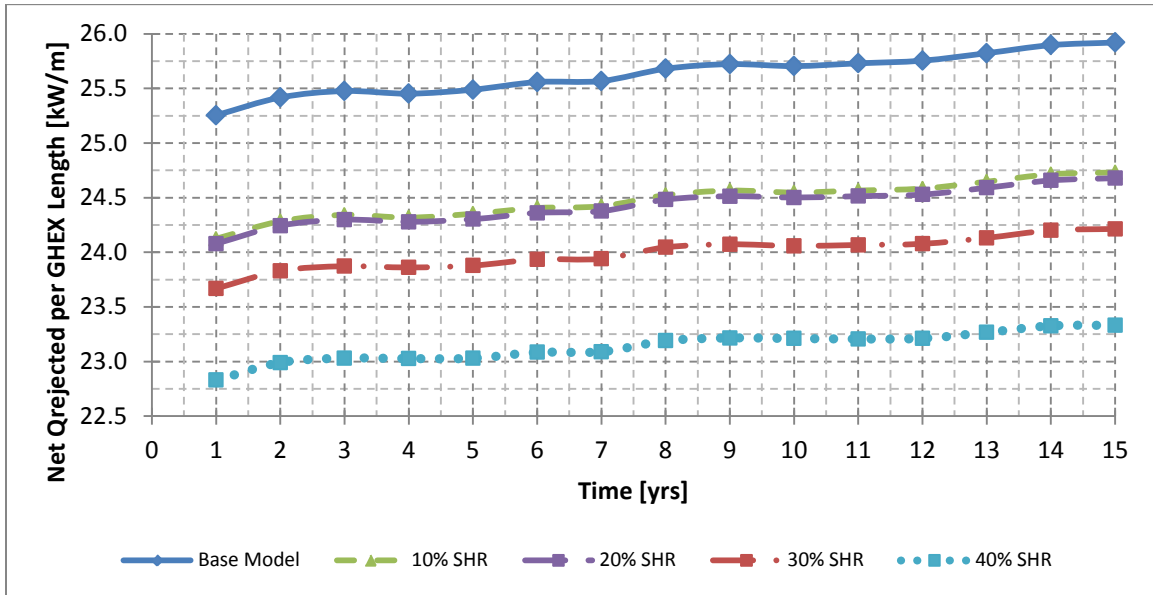


Figure 168: Comparison of the ratio of net annual heat rejected per unit GHEX length for the SHR test

An explanation for the oscillations in total cooling from year to year (as seen in Figure 166), is also unclear. One possible explanation is that on/off control increases cooling and heating overshoot in the zones. Cooling and heating overshoot potentially causes a lack of consistency from day to day and year to year, as the zone temperature at any particular time-step is not solely based on the external weather loads and internal heat sources.

The total annual heating values for each test are shown in Figure 169. Through year 13, all five test cases show similar responses for total annual heating. Increased EWT values in year 14 of the base model cause heat pump shutdown, resulting in lower annual heating totals. All of the SHR test cases behave as expected relative to each other; the 40% SHR case, which as the lowest EWT values, has the lowest total heating capacity and lowest annual heating totals. Moving to the 30% SHR case, the 20% SHR case and the 10% SHR case increases the EWT each time, resulting in slightly higher total heating capacity and a slightly higher total annual heating value. Data for this figure can be found in Appendix A.12.

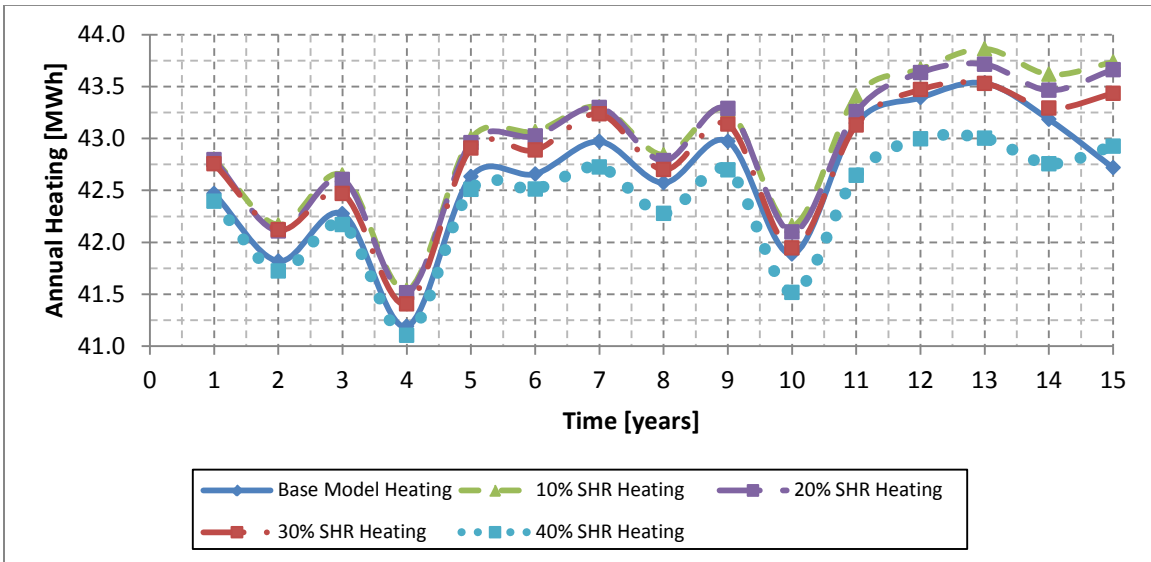


Figure 169: Comparison of total annual heating for the SHR test

The time out-of-setpoint for the SHR test cases is shown in Figure 170. All of the test cases show similar increases and decreases in time out-of-setpoint from year to year until year 14. In year 14, heat pump shutdown in the base model causes increased time out-of-setpoint. None of the SHR test cases exhibit the heat pump shutdown behavior.

The base model increases from 81hrs to 386hrs, a 376% increase, the base model increases from 81hrs to 386hrs, a 377% increase. The 10% SHR case increases from 36hrs to 59hrs, a 64% increase. The 20% SHR case increases from 38hrs to 56hrs, a 47%

increase. The 30% SHR case increases from 40hrs to 54hrs, a 35% increase. Finally, the 40% SHR case increases from 87hrs to 121hrs, a 39% increase. Data for this figure can be found in Appendix A.12.

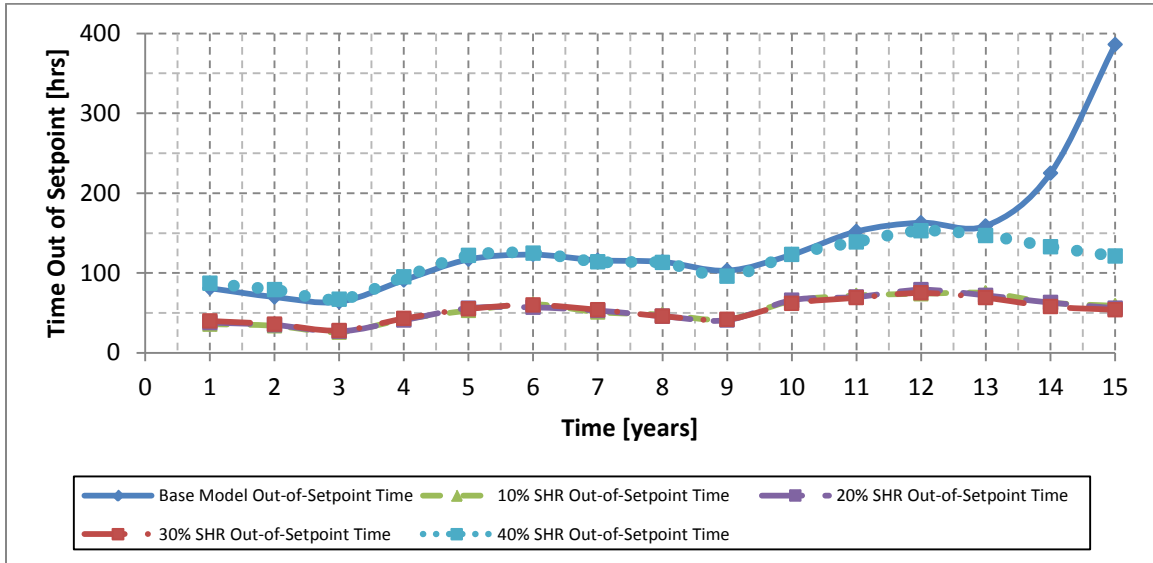


Figure 170: Comparison of annual time out-of-setpoint for the SHR test

The annual net heat rejected to the ground loop for each test case is shown in Figure 171. This figure shows the effect of SHR in the simulations. The 10% SHR case diverts 10% of heat rejected by the heat pumps to an ideal supplementary heat rejection device, such as a cooling tower, reducing the net heat rejected to the ground loop to 90% of the base model. The 20% SHR case, 30% SHR case and 40% SHR case similarly divert 20%, 30% and 40% of heat rejected by the heat pumps to an ideal SHR device, respectively. The smaller heat load rejected to the ground loop allows for the smaller GHEX installations shown in Table 71. Additional heat rejection and heat absorption data can be found in Appendix A.12.

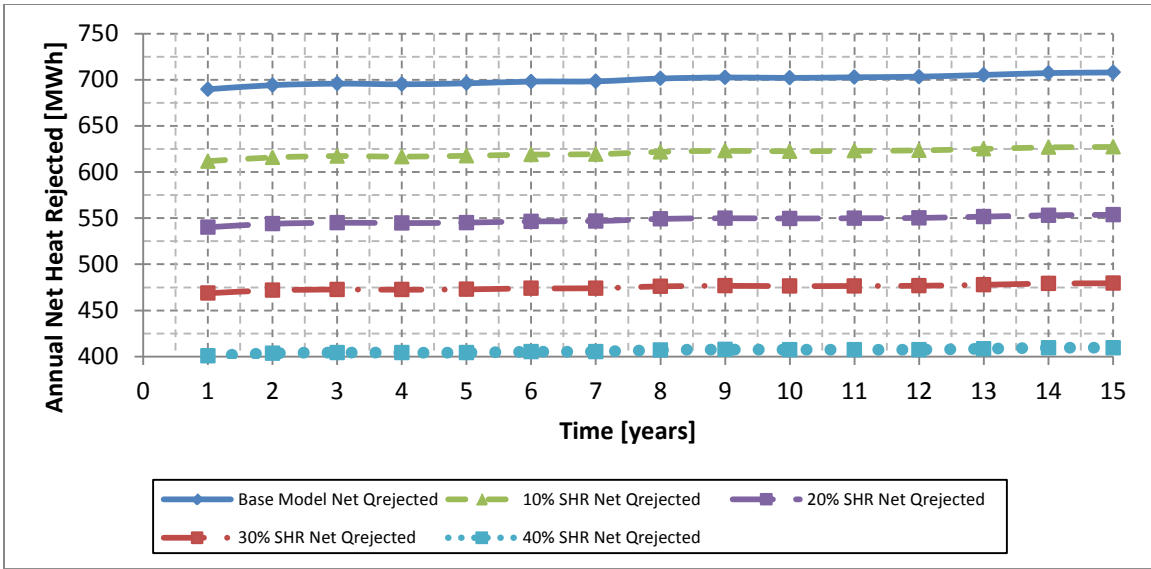


Figure 171: Comparison of annual net heat rejected to the ground loop for the SHR test

The total annual power usage for cooling is shown in Figure 172. The power usage increases as EWT increases for all of the test cases. Over the 15year simulation, the test case with the highest EWT experienced the greatest increase in total annual power usage for cooling, and the test case with the lowest EWT experienced the smallest increase in total power usage. The cooling power usage in the base model increased by 20.6% compared to 19.3% for the 10% SHR case, 18.5% for the 20% SHR case, 16.5% for the 30% SHR case and 15.4% for the 40% SHR case. Thus, increasing the SHR by 10% decreased the 15year cooling power usage from 2.059GWh to 2.031GWh, a 1.34% reduction. By comparison, the 20% SHR case reduced the 15year cooling power usage from 4 2.030GWh, a 1.41% reduction, the 30% SHR case reduced the 15year cooling power usage to 2.019GWh, a 1.95% reduction, and the 40% SHR case reduced the 15year cooling power usage to 2.033GWh, a 1.26% reduction. Data for the cooling power usage can be found in Appendix A.12.

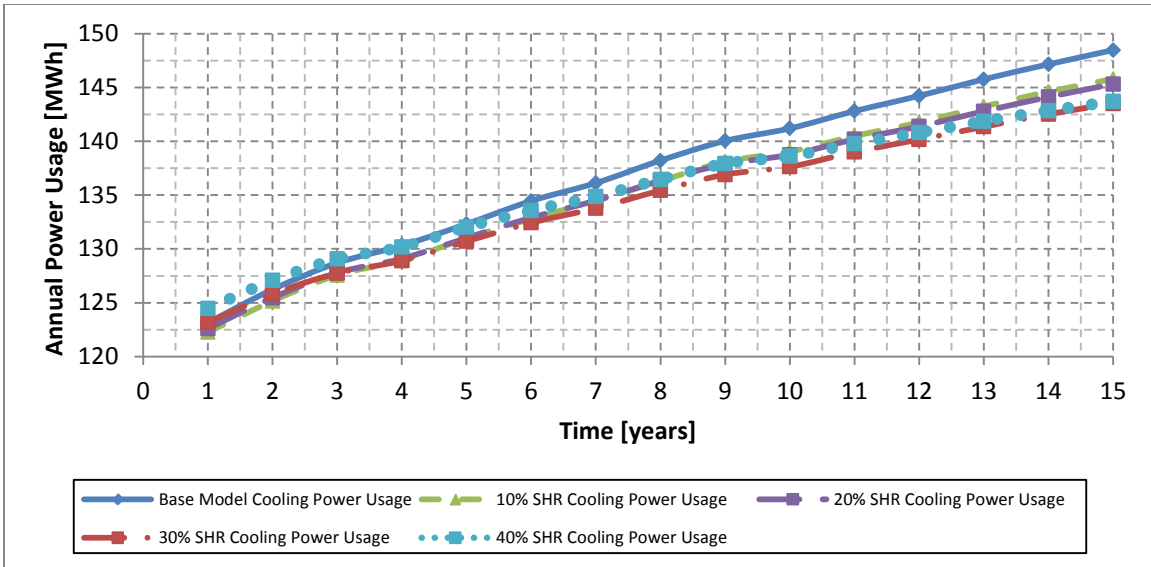


Figure 172: Comparison of total annual cooling power usage for the SHR test

The total annual power usage for heating is shown in Figure 173. The energy used for heating increases gradually throughout the 15-year interval. The increased energy usage is a result of increased EWT; as the EWT increases so does the power usage during heating. The test cases with greater SHR show a smaller increase in total annual heating across the 15-year simulation than the test cases with smaller SHR values.

The base model was the only test case to show a sharp decline in annual power usage during year 15, indicating that none of the SHR test cases experience heat pump shutdown due to excessively high EWT. Data for the heating power usage can be found in Appendix A.12.

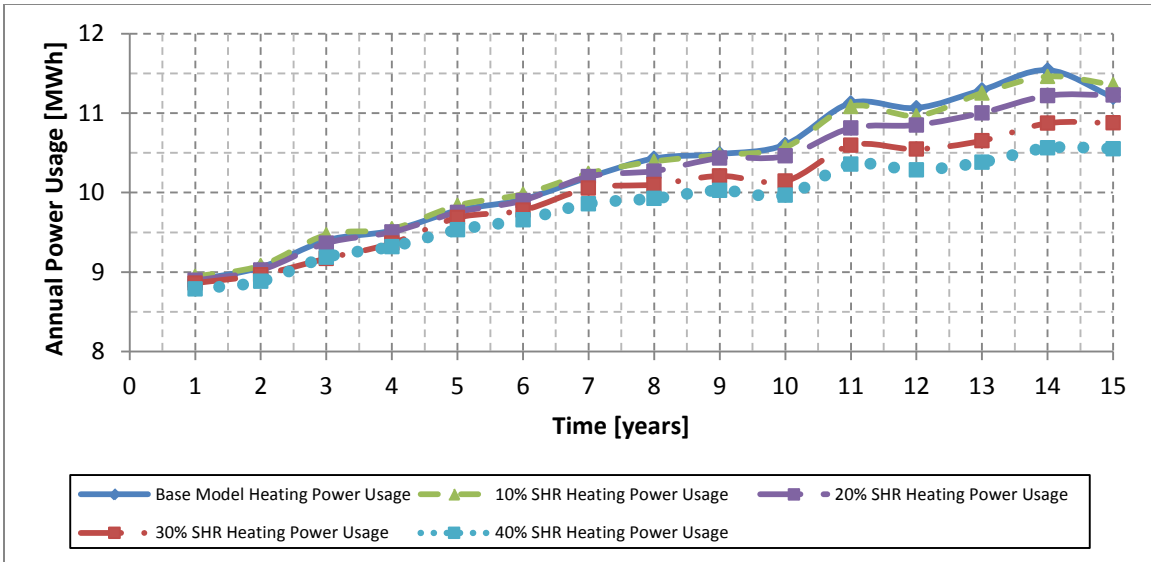


Figure 173: Comparison of total annual heating power usage for the SHR test

The increasing electricity usage values during the simulation in steady decline for heat pump efficiency, as shown in Figure 174.

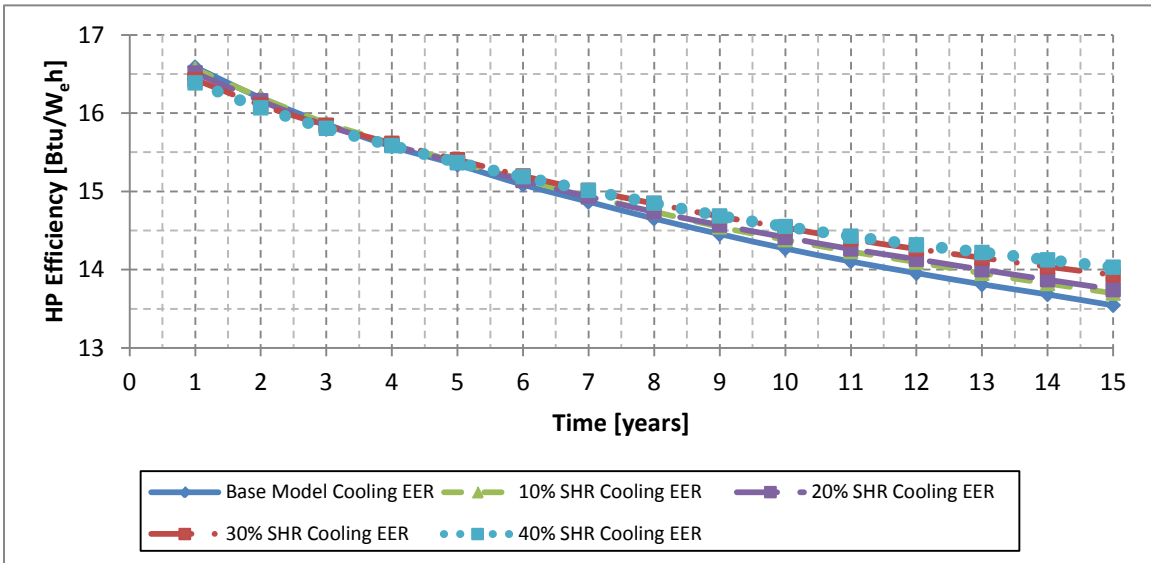


Figure 174: Comparison of average annual EER for the SHR test

The figure shows that the test cases with greater SHR experience a smaller decline in EER over the 15year simulation than the test cases with smaller SHR. After 15years of simulation the 40% SHR case had the smallest decline in SHR, decreasing from 16.4Btu/W_eh to 14.0Btu/W_eh, a 14.4% decline. In contrast, the 30% SHR case decreased from 16.4Btu/W_eh to 13.9Btu/W_eh (a 15.2% decline), the 20% SHR case decreased from 16.5Btu/W_eh to 13.7Btu/W_eh (a 16.7% decline), the 10% SHR case decreased from 16.6Btu/W_eh to 13.7Btu/W_eh (a 17.3% decline) and the base model decreased from 16.6Btu/W_eh to 13.5Btu/W_eh (an 18.3% decline). Data for all of the test cases are shown in Table 73.

Table 73: Data for the annual average EER in the SHR test

Time [years]	Base Model [Btu/Wh]	10% SHR [Btu/Wh]	20% SHR [Btu/Wh]	30% SHR [Btu/Wh]	40% SHR [Btu/Wh]
1	16.6	16.6	16.5	16.4	16.4
2	16.2	16.2	16.2	16.1	16.1
3	15.9	15.9	15.8	15.8	15.8
4	15.6	15.6	15.6	15.6	15.6
5	15.3	15.4	15.4	15.4	15.4
6	15.1	15.2	15.1	15.2	15.2
7	14.9	14.9	14.9	15.0	15.0
8	14.7	14.7	14.7	14.8	14.8
9	14.5	14.5	14.6	14.7	14.7
10	14.3	14.4	14.4	14.5	14.6
11	14.1	14.2	14.3	14.4	14.4
12	14.0	14.1	14.1	14.3	14.3
13	13.8	14.0	14.0	14.2	14.2
14	13.7	13.8	13.9	14.0	14.1
15	13.5	13.7	13.7	13.9	14.0
Abs. Change	-3.0	-2.9	-2.8	-2.5	-2.4
% Change	-18.3%	-17.3%	-16.7%	-15.2%	-14.4%
% per Year	-1.31%	-1.24%	-1.20%	-1.08%	-1.03%

The heat pump efficiency in heating mode, measured in COP, is shown in Figure 175. All of the tests show a general decline in COP over time, despite the fact that increasing EWT causes COP to increase. The reason for this discrepancy is heating overshoot, as was previously discussed in Section 6.4.5. Time-step data of this effect is shown in Section 4.8.

Similarly to EER, the test cases with the larger SHR show better efficiency than the test cases with smaller SHR. Over the 15 year simulation, the 40% SHR case has the highest COP, beginning at $4.96 W_t h / W_e h$ and ending at $4.65 W_t h / W_e h$ (a 6.2% reduction). By comparison, the 30% SHR case initially has a COP of $4.96 W_t h / W_e h$ and ends at $4.60 W_t h / W_e h$ (a 7.2% reduction), the 20% SHR case initially has a COP of $4.96 W_t h / W_e h$ and ends at $4.51 W_t h / W_e h$ (a 9.0% reduction), the 10% SHR case initially has a COP of $4.96 W_t h / W_e h$ and ends at $4.48 W_t h / W_e h$ (a 9.7% reduction) and the base model initially has a COP of $4.96 W_t h / W_e h$ and ends at $4.41 W_t h / W_e h$ (an 11.0% reduction). Data for the COP in all test cases can be found in Appendix A.12.

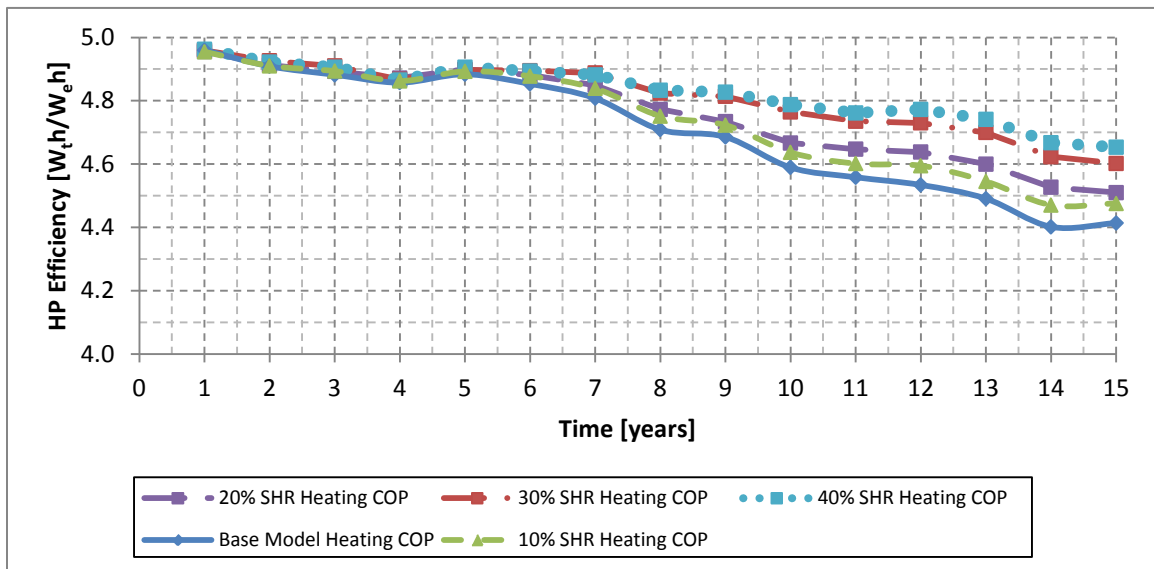


Figure 175: Comparison of annual average COP for the SHR test

A summary of the results for the supplemental heat rejection test is shown in Table 74. The savings associated with each SHR test do not include the additional capital cost required for the SHR device itself.

Table 74: Summary of results for SHR test

Test Case	Installation Costs [\$]	15-Year Operation Costs [\$]	15-Year Savings [\$]	Average Annual Time Out-of-Setpoint [hrs]
Base Model	627,200	253,459	N/A	139
10% SHR	582,400	250,312	47,947	53
20% SHR	515,200	249,951	115,508	53
30% SHR	454,720	248,336	177,603	53
40% SHR	403,200	249,668	227,791	114

These results show that considerable cost savings can be realized through the use of a supplemental heat rejection system (note that these savings do not include any costs associated with the SHR device; installation costs, operating costs or maintenance costs). Not only did the SHR systems enable the construction of shorter GHEX installations that significantly reduced GSHP installation costs, increasing the size of the SHR system improved the operational efficiency of the entire HVAC system. Both the installation costs and the operational costs show an inflection point between 10% and 30% SHR. The marginal installation savings are \$44,800 for the 10% SHR system, \$67,200 for the 20% SHR system, \$60,480 for the 30% SHR system and \$51,520 for the 40% SHR. The marginal operational savings are \$3,147 for the 10% SHR system, \$362 for the 20% SHR system, \$1,615 for the 30% SHR system and -\$1,333 for the 40% SHR.

Chapter 8 Conclusions

The objective of this research was to provide an integrated building load and ground source heat pump (GSHP) model that can be used to evaluate new technologies, different control approaches and different system designs for GSHP systems and heating, ventilation and air conditioning (HVAC) systems with a specific focus on commercial GSHP installations in the southwest and southcentral United States. To this end, the model was developed for a 3-story commercial office building, 15 heat pumps, an HVAC system and a vertically bored ground heat exchanger (GHEX) arranged in a 10x16 borefield.

The building-load model was developed in HAMBASE, which simulates the thermal and hygric response of each zone in the building to external weather and internal loads. The building-load model was validated using the ASHRAE 140-2007 Standard Method of Test for the Evaluation of Building Energy Analysis Computer Programs and with simulations from EnergyPlus.

The heat pump model was developed as a performance map, based on data commonly provided by heat pump manufacturers. This approach allows for easy expansion of the number and type of heat pump models supported.

The GHEX model, developed by Oklahoma State University researchers, accurately represents the interaction between boreholes and ground temperature response over short and long time-intervals. The GHEX model also maintains computational efficiency through the use of temporal superposition, and is easily altered due to its use of GLHEPRO files for input parameters.

These component models were integrated in the Matlab® Simulink® modeling environment, which allows for model modification and expansion. Additional component models of the building plenum and ground loop header, for example, were created and easily integrated due to Simulink's® graphical and modular nature. Simulation of the integrated model couples the building temperature and humidity to the thermostat, the heat pump and subsequently the ground loop. The dynamic response of each subsystem

can then be tracked and evaluated for both individual and system-level optimization. The integrated model is computationally expensive: a single year of simulation requires approximately 7.5hours and a 15year simulation takes approximately 118hours on a computer which has two six-core, hyperthreading 3.33GHz Xeon processors with 24GB of shared memory (shared between 9 machines).

Long time-interval simulations with durations of 15years were completed for the integrated model. These simulations showed the interconnectedness of the component models and the integrated model's ability to calculate and use changes in environmental parameters over time. During the 15year simulations using Austin, Texas-based environmental and geological conditions, the base-case office building experienced considerably greater cooling loads than heating loads, resulting in a net heat rejection to the GHEX and corresponding ground heating over time. The ground heating caused an increase in the total power usage of the heat pump and a decline in the total cooling ability of the heat pump. The increased power usage resulted in lower heat pump efficiency and higher operating costs. The decreased total cooling ability caused an increase in building temperature and time above the cooling setpoint.

The results summarized above were for the base-case model, which represents one possible design approach. Other design approaches could have been used, so sensitivity studies were performed to evaluate the effects of design parameters on total system cost and efficiency. These studies showed that: small changes in the total GHEX length resulted in significant changes to the total system cost with minimal impact on total system performance; increased borehole spacing significantly improved system performance with no additional system cost; supplemental heat rejection significantly reduced installation costs and improved system performance; industry-recommended ground loop design cutoff temperatures properly sized the GHEX system; and, while cooling is the most significant driver of cost of operation for an office building in the southwest and southcentral United States, heating was the limiting design case for GHEX sizing since the entering water temperature limit during heating ($32.2^{\circ}\text{C}/90^{\circ}\text{F}$) was lower than that for cooling ($48.9^{\circ}\text{C}/120^{\circ}\text{F}$).

Incorporating the results of these sensitivity studies will reduce installation costs and operating costs for GSHP systems in Texas and other hot, arid regions of the United States, making GSHP systems more accessible and competitive with other HVAC technologies. The greater overall efficiency of GSHP systems compared to other HVAC systems means that greater adoption of GSHP systems will reduce the growing demand for electricity worldwide and reduce the environmental effects of electricity generation. In addition, integrated models such as the one developed in this paper will help to further improve GSHP system design, ensuring that appropriately sized GSHP systems are installed, thus sustaining their effectiveness and low cost of operation through many years of use.

8.1. Recommendations for Future Work

The integrated model developed in this thesis offers an environment for considerable further research. The following model improvements are recommended:

- Multi-speed control of fans and water pumps
- Continuously variable speed control of fans and water pumps
- Eliminate the one-minute response lag

The following tests are proposed:

- Compare the efficiency of a small GHEX dedicated to each floor of the building to the efficiency of one large GHEX for the entire building.
- Create 1 GHEX installation with total length L . Create n GHEX installations with individual length L/n , and rotate through each installation for one year while letting the others recover. Compare the operational efficiency of the two approaches.

Appendix

A.1. Additional Load Profiles

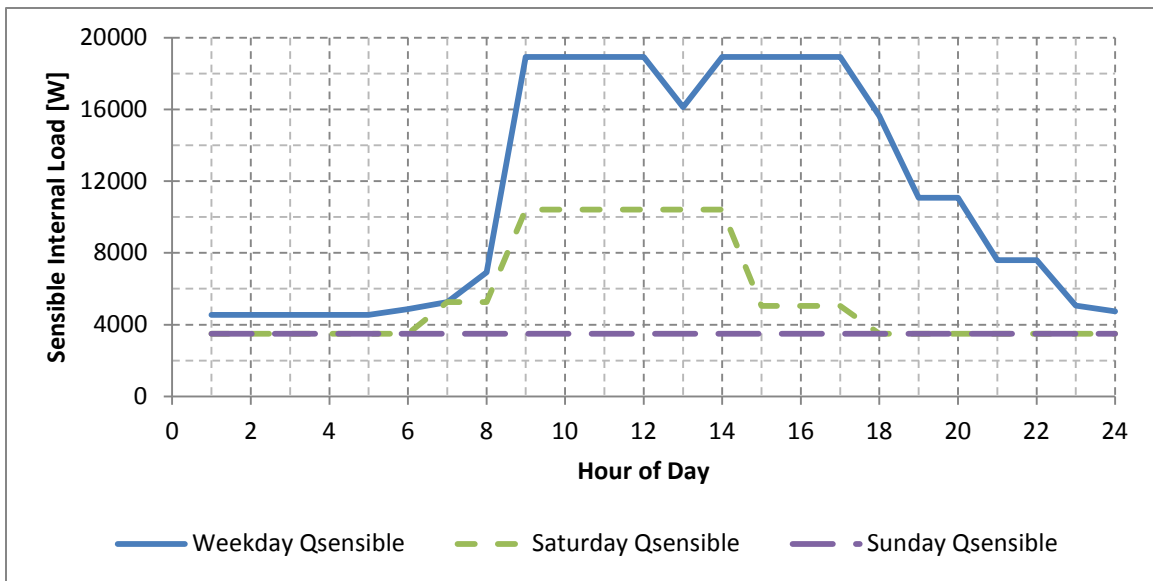


Figure 176: Sensible internal load profiles for Core2 and Core3

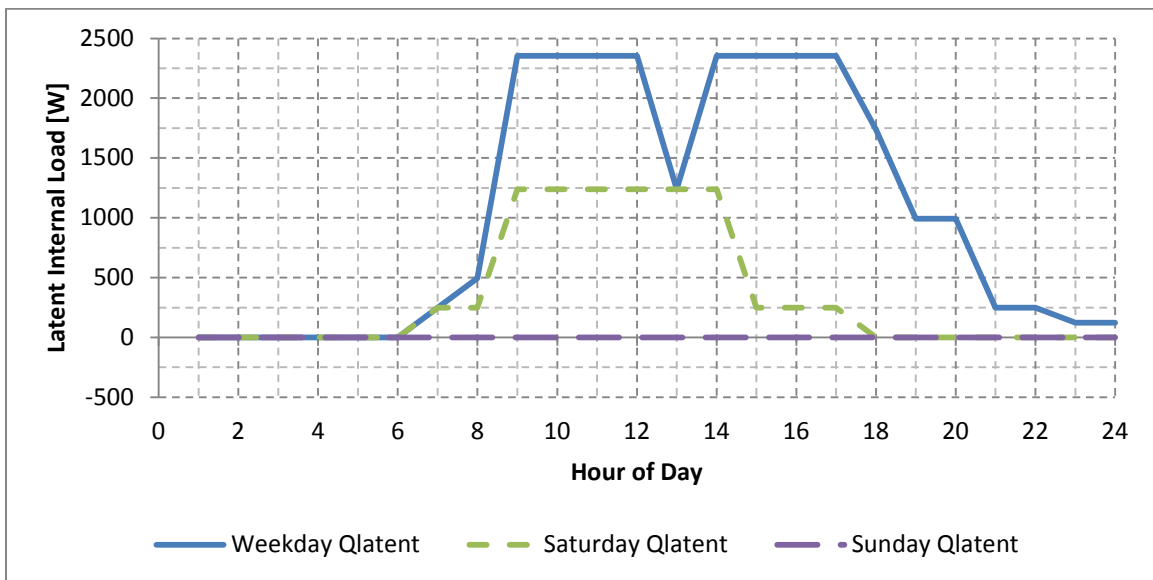


Figure 177: Latent internal load profiles for Core2 and Core3

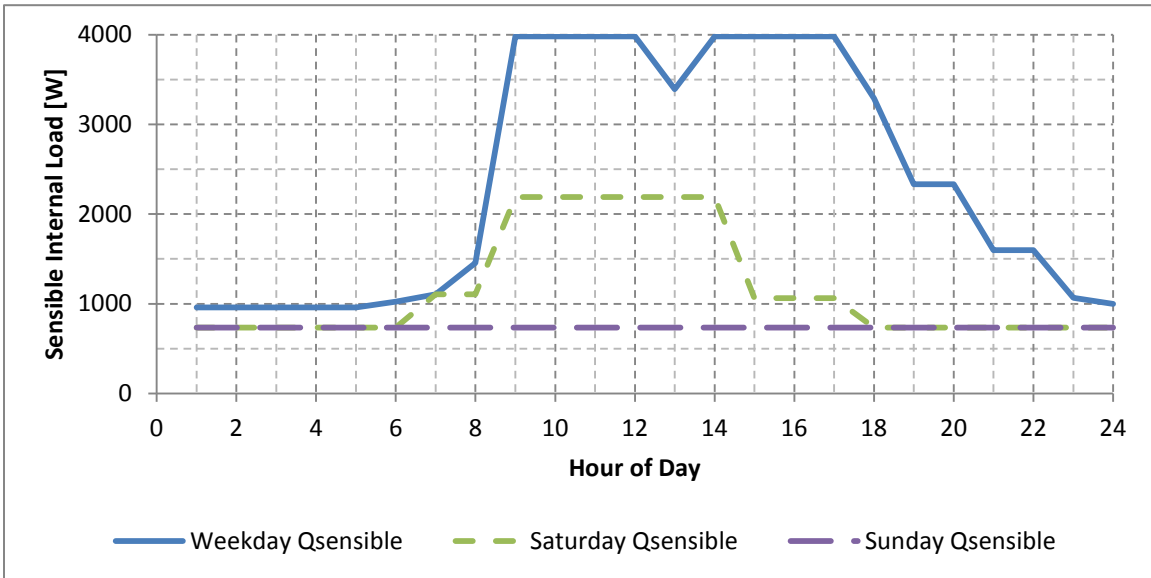


Figure 178: Sensible internal load profiles for North and South zones

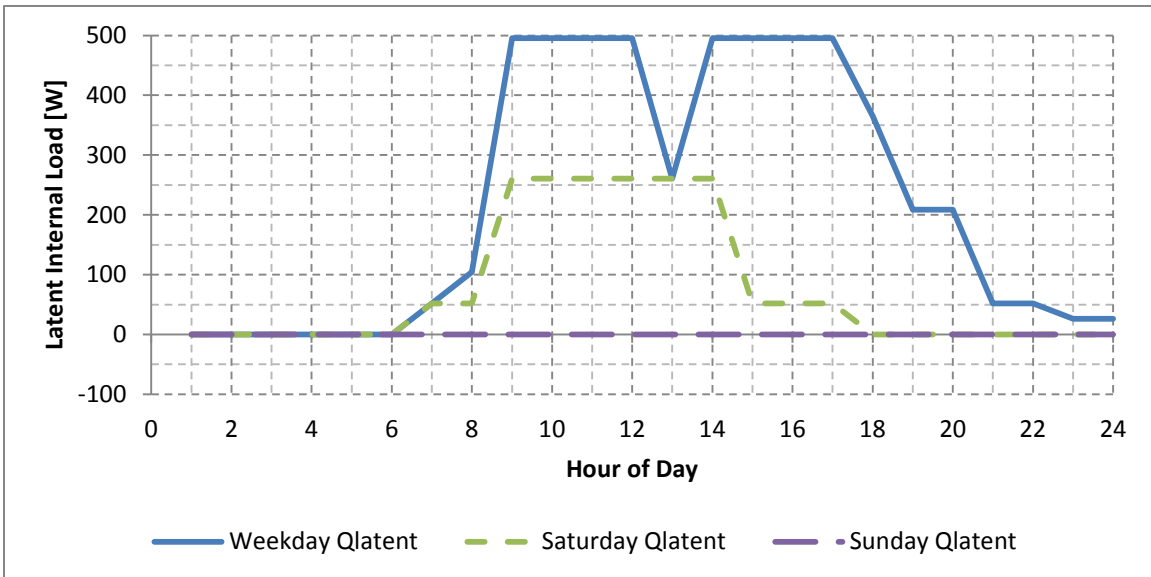


Figure 179: Latent internal load profiles for North and South zones

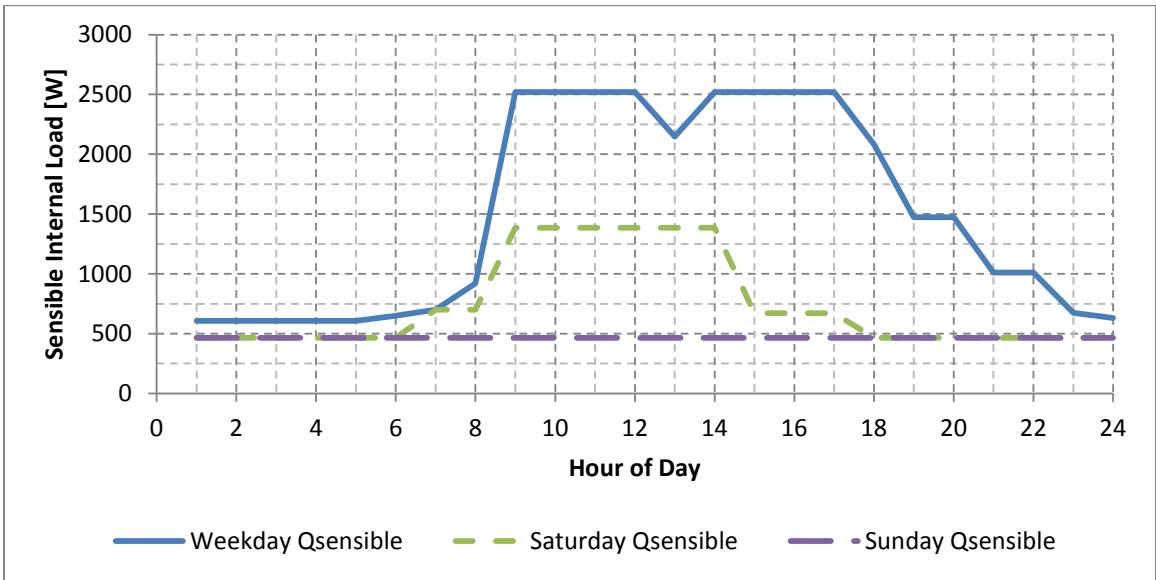


Figure 180: Sensible internal load profiles for East and West zones

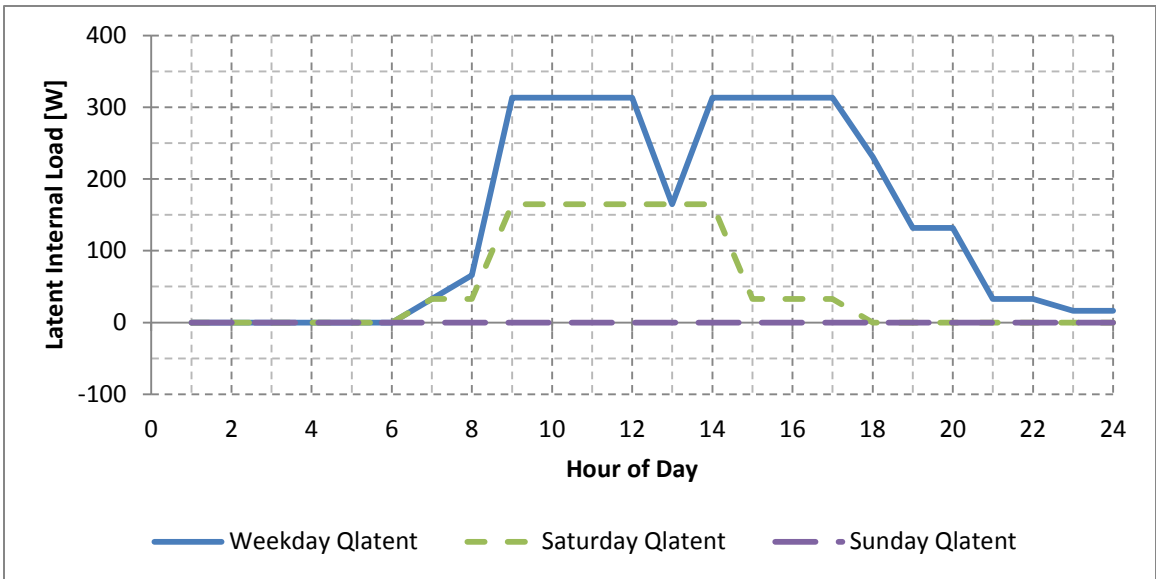


Figure 181: Latent internal load profiles for East and West zones

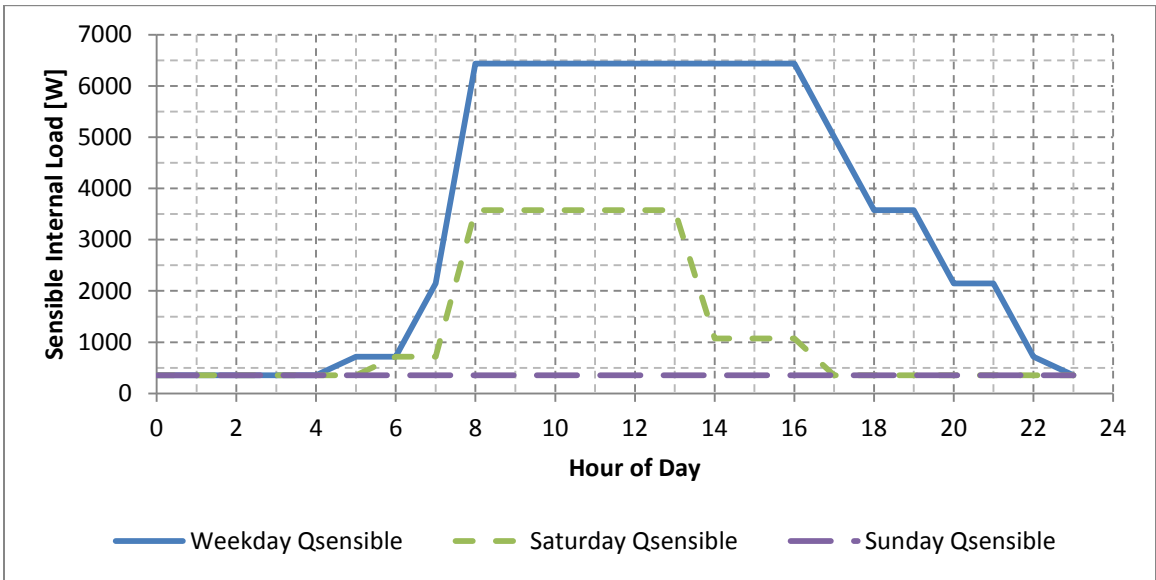


Figure 182: Sensible internal load profiles for Plenum zones

Note: Plenum zones do not experience internal latent loads.

A.2. Additional Performance Map Data

The following figure shows the entire interpolation and correction process for performance map inlet conditions.

Entering Air Temp DB 75 F NOTES: 1) Correction Factors are From Matlab and Table Values are directly taken
 Entering Water Temp 86 F from the provided correction factor tables 2) All Interpolation is done in the Excel
 GPM 13 GPM Spreadsheet 3) Error on Correction Factors includes error on curve fitting
 Airflow 1313.2 CFM
 Entering Air Temp WB 66.23 F

Interpolation Data				Cooling				Heating		
EWT	Water Flow Rate	Air Flow Rate		Total Capacity	Sensible Capacity	Power	Heat Rejected	Capacity	Power	Heat Extracted
F	GPM	CFM		kBtuh	kBtuh	kW	kBtuh	kBtuh	kW	kBtuh
85	7.5	1465		56.9	37.4	4.44	72.1	78.1	5.15	60.4
85	7.5	1950		59.3	44.8	4.59	75	80.1	4.71	64
85	11.3	1465		59.1	38.3	4.16	73.3	81.6	5.23	63.5
85	11.3	1950		61.6	45.8	4.3	76.3	83.7	4.79	67.4
85	15	1465		60.2	38.7	4.03	73.9	83.4	5.28	65.1
85	15	1950		62.7	46.3	4.17	76.9	85.6	4.83	69.1
90	7.5	1465		55.2	36.8	4.66	71.2	81	5.22	63
90	7.5	1950		57.5	44	4.82	74	83.2	4.77	66.9
90	11.3	1465		57.5	37.7	4.37	72.4	84.5	5.3	66.2
90	11.3	1950		59.9	45.1	4.51	75.3	86.8	4.85	70.2
90	15	1465		58.6	38.1	4.23	73.1	86.3	5.35	67.7
90	15	1950		61.1	45.6	4.37	76	88.6	4.89	71.9

Step 1: Interpolation for T_{WATER,IN}				Cooling				Heating		
EWT	Water Flow Rate	Air Flow Rate		Total Capacity	Sensible Capacity	Power	Heat Rejected	Capacity	Power	Heat Extracted
F	GPM	CFM		kBtuh	kBtuh	kW	kBtuh	kBtuh	kW	kBtuh
86	7.5	1465		56.56	37.28	4.484	71.92	78.68	5.164	60.92
86	7.5	1950		58.94	44.64	4.636	74.8	80.72	4.722	64.58
86	11.3	1465		58.78	38.18	4.202	73.12	82.18	5.244	64.04
86	11.3	1950		61.26	45.66	4.342	76.1	84.32	4.802	67.96
86	15	1465		59.88	38.58	4.07	73.74	83.98	5.294	65.62
86	15	1950		62.38	46.16	4.21	76.72	86.2	4.842	69.66

Step 2: Interpolation for V_{WATER}				Cooling				Heating		
EWT	Water Flow Rate	Air Flow Rate		Total Capacity	Sensible Capacity	Power	Heat Rejected	Capacity	Power	Heat Extracted
F	GPM	CFM		kBtuh	kBtuh	kW	kBtuh	kBtuh	kW	kBtuh
86	13	1465		59.2854	38.3638	4.1414	73.4049	83.0070	5.2670	64.7659
86	13	1950		61.7746	45.8897	4.2814	76.3849	85.1838	4.8204	68.7411

Step 3: Correction Factors for V_{AIR}				Cooling				Heating		
	Air Flow Ratio			Total Capacity	Sensible Capacity	Power	Heat Rejected	Capacity	Power	Heat Extracted
Correction Factc	0.6734			0.9924	0.9583	0.9907	0.9920	0.9940	1.0169	0.9880
Table Values				0.9923	0.9578	0.9906	0.9920	0.9940	1.0167	0.9880
Error				-0.01%	-0.05%	-0.01%	0.00%	0.00%	-0.02%	0.00%
Corrected Value	1313.2			61.3051	43.9761	4.2415	75.7738	84.6727	4.9018	67.9162

Step 4: Correction Factors for Entering Air Conditions				Cooling- Based on T_{AIR,WET}				Heating - Based on T_{AIR,DRY}		
				Total Capacity	Sensible Capacity	Power	Heat Rejected	Capacity	Power	Heat Extracted
Correction Factc				0.9860	0.8137	1.0003	0.9873	0.9892	1.0558	0.9719
Table Values				0.9882	0.8152	0.999	0.9903	0.9883	1.0556	0.9706
Error				0.22%	0.18%	-0.13%	0.30%	-0.09%	-0.02%	-0.13%
Corrected Value				60.4468	35.7834	4.2428	74.8115	83.7582	5.1754	66.0077

Figure 183: Performance map data fitting process

A.3. Inlet Air Correction Factors

The heat pump performance map assumes an inlet air condition of 19.4°C T_{wb} (67°F), 26.7°C T_{db} (80°F) during cooling mode. For inlet air that does not match, the correction table shown in Figure 42 is used. The correction factors are shown as a function of inlet wet bulb temperature in Figure 184.

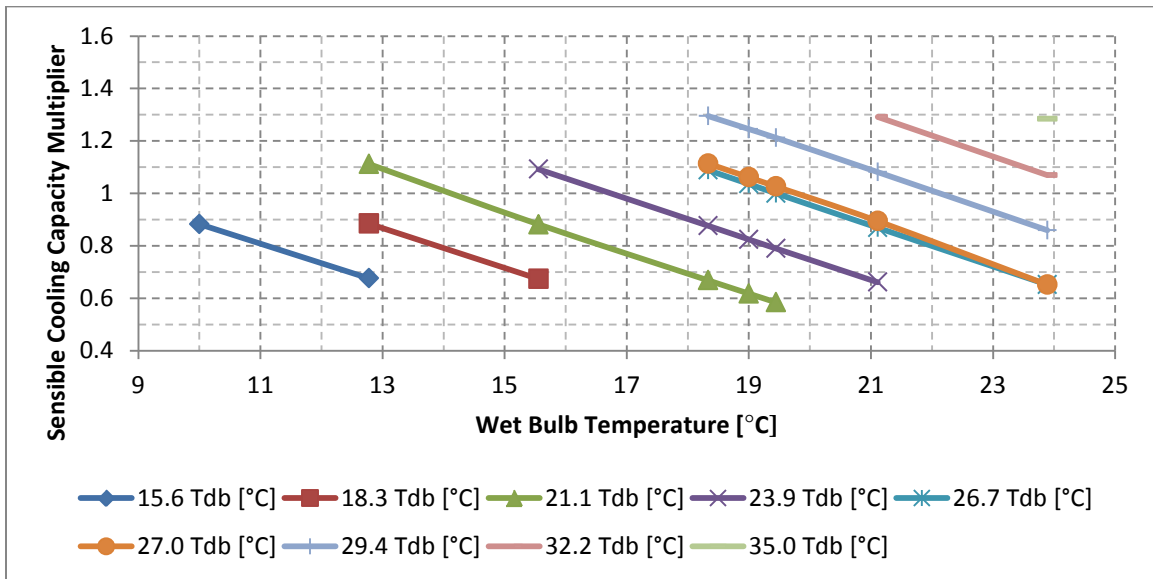


Figure 184: Inlet air correction factors provided by ClimateMaster

Extra data points were generated using extrapolation, as shown in Figure 185.

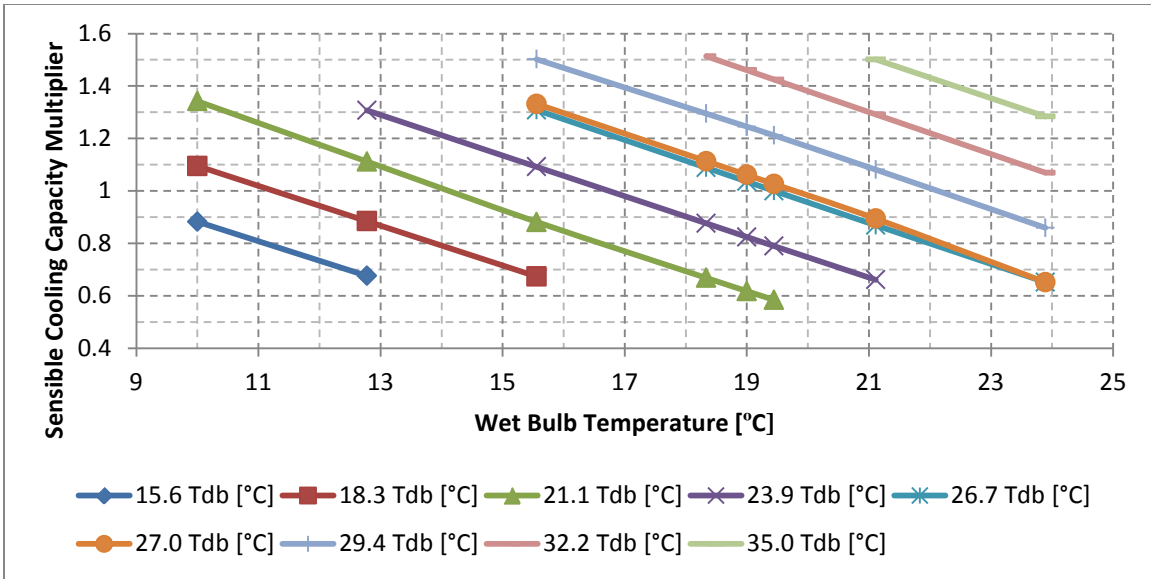


Figure 185: Inlet air correction factors for heat pump performance map

A.4. Additional GLHEPRO Data

The following sections describe the use of GLHEPRO as a ground loop sizing tool in this model. A detailed explanation of the general use of GLHEPRO can be found at the GLHEPRO website, hosted by Oklahoma State University (2007a), or using the GLHEPRO 4.0 Users' Guide (Oklahoma State University, 2007b)

A.4.1. Peak Load Analysis Tool

The peak load analysis tool included with GLHEPRO converts hourly building loads into monthly peak load values, which are in turn used to size the ground loop. The peak load values consist of a magnitude and a duration. The peak heating and peak cooling magnitudes are calculated by month, while the duration is a constant value for the year (Oklahoma State University, 2007b, p. 80).

A year of HAMBASE hourly heating and cooling values for every zone was summed to create an hourly cooling and heating total for the medium office building. The year of hourly building totals combined with the secondary parameters shown in Figure 186 as the inputs to the peak load analysis tool.

System Sizing		U-Tube Size	
Borehole Depth [ft]	400	Inner Diameter [in]	1.38
Borehole Radius [in]	2.50038	Outer Diameter [in]	1.66
Thermal Conductivities		Volumetric Heat Capacities	
Pipe [Btu/(hr*ft*F)]	0.22501415	Pipe [Btu/(ft^3*F)]	23
Grout [Btu/(hr*ft*F)]	1	Grout [Btu/(ft^3*F)]	58.16391
Ground [Btu/(hr*ft*F)]	1.2	Ground [Btu/(ft^3*F)]	22.99
		Fluid [Btu/(ft^3*F)]	62.21943
Convection Coefficient [Btu/(hr*ft^2*F)]	47.59		
Borehole Thermal Resistance [(hr*ft*F)/Btu]	0.3172		

OK

Figure 186: Secondary parameters used in the GLHEPRO peak load analysis tool

The tool then generated the normalized temperature responses shown in Figure 187 and Figure 188. The normalized temperature response that peaked closest to 1.0 was chosen as the most appropriate duration; thus a duration of 9hr and 3hr was chosen for cooling and heating respectively.

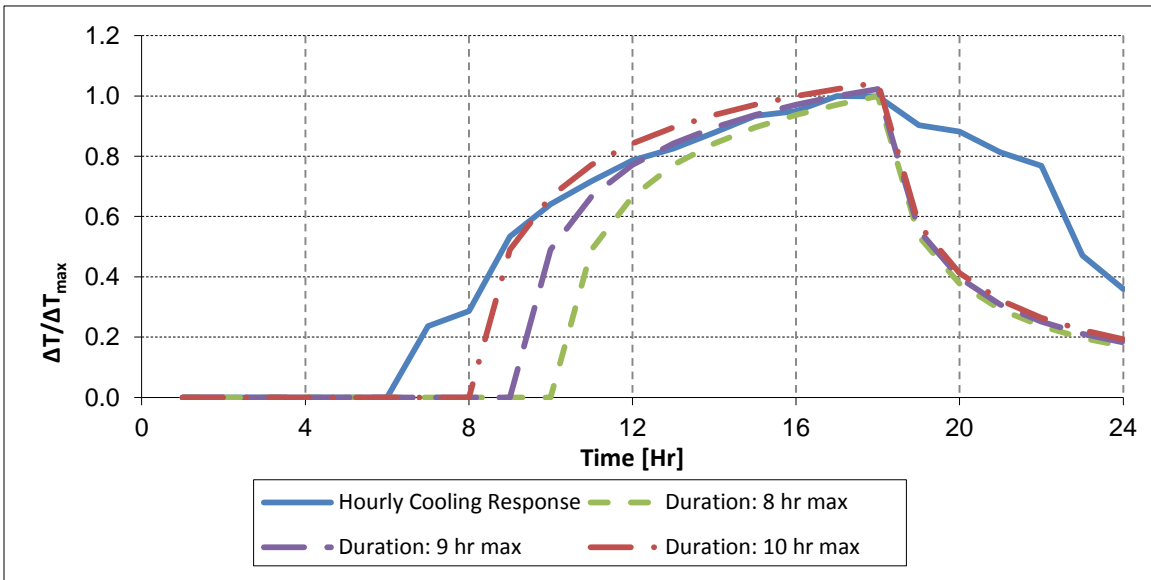


Figure 187: GLHEPRO normalized temperature response for peak cooling load

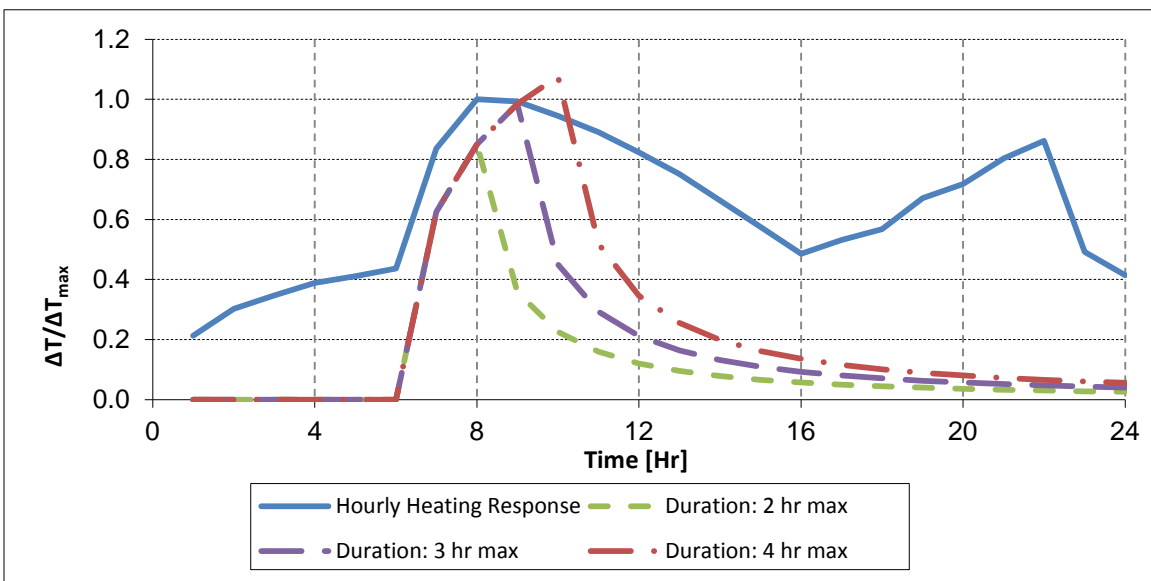


Figure 188: GLHEPRO normalized temperature response for peak heating load

With the durations chosen, the peak load analysis tool generated monthly total loads and peak loads, which were then used as an input to GLHEPRO. These values are shown in Figure 189.

Monthly Loads

Heating	Cooling
<input type="checkbox"/> Average over duration	<input type="checkbox"/> Average over duration
<input checked="" type="checkbox"/> Maximum during duration	<input checked="" type="checkbox"/> Maximum during duration
Duration: 3	Duration: 9

Note that it is not necessarily the case that the best method for heating and cooling (average or maximum) will be the same.

Get Summary Data

	Total Loads [1000 Btu]		Peak Loads [1000 Btu/h]	
	Heating	Cooling	Heating	Cooling
January	53639	29363	801	560
February	22230	31646	649	629
March	11356	87415	546	841
April	815	166399	287	972
May	280	227660	91	1054
June	0	299794	0	1089
July	0	341319	0	1112
August	0	323535	0	1135
September	141	234544	66	1049
October	448	182926	181	1080
November	7122	86164	323	940
December	52866	40821	874	658

Figure 189: Monthly total loads and peak loads generated by the peak load analysis tool

A.4.2. Use of GLHEPRO

The following figures show the inputs used to generate the base case ground loop file in GLHEPRO. Figure 190 shows the main screen inputs. Figure 191 shows the ground loop dimensions. Figure 192 shows the monthly total and peak heating and cooling loads. More detailed explanation of how to use GLHEPRO to create a ground loop file can be found in the GLHEPRO Users' Manual (Oklahoma State University, 2007b).

The screenshot shows the main input screen of the GLHEPRO software. The window title is "glhepro - OfficeGloop_2013_07_17-10Wx16Lx20Rx560Dborefield-90F.gli". The interface includes a menu bar (File, Loads, Units, Action, Help, Register) and a toolbar with various icons. The main content area is organized into four sections:

- Borehole Parameters:**
 - Active Borehole Depth: 561.1 ft
 - Borehole Diameter: 5 in
 - Borehole Thermal Resistance: 0.178 °F/(Btu/(hr*ft))
 - Borehole Spacing: 20 ft
 - Borehole Geometry: LARGE RECTANGLE 160 : 16 x 10
- Ground Parameters:**
 - Soil type currently entered :
 - Thermal Conductivity of the ground: 1.2 Btu/(hr*ft*°F)
 - Volumetric heat capacity of the ground: 34.94 Btu/(°F*ft^3)
 - Undisturbed ground temperature: 72 °F
- Fluid Parameters:**
 - Total flow rate for entire system: 319.9 gal/min
 - Fluid Type: Pure Water
 - Average Temperature: 68°F
 - Fluid Concentration: 0%

Freezing Point	Density	Volumetric Heat Capacity	Conductivity	Viscosity
°F	lb/ft^3	Btu/(F.ft^3)	Btu/(h.ft.F)	lbm/(ft.h)
32.00	62.31	62.228	0.3425	2.423
- Heat Pump:**
 - Heat Pump Selected: ClimateMaster TS060_PSC_MOTOR@11.3GPM_1465CI

Figure 190: Main screen of GLHEPRO for the base model simulation

G-Function and Borehole Resistance Calculator

U-Tube | Double U-Tube | Concentric Tube

Borehole Diameter (d): in

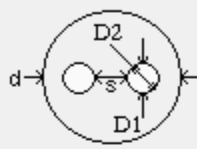
Shank Spacing (s): in

U-Tube Inside Diameter (D1): in

U-Tube Outside Diameter (D2): in

Volumetric Flow Rate/borehole: gal/min

Fluid Factor: Unitless (multiply fluid in the system by this amount)



Volumetric Heat Capacities

Soil: Btu/(°F*ft³)

Grout: Btu/(°F*ft³)

Pipe: Btu/(°F*ft³)

Conductivities

Soil: Btu/(hr*ft*°F)

Grout: Btu/(hr*ft*°F)

Pipe: Btu/(hr*ft*°F)

Options for specifying the Fluid Convection Coefficient

Option 1 Convection Coefficient Btu/(hr*ft²*°F)

Option 2

Fluid Type: **Pure Water** Fluid Concentration: **0%**
Average Temperature: **68°F**

Select Fluid	Freezing Point °F	Density lb/ft ³	Volumetric Heat Capacity Btu/(F.ft ³)	Conductivity Btu/(h.ft.F)	Viscosity lbm/(ft.h)
	32.00	62.31	62.228	0.3425	2.423

Borehole Resistance °F/(Btu/(hr*ft))

Figure 191: G-function and borehole resistance screen for the base model simulation

Edit Loads on Heat Pump

Load on Heat pump

Month	Total Heating 1000 Btu	Total Cooling 1000 Btu	Peak Heating 1000 Btu/hr	Peak Cooling 1000 Btu/hr
January	53639	29363	801	560
February	22230	31646	649	629
March	11356	87415	546	841
April	815	166399	287	972
May	280	227660	91	1054
June	0	299794	0	1089
July	0	341319	0	1112
August	0	323535	0	1135
September	141	234544	66	1049
October	448	182926	181	1080
November	7122	86164	323	940
December	52866	40821	874	658

Duration of Peak Loads

Number of Peak heating hours : 3 Number of Peak Cooling hours : 9

Clear Loads Copy Paste Cancel OK

Figure 192: Heat pump load screen for the base model simulation

A.5. Additional Validation Tests

A.5.1. Test Set 8: Open-Loop, Ambient Temperature and Relative Humidity-Sine, No Internal Loads

The constant weather file was altered to create a temperature and relative humidity-sine input. The TMY3 data was reviewed to find a representative summer day. A sine-wave was then fit to the temperature data and relative humidity data, as shown in Figure 203. The remainder of the constant weather file from Table 32 remained unchanged. Internal loads were turned off. The thermostat was disengaged, eliminating HVAC operation.

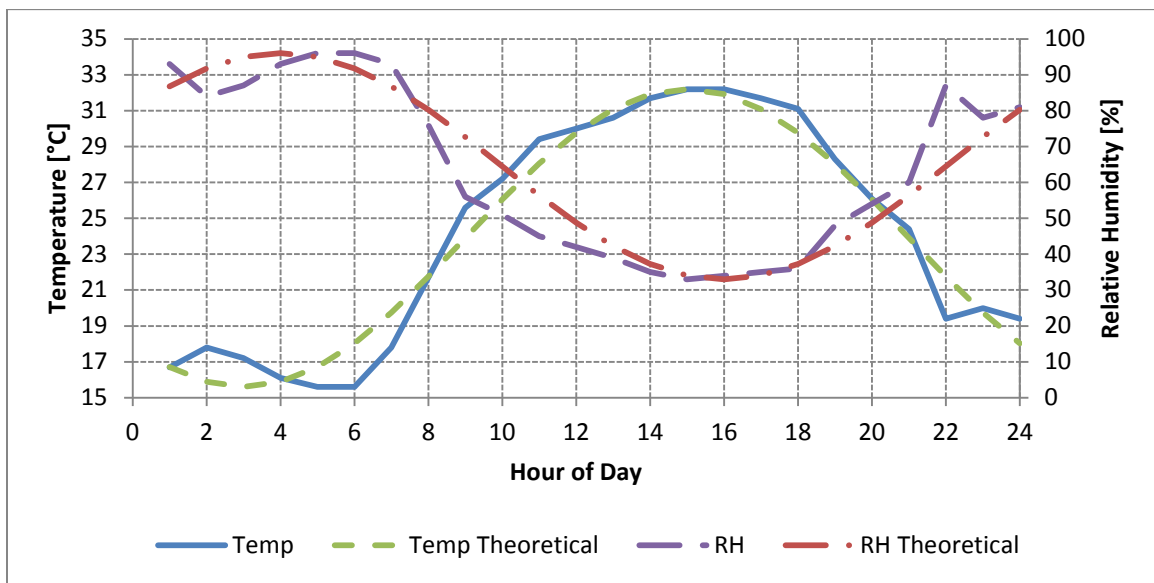


Figure 193: Temperature and relative humidity curves for 8/16/2004

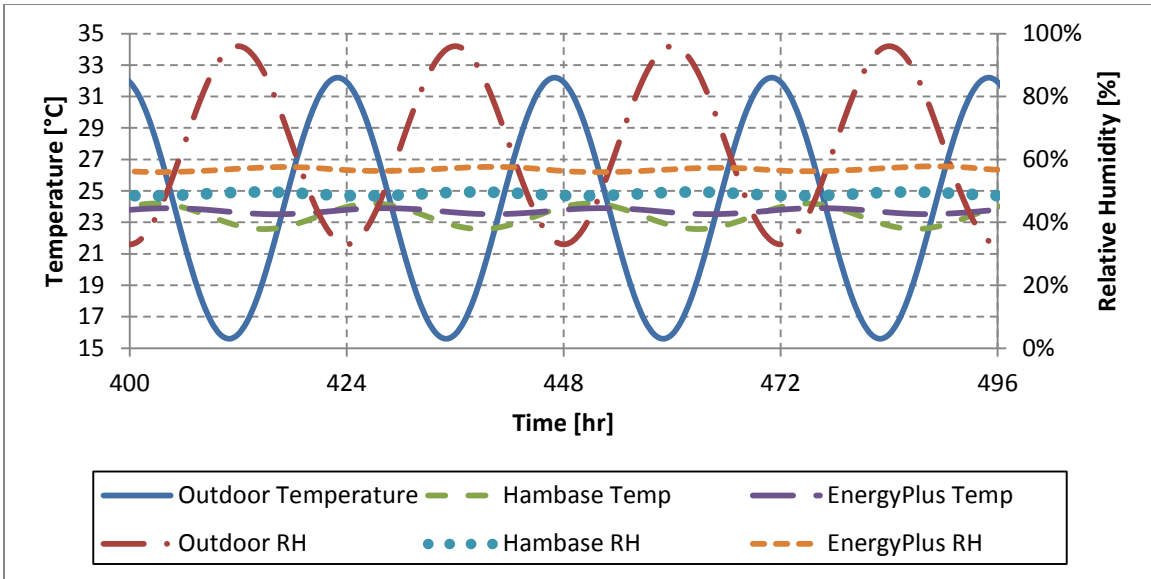


Figure 194: Open-loop response of Core1 to temperature and RH-sine input

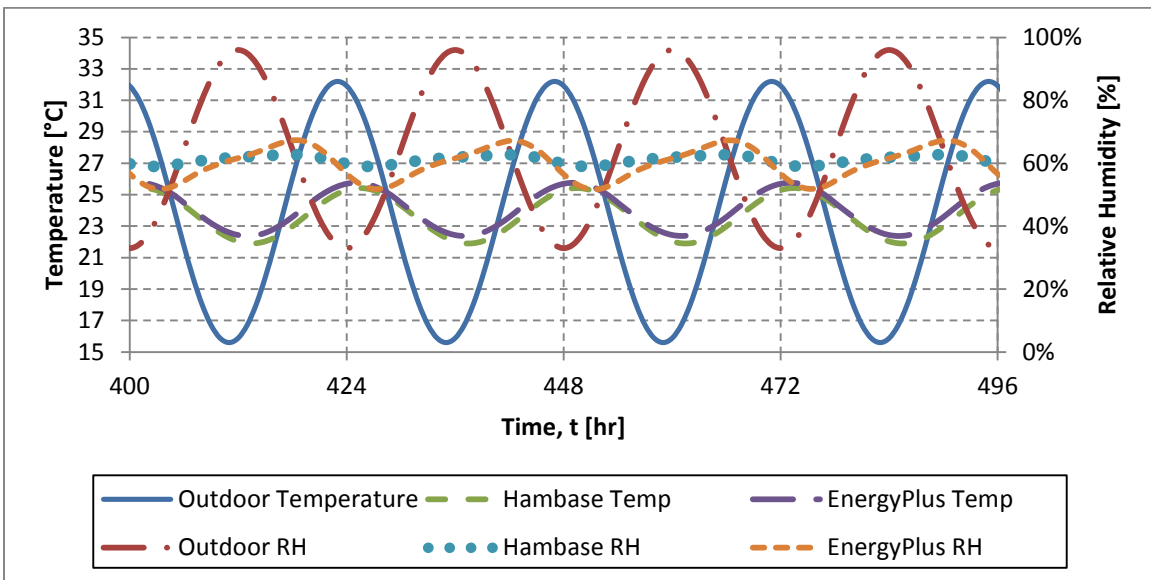


Figure 195: Open-loop response of East2 to temperature and RH-sine input

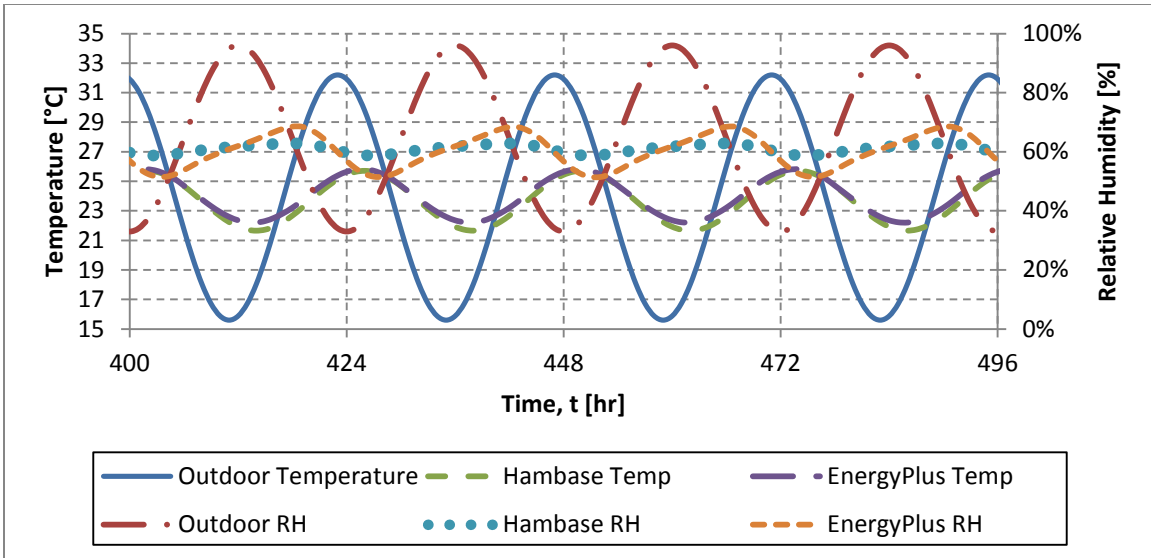


Figure 196: Open-loop response of South3 to temperature and RH-sine input

Table 75: Temperature results for open-loop temperature and RH-sine input

Zone	Steady-State Max. Temperature [°C]		Steady-State Min. Temperature [°C]		Steady-State Avg. Temperature [°C]	
	HB	EP	HB	EP	HB	EP
Core1	24.2	24.2	22.6	22.6	23.4	23.7
South1	26.2	26.2	20.9	20.9	23.6	23.6
East1	26.2	26.2	20.9	20.9	23.6	23.6
North1	26.2	26.2	20.9	20.9	23.6	23.6
West1	26.2	26.2	20.9	20.9	23.6	23.6
Plenum1	24.6	24.6	22.5	22.5	23.6	24.1
Core2	24.0	24.0	23.2	23.2	23.6	24.3
South2	25.4	25.4	21.9	21.9	23.7	24.1
East2	25.4	25.4	21.9	21.9	23.7	24.1
North2	25.4	25.4	21.9	21.9	23.7	24.1
West2	25.4	25.4	21.9	21.9	23.7	24.1
Plenum2	24.4	24.4	22.9	22.9	23.7	24.3
Core3	24.5	24.5	22.8	22.8	23.7	24.2
South3	25.7	25.7	21.7	21.7	23.7	24.0
East3	25.7	25.7	21.6	21.6	23.7	24.0
North3	25.7	25.7	21.7	21.7	23.7	24.0
West3	25.7	25.7	21.6	21.6	23.7	24.0
Plenum3	26.3	26.3	20.9	20.9	23.7	23.9
Average	25.4	25.4	21.8	21.8	23.6	24.0

Table 76: Relative humidity results for open-loop temperature and RH-sine input

Zone	Steady-State Max RH [%]		Steady-State Min RH [%]		Steady-State Amplitude (Max-Min) [%]	
	HB	EP	HB	EP	HB	EP
Core1	50%	58%	48%	56%	1%	2%
South1	64%	69%	58%	54%	6%	15%
East1	64%	69%	58%	53%	6%	16%
North1	64%	69%	58%	54%	6%	15%
West1	64%	69%	58%	53%	6%	16%
Plenum1	63%	64%	61%	57%	2%	7%
Core2	49%	56%	49%	54%	0%	2%
South2	63%	67%	59%	52%	4%	15%
East2	63%	67%	59%	52%	4%	16%
North2	63%	67%	59%	52%	4%	15%
West2	63%	67%	59%	52%	4%	16%
Plenum2	62%	63%	61%	56%	2%	7%
Core3	50%	58%	49%	53%	1%	5%
South3	63%	69%	59%	51%	4%	17%
East3	63%	69%	59%	51%	4%	18%
North3	63%	68%	59%	51%	4%	17%
West3	63%	69%	59%	51%	4%	18%
Plenum3	72%	77%	54%	45%	17%	32%
Average	61%	66%	57%	53%	4%	14%

A.5.2. Test Set 9: Open-Loop Direct Normal Irradiance-Sine, No Internal Loads

The constant weather file was altered to create a DNI (direct normal irradiance) sine input. The TMY3 data was reviewed to find a representative summer day. A sine-wave was then fit to the DNI data, as shown in Figure 197. The remainder of the constant weather file from Table 32 remained unchanged. Internal loads were turned off. The thermostat was disengaged, eliminating HVAC operation.

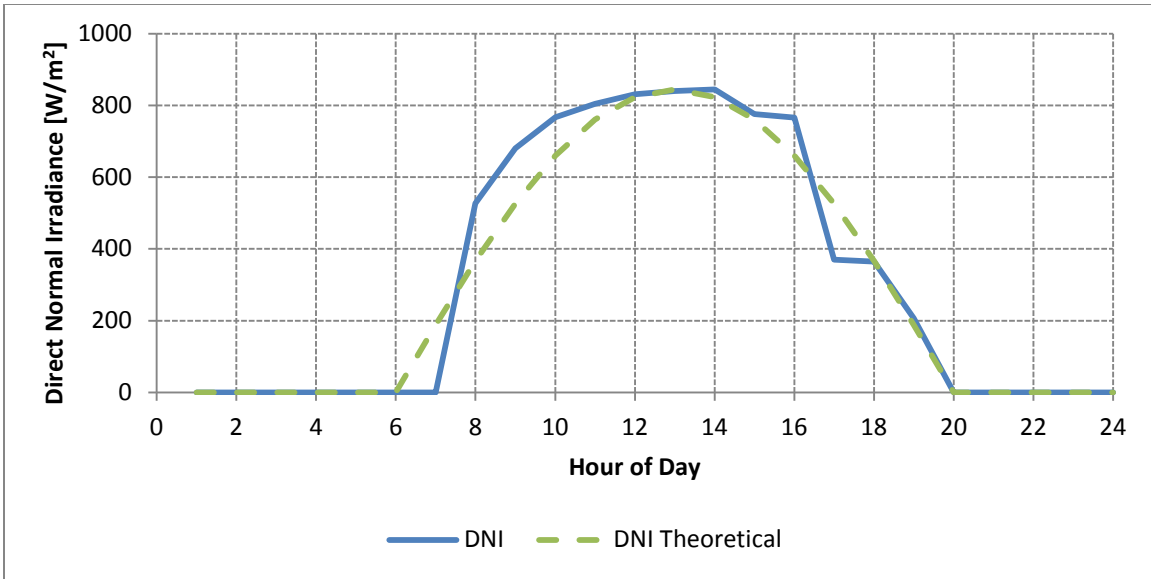


Figure 197: Direct normal irradiance curves for 8/16/2004

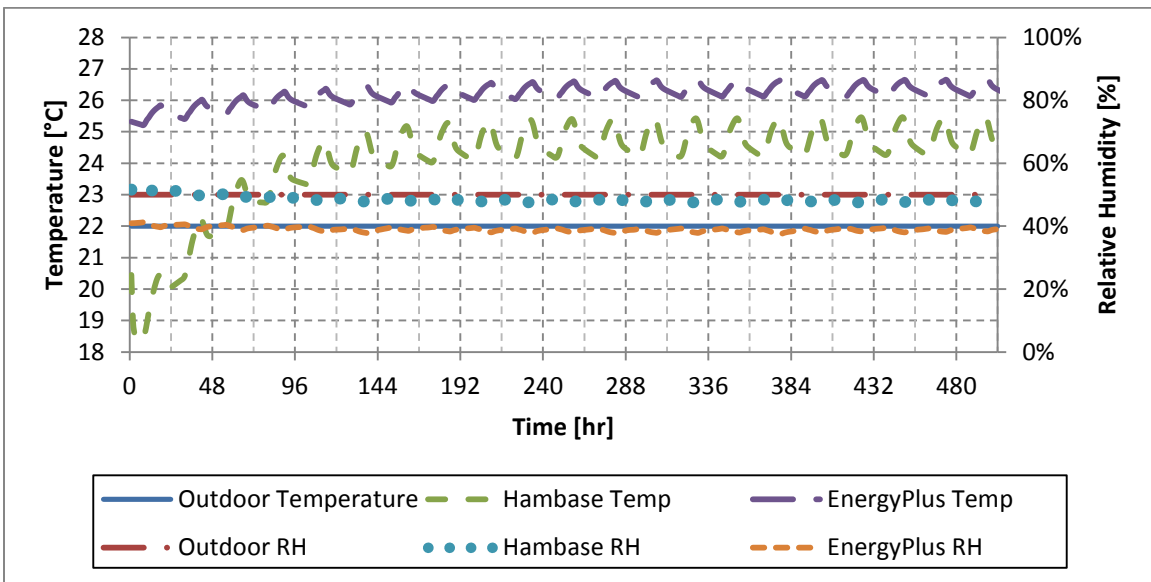


Figure 198: Open-loop response of Core1 to DNI-sine input

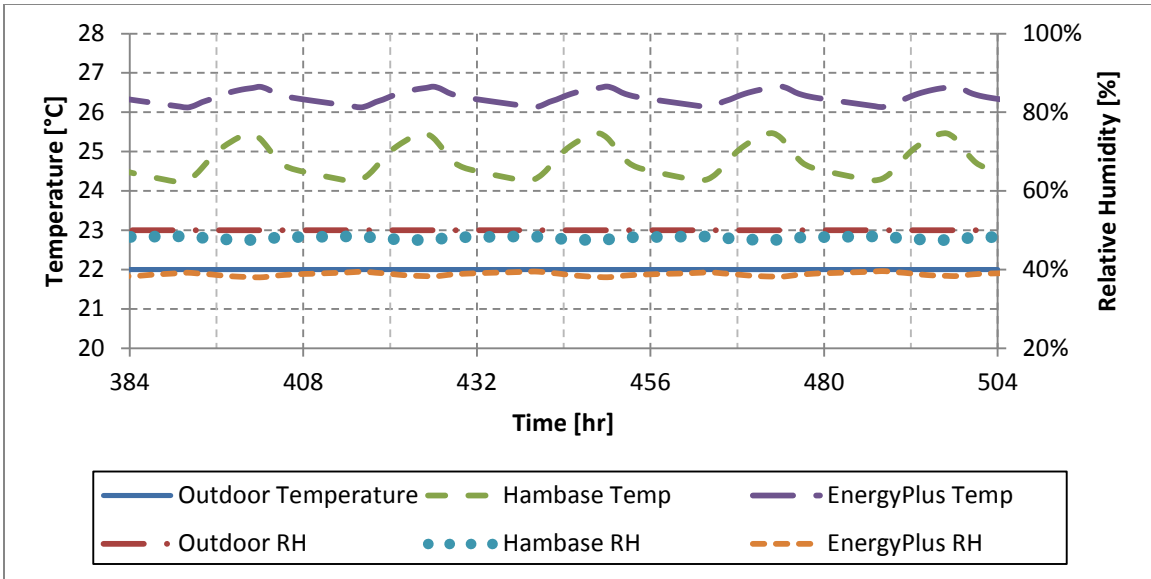


Figure 199: Open-loop steady-state response of Core1 to DNI-sine input

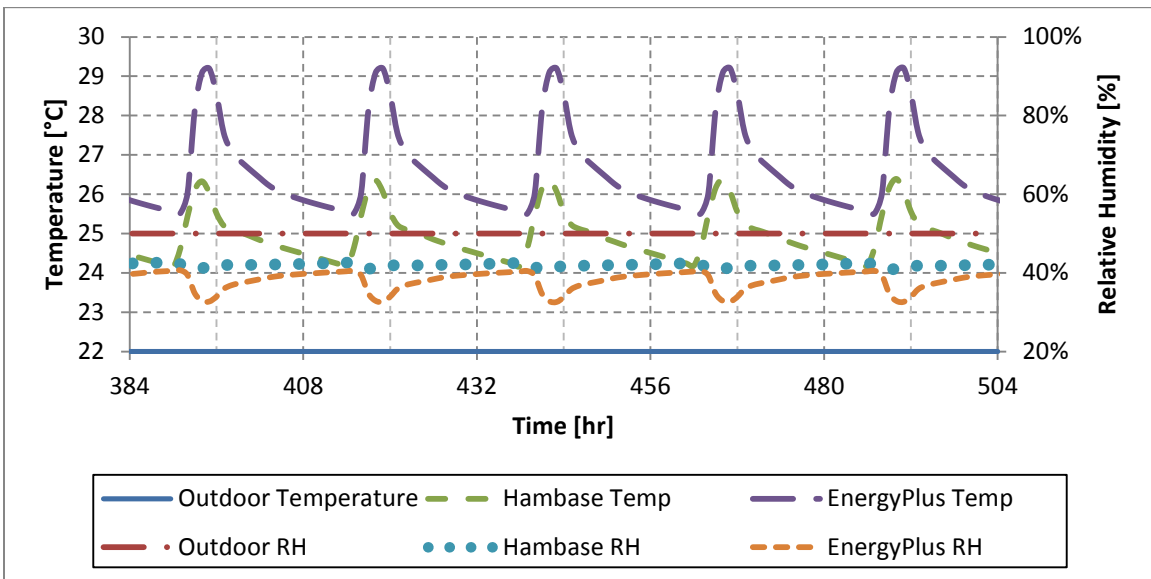


Figure 200: Open-loop steady-state response of East2 to DNI-sine input

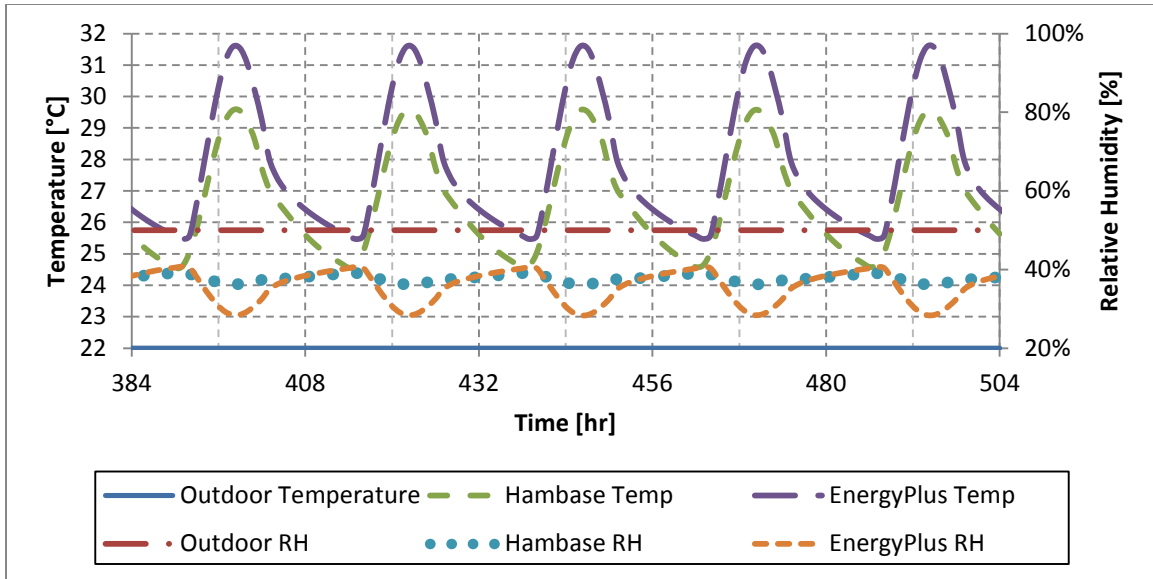


Figure 201: Open-loop steady-state response of South3 to DNI-sine input

Table 77: Temperature results for open-loop DNI-sine input

Zone	Steady-State Max Temperature [°C]		Steady-State Min Temperature [°C]		Steady-State Amplitude (Max-Min) [°C]	
	HB	EP	HB	EP	HB	EP
Core1	25.46	26.66	24.25	26.12	1.21	0.54
South1	30.42	32.45	23.76	25.97	6.66	6.48
East1	26.81	29.01	23.43	24.95	3.38	4.06
North1	24.26	25.18	23.33	24.55	0.93	0.63
West1	28.96	29.16	23.52	25.02	5.44	4.14
Plenum1	26.10	27.33	24.44	26.43	1.66	0.90
Core2	25.70	27.45	25.07	26.94	0.62	0.52
South2	29.16	32.25	24.40	26.00	4.76	6.25
East2	26.39	29.21	24.17	25.51	2.22	3.69
North2	24.60	25.95	24.09	25.41	0.52	0.54
West2	28.01	29.38	24.20	25.57	3.81	3.81
Plenum2	26.27	27.34	25.12	26.56	1.15	0.78
Core3	27.20	27.12	25.24	26.17	1.96	0.95
South3	29.57	31.60	24.56	25.47	5.01	6.13
East3	26.44	28.43	24.32	24.99	2.12	3.44
North3	25.69	25.64	24.18	24.88	1.52	0.76
West3	29.00	28.96	24.29	25.03	4.71	3.92
Plenum3	30.73	26.79	24.08	24.38	6.65	2.41
Average	27.27	28.33	24.25	25.55	3.02	2.77

Table 78: Relative humidity results for open-loop DNI-sine input

Zone	Steady-State Max RH [%]		Steady-State Min RH [%]		Steady-State Amplitude (Max-Min) [%]	
	HB	EP	HB	EP	HB	EP
Core1	48%	40%	48%	38%	1%	2%
South1	42%	39%	36%	27%	5%	12%
East1	44%	42%	41%	33%	3%	9%
North1	45%	43%	45%	41%	1%	2%
West1	44%	42%	39%	33%	4%	9%
Plenum1	42%	38%	41%	36%	1%	2%
Core2	49%	38%	48%	36%	0%	1%
South2	40%	39%	37%	27%	3%	12%
East2	43%	41%	41%	33%	2%	8%
North2	44%	41%	43%	39%	0%	1%
West2	42%	40%	40%	32%	2%	8%
Plenum2	40%	38%	40%	36%	1%	2%
Core3	49%	39%	47%	37%	1%	2%
South3	39%	41%	36%	28%	3%	12%
East3	42%	42%	40%	34%	1%	8%
North3	42%	42%	42%	40%	1%	2%
West3	41%	42%	38%	33%	3%	9%
Plenum3	42%	43%	34%	38%	8%	6%
Average	43%	41%	41%	35%	2%	6%

A.5.3. Test Set 10: Open-Loop, Diffuse Horizontal Irradiance-Sine, No Internal Loads

The constant weather file was altered to create a DHI (diffuse horizontal irradiance) sine input. The TMY3 data was reviewed to find a representative summer day. A sine-wave was then fit to the DHI data, as shown in Figure 202. The remainder of the constant weather file from Table 32 remained unchanged. Internal loads were turned off. The thermostat was disengaged, eliminating HVAC operation.

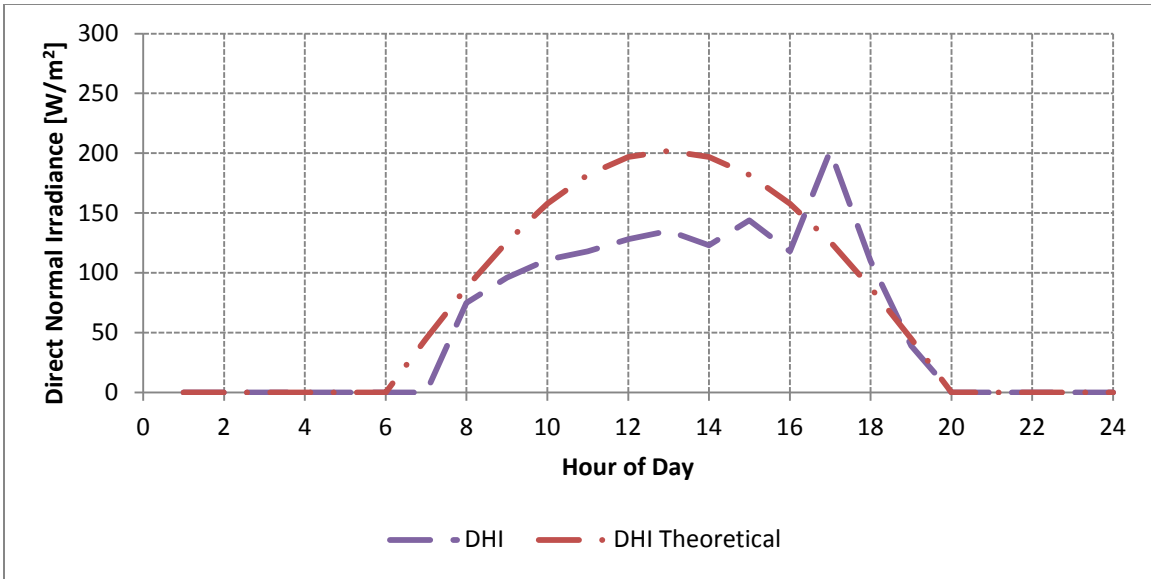


Figure 202: Diffuse horizontal irradiance curves for 8/16/2004

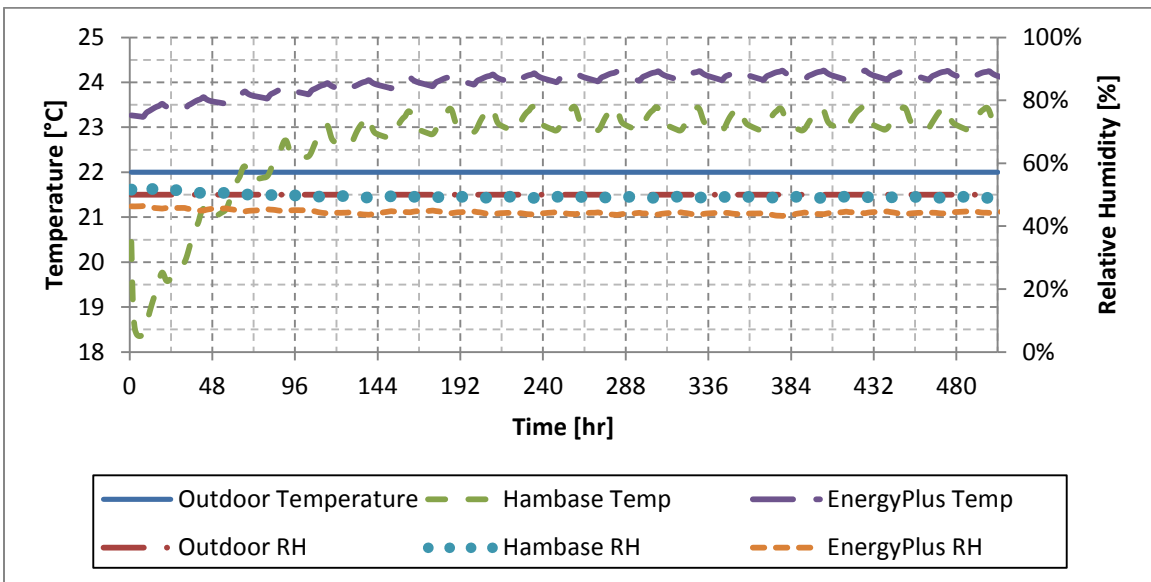


Figure 203: Open-loop response of Core1 to DHI-sine input

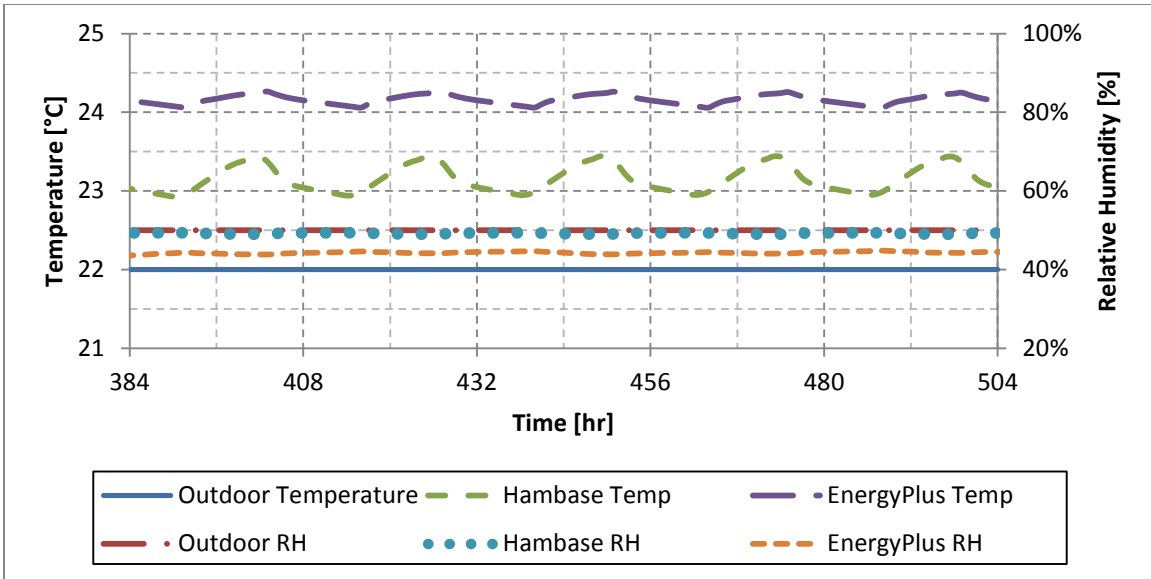


Figure 204: Open-loop steady-state response of Core1 to DHI-sine input

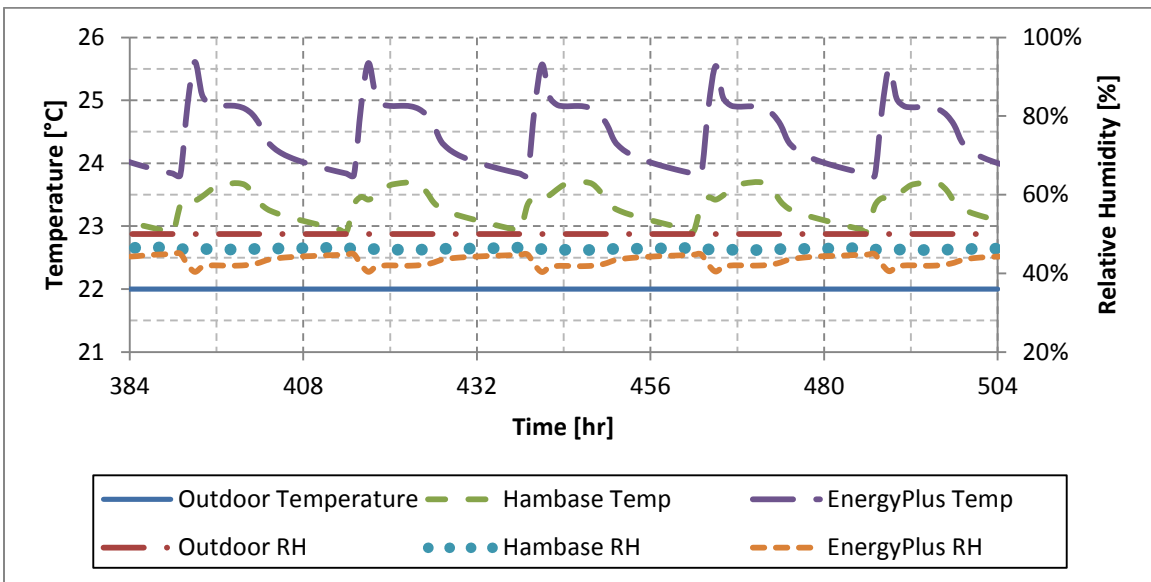


Figure 205: Open-loop steady-state response of East2 to DHI-sine input

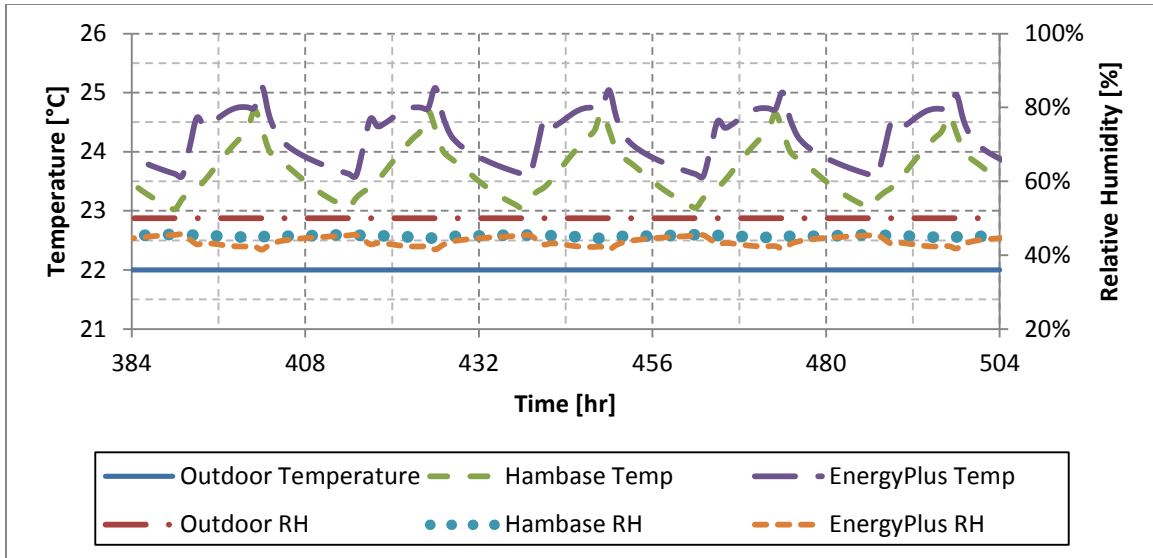


Figure 206: Open-loop steady-state response of South3 to DHI-sine input

Table 79: Temperature results for open-loop DHI-sine input

Zone	Steady-State Max Temperature [°C]		Steady-State Min Temperature [°C]		Steady-State Amplitude (Max-Min) [°C]	
	HB	EP	HB	EP	HB	EP
Core1	23.44	24.26	22.94	24.05	0.50	0.21
South1	24.42	25.04	22.63	23.50	1.79	1.55
East1	23.71	25.37	22.59	23.42	1.13	1.94
North1	23.65	24.36	22.58	23.36	1.07	1.00
West1	25.23	25.65	22.63	23.45	2.60	2.20
Plenum1	23.72	24.60	23.01	24.27	0.71	0.33
Core2	23.58	24.82	23.32	24.61	0.26	0.21
South2	24.25	25.30	22.96	23.87	1.29	1.43
East2	23.70	25.59	22.92	23.80	0.78	1.79
North2	23.64	24.70	22.92	23.81	0.72	0.89
West2	24.76	25.83	22.96	23.83	1.79	1.99
Plenum2	23.84	24.71	23.37	24.39	0.47	0.32
Core3	24.28	24.60	23.42	24.17	0.87	0.43
South3	24.69	25.08	23.05	23.58	1.64	1.50
East3	24.04	25.17	23.01	23.51	1.04	1.66
North3	23.99	24.43	23.00	23.51	0.99	0.91
West3	25.19	25.56	23.03	23.54	2.16	2.03
Plenum3	25.83	24.15	22.83	23.12	2.99	1.03
Average	24.22	24.96	22.95	23.77	1.27	1.19

Table 80: Relative humidity results for open-loop DHI-sine input

Zone	Steady-State Max RH [%]		Steady-State Min RH [%]		Steady-State Amplitude (Max-Min) [%]	
	HB	EP	HB	EP	HB	EP
Core1	49%	45%	49%	44%	0%	1%
South1	47%	46%	45%	42%	2%	4%
East1	47%	46%	46%	41%	1%	5%
North1	48%	46%	47%	43%	1%	3%
West1	47%	46%	44%	40%	3%	6%
Plenum1	46%	44%	46%	43%	0%	1%
Core2	49%	43%	49%	42%	0%	1%
South2	46%	45%	45%	41%	1%	4%
East2	47%	45%	46%	40%	1%	5%
North2	47%	45%	46%	42%	1%	3%
West2	46%	45%	45%	40%	1%	5%
Plenum2	46%	43%	45%	42%	0%	1%
Core3	49%	45%	49%	43%	0%	2%
South3	46%	45%	44%	42%	1%	4%
East3	46%	46%	45%	41%	1%	4%
North3	46%	46%	45%	43%	1%	3%
West3	46%	46%	44%	40%	2%	5%
Plenum3	46%	47%	42%	44%	4%	3%
Average	47%	45%	46%	42%	1%	3%

A.5.4. Test Set 11: Open-Loop, Constant Weather, People Loads

The internal load profile for people was set to a constant value of the peak people load. The remaining internal loads were turned off. The constant weather file from Table 32 was used. The thermostat was disengaged, eliminating HVAC operation.

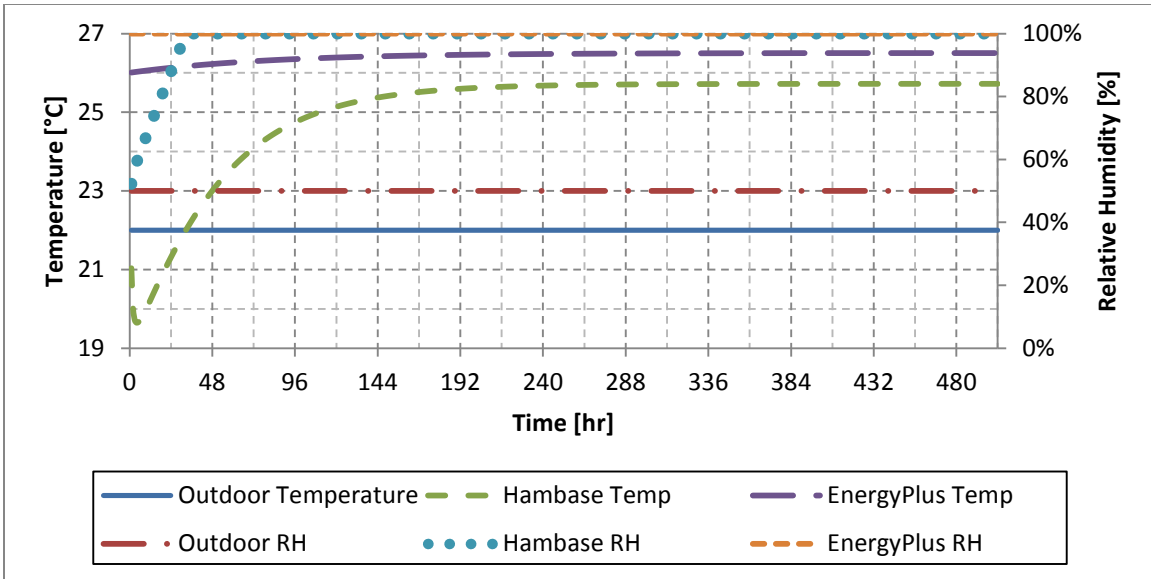


Figure 207: Open-loop response of Core1 to constant people input

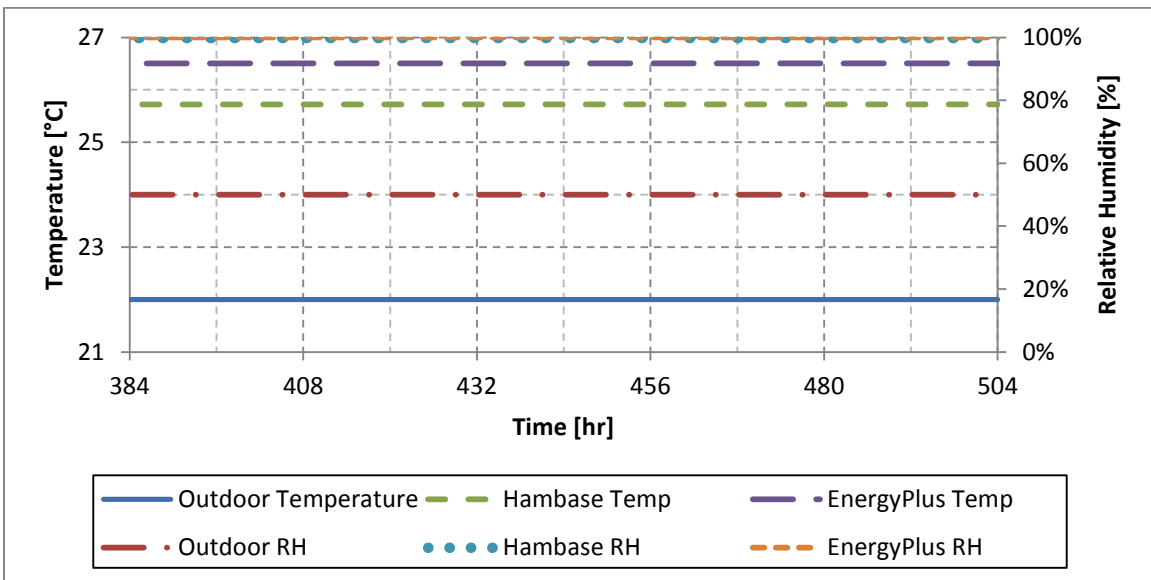


Figure 208: Open-loop steady-state response of Core1 to constant people input

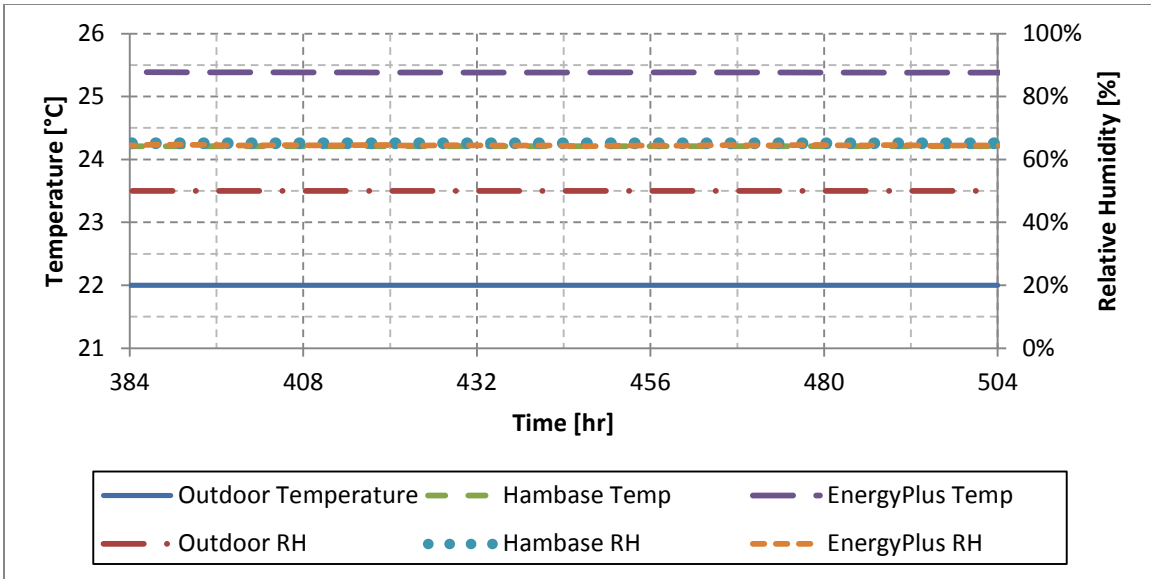


Figure 209: Open-loop steady-state response of East2 to constant people input

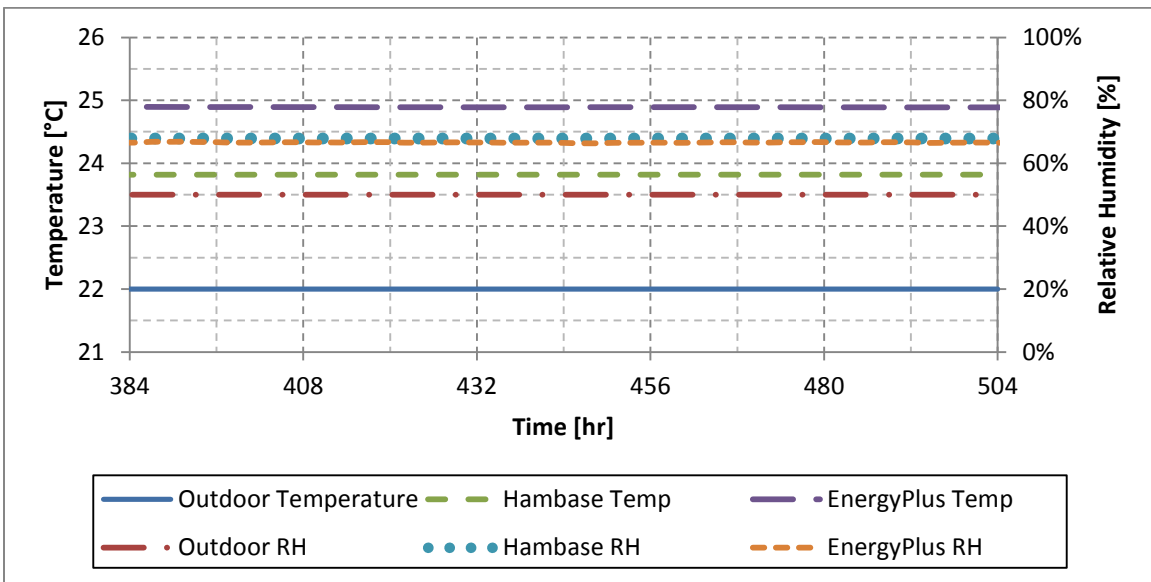


Figure 210: Open-loop steady-state response of South3 to constant people input

Table 81: Temperature results for open-loop constant people input

Zone	HAMBASE Steady-State Temperature [°C]	EnergyPlus Steady-State Temperature [°C]	Absolute Error HB – EP [°C]	Percent Error (HB – EP) / EP [%]
Core1	25.72	26.50	-0.78	-3.0%
South1	24.09	25.01	-0.92	-3.7%
East1	24.04	24.94	-0.91	-3.6%
North1	24.09	25.03	-0.94	-3.8%
West1	24.04	24.94	-0.91	-3.6%
Plenum1	24.77	25.71	-0.93	-3.6%
Core2	25.40	26.84	-1.44	-5.4%
South2	24.25	25.46	-1.21	-4.7%
East2	24.21	25.38	-1.17	-4.6%
North2	24.25	25.47	-1.22	-4.8%
West2	24.21	25.38	-1.17	-4.6%
Plenum2	24.54	25.63	-1.09	-4.2%
Core3	24.79	26.06	-1.27	-4.9%
South3	23.82	24.89	-1.07	-4.3%
East3	23.78	24.83	-1.05	-4.2%
North3	23.82	24.90	-1.08	-4.3%
West3	23.78	24.83	-1.05	-4.2%
Plenum3	23.53	23.94	-0.41	-1.7%
Average	24.28	25.32	-1.03	-4.1%

Table 82: Relative humidity results for open-loop constant people input

Zone	HAMBASE Steady-State RH [%]	EnergyPlus Steady-State RH [%]	Absolute Error HB – EP [%]	Percent Error (HB – EP) / EP [%]
Core1	100%	100%	0.0%	0.0%
South1	67%	67%	0.3%	0.4%
East1	66%	65%	0.4%	0.6%
North1	67%	66%	0.3%	0.4%
West1	66%	65%	0.4%	0.6%
Plenum1	42%	40%	2.2%	5.4%
Core2	100%	100%	0.0%	0.0%
South2	66%	66%	0.4%	0.6%
East2	65%	65%	0.5%	0.8%
North2	66%	66%	0.4%	0.7%
West2	65%	65%	0.5%	0.8%
Plenum2	43%	40%	2.6%	6.3%
Core3	100%	100%	0.0%	0.0%
South3	68%	67%	1.1%	1.7%
East3	67%	66%	1.2%	1.9%
North3	68%	67%	1.1%	1.7%
West3	67%	66%	1.2%	1.9%
Plenum3	46%	45%	1.1%	2.4%
Average	68%	67%	0.8%	1.5%

A.5.5. Test Set 13: Open-Loop, Constant Weather, Equipment Loads

The internal load profile for equipment was set to a constant value of the peak equipment load. The remaining internal loads were turned off. The constant weather file from Table 32 was used. The thermostat was disengaged, eliminating HVAC operation.

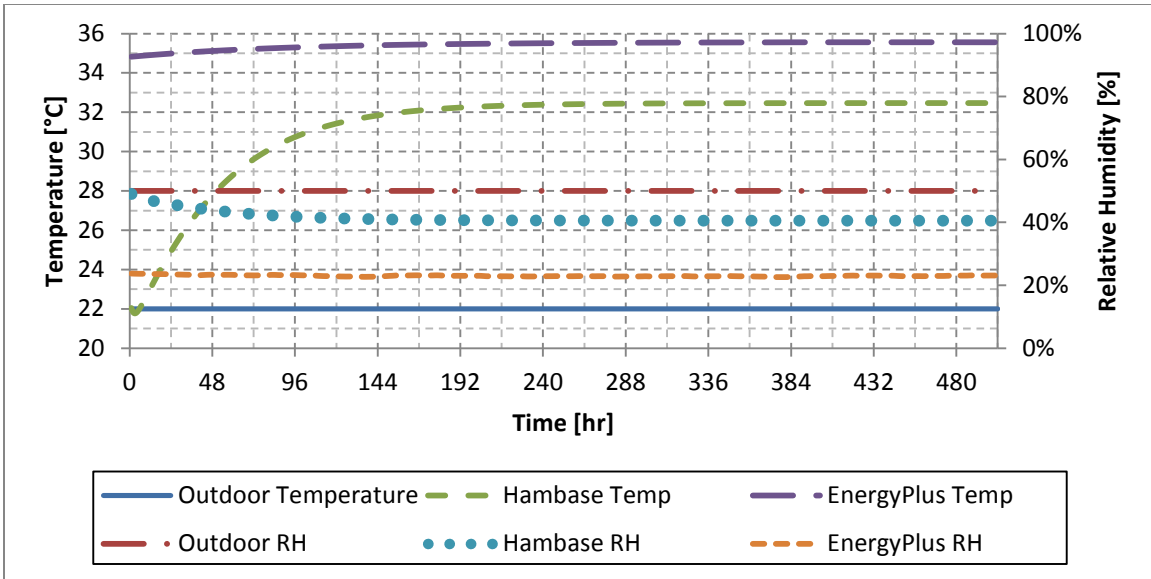


Figure 211: Open-loop response of Core1 to constant equipment input

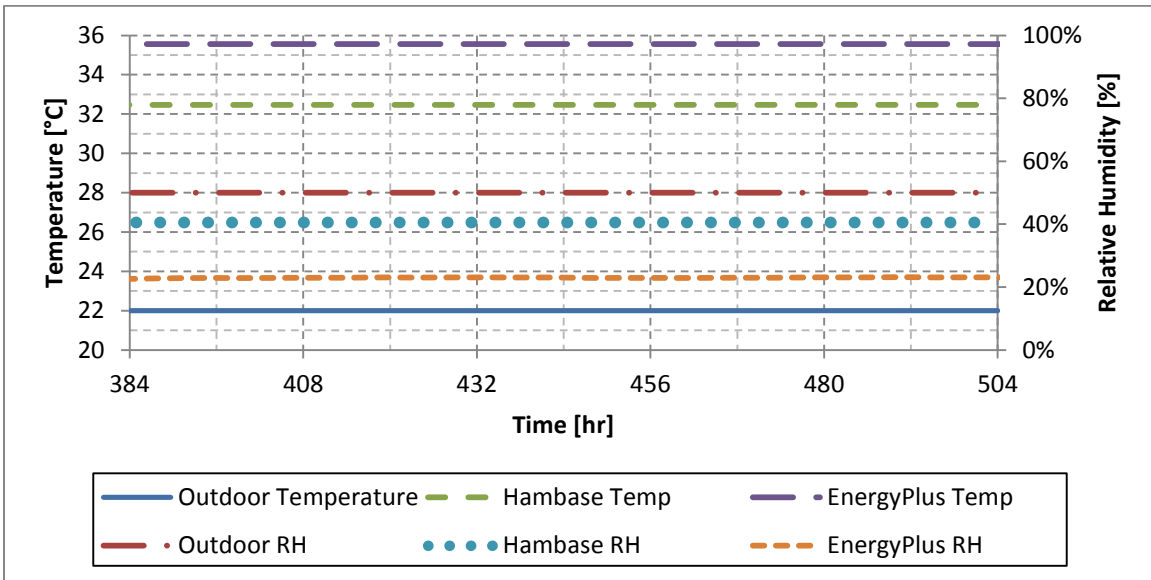


Figure 212: Open-loop steady-state response of Core1 to constant equipment input

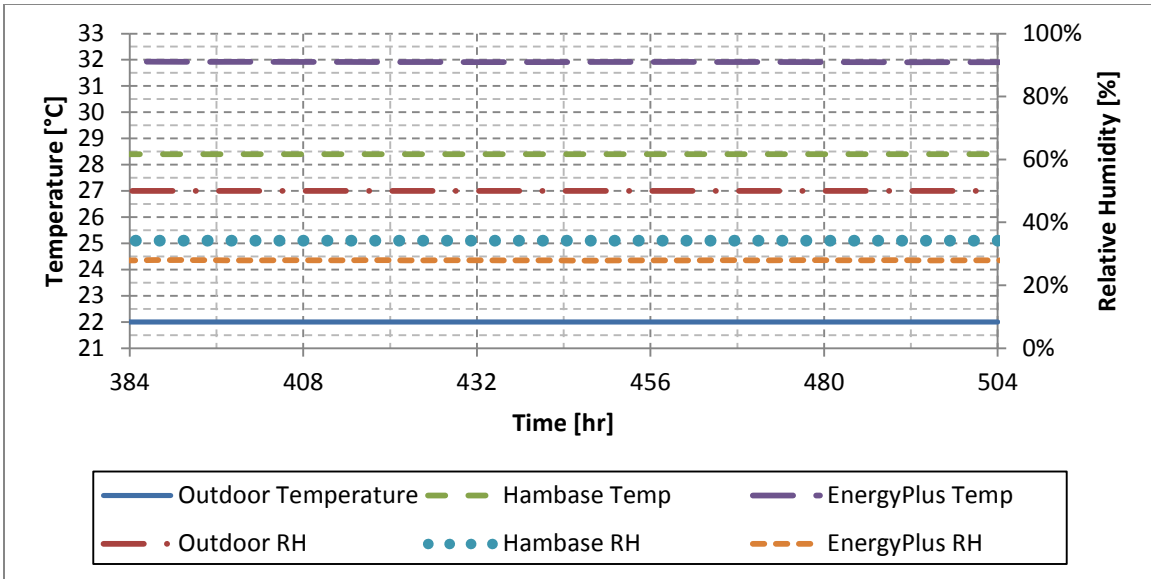


Figure 213: Open-loop steady-state response of East2 to constant equipment input

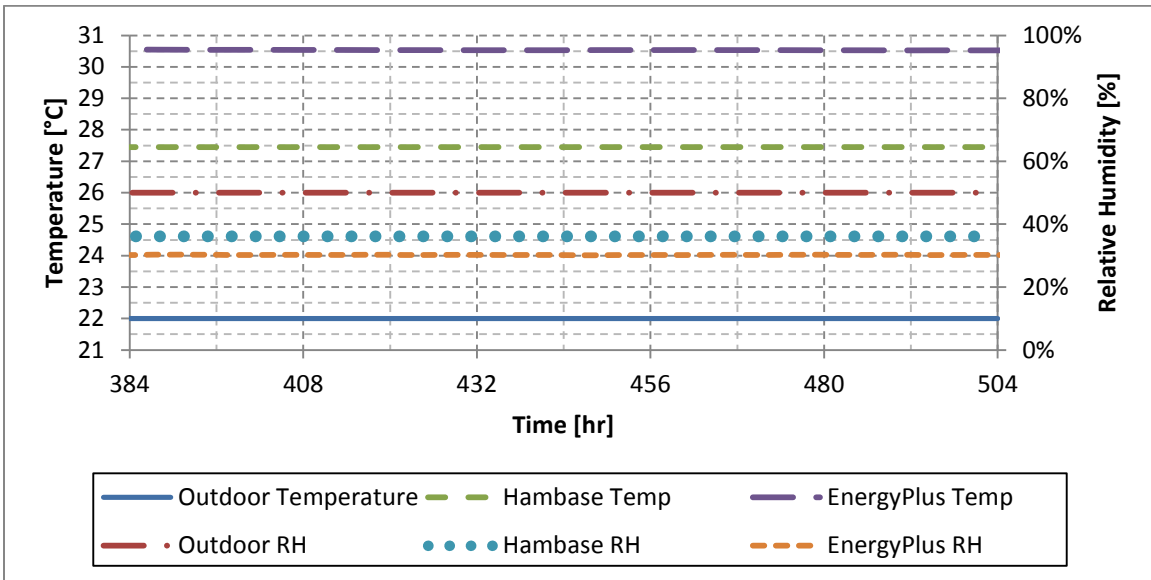


Figure 214: Open-loop steady-state response of South3 to constant equipment input

Table 83: Temperature results for open-loop constant people input

Zone	HAMBASE Steady-State Temperature [°C]	EnergyPlus Steady-State Temperature [°C]	Absolute Error HB – EP [°C]	Percent Error (HB – EP) / EP [%]
Core1	32.47	35.56	-3.09	-8.7%
South1	27.99	31.19	-3.20	-10.3%
East1	27.85	30.99	-3.14	-10.1%
North1	27.99	31.22	-3.23	-10.4%
West1	27.85	30.99	-3.14	-10.1%
Plenum1	29.92	33.34	-3.42	-10.3%
Core2	31.69	36.04	-4.35	-12.1%
South2	28.50	32.15	-3.65	-11.3%
East2	28.40	31.92	-3.52	-11.0%
North2	28.50	32.14	-3.64	-11.3%
West2	28.40	31.92	-3.52	-11.0%
Plenum2	29.40	32.85	-3.45	-10.5%
Core3	30.19	33.75	-3.56	-10.5%
South3	27.45	30.54	-3.09	-10.1%
East3	27.36	30.35	-2.99	-9.9%
North3	27.45	30.52	-3.07	-10.1%
West3	27.36	30.35	-2.99	-9.9%
Plenum3	26.87	28.51	-1.65	-5.8%
Average	28.65	31.91	-3.26	-10.2%

Table 84: Relative humidity results for open-loop constant people input

Zone	HAMBASE Steady-State RH [%]	EnergyPlus Steady-State RH [%]	Absolute Error HB – EP [%]	Percent Error (HB – EP) / EP [%]
Core1	41%	23%	17.4%	75.1%
South1	35%	29%	5.8%	19.9%
East1	35%	30%	5.8%	19.5%
North1	35%	29%	5.9%	20.2%
West1	35%	30%	5.8%	19.5%
Plenum1	31%	26%	5.5%	21.1%
Core2	44%	23%	21.4%	94.9%
South2	34%	28%	6.3%	22.9%
East2	34%	28%	6.2%	22.1%
North2	34%	28%	6.3%	22.8%
West2	34%	28%	6.2%	22.1%
Plenum2	32%	27%	5.7%	21.3%
Core3	45%	26%	19.2%	74.8%
South3	36%	30%	5.8%	19.2%
East3	36%	31%	5.7%	18.6%
North3	36%	30%	5.8%	19.1%
West3	36%	31%	5.7%	18.6%
Plenum3	37%	34%	3.4%	9.9%
Average	36%	28%	8.0%	30.1%

A.5.6. Closed-Loop Heating and Cooling Data

Data from the closed-loop validation test are shown in the following tables. Table 85 shows data for the annual heating and annual cooling totals by zone for HAMBASE and EnergyPlus. These data are used in Figure 91 and Figure 92.

Table 85: HAMBASE and EnergyPlus annual heating and cooling data

Zone	Annual Heating [MWh]				Annual Total Cooling [MWh]			
	HB	EP	Diff.	%Diff.	HB	EP	Diff.	%Diff.
Core1	0.2	0.0	0.1	476%	-103.3	-84.9	-18.3	22%
South1	3.0	1.0	2.1	216%	-32.5	-20.8	-11.8	57%
East1	2.3	1.5	0.8	51%	-20.5	-14.6	-5.9	40%
North1	3.8	1.2	2.6	219%	-28.3	-15.4	-12.8	83%
West1	2.6	2.2	0.4	17%	-26.4	-18.0	-8.4	47%
Plenum1	0.0	0.0	0.0	N/A	0.0	0.0	0.0	N/A
Core2	0.7	0.2	0.5	238%	-76.6	-72.1	-4.5	6%
South2	3.1	1.3	1.8	136%	-32.3	-25.7	-6.6	26%
East2	2.4	1.9	0.4	21%	-21.1	-17.7	-3.4	19%
North2	3.9	1.8	2.2	124%	-29.4	-20.3	-9.1	45%
West2	2.6	2.6	0.0	0%	-26.5	-20.8	-5.7	27%
Plenum2	0.0	0.0	0.0	N/A	0.0	0.0	0.0	N/A
Core3	1.7	2.2	-0.5	-24%	-85.9	-81.9	-4.0	5%
South3	4.3	2.4	1.9	78%	-34.3	-27.2	-7.0	26%
East3	3.2	2.7	0.4	16%	-22.8	-18.4	-4.4	24%
North3	5.3	3.3	1.9	57%	-32.2	-22.4	-9.8	44%
West3	3.6	3.9	-0.3	-8%	-28.2	-22.0	-6.2	28%
Plenum3	0.0	0.0	0.0	N/A	0.0	0.0	0.0	N/A
Total	42.6	28.3	14.2	50%	-600.4	-482.4	-118.0	24%

Table 86 shows data for the annual sensible cooling and annual latent cooling totals by zone for HAMBASE and EnergyPlus. These data are used in Figure 93 and Figure 94.

Table 86: HAMBASE and EnergyPlus annual sensible and latent cooling data

Zone	Annual Sensible Cooling [MWh]				Annual Latent Cooling [MWh]			
	HB	EP	Diff	%Diff.	HB	EP	Diff	%Diff.
Core1	-76.8	-75.1	-1.7	2%	-26.5	-9.9	-16.6	168%
South1	-26.5	-18.4	-8.1	44%	-6.1	-2.4	-3.7	156%
East1	-15.1	-12.8	-2.2	17%	-5.4	-1.8	-3.6	200%
North1	-20.9	-13.5	-7.4	55%	-7.4	-1.9	-5.5	287%
West1	-20.0	-15.9	-4.2	26%	-6.4	-2.2	-4.2	194%
Plenum1	0.0	0.0	0.0	N/A	0.0	0.0	0.0	N/A
Core2	-54.9	-63.6	8.7	-14%	-21.7	-8.6	-13.2	154%
South2	-25.9	-22.8	-3.1	13%	-6.4	-2.9	-3.6	124%
East2	-15.4	-15.6	0.2	-1%	-5.7	-2.1	-3.6	173%
North2	-21.5	-17.9	-3.6	20%	-7.9	-2.4	-5.5	228%
West2	-19.8	-18.4	-1.5	8%	-6.7	-2.4	-4.2	175%
Plenum2	0.0	0.0	0.0	N/A	0.0	0.0	0.0	N/A
Core3	-63.6	-69.7	6.1	-9%	-22.3	-12.2	-10.1	82%
South3	-28.9	-23.4	-5.5	23%	-5.4	-3.8	-1.6	42%
East3	-17.3	-15.6	-1.7	11%	-5.5	-2.8	-2.7	96%
North3	-24.6	-19.0	-5.6	30%	-7.6	-3.4	-4.2	123%
West3	-22.1	-18.8	-3.3	18%	-6.1	-3.2	-2.9	91%
Plenum3	0.0	0.0	0.0	N/A	0.0	0.0	0.0	N/A
Total	-453.3	-420.4	-32.8	8%	-147.1	-62.0	-85.1	137%

The peak heating for HAMBASE and EnergyPlus is shown by zone in Figure 215. The peak heating values for HAMBASE are greater than in EnergyPlus for all zones except Core3. A zone by zone comparison using the 521% range from ASHRAE 140-2007 shows that all zones, as well as the total for the building, fall within the range (as seen in Table 87).

The peak cooling for HAMBASE and EnergyPlus is shown by zone in Figure 216. The peak cooling values for HAMBASE are greater than in EnergyPlus for all zones. A zone by zone comparison using the 60% range from ASHRAE 140-2007 shows that Core1, South1, North1, South2, North2 and North3 fall outside of the range (as seen in Table 87). The average peak cooling for all zones is also outside the range. This comparison is of limited use however; the peak conditioning is limited by the

HVAC equipment. As long as the equipment is similarly sized and both models experience at least one time-step with full heating/cooling, the peak values will be in close alignment.

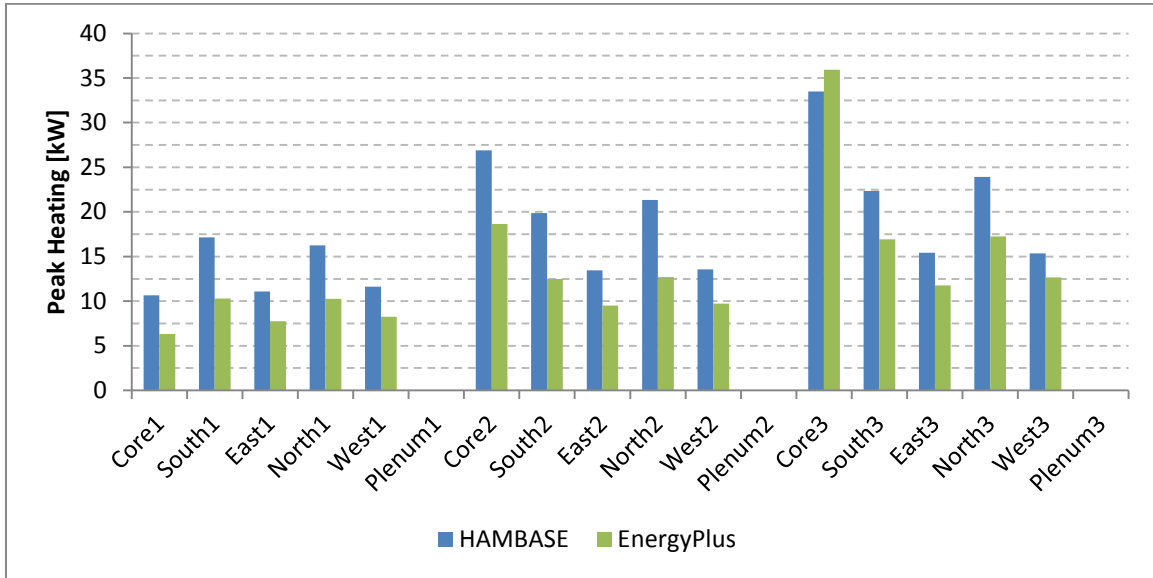


Figure 215: Comparison of HAMBASE and EnergyPlus peak heating

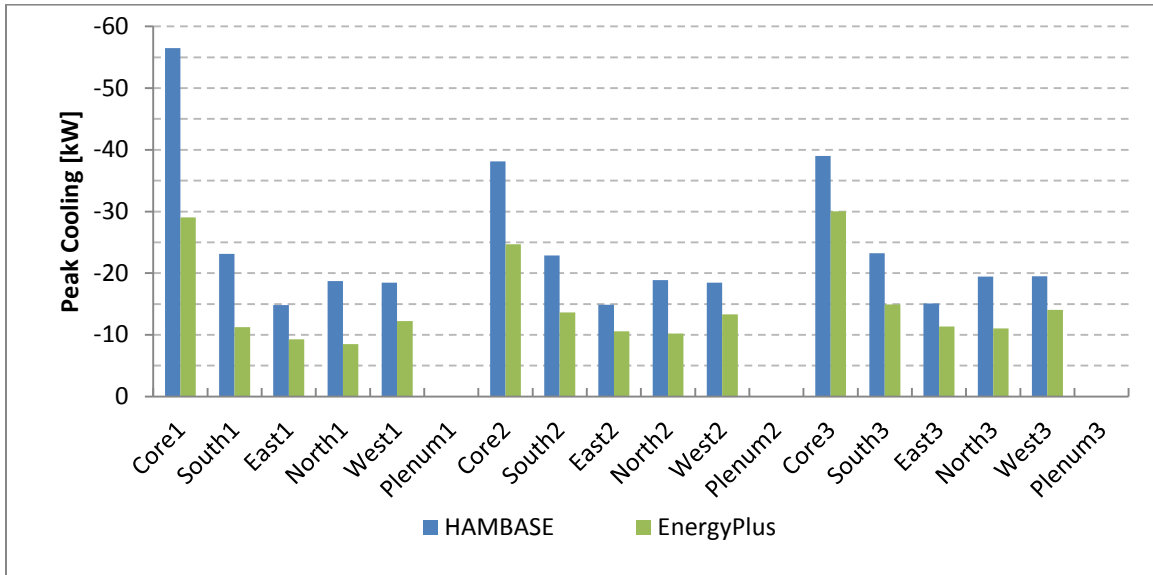


Figure 216: Comparison of HAMBASE and EnergyPlus peak total cooling

Table 87: HAMBASE and EnergyPlus peak heating and cooling data

Zone	Peak Heating [kW]				Peak Total Cooling [kW]			
	HB	EP	Diff.	%Diff.	HB	EP	Diff.	%Diff.
Core1	10.7	6.3	4.4	69%	-56.5	-29.0	-27.5	95%
South1	17.1	10.3	6.8	66%	-23.2	-11.2	-11.9	106%
East1	11.1	7.8	3.3	43%	-14.8	-9.3	-5.6	60%
North1	16.3	10.3	6.0	58%	-18.7	-8.5	-10.2	120%
West1	11.6	8.3	3.4	41%	-18.5	-12.2	-6.3	51%
Plenum1	0.0	0.0	0.0	N/A	0.0	0.0	0.0	N/A
Core2	26.9	18.6	8.2	44%	-38.1	-24.7	-13.4	54%
South2	19.9	12.5	7.4	59%	-22.9	-13.6	-9.2	68%
East2	13.5	9.5	4.0	42%	-14.9	-10.6	-4.3	41%
North2	21.3	12.7	8.7	68%	-18.9	-10.2	-8.6	84%
West2	13.6	9.7	3.9	40%	-18.5	-13.3	-5.2	39%
Plenum2	0.0	0.0	0.0	N/A	0.0	0.0	0.0	N/A
Core3	33.5	35.9	-2.4	-7%	-39.0	-30.0	-9.0	30%
South3	22.3	16.9	5.4	32%	-23.2	-15.0	-8.3	55%
East3	15.4	11.8	3.6	31%	-15.1	-11.4	-3.7	33%
North3	23.9	17.2	6.7	39%	-19.4	-11.0	-8.4	76%
West3	15.3	12.7	2.7	21%	-19.5	-14.0	-5.5	39%
Plenum3	0.0	0.0	0.0	N/A	0.0	0.0	0.0	N/A
Average	15.1	11.1	4.0	36%	-20.1	-12.5	-7.6	61%

The peak sensible cooling and peak latent cooling for HAMBASE and EnergyPlus are shown by zone in Figure 217 and Figure 218, respectively. The peak sensible cooling and latent cooling values for HAMBASE are greater than in EnergyPlus for all zones. A zone by zone comparison using the 60% range from ASHRAE 140-2007 shows that South1, North1 and North3 fall outside of the range for sensible cooling, while almost every zone falls outside the range for latent cooling (as seen in Table 88). The average peak sensible cooling for all zones falls within the 60% range, while the average peak latent cooling falls outside.

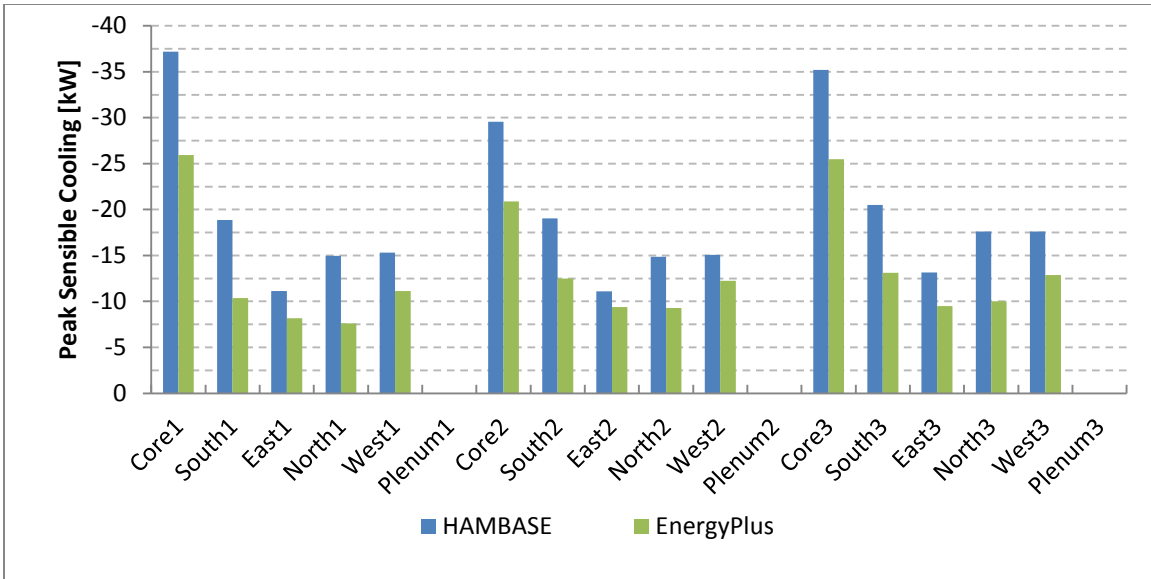


Figure 217: Comparison of HAMBASE and EnergyPlus peak sensible cooling

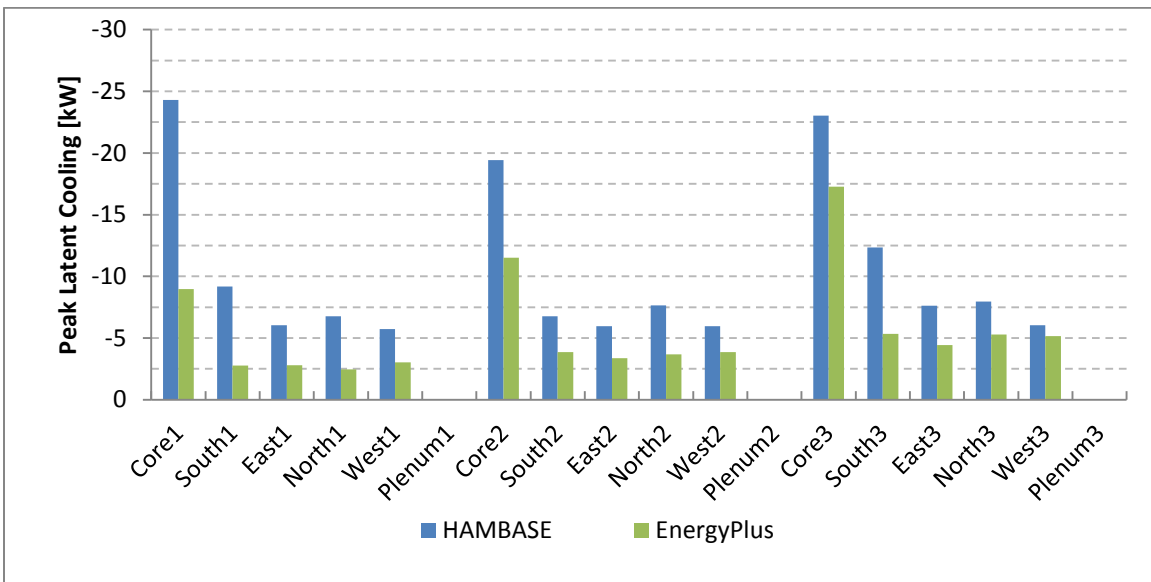


Figure 218: Comparison of HAMBASE and EnergyPlus peak latent cooling

Table 88: HAMBASE and EnergyPlus peak sensible and latent data

Zone	Peak Sensible Cooling [kW]				Peak Latent Cooling [kW]			
	HB	EP	Diff	%Diff.	HB	EP	Diff	%Diff.
Core1	-37.2	-25.9	-11.2	43%	-24.3	-9.0	-15.3	171%
South1	-18.9	-10.4	-8.5	82%	-9.2	-2.8	-6.4	232%
East1	-11.1	-8.2	-3.0	36%	-6.0	-2.8	-3.3	117%
North1	-15.0	-7.6	-7.3	97%	-6.8	-2.5	-4.3	176%
West1	-15.3	-11.1	-4.2	37%	-5.7	-3.0	-2.7	90%
Plenum1	0.0	0.0	0.0	N/A	0.0	0.0	0.0	N/A
Core2	-29.6	-20.9	-8.7	42%	-19.4	-11.5	-7.9	69%
South2	-19.0	-12.5	-6.5	52%	-6.8	-3.9	-2.9	76%
East2	-11.1	-9.4	-1.7	18%	-6.0	-3.4	-2.6	77%
North2	-14.9	-9.3	-5.6	60%	-7.6	-3.7	-4.0	108%
West2	-15.1	-12.3	-2.8	23%	-6.0	-3.8	-2.1	55%
Plenum2	0.0	0.0	0.0	N/A	0.0	0.0	0.0	N/A
Core3	-35.2	-25.5	-9.7	38%	-23.0	-17.3	-5.8	33%
South3	-20.5	-13.1	-7.4	56%	-12.3	-5.3	-7.0	131%
East3	-13.1	-9.5	-3.6	38%	-7.6	-4.4	-3.2	72%
North3	-17.6	-10.0	-7.6	76%	-8.0	-5.3	-2.7	50%
West3	-17.6	-12.9	-4.7	37%	-6.1	-5.2	-0.9	17%
Plenum3	0.0	0.0	0.0	N/A	0.0	0.0	0.0	N/A
Average	-291.1	-198.5	-92.6	47%	-154.8	-83.8	-71.0	85%

A.6. Additional Hourly Data for the Base Model

This section contains additional hourly average data for the base model.

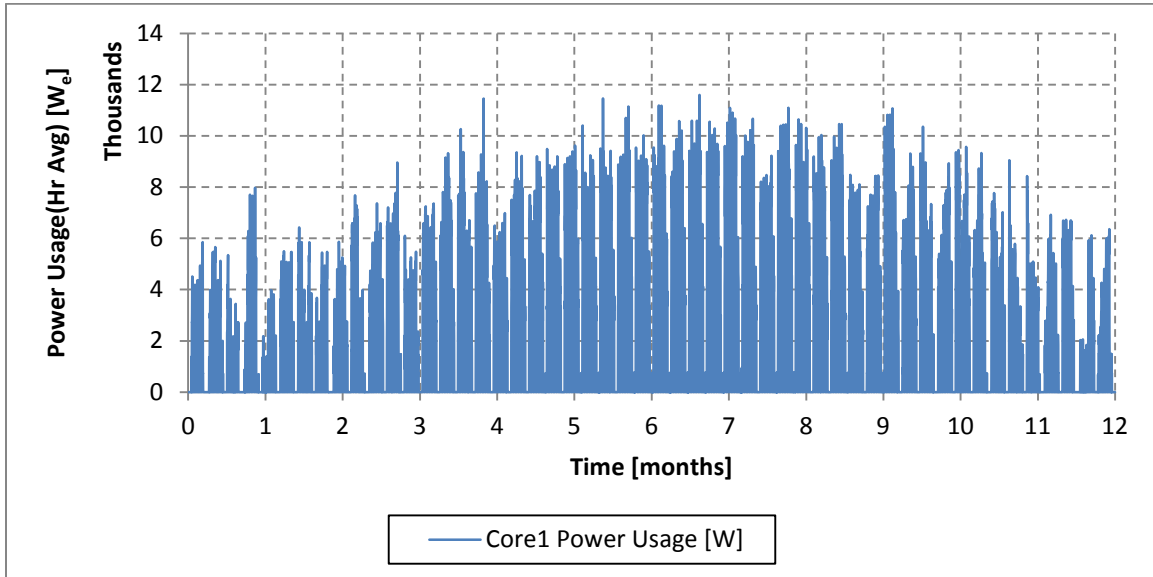


Figure 219: Hourly average power usage by the Core1 heat pump for the first 12 months of simulation

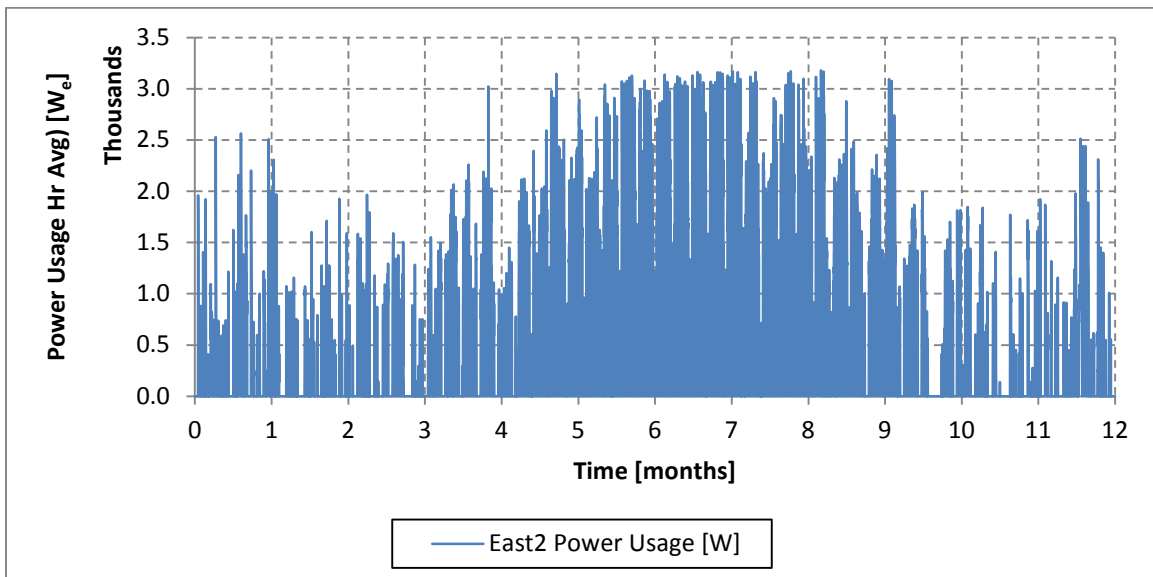


Figure 220: Hourly average power usage by the East2 heat pump for the first 12 months of simulation

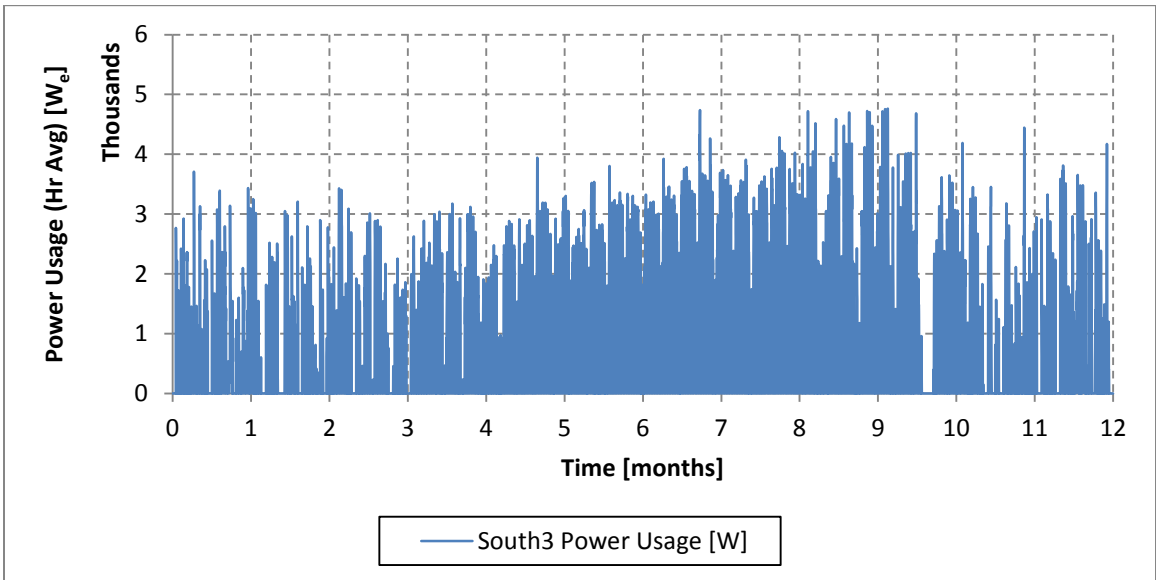


Figure 221: Hourly average power usage by the South3 heat pump for the first 12 months of simulation

A.7. Additional Monthly Data for the Base Model

This section contains additional monthly data for the base model.

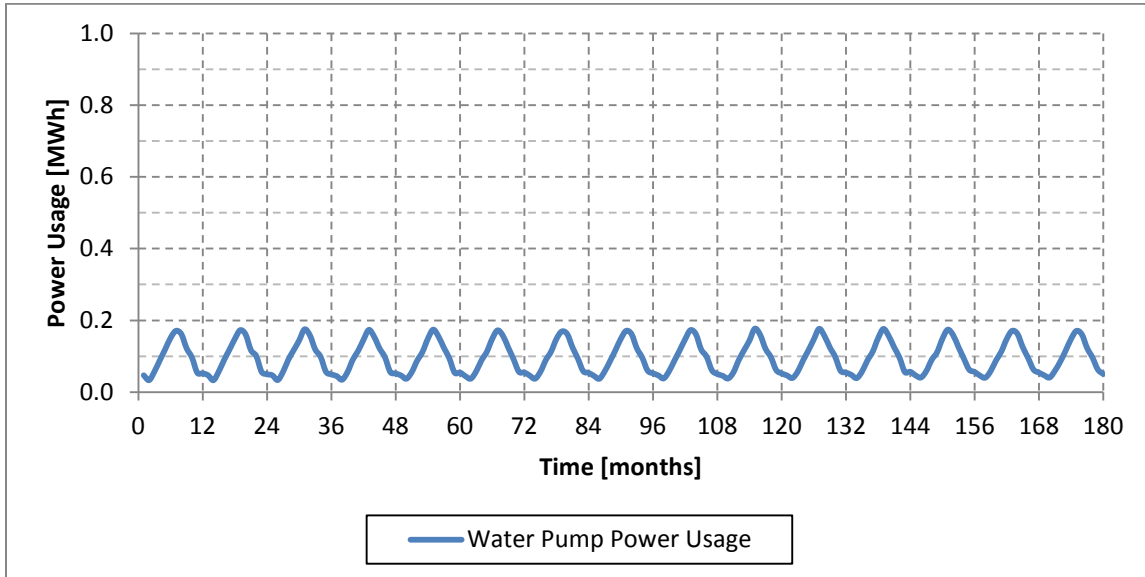


Figure 222: Monthly average power usage by the water pumps during 15 years of simulation

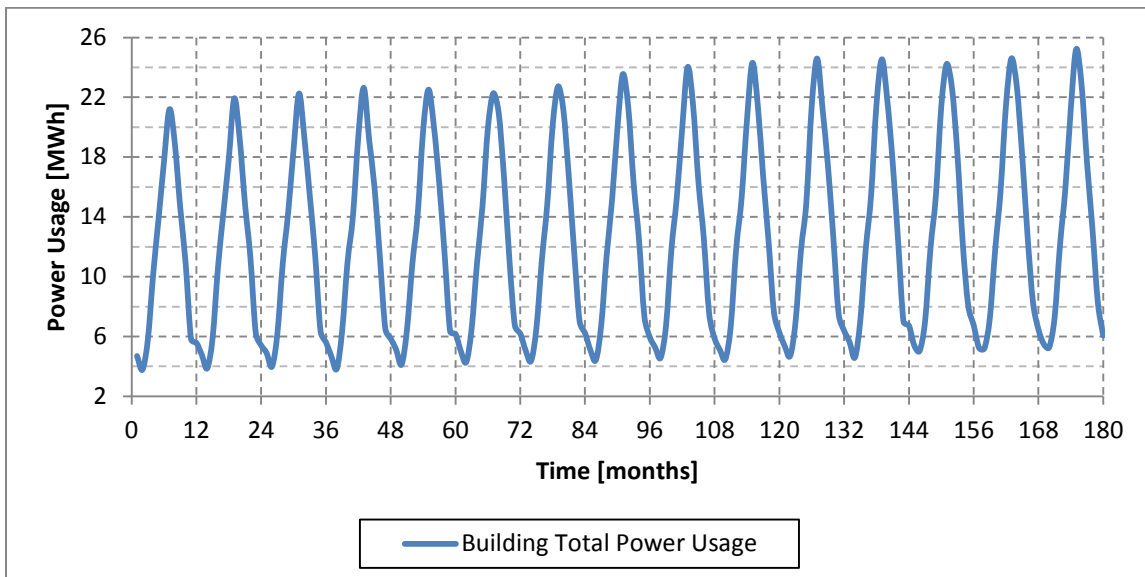


Figure 223: Monthly average power usage by the building during 15 years of simulation

A.8. Additional Annual Data for the Base Model

This section contains additional annual data for the base model.

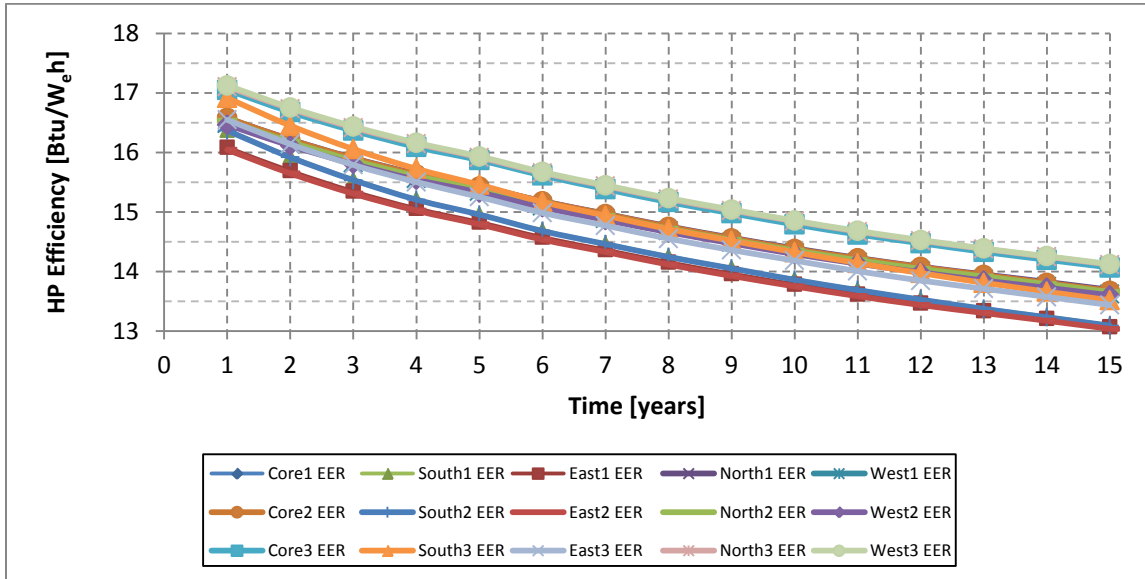


Figure 224: Annual average cooling EER of all zones in the base model for 15 years

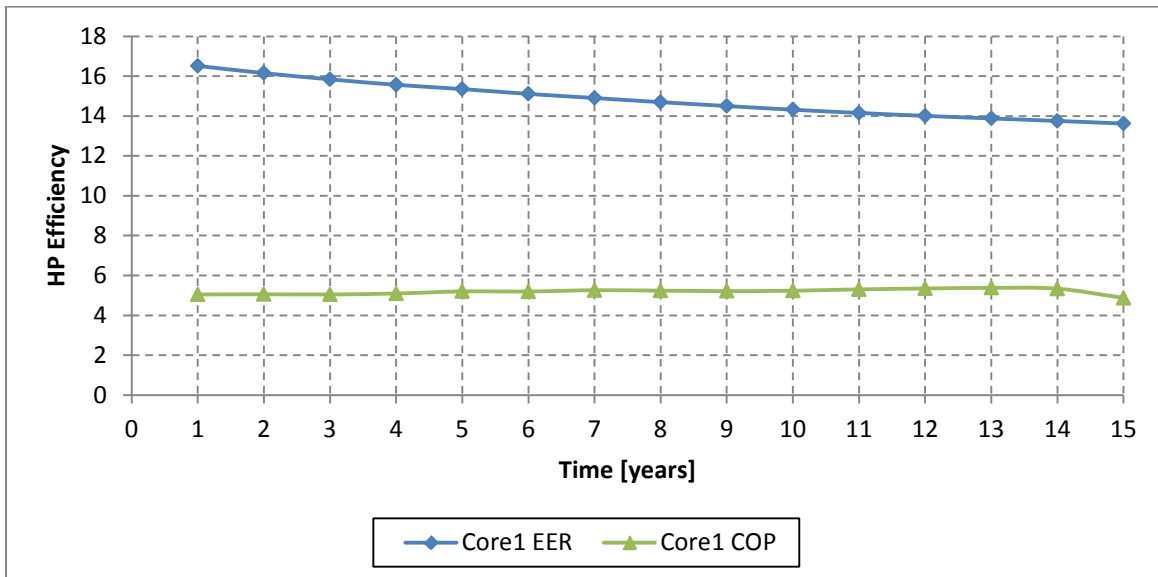


Figure 225: Annual average Core1 heat pump efficiency in the base model for 15 years

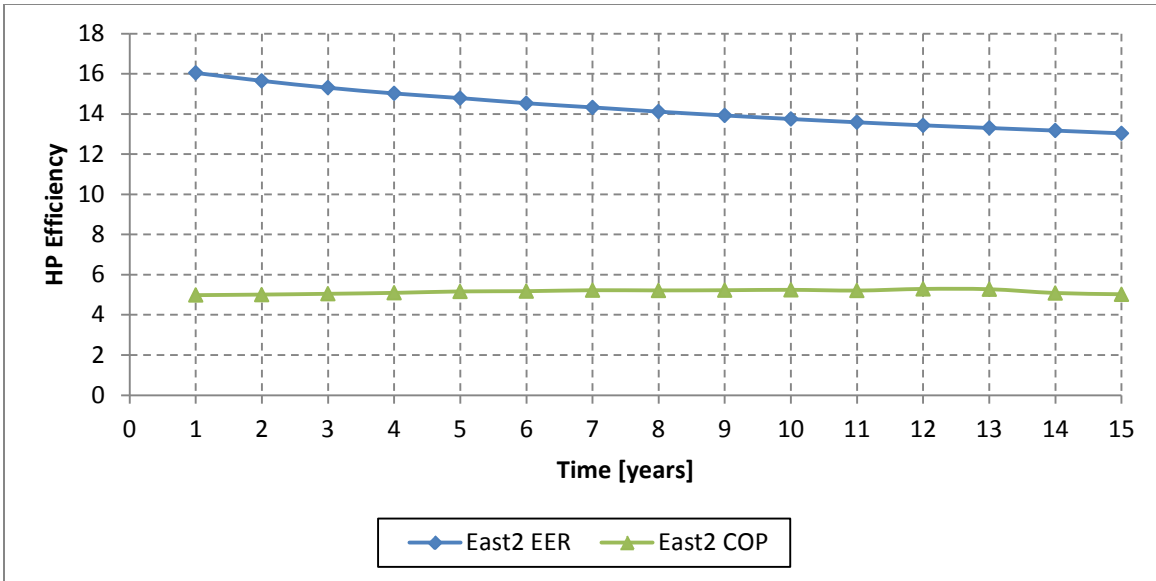


Figure 226: Annual average East2 heat pump efficiency in the base model for 15 years

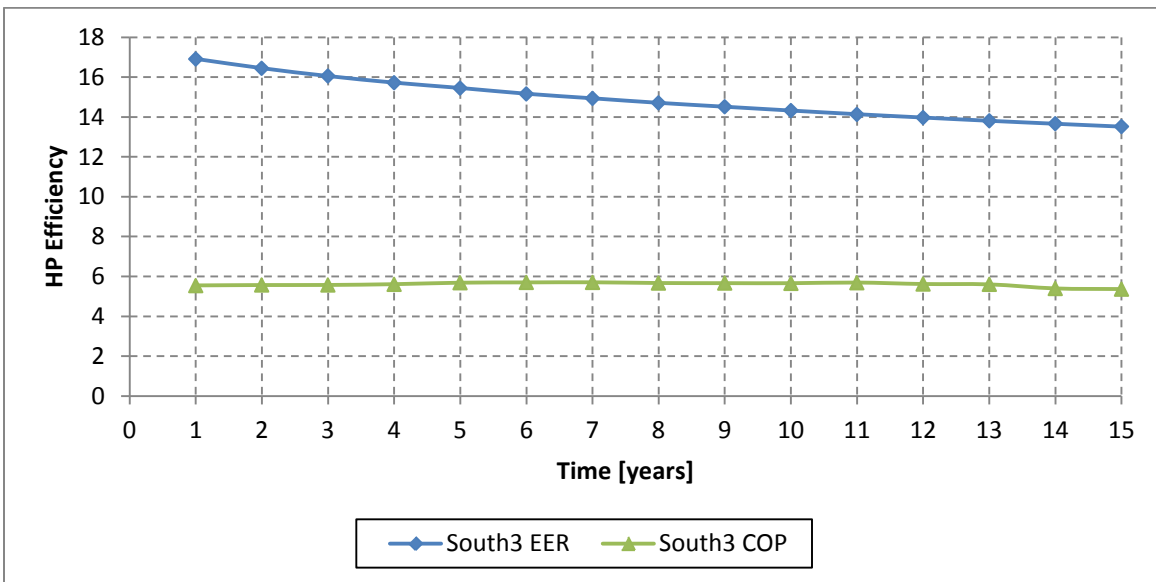


Figure 227: Annual average South3 heat pump efficiency in the base model for 15 years

A.9. Additional Data for the EWT Cutoff Sensitivity Study

This section contains additional data for the EWT cutoff sensitivity study.

Table 89: Data for the minimum annual EWT for the EWT cutoff test

Time [years]	Base Model (90F Case) [°C]	95F Case [°C]	100F Case [°C]	105F Case [°C]	110F Case [°C]	115F Case [°C]	120F Case [°C]
1	20.5	20.5	20.5	20.3	19.9	19.6	19.6
2	21.3	21.5	21.5	21.7	21.9	21.8	22.0
3	22.3	23.0	22.9	23.2	23.5	23.7	23.7
4	23.3	24.0	24.2	24.7	25.3	25.6	25.6
5	23.6	24.6	24.7	25.5	25.9	25.9	26.3
6	24.8	25.4	25.7	26.4	26.9	27.7	27.5
7	25.0	26.0	26.2	27.3	28.0	28.0	28.6
8	25.6	26.5	27.1	28.0	28.1	28.8	29.2
9	26.2	27.2	27.7	28.6	29.9	30.4	30.6
10	26.6	27.9	28.2	28.8	31.0	31.5	31.6
11	27.0	28.6	28.9	29.8	32.3	32.7	33.1
12	27.2	28.6	28.9	31.1	32.4	33.2	33.2
13	27.6	28.7	30.0	31.7	33.1	33.8	34.1
14	28.1	29.3	30.2	31.5	33.1	33.3	33.1
15	28.6	29.1	31.1	32.6	33.8	34.5	35.0
Abs. Change %	8.1	8.6	10.6	12.3	13.9	15.0	15.4
Change % per Year	39.7%	42.2%	51.6%	60.7%	70.1%	76.3%	78.7%
	2.83%	3.01%	3.69%	4.34%	5.00%	5.45%	5.62%

Table 90: Data for the total annual cooling in the EWT cutoff test

Time [years]	Base Model (90F Case) [MWh]	95F Case [MWh]	100F Case [MWh]	105F Case [MWh]	110F Case [MWh]	115F Case [MWh]	120F Case [MWh]
1	-600.2	-599.5	-598.9	-598.3	-597.6	-597.0	-596.0
2	-600.9	-600.1	-599.3	-598.4	-597.3	-596.4	-595.3
3	-600.3	-599.2	-598.3	-597.0	-595.7	-594.6	-593.4
4	-596.9	-595.8	-594.6	-593.0	-591.6	-590.2	-588.8
5	-597.2	-595.7	-594.3	-592.6	-590.8	-589.2	-587.6
6	-596.9	-595.2	-593.7	-591.7	-589.9	-587.8	-586.2
7	-595.6	-593.7	-592.3	-590.3	-587.8	-584.2	-581.4
8	-596.0	-594.0	-592.5	-590.3	-587.0	-582.4	-578.4
9	-595.8	-593.8	-592.2	-589.2	-584.1	-577.0	-575.0
10	-593.0	-590.9	-589.0	-584.0	-575.6	-573.0	-571.1
11	-592.9	-590.6	-588.4	-581.8	-574.3	-571.6	-569.7
12	-592.5	-590.0	-586.9	-576.1	-573.1	-570.4	-568.5
13	-592.8	-589.7	-584.6	-575.7	-572.5	-569.9	-568.0
14	-592.8	-588.5	-581.3	-576.4	-573.1	-570.4	-568.4
15	-592.1	-586.5	-579.1	-575.6	-572.2	-569.5	-567.5
Abs. Change %	-8.2	-13.0	-19.8	-22.7	-25.4	-27.4	-28.5
Change % per Year	-1.4%	-2.2%	-3.3%	-3.8%	-4.2%	-4.6%	-4.8%
	-0.10%	-0.15%	-0.24%	-0.27%	-0.30%	-0.33%	-0.34%

Table 91: Data for the total annual heating in the EWT cutoff test

Time [years]	Base Model (90F Case) [MWh]	95F Case [MWh]	100F Case [MWh]	105F Case [MWh]	110F Case [MWh]	115F Case [MWh]	120F Case [MWh]
1	42.5	42.5	42.4	42.5	42.5	42.5	42.5
2	41.8	41.9	41.9	42.0	42.0	42.0	42.0
3	42.3	42.4	42.4	42.5	42.5	42.6	42.6
4	41.2	41.3	41.4	41.4	41.6	41.7	41.7
5	42.6	42.8	42.8	43.0	43.1	43.3	43.2
6	42.7	42.8	42.9	43.1	43.3	43.1	42.6
7	43.0	43.2	43.3	43.5	43.3	36.9	26.0
8	42.6	42.8	42.8	43.1	40.3	23.5	14.1
9	43.0	43.2	43.3	42.9	25.0	0.7	0.0
10	41.9	42.2	42.4	35.6	0.8	0.0	0.0
11	43.1	43.3	43.1	23.7	0.0	0.0	0.0
12	43.4	43.0	39.8	0.0	0.0	0.0	0.0
13	43.5	42.1	25.0	0.0	0.0	0.0	0.0
14	43.2	38.3	9.3	0.0	0.0	0.0	0.0
15	42.7	32.9	0.0	0.0	0.0	0.0	0.0
Abs. Change %	0.2	-9.5	-42.4	-42.5	-42.5	-42.5	-42.5
Change % per Year	0.6%	-22.4%	100.0%	100.0%	100.0%	100.0%	100.0%
	0.04%	-1.60%	-7.14%	-7.14%	-7.14%	-7.14%	-7.14%

Table 92: Data for the total annual time out-of-setpoint in the EWT cutoff test

Time [years]	Base Model (90F Case) [hr]	95F Case [hr]	100F Case [hr]	105F Case [hr]	110F Case [hr]	115F Case [hr]	120F Case [hr]
1	81	84	90	102	108	121	138
2	70	77	96	110	122	132	153
3	64	73	86	103	120	138	159
4	91	102	117	138	164	190	214
5	117	130	160	182	211	248	325
6	123	143	169	200	233	451	691
7	116	143	169	206	418	2672	4952
8	114	136	173	240	1652	5773	8515
9	103	127	153	470	5093	12360	12618
10	123	157	194	2657	12519	12807	12858
11	152	211	397	5899	13040	13111	13188
12	163	500	1788	12536	12612	12688	12753
13	159	971	5313	12702	12785	12848	12927
14	225	2381	10076	12712	12786	12883	12953
15	386	4152	12421	12521	12594	12695	12784
Abs. Change	305	4068	12331	12419	12486	12574	12646
% Change	377%	4843%	13701%	12176%	11561%	10392%	9164%
% per Year	26.9%	345.9%	978.7%	869.7%	825.8%	742.3%	654.6%

Table 93: Data for the total annual cooling power usage in the EWT cutoff test

Time [years]	Base Model (90F Case) [MWh]	95F Case [MWh]	100F Case [MWh]	105F Case [MWh]	110F Case [MWh]	115F Case [MWh]	120F Case [MWh]
1	123.1	124.8	126.7	128.4	130.2	131.9	134.5
2	126.2	128.5	130.7	133.4	136.1	138.7	141.6
3	128.7	131.5	134.2	137.6	141.2	144.5	147.5
4	130.3	133.6	136.8	141.0	144.9	148.6	152.2
5	132.3	136.3	139.9	144.5	149.0	153.4	157.4
6	134.5	138.9	142.8	147.8	153.0	157.7	161.6
7	136.1	141.1	145.1	150.6	156.3	160.8	164.2
8	138.2	143.5	147.8	153.9	159.8	163.9	168.2
9	140.0	145.5	150.2	156.8	162.2	166.7	171.7
10	141.2	146.9	151.8	158.1	163.2	169.3	174.5
11	142.8	148.7	153.9	160.0	166.0	172.5	177.6
12	144.2	150.4	155.7	161.3	168.8	175.6	180.7
13	145.8	152.2	157.1	163.5	171.6	178.5	183.7
14	147.1	153.6	158.4	166.4	174.7	181.7	187.0
15	148.5	154.7	160.0	168.6	177.2	184.4	189.6
Abs. Change %	25.3	29.8	33.3	40.3	47.1	52.5	55.1
Change % per Year	20.6%	23.9%	26.3%	31.4%	36.2%	39.8%	40.9%
	1.47%	1.71%	1.88%	2.24%	2.58%	2.84%	2.92%

Table 94: Data for the total annual heating power usage in the EWT cutoff test

Time [years]	Base Model (90F Case) [MWh]	95F Case [MWh]	100F Case [MWh]	105F Case [MWh]	110F Case [MWh]	115F Case [MWh]	120F Case [MWh]
1	8.9	8.9	8.9	8.9	9.0	9.1	9.0
2	9.1	9.2	9.3	9.3	9.4	9.5	9.4
3	9.4	9.6	9.5	9.8	9.8	9.9	9.9
4	9.5	9.6	9.7	9.9	10.1	10.3	10.3
5	9.8	10.0	10.1	10.3	10.6	10.9	10.8
6	9.9	10.1	10.2	10.5	10.9	11.1	10.8
7	10.2	10.6	10.7	11.0	11.2	9.3	7.1
8	10.4	10.7	10.9	11.4	10.6	6.5	3.7
9	10.5	10.9	11.1	11.2	6.9	0.1	0.0
10	10.6	11.1	11.4	9.3	0.2	0.0	0.0
11	11.1	11.6	11.7	6.6	0.0	0.0	0.0
12	11.1	11.4	10.5	0.0	0.0	0.0	0.0
13	11.3	10.9	6.8	0.0	0.0	0.0	0.0
14	11.5	9.4	2.3	0.0	0.0	0.0	0.0
15	11.2	7.5	0.0	0.0	0.0	0.0	0.0
Abs. Change	2.3	-1.4	-8.9	-8.9	-9.0	-9.1	-9.0
% Change % per Year	25.8%	-15.3%	-100.0%	-100.0%	-100.0%	-100.0%	-100.0%
	1.85%	-1.09%	-7.14%	-7.14%	-7.14%	-7.14%	-7.14%

Table 95: Data for the annual average COP in the EWT cutoff test

Time [years]	Base Model (90F Case)	95F Case	100F Case	105F Case	110F Case	115F Case	120F Case
	[Wh/Wh]	[Wh/Wh]	[Wh/Wh]	[Wh/Wh]	[Wh/Wh]	[Wh/Wh]	[Wh/Wh]
1	5.0	5.0	5.0	5.0	4.9	4.9	4.9
2	4.9	4.9	4.9	4.9	4.9	4.9	4.9
3	4.9	4.9	4.9	4.9	4.8	4.8	4.8
4	4.9	4.8	4.8	4.8	4.7	4.7	4.7
5	4.9	4.8	4.8	4.8	4.7	4.6	4.6
6	4.9	4.8	4.8	4.7	4.6	4.5	4.5
7	4.8	4.7	4.7	4.6	4.5	4.5	4.4
8	4.7	4.6	4.6	4.4	4.4	4.3	4.4
9	4.7	4.6	4.5	4.4	4.2	5.0	0.0
10	4.6	4.5	4.4	4.4	4.9	0.0	0.0
11	4.6	4.4	4.4	4.2	0.0	0.0	0.0
12	4.5	4.4	4.4	0.0	0.0	0.0	0.0
13	4.5	4.4	4.3	0.0	0.0	0.0	0.0
14	4.4	4.5	4.5	0.0	0.0	0.0	0.0
15	4.4	4.7	0.0	0.0	0.0	0.0	0.0
Abs. Change %	-0.5	-0.3	-5.0	-5.0	-4.9	-4.9	-4.9
Change % per Year	-11.0%	-5.5%	-100.0%	-100.0%	-100.0%	-100.0%	-100.0%
	-0.79%	-0.39%	-7.14%	-7.14%	-7.14%	-7.14%	-7.14%

A.10. Additional Data for the Borehole Spacing Study

This section contains additional data for the borehole spacing sensitivity study.

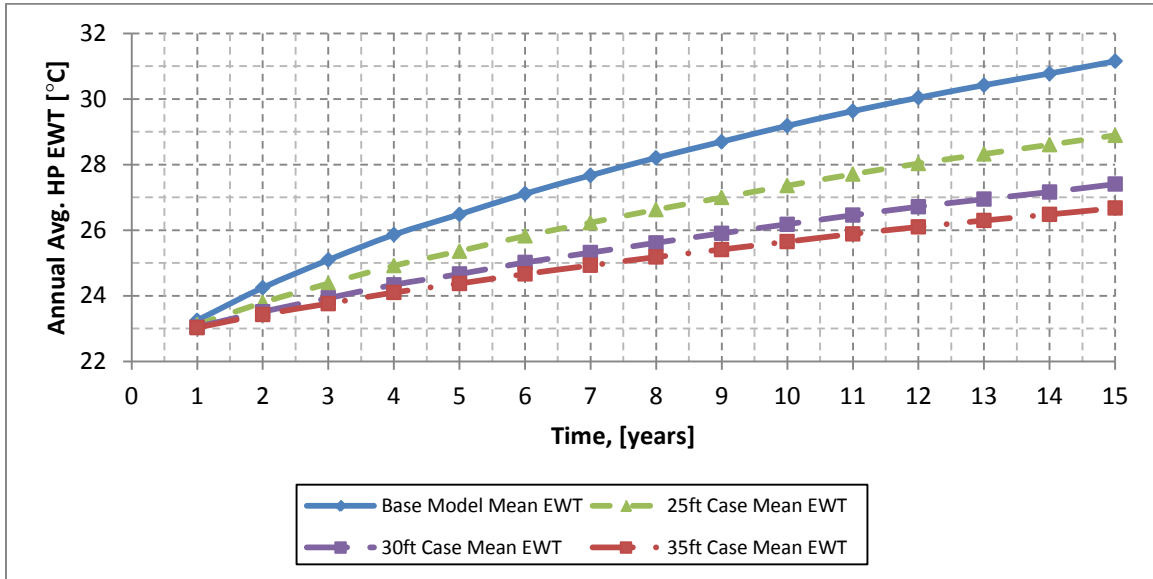


Figure 228: Comparison of average annual EWT for the borehole spacing test

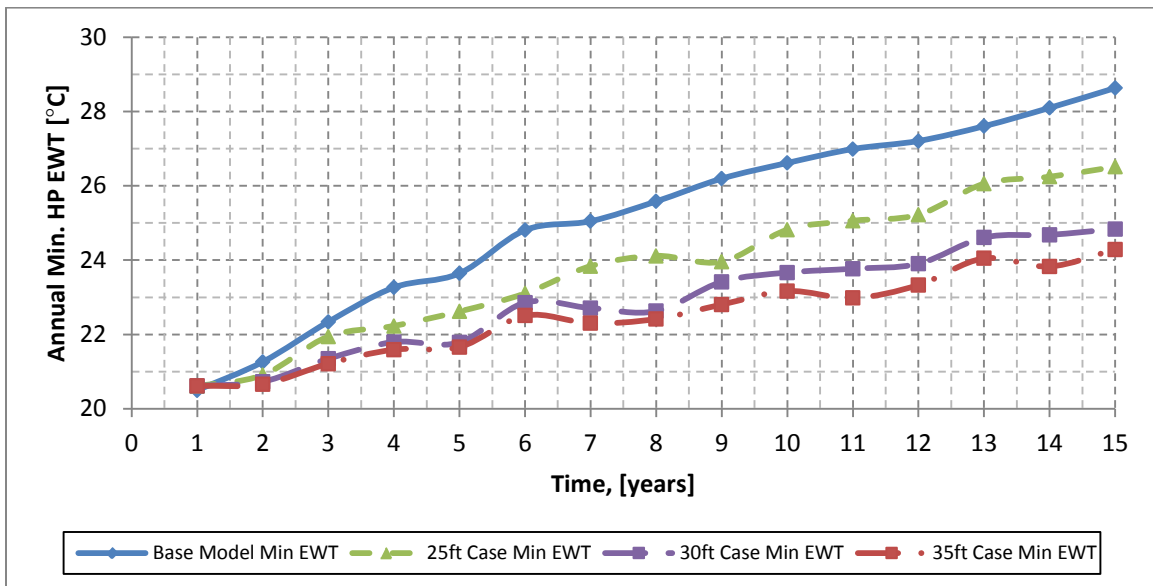


Figure 229: Comparison of minimum annual EWT for the borehole spacing test

Table 96: Data for the average annual EWT for the borehole spacing test

Time [years]	Base Model (20ft Case) [°C]	25ft Case [°C]	30ft Case [°C]	35ft Case [°C]
1	23.3	23.1	23.1	23.0
2	24.2	23.8	23.5	23.4
3	25.1	24.4	23.9	23.8
4	25.9	24.9	24.3	24.1
5	26.5	25.4	24.7	24.4
6	27.1	25.8	25.0	24.7
7	27.7	26.2	25.3	24.9
8	28.2	26.6	25.6	25.2
9	28.7	27.0	25.9	25.4
10	29.2	27.4	26.2	25.7
11	29.6	27.7	26.5	25.9
12	30.0	28.0	26.7	26.1
13	30.4	28.3	26.9	26.3
14	30.8	28.6	27.2	26.5
15	31.1	28.9	27.4	26.7
Abs. Change	7.9	5.8	4.4	3.6
% Change	34.0%	24.9%	18.9%	15.8%
% per Year	2.43%	1.78%	1.35%	1.13%

Table 97: Data for the minimum annual EWT for the borehole spacing test

Time [years]	Base Model (20ft Case) [°C]	25ft Case [°C]	30ft Case [°C]	35ft Case [°C]
1	20.5	20.6	20.6	20.6
2	21.3	20.9	20.7	20.7
3	22.3	21.9	21.3	21.2
4	23.3	22.2	21.8	21.6
5	23.6	22.6	21.8	21.7
6	24.8	23.1	22.9	22.5
7	25.0	23.8	22.7	22.3
8	25.6	24.1	22.6	22.4
9	26.2	24.0	23.4	22.8
10	26.6	24.8	23.7	23.2
11	27.0	25.1	23.8	23.0
12	27.2	25.2	23.9	23.3
13	27.6	26.1	24.6	24.0
14	28.1	26.2	24.7	23.8
15	28.6	26.5	24.8	24.3
Abs. Change	8.1	5.9	4.2	3.7
% Change	39.7%	28.6%	20.5%	17.8%
% per Year	2.83%	2.05%	1.46%	1.27%

Table 98: Data for the total annual cooling for the borehole spacing test

Time [years]	Base Model (20ft Case) [MWh]	25ft Case [MWh]	30ft Case [MWh]	35ft Case [MWh]
1	-600.2	-600.3	-600.4	-600.4
2	-600.9	-601.4	-601.6	-601.8
3	-600.3	-601.0	-601.4	-601.6
4	-596.9	-597.9	-598.5	-598.7
5	-597.2	-598.5	-599.2	-599.6
6	-596.9	-598.4	-599.2	-599.5
7	-595.6	-597.4	-598.4	-598.8
8	-596.0	-598.0	-599.1	-599.5
9	-595.8	-597.9	-599.1	-599.7
10	-593.0	-595.2	-596.6	-597.1
11	-592.9	-595.3	-596.8	-597.5
12	-592.5	-595.1	-596.8	-597.5
13	-592.8	-595.4	-597.2	-598.0
14	-592.8	-595.5	-597.4	-598.2
15	-592.1	-595.1	-596.9	-597.8
Abs. Change	-8.2	-5.2	-3.4	-2.6
% Change	-1.4%	-0.9%	-0.6%	-0.4%
% per Year	-0.10%	-0.06%	-0.04%	-0.03%

Table 99: Data for the total annual heating for the borehole spacing test

Time [years]	Base Model (20ft Case) [MWh]	25ft Case [MWh]	30ft Case [MWh]	35ft Case [MWh]
1	42.5	42.4	42.4	42.4
2	41.8	41.8	41.7	41.7
3	42.3	42.1	42.0	42.1
4	41.2	41.1	41.0	40.9
5	42.6	42.5	42.3	42.3
6	42.7	42.4	42.3	42.2
7	43.0	42.7	42.6	42.4
8	42.6	42.3	42.1	42.0
9	43.0	42.6	42.5	42.4
10	41.9	41.5	41.2	41.2
11	43.1	42.7	42.4	42.3
12	43.4	43.0	42.6	42.6
13	43.5	43.0	42.7	42.6
14	43.2	42.7	42.5	42.4
15	42.7	42.9	42.7	42.5
Abs. Change	0.2	0.5	0.3	0.1
% Change	0.6%	1.2%	0.6%	0.2%
% per Year	0.04%	0.09%	0.05%	0.01%

Table 100: Data for the annual time out-of-setpoint for the borehole spacing test

Time [years]	Base Model (20ft Case) [hr]	25ft Case [hr]	30ft Case [hr]	35ft Case [hr]
1	81	76	76	80
2	70	65	61	66
3	64	58	54	55
4	91	81	77	75
5	117	102	101	92
6	123	110	107	101
7	116	101	92	91
8	114	96	84	80
9	103	83	71	67
10	123	109	87	91
11	152	120	105	100
12	163	134	116	111
13	159	126	105	105
14	225	119	103	94
15	386	103	87	79
Abs. Change	305.0	27.0	11.0	-1.0
% Change	376.5%	35.5%	14.5%	-1.3%
% per Year	26.90%	2.54%	1.03%	-0.09%

Table 101: Data for the total annual cooling power usage for the borehole spacing test

Time [years]	Base Model (20ft Case) [MWh]	25ft Case [MWh]	30ft Case [MWh]	35ft Case [MWh]
1	123.1	122.8	122.6	122.5
2	126.2	125.0	124.2	124.0
3	128.7	126.7	125.4	125.0
4	130.3	127.6	126.0	125.4
5	132.3	129.1	127.1	126.3
6	134.5	130.5	128.2	127.2
7	136.1	131.6	128.9	127.8
8	138.2	133.0	130.0	128.8
9	140.0	134.3	131.0	129.6
10	141.2	135.0	131.3	129.7
11	142.8	136.2	132.2	130.5
12	144.2	137.4	133.0	131.2
13	145.8	138.5	133.9	131.9
14	147.1	139.6	134.8	132.6
15	148.5	140.6	135.6	133.2
Abs. Change	25.3	17.9	13.0	10.7
% Change	20.6%	14.5%	10.6%	8.7%
% per Year	1.47%	1.04%	0.76%	0.62%

Table 102: Data for the total annual heating power usage for the borehole spacing test

Time [years]	Base Model (20ft Case) [MWh]	25ft Case [MWh]	30ft Case [MWh]	35ft Case [MWh]
1	8.9	8.8	8.8	8.8
2	9.1	8.9	8.8	8.8
3	9.4	9.1	9.0	9.0
4	9.5	9.3	9.1	8.9
5	9.8	9.5	9.2	9.1
6	9.9	9.6	9.4	9.1
7	10.2	9.8	9.6	9.3
8	10.4	9.9	9.5	9.4
9	10.5	10.0	9.7	9.5
10	10.6	9.9	9.6	9.5
11	11.1	10.4	10.0	9.8
12	11.1	10.3	9.8	9.7
13	11.3	10.4	9.9	9.8
14	11.5	10.5	10.1	9.9
15	11.2	10.5	10.1	9.9
Abs. Change	2.3	1.7	1.3	1.0
% Change	25.8%	19.4%	14.7%	11.7%
% per Year	1.85%	1.39%	1.05%	0.83%

Table 103: Data for the annual average COP for the borehole spacing test

Time [years]	Base Model (20ft Case) [Wh/Wh]	25ft Case [Wh/Wh]	30ft Case [Wh/Wh]	35ft Case [Wh/Wh]
1	4.96	4.96	4.96	4.96
2	4.9	4.9	4.9	4.9
3	4.9	4.9	4.9	4.9
4	4.9	4.9	4.9	4.9
5	4.9	4.9	4.9	4.9
6	4.9	4.9	4.9	4.9
7	4.8	4.9	4.9	4.9
8	4.7	4.8	4.9	4.9
9	4.7	4.8	4.9	4.9
10	4.6	4.8	4.9	4.9
11	4.6	4.8	4.9	4.9
12	4.5	4.8	4.9	4.9
13	4.5	4.8	4.9	4.9
14	4.4	4.7	4.8	4.8
15	4.41	4.66	4.80	4.85
Abs. Change	-0.5	-0.3	-0.2	-0.1
% Change	-11.0%	-6.0%	-3.3%	-2.3%
% per Year	-0.79%	-0.43%	-0.24%	-0.17%

A.11. Additional Data for the Borehole Depth Study

This section contains additional data for the borehole depth sensitivity study.

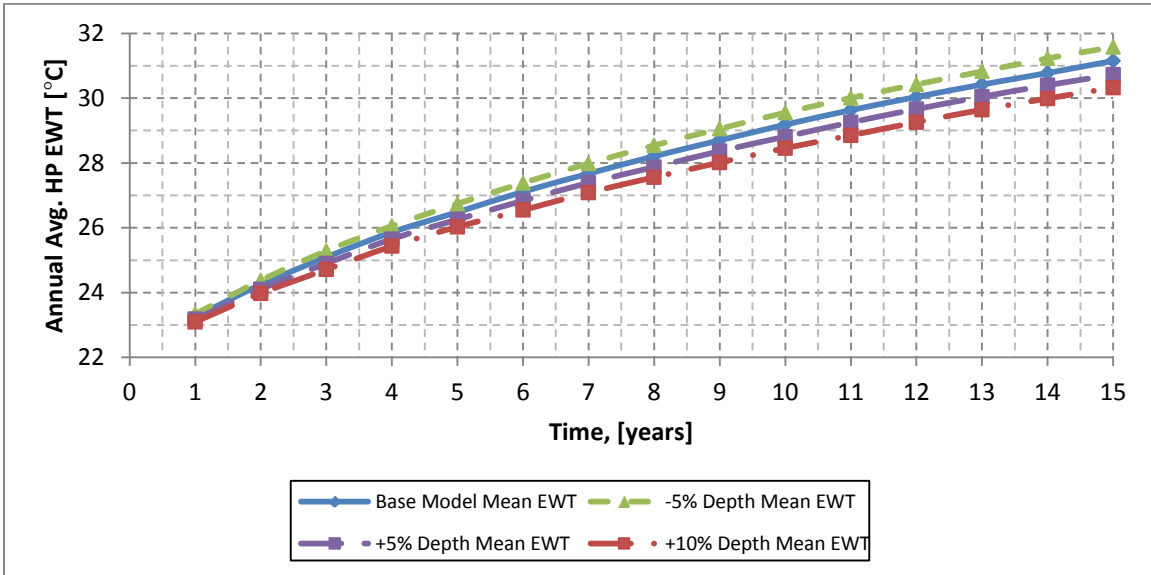


Figure 230: Comparison of average annual EWT for the borehole depth test

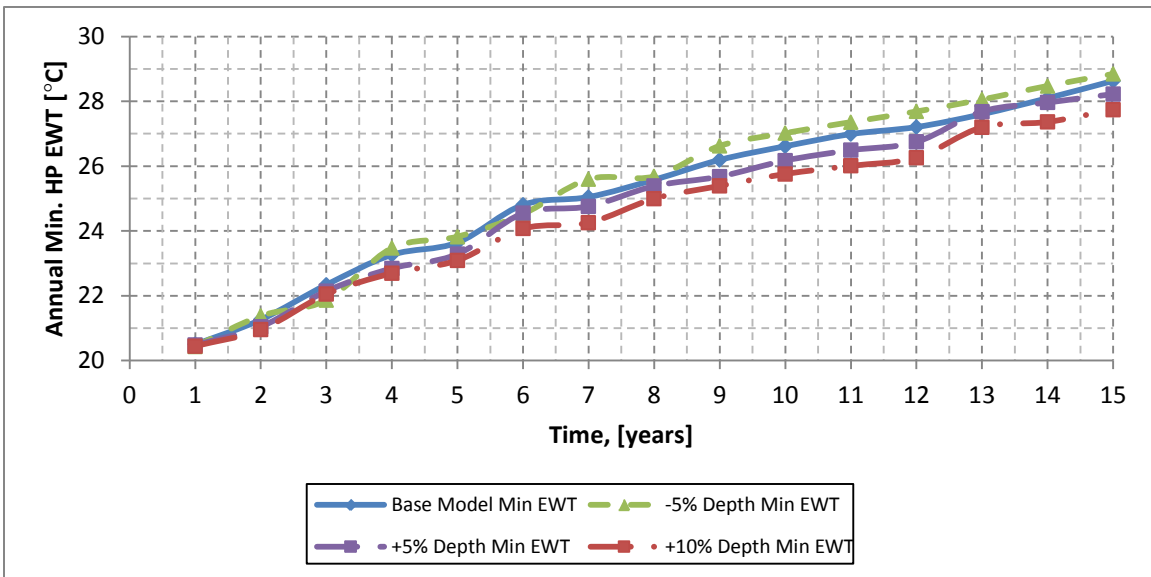


Figure 231: Comparison of minimum annual EWT for the borehole depth test

Table 104: Data for the average annual EWT for the borehole depth test

Time [years]	Base Model (171m Depth) [°C]	-5% Case (162m Depth) [°C]	+5% Case (180m Depth) [°C]	+10% Case (188m Depth) [°C]
1	23.3	23.3	23.2	23.1
2	24.2	24.4	24.1	24.0
3	25.1	25.3	24.9	24.7
4	25.9	26.1	25.7	25.4
5	26.5	26.7	26.3	26.0
6	27.1	27.4	26.8	26.5
7	27.7	28.0	27.4	27.1
8	28.2	28.5	27.9	27.6
9	28.7	29.1	28.4	28.0
10	29.2	29.6	28.8	28.5
11	29.6	30.0	29.3	28.9
12	30.0	30.4	29.7	29.3
13	30.4	30.8	30.0	29.6
14	30.8	31.2	30.4	30.0
15	31.1	31.6	30.7	30.3
Abs. Change	7.9	8.2	7.5	7.2
% Change	34.0%	35.3%	32.5%	31.3%
% per Year	2.43%	2.52%	2.32%	2.23%

Table 105: Data for the minimum annual EWT for the borehole depth test

Time [years]	Base Model (171m Depth) [°C]	-5% Case (162m Depth) [°C]	+5% Case (180m Depth) [°C]	+10% Case (188m Depth) [°C]
1	20.5	20.4	20.5	20.4
2	21.3	21.4	21.0	21.0
3	22.3	21.9	22.1	22.0
4	23.3	23.5	22.8	22.7
5	23.6	23.8	23.3	23.1
6	24.8	24.5	24.5	24.1
7	25.0	25.6	24.8	24.3
8	25.6	25.7	25.4	25.0
9	26.2	26.6	25.7	25.4
10	26.6	27.0	26.2	25.8
11	27.0	27.4	26.5	26.0
12	27.2	27.7	26.7	26.3
13	27.6	28.1	27.7	27.2
14	28.1	28.5	28.0	27.4
15	28.6	28.8	28.2	27.7
Abs. Change	8.1	8.4	7.7	7.3
% Change	39.7%	41.1%	37.8%	35.7%
% per Year	2.83%	2.94%	2.70%	2.55%

Table 106: Data for the total annual cooling for the borehole depth test

Time [years]	Base Model (171m Depth) [MWh]	-5% Case (162m Depth) [MWh]	+5% Case (180m Depth) [MWh]	+10% Case (188m Depth) [MWh]
1	-600.2	-600.0	-600.3	-600.5
2	-600.9	-600.8	-601.2	-601.3
3	-600.3	-600.0	-600.5	-600.8
4	-596.9	-596.7	-597.2	-597.4
5	-597.2	-596.9	-597.5	-597.8
6	-596.9	-596.5	-597.3	-597.7
7	-595.6	-595.2	-596.1	-596.5
8	-596.0	-595.5	-596.5	-596.9
9	-595.8	-595.3	-596.3	-596.7
10	-593.0	-592.5	-593.5	-594.0
11	-592.9	-592.3	-593.4	-593.9
12	-592.5	-591.9	-593.0	-593.6
13	-592.8	-592.2	-593.3	-593.9
14	-592.8	-592.0	-593.4	-593.9
15	-592.1	-591.1	-592.8	-593.4
Abs. Change	-8.2	-8.9	-7.5	-7.0
% Change	-1.36%	-1.49%	-1.25%	-1.17%
% per Year	-0.10%	-0.11%	-0.09%	-0.08%

Table 107: Data for the total annual heating for the borehole depth test

Time [years]	Base Model (171m Depth) [MWh]	-5% Case (162m Depth) [MWh]	+5% Case (180m Depth) [MWh]	+10% Case (188m Depth) [MWh]
1	42.5	42.5	42.5	42.4
2	41.8	41.8	41.8	41.8
3	42.3	42.3	42.3	42.3
4	41.2	41.2	41.2	41.1
5	42.6	42.7	42.6	42.6
6	42.7	42.8	42.7	42.6
7	43.0	43.0	42.9	42.9
8	42.6	42.6	42.5	42.3
9	43.0	43.1	42.9	42.9
10	41.9	42.0	41.7	41.7
11	43.1	43.2	43.0	42.9
12	43.4	43.5	43.3	43.2
13	43.5	43.6	43.4	43.3
14	43.2	42.6	43.3	43.1
15	42.7	41.6	43.2	43.3
Abs. Change	0.2	-0.8	0.8	0.9
% Change	0.6%	-1.9%	1.8%	2.1%
% per Year	0.04%	-0.14%	0.13%	0.15%

Table 108: Data for the total annual time out-of-setpoint for the borehole depth test

Time [years]	Base Model (171m Depth) [hr]	-5% Case (162m Depth) [hr]	+5% Case (180m Depth) [hr]	+10% Case (188m Depth) [hr]
1	81	78	73	76
2	70	75	65	66
3	64	67	57	57
4	91	93	88	87
5	117	124	110	105
6	123	127	123	115
7	116	119	112	107
8	114	122	110	106
9	103	107	100	91
10	123	134	125	119
11	152	151	140	134
12	163	174	156	147
13	159	177	151	138
14	225	576	143	133
15	386	914	175	122
Abs. Change	305.0	836.0	102.0	46.0
% Change	377%	1072%	140%	61%
% per Year	26.90%	76.56%	9.98%	4.32%

Table 109: Data for the total annual cooling power usage for the borehole depth test

Time [years]	Base Model (171m Depth) [MWh]	-5% Case (162m Depth) [MWh]	+5% Case (180m Depth) [MWh]	+10% Case (188m Depth) [MWh]
1	123.1	123.5	122.8	122.4
2	126.2	126.7	125.7	125.2
3	128.7	129.4	128.0	127.4
4	130.3	131.0	129.6	128.8
5	132.3	133.3	131.5	130.7
6	134.5	135.5	133.4	132.4
7	136.1	137.4	135.1	133.9
8	138.2	139.5	136.9	135.7
9	140.0	141.4	138.8	137.4
10	141.2	142.6	139.7	138.4
11	142.8	144.2	141.4	139.8
12	144.2	145.7	142.8	141.3
13	145.8	147.3	144.3	142.7
14	147.1	148.9	145.7	144.1
15	148.5	150.1	146.8	145.3
Abs. Change	25.3	26.6	24.0	22.8
% Change	20.6%	21.5%	19.6%	18.6%
% per Year	1.47%	1.54%	1.40%	1.33%

Table 110: Data for the total annual heating power usage for the borehole depth test

Time [years]	Base Model (171m Depth) [MWh]	-5% Case (162m Depth) [MWh]	+5% Case (180m Depth) [MWh]	+10% Case (188m Depth) [MWh]
1	8.9	8.9	8.9	8.9
2	9.1	9.1	9.0	9.0
3	9.4	9.4	9.4	9.4
4	9.5	9.6	9.4	9.4
5	9.8	9.8	9.7	9.7
6	9.9	10.1	9.9	9.8
7	10.2	10.3	10.1	10.0
8	10.4	10.5	10.3	10.1
9	10.5	10.6	10.4	10.4
10	10.6	10.7	10.5	10.4
11	11.1	11.3	11.0	10.8
12	11.1	11.3	10.9	10.7
13	11.3	11.4	11.0	11.0
14	11.5	11.4	11.5	11.2
15	11.2	10.7	11.3	11.3
Abs. Change	2.3	1.8	2.4	2.4
% Change	25.8%	20.6%	26.4%	26.5%
% per Year	1.85%	1.47%	1.89%	1.89%

Table 111: Data for the annual average COP for the borehole depth test

Time [years]	Base Model (171m Depth) [Wh/Wh]	-5% Case (162m Depth) [Wh/Wh]	+5% Case (180m Depth) [Wh/Wh]	+10% Case (188m Depth) [Wh/Wh]
1	4.96	4.96	4.96	4.95
2	4.9	4.9	4.9	4.9
3	4.9	4.9	4.9	4.9
4	4.9	4.9	4.9	4.9
5	4.9	4.9	4.9	4.9
6	4.9	4.8	4.9	4.9
7	4.8	4.8	4.8	4.8
8	4.7	4.7	4.7	4.8
9	4.7	4.6	4.7	4.7
10	4.6	4.5	4.6	4.7
11	4.6	4.5	4.6	4.6
12	4.5	4.5	4.6	4.6
13	4.5	4.5	4.5	4.6
14	4.4	4.4	4.4	4.5
15	4.41	4.45	4.45	4.47
Abs. Change	-0.5	-0.5	-0.5	-0.5
% Change	-11.0%	-10.2%	-10.3%	-9.9%
% per Year	-0.79%	-0.73%	-0.73%	-0.70%

A.12. Additional Data for the SHR Study

This section contains additional data for the supplemental heat rejection study.

10% SHR GLHEPRO Loads

Monthly Loads

Heating Average over duration
 Heating Maximum during duration
 Duration: 3

Cooling Average over duration
 Cooling Maximum during duration
 Duration: 9

Note that it is not necessarily the case that the best method for heating and cooling (average or maximum) will be the same.

Get Summary Data

	Total Loads [1000 Btu]		Peak Loads [1000 Btu/h]	
	Heating	Cooling	Heating	Cooling
January	48275	26426	721	504
February	20007	28481	584	567
March	10220	78673	492	757
April	734	149759	259	874
May	252	204894	82	948
June	0	269815	0	980
July	0	307187	0	1001
August	0	291182	0	1022
September	127	211090	59	944
October	403	164633	163	972
November	6409	77548	290	846
December	47579	36739	787	592

20% SHR GLHEPRO Loads

Monthly Loads

Heating Average over duration
 Heating Maximum during duration
 Duration: 3

Cooling Average over duration
 Cooling Maximum during duration
 Duration: 9

Note that it is not necessarily the case that the best method for heating and cooling (average or maximum) will be the same.

Get Summary Data

	Total Loads [1000 Btu]		Peak Loads [1000 Btu/h]	
	Heating	Cooling	Heating	Cooling
January	42911	23490	641	448
February	17784	25317	519	504
March	9085	69932	437	673
April	652	133119	230	777
May	224	182128	72	843
June	0	239835	0	871
July	0	273055	0	890
August	0	258828	0	908
September	113	187635	53	839
October	359	146341	145	864
November	5697	68931	258	752
December	42293	32657	699	526

30% SHR GLHEPRO Loads

Monthly Loads

Heating Average over duration
 Heating Maximum during duration
 Duration: 3

Cooling Average over duration
 Cooling Maximum during duration
 Duration: 9

Note that it is not necessarily the case that the best method for heating and cooling (average or maximum) will be the same.

Get Summary Data

	Total Loads [1000 Btu]		Peak Loads [1000 Btu/h]	
	Heating	Cooling	Heating	Cooling
January	37547	20554	561	392
February	15561	22152	454	441
March	7949	61190	382	588
April	571	116480	201	680
May	196	159362	63	737
June	0	209856	0	762
July	0	238923	0	779
August	0	226475	0	795
September	99	164181	46	734
October	314	128048	127	756
November	4985	60315	226	658
December	37006	28575	612	461

40% SHR GLHEPRO Loads

Monthly Loads

Heating Average over duration
 Heating Maximum during duration
 Duration: 3

Cooling Average over duration
 Cooling Maximum during duration
 Duration: 9

Note that it is not necessarily the case that the best method for heating and cooling (average or maximum) will be the same.

Get Summary Data

	Total Loads [1000 Btu]		Peak Loads [1000 Btu/h]	
	Heating	Cooling	Heating	Cooling
January	32183	17618	481	336
February	13338	18987	389	378
March	6813	52449	328	504
April	489	99840	172	583
May	168	136596	54	632
June	0	179877	0	654
July	0	204792	0	667
August	0	194121	0	681
September	85	140726	40	629
October	269	109756	108	648
November	4273	51699	194	564
December	31720	24493	524	395

Figure 232: GLHEPRO sizing loads for the SHR test

Table 112: GLHEPRO total monthly cooling design loads for the SHR test

Month	Base Model [MWh]	10% SHR [MWh]	20% SHR [MWh]	30% SHR [MWh]	40% SHR [MWh]
January	8.61	7.75	6.88	6.02	5.16
February	9.27	8.35	7.42	6.49	5.56
March	25.62	23.06	20.50	17.93	15.37
April	48.77	43.89	39.02	34.14	29.26
May	66.72	60.05	53.38	46.71	40.03
June	87.86	79.08	70.29	61.51	52.72
July	100.03	90.03	80.03	70.02	60.02
August	94.82	85.34	75.86	66.38	56.89
September	68.74	61.87	54.99	48.12	41.24
October	53.61	48.25	42.89	37.53	32.17
November	25.25	22.73	20.20	17.68	15.15
December	11.96	10.77	9.57	8.37	7.18
Total	601.29	541.16	481.03	420.90	360.77

Table 113: GLHEPRO total monthly heating design loads for the SHR test

Month	Base Model [MWh]	10% SHR [MWh]	20% SHR [MWh]	30% SHR [MWh]	40% SHR [MWh]
January	15.72	14.15	12.58	11.00	9.43
February	6.52	5.86	5.21	4.56	3.91
March	3.33	3.00	2.66	2.33	2.00
April	0.24	0.22	0.19	0.17	0.14
May	0.08	0.07	0.07	0.06	0.05
June	0.00	0.00	0.00	0.00	0.00
July	0.00	0.00	0.00	0.00	0.00
August	0.00	0.00	0.00	0.00	0.00
September	0.04	0.04	0.03	0.03	0.02
October	0.13	0.12	0.11	0.09	0.08
November	2.09	1.88	1.67	1.46	1.25
December	15.49	13.94	12.40	10.85	9.30
Total	43.64	39.28	34.91	30.55	26.18

Table 114: GLHEPRO peak monthly cooling design loads for the SHR test

Month	Base Model [kW]	10% SHR [kW]	20% SHR [kW]	30% SHR [kW]	40% SHR [kW]
January	164.1	147.7	131.3	114.9	98.5
February	184.5	166.0	147.6	129.1	110.7
March	246.4	221.7	197.1	172.5	147.8
April	284.7	256.3	227.8	199.3	170.8
May	308.8	277.9	247.0	216.1	185.3
June	319.2	287.3	255.4	223.5	191.5
July	326.0	293.4	260.8	228.2	195.6
August	332.7	299.4	266.1	232.9	199.6
September	307.3	276.6	245.8	215.1	184.4
October	316.6	284.9	253.3	221.6	189.9
November	275.4	247.8	220.3	192.8	165.2
December	192.9	173.6	154.3	135.0	115.7
Average	271.55	244.39	217.24	190.08	162.93

Table 115: GLHEPRO peak monthly heating design loads for the SHR test

Month	Base Model [kW]	10% SHR [kW]	20% SHR [kW]	30% SHR [kW]	40% SHR [kW]
January	234.7	211.2	187.8	164.3	140.8
February	190.1	171.1	152.1	133.0	114.0
March	160.1	144.1	128.1	112.1	96.1
April	84.2	75.8	67.4	58.9	50.5
May	26.5	23.9	21.2	18.6	15.9
June	0.0	0.0	0.0	0.0	0.0
July	0.0	0.0	0.0	0.0	0.0
August	0.0	0.0	0.0	0.0	0.0
September	19.4	17.4	15.5	13.6	11.6
October	53.0	47.7	42.4	37.1	31.8
November	94.6	85.1	75.6	66.2	56.7
December	256.2	230.6	205.0	179.3	153.7
Average	93.23	83.91	74.59	65.26	55.94

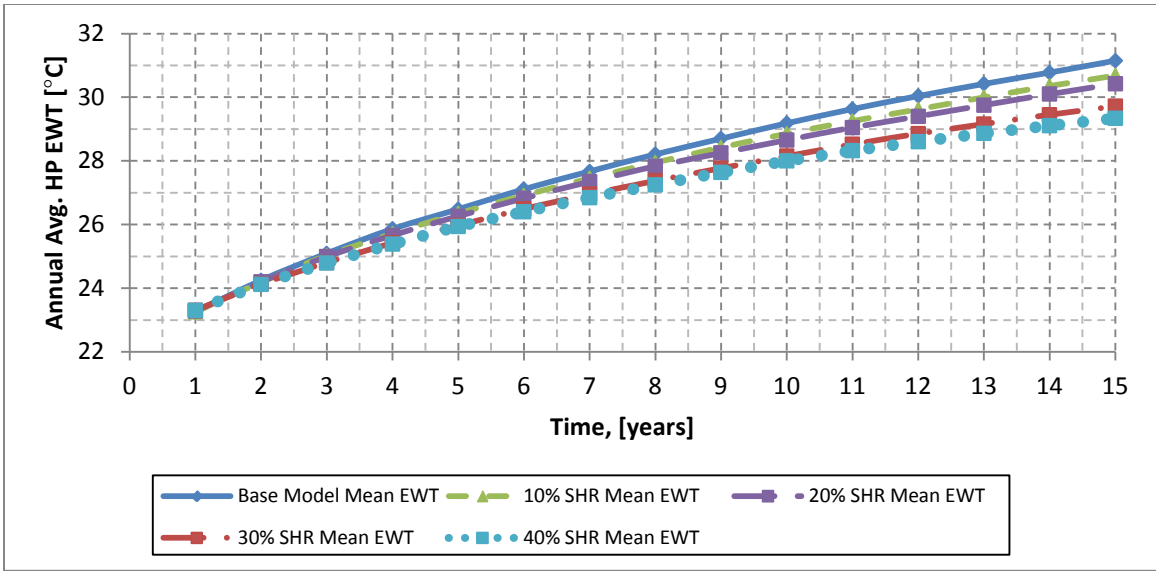


Figure 233: Comparison of average annual EWT for the SHR test

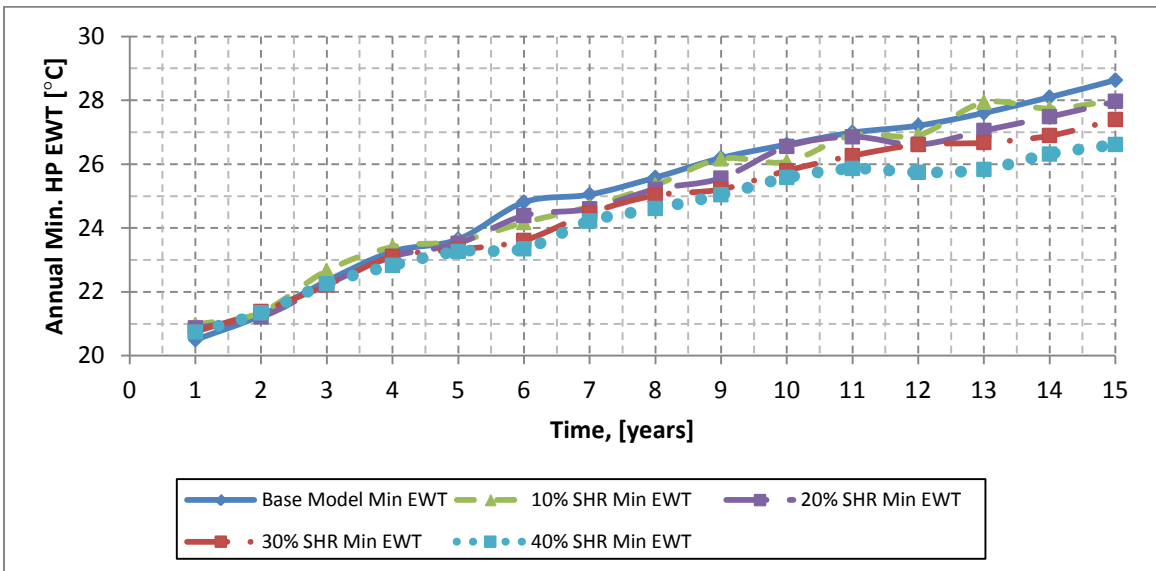


Figure 234: Comparison of minimum annual EWT for the SHR test

Table 116: Data for the average annual EWT for the SHR test

Time [years]	Base Model [°C]	10% SHR [°C]	20% SHR [°C]	30% SHR [°C]	40% SHR [°C]
1	23.3	23.3	23.3	23.3	23.3
2	24.2	24.2	24.2	24.1	24.1
3	25.1	25.0	25.0	24.8	24.8
4	25.9	25.7	25.7	25.4	25.4
5	26.5	26.4	26.3	26.0	25.9
6	27.1	26.9	26.8	26.5	26.4
7	27.7	27.5	27.3	27.0	26.8
8	28.2	27.9	27.8	27.4	27.2
9	28.7	28.4	28.2	27.8	27.6
10	29.2	28.9	28.7	28.1	28.0
11	29.6	29.3	29.0	28.5	28.3
12	30.0	29.6	29.4	28.9	28.6
13	30.4	30.0	29.8	29.2	28.9
14	30.8	30.4	30.1	29.5	29.1
15	31.1	30.7	30.4	29.7	29.3
Abs. Change	7.9	7.4	7.1	6.4	6.0
% Change	34.0%	31.9%	30.6%	27.5%	25.9%
% per Year	2.43%	2.28%	2.19%	1.96%	1.85%

Table 117: Data for the minimum annual EWT for the SHR test

Time [years]	Base Model [°C]	10% SHR [°C]	20% SHR [°C]	30% SHR [°C]	40% SHR [°C]
1	20.5	21.0	20.9	20.8	20.7
2	21.3	21.4	21.2	21.4	21.3
3	22.3	22.7	22.2	22.2	22.3
4	23.3	23.4	23.1	23.1	22.8
5	23.6	23.6	23.5	23.3	23.3
6	24.8	24.2	24.4	23.6	23.3
7	25.0	24.7	24.6	24.5	24.2
8	25.6	25.3	25.2	25.0	24.6
9	26.2	26.2	25.6	25.2	25.0
10	26.6	26.1	26.6	25.8	25.6
11	27.0	26.9	26.9	26.3	25.9
12	27.2	26.9	26.6	26.6	25.7
13	27.6	27.9	27.1	26.7	25.8
14	28.1	27.7	27.5	26.9	26.3
15	28.6	28.0	28.0	27.4	26.6
Abs. Change	8.1	7.0	7.1	6.6	5.9
% Change	39.7%	33.5%	34.0%	32.0%	28.3%
% per Year	2.83%	2.39%	2.43%	2.28%	2.02%

Table 118: Data for the total annual cooling for the SHR test

Time [years]	Base Model [MWh]	10% SHR [MWh]	20% SHR [MWh]	30% SHR [MWh]	40% SHR [MWh]
1	-600.2	-595.2	-595.1	-594.9	-599.7
2	-600.9	-596.1	-596.0	-595.9	-600.7
3	-600.3	-595.5	-595.5	-595.4	-600.2
4	-596.9	-592.3	-592.2	-592.2	-597.0
5	-597.2	-592.6	-592.5	-592.7	-597.3
6	-596.9	-592.2	-592.2	-592.5	-597.2
7	-595.6	-591.1	-591.1	-591.4	-596.2
8	-596.0	-591.5	-591.6	-592.0	-596.7
9	-595.8	-591.3	-591.4	-591.8	-596.6
10	-593.0	-588.6	-588.7	-589.1	-593.9
11	-592.9	-588.5	-588.7	-589.1	-593.9
12	-592.5	-588.3	-588.4	-588.8	-593.8
13	-592.8	-588.5	-588.7	-589.1	-594.2
14	-592.8	-588.6	-588.7	-589.3	-594.3
15	-592.1	-588.1	-588.3	-588.9	-593.9
Abs. Change	-8.2	-7.1	-6.8	-6.0	-5.8
% Change	-1.36%	-1.20%	-1.14%	-1.01%	-0.97%
% per Year	-0.10%	-0.09%	-0.08%	-0.07%	-0.07%

Table 119: Data for the total annual time in cooling operation for the SHR test

Time [years]	Base Model [1000·hrs]	10% SHR [1000·hrs]	20% SHR [1000·hrs]	30% SHR [1000·hrs]	40% SHR [1000·hrs]
1	49.8	49.6	49.6	49.6	49.8
2	49.6	49.4	49.4	49.4	49.6
3	49.6	49.4	49.4	49.4	49.6
4	49.6	49.4	49.4	49.4	49.5
5	49.3	49.1	49.1	49.2	49.3
6	49.4	49.3	49.3	49.3	49.5
7	49.8	49.6	49.6	49.6	49.8
8	49.6	49.4	49.4	49.4	49.5
9	49.6	49.5	49.5	49.4	49.6
10	49.6	49.4	49.4	49.4	49.6
11	49.7	49.4	49.4	49.4	49.6
12	49.3	49.1	49.2	49.1	49.3
13	50.0	49.8	49.8	49.7	49.9
14	49.6	49.5	49.4	49.4	49.6
15	49.6	49.4	49.4	49.4	49.5
Abs. Change	-0.2	-0.2	-0.2	-0.2	-0.2
% Change	-0.4%	-0.4%	-0.4%	-0.5%	-0.5%
% per Year	-0.03%	-0.03%	-0.03%	-0.03%	-0.03%

Table 120: Data for the ratio of net annual heat rejected per unit GHEX length for the SHR test

	Base Model	10% SHR	20% SHR	30% SHR	40% SHR
GHEX Length [m]	27310.1	25359.4	22433.3	19799.8	17556.5
Time [years]	Heat Rejected per GHEX Length [kW/m]				
1	25.3	24.1	24.1	23.7	22.8
2	25.4	24.3	24.2	23.8	23.0
3	25.5	24.3	24.3	23.9	23.0
4	25.5	24.3	24.3	23.9	23.0
5	25.5	24.4	24.3	23.9	23.0
6	25.6	24.4	24.4	23.9	23.1
7	25.6	24.4	24.4	23.9	23.1
8	25.7	24.5	24.5	24.0	23.2
9	25.7	24.6	24.5	24.1	23.2
10	25.7	24.5	24.5	24.1	23.2
11	25.7	24.6	24.5	24.1	23.2
12	25.8	24.6	24.5	24.1	23.2
13	25.8	24.6	24.6	24.1	23.3
14	25.9	24.7	24.7	24.2	23.3
15	25.9	24.7	24.7	24.2	23.3
Abs. Change	0.7	0.6	0.6	0.5	0.5
% Change	2.6%	2.5%	2.5%	2.3%	2.2%
% per Year	0.19%	0.18%	0.18%	0.16%	0.16%

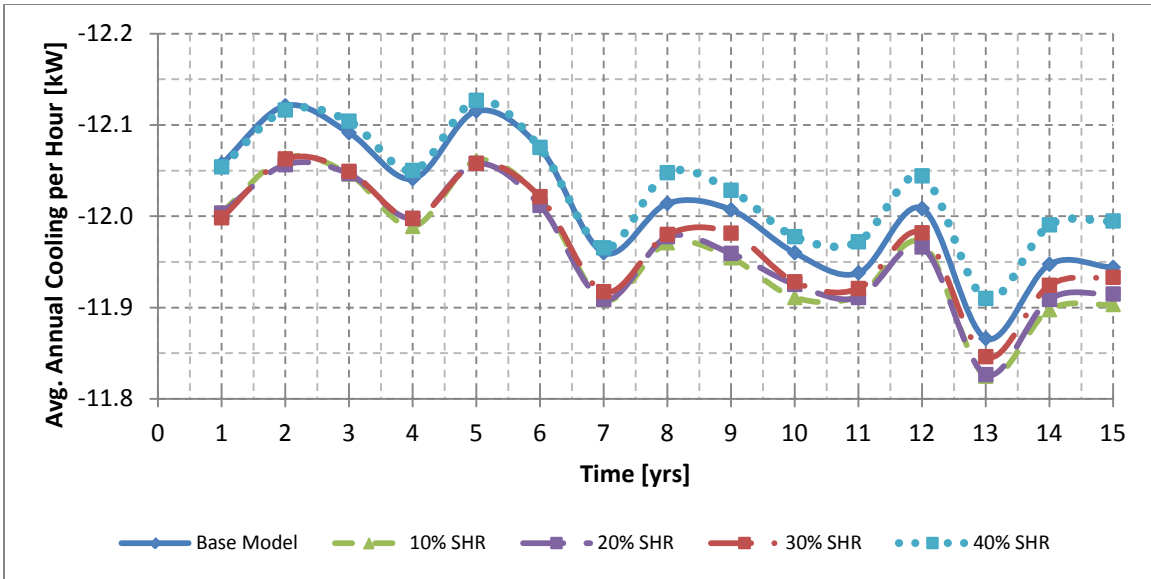


Figure 235: Comparison of the ratio of net annual cooling provided per hour of cooling operation for the SHR test

Table 121: Data for the ratio of net annual cooling provided per hour of cooling operation for the SHR test

Time [years]	Base Model [kW]	10% SHR [kW]	20% SHR [kW]	30% SHR [kW]	40% SHR [kW]
1	-12.06	-12.00	-12.00	-12.00	-12.05
2	-12.12	-12.06	-12.06	-12.06	-12.12
3	-12.09	-12.05	-12.05	-12.05	-12.10
4	-12.04	-11.99	-12.00	-12.00	-12.05
5	-12.12	-12.06	-12.06	-12.06	-12.13
6	-12.07	-12.02	-12.01	-12.02	-12.08
7	-11.96	-11.91	-11.91	-11.92	-11.97
8	-12.01	-11.97	-11.98	-11.98	-12.05
9	-12.01	-11.95	-11.96	-11.98	-12.03
10	-11.96	-11.91	-11.93	-11.93	-11.98
11	-11.94	-11.91	-11.91	-11.92	-11.97
12	-12.01	-11.97	-11.97	-11.98	-12.04
13	-11.87	-11.82	-11.83	-11.85	-11.91
14	-11.95	-11.90	-11.91	-11.92	-11.99
15	-11.94	-11.90	-11.91	-11.93	-11.99
Abs. Change	-0.1	-0.1	-0.1	-0.1	-0.1
% Change	-0.9%	-0.8%	-0.7%	-0.5%	-0.5%
% per Year	-0.07%	-0.06%	-0.05%	-0.04%	-0.04%

Table 122: Data for the total annual heating for the SHR test

Time [years]	Base Model [MWh]	10% SHR [MWh]	20% SHR [MWh]	30% SHR [MWh]	40% SHR [MWh]
1	42.5	42.8	42.8	42.8	42.4
2	41.8	42.2	42.1	42.1	41.7
3	42.3	42.6	42.6	42.5	42.2
4	41.2	41.5	41.5	41.4	41.1
5	42.6	43.0	43.0	42.9	42.5
6	42.7	43.1	43.0	42.9	42.5
7	43.0	43.3	43.3	43.2	42.7
8	42.6	42.8	42.8	42.7	42.3
9	43.0	43.3	43.3	43.1	42.7
10	41.9	42.2	42.1	41.9	41.5
11	43.1	43.4	43.3	43.1	42.6
12	43.4	43.7	43.6	43.5	43.0
13	43.5	43.9	43.7	43.5	43.0
14	43.2	43.6	43.5	43.3	42.8
15	42.7	43.7	43.7	43.4	42.9
Abs. Change	0.2	0.9	0.9	0.7	0.5
% Change	0.6%	2.2%	2.0%	1.6%	1.3%
% per Year	0.04%	0.16%	0.14%	0.11%	0.09%

Table 123: Data for the total annual time out-of-setpoint for the SHR test

Time [years]	Base Model [hr]	10% SHR [hr]	20% SHR [hr]	30% SHR [hr]	40% SHR [hr]
1	81	36	38	40	87
2	70	34	35	36	79
3	64	26	27	28	67
4	91	42	41	43	95
5	117	53	56	55	122
6	123	61	57	60	125
7	116	51	53	54	114
8	114	48	46	46	113
9	103	42	41	42	96
10	123	65	66	62	123
11	152	72	70	69	139
12	163	74	79	75	153
13	159	75	72	69	147
14	225	63	63	58	133
15	386	59	56	54	121
Abs. Change	305.0	23.0	18.0	14.0	34.0
% Change	377%	64%	47%	35%	39%
% per Year	26.90%	4.56%	3.38%	2.50%	2.79%

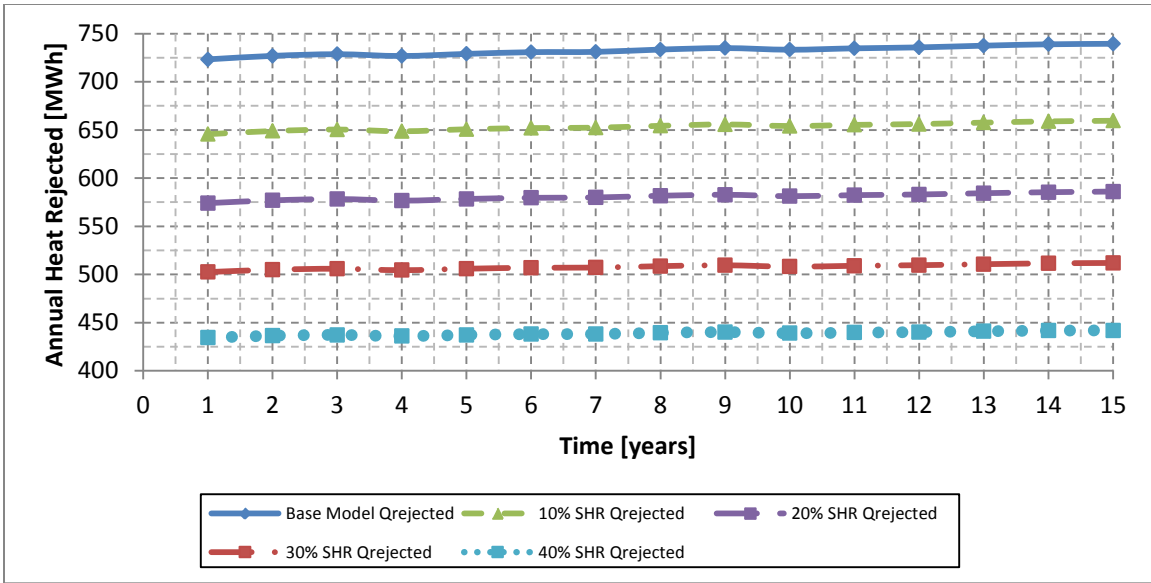


Figure 236: Comparison of heat rejected to the ground loop during cooling for the SHR test

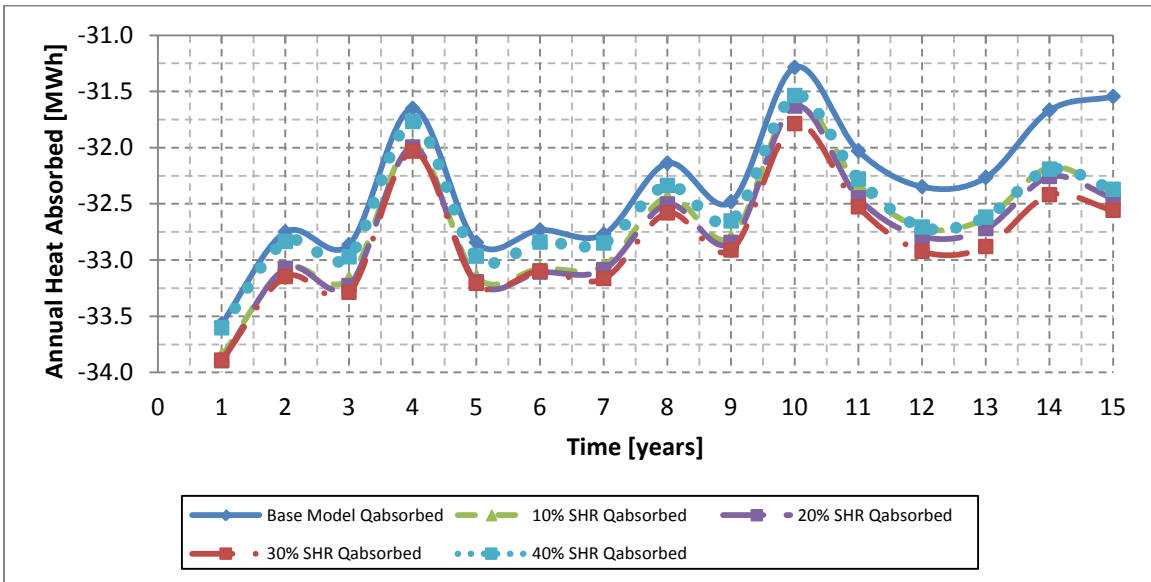


Figure 237: Comparison of heat absorbed from the ground loop during heating for the SHR test

Table 124: Data for the annual net heat rejected to the ground loop for the SHR test

Time [years]	Base Model [MWh]	10% SHR [MWh]	20% SHR [MWh]	30% SHR [MWh]	40% SHR [MWh]
1	689.7	611.8	574.1	468.6	400.8
2	694.1	615.8	576.9	471.8	403.6
3	695.7	617.3	578.3	472.7	404.3
4	695.1	616.7	576.7	472.4	404.3
5	696.1	617.6	578.4	472.8	404.3
6	698.0	618.9	579.6	473.9	405.3
7	698.3	619.3	579.9	474.0	405.4
8	701.3	621.9	581.7	476.1	407.1
9	702.5	622.9	582.8	476.6	407.6
10	702.0	622.5	581.3	476.3	407.5
11	702.7	623.0	582.4	476.5	407.4
12	703.3	623.4	583.0	476.7	407.5
13	705.2	625.0	584.4	477.8	408.5
14	707.2	626.7	585.4	479.2	409.5
15	707.9	627.2	586.1	479.4	409.6
Abs. Change	18.2	15.4	12.0	10.8	8.8
% Change	2.6%	2.5%	2.1%	2.3%	2.2%
% per Year	0.19%	0.18%	0.15%	0.16%	0.16%

Table 125: Data for the total annual cooling power usage for the SHR test

Time [years]	Base Model [MWh]	10% SHR [MWh]	20% SHR [MWh]	30% SHR [MWh]	40% SHR [MWh]
1	123.1	122.3	122.6	123.2	124.5
2	126.2	125.2	125.5	125.8	127.1
3	128.7	127.6	127.8	127.7	129.1
4	130.3	128.9	129.1	128.9	130.2
5	132.3	131.0	131.0	130.7	132.0
6	134.5	132.8	132.9	132.4	133.6
7	136.1	134.5	134.5	133.8	134.9
8	138.2	136.3	136.3	135.4	136.5
9	140.0	138.1	137.9	136.9	137.9
10	141.2	139.0	138.7	137.6	138.6
11	142.8	140.5	140.2	139.0	139.8
12	144.2	141.7	141.4	140.2	140.8
13	145.8	143.2	142.8	141.3	141.9
14	147.1	144.6	144.1	142.5	142.9
15	148.5	145.8	145.3	143.5	143.7
Abs. Change	25.3	23.5	22.7	20.3	19.2
% Change	20.6%	19.3%	18.5%	16.5%	15.4%
% per Year	1.47%	1.38%	1.32%	1.18%	1.10%

Table 126: Data for the total annual heating power usage for the SHR test

Time [years]	Base Model [MWh]	10% SHR [MWh]	20% SHR [MWh]	30% SHR [MWh]	40% SHR [MWh]
1	8.9	8.9	8.9	8.9	8.8
2	9.1	9.1	9.0	9.0	8.9
3	9.4	9.5	9.4	9.2	9.2
4	9.5	9.5	9.5	9.4	9.3
5	9.8	9.8	9.8	9.7	9.5
6	9.9	10.0	9.9	9.8	9.7
7	10.2	10.2	10.2	10.1	9.9
8	10.4	10.4	10.3	10.1	9.9
9	10.5	10.5	10.4	10.2	10.0
10	10.6	10.6	10.5	10.1	10.0
11	11.1	11.1	10.8	10.6	10.4
12	11.1	11.0	10.9	10.5	10.3
13	11.3	11.3	11.0	10.7	10.4
14	11.5	11.5	11.2	10.9	10.6
15	11.2	11.4	11.2	10.9	10.6
Abs. Change	2.3	2.4	2.3	2.0	1.8
% Change	25.8%	27.0%	26.2%	22.7%	20.1%
% per Year	1.85%	1.93%	1.87%	1.62%	1.43%

Table 127: Data for the annual average COP for the SHR test

Time [years]	Base Model [Wh/Wh]	10% SHR [Wh/Wh]	20% SHR [Wh/Wh]	30% SHR [Wh/Wh]	40% SHR [Wh/Wh]
1	4.96	4.95	4.96	4.96	4.96
2	4.9	4.9	4.9	4.9	4.9
3	4.9	4.9	4.9	4.9	4.9
4	4.9	4.9	4.9	4.9	4.9
5	4.9	4.9	4.9	4.9	4.9
6	4.9	4.9	4.9	4.9	4.9
7	4.8	4.8	4.8	4.9	4.9
8	4.7	4.8	4.8	4.8	4.8
9	4.7	4.7	4.7	4.8	4.8
10	4.6	4.6	4.7	4.8	4.8
11	4.6	4.6	4.6	4.7	4.8
12	4.5	4.6	4.6	4.7	4.8
13	4.5	4.5	4.6	4.7	4.7
14	4.4	4.5	4.5	4.6	4.7
15	4.41	4.48	4.51	4.60	4.65
Abs. Change	-0.5	-0.5	-0.4	-0.4	-0.3
% Change	-11.0%	-9.7%	-9.0%	-7.2%	-6.2%
% per Year	-0.79%	-0.69%	-0.64%	-0.51%	-0.44%

Bibliography

- ASHRAE. (2007). *Standard Method of Test for the Evaluation of Building Energy Analysis Computer Programs*. Atlanta, GA: American Society of Heating, Refrigerating and Air-Conditioning Engineers.
- ASHRAE 2009 Fundamentals Handbook. (2009). 1791 Tullie Cir, N.E., Atlanta, GA 30329: American Society of Heating, Refrigerating and Air-Conditioning Engineers.
- ASHRAE. (2013). *Ventilation for Acceptable Indoor Air Quality*. Atlanta, GA: American Society of Heating, Refrigerating and Air-Conditioning Engineers.
- Bennet, J., Claesson, J., & Hellström, G. (1987). *Multipole method to compute the conductive heat flows to and between pipes in a composite cylinder*. Lund, Sweden: Lund University.
- CANMET Energy Technology Centre. (2002). *Commercial Earth Energy Systems: A Buyer's Guide*. Her Majesty the Queen in Right of Canada. Retrieved from <http://canmetenergy.nrcan.gc.ca/sites/canmetenergy.nrcan.gc.ca/files/files/pubs/M92-251-2002E.pdf>
- Carslaw, H. S., & Jaeger, J. C. (1946). *Conduction of heat in solids*. Oxford, UK: Clarendon Press.
- Chen, Y., Halm, N. P., Braun, J. E., & Groll, E. A. (2002). Mathematical modeling of scroll compressors-part II: overall scroll compressor modeling. *International Journal of Refrigeration*, 25, 751-764.
- Chen, Y., Halm, N. P., Groll, E. A., & Braun, J. E. (2002). Mathematical modeling of scroll compressors-part I: compression process modeling. *International Journal of Refrigeration*, 25, 731-750.
- Claesson, J., & Hellström, G. (2011). Multipole method to calculate borehole thermal resistances in a borehole heat exchanger. *HVAC & R Research*, 17(6), 895-911.
- ClimateMaster. (2010, Sept. 24). Tranquility® 20 (TS) Series. *Residential Products Technical Guide*. ClimateMaster.

- Department of the Built Environment at Eindhoven University of Technology. (2012, 11 4). *Hamlab*. Retrieved from BPS Wiki:
<http://archbps1.campus.tue.nl/bpswiki/index.php/Hamlab>
- Energy Design Update. (2013, Feb). Taking stock of heat pumps: Steve Kavanaugh talks measuring real ground source heat pump costs and performance against projected cost and performance. (33.2), pp. 13-16.
- Eskilson, P. (1987). *Thermal Analysis of Heat Extraction Boreholes*. Lund, Sweden: University of Lund.
- Fischer, S. K., & Rice, C. K. (1983). *The Oak Ridge heat pump models: I. a steady-state computer design model for air-to-air heat pumps*. Oak Ridge, TN: Oak Ridge National Laboratory.
- Garca-Valladaresa, O., Perez-Segarrab, C., & Rigola, J. (2004). Numerical simulation of double-pipe condensers and evaporators. *International Journal of Refrigeration*, 27, 656-670.
- Gaspredes, J. L. (2011, Dec). *Development of an Integrated Building Load-Ground Source Heat Pump Model as a Test Bed to Assess Short- and Long-Term Heat Pump and Ground Loop and Ground Loop*. Austin, Texas: University of Texas at Austin.
- Hammond, M. (2011, Nov). Climatemaster Technical Trainer. (G. Masada, J. Gaspredes, & J. Blair, Interviewers)
- Hellström, G. (1991). *Ground heat storage: Thermal analyses of duct storage systems*. Sweden: Department of Mathematical Physics, Lund University.
- Hughes, P. J. (2008). *Geothermal (ground-source) heat pumps: Market status, barriers to adoption, and actions to overcome barriers*. Oak Ridge National Laboratory.
- Hughes, P., & Pratsch, L. (2001). *Technical and Market Results of Major U.S. Geothermal Heat Pump Programs*. U.S. Department of Energy, Office of Energy Efficiency and Renewable Energy. Oak Ridge: U.S. Department of Energy. Retrieved from <http://web.ornl.gov/~webworks/cppr/y2001/pres/113275.pdf>

- Ingersoll, L. R., & Plass, H. J. (1948). Theory of the ground pipe heat source for the heat pump. *Heating, Piping & Air Conditioning*.
- Ingersoll, L. R., Zobel, O. J., & Ingersoll, A. C. (1954). *Heat conduction with engineering, geological, and other applications*. New York: McGraw-Hill.
- International Energy Agency. (2012). *2012 Key World Energy Statistics*. International Energy Agency. Paris, France: OECD/IEA. Retrieved June 26, 2013, from <http://www.iea.org/publications/freepublications/publication/kwes.pdf>
- International Ground Source Heat Pump Association. (2009). *Ground Source Heat Pump Residential and Light Commercial Design and Installation Guide*. Stillwater: Oklahoma State University.
- Judge, J., & Radermacher, R. (1997). A heat exchanger model for mixtures and pure refrigerant cycle simulations. *International Journal of Refrigeration*, 20(4), 244-255.
- Kavanaugh, S. P. (1985). *Simulation and experimental verification of vertical ground-coupled heat pump systems*. Stillwater, Oklahoma: Oklahoma State University.
- Kavanaugh, S., Green, M., & Mescher, K. (2012, Oct). Long-Term Commercial GSHP Performance Part 4: Installation Costs. *ASHRAE Journal*, 26-38.
- Kohl, T., & Hopkirk, R. J. (1995). "FRACTure" - A simulation code for forced fluid flow and transport in fractured, porous rock. *Geothermics*, 24(3), 333-343.
- Lee, A. H., & Jones, J. W. (1997). Analytical model of a residential desuperheater. *Applied Energy*, 57(4), 271-285.
- Lund, J. W., Freeston, D. H., & Boyd, T. L. (2011). Direct utilization of geothermal energy 2010 worldwide review. *Geothermics*(40), 159-180.
- Muller, N. Z., Mendelsohn, R., & Nordhaus, W. (2011, Aug). Environmental Accounting for Pollution in the United States Economy. *The American Economic Review*, 101(5), 1649-1675. Retrieved Feb 17, 2014, from <http://www.jstor.org/stable/23045618>

- Muraya, N. K., O'Neal, D. L., & Heffington, W. M. (1996). Thermal interference of adjacent legs in a vertical u-tube heat exchanger for a ground-coupled heat pump. *ASHRAE Transactions*, 102(2), 12-21.
- Navigant Consulting, Inc. (2009). *Ground-Source Heat Pumps: Overview of Market Status, Barriers to Adoption, and Options for Overcoming Barriers*. Office of Energy Efficiency and Renewable Energy, U.S. Department of Energy. U.S. Department of Energy. Retrieved July 13, 2013, from http://www1.eere.energy.gov/geothermal/pdfs/gshp_overview.pdf
- NREL. (2009, Mar 10). *1991-2005 Update: Typical Meteorological Year 3*. Retrieved March 21, 2013, from National Solar Radiation Data Base: http://rredc.nrel.gov/solar/old_data/nsrdb/1991-2005/tmy3/
- Oklahoma State University. (2007a, Oct 25). *GLHEPRO Overview*. (J. R. Cullin, Editor) Retrieved Apr 12, 2014, from GLHEPRO for Windows: <http://www.hvac.okstate.edu/glhepro/>
- Oklahoma State University. (2007b, Oct 25). *GLHEPRO 4.0 For Windows: Users' Guide*. Retrieved from GLHEPRO 4.0 For Windows: <http://www.hvac.okstate.edu/glhepro/Manualv4.pdf>
- Pacheco-Vega, A., Sen, M., Yang, K. T., & McClain, R. L. (2001). Neural network analysis of fin-tube refrigerating heat exchanger with limited experimental data. *International Journal of Heat and Mass Transfer*, 44, 763-770.
- Rees, D. F. (2005). Modeling ground source heat pump systems in a building energy simulation program (EnergyPlus). *9th International IBPSA Conference*, (pp. 311-318). Montreal, Canada.
- Rottmayer, S. P., Beckman, W. A., & Mitchell, J. W. (1997). Simulation of a single vertical u-tube ground heat exchanger in an infinite medium. *ASHRAE Transactions*, 103(3), 651-659.
- Schijndel, A. W. (2007). *Integrated Heat Air and Moisture Modeling and Simulation*. Eindhoven University of Technology. Eindhoven, The Netherlands: Eindhoven University Press.

- Spitler, J. (2005). Ground Source Heat Pump System Research – Past, Present and Future (Editorial). *International Journal of HVAC&R Research*, 11(2), 165-167.
- Spitler, J. D., & Cullin, J. (2008). Misconceptions regarding design of ground-source heat pump systems. *Proceedings of the World Renewable Energy congress*. Glasgow, Scotland: Elsevier.
- The MathWorks, Inc. (2012, Feb 9). Product Help. *Matlab 2012a*. MathWorks.
- The World Bank. (2013). *World DataBank*. Retrieved Jun 23, 2013, from The World Bank: <http://databank.worldbank.org/data/views/reports/tableview.aspx>
- U.S. Department of Energy. (2010, Sept 30). *Commercial Reference Building Initiative*. Retrieved Sept 15, 2011, from U.S. Department of Energy Web site: http://www1.eere.energy.gov/buildings/commercial_initiative/new_construction.html
- U.S. Department of Energy. (2012, Jun 24). *Energy Saver: Geothermal Heat Pumps*. Retrieved Jul 15, 2013, from Energy.gov: <http://energy.gov/energysaver/articles/geothermal-heat-pumps>
- U.S. Department of Energy. (2013, Sept 29). *U.S. States: State Profiles and Energy Estimates*. Retrieved from Rankings: Average Retail Price of Electricity to Residential Sector, June 2013 (cents/kWh): <http://www.eia.gov/state/rankings/?sid=US#/series/31>
- U.S. Energy Information Administration. (2012). *Annual Energy Outlook 2012 with Projections to 2035*. U.S. Department of Energy, U.S. Energy Information Administration. Washington, DC: U.S. Department of Energy. Retrieved from www.eia.gov/forecasts/aeo
- United States Government Accountability Office. (Apr 2012). *Air Emissions and Electricity Generation at U.S. Power Plants*. Washington, DC: U.S. GAO. Retrieved Feb 17, 2014, from <http://www.gao.gov/assets/600/590188.pdf>
- Wang, B., Li, X., & Shi, W. (2005). A general geometrical model of scroll compressors based on discretional initial angles of involute. *International Journal of Refrigeration*(28), 958-966.

- Winandy, E., & Claudio Saavedra O, a. J. (2002). Experimental analysis and simplified modelling of a hermetic scroll refrigeration compressor. *Applied Thermal Engineering*, 22(2), 107-120.
- Wit, M. d. (2006). HAMBASE: Heat, Air and Moisture model for Building And Systems Evaluation. *Bouwstenen*(100).
- Wit, M. d. (2009, Jul). *HAMBASE: Part I Theory*. Retrieved Jul 29, 2013, from BPSwiki: Hamlab-Wiki page of the Computational Building Physics Group at the Department of the Built Environment of the Eindhoven University of Technology: http://archbps1.campus.tue.nl/bpswiki/images/3/3a/Hambasetheorydec_2009.pdf
- Wit, M. d. (2009, Oct). *HAMBASE: Part II Input and Output*. Retrieved Jul 29, 2013, from BPSwiki: Hamlab-Wiki page of the Computational Building Physics Group at the Department of the Built Environment of the Eindhoven University of Technology: http://archbps1.campus.tue.nl/bpswiki/images/7/75/Hambaseinoutputdec_2009.pdf
- Wit, M. d., & Driessen, H. (1988). ELAN - A Computer Model for Building Energy Design. *Building and Environment*, 23(4), 285-289.
- Xu, X. (2007). *Simulation and Optimal Control of Hybrid Ground Source Heat Pump Systems*. Stillwater, Oklahoma: Oklahoma State University.
- Yavuzturk, C. (1999). *Modeling of Vertical Ground Loop Heat Exchangers for Ground Source Heat Pump Systems*. Stillwater, Oklahoma: Oklahoma State University.
- Young, T. R. (2004). *Development, verification, and design analysis of the borehole fluid thermal mass model for approximating short term borehole thermal response*. Stillwater, Oklahoma: Oklahoma State University.
- Zeng, H., Diao, N., & Fang, Z. (2003). Efficiency of vertical geothermal heat exchangers in the ground source heat pump system. *Journal of Thermal Science*, 12(1), 77-81.